25/1/95 19.34

29/1/95 19.55

30/1/95 17.48

30 JAN 1995
20.59

8 FEB
17.11

9 FEB
18.33

13/2/95
4pm

16/2
16.45

23 FEB 1995
20.59

~~20/2/95~~
2/3/95
20.59

30.4.95
7.59 pm

6/5 - 17.00

11/5 - 16.51

12/5 - 17.59

16/6 17.59

ProQuest LLC.
789 East Eisenhower Parkway
P.O. Box 1346
Ann Arbor, MI 48106 – 1346

OPTIMISATION OF PLASTOHYDRODYNAMIC SYSTEM OF WIRE DRAWING USING POLYMER MELTS.

by

Hossein Parvinmehr BSc.

A thesis submitted to the COUNCIL FOR NATIONAL ACADEMIC AWARD in partial fulfilment for the degree of DOCTOR OF PHILOSOPHY

Department of Mechanical and Production Engineering,
Sheffield City Polytechnic. (Sponsoring Establishment)

Arthur Lee and Sons Ltd. (Collaborating Establishment)

December 1983

CONTENTS PAGE

LIST OF FIGURES PAGE

LIST OF PLATES PAGE

ACKNOWLEDGEMENTS

The author gratefully acknowledges his appreciation for the continual assistance and invaluable suggestions proffered by Dr. G. R. Symmons and Dr. M. S. J. Hashmi without whose supervision this work could not have been accomplished.

The technical assistance offered by Mr R. Teasdale and his staff was received with gratitude and particular thanks go to Mr D. McKay, Mr R. Wilkinson and Mr M. Jackson for their co-operation during the duration of this work.

A final acknowledgement is paid to the Arthur Lee and Sons Ltd., Sheffield, for their active collaborations.

DECLARATION

The author declares that no part of this work has been submitted in support of another degree or qualification to this or any other establishment. The author further declares that he has not been a registered candidate or enrolled student for another award of the CNAA or other academic or professional institution during the course of the research programme.

H. Parvinmehr

ABSTRACT

OPTIMISATION OF PLASTOHYDRODYNAMIC SYSTEM OF WIRE DRAWING USING POLYMER MELTS.

H. Parvinmehr

A feasibility study carried out on the wire drawing system consisting of a reduction die preceded by a pressure tube and polymer melt lubrication, led to the introduction of the die-less wire drawing process. The conventional reduction die is altogether replaced by a die-less unit of stepped bore configuration. The deformation is induced by means of an effective die which is formed as a result of hydrodynamic pressures generated in the unit due to the motion of the wire and viscous action of the polymer melt. The dimensions of the unit are such that the smallest bore size is greater than the incoming wire diameter, metal to metal contact, therefore is eliminated, removing some of the disadvantages encountered in a conventional wire drawing process.

An extensive experimental study has been under taken which showed that the deformation in the wire was much higher at slower drawing speeds and the obtainable percentage reduction in area reduced at higher drawing speeds. However, use of a higher viscosity polymer melt and/or a multi-unit drawing system has resulted in higher deformation of the wire at higher drawing speeds.

An analysis has been developed for predicting the length of the deformation zone, shape of the effective die and percentage reduction in area based on an empirical expression relating shear stress and shear rate of the polymer melt. The theory incorporates the pressure coefficient of viscosity derived from the available data, the limiting shear stress which manifests itself as slip in the polymer melt and the strain hardening and the strain rate sensitivity of the wire material.

Results from the analysis appears to under estimate the experimental results at slower drawing speeds and over estimate the experimental results at higher drawing speeds.

NOTATION

$\acute{P}_1$	pressure gradient in the first section of the unit prior to the deformation of wire.
$\acute{P}_2$	pressure gradient in the second part of the unit prior to the deformation of wire
τ_1	shear stress in the melt in the first part of unit
τ_2	shear stress in the melt in the second part of unit
K	non-Newtonian factor
τ_{c_1}	shear stress on the wire in the first section of the unit prior to deformation
τ_{c_2}	shear stress on the wire in the second section of the unit prior to deformation
τ_{ca}	critical shear stress
η_o	initial viscosity of polymer melt
a	viscosity constant
b	pressure coefficient of viscosity
$\acute{V}$	velocity of wire prior to deformation
Q_1	flow of polymer in the first section of the unit
Q_2	flow of polymer in the second section of the unit
U_1	velocity of polymer in the first section of the unit
U_2	velocity of polymer in the second section of the unit
P_m	pressure at the step

h_1	radial gap in the first section of the unit prior to deformation of wire
h_2	radial gap in the second section of the unit prior to deformation of wire
l_1	length of the first section of the unit
l_2	length of the second section of the unit
V_s	wire speed at commencement of slip
$\dot{\gamma}$	apparent shear rate in the first section of the unit
X_1	yielding position of wire
σ_{x1}	axial stress in the wire at commencement of plastic deformation
P_1	radial pressure in the melt at commencement of plastic deformation
D_1	original diameter of wire
σ_r	radial stress in the wire
D_i	wire diameter in the deformation zone
h_i	radial gap in the deformation zone
α	semi-angle of the effective die
Δx	step size in the deformation zone
B	slope of the deformation line within Δx
τ_{ci}	shear stress on the wire in the deformation zone
σ_{xi}	axial stress in the deformation zone
P_i	pressure in the melt in the deformation zone

Q_i flow of polymer in the deformation zone

V_i velocity of wire in the deformation zone

Y_o initial yield stress in the wire

K_o strain hardening constant

n strain hardening index

Y_i yield stress in the deformation zone

V_d velocity of wire at the end of deformation zone

S_i dynamic/static stress ratio

h_3 polymer coating thickness

Note : percentage reduction in area is given by; $\frac{D_1^2 - D_2^2}{D_1^2}$

SUBSCRIPTS:

1 first section of the unit

2 second section of the unit

i deformation zone

r denotes radial direction

x denotes axial direction

1 inch = 25.4 mm
1 foot = 12 inches
1 bar = 10^5 N/m^2
1 psi = 6897.11 N/m^2

CHAPTER 1: Introduction.

1.1- The Wire Drawing Process.

1.2- The Historical Background Of Hydrodynamic Lubrication.

1.3- Introduction Of Polymer Melt As A Lubricant In Wire Drawing.

1.4- Background Development Leading To The Design Of The Pressure Reduction Units And The Scope Of The Present Work.

1.1- The Wire Drawing Process

Conventional wire drawing is the process of pulling the wire through a trumpet shaped die to produce a reduction in diameter. The principal purpose of wire drawing is to consistently reduce wire to a specific size with acceptable metallurgical properties.

The process is usually carried out employing tungsten carbide dies. Diamond dies however, are used especially for finer wires. When the wire is drawn cold, the deformation of metal produces a very high drawing load which makes the presence of a lubricant essential. Generally two types of lubrication methods are used in wire drawing depending upon the material and size of the wire. These are:

i)- "Wet Drawing" in which the entire apparatus is submerged in a bath of lubricant. This type of lubrication is usually employed for wire diameters of less than 0.5mm.

ii)- "Dry Drawing" refers to a system in which the wire is passed through a box of soap powder before entering the die. To facilitate the pick up of soap powder, the wire is passed through the lime liquid, borax or other alkaline substances. Dry drawing is usually used for wire diameters of more than 0.5mm.

In conventional wire drawing, friction between the wire and the die is of the boundary type where metal to metal contact takes place inspite of the presence of a lubricant, resulting in die wear.

Hydrodynamic lubrication however, refers to a regime where a thick lubricant film separates two metal surfaces previously in contact. To create such a regime, certain wire speed and lubricant pressure must be reached and maintained in order to keep the surfaces continously apart. Prior to hydrodynamic lubrication, boundary lubrication is the dominant regime. The film thickness produced in dry drawing is greater than that in boundary lubrication but less than that in hydrodynamic lubrication, "Quasi-Hydrodynamic" (1,2).**

Attempts were made (2,3) to ascertain the mean die pressure by means of the split-die technique in order to estimate the die wear. The radial force tending to separate the two halves of the die was measured concurrently with the drawing force. It was shown that there is an optimum die angle for a given reduction in area for which drawing force is the least.

Boundary lubrication methods have been used for the wire drawing process since the inception of the process itself. However, the tasks of producing satisfactory physical properties of the drawn wire to meet the demand for increased production and quality of product are proving to be beyond the scope of these traditional lubrication methods. Therefore, other means of lubrication are being investigated.

**- Numbers in brackets refer to references which may be found in chapter 9.

1.2- The Historical Background Of Hydrodynamic Lubrication

In the past, both the die angle and the lubricant were selected by means of trial and error to ensure that the best possible results were obtained. As demand for higher quality wire increased, better lubrication proved necessary to promote efficiency, surface finish, quality, heat dissipation and loss of production time. The latter may be summarized as:

1- Reduced drawing time.
2- Reduction of the number of interpass heat treatments.
3- Elimination of pre-drawing time.
4- Reduction of down time due to changing dies because of excessive wear.

Recently, attempts have been made to introduce more theoretical background to the process which will hopefully enable greater understanding of the mechanism of the process, leading to more improved and efficient systems. Christopherson and Naylor (4) pioneered the development of hydrodynamic lubrication in wire drawing. They employed a long tube, with very close tolerances, attached to the front end of a conventional die as shown in figure 1. Oil was used for lubrication purposes, and as the wire was pulled through the die, it pressurized the lubricant by viscous action and fed into the die inlet. Christopherson and Naylor reasoned that if this pressure is high enough at the die inlet, metal to metal contact can be prevented. Experimental results provided by them showed evidence of

deformation of wire in the tube before the die entrance. Although it was shown that hydrodynamic lubrication was achieved under the designed conditions, the pressure nozzle had to be placed vertical and was of such a length that the wire industry found it too inconvenient to put it into practice.

Wistreich (5) conducted experimental work on the forced lubrication based on a pressure tube system. Soap powder was used as the lubricant in a short nozzle (2 inch. length) which was attached to the entry side of the die. The experimental results showed that the speed, temperature and the tube gap had a direct effect on the property of the film thickness produced. He also showed that when the soap powder was replaced by oil, an increase rather than the decline of film thickness was observed. The schematic diagram of the (BISRA) unit is shown in figure 2.

Tattersall (6) published a detailed analysis of plasto-hydrodynamic lubrication in wire drawing taking some rheological and metallurgical properties of the process into account. Results from experiment and theory showed that these were in reasonable agreement. More recently Chu (7), using the work of Tattersall has presented charts for inlet tube design.

Theoretical analysis of the high speed strip drawing process by Bloor etal (8) predicted that film thickness of the order of 10^{-4} in. were attainable using tapered dies and mineral oil as a lubricant. The experimental process was carried out at speeds of up to 9000 ft/min with conventional drawing dies. These authors concluded that at the higher drawing speeds the worked material and die

surfaces were protected by a hydrodynamic film as exhibited by the surface quality of the material after drawing.

Apart from the consideration of the inlet tube one of the main themes of the analysis presented by other workers (9,10,11) has been the study of the theoretical film thickness which would be developed under representative practical drawing conditions. An improvement in lubrication was reported by Middlemiss (12) using an externally pressurized lubrication system. The unit consisted of two dies separated by a narrow tube which was connected to a hydraulic pump to pressurize the lubricant in order to assist the formation of hydrodynamic film at the beginning of the drawing process. The wire was first passed through an ironing die which acted as a seal and then through the reduction die. A section view of the unit is shown in figure 3. This pre-pressurized lubrication method was reported to work successfully for the reduction die but the ironing die was worn severely due to lack of lubrication.

Further evidence of improvement in lubrication and machine efficiency was observed when the ironing die was replaced by a short pressure tube with very fine tolerances. The system was still provided with pressurized lubricant and the action of the tube was to reduce the oil leakage. As soon as steady state lubrication was reached, the hydraulic pump was dispensed with in order to reduce the cost of operation. The modified unit is shown in figure 4.

Double die arrangements were further developed by Orlov etal (13). Their version of the pressure nozzle/die is shown in figure 5. This arrangement differs from

Middlemiss's unit in that the pressure die takes over the function of the pump by the motion of the wire. The lubricant is transported into the chamber formed by the exit cone of the pressure die and the entry part of the drawing die, where the pressurized lubricant provides the hydrodynamic lubrication during drawing. Although, it was claimed that the efficiency was increased by 53%, die life was improved by 500%, and the electrical power consumption was reduced by 45%, there was however, a lack of substantial experimental evidence.

1.3- Introduction Of Polymer Melt As A Lubricant In Wire Drawing

Polymers have been considered as a lubricant previously and were used in other processes such as hydrostatic extrusion and deep drawing. The reason for this type of lubrication stems from the desire to have an alternative lubrication system which has very different characteristics from those currently in use. One of the advantages that a polymer melt can offer is its high viscosity which conventional lubricants fail to provide at higher temperatures.

The use of a polymer melt as a lubricant in wire drawing was suggested by Symmons and Thompson (14) to investigate the adherence of the polymer coat onto the drawn wire. Although hydrodynamic lubrication of wire was claimed to be achieved successfully, the adhesion between the wire and the polymer was reported to be unsatisfactory. Stevens (15) conducted a limited experimental work in wire

drawing and polymer melt lubrication investigating the coating properties of the polymer. Practical results showed a decrease in the coating thickness with increasing speed which gave some correlation with his newtonian solution. Crampton (16) carried out an indepth study of the wire drawing process based on the similar unit adopted by Stevens again using polymer melt as a lubricant. The apparatus consisted of a pressure tube connected to the forward end of a conventional die. The polymer melt was dragged into the tube by the motion of the wire, generating high pressures which resulted in hydrodynamic lubrication and coating of wire during the drawing process. A section view of the unit is shown in figure 6. The lubrication ability of the polymer melt was theoretically and experimentally examined by changing various parameters such as polymer temperature, wire material, drawing speed etc. and computer assisted, plasto-hydrodynamic non-newtonian solution was shown to be in some agreement with the experimental results.

1.4- Background Development Leading To The Design Of The Pressure Reduction Units And The Scope Of The Present Work

The application of the pressure tube in wire drawing was originated to overcome the difficulties associated with using oil or soap lubricant. Although successful attempts were made to introduce hydrodynamic lubrication, the following areas of inconvenience in wire drawing still exist:

i)- The need for a leader wire.

ii)- Start up problems during which the wire may snap.

iii)- Severe die wear prior to the establishment of hydrodynamic lubrication.

When polymer melt was introduced in conjunction with the pressure tube, it was thought that it would provide a novel lubrication system which would give partial solutions to the existing problems. The initial researchers (14,15,16) showed that in addition to above difficulties, other limitations were also present:

i)- Up to certain drawing speeds "Bamboo" effect was observed on the polymer coating with subsequent necking of the wire.

ii)- Polymer coating thickness on the wire reduced by increasing the drawing speed.

A careful study of previous works was undertaken to develop a system in order to eliminate some of the limitations and difficulties inherent in the wire drawing process. Crampton (16) showed that during drawing, deformation of wire took place before the die entrance due to the high pressure generated in the pressure tube. It was then thought that under certain geometrical configurations it might be possible to remove the reduction die and still generate the necessary pressure by the polymer melt to reduce the wire diameter. The feasibility study showed that, in the absence of the die, units capable of deforming the wire could be operated to some

degree of success. Hence two reduction units were designed and manufactured, one being of stepped and the other being of tapered bore. Dimensions of the units were chosen in a fashion that a narrow gap was present between the wire and the smallest diameter of either units, preventing metal to metal contact taking place. This immediately solved the problem of a leader wire which was absolutely necessary prior to drawing process in the case of conventional wire drawing. Initially an experimental programme was conducted to examine the performance of the pressure reduction units. The obtained results confirmed successful achievements in the die-less wire drawing where many difficulties associated with this deforming process were completely eliminated ie die and consequently die wear, start up problems, breakage etc. The only observed limitation was the fact that at increasing drawing speeds the performance of both units, in terms of the obtainable reduction in area, decreased. Since the design and manufacturing of the stepped bore reduction unit proved simpler, an extensive experimental and theoretical work was carried out for this unit.

The objectives of the present work are to fulfil the following points:

1- To provide an improved theoretical solution, taking detailed rheological and metallurgical properties of the polymer melt and the wire into account.

2- To investigate the performance of the unit in detail and to examine the correlation between the experimental and theoretical results.

3- To examine the product from the present system and compare the results with those wires drawn using the conventional drawing process, and critically evaluate the new system in the light of industrial practice and requirement.

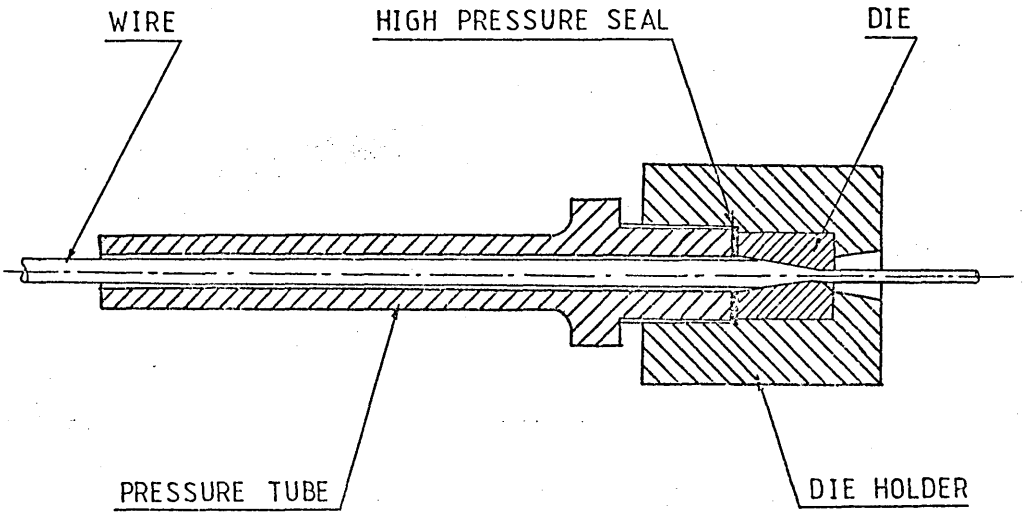

FIG 1 : TYPICAL PRESSURE TUBE AND DIE

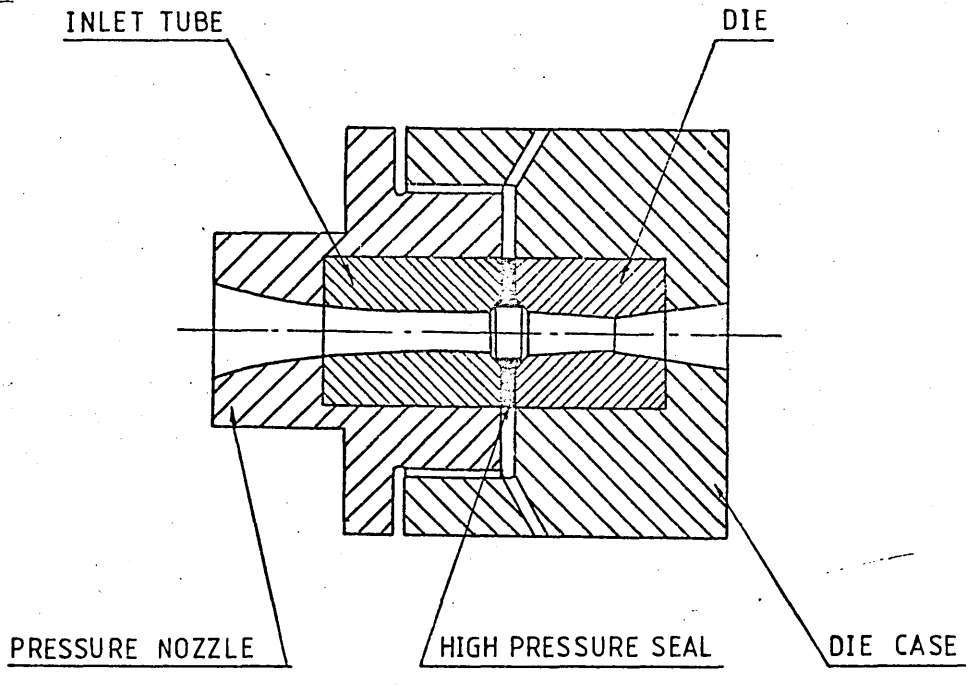

FIG 2 : NOZZLE - DIE UNIT (BISRA)

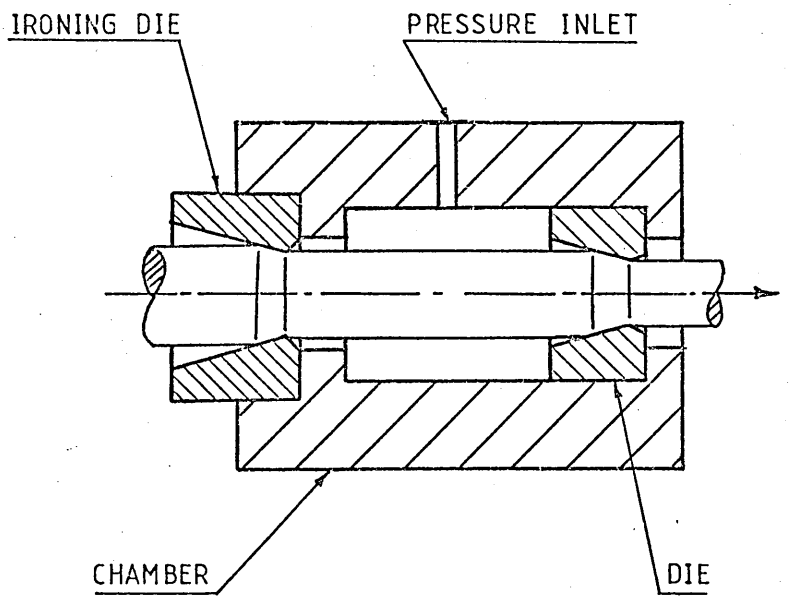

FIG 3 : PRESSURIZED CHAMBER

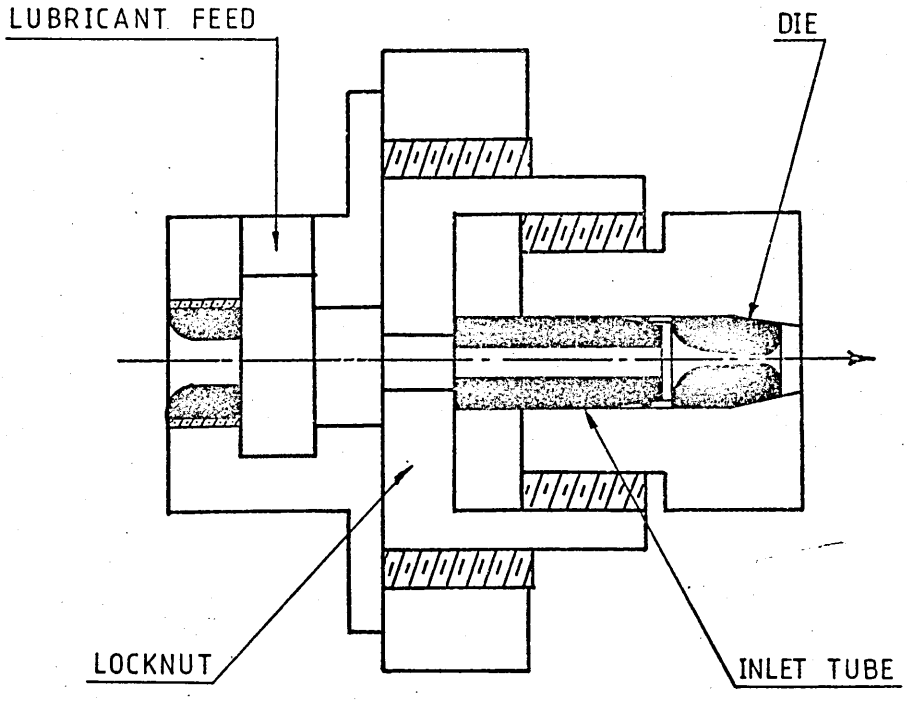

FIG 4 : HIGH PRESSURE DIE UNIT

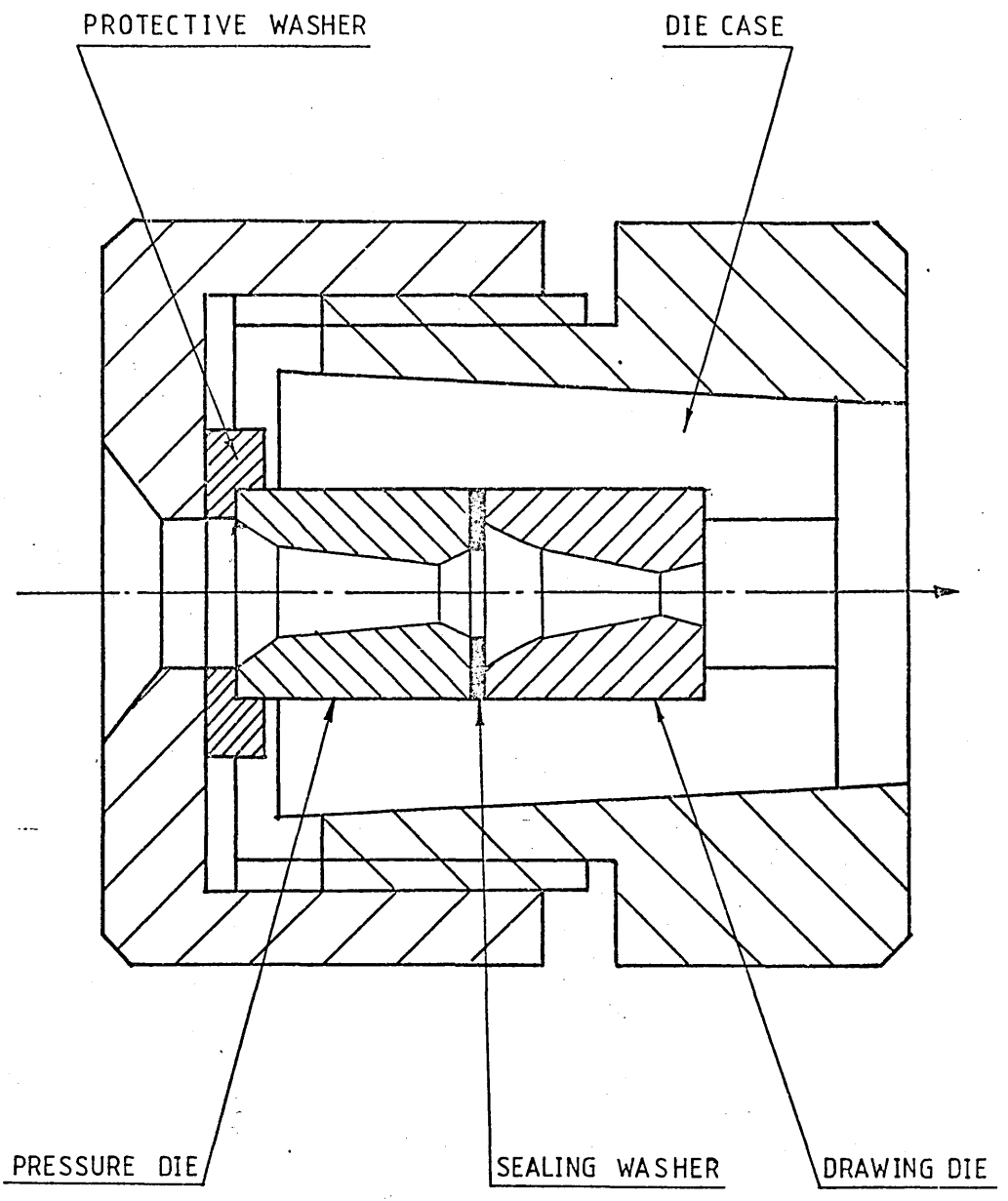

FIG 5 : DOUBLE DIE UNIT

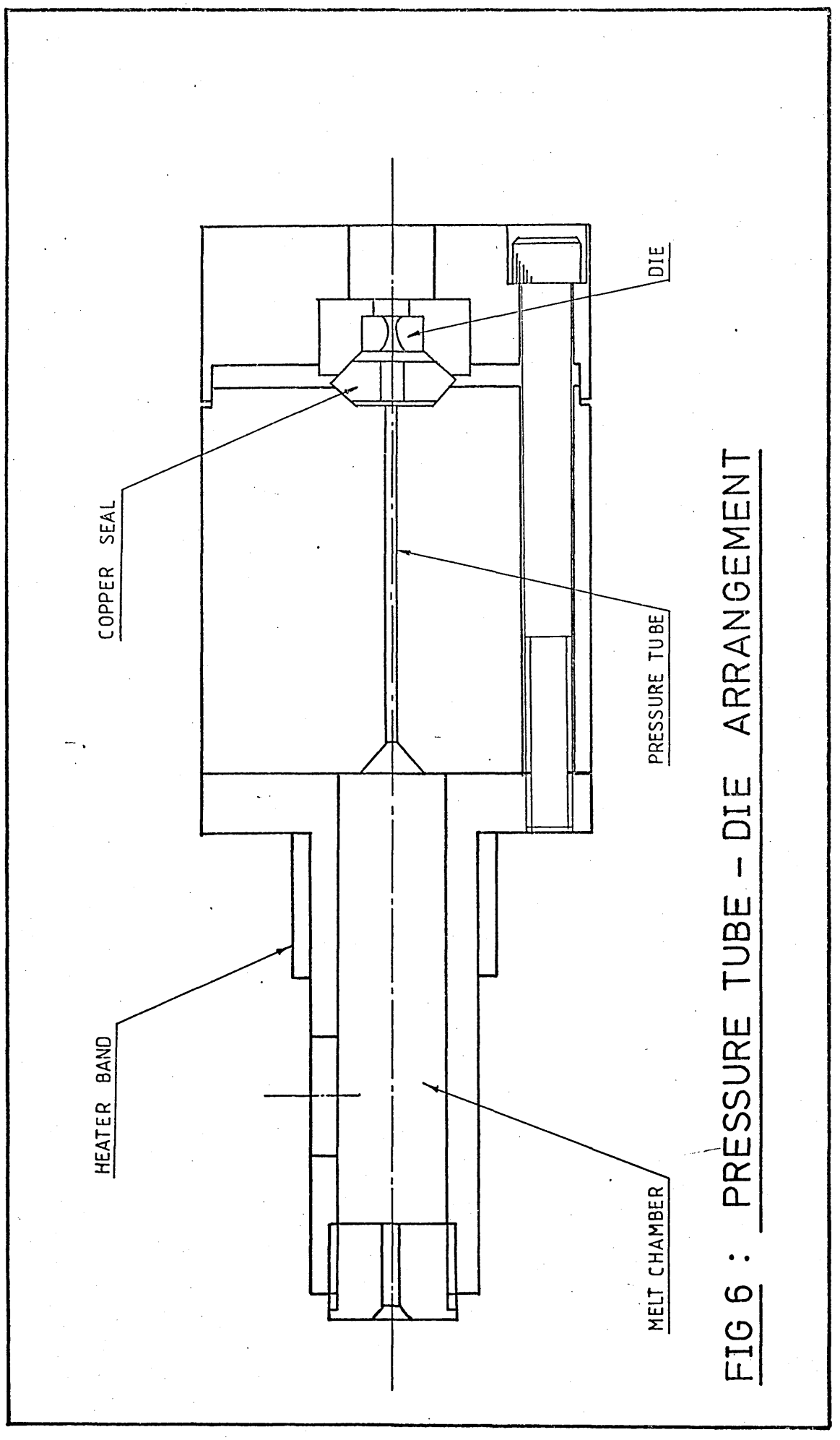

FIG 6 : PRESSURE TUBE - DIE ARRANGEMENT

CHAPTER 2: Rheology Of Polymer Melts.

2.1- Introduction.

2.2- Temperature Dependent Viscosity.

2.3- Stress-Strain Dependent Viscosity.

2.3.1- Critical Shear Stress.

2.3.2- Shark Skin.

2.4- Pressure Dependent Viscosity.

2.5- Effect Of Polymer Flow Characteristics.

2.1- Introduction

Rheology of polymer melt describes the flow characteristics of the material. Polymers generally consist of very long molecules and the atoms making these long chains are carbon and hydrogen atoms. The links between the atoms form a definite angle with each other, depending mainly on the linking atoms but usually a little over 100°. In most cases the molecular segments, if they have sufficient energy, can rotate about these links. One of the most common forces of attraction between the molecules is the Van der Waals forces and polymers with this type of bonding are commonly called Thermoplastic polymers. Another form of bonding between the molecules is cross-linking which is refered to Thermosetting polymers. In Thermoplastic polymers long molecules take up a non-random configuration under the stress which would be partially recovered when stress is removed (Thermosetting polymers show brittle behaviour). If the stress applied together with a temperature increase is high enough to overcome the Van der Waals forces, a relative molecular motion takes place causing the polymer to flow. The ease of flow will depend on the mobility of the molecular chains and the forces holding them together.

The flow characteristics of the polymer melts are influenced by many factors which are described in this chapter in relation to the present work.

2.2- Temperature Dependent Viscosity

An increase in temperature generally decreases the viscosity of the fluids. This effect vastly differs for different types of polymers. Figure 7 shows typical changes in viscosity against the reciprocal of absolute temperature at zero shear rates. The slope of each line measures the activation energy for each polymer. Temperature increase in polymers with higher activation energies has more deterioration effect on viscosity compared to those of lower activation energies. This energy is a function of polarity in polymers and the most non-polar polymers such as polyethylene with very small inter-molecular forces have low activation energy.

Dienes (17) believed that as the temperature increases the molecular arrangements within the polymer change more towards random configuration, therefore it becomes easier for the polymer to flow at higher temperatures. Attempts have also been made (18) to explain the difference in temperature dependence of viscosity between different polymers. It was indicated that the variation of viscosity with temperature is a function of the difference between the melt temperature and the glass transition temperature of the polymer.

Polymers used for the experimental tests were an ICI polyethylene polymer (Alkathene WVG23) and a Shell polypropylene (KM61) with specific densities of 0.913 and 0.908 respectively. Figure 8 shows the variation of viscosity versus temperatures for both polymers at zero shear rate. These graphs do not represent the complete

behaviour since viscosity measurements are affected by pressure, shear rate, temperature etc. and it is necessary to include these effects on viscosity of polymer melts.

2.3- Stress-Strain Dependent Viscosity

Newtonian fluids under shear stress condition exhibit linear relationship with shear rate where the slope of the line represents the viscosity of the fluids. Pseudo-plastic fluids however, show non-linear behaviour under similar conditions where stress deterioration is noticed owing to increasing shear rate. This phenomenon is called shear-thinning effect which is one of the most important flow properties of the polymer melts. The opposite rheological effect to shear-thinning is shear-thickening, commonly called dilatant behaviour. Although no polymer melts have been found to be dilated under any conditions, certain polymer solutions have been reported to exhibit dilatant behaviour (19). Figures 9 and 10 show the effect of shear rate on viscosity where the influence of temperature may be noticed. These curves were produced by extruding polymer melts (Alkathene WVG23 and polypropylene KM61) through an extrusion rheometer at different temperatures. Details of equipments and calculations are provided in Appendix 1. The viscosity of the polymer may be calculated at any known shear rate by measuring the slope of the curve. Clegg (20) showed that the length and diameter of the extrusion die had very little effect on the flow of the polymer when low density polythene was used. Another way of representing the effect of shear rate on viscosity is

shown in figures 11 and 12 from which viscosity can be read directly, (in the case of Newtonian fluids, straight horizontal lines would be produced).

2.3.1- Critical Shear Stress

Critical shear stress is the stress at which the uniformity of the flow of the polymer melt ceases to exist. Many workers (20 to 25) investigated this phenomenon and showed that certain flow defects are associated with polymer melts at critical shear stress. The flow irregularities were shown to take the form of Spiral, Ripple, Bamboo, Zig Zag or Hilex for different types of polymers. Non-uniformity of the flow for polypropylene KM61 was observed while being extruded at 200° C at shear stress of 3.2×10^5 N/m^2 as shown in figure 10. The extruded polymer showed random shape. This phenomemon for polypropylene, at higher temperatures, and Alkathene WVG23 polymer was not detected during the extrusion process.

The terms "Melt fracture", "Elastic turbulance" and "Flow distortion" have been used to describe this effect. However, there is a general agreement on the following points:

1- Critical Shear Stress (CSS) is independent of die length and diameter.
2- CSS has values in the region of 0.1 - 1.0 MN/m^2 for most polymers.
3- CSS does not vary widely with temperature.

Also at critical shear stress, the following observations were made by the above authors:

1- A discontinuity in the viscosity shear stress curves occured.
2- The flow defect always took place when non-Newtonian fluids were involved.
3- The critical shear stress was shown by cinematography method to take place in the die.

A careful study of polymer flow was conducted by Benbow and Lamb (26) who showed, employing a transparent die and coloured polymer, that slip occured at the die wall when critical shear stress was reached. Experiments carried out by them showed that the critical shear stress was affected by die materials where different flow characteristics were observed for each material. Results from brass and silver steel dies were compared using Alkathene polymer. It was shown that for brass die, there is a change in slope of shear stress-shear rate curve at the onset of flow distorsion, whereas silver steel die exhibited a smooth flow curve. Also the silver steel die results indicated a critical shear stress independent of temperature whilst the brass die showed a slight increase in critical stress with temperature.

Lupton and Regester (27) reported that for a linear polyethylene of unit melt index the flow rate increased by a factor of four without any appreciable change in the differential pressure. They suggested that the flow behaviour depended upon the length/diameter ratio and

believed that slip on the die wall was the cause of the discontinuity in the flow of the polymer. Westover (28) carried out a study of polymer slip on an ultra high molecular weight linear polyethylene incorporating hydrostatic pressure. Two interesting observations were made:

1- Flow rate above the critical shear stress increased rather than decreasing as for most of the polymers.
2- The critical shear stress occured at lower shear rate as the hydrostatic pressure upon the melt increased.

Westover concluded that the basic concepts of maximum shear stress, apparent shear rate and viscosity are invalid after slip occurs and that Rabinowitsch (35) equation becomes inapplicable.

2.3.2- Shark-Skin

Shark-skin is another flow defect which occurs at shear stresses below critical value and figure 10 clearly shows these differences for polypropylene polymer. This flow distorsion manifests itself in regular ridges perpendicular to the flow direction. The possible mechanism of shark-skin has been described as the surface failure of the melt caused by the outer layer of the polymer accelerating away from a relatively stationary bank of polymer held near the die exit plane. Cyclic build-up and release of surface tensile forces in the extrudate was suggested that must rise from a particular balance

between the elastic and viscous properties of the melt (18,24).

To investigate the source of shark-skin, Benbow and Lamb (26) carried out an experiment employing a thin walled wood's metal die, extruding silicone gum through, at a stress sufficient to give pronounced shark-skin. To examine the extruding polymer, the die was melted in boiling water and it was found that the polymer surface in the die was smooth, thus showing that the stresses causing shark-skin were produced at the die exit. A schematic representation of the shark-skin mechanism is shown in figure 13. Also plates 11 to 16 show shark-skin produced on polymer coatings during the drawing process.

2.4- Pressure Dependent Viscosity

The influence of pressure on the polymer melts and the consequence changes of apparent viscosity and other flow properties are not as well understood as the effect of temperature and shear rate. Compressibility of polymers was investigated by Maxwell and Matsuoka (29) and they showed that polymers are compressible fluids and the compressibility varies with the pressure rate, temperature and the polymer type. They reported a 2.5% permanent change in the density of polyethylene under high pressures.

Viscosity, by definition, is the internal resistance to shearing stress due to inter molecular forces of attraction. It was thought that when the molecular attractions are encouraged, the apparent viscosity of the polymers, which is one of the most important properties

of these materials, may be increased. Studies by Maxwell and Jung (30) on polyethylene and polystyrene showed a non-linear increase of viscosity due to high pressure at constant shear rate. At the pressure of 150 MN/m^2, molten polystyrene was reported to act like a solid plug. Other workers (28,31,32) have also confirmed the increasing effect of pressure on viscosity of polymer melts. It was pointed out that a pressure increase of 160 MN/m^2 causes a viscosity change by a factor of over one hundred for polystyrene and a factor of five for polyethylene. Cogswell (33) suggested that the effect of the increase in pressure may be linked to that due to a drop in temperature. Experimental results reported by Cogswell on low density polyethylene showed an increase in pressure of 100 MN/m^2 had the same effect on viscosity as that due to a drop in temperature of 53 $^{\circ}C$ within the melt range.

One of the most comprehensive studies of the effect of pressure on different polymer melts was conducted by Westover (34) based on a similar device used by Maxwell and Matsuoka (29). Most of the experimental work carried out by Westover was on a branched 0.92 density polyethylene with pressure varying from 14 MN/m^2 to 170 MN/m^2.

Since the data provided by Westover were found to be most comprehensive, these have been used to determine the pressure coefficient of viscosity in the present analysis. Figure 14 shows the effect of pressure on shear stress-shear rate curves and figure 15 shows how shear rate effects the influence of pressure on viscosity.

2.5- The Effect Of Polymer Flow Characteristics

In the present work polymer melt is subjected to very high shear rates and pressures, much greater than those capable of being investigated in any extrusion rheometer. Crampton (16) concluded that the decrease in coating thickness was due to the presence of a critical shear stress at low shear rates. It is however believed that, the poor performance of the units at higher drawing speeds is related to a combination of factors such as shear rate, melt flow instability, partial crystallization, compressibility etc. and not the critical shear stress alone.

The formation of shark skin is thought to take place at the exit end of the unit, therefore, this effect on the performance of the system is neglected. Furthermore, little is known about the crystallization and compressibility of the polymers at high pressures, therefore more investigation is needed to understand these effects fully.

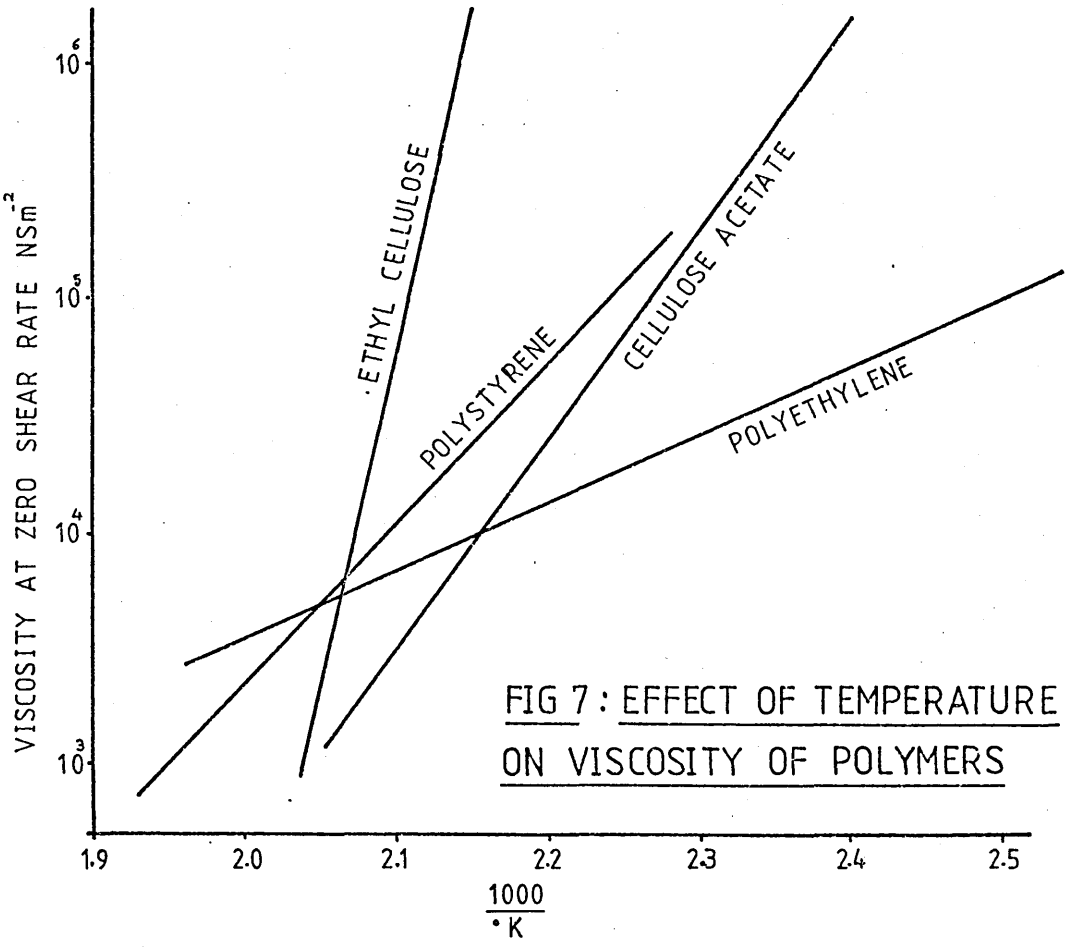

FIG 7 : EFFECT OF TEMPERATURE ON VISCOSITY OF POLYMERS

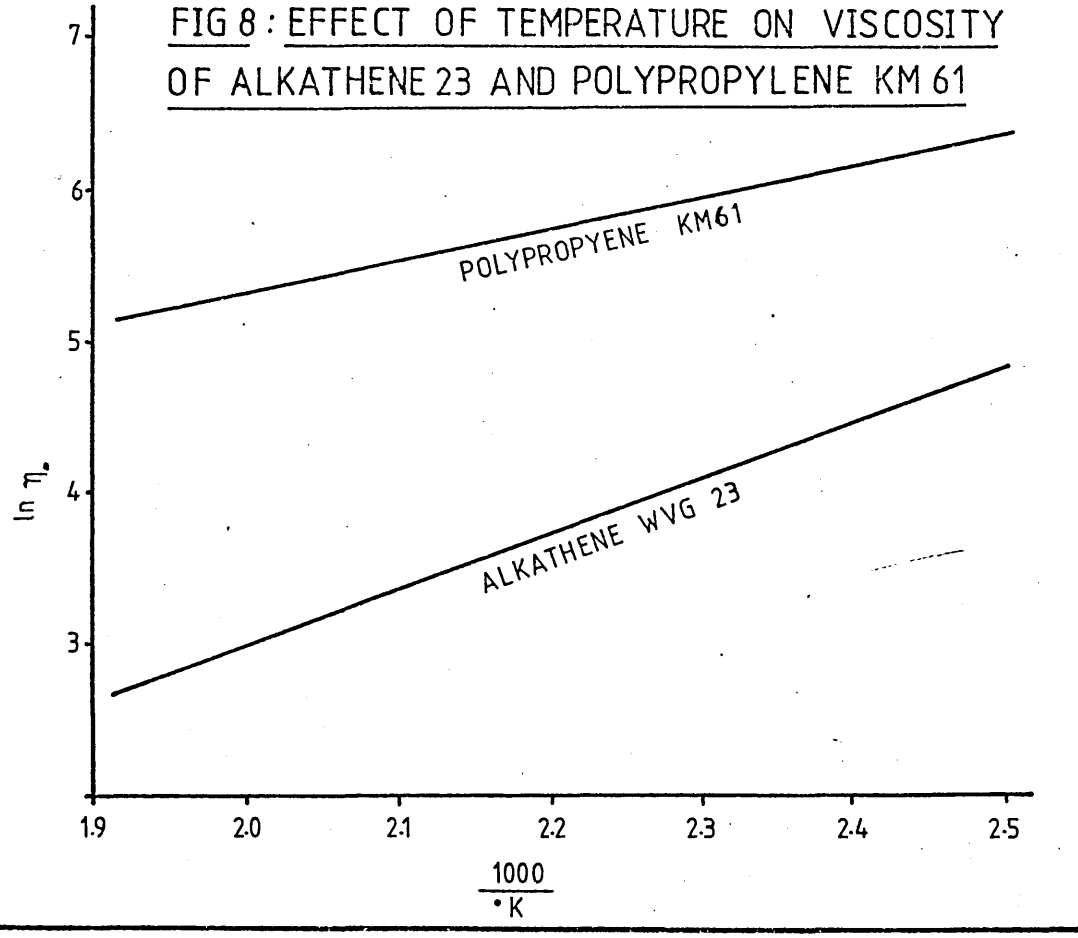

FIG 8 : EFFECT OF TEMPERATURE ON VISCOSITY OF ALKATHENE 23 AND POLYPROPYLENE KM 61

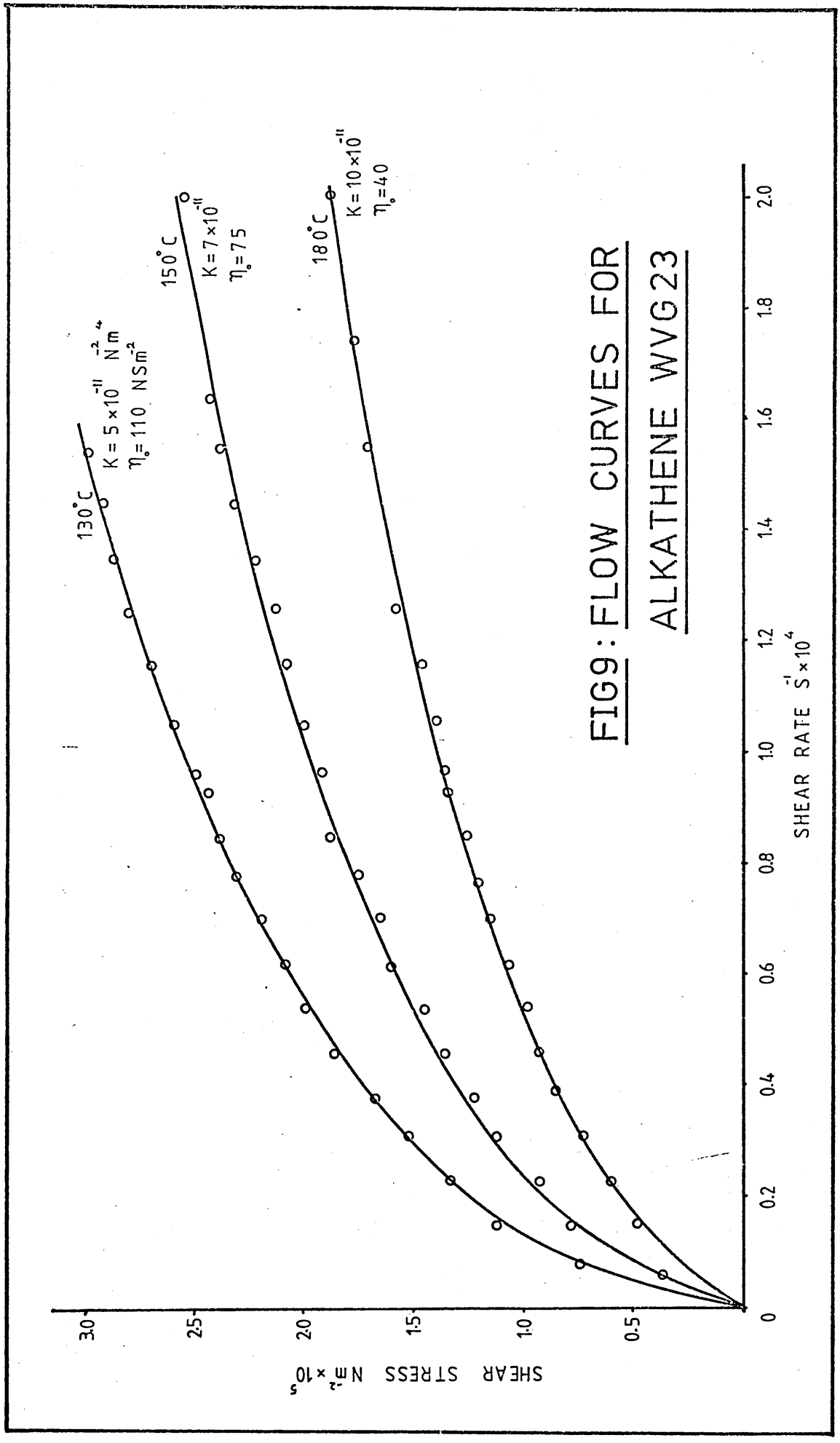

FIG9: FLOW CURVES FOR ALKATHENE WVG23

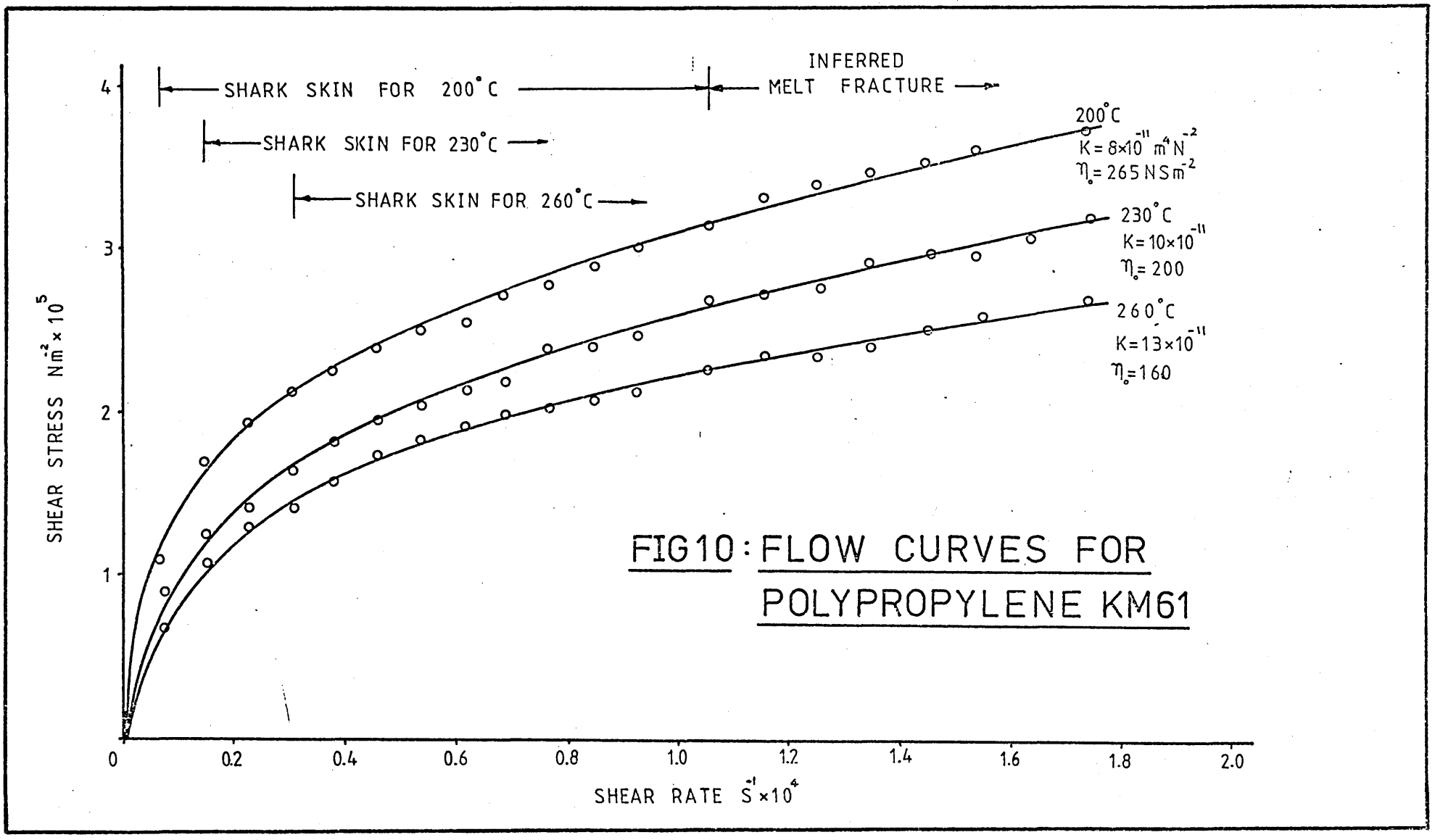

FIG10: FLOW CURVES FOR POLYPROPYLENE KM61

FIG 11: EFFECT OF SHEAR RATE ON VISCOSITY OF ALKATHENE WVG23

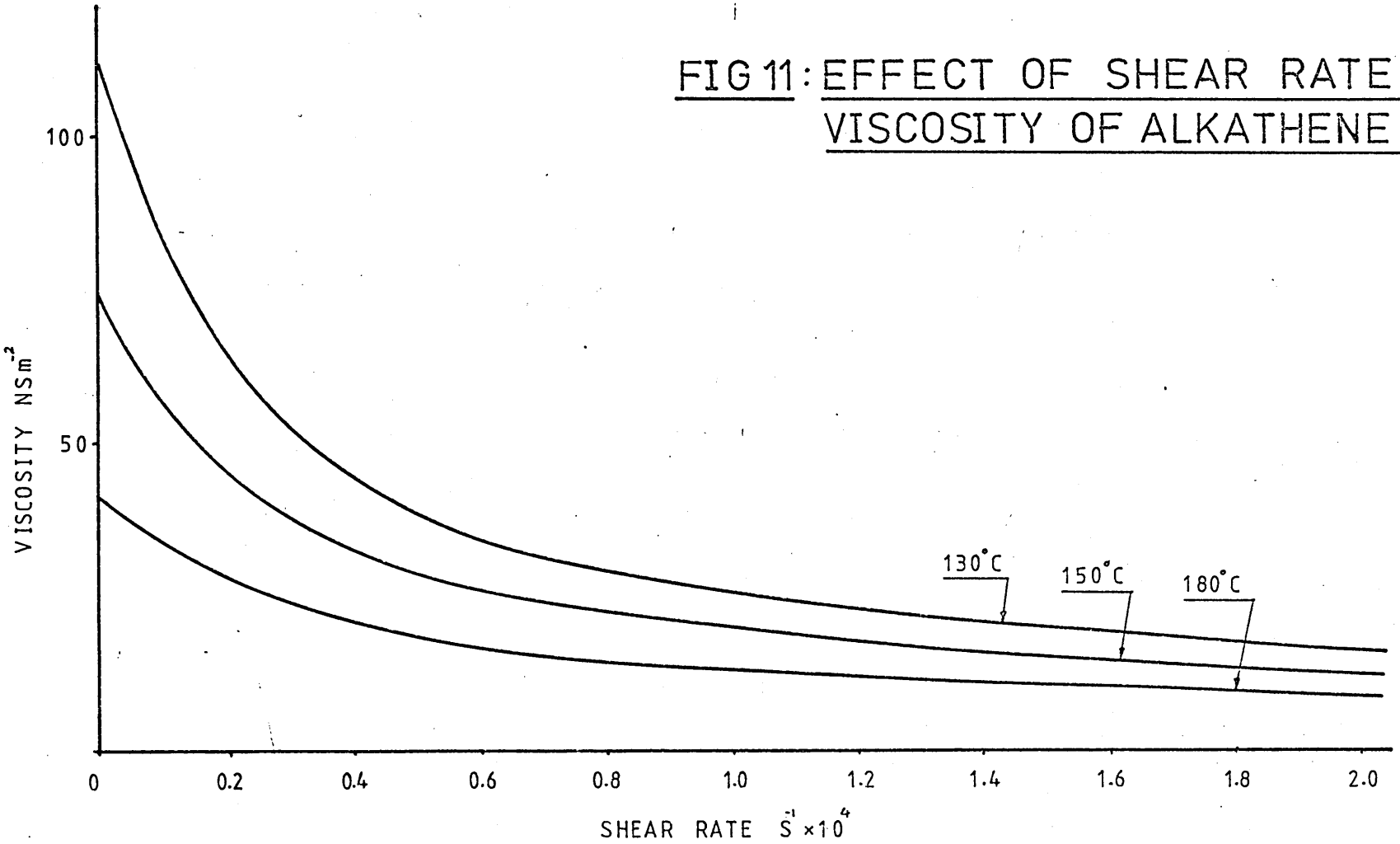

FIG 12: EFFECT OF SHEAR RATE ON VISCOSITY OF POLYPROPYLENE KM61

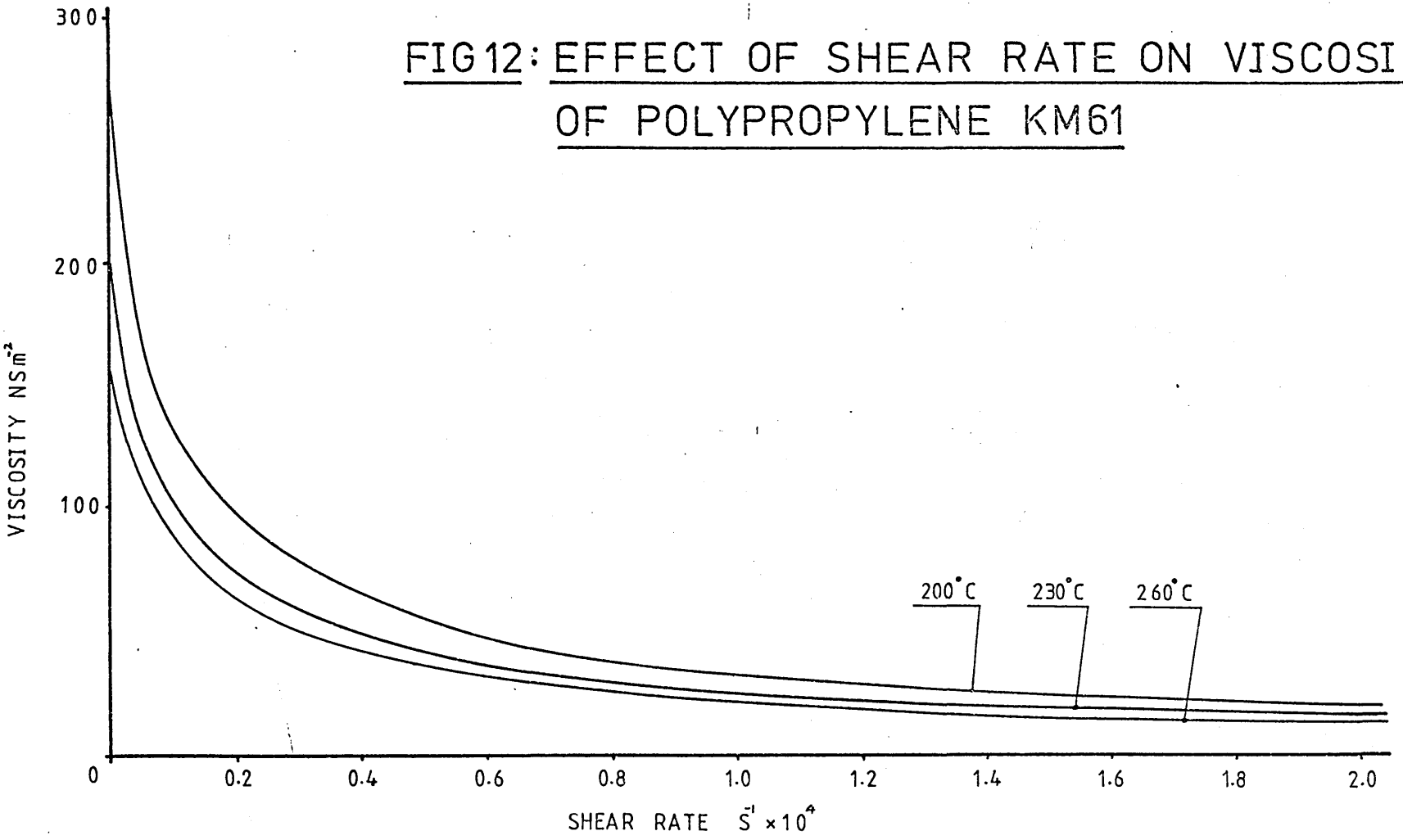

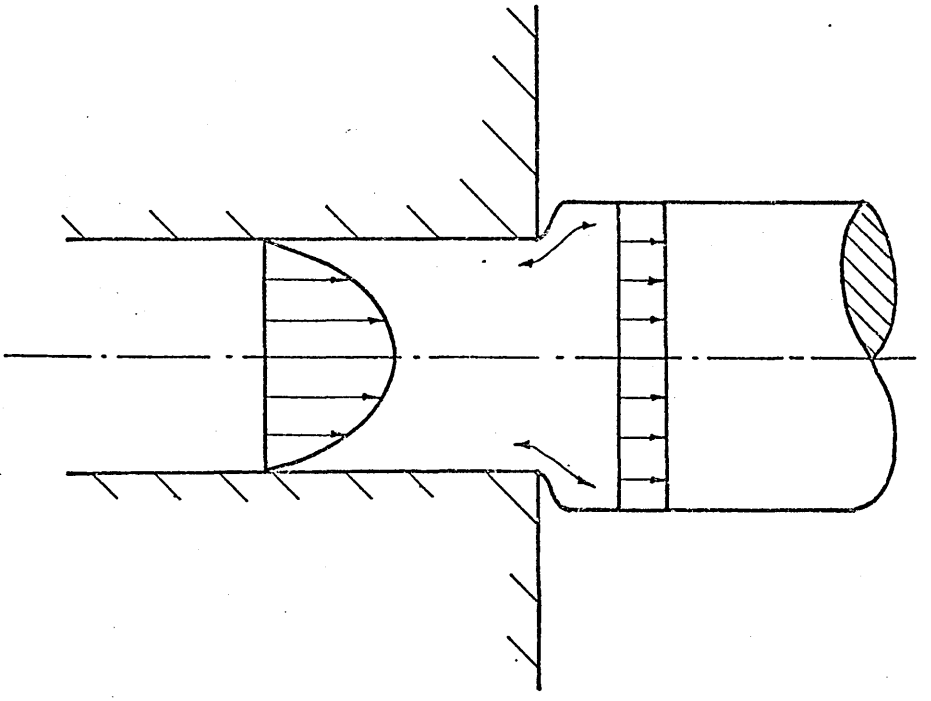

FIG 13 : A POSSIBLE MECHANISM OF SHARKSKIN

AFTER BRYDSON(18)

FIG14 : FLOW CURVES FOR 0.92 POLYETHYLENE AT 130°C

AFTER WESTOVER(34)

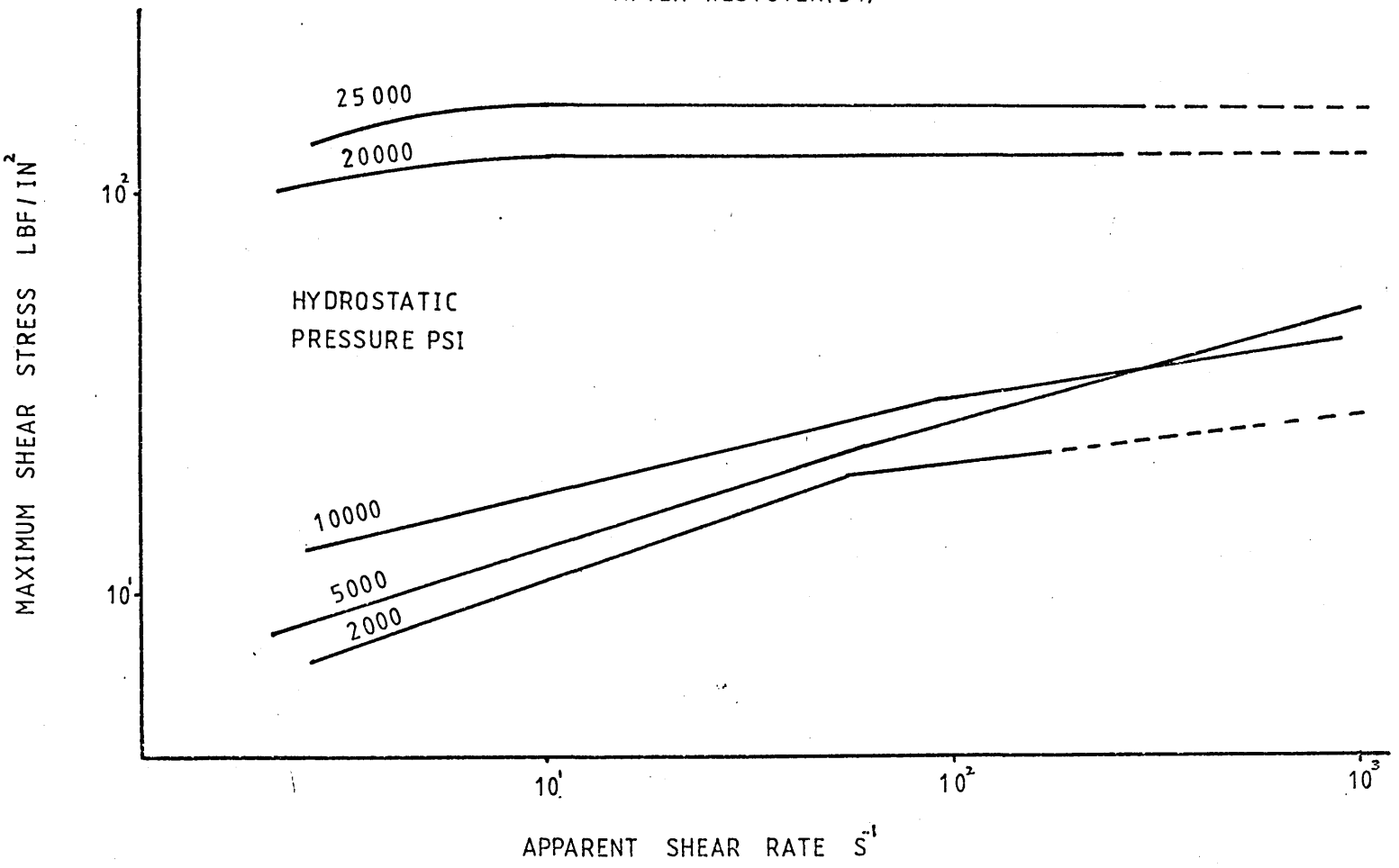

FIG 15 : VISCOSITY VERSUS PRESSURE FOR DIFFERENT SHEAR RATES

(0·92 POLYETHYLENE 130°C)

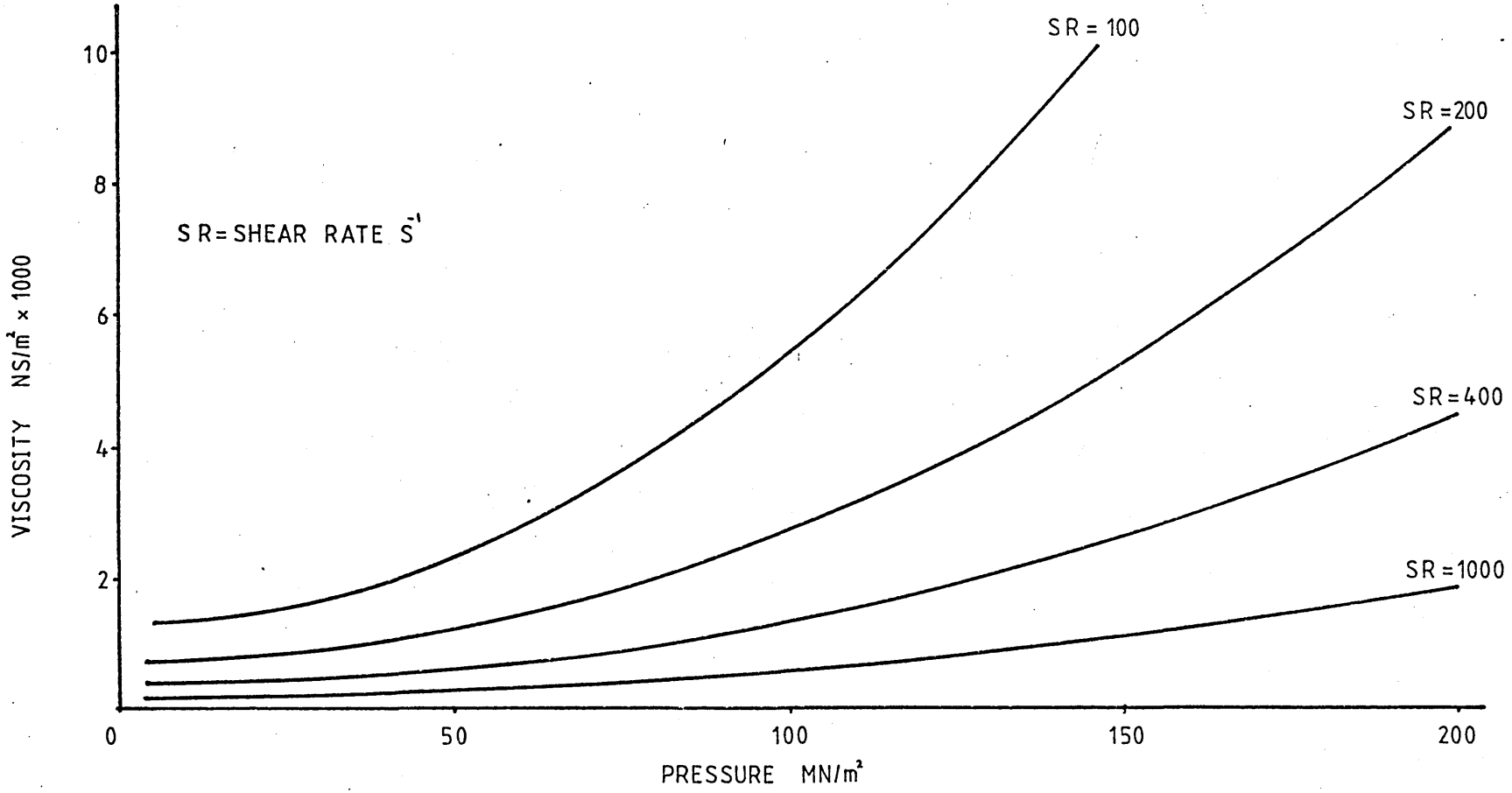

CHAPTER 3: Description Of The Experimental Equipment And Design And Development Of The Die-less Units.

3.1- Description Of The Experimental Equipments.

3.2- Modification To The Existing Rig.

3.3- Design And Development Of The Pressure Reduction Units.

3.4- Further Modifications To The Existing Rig.

3.5- Experimental Procedure And Difficulties Encountered.

3.6- Wire Preparation.

3.1- Description Of The Experimental Equipments

Initial tests were carried out using the existing drawing bench originally designed by Stevens (15) and later modified by Crampton (16). A full description of the apparatus is given below.

The drawing bench consisted of interchangeable bull blocks of 50, 100 and 300mm diameter, driven by a Shraga 3-phase electric motor (type BTH 18/4.5hp VSC.) capable of running at speeds infinitely variable between 550 and 2200 revolutions per minute. The power was transmitted from the motor to the bull block via a flexible type tyre coupling (Fenner F80), a 29:3 reduction worm gear box (Croft type 41/551/05) and a coupling clutch (Broadbent type DP25) which enabled the bull block to be engaged when the electric motor was running at the required speed, thus providing a rapid build up to full speed. The above arrangements facilitated drawing speeds infinitely variable between 0.2 m/s to 4.0 m/s.

The above equipment were mounted on a suitable bench of welded steel construction and guarding were placed around all the moving parts to provide adequate safety.

The drawing load was measured by attaching a strain gauge bridge on the reduced part of the bull block shaft. A mercury cell transmitter (Vibro-meter Sa type 4MTA/T) was used to connect the gauges on the rotating shaft to the UV recorder through a Sangmo direct reading transducer meter (type C52). The unit was also able to measure the rotational speed of the bull block by the use of a magnetic sensor fitted into the body of the transmitter. The output

from the strain gauge bridge was fed, via the transmitter to the UV recorder and the output from the magnetic sensor passed through an amplifier before being fed into a digital counter which gave a visual display of the rotational speed.

The polymer was heated by means of an electric heater band and the temperature was controlled thermostatically within $\pm 4^{\circ}C$ of the set temperature using thermocouples connected to a digital meter.

The pressure tube/die unit consisted of a polymer melt reservoir, pressure tube and die, held together with three sockets headed cap screws. A copper seal was incorporated between the die and the pressure tube to prevent leakage. The schematic diagram of this unit is shown in figure 6 . The wire coil was placed at the side of the drawing bench on a purpose built stand and a heavy ring was placed over the coil thus preventing the wire from becoming entangled. Guides and a freely rotating pulley was used to turn the wire through a right angle so that a horizontal feed to the pressure tube was achieved.

3.2- Modification To The Existing Rig

As the experimental work progressed it became necessary to investigate the performance of the unit at speeds slower than the drawing bench could facilitate. By reducing the diameter of the smallest bull block from 50mm to 20mm, the minimum drawing speed was reduced to 0.05 m/s. Plate 5 shows the modified bull block.

3.3- Design And Development Of The Pressure Reduction Units

The principal objective of the experimental programme was to optimise the existing wire drawing system with polymer melt lubrication. Some initial experimental work was conducted by extending Crampton's research to enhance better understanding of the principles of the process during which the following limitations and problems were encountered:

i)- A leader wire was found absolutely necessary before the drawing process could commence.

ii)- Wire breakage was repeatedly occuring before full drawing speed was reached.

iii)- Die wear prior to hydrodynamic lubrication was noticed.

iv)- Non-uniform wire was produced owing to "Bamboo" effect.

v)- The coating thickness on the wire was reduced at higher drawing speeds.

The desire to overcome these limitations stimulated the thought that a system may be developed to provide solutions to some of the difficulties. A careful study of the previous researches was then undertaken in order to analyse the mechanism of the process in more detail. By cutting the wire during drawing Crampton (16) showed that the deformation was commencing inside the pressure tube well before the die entrance. The deformation of the wire was shown to take place in a manner as if a variable angle

die was used. These observations gave way to conclusions that as the result of high pressures an effective die was formed by the polymer inside the pressure tube and that the reduction die was acting as a seal controlling the flow of the polymer. Since the die was found to be performing as a means of generating high pressures in the tube, it was then thought that under a special geometrical configuration, it may be possible to eliminate the die from the unit and still generate the necessary pressure within the tube to deform the wire. The suggestion that a die-less wire drawing unit may be developed to reduce the wire diameter by the hydrodynamic action of the polymer lubricant became a dominant objective in optimising the system to meet industrial requirements.

Theoretical argu ments revealed that such a device had to be dimensionally greater than the nominal wire diameter in order to eliminate some of the existing problems in the conventional wire drawing process. With the concept of the die-less wire drawing in mind, a number of designs were considered to examine the feasibility of such a system.

First it was thought that a suitable tube with its diameter slightly bigger than the undeformed wire could be used instead of the pressure tube thus providing a gap to prevent metal to metal contact during initial insertion of the wire. If the tube was then subjected to external pressures to cause the diameter of the tube to become smaller than the wire, it would result in deformation of the wire due to the effect of the hydrodynamic lubrication. A simple calculation showed that the magnitude

of the required pressure was impractical to achieve for the desired dimensional changes.

Another idea of die-less wire drawing stemmed from the concept of thermal expansion. It is well known that the variation of temperature causes dimensional changes. This led to the idea that a tube with its diameter initially smaller than wire would increase in size when heated, thus providing a gap between the wire and the tube so preventing metal to metal contact. With the commencement of the drawing process, the tube would then be cooled to reduce the gap and induce deformation of wire under hydrodynamic lubrication condition. Calculations for the necessary expansion of the tube indicated that an extremely large temperature rise was required to cause the satisfactory dimensional changes. The above methods were soon abandoned due to their inconveniences.

The third attempt produced a unit the schematic diagram of which is shown in figure 16. It consisted of two parts, a stepped bore cylindrical body and a special purpose nut. The external diameter of the main cylindrical body was reduced once to match the internal diameter of the threaded nut and again to a smaller size which then gradually tapered down over a certain length. This tapering length of the main body was slitted into four equal segments to achieve variable bore size by tightening the nut. This nut had a parallel bore with internal thread to match with the externally threaded part of the main body and a length having tapered bore which progressively squeezes the segmented part of the main body upon gradual tightening action. The idea being that without any

tightening action of the nut, the wire could be inserted freely through the bore of the main body and once the drawing process is started the nut would be tightened to reduce the bore size, thus giving rise to hydrodynamic pressure and hence deforming the wire.

During the initial test runs it was found that reduction in diameter of the copper wire took place without tightening the nut over the main body. It was also observed that the drawing speed had significant influence on the performance of the unit. It was then realised that the pressure produced by the stepped configuration was the main reason for causing reduction in the wire diameter, even though the smallest bore size was larger than the undeformed wire diameter. Subsequently two die-less reduction units were designed and manufactured, one of taper bore and the other of stepped bore, the principal operating concepts for both units being:

i)- The hydrodynamic action of the lubricant generated the effective die.

ii)- The pressure was generated by the geometrical configurations of the units and was speed dependent.

iii)- Manufacturing the units were relatively simple.

iv)- Since the smallest bore size of each unit was greater than the undeformed wire, metal to metal contact was totally eliminated and initial insertion of the wire was no longer a problem.

Initial investigations which were conducted to examine the performance of these die-less units showed successful operation of each unit and gave rise to the invention of the die-less wire drawing where total prevention of metal to metal contact was achieved, thus completely eliminating several technical problems associated with the conventional wire drawing process. The only limitation observed was that at higher drawing speeds reduction in area of the wire was found to be comparatively lower. The design and performance of the stepped bore reduction unit were found to be favourable over the tapered bore unit and hence, extensive experimental work and subsequently theoretical analysis was carried out for this unit. Figures 17 and 18 show the dimensional details of both of these units. Also section views of the stepped and tapered bore units are shown in plates 6 and 7 respectively.

As the experimental work progressed it became necessary to measure the distribution of pressure along the inside bore of each of these units. Piezo-electric quartz pressure transducers (Kistler type 6203) were mounted on the units (four on the stepped bore reduction unit and three on the tapered bore reduction unit) which enabled the pressure variation along each unit to be estimated. The output from the transducers were fed into the UV recorder via charge amplifiers. The schematic diagrams in figures 19 and 20 and also plate 8 show the arrangements.

3.4- Further Modifications To The Existing Rig

On the existing drawing bench the drawing load was measured by a strain gauge bridge attached on the bull block shaft. The output from this bridge, when recorded on a UV recorder, appeared to be oscillatory because the weight of the clutch assembly was supported by the shaft thus producing an alternating bending moment. Subsequently, a robust frame was designed and manufactured, one end of which was fixed onto the platform of the drawing bench and the other end had facilities for the die-less reduction units to be rigidly fixed to it by means of socket headed cap screws. Strain gauges were attached to a member of the support frame to detect the amount of deflection and when calibrated, gave a direct reading of the drawing load on the UV recorder. This method of measuring the drawing load completely eliminated the problem of oscillatory trace and enabled the load to be measured more accurately. Plate 9 shows the support frame and the strain gauges attached on it.

A magnetic sensor was used to obtain the drawing speed. However, it was found that a hand tachogenerator allowed the measurement of the rotational speed of the bull block to be taken more accurately and conveniently. Therefore, the sensor/transmitter unit was discarded and a hand tachogenerator was used for this purpose.

The polymer melt chamber could only store a limited amount of polymer and hence proved to be inadequate for a complete series of tests. To carry out multiple tests, fresh polymer granules had to be fed into the chamber

frequently and this caused at least fifteen minutes delay for the polymer melt to reach the steady state temperature before further tests could be undertaken. It was also noticed that the flow of polymer was restricted during the test runs due to its relatively higher viscosity and the narrow gap through which the flow should take place. Scattered results from the copper wire tests confirmed that insufficient and irregular flow of polymer was occuring. To overcome this problem a hopper was designed, manufactured and welded onto the melt chamber, having sufficient capacity to hold enough polymer for a complete set of results. The hopper was heated by an electric heater band and the temperature of the polymer was controlled thermostatically at the set temperature equal to that of the melt chamber. The hopper was also connected to a pressurized air supply of 100 psi via a 2-way servo valve. A copper seal was incorporated between the air supplying device and the hopper to prevent cooling effect on the polymer melt due to air leakage. With the servo valve on forward position, air pressure was activated onto the free polymer surface, helping the polymer to flow with the wire into the units. Further tests showed that the new air assisted feed mechanism significantly improved the performance of the units. Figure 21 shows the integrated polymer container and also plates 8,9 and 10 show the final arrangements of the air and polymer feed assembly. The new polymer melt container was held on the forward entry of the units by means of three socket headed cap screws. Figure 22 shows the final form of the feed mechanism which worked satisfactorily throughout the course of the experimental tests.

3.5- Experimental Procedure And Difficulties Encountered

The following procedure was followed before carrying out any test. The heater bands on the hopper and melt chamber were first switched on and were controlled thermostatically to maintain the temperature at the pre-set level. Other instrumentations were also switched on and the hopper was supplied with an adequate amount of fresh granules. The polymer granules in the hopper and melt chamber melted very quickly but the unit was allowed two hours to reach the steady state temperature level. The pressure reduction unit was not heated, therefore, a temperature gradient was present, decreasing from the set value at the forward entry point of the unit to some lower temperature (usually 40°C less than the set temperature) at the exit end. When steady state temperature was reached the semi-solid polymer left from the previous test was removed from the unit using a smaller diameter drill. Wire from the coil placed on the stand next to the drawing bench was passed through the guides and over the pulley before being inserted and pulled through the unit and then wound onto the bull block. The electric motor was started and set running at desired speed (the motor speed was adjusted by altering the position of the commutator brushes). Charge amplifiers for the pressure transducers were switched to "long time" positions which gave a steady and uniform reading through the run. Paper drive on the UV recorder was set in motion and air pressure was put on before engaging the clutch. While the wire was being drawn, rotational speed of the bull block was measured

using a hand held tachogenerator. When a reasonable length of wire was drawn (between 5 to 15 metres depending on the drawing speed), the clutch was disengaged. Air valve, UV paper drive and charge amplifiers were switched back to their original positions. Test number was recorded on the data sheet and UV paper for subsequent collection and analysis. An identification tag was also placed on the drawn wire. The speed of the electric motor was then increased in suitable steps and the procedure was repeated for each speed increment. At the end of each run a qualitative assessment of the polymer coating was made and remarks were recorded on data sheet. When analysing the experimental results the traces for loads and pressures on the UV paper were measured and recorded on the data sheet for each test. A typical UV trace is shown in figure 23. The wire was then unwound from the bull block and for each test run, four samples were collected (about 400mm length), one from the leading end, two from the intermediate positions and one from the tail end of the drawn wire and put into marked envelopes. Each sample was later cut in half. One half was used to determine the coating thickness and the percentage reduction in area and the other half was kept as reserve for any subsequent future references. In order to measure the percentage reduction in area, the diameter of the piece of wire was measured in four places after stripping off the polymer coating. The coating was later weighted and since the density of the polymer was known and the length of the sample could be easily measured, the thickness of the polymer coat could be calculated. The average values of percentage reduction in area and the

coating thickness were taken from the four samples and the results were plotted against the drawing speed.

Strain gauges were calibrated before each set of tests using known weights hung over the pulley and attached to the support frame. Pressure transducers were also checked regularly using a Budenberg Gauge Tester in order to examine the accuracy of the obtained readings.

3.6- Wire Preparation.

The received wire coils were protected by waterproof materials. In the case of mild steel wire, a layer of grease was also applied on the wire surface by the supplier to prevent corrosion. This layer of protective oil had to be removed before tests could be carried out for this wire. Therefore, the coil was first washed in a paraffin bath and was left to dry. The coil was then washed in a concentrated bath of hydrochloric acid to remove other substances from the wire surface and finally rinsed in a water bath. The wet coil of wire was then quickly dried using a hot air blower machine. This treatment was carried out for mild steel wire only since copper and stainless steel wires were received in dry and clean conditions.

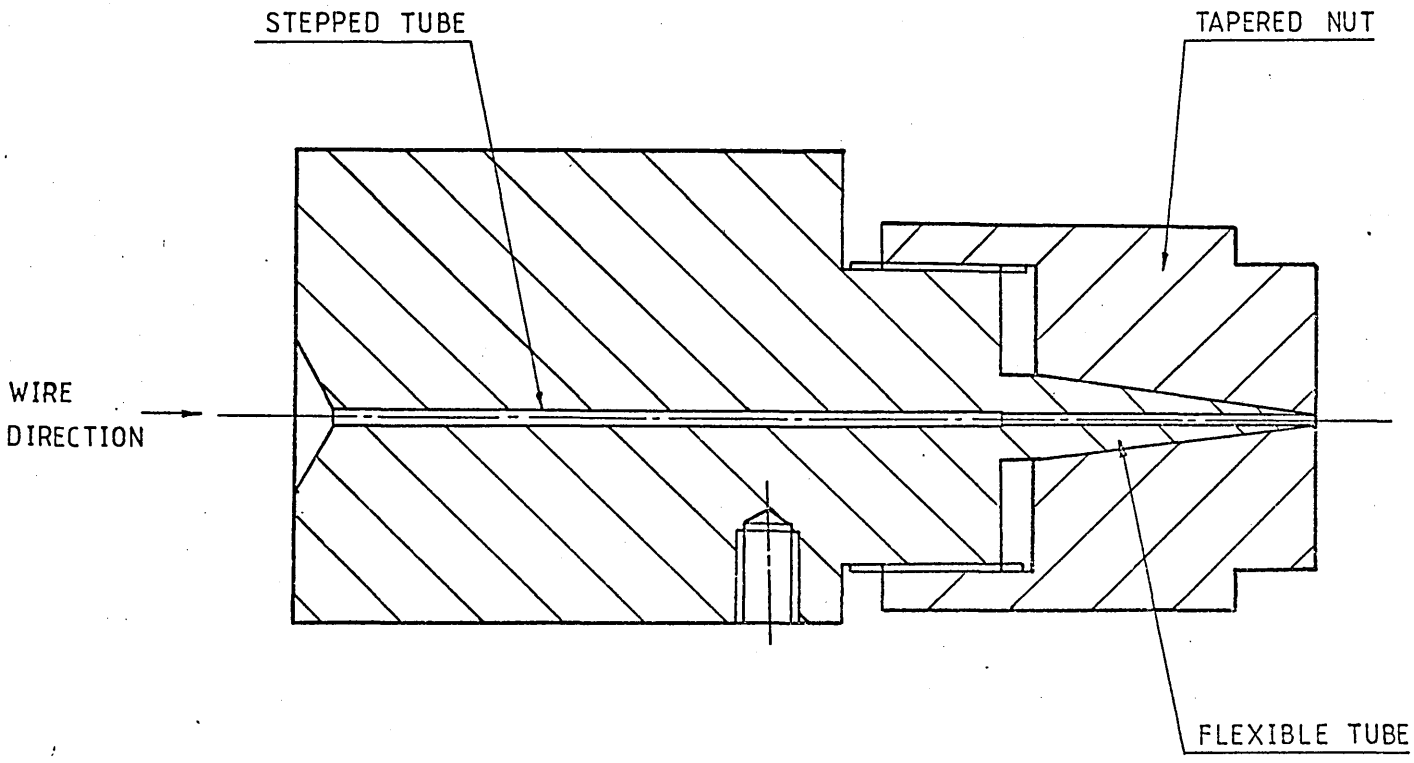

FIG16 : VARIABLE DIAMETER UNIT

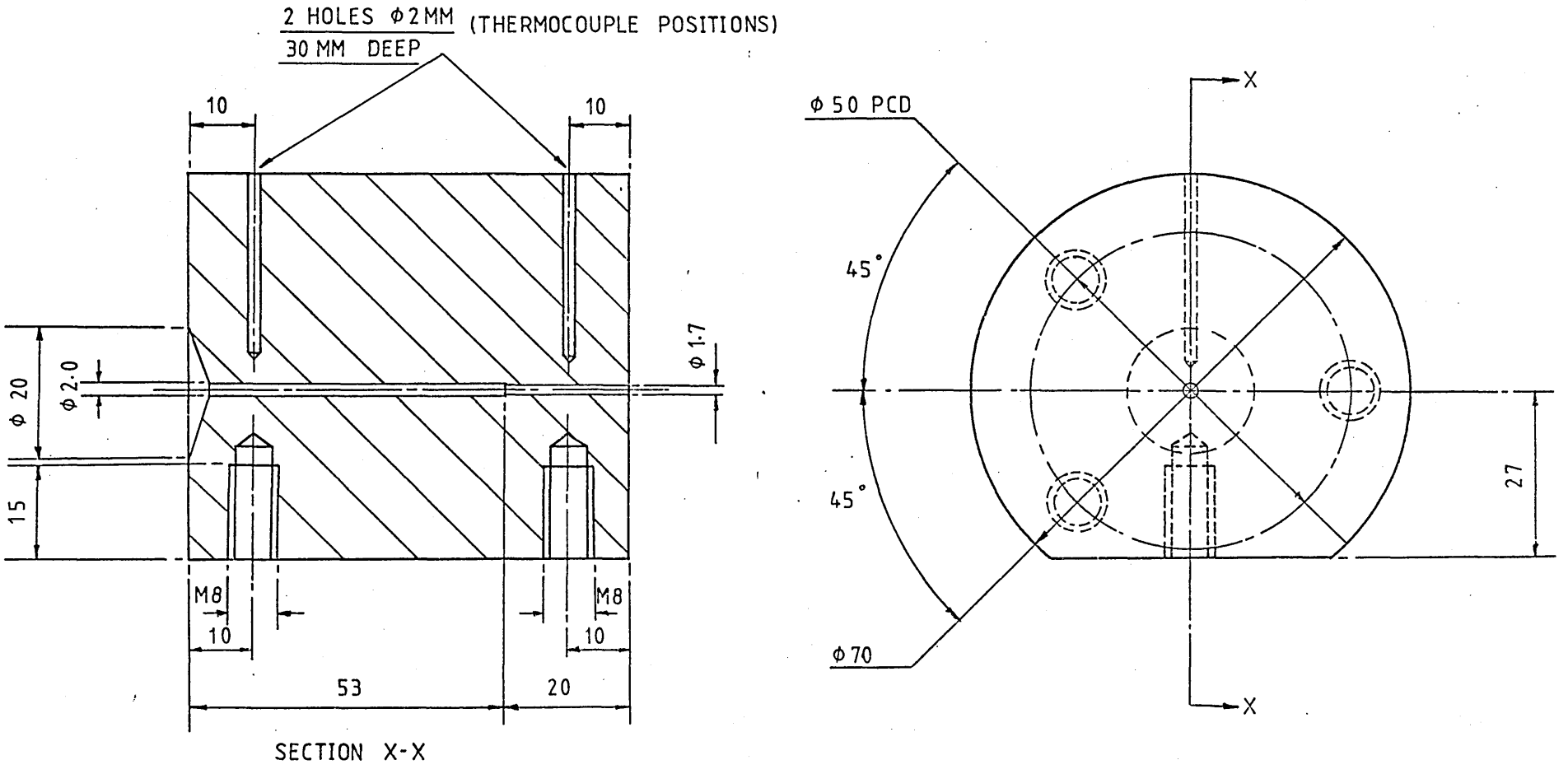

FIG 17: STEPPED BORE REDUCTION UNIT

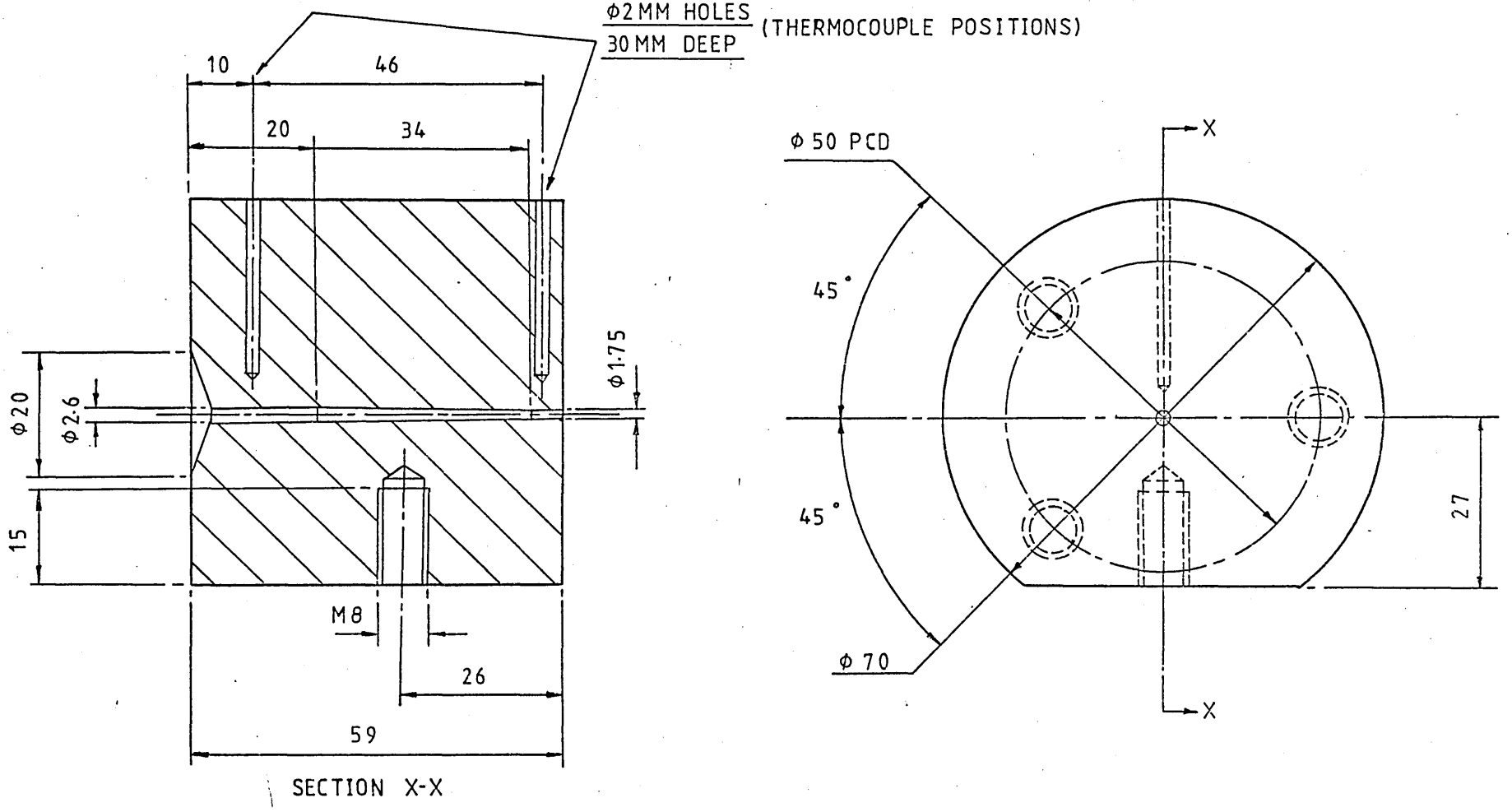

FIG18 : TAPERED BORE REDUCTION UNIT

FIG 19 : STEPPED BORE REDUCTION UNIT ASSEMBLY

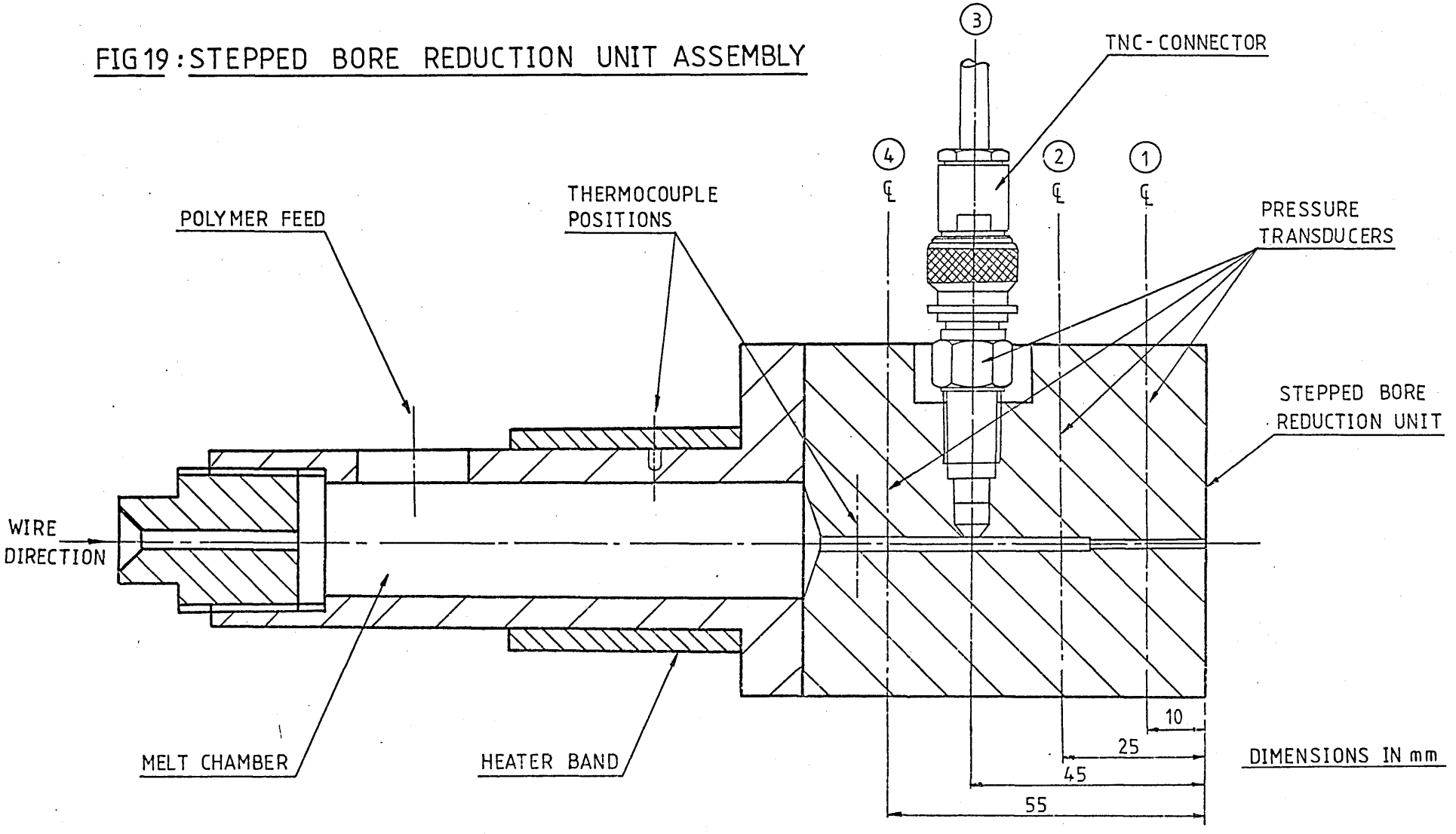

FIG 20 : TAPERED BORE REDUCTION UNIT ASSEMBLY

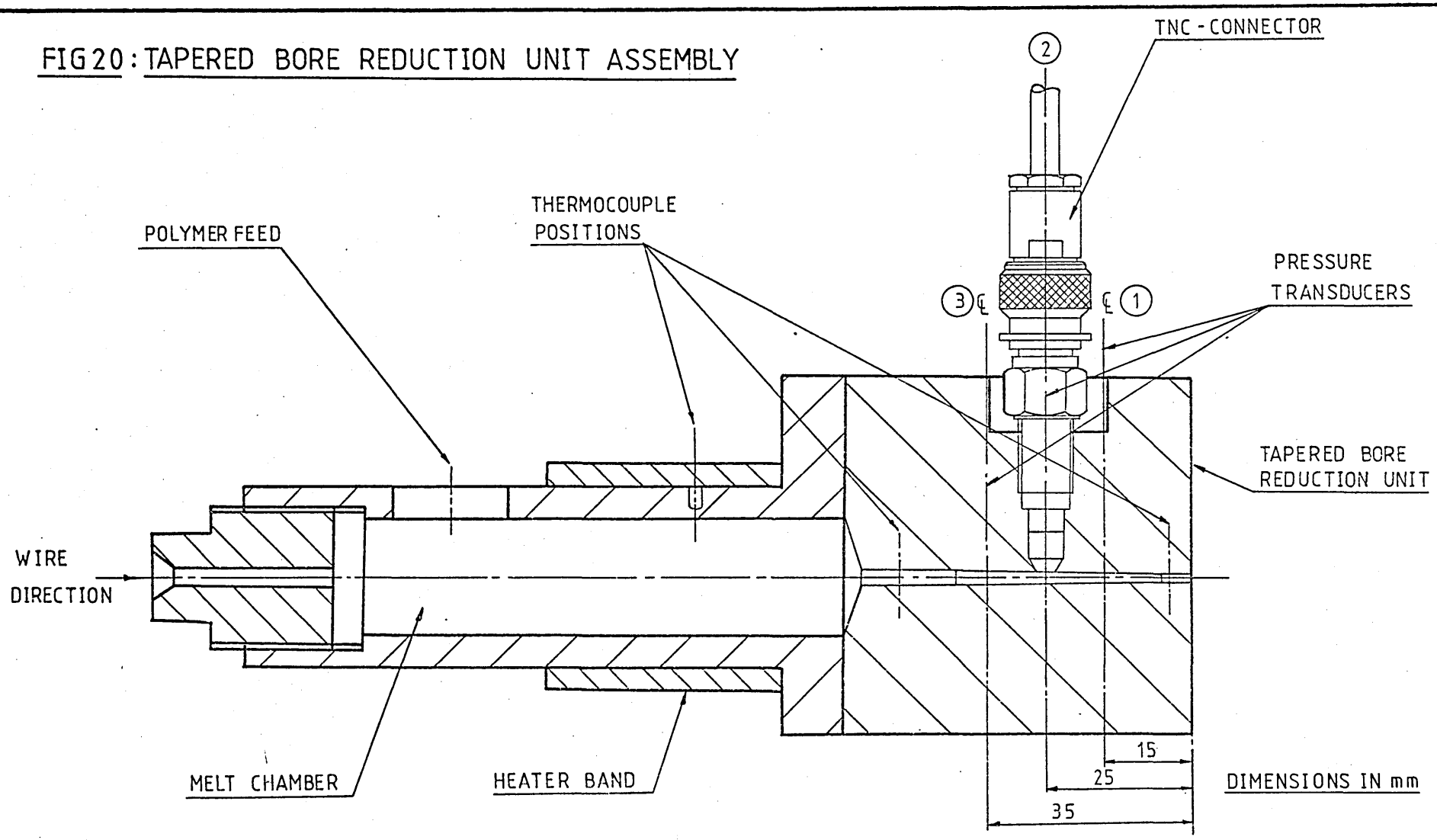

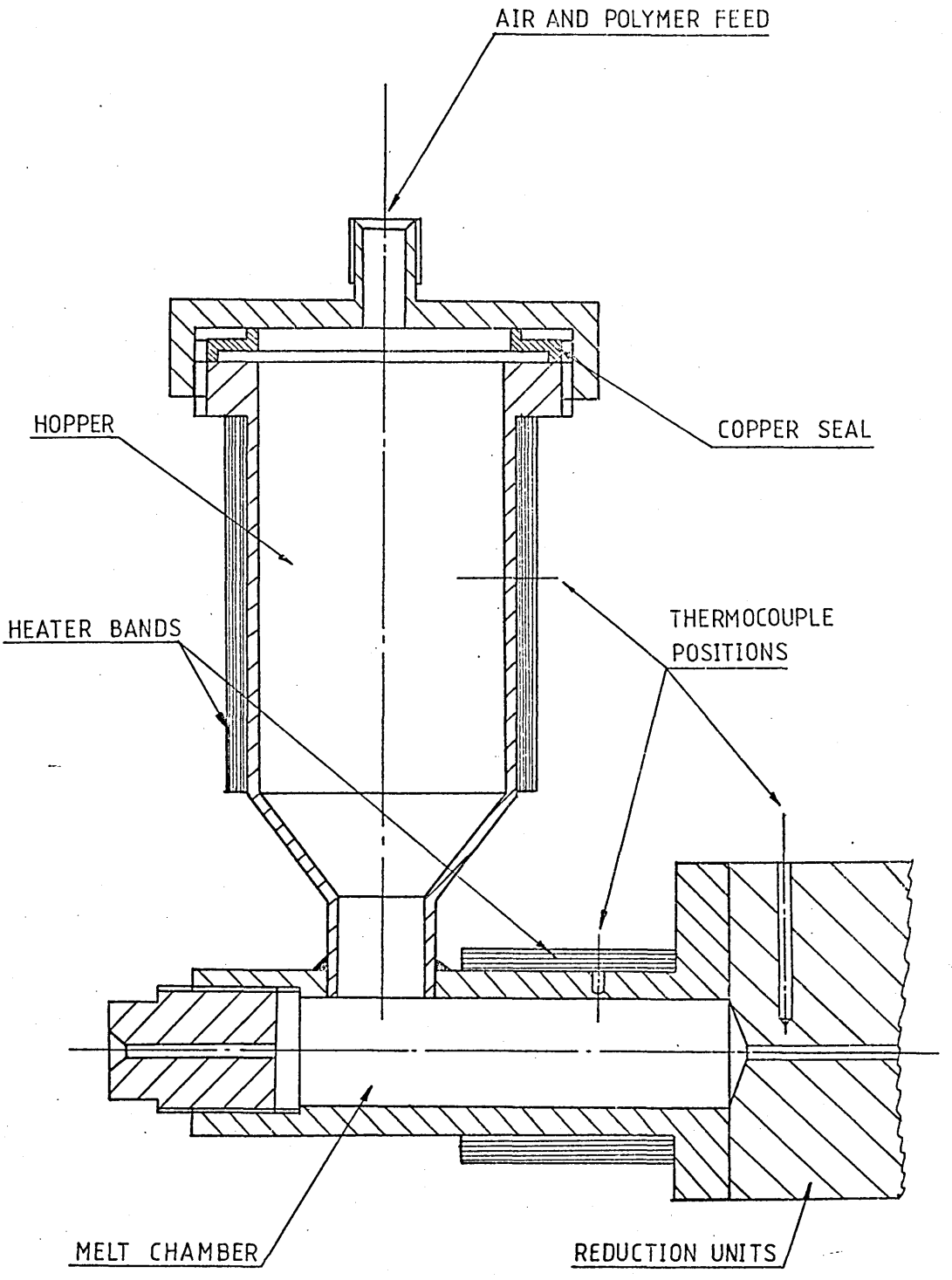

FIG 21 : AIR ASSISTED POLYMER FEED ASSEMBLY

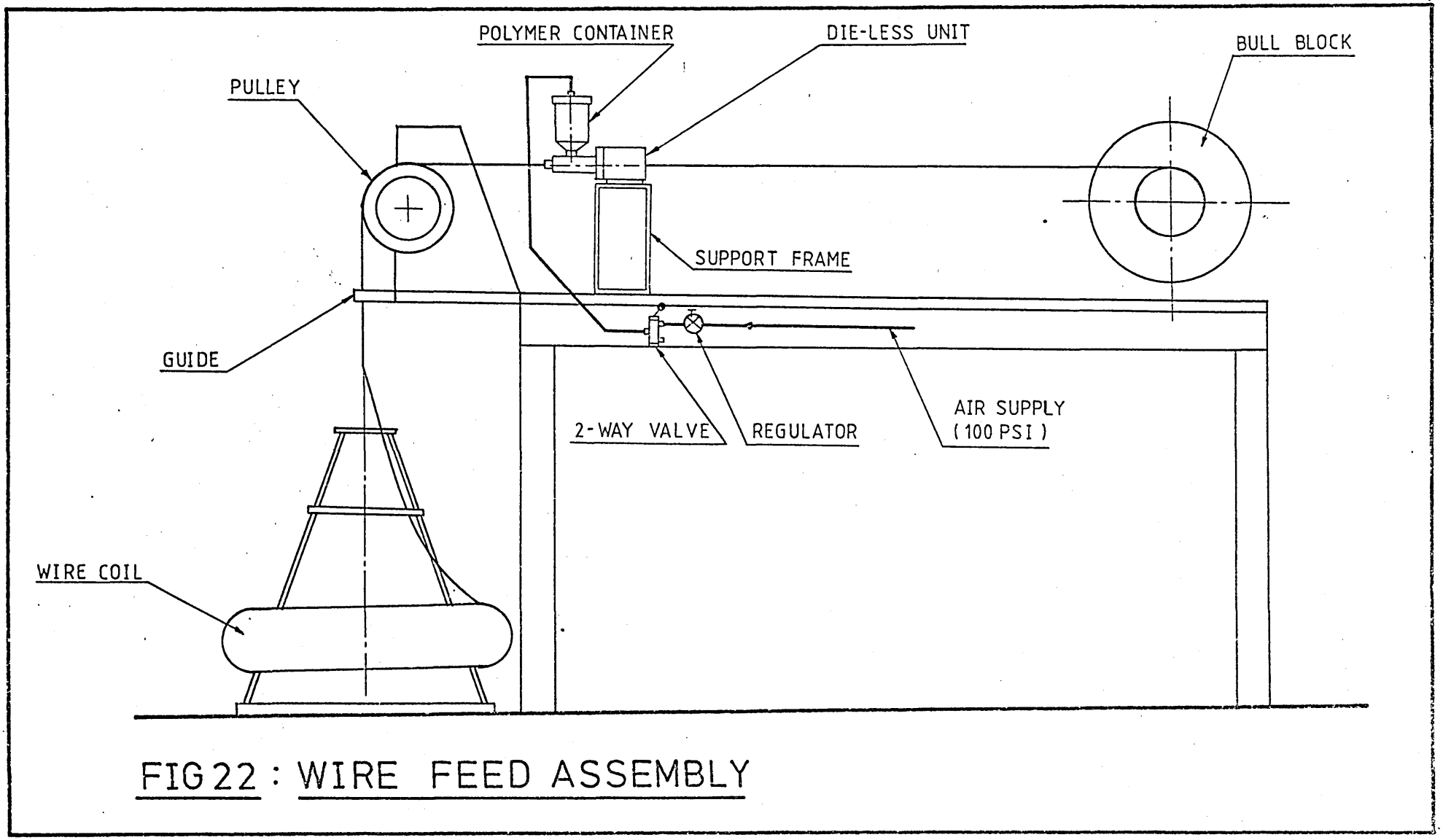

FIG 22 : WIRE FEED ASSEMBLY

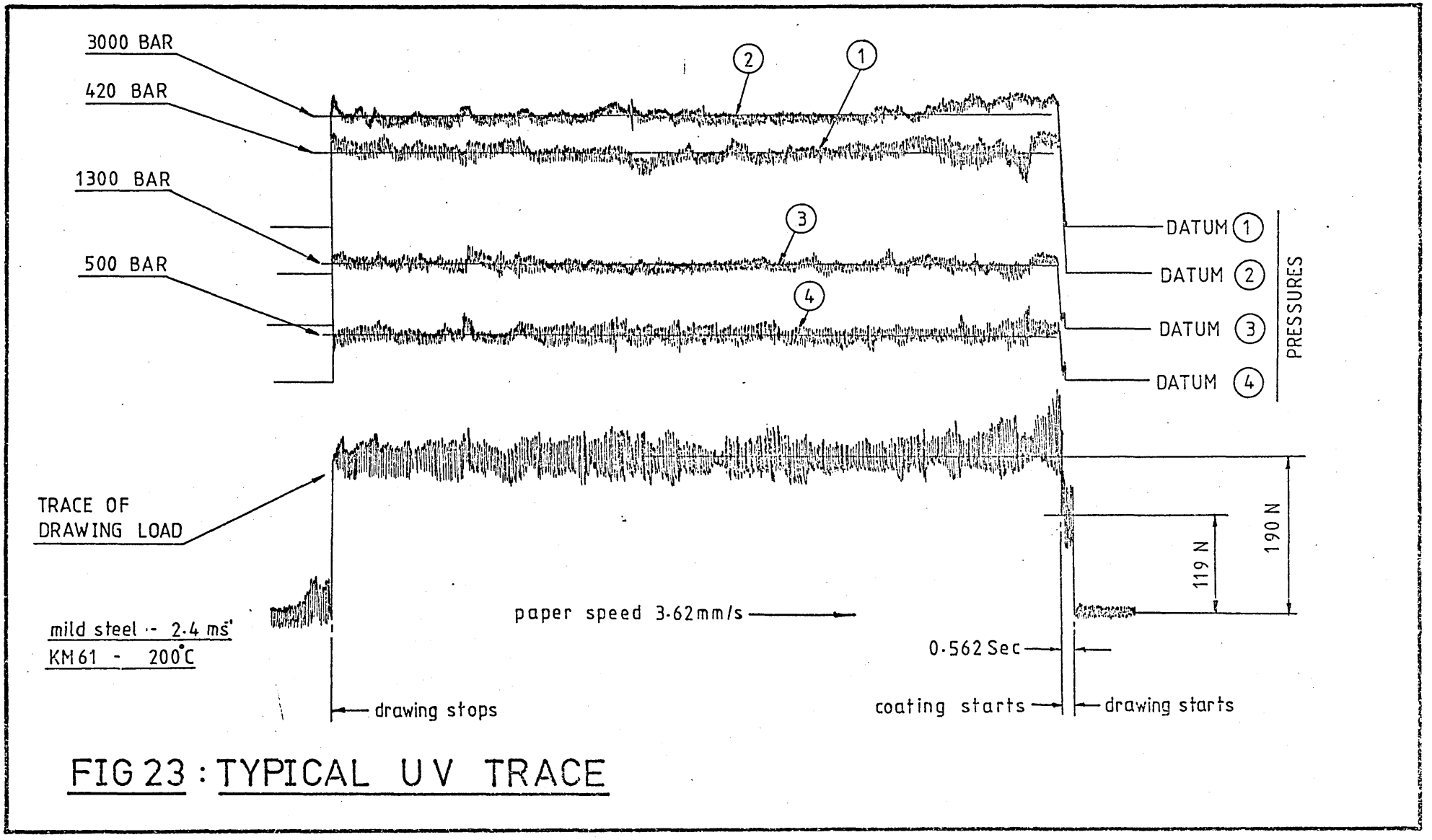

FIG 23 : TYPICAL UV TRACE

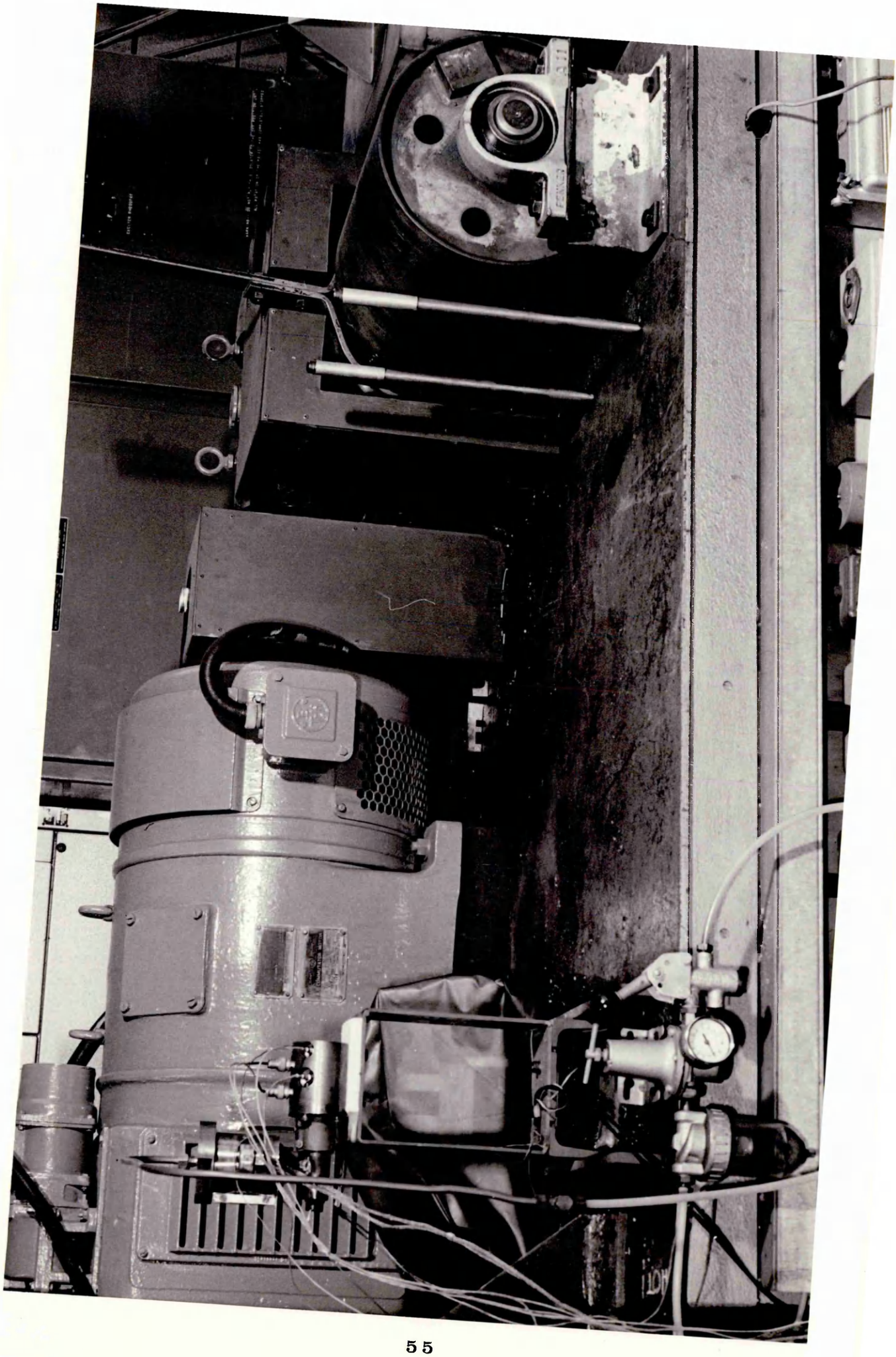

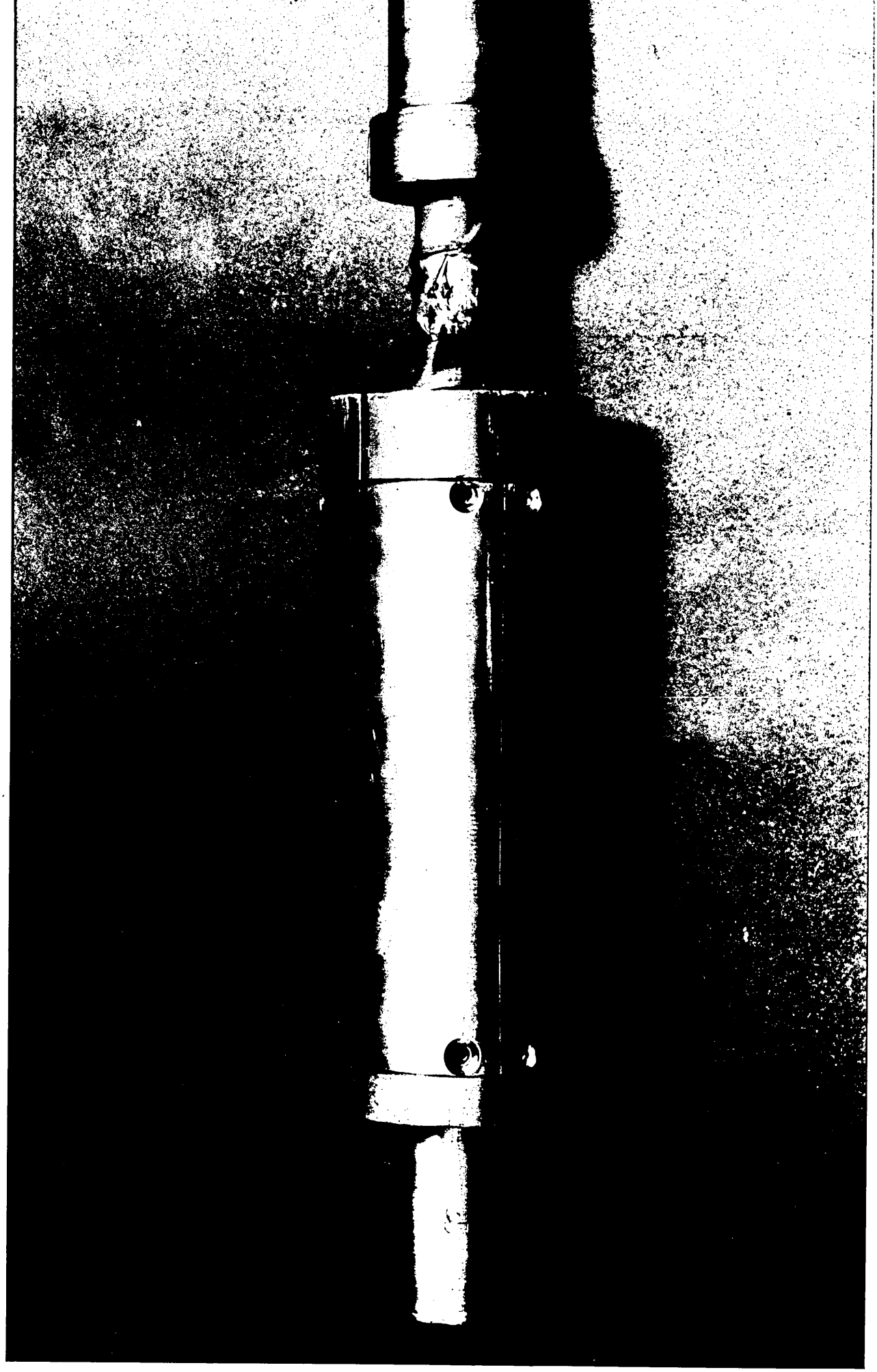

Southern Instruments

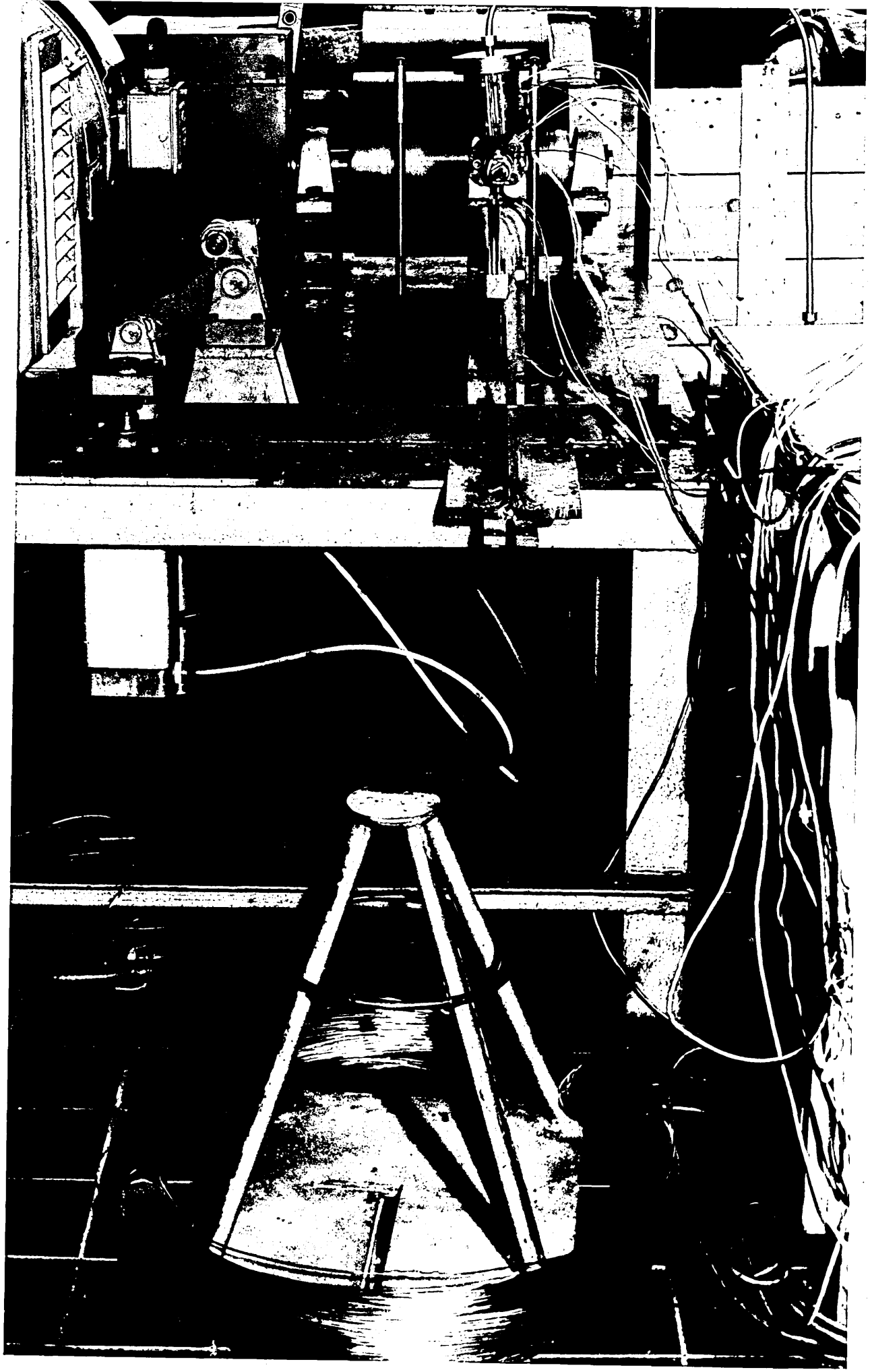

REMOVEABLE
BRACKETS

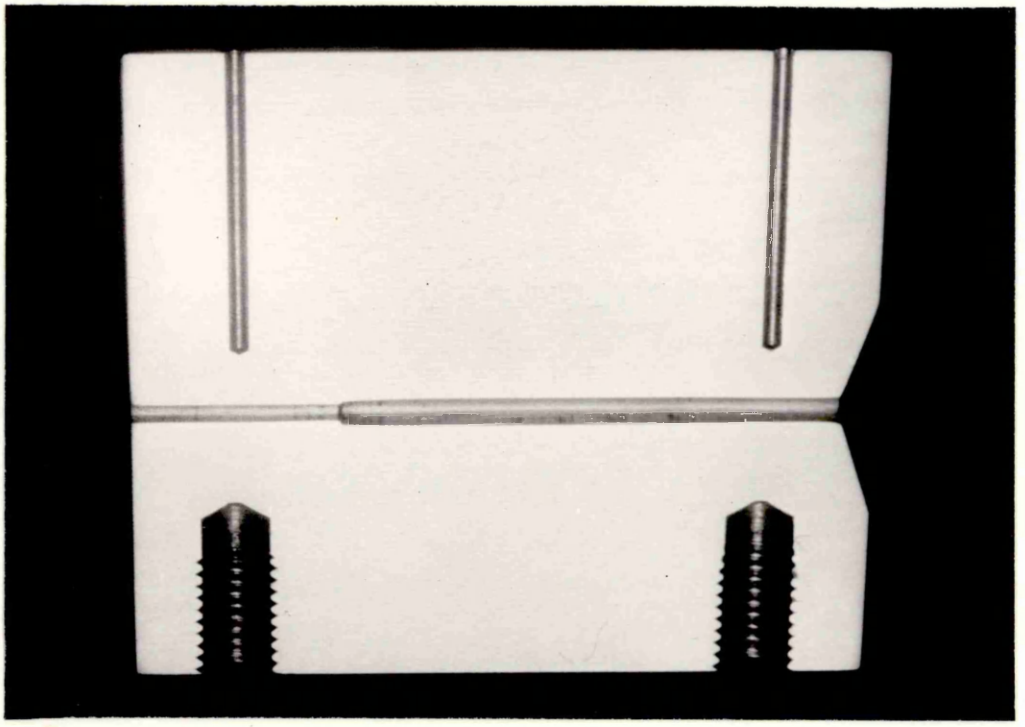

PLATE 6 : SECTION VIEW OF THE STEPPED BORE REDUCTION UNIT

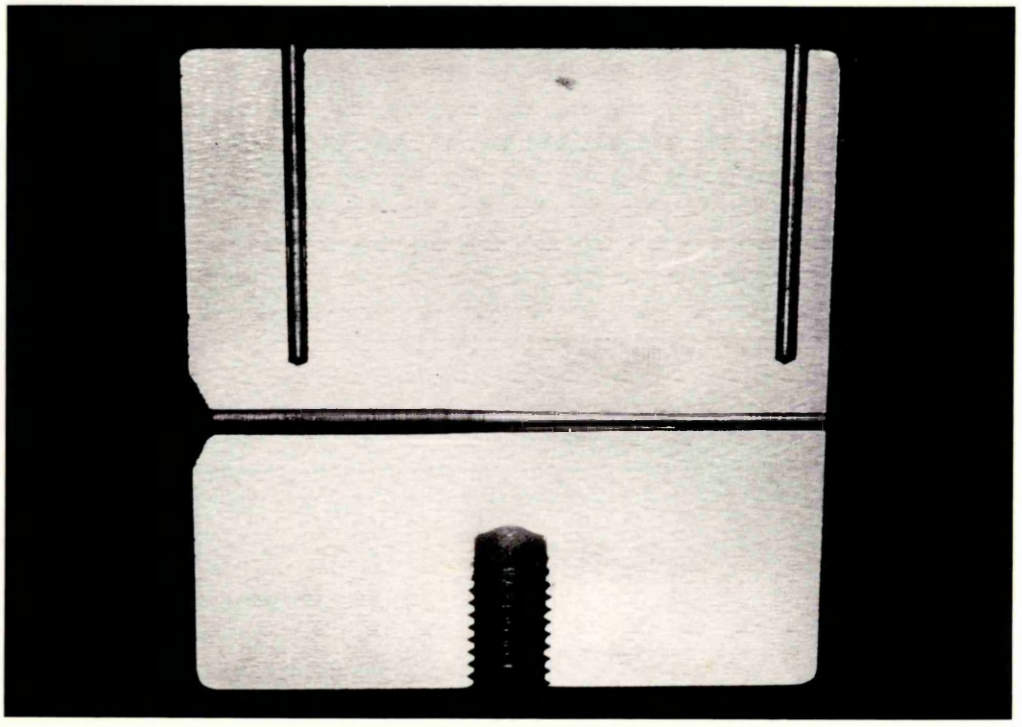

PLATE 7 : SECTION VIEW OF THE TAPERED BORE REDUCTION UNIT

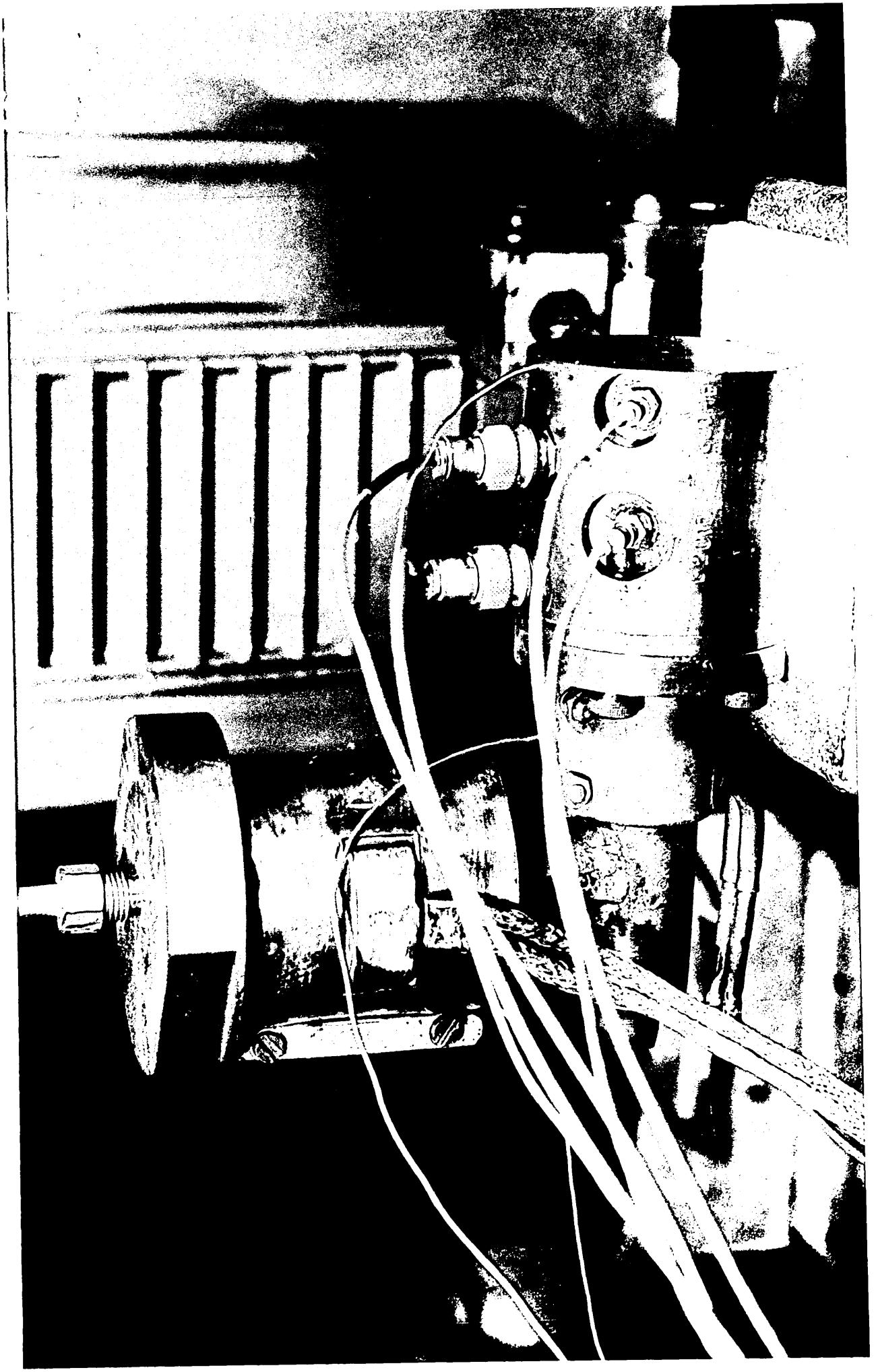

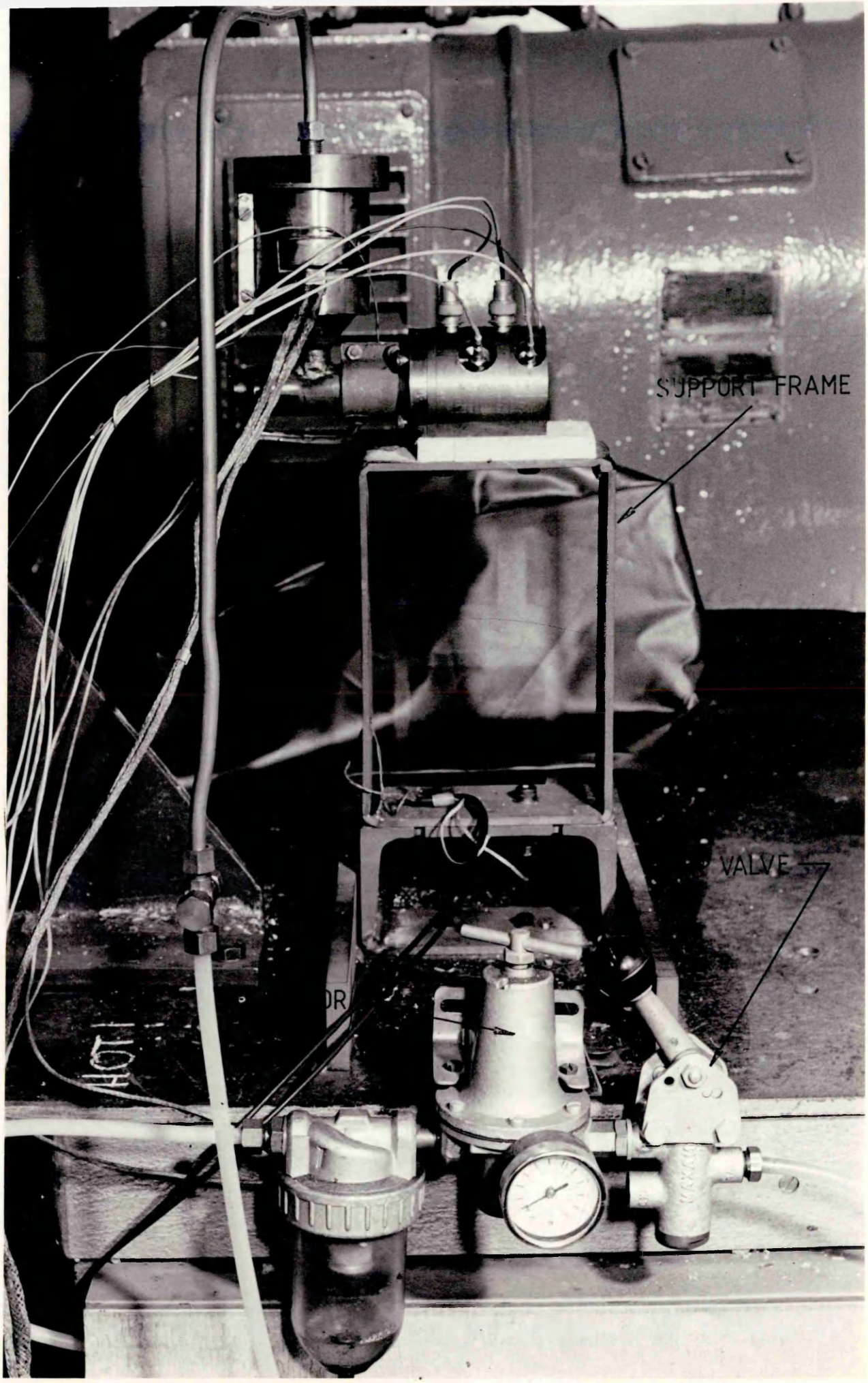
SUPPORT FRAME
VALVE

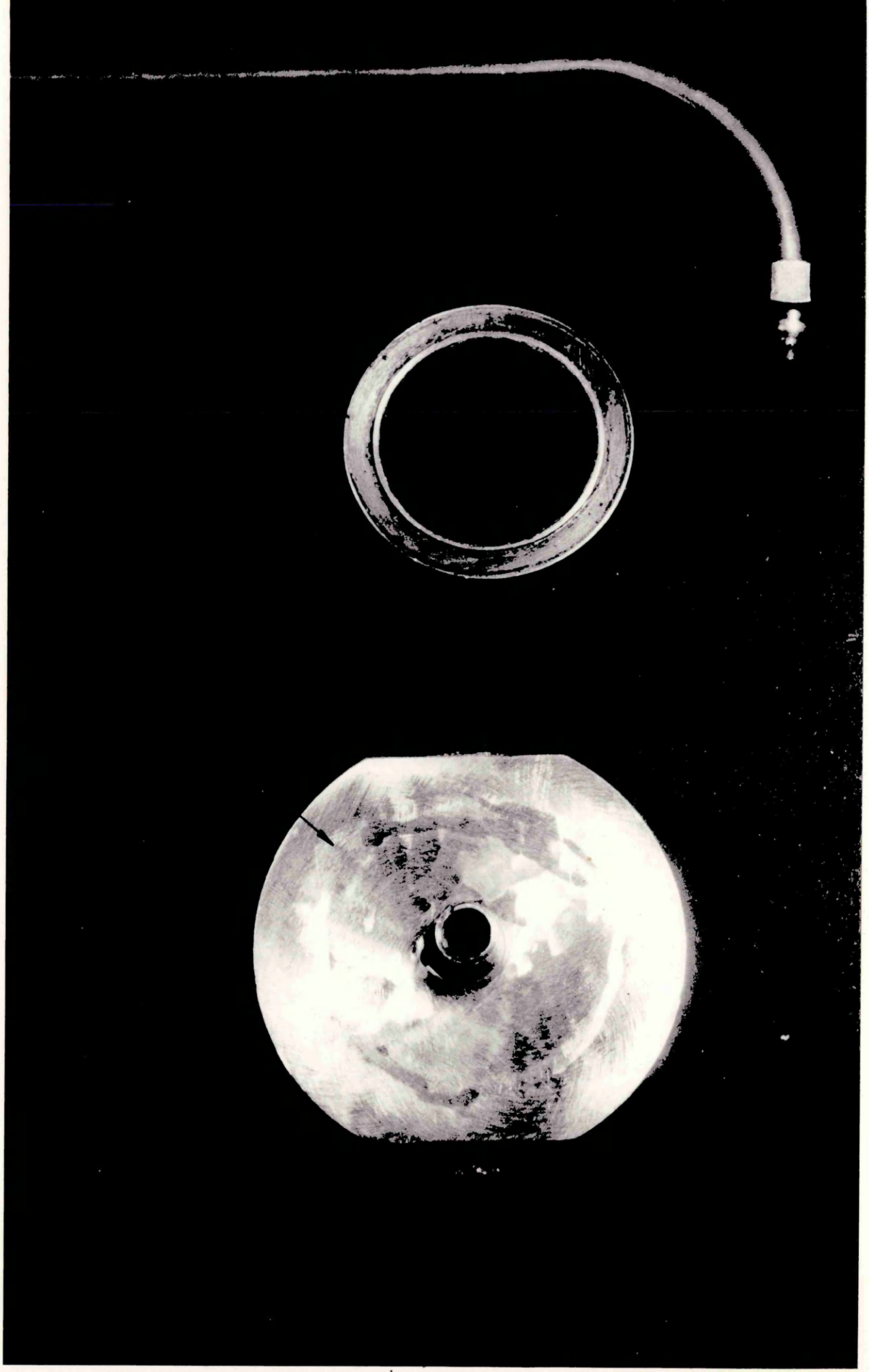

CHAPTER 4: Experimental Results Obtained Using The Stepped Bore Reduction Unit.

4.1- Introduction.

4.2- Determination Of The Yield Characteristics Of The Wire.

4.3- Experimental Results.

4.3.1- Results Of Pressure.

4.3.2- Results Of Drawing Load Versus Drawing Speed.

4.3.3- Results Of Coating Thickness Versus Drawing Speed.

4.3.4- Results Of Percentage Reduction In Area Versus Drawing Speed.

4.4- Determination Of The Deformation Profile.

4.5- Evaluation Of The Product Quality.

4.5.1- Roundness Test.

4.5.2- Examination Of The Uniformity Of The Wire Diameter.

4.5.3- Micro-Examination Of The Surface Finish Of The Wire.

4.6- Results Of Multi-Pass Tests.

4.1- Introduction.

Two types of pressure chambers were used to explore and study the die-less drawing process, one being of stepped bore and the other of tapered bore configurations. The initial tests with the stepped bore reduction unit showed higher deformations and also proved to be analytically simpler than the tapered bore reduction unit, therefore extensive experimental tests were conducted using this unit.

Two different types of polymers were used as pressure medium for the tests, polyethylene (Alkathene WVG 23) polymer produced by ICI and polypropylene KM 61 polymer produced by Shell.

A limited number of experimental tests were carried out with the tapered bore reduction unit using Alkathene WVG 23 polymer as a pressure medium. Since the investigation was mainly aimed at optimising the drawing process with the stepped bore reduction unit, this chapter is devoted entirely to the results obtained therefrom. The results obtained using the tapered bore reduction unit are therefore provided in Appendix 2 for convenience.

Qualitative tests were also conducted to evaluate and compare the quality of the wires drawn using the stepped bore reduction unit and wires drawn with the conventional reduction die. These tests involved, i)- examination of the wire surface employing a micro-photography technique, ii)- investigation of the uniformity of the wire diameter over long drawn length and iii)- roundness tests of the cross section of the wires.

In addition to the above, a multi-unit drawing system

was simulated by redrawing the wire through the same unit a number of times. The results of these tests are also provided in this chapter.

Wire materials selected for the experimental tests were copper, mild steel and 18/8 stainless steel of 1.6mm nominal diameter.

4.2- Determination Of The Yield Characteristics Of The Wires.

The yield characteristics of the wires were determined using a Hounsfield Tensometer. Small samples of the wires with L/D = 1 were subjected to uniaxial compression. The contact surfaces between the specimen and the plates were lubricated in order to minimise the frictional effects. Readings of loads and compressions were taken at close intervals throughout the tests. Knowing the initial length and diameter of the specimen, true stress and natural strain values were calculated assuming constant volume and ignoring the "Barrelling" effect. At least three compression tests were carried out for each wire material and the results are shown in figures 24 to 26 which are assumed to take the form;

$$Y = Y_o + K_o \epsilon^n$$

where,

Y_o = initial yield stress N/m^2.

K_o = strain hardening constant N/m^2.

n = strain hardening index.

ϵ = natural strain.

Using the experimental results, the above parameters were evaluated, by curve fitting, for each wire. These are;

for copper wire,

$$Y = (0.5 \times 10^8) + (4.4 \times 10^8)\,\epsilon^{0.52} \quad N/m^2$$

for mild steel wire,

$$Y = (1.0 \times 10^8) + (6.4 \times 10^8)\,\epsilon^{0.41} \quad N/m^2$$

and for 18/8 stainless steel wire,

$$Y = (0.5 \times 10^8) + (9.6 \times 10^8)\,\epsilon^{0.44} \quad N/m^2$$

FIG24 : THE YIELD CHARACTERISTICS OF THE COPPER WIRE

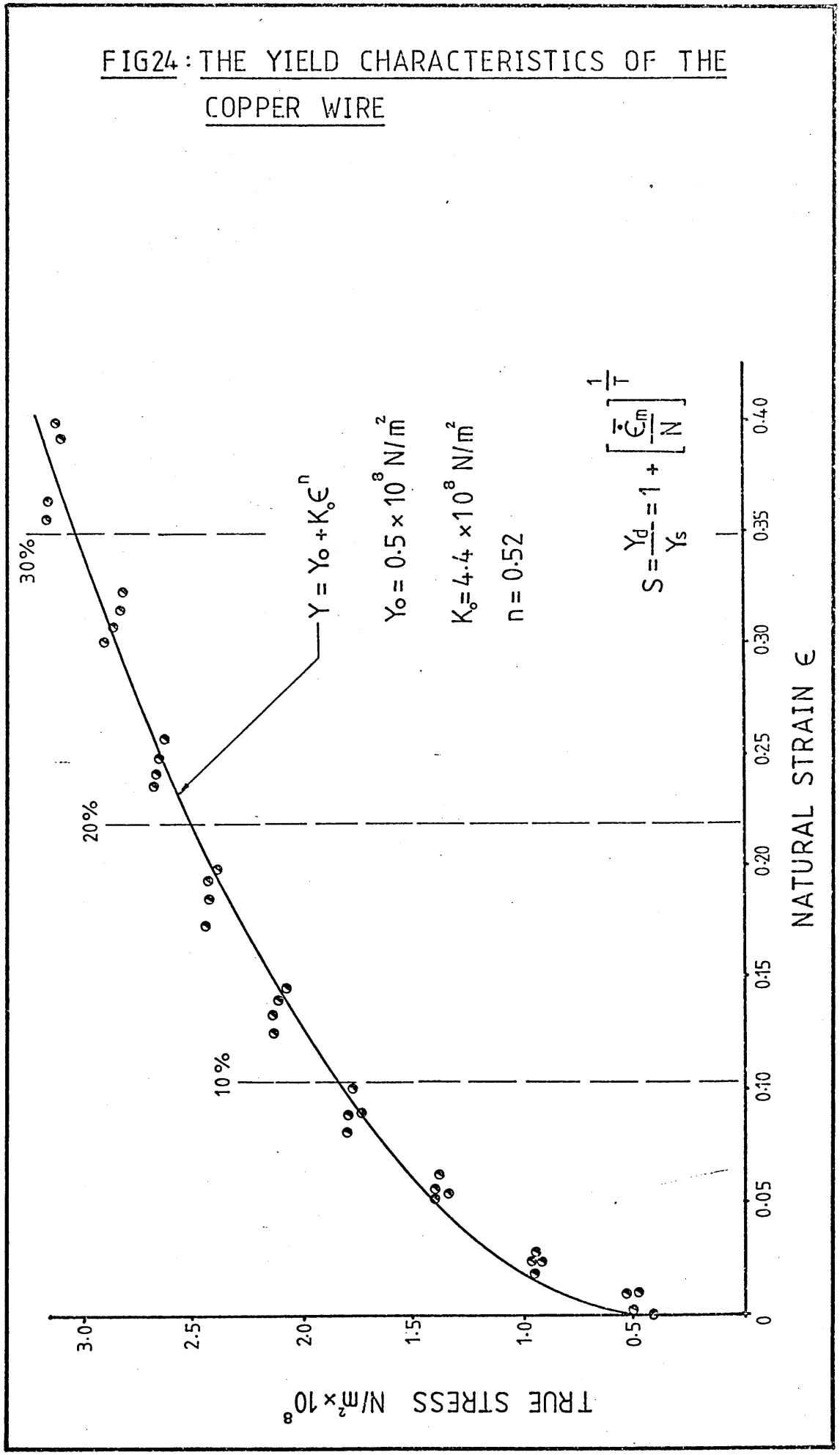

FIG25 : THE YIELD CHARACTERISTICS OF THE MILD STEEL WIRE

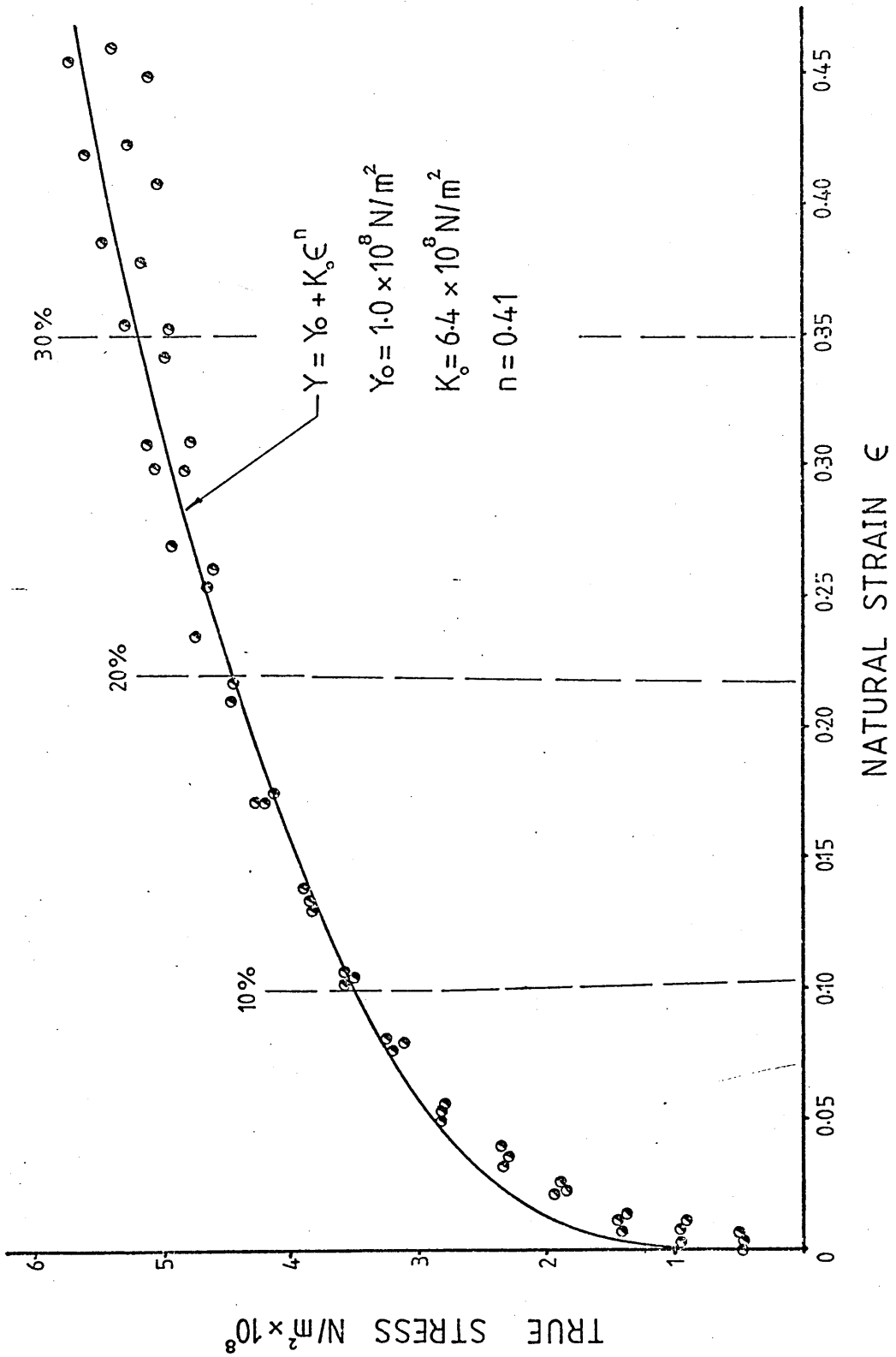

FIG 26 : THE YIELD CHARACTERISTICS OF THE 18/8 STAINLESS STEEL WIRE

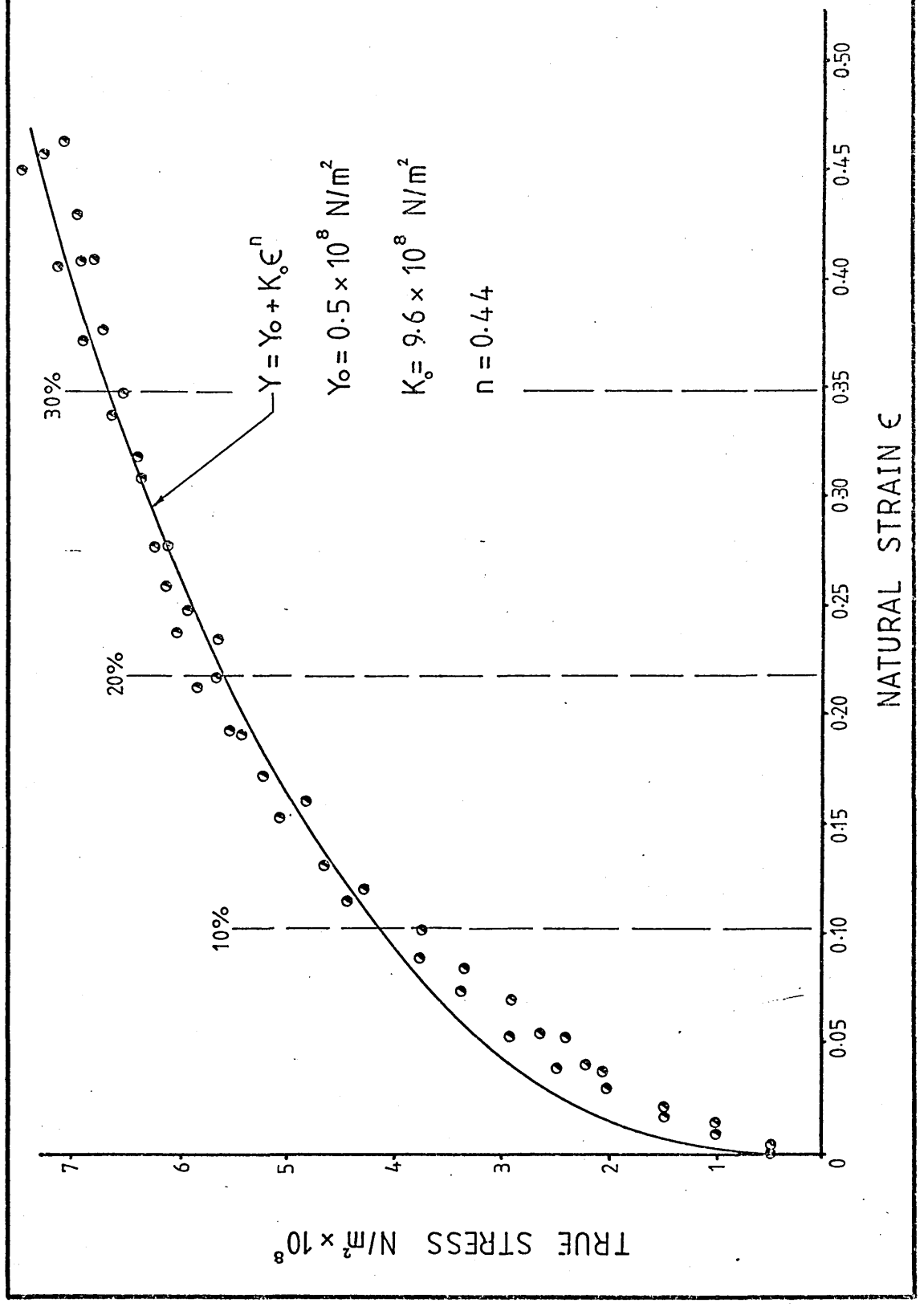

4.3- Experimental Results.

Experimental results obtained using the stepped bore reduction unit are presented in graphical forms in this section. Dimensional details of the pressure chamber used for the tests are shown in the schematic diagram below and are as follows;

l_1 = 50mm

l_2 = 20mm

l_1/l_2 = 2.5

h_1 = 0.2mm

h_2 = 0.05mm

h_1/h_2 = 4.0

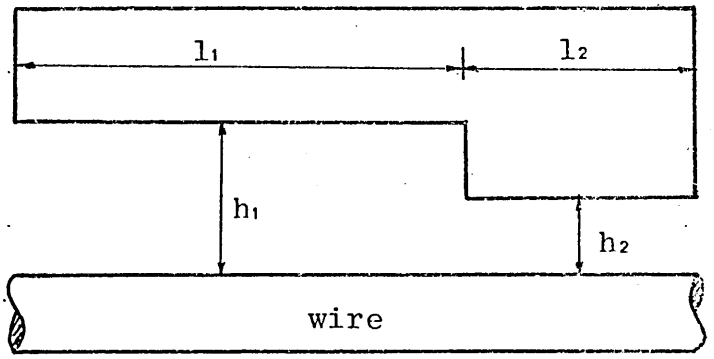

The exit diameter of the unit was later increased to 1.8mm (see figure 17) which increased the gap in the second part by 0.1mm. This introduced a new gap ratio of 2.0 which was half of the original value.

4.3.1- Results Of Pressure.

The generated pressures in the stepped bore reduction unit were measured by means of pressure transducers mounted on the unit. The results of pressures are divided into two sections, i)- the pressure variations versus speed and ii)- the pressure profiles in the unit. Numbers on each figure refers to the locations of the pressure transducers as shown in figure 19.

i)- Results of pressure versus speed.

Figure 27 shows the pressure variations versus speed for copper wire using WVG 23 polymer at the temperature of 180°C. For drawing speeds in excess of about 0.5 m/s the pressure readings were found to be approximately constant for all but position 1 where pressure was found to reduce as the drawing speed was increased. The maximum pressures for positions 3 and 1 were observed to occur at drawing speeds of about 0.2 m/s and 0.3 m/s respectively.

Figure 28 shows the pressures measured for copper wire versus speed with WVG 23 polymer at 130°C. At this polymer temperature more scattered results were produced. Again at higher drawing speeds approximately constant pressures were recorded. These trends were slightly changed at lower speeds and generally higher pressures were measured compared to those shown in figure 27.

Figure 29 gives the pressures measured for copper wire with KM 61 polymer at temperature of 200°C. Trends of the results for this polymer were significantly changed compared to those in figure 28. Flow of polymer commenced at about 0.4 m/s after which pressures decreased at all positions as the drawing speed was increased. Turning points in the pressure curves were noticed for all positions which occured at different speeds. These speeds were about 0.9 m/s for position 1, 0.7 m/s for position 2, 1.1 m/s for position 3,and 1.2 m/s for position 4. The magnitudes of the pressures were found to be close to those shown in figure 28.

Figure 30 shows the pressure variations for 18/8 stainless steel wire drawn with WVG 23 polymer at 130°C. At

higher drawing speeds the pressure magnitudes at all positions remained approximately constant. At lower drawing speeds however, pressures decreased as the drawing speed was decreased. A discontinuity was observed for the pressures at position 2 corresponding to the drawing speed of about 0.8 m/s where pressure was found to reduce by about 49%.

Figure 31 shows the measured pressures versus speed for 18/8 stainless steel wire drawn with KM 61 polymer at 200°C. Flow of this polymer took place at about 0.2 m/s after which positions 2 and 3 showed an increase and position 1 showed a decrease in the pressure. The magnitudes of the generated pressures at lower drawing speeds were similar to those shown in figure 30. The pressures reduced as speed was increased except for position 1, where the recorded pressures showed approximately constant values.

Figure 32 shows the pressures measured for mild steel wire versus speed with WVG 23 polymer at 130°C. The general trends of the results were found to be similar to those shown in figure 30 with the exception that at lower drawing speeds the pressures at all but position 3, increased with increasing speed. At position 3 the pressure decreased as the drawing speed was increased.

Figure 33 shows the pressure variations versus speed for mild steel wire using KM 61 polymer at the temperature of 200°C. Higher pressures were recorded with this polymer compared to those in figure 32 especially at lower drawing speeds. Pressures at position 2 remained reasonably constant as the drawing speed was increased but the pressures at positions 1 and 4 decreased gradually to

nearly the same magnitude. Pressures measured at position 3 showed two maximum points at about 0.2 m/s and 2 m/s and a turning point at about 0.7 m/s.

Figure 34 is showing the variations of pressure versus speed for mild steel wire with KM 61 polymer at 200°C. These results were obtained when the gap ratio was reduced to 2. The general trends were found to change compared to those in figure 33. Pressures measured at positions 2 and 4 increased as the drawing speed was increased and reached a maximum at about 1.5 m/s and 0.8 m/s respectively. Both positions showed a reduction in the pressure as the drawing speed was increased further. At slower speeds, the pressures for positions 3 and 1 reduced as the drawing speed was increased. Turning points were observed at about 0.3 m/s for position 3 and 0.4 m/s for position 1. Maximum pressures were also measured for these two positions at about 1.3 m/s.

ii)- Results of pressure profiles.

Pressure profiles in the stepped bore reduction unit are also shown in figures 35 to 42, at four typical drawing speeds. These results exhibited similar trends with slight differences as the conditions were altered. Pressures were found to increase from the entry point of the unit towards the step and decrease after the step. It may be noted that pressures at the step could not be measured since it was found difficult to mount a pressure transducer there without damaging the step configuration.

Figures 35 to 37 show the pressure profiles for the

copper wire, with WVG 23 polymer and melt temperature of 180°C (figure 35). Pressure profiles showed very little change in the first part of the unit as the drawing speed was increased. When the melt temperature of the WVG 23 polymer was reduced to 130°C, higher pressures were recorded at the step and magnitudes of the pressures reduced as the speed was increased (figure 36). At the drawing speed of 0.5 m/s, approximately a linear pressure profile was produced. Pressure profiles using KM 61 polymer at the temperature of 200°C was found to vary more towards the entry point of the unit rather than at the step as shown in figure 37. Magnitudes of the pressures recorded using KM 61 polymer were similar to those shown in figure 36.

Figures 38 and 39 show the pressure profiles for the 18/8 stainless steel wire when WVG 23 polymer and KM 61 polymer were used at melt temperatures of 130°C and 200°C respectively. The reduction in the pressure (especially at position 2) as the drawing speed was increased is clearly shown in both cases. At higher drawing speeds more linear pressure profiles were produced with WVG 23 polymer.

Figures 40 to 42 show the pressure profiles for the mild steel wire. The WVG 23 polymer at the temperature of 130°C showed similar trends to those of figure 38. These profiles are shown in figure 40. When the KM 61 polymer was used as a pressure medium at 200°C, little changes were observed in the pressure profiles as the drawing speed was increased. Higher pressures were recorded for this polymer as shown in figure 41. Introduction of the new gap ratio ($h_1/h_2 = 2.0$) caused the pressure to reduce

and the drawing speed was found to have even more reducing effect on the generated pressures compared to those in figure 41. These results are shown in figure 42.

FIG 27 : PRESSURE V SPEED FOR COPPER WIRE WITH WVG23 AT 180°C

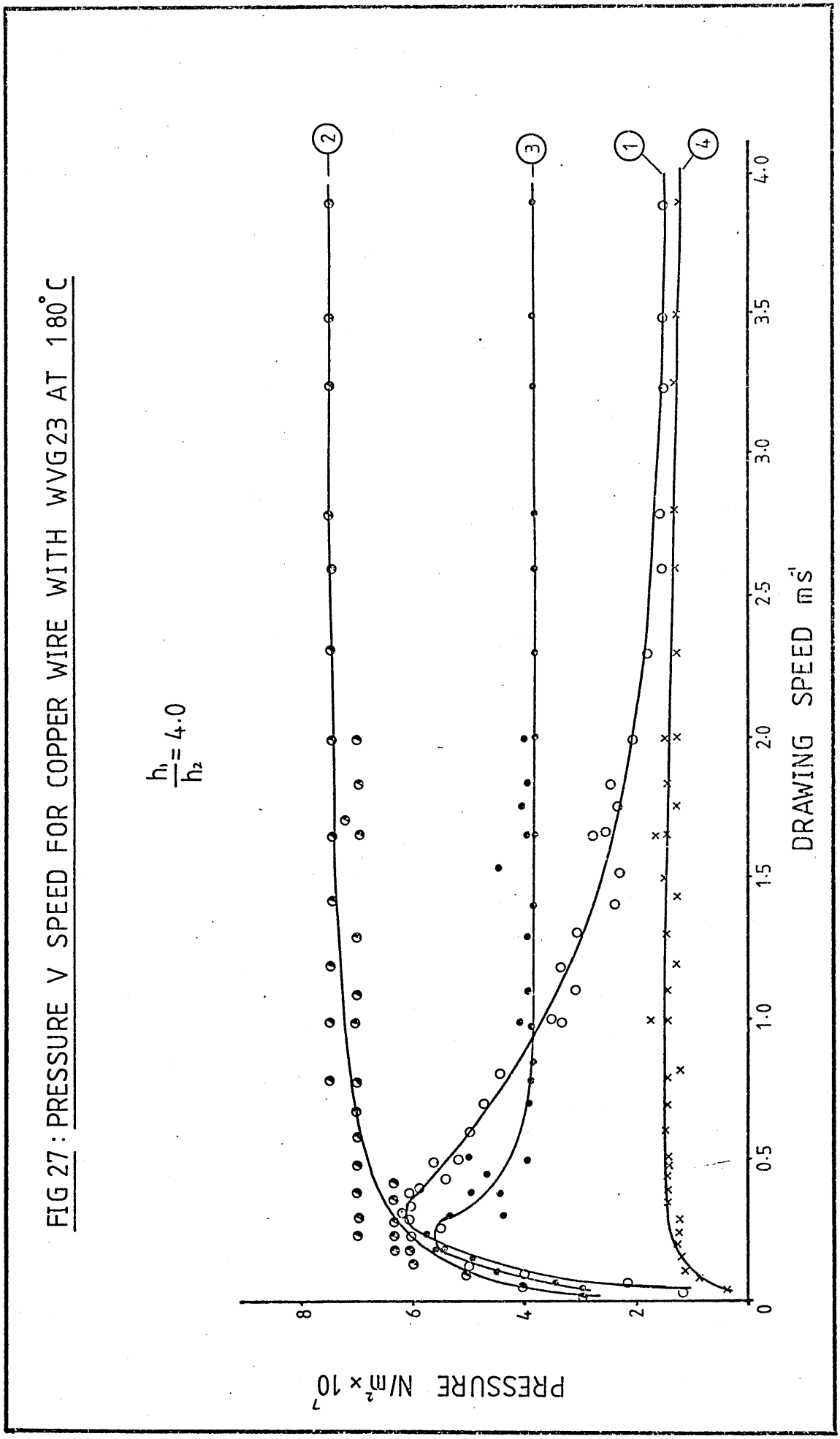

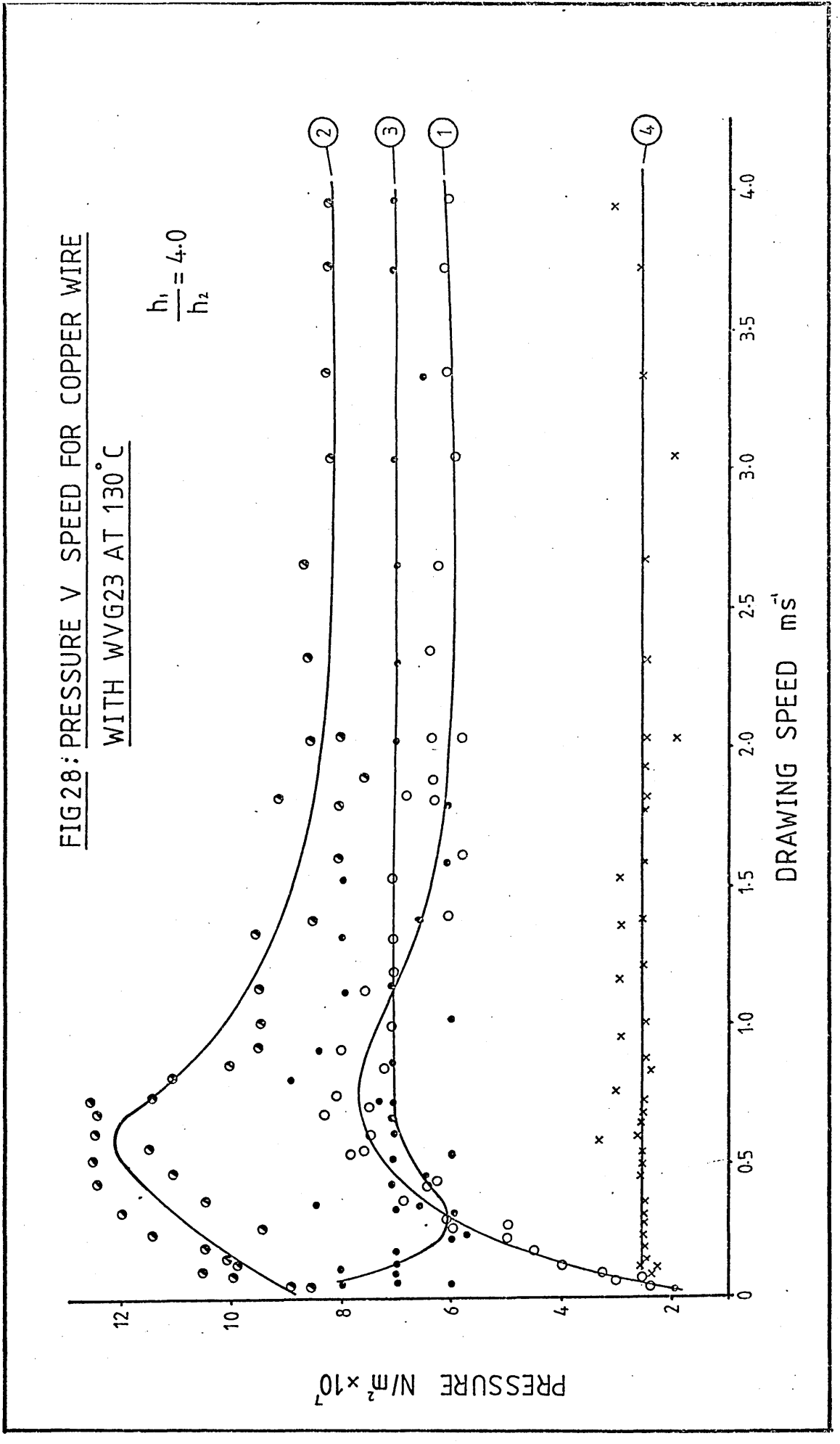
FIG 28: PRESSURE V SPEED FOR COPPER WIRE
WITH WVG23 AT 130°C
$\frac{h_1}{h_2} = 4.0$
PRESSURE N/m² ×10⁷
DRAWING SPEED ms⁻¹
12
10
8
6
4
2
0
0·5
1·0
1·5
2·0
2·5
3·0
3·5
4·0
1
2
3
4

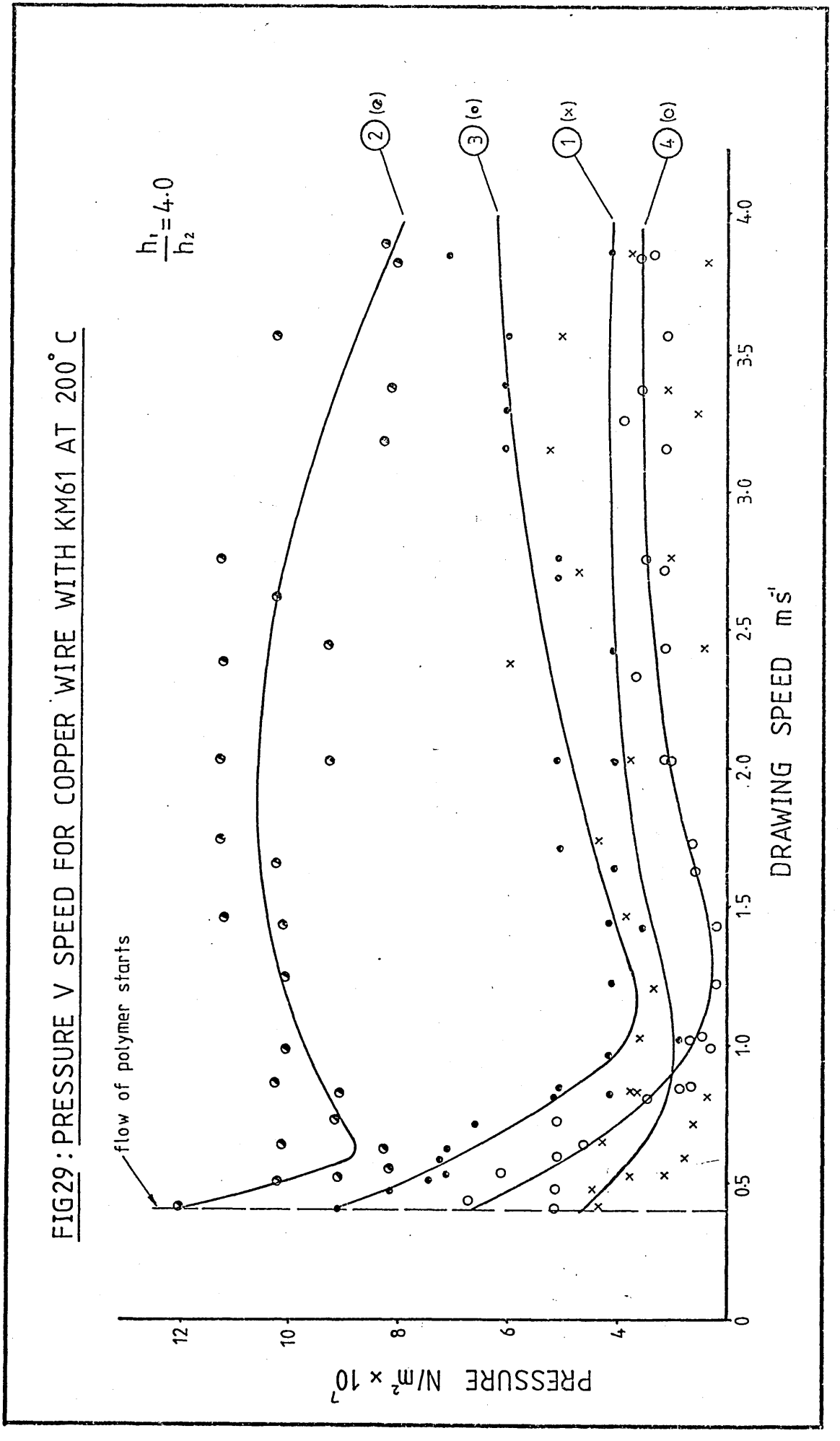
FIG29: PRESSURE V SPEED FOR COPPER WIRE WITH KM61 AT 200°C
$\frac{h_1}{h_2}$=4.0
2 (@)
3 (o)
1 (x)
4 (o)
flow of polymer starts
PRESSURE N/m² × 10⁷
DRAWING SPEED ms⁻¹
0
4
6
8
10
12
0·5
1·0
1·5
2·0
2·5
3·0
3·5
4·0

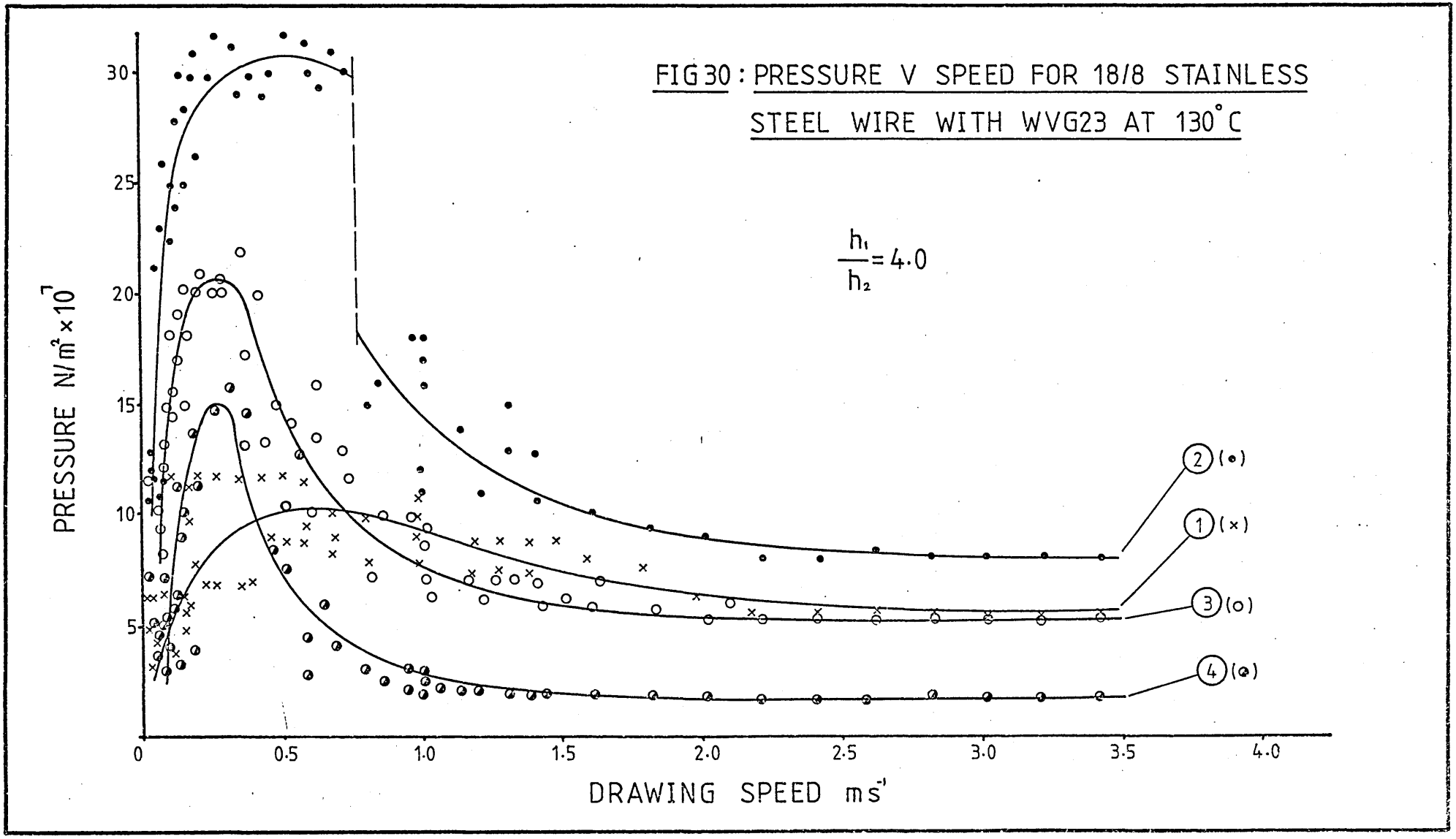
FIG 30 : PRESSURE V SPEED FOR 18/8 STAINLESS STEEL WIRE WITH WVG23 AT 130°C
$\frac{h_1}{h_2} = 4.0$
PRESSURE N/m² × 10⁷
30
25
20
15
10
5
0
0.5
1.0
1.5
2.0
2.5
3.0
3.5
4.0
DRAWING SPEED ms⁻¹
2 (•)
1 (×)
3 (o)
4 (⊘)

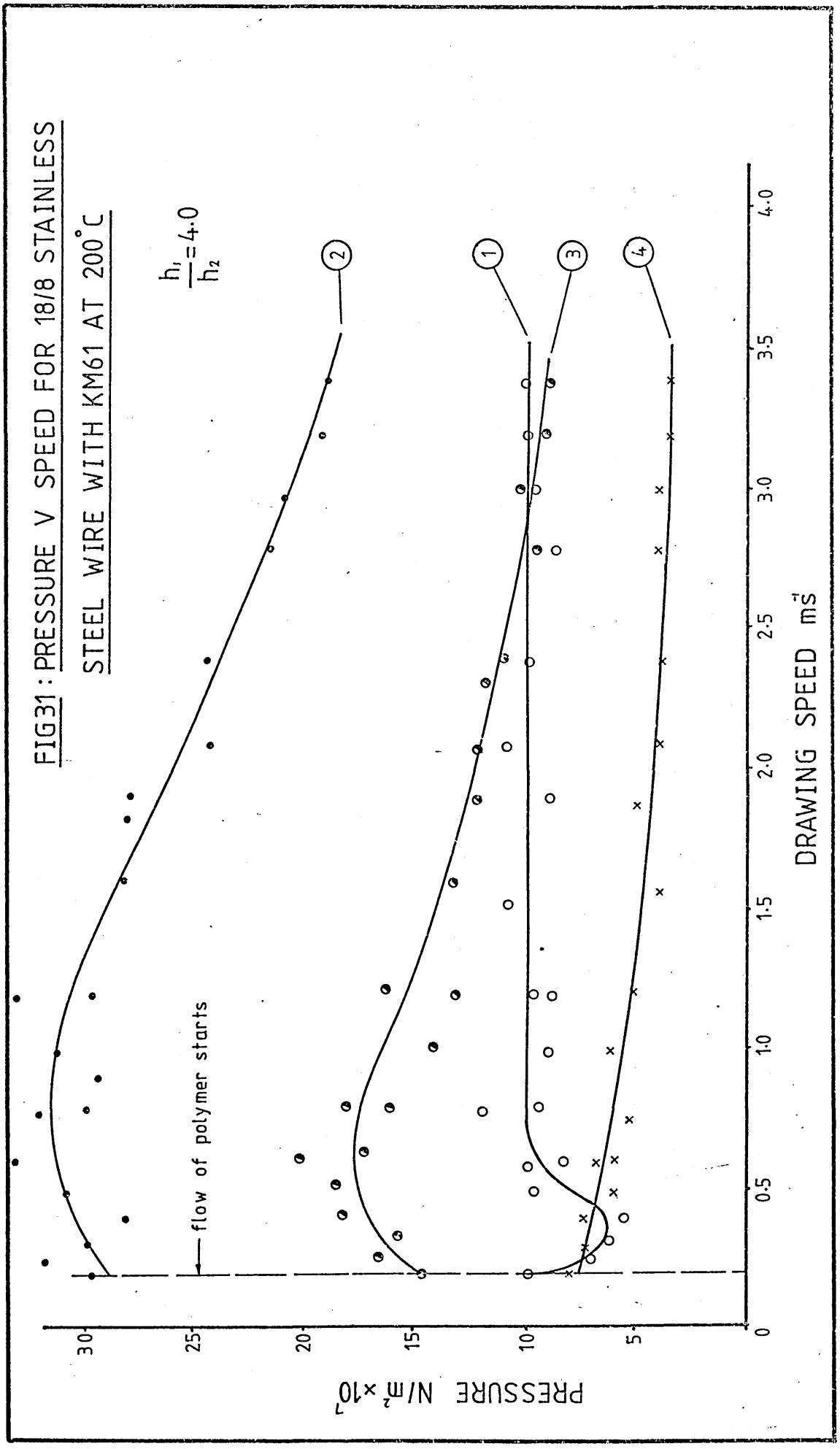
FIG 31 : PRESSURE V SPEED FOR 18/8 STAINLESS STEEL WIRE WITH KM61 AT 200°C
h1/h2 = 4.0
flow of polymer starts
PRESSURE N/m² ×10⁷
DRAWING SPEED ms⁻¹
0
0.5
1.0
1.5
2.0
2.5
3.0
3.5
4.0
5
10
15
20
25
30
1
2
3
4

FIG 32 : PRESSURE V SPEED FOR MILD STEEL WIRE WITH WVG23 AT 130°C

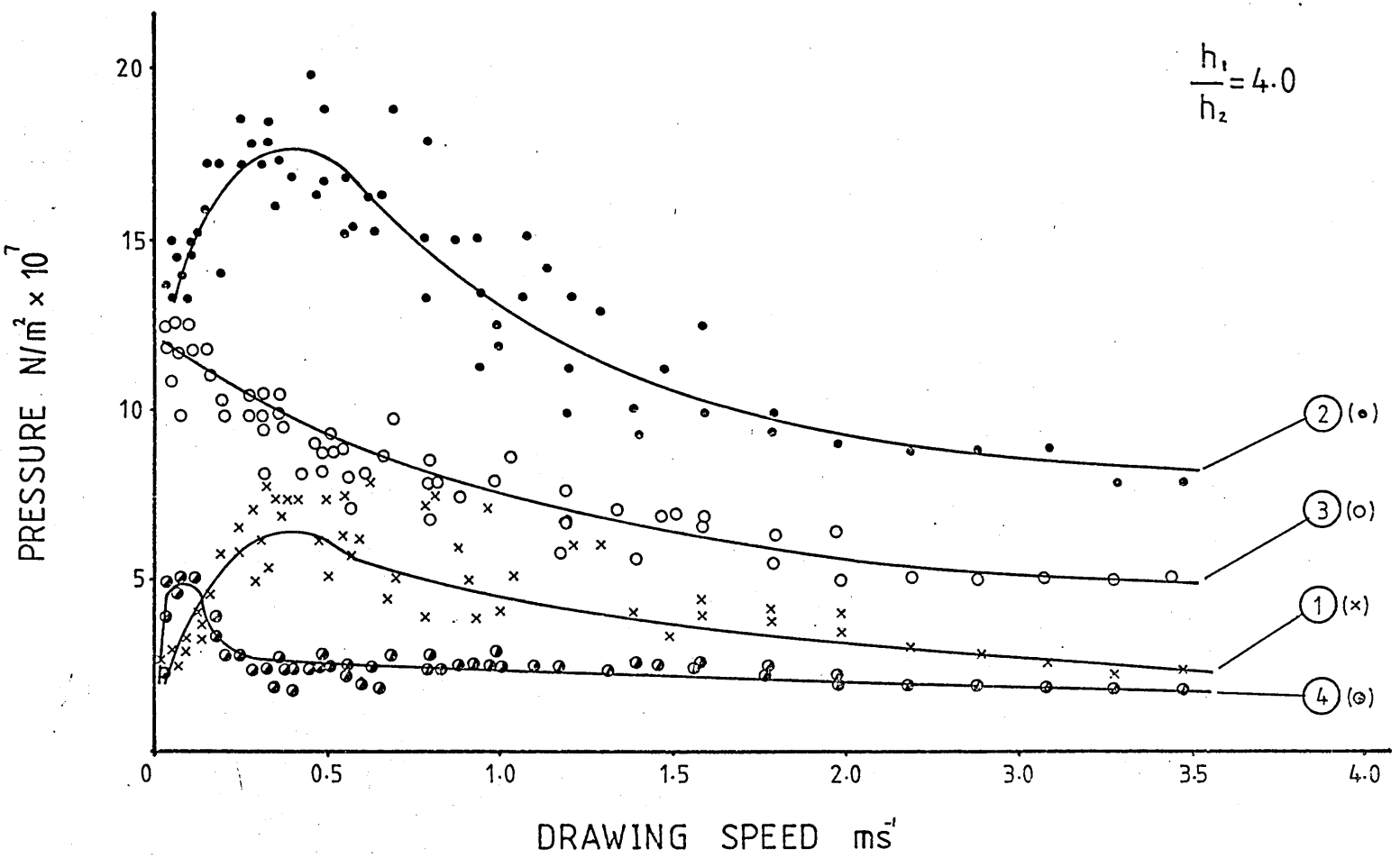

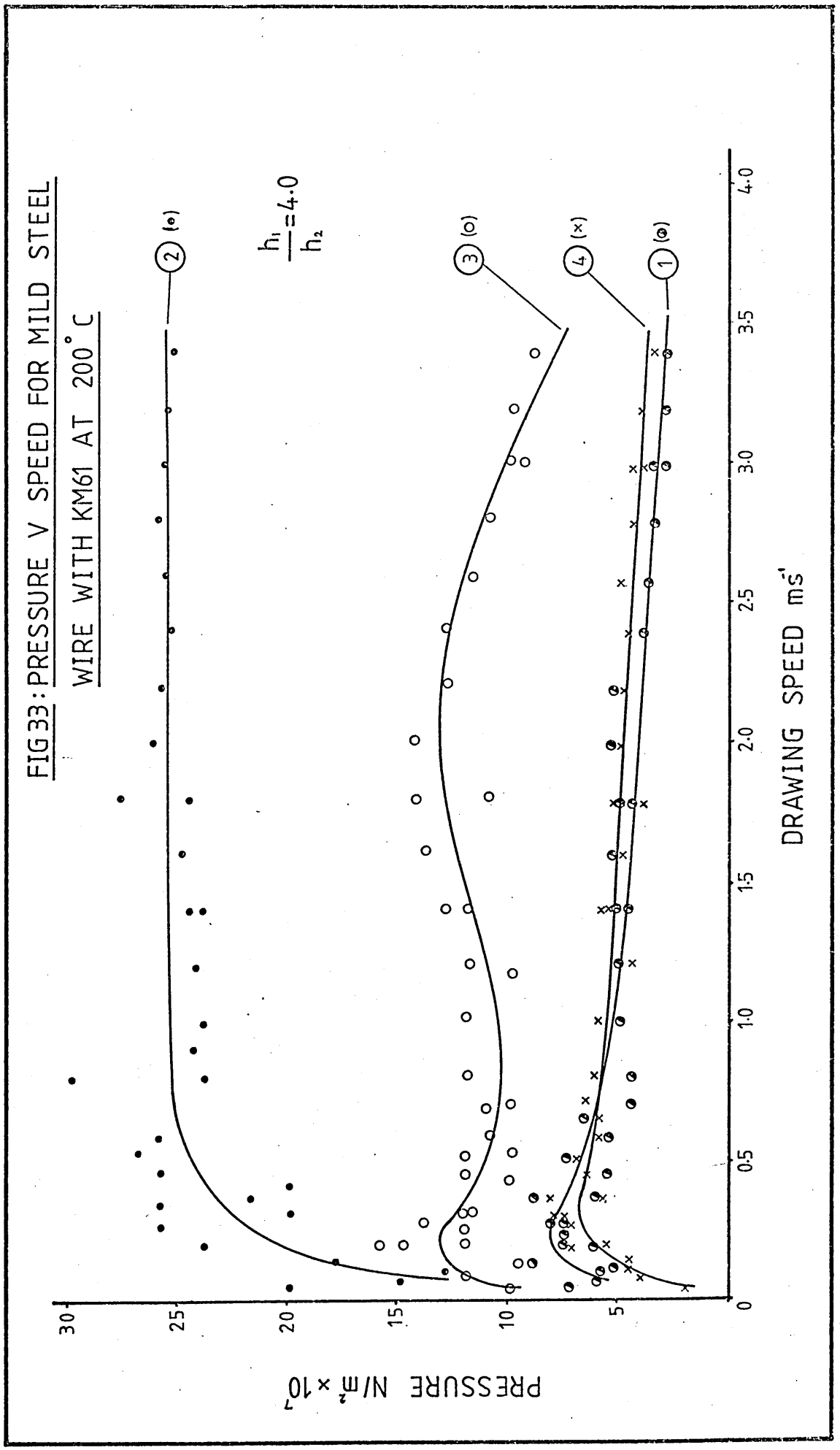
FIG 33: PRESSURE V SPEED FOR MILD STEEL WIRE WITH KM61 AT 200°C
$\frac{h_1}{h_2}$=4.0
(2) (•)
(3) (○)
(4) (×)
(1) (⊙)
PRESSURE N/m² × 10⁷
DRAWING SPEED ms⁻¹
30
25
20
15
10
5
0
0.5
1.0
1.5
2.0
2.5
3.0
3.5
4.0

FIG 34 : PRESSURE V SPEED FOR MILD STEEL WIRE WITH KM61 AT 200°C

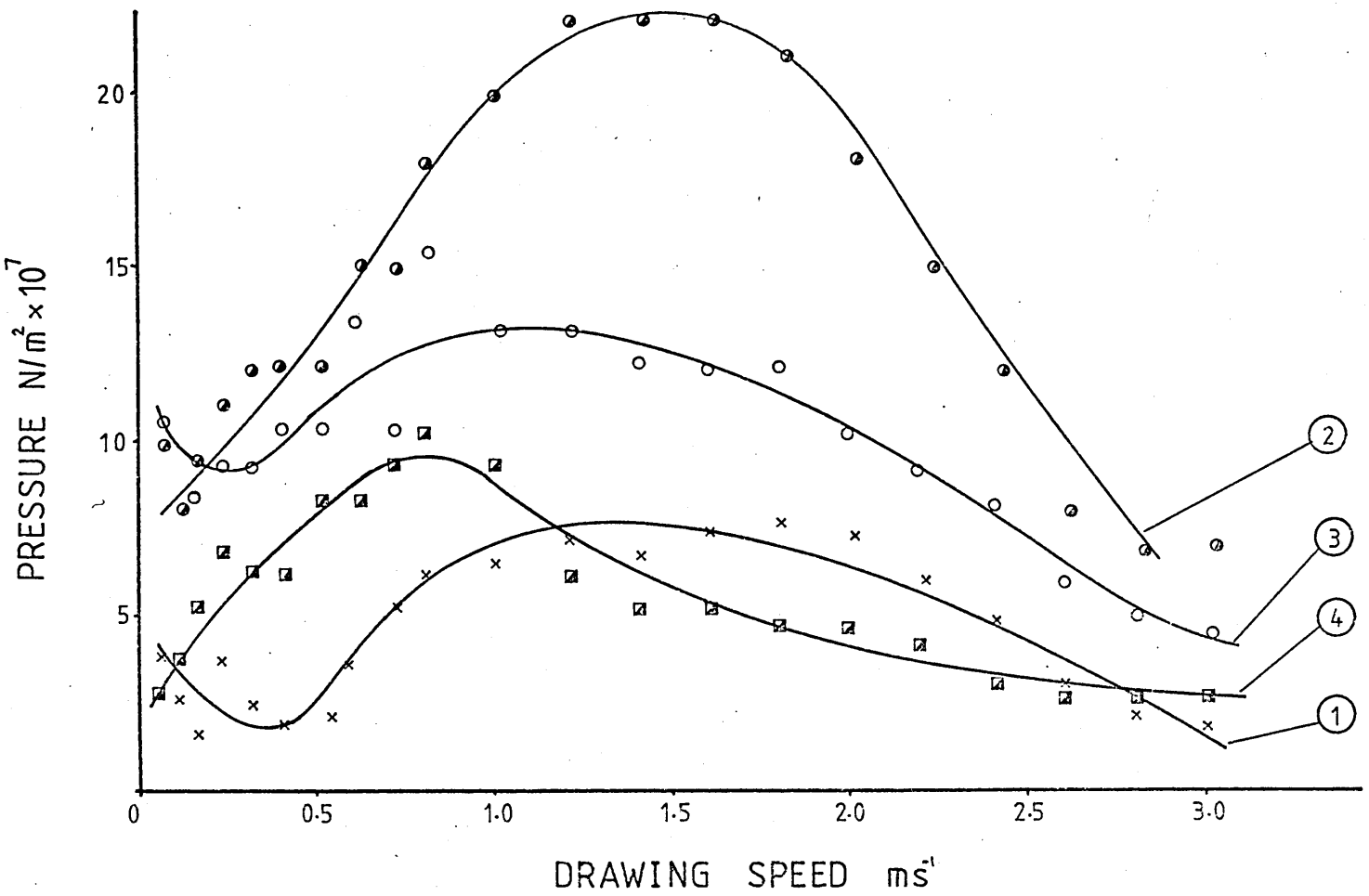

FIG 35: PRESSURE DISTRIBUTIONS FOR COPPER WIRE WITH WVG23 AT 180°C

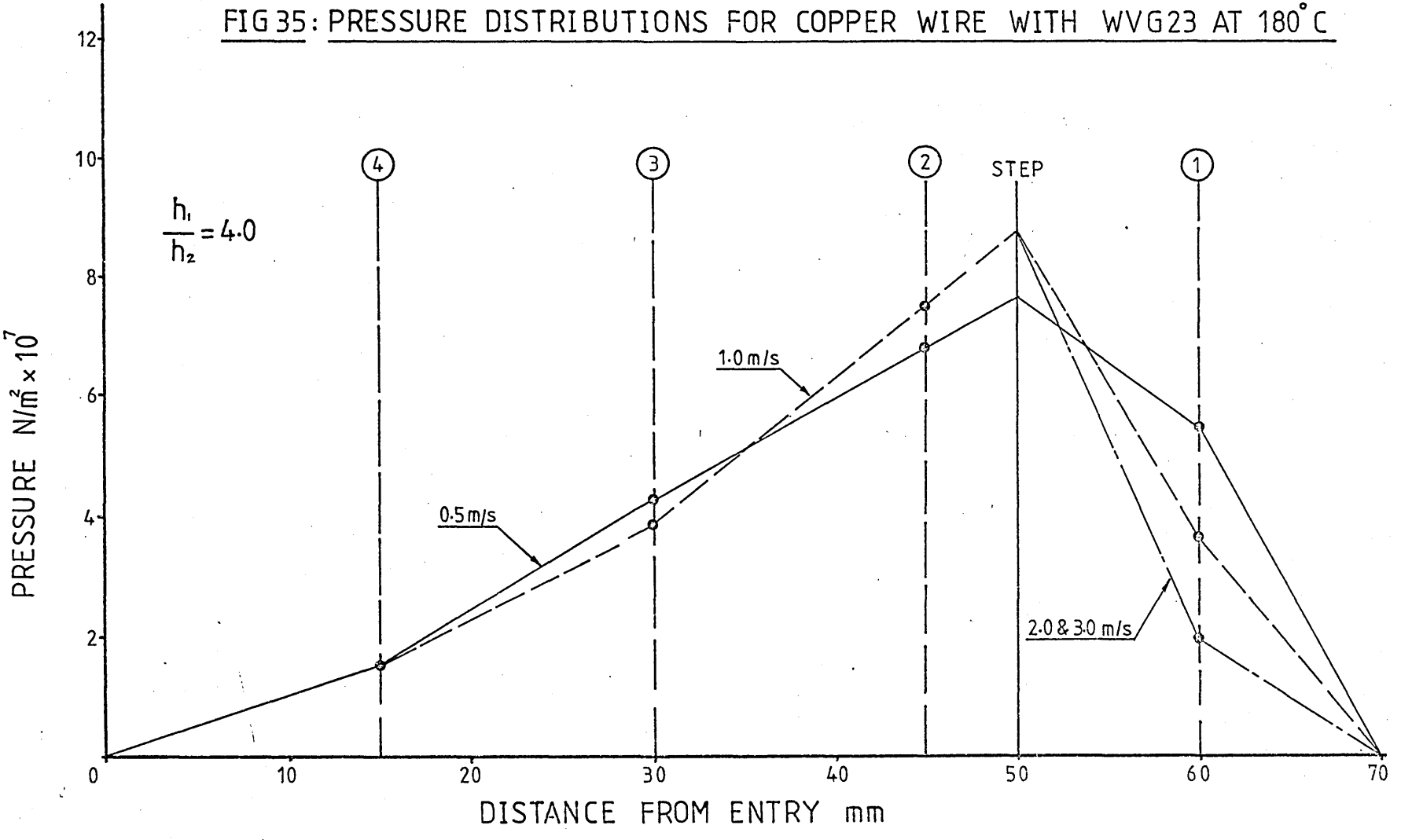

FIG36 : PRESSURE DISTRIBUTIONS FOR COPPER WIRE WITH WVG23 AT 130°C

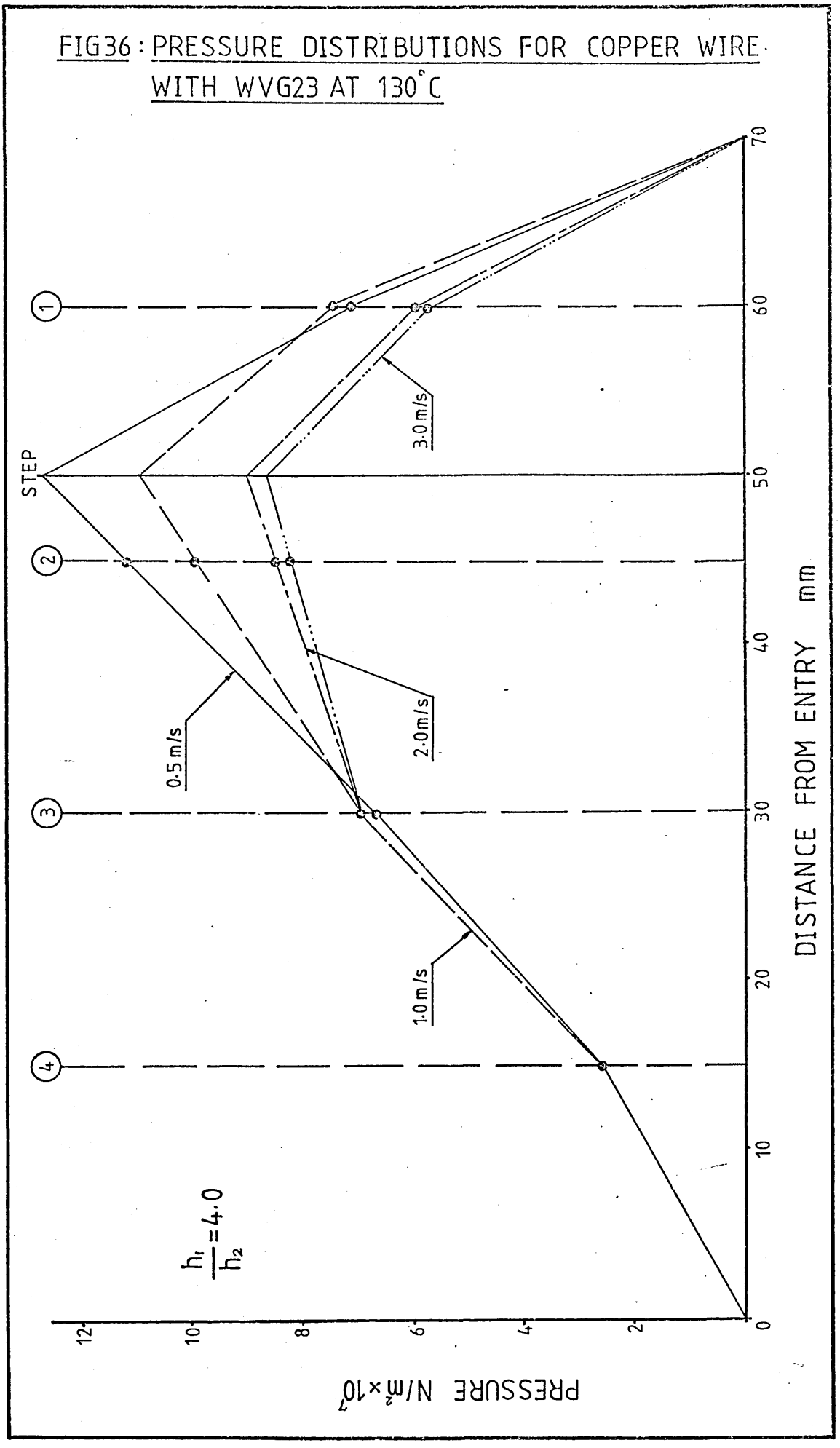

FIG 37: PRESSURE DISTRIBUTIONS FOR COPPER WIRE WITH KM61 AT 200°C

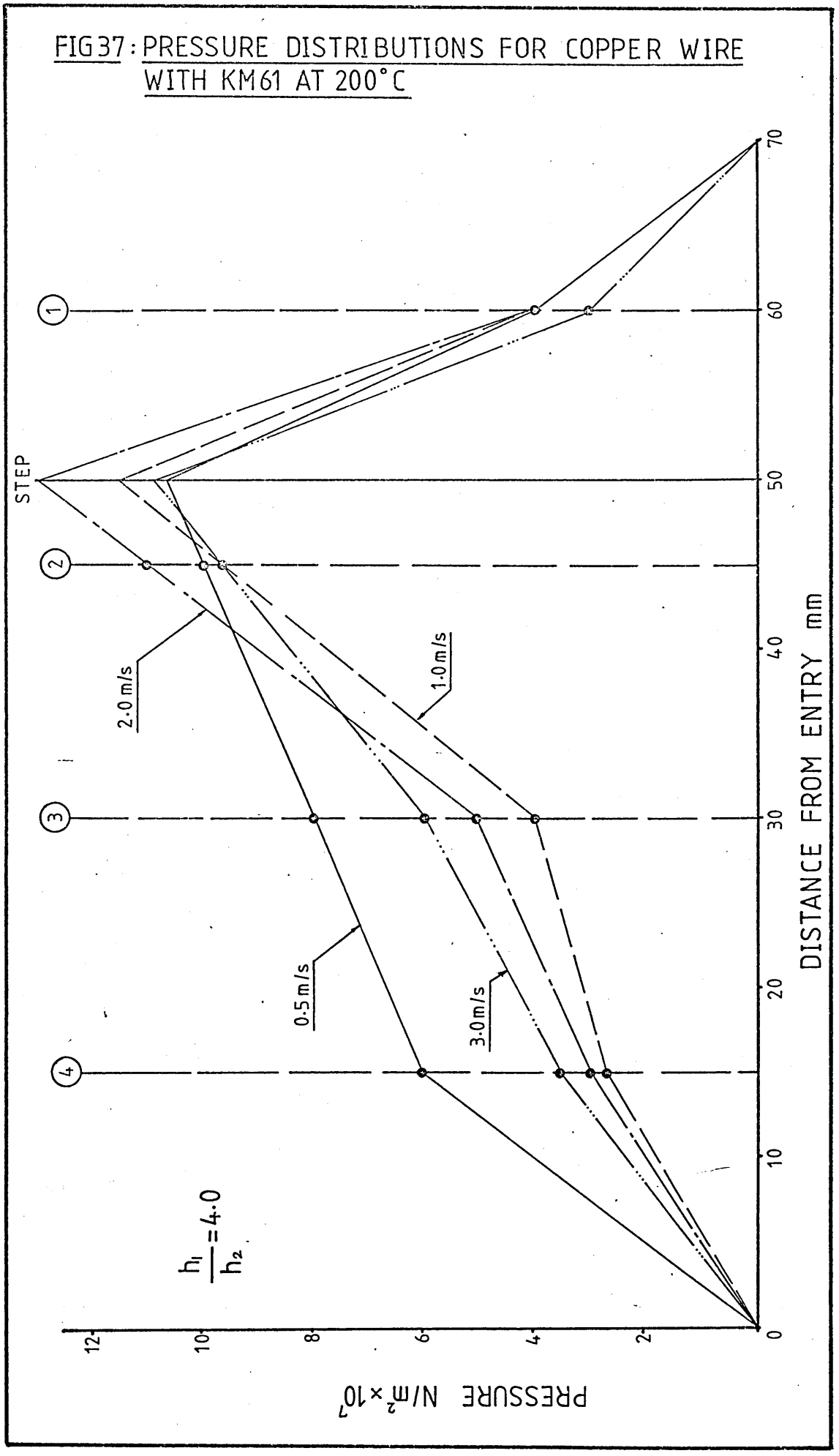

FIG38: PRESSURE DISTRIBUTIONS FOR 18/8 STAINLESS STEEL WIRE WITH WVG23 AT 130°C

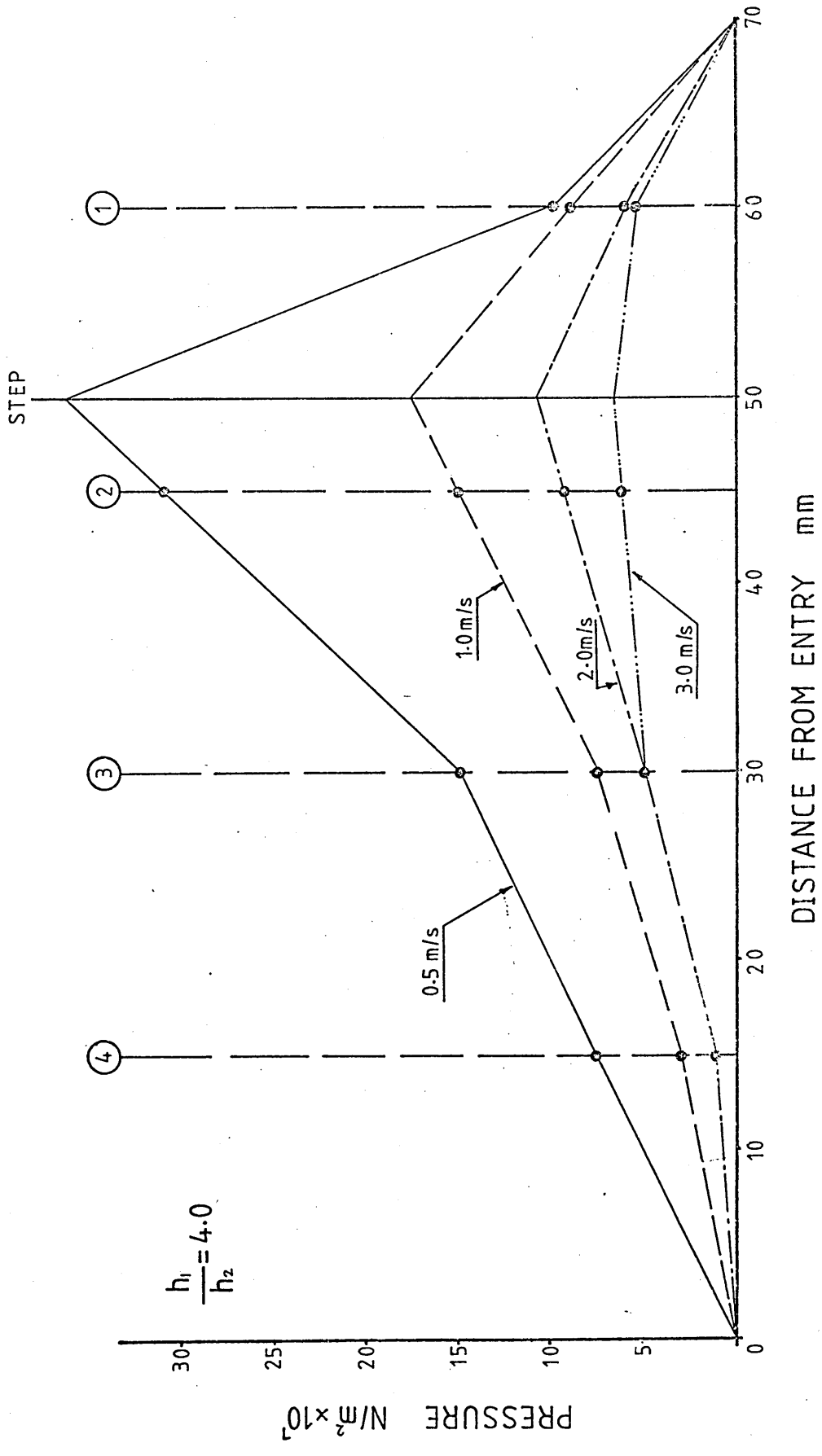

FIG39: PRESSURE DISTRIBUTIONS FOR 18/8 STAINLESS STEEL WIRE WITH KM61 AT 200°C

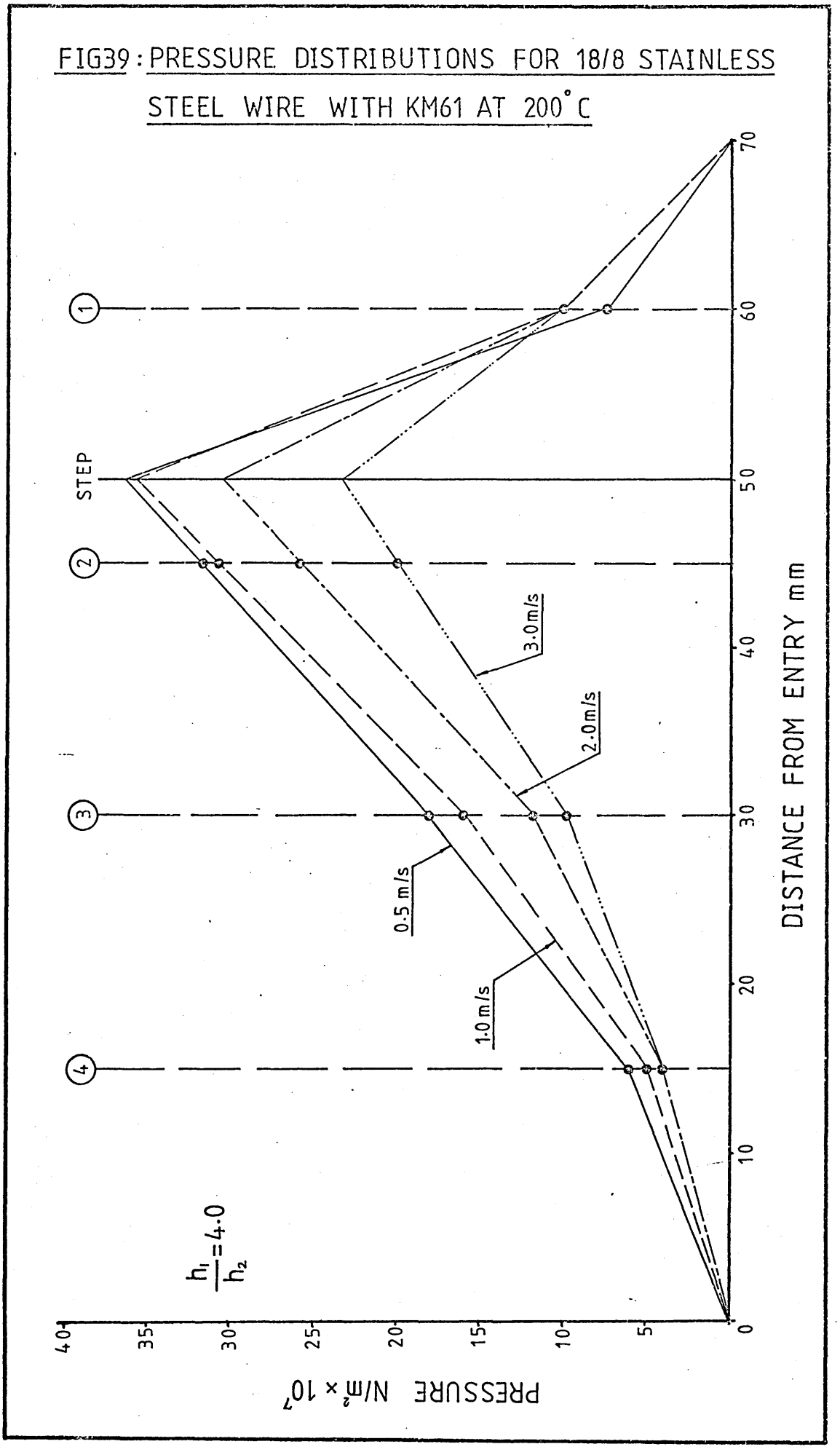

FIG40 : PRESSURE DISTRIBUTIONS FOR MILD STEEL WIRE WITH WVG 23 AT 130°C

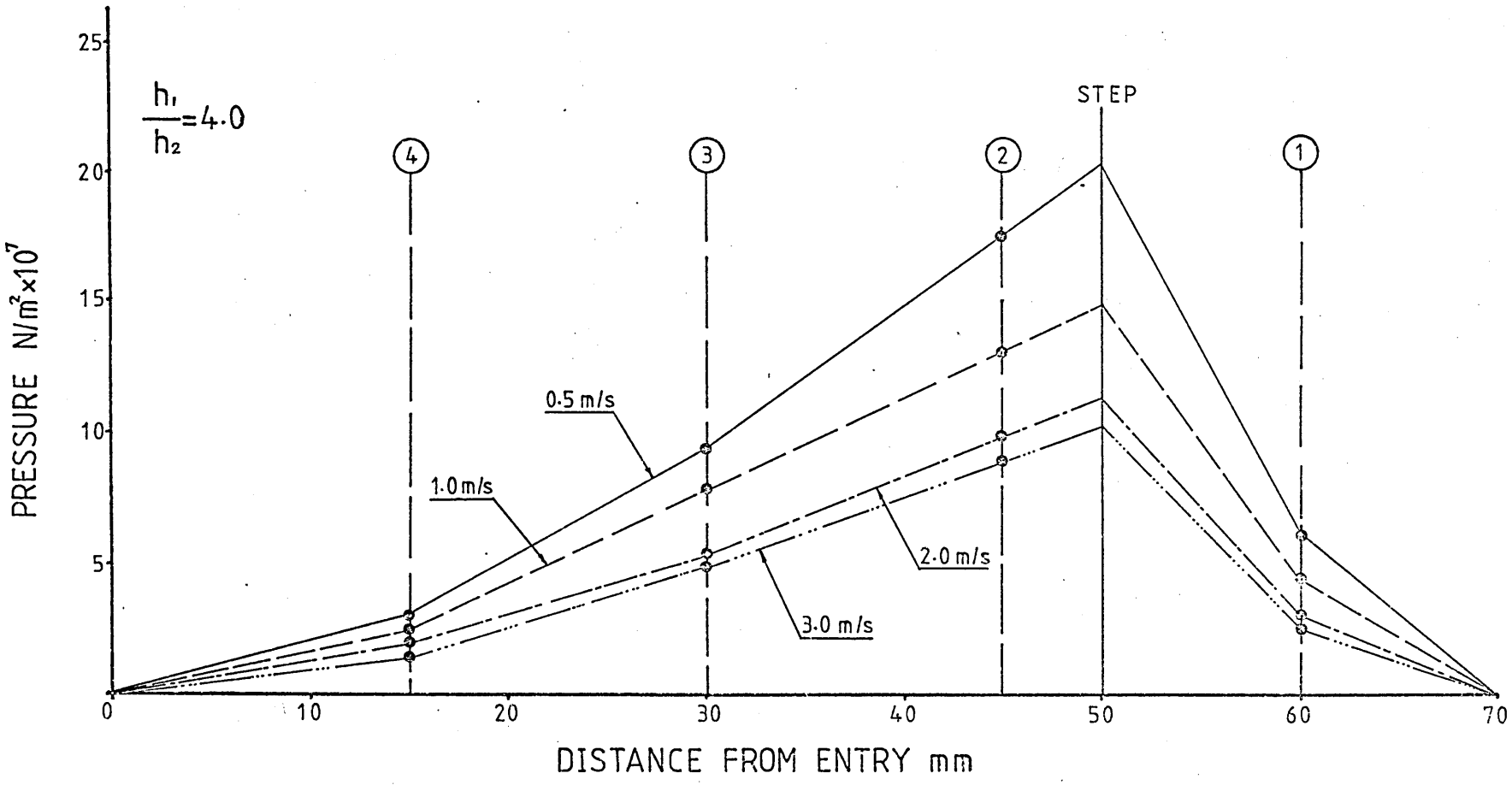

FIG41 : PRESSURE DISTRIBUTIONS FOR MILD STEEL WIRE WITH KM61 AT 200°C

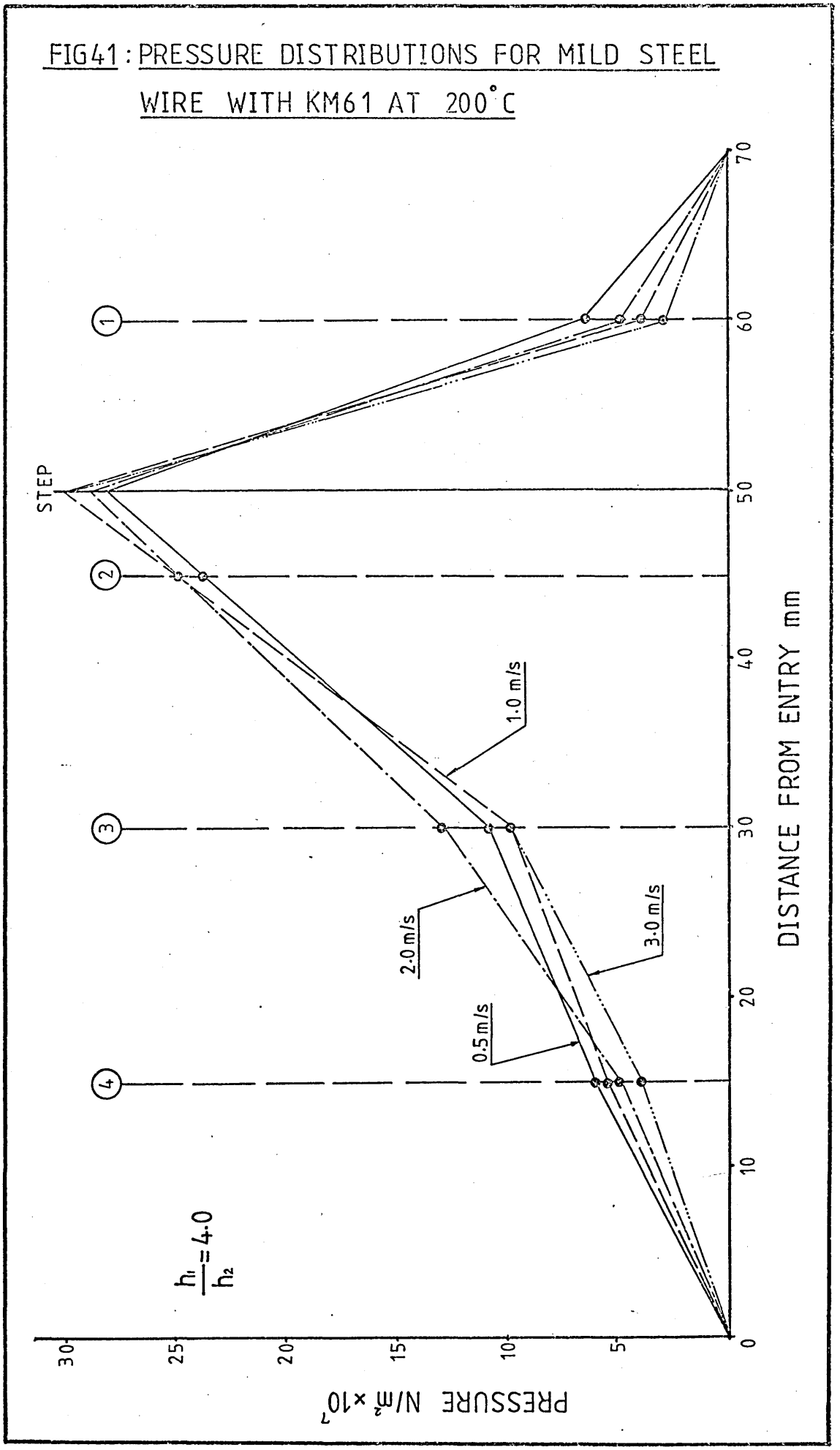

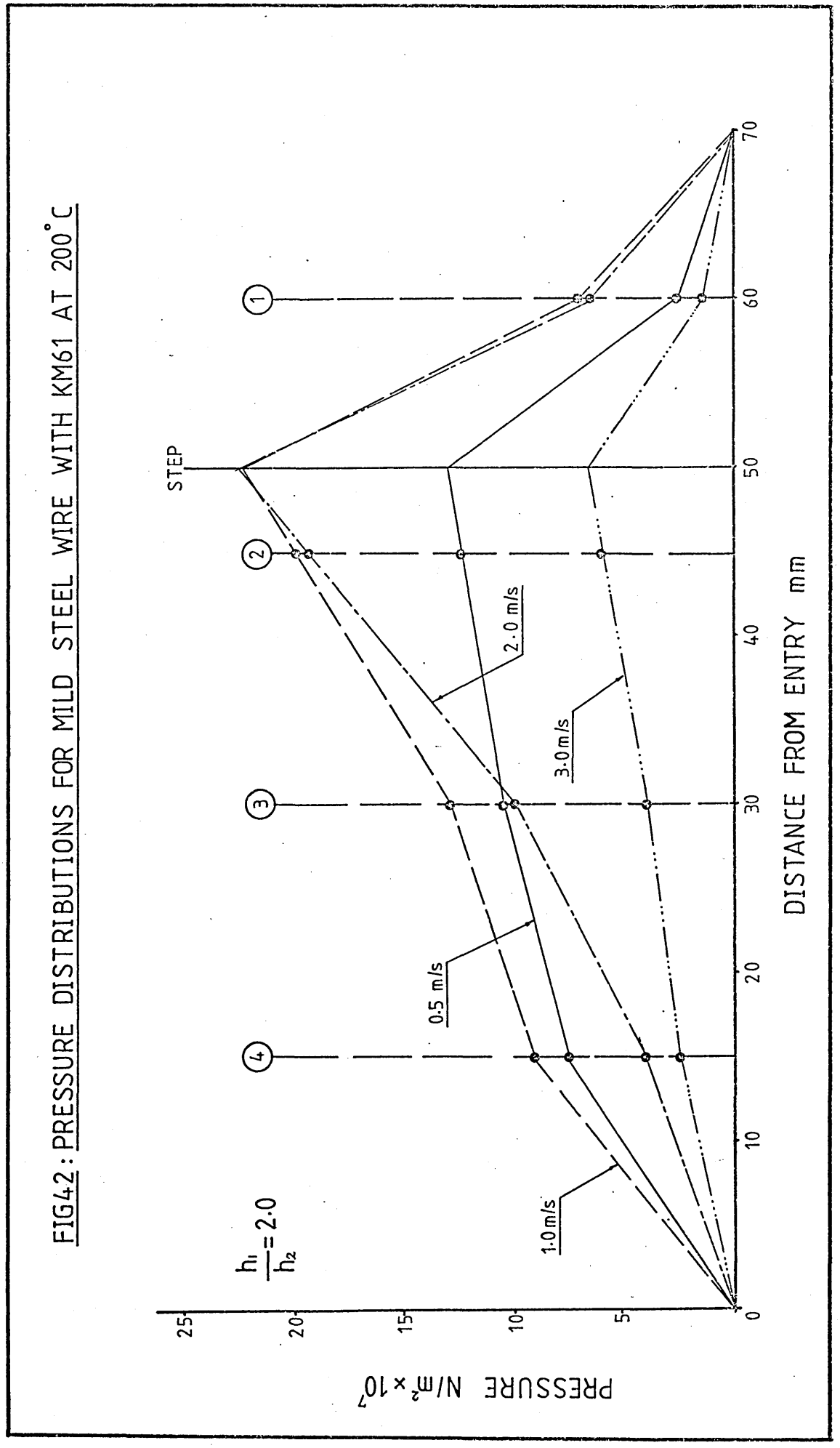

FIG42 : PRESSURE DISTRIBUTIONS FOR MILD STEEL WIRE WITH KM61 AT 200°C

4.3.2- Results Of Drawing Load Versus Drawing Speed.

Drawing loads were measured by attaching strain gauges on the support frame as shown in plate 9. The deflection of this frame produced a trace on U.V. paper which indicated the magnitude of the drawing load. A typical U.V. trace produced during the tests is shown in figure 23.

Figure 43 shows the variations in the drawing load versus speed for copper wire with WVG 23 polymer at two different temperatures (130°C and 180°C). Approximately constant drawing loads were measured at speeds in excess of 1.0 m/s for both melt temperatures. At lower drawing speeds, the drawing loads reduced as the drawing speed was reduced. At the temperature of 130°C, generally higher drawing loads were measured and a maximum point was observed at about 0.12 m/s.

Figure 44 shows the drawing loads measured for different wire materials versus drawing speed using WVG 23 polymer at 130°C. As the drawing speed was increased the drawing loads for the copper and the 18/8 stainless steel wires were increased. A maximum drawing load was noted for the stainless steel wire at 0.3 m/s and similarly a maximum drawing load at about 0.15 m/s for the copper wire. As the drawing speed was increased further, the recorded results for both wires reduced. The drawing loads for mild steel wire reduced as the drawing speed was increased and comparatively lower results were recorded.

Figure 45 shows the drawing loads measured for different wire materials with KM 61 polymer at the

temperature of 200°C. Flow of this polymer commenced at about 0.4 m/s for copper and at about 0.2 m/s for 18/8 stainless steel wire. Below these speeds, random results were recorded. Drawing loads for all the wire materials decreased as the drawing speed was increased. Again drawing loads measured for mild steel wire showed lower magnitudes compared to the other two materials.

Figure 46 shows the drawing loads measured for the mild steel wire with two different gap ratios using KM 61 polymer at the temperature of 200°C. Drawing loads were reduced as the drawing speed was increased. At speeds in excess of 1.0 m/s, for the gap ratio of 4.0, approximately constant drawing loads were measured (about 200 N). For smaller gap ratio, comparatively higher drawing loads were recorded at lower drawing speeds and lower drawing loads at higher drawing speeds.

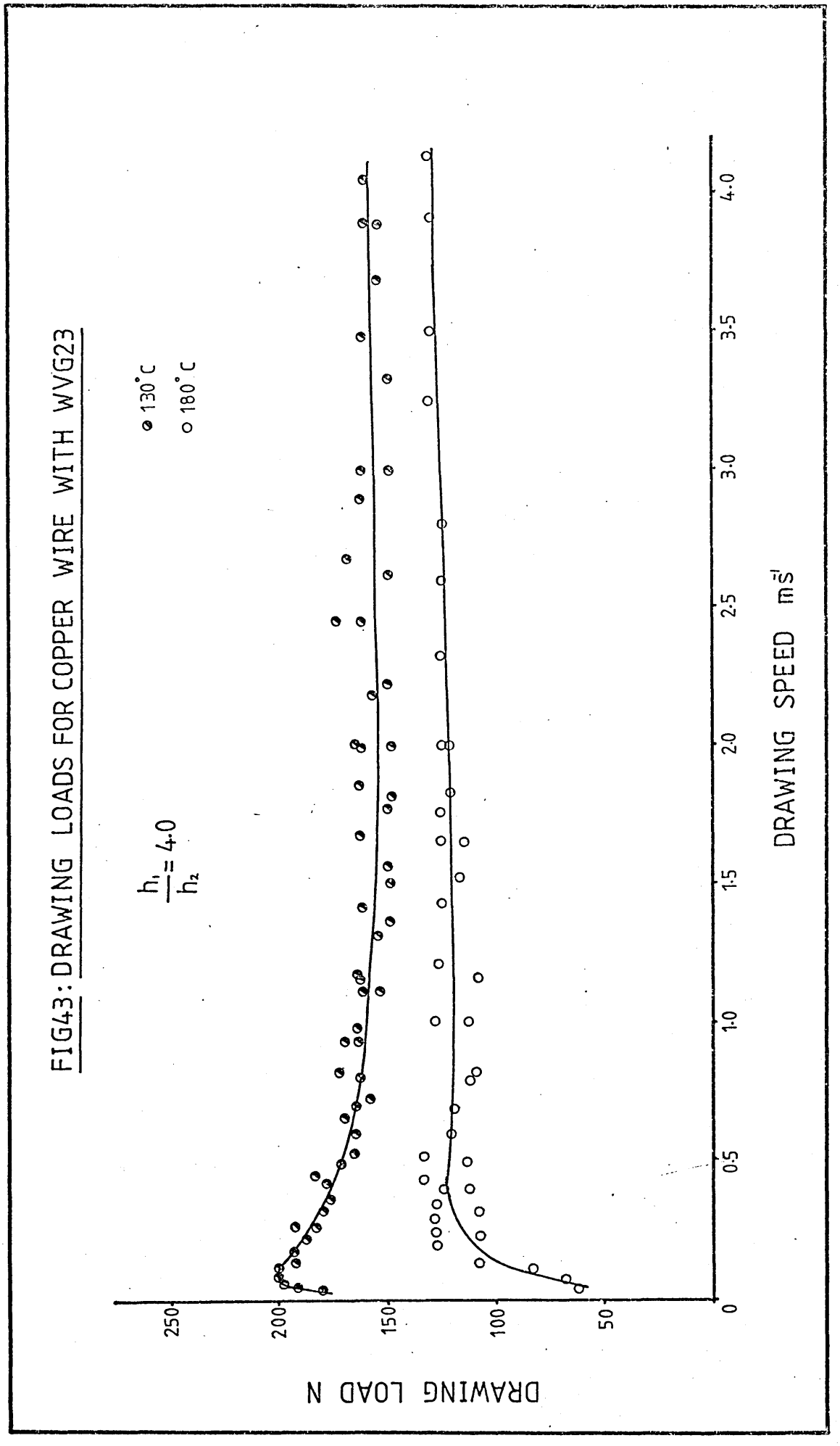
FIG43: DRAWING LOADS FOR COPPER WIRE WITH WVG23
$\frac{h_1}{h_2} = 4.0$
● 130°C
○ 180°C
DRAWING LOAD N
250
200
150
100
50
0
0·5
1·0
1·5
2·0
2·5
3·0
3·5
4·0
DRAWING SPEED ms⁻¹

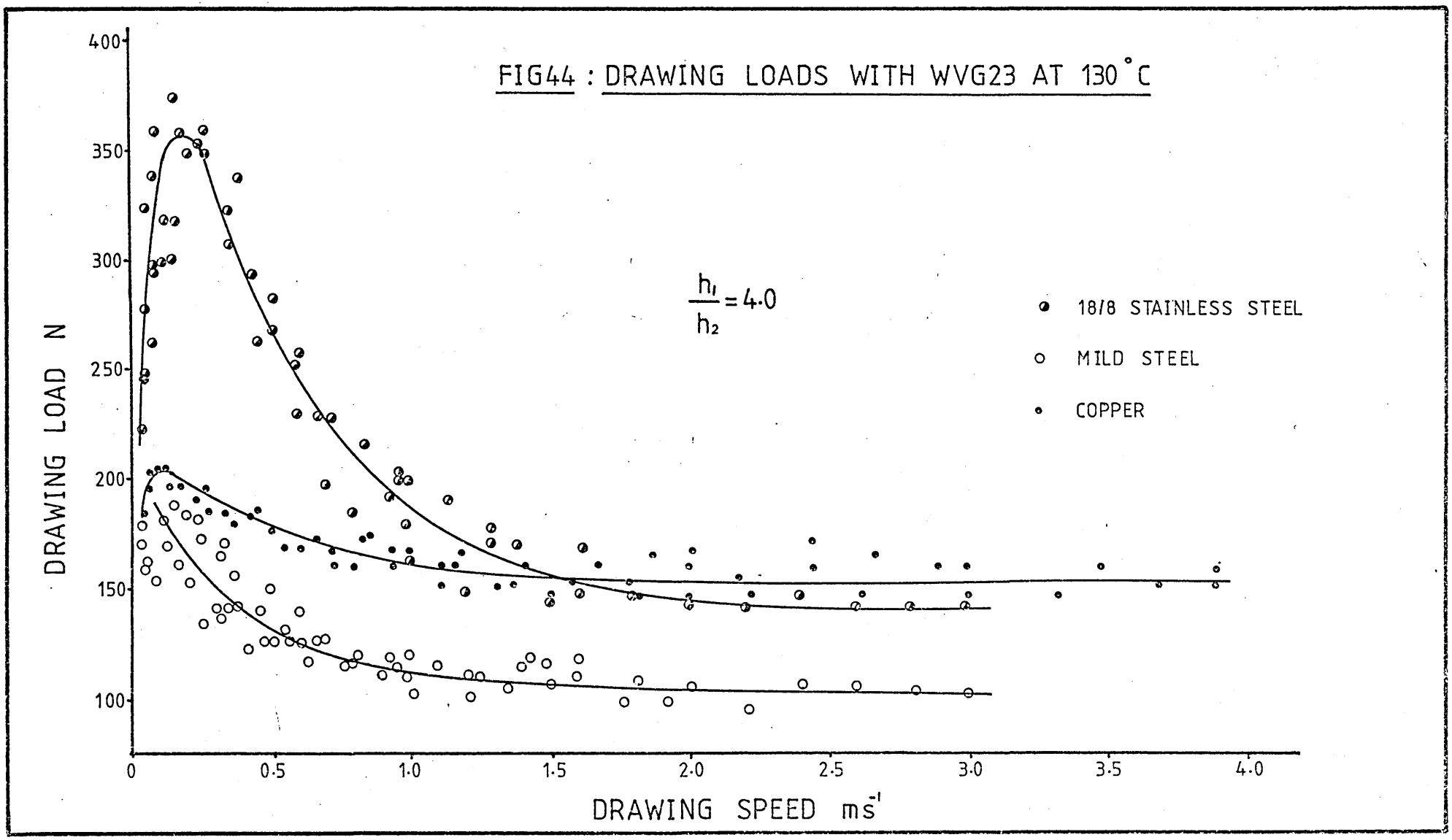
FIG44 : DRAWING LOADS WITH WVG23 AT 130 °C
DRAWING LOAD N
400
350
300
250
200
150
100
0
0·5
1·0
1·5
2·0
2·5
3·0
3·5
4·0
DRAWING SPEED ms⁻¹
h1/h2 = 4·0
18/8 STAINLESS STEEL
MILD STEEL
COPPER

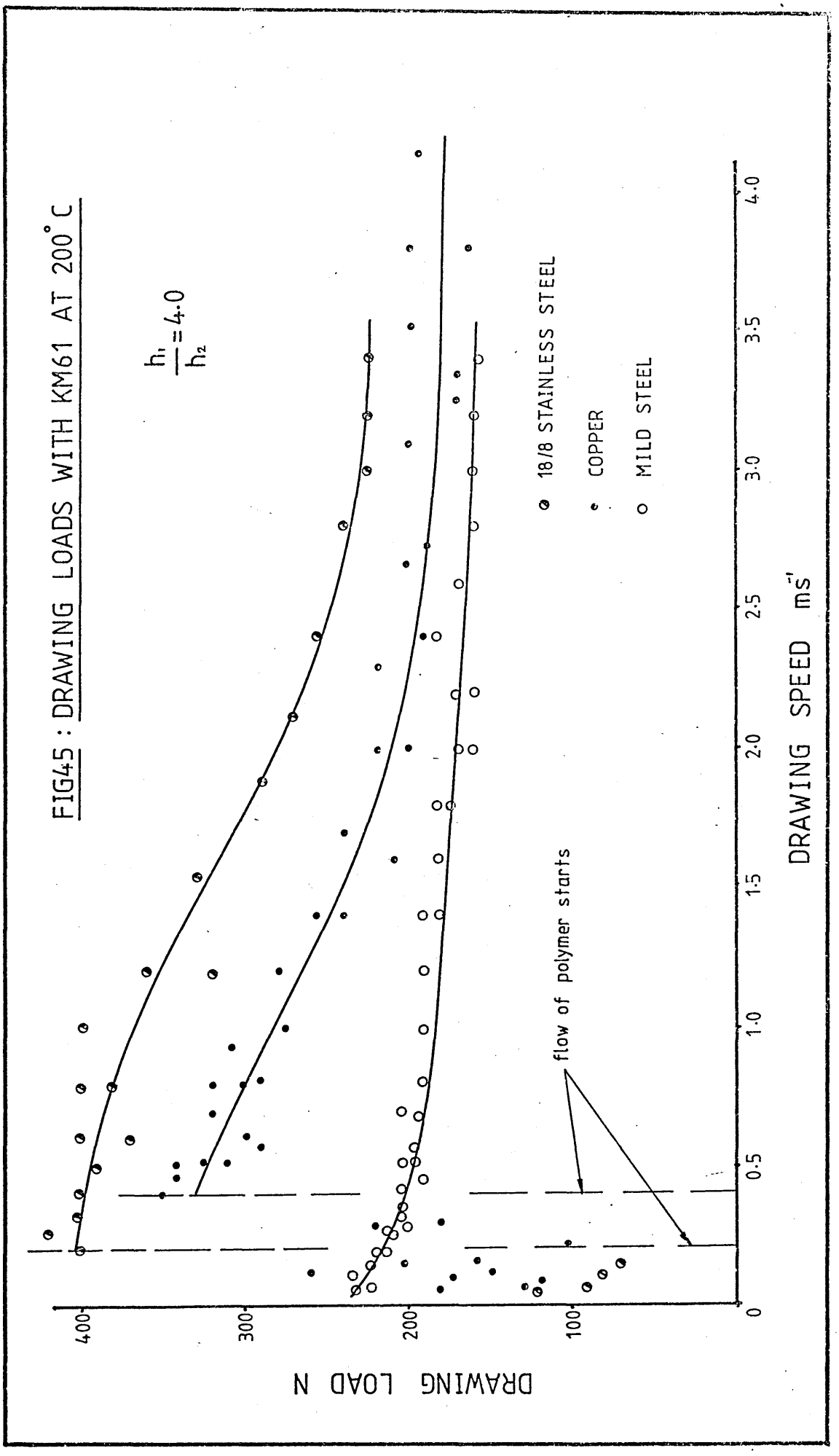
FIG45 : DRAWING LOADS WITH KM61 AT 200°C
h1/h2 = 4.0
18/8 STAINLESS STEEL
COPPER
MILD STEEL
flow of polymer starts
DRAWING LOAD N
DRAWING SPEED ms⁻¹
400
300
200
100
0
0.5
1.0
1.5
2.0
2.5
3.0
3.5
4.0

FIG46 : DRAWING LOADS FOR MILD STEEL WIRE WITH KM61 AT 200°C

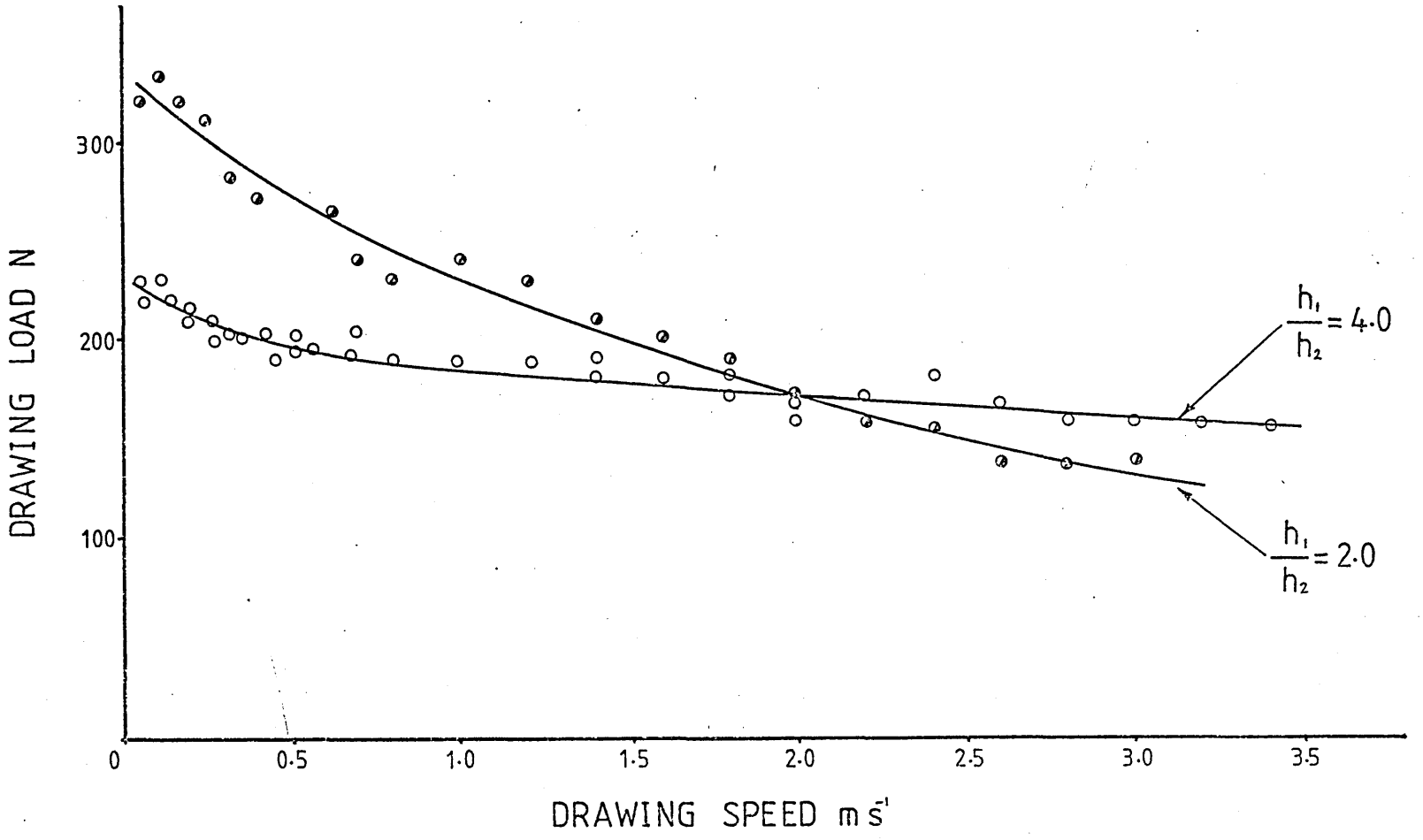

4.3.3- Results Of Coating Thickness Versus Drawing Speed.

Qualitative assesments of the polymer coatings were made after each test which showed uniform and continuous layer of polymer were deposited on the wires with generally poor adhesion.

Figure 47 shows the coating thickness produced on the copper wire drawn with WVG 23 polymer at 130°C and 180°C. At slower drawing speeds, coating thickness increased as the drawing speed was increased. At drawing speeds in excess of about 1.5 m/s approximately constant coating thickness was measured. Shark-skin was observed on the coatings up to speeds where maximum thickness was measured. The thickness of polymer coatings at lower temperature was found to be greater than those at higher temperature. A typical shark-skin formed on the coating of the copper wire is shown in plate 11.

Figure 48 gives the coating thickness obtained with WVG 23 polymer at 130°C for different wire materials. The general trends of the results are similar to those in figure 47 except for 18/8 stainless steel wire in which a discontinuity was observed in the coating thickness at drawing speed of about 0.8 m/s. Shark-skin was produced on the coatings of all the wires upto speeds where maximum thickness were measured. Note that at drawing speeds in excess of 1.5 m/s the thickness of the polymer on the stainless steel wire reduced below the gap which existed between the wire and the unit (0.05mm). Also the coating thickness measured on the mild steel wire reduced to the thickness of the gap in the unit.

Figure 49 shows the measured coating thickness when KM 61 polymer was used at 200°C for different wire materials. The characteristics of the results were altered compared to those in figure 48. For copper wire, the flow of polymer and hence coating of wire commenced at about 0.4 m/s. Shark-skin was observed on the polymer immediately after the flow occured upto drawing speed of about 1.0 m/s. Coating thickness on the copper wire reduced gradually as drawing speed was increased. Plate 12 shows a typical shark-skin on the coating of copper wire drawn with KM 61 polymer.

The measured coating thickness on the stainless steel wire was found to have similar trend to those of copper wire. Flow of polymer commenced at about 0.2 m/s and shark-skin on the coating was observed upto drawing speed of 1.9 m/s. Plate 16 shows the shark-skin formed on the coating of this wire.

Results of coating thickness on the mild steel wire showed a rather different trend than the other two materials. Upto the drawing speed of 0.3 m/s smooth coating was produced which decreased as the drawing speed was increased. From drawing speed of 0.3 m/s to 1.6 m/s, traces of shark-skin was observed on the coatings and in this region, appoximately constant thickness was measured. At drawing speeds in excess of 1.6 m/s, again smooth coatings were deposited on the wire and the thickness decreased as the drawing speed was increased further. Plate 14 shows shark-skin on the mild steel wire.

Figure 50 shows the effect of two different gap ratios on the thickness of polymer coating with KM 61 polymer at

200° C. Mild steel wire was used for these experiments. The results of coating thickness for the gap ratio of 4.0 are the same as those described for mild steel wire in figure 49. The coating thickness measured for the gap ratio of 2.0 reduced gradually as the drawing speed was increased. Note that thicker polymer coatings were obtained at higher drawing speeds for the smaller gap ratio.

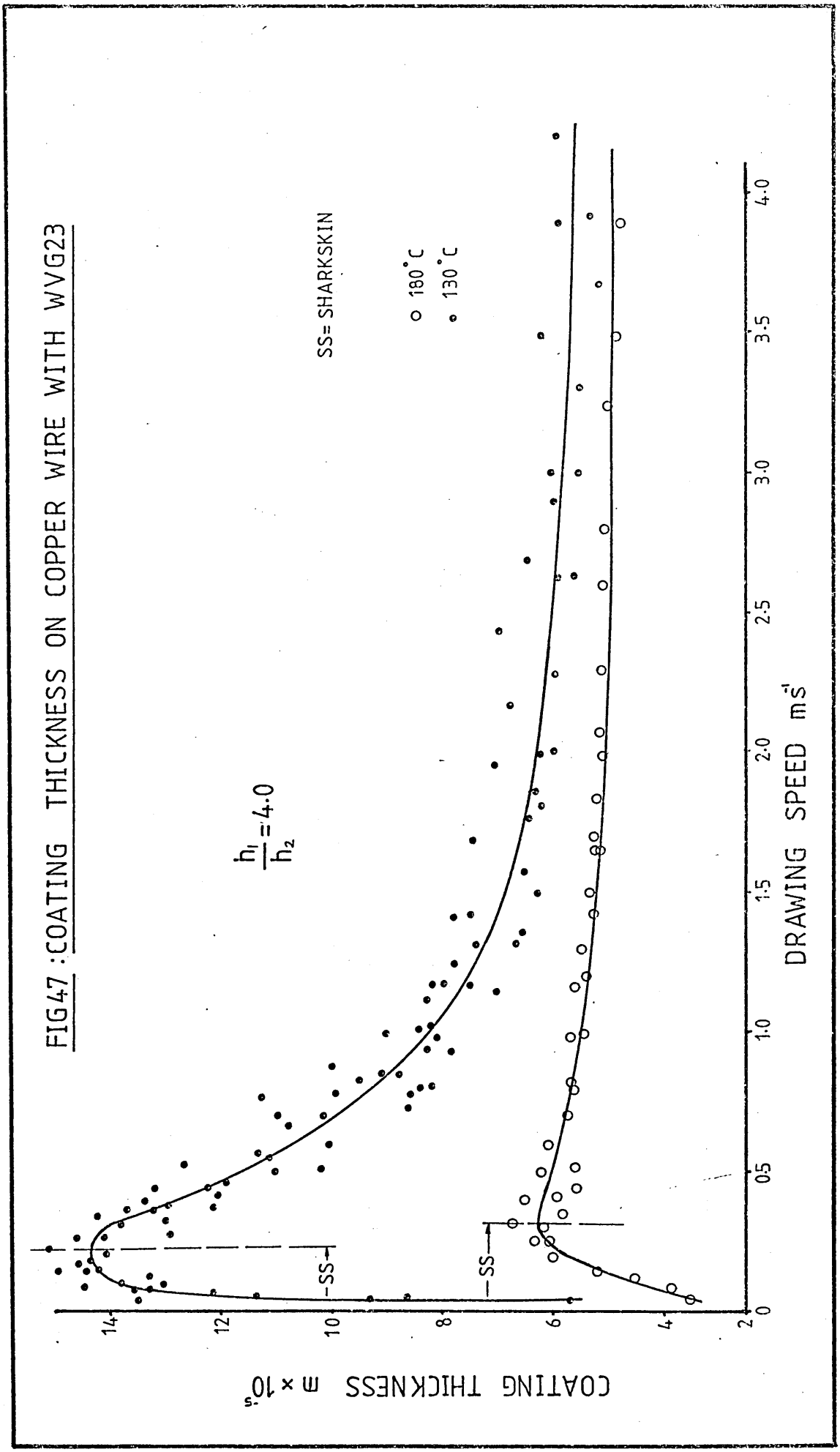
FIG47 :COATING THICKNESS ON COPPER WIRE WITH WVG23
SS= SHARKSKIN
o 180°C
• 130°C
$\frac{h_1}{h_2}$=4.0
SS
SS
COATING THICKNESS m x 10⁵
DRAWING SPEED ms⁻¹
14
12
10
8
6
4
2
0
0.5
1.0
1.5
2.0
2.5
3.0
3.5
4.0

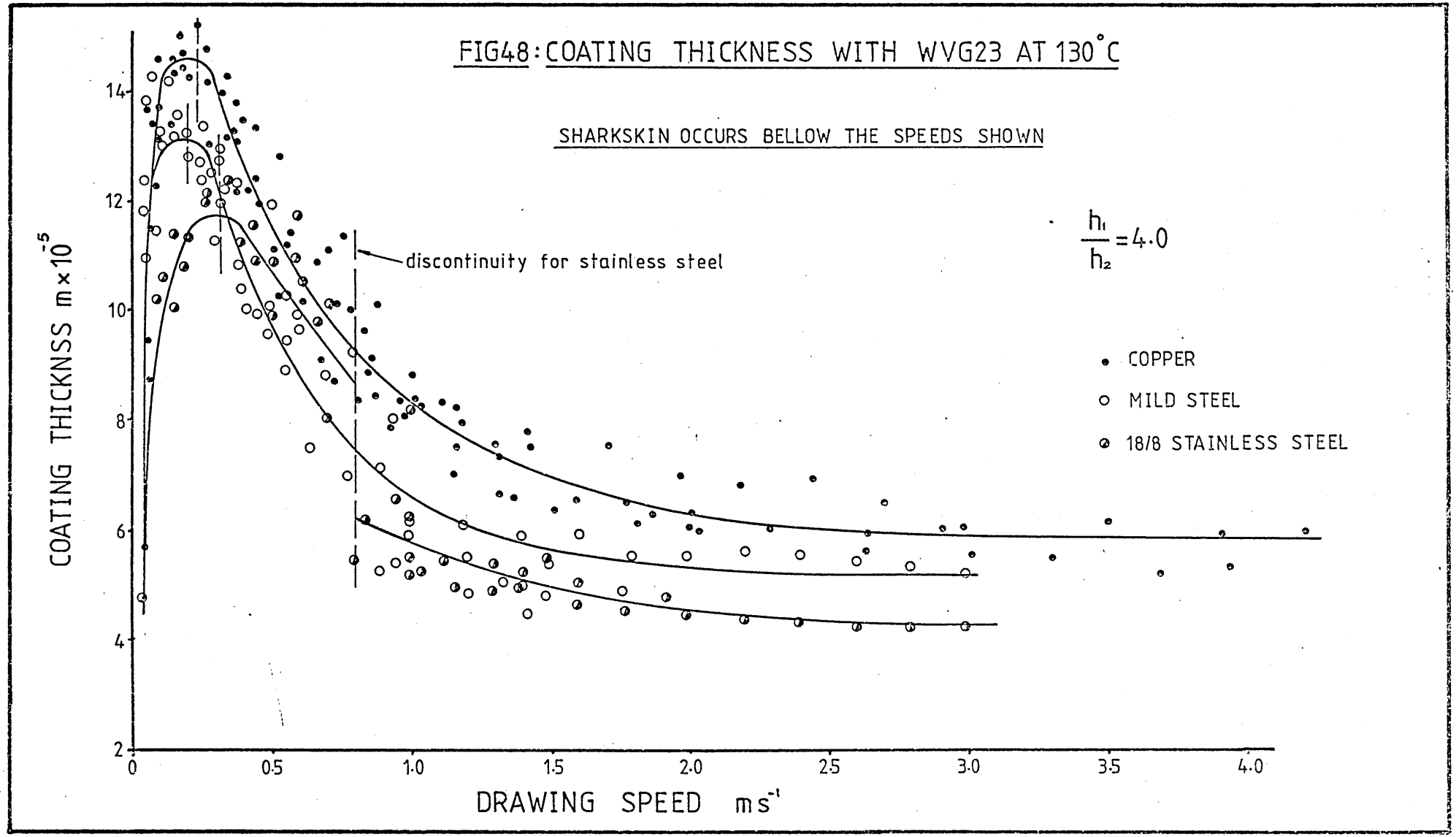
FIG48: COATING THICKNESS WITH WVG23 AT 130°C
SHARKSKIN OCCURS BELLOW THE SPEEDS SHOWN
discontinuity for stainless steel
h1/h2 = 4.0
COPPER
MILD STEEL
18/8 STAINLESS STEEL
COATING THICKNSS m x 10^-5
DRAWING SPEED m s^-1
2
4
6
8
10
12
14
0
0.5
1.0
1.5
2.0
2.5
3.0
3.5
4.0

FIG49: COATING THICKNESS WITH KM61 AT 200°C

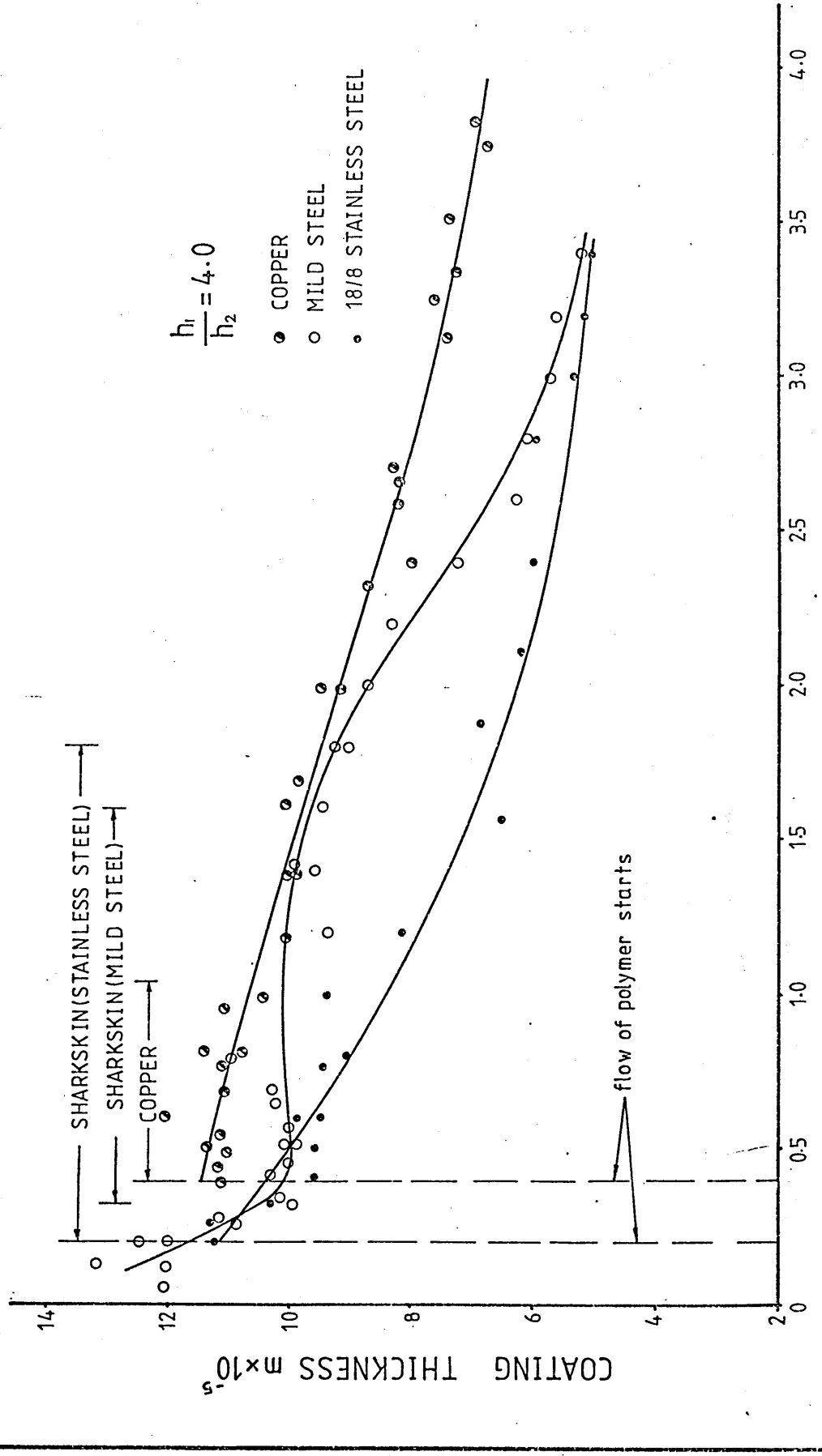

FIG50: COATING THICKNESS ON MILD STEEL WIRE WITH KM61 AT 200°C

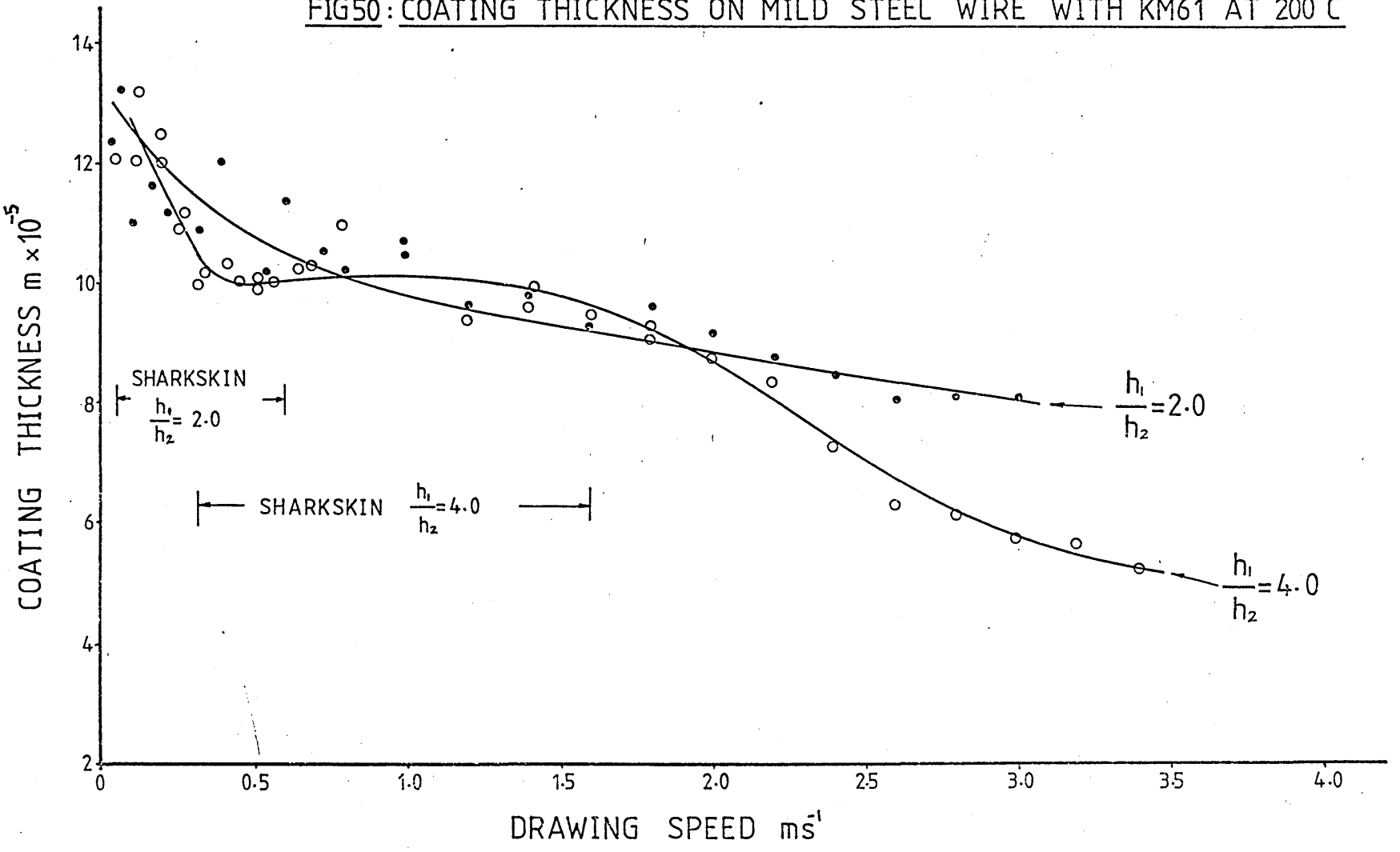

PLATE 11 : SHARKSKIN ON COPPER WIRE COATING WITH WVG23 (130°C - 0·15 m/s)

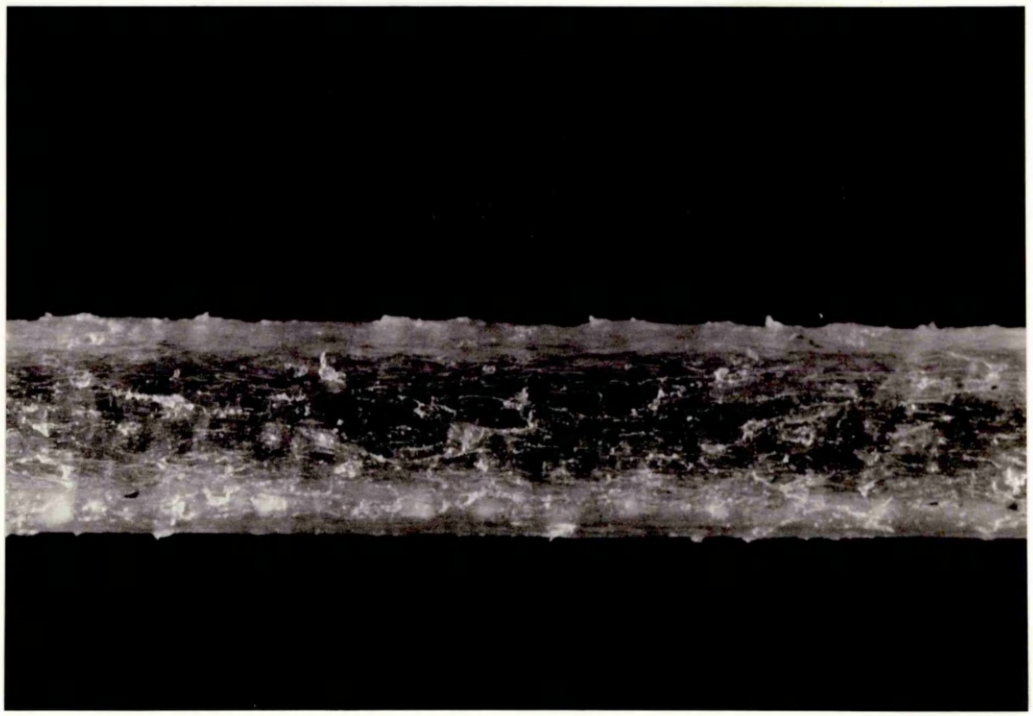

PLATE 12 : SHARKSKIN ON COPPER WIRE COATING WITH KM61 (200°C - 0·6 m/s)

PLATE 13 : SHARKSKIN ON MILD STEEL WIRE COATING WITH WVG23 (130°C - 0·12 m/s)

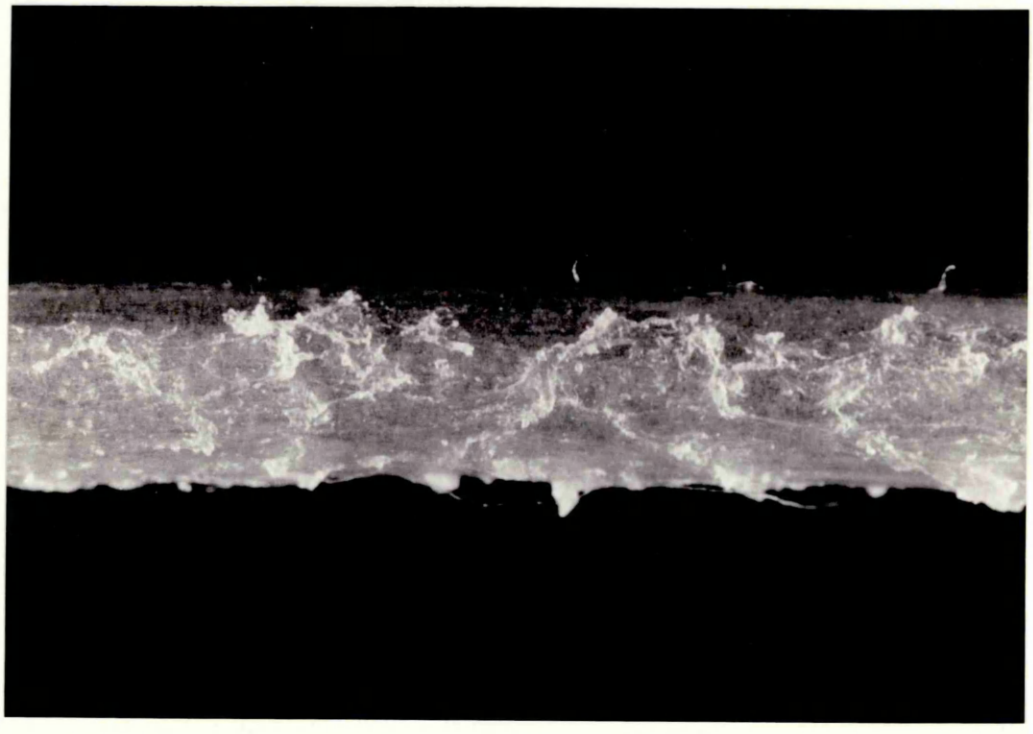

PLATE 14 : SHARKSKIN ON MILD STEEL WIRE COATING WITH KM61 (200°C - 1·2 m/s)

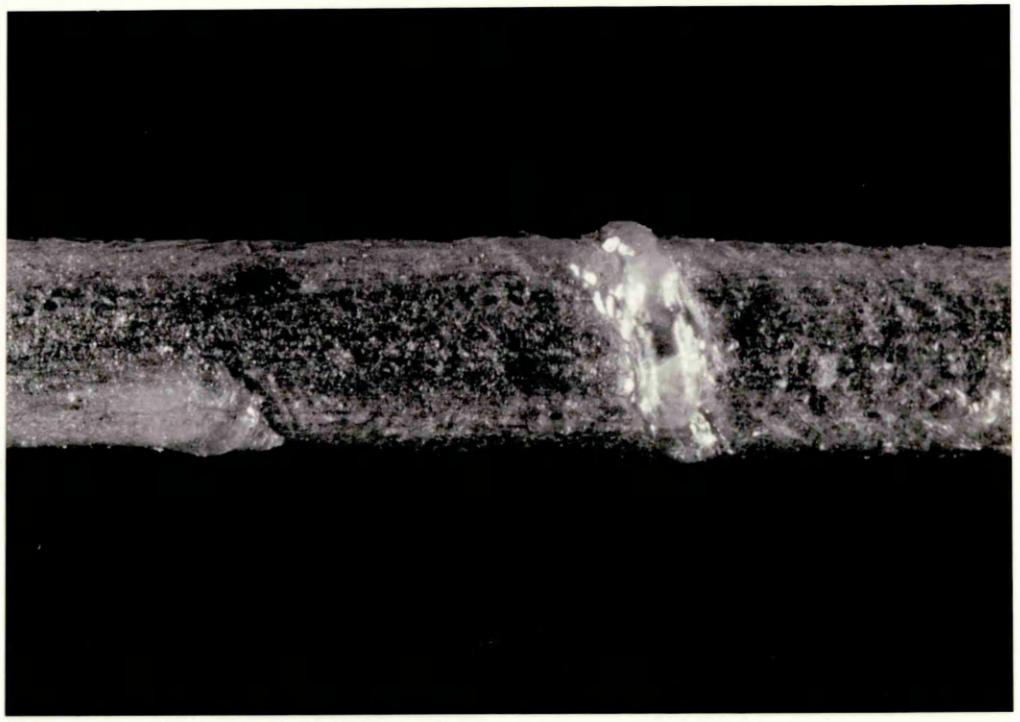

PLATE 15 : SHARKSKIN ON 18/8 STAINLESS STEEL WIRE COATING WITH WVG23 (130°C - 0·2 m/s)

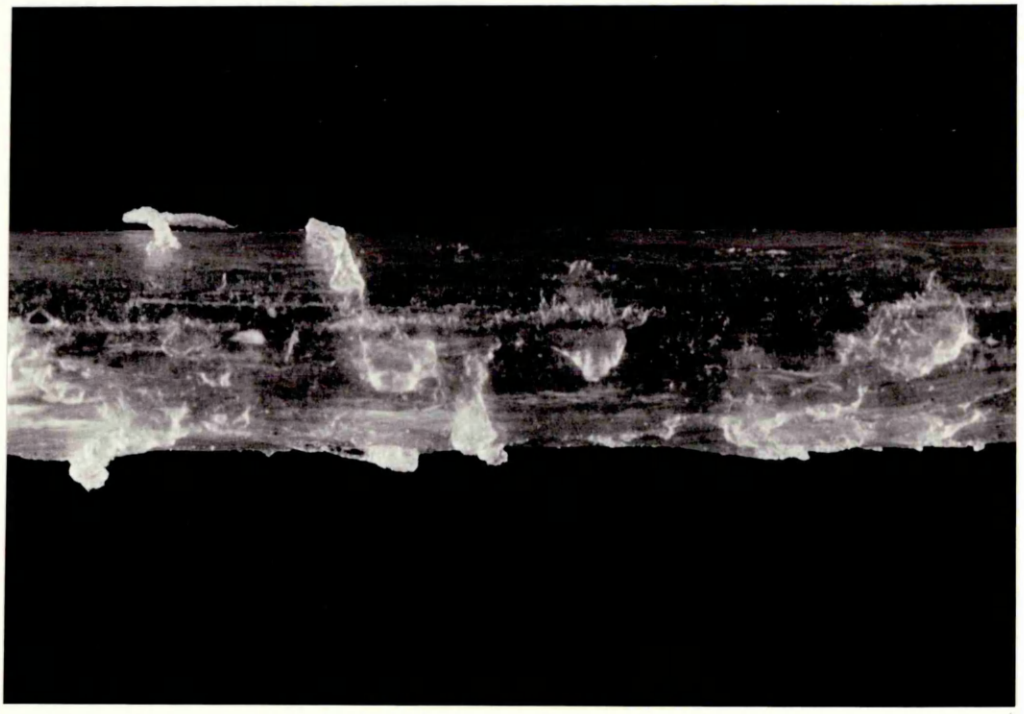

PLATE 16 : SHARKSKIN ON 18/8 STAINLESS STEEL WIRE COATING WITH KM61 (200°C - 0·8 m/s)

4.3.4- Results Of Percentage Reduction In Area Versus Drawing Speed.

Figure 51 shows the percentage reduction in area for the copper wire using WVG 23 polymer at 130° C and 180° C. At slower drawing speeds, the deformation of wire increased as the speed was increased for both polymer temperatures. A maximum reduction in area was noted for the melt temperature of 130° C at about 0.2 m/s and similarly at 0.3 m/s, a maximum point was observed for the temperature of 180° C. As the drawing speed was increased further, the reduction in area for lower melt temperature reduced to about 7% at 4.0 m/s. Higher polymer temperature showed approximately constant deformation in the wire at speeds in excess of 1.0 m/s.

Figure 52 shows the percentage reduction in area measured for different wire materials using WVG 23 polymer at 130° C. At lower drawing speeds, the general trends were found to be the same as those in figure 51. There was a marked difference between the results of copper wire and the other two materials. Deformation of mild steel wire ceased at about 1.0 m/s and at slightly higher drawing speeds (1.4 m/s) the stainless steel wire was no longer deformed as the speed was increased. Also the results of reduction in area for stainless steel wire showed a discontinuity at about 0.8 m/s,a pattern which has been observed for the results of coating thickness and pressure (position 2) as shown in figures 48 and 30 respectively.

Figure 53 gives the percentage reduction in area

measured for different wire materials drawn with KM 61 polymer at 200° C. This polymer produced higher deformation in wires at higher speeds compared to those obtained using WVG 23 polymer (see figure 52). Flow of polymer commenced at about 0.4 m/s for copper wire and below this speed, wire was reduced randomly. After commencement of the flow of the polymer melt, an increase in the percentage reduction in area was observed which eventually reached a maximum at about 0.6 m/s (22%). Further increase in the drawing speed caused the deformation of the wire to reduce.

Flow of KM 61 polymer for the stainless steel wire began at about 0.2 m/s and again the wire diameter was found to reduce randomly below this speed. The percentage reduction in area reduced as the drawing speed was increased further and the deformation of wire ceased at about 3.4 m/s which was about 60% improvement in the limiting drawing speed, compared to the limiting speed shown in figure 52.

The trend of the results of the percentage reduction in area measured for the mild steel wire was similar to those of corresponding coat thickness (see figure 49). Deformation of the wire ceased at drawing speed of about 3.0 m/s which when compared with figure 52, showed about 66% increase in the limiting drawing speed.

Figure 54 shows the effect of the gap ratio on the performance of the stepped bore reduction unit when mild steel wire was drawn using KM 61 polymer at 200° C. The results obtained with the higher gap ratio were the same as those described in figure 53. The amount of reduction in the mild steel wire was found to be the same in the case of both gap ratios at lower drawing speeds. At higher

drawing speeds, the percentage reduction in area obtained for the smaller gap ratio reduced as the speed was increased and eventually became zero at about 2.2 m/s.

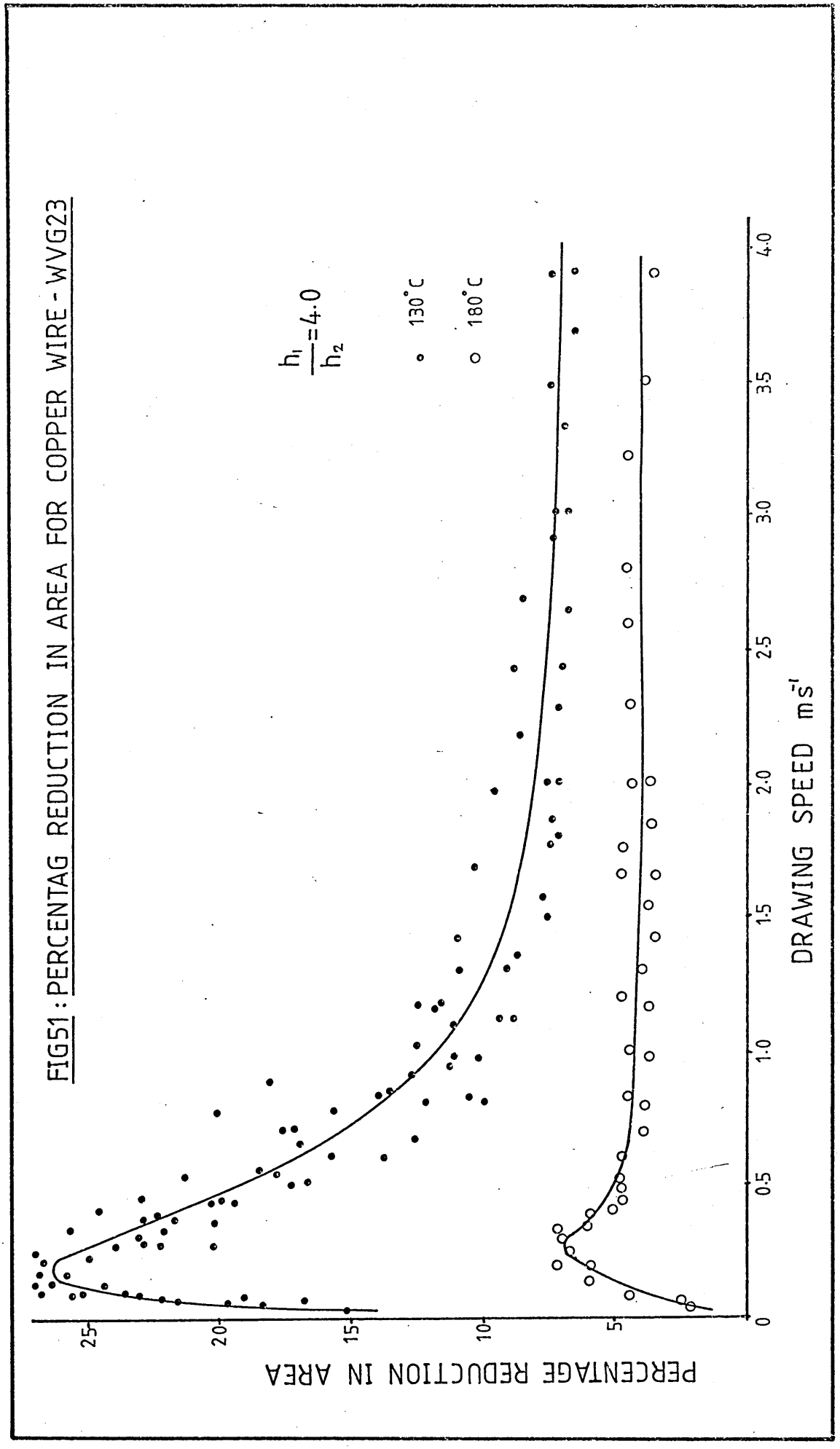
FIG51 : PERCENTAG REDUCTION IN AREA FOR COPPER WIRE - WVG23
$\frac{h_1}{h_2}$=4.0
130°C
180°C
PERCENTAGE REDUCTION IN AREA
DRAWING SPEED ms⁻¹
0
0.5
1.0
1.5
2.0
2.5
3.0
3.5
4.0
5
10
15
20
25

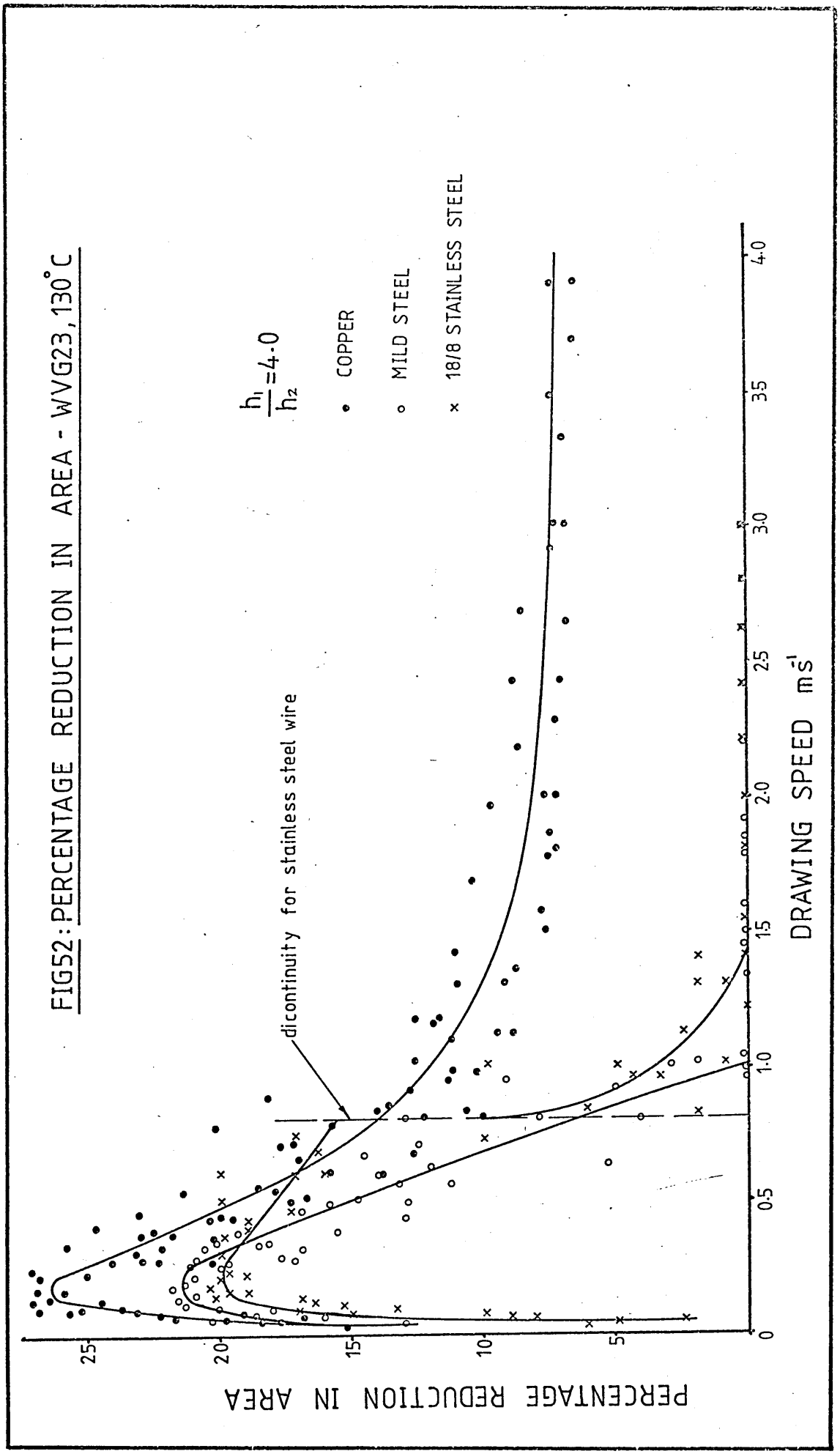
FIG52: PERCENTAGE REDUCTION IN AREA - WVG23, 130°C
$\frac{h_1}{h_2}$=4.0
COPPER
MILD STEEL
18/8 STAINLESS STEEL
dicontinuity for stainless steel wire
PERCENTAGE REDUCTION IN AREA
DRAWING SPEED ms⁻¹
0
5
10
15
20
25
0.5
1.0
1.5
2.0
2.5
3.0
3.5
4.0

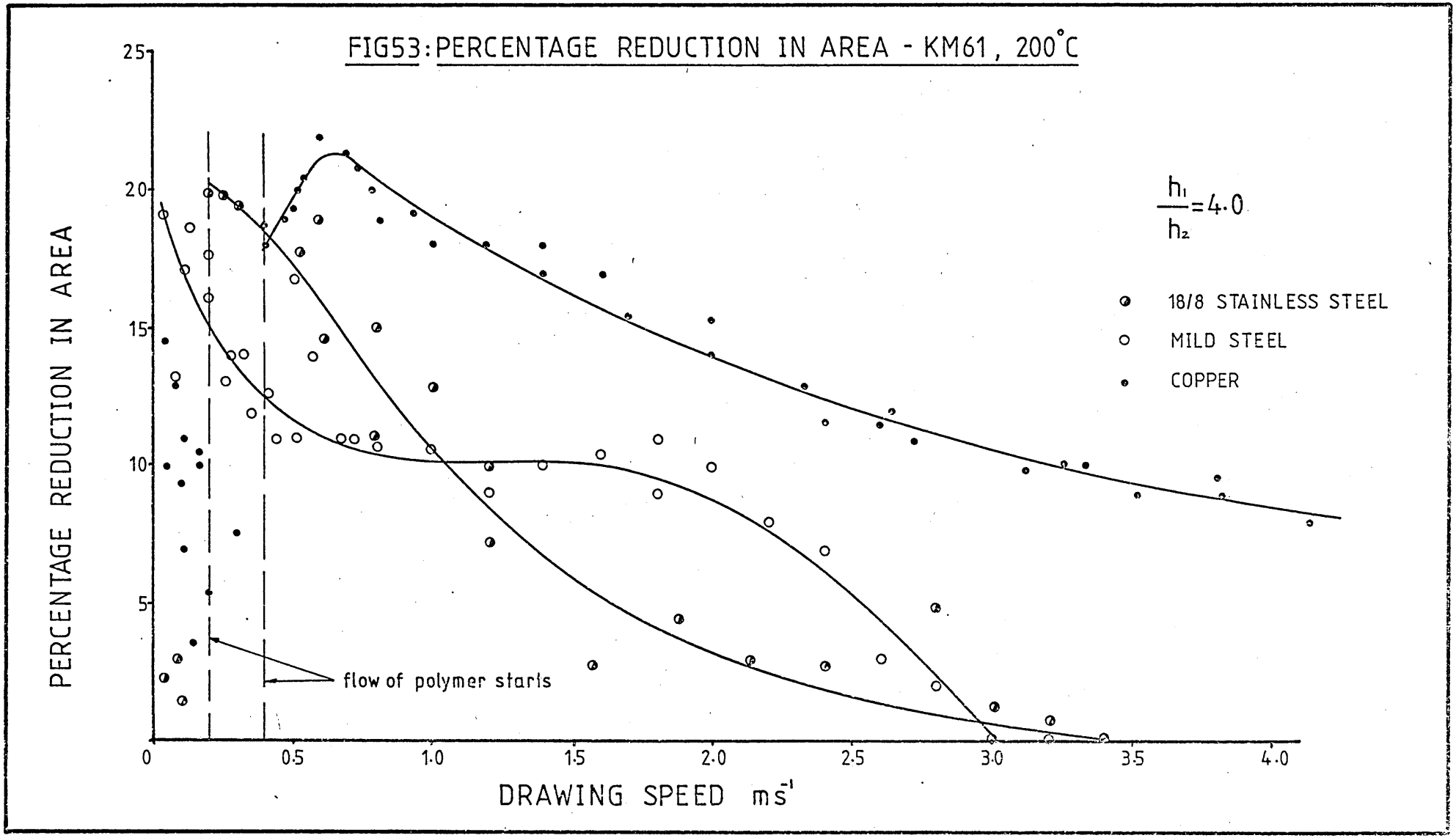
FIG53: PERCENTAGE REDUCTION IN AREA - KM61, 200°C
PERCENTAGE REDUCTION IN AREA
25
20
15
10
5
0
0·5
1·0
1·5
2·0
2·5
3·0
3·5
4·0
DRAWING SPEED ms⁻¹
h1/h2 = 4·0
18/8 STAINLESS STEEL
MILD STEEL
COPPER
flow of polymer starts

FIG54: PERCENTAGE REDUCTION IN AREA FOR MILD STEEL WIRE - KM61, 200°C

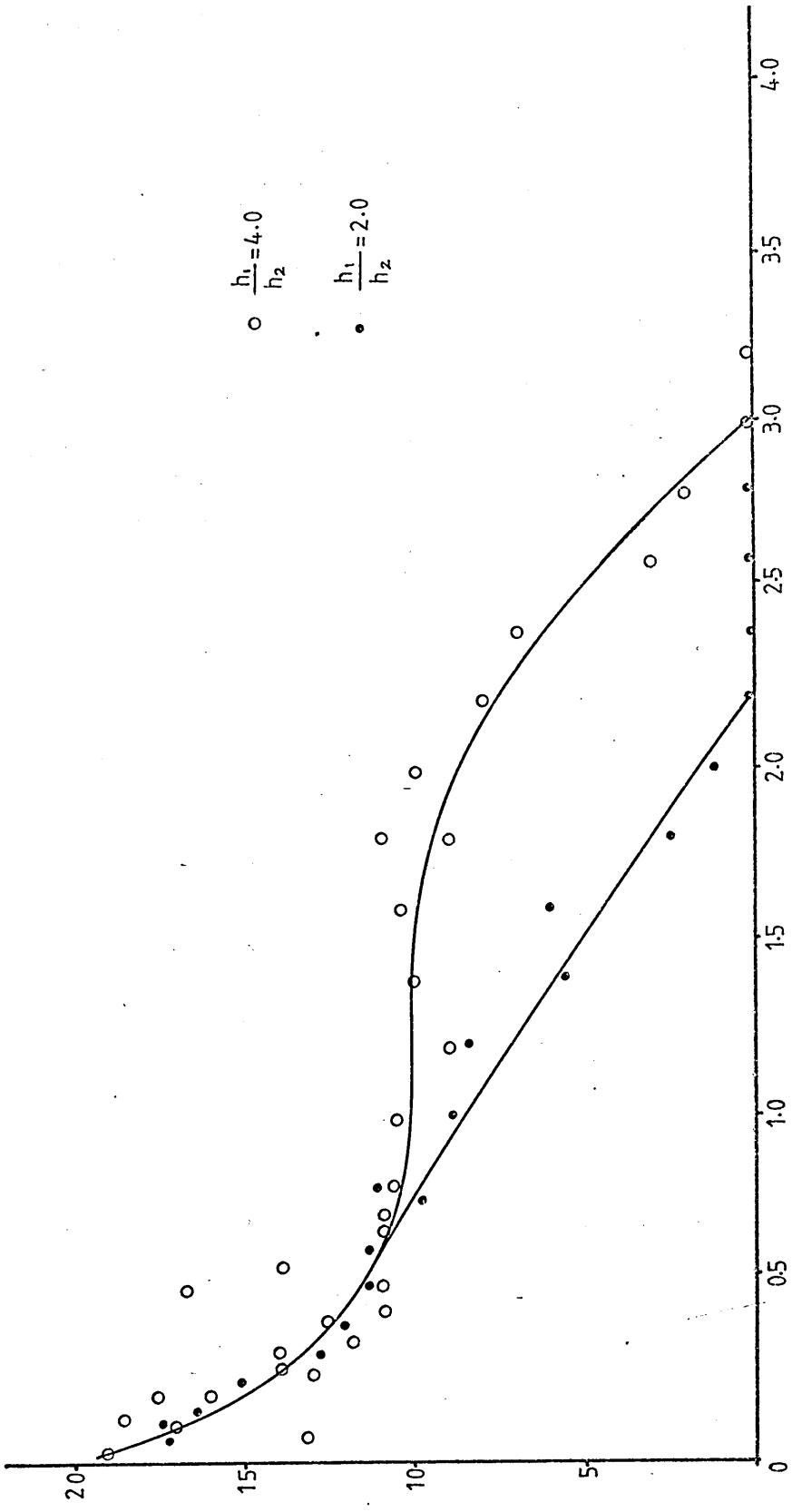

4.4- Determination Of The Deformation Profiles.

Tests were conducted to examine the deformation profiles of the wires under-going the drawing process. While the wire was being drawn, the process was deliberately shortened by cutting the wire between the unit and the bull block. The wire was then marked at the exit point of the unit and pulled out for investigations.

The diameter of the wire was measured at two millimetre intervals from the exit position using a Societ Genevoise travelling microscope (type MU 2148). This test was repeated for different wire materials and at different speeds, using WVG 23 polymer at temperature of 130° C. Results are shown in figures 55 to 57 which clearly exhibit the shapes of the effective dies formed in the unit.

The measured profiles showed, in some cases, that either the deformation of wire ceased before or terminated after the step**. These differences could have arisen due to motion of polymer and other forces exerted on the wire at the instant when the process was severed.

Figure 55 shows the effective dies measured for copper wire at three different speeds. The position of yield of the wire, at 1.0 m/s and 0.05 m/s, was found to occur at 30 mm in the unit. At 0.2 m/s however, the deformation zone commenced at about 35 mm from the entry of the unit.

Figure 56 shows three deformation profiles for mild steel wire. The position of yield for this wire was measured at about 35 mm in the unit for drawing speeds of 0.3 m/s and 0.5 m/s. The length of the deformation zone was slightly increased when the drawing speed was reduced to 0.05 m/s.

**-The deformation was expected to cease at the step.

Figure 57 shows the profiles of the effective dies measured for 18/8 stainless steel wire. The yielding positions in the unit were found to take place at 38 mm, 25mm and 35 mm at drawing speeds of 0.1 m/s, 0.2 m/s and 0.6 m/s respectively.

FIG55 : DEFORMATION PROFILES FOR COPPER WIRE WITH WVG23 , 130°C

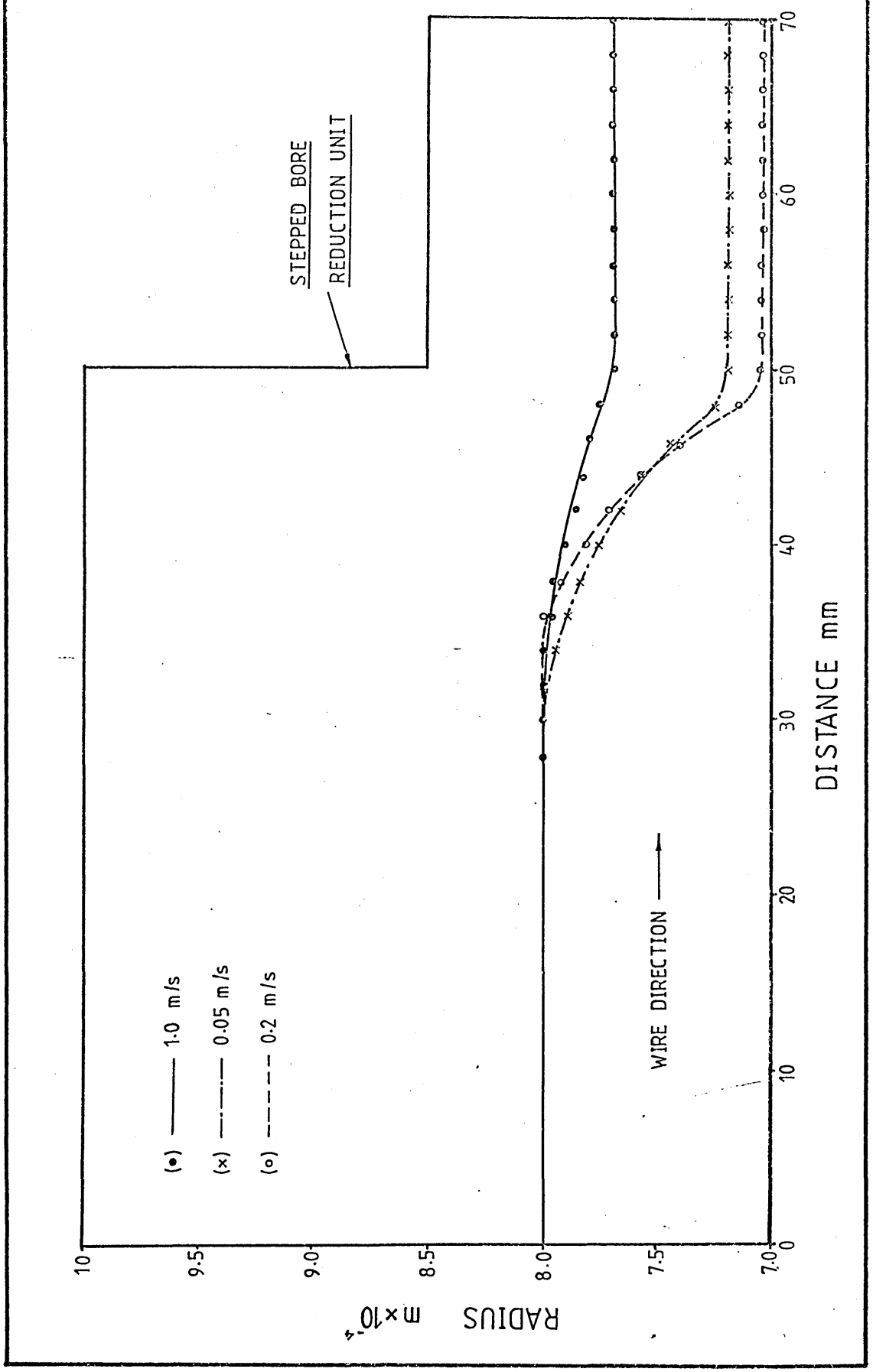

FIG56: DEFORMATION PRFILES FOR MILD STEE WIRE WITH WVG23, 130°C

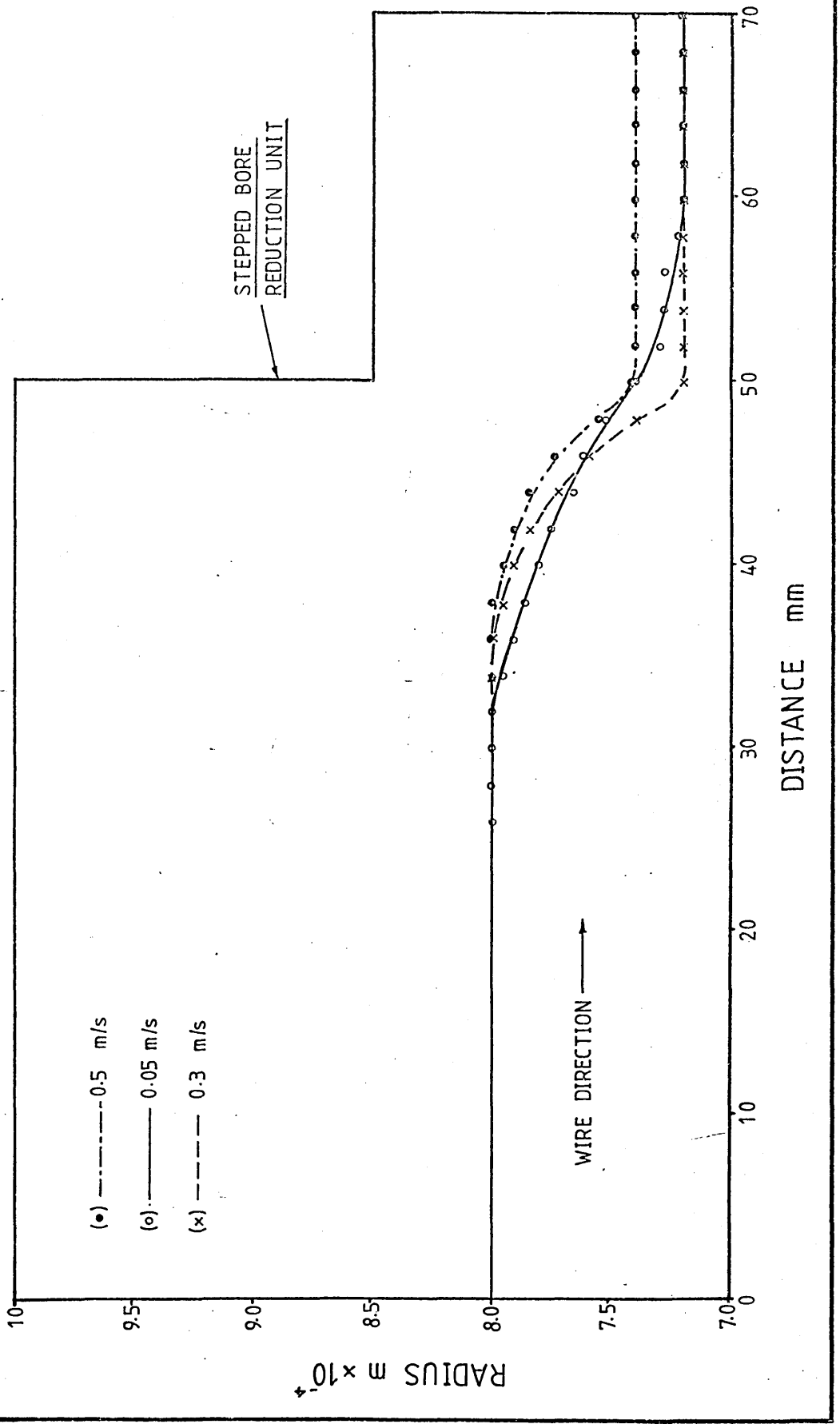

FIG57: DEFORMATION PROFILES FOR 18/8 STAINLESS STEEL WIRE WITH WVG23, 130°C

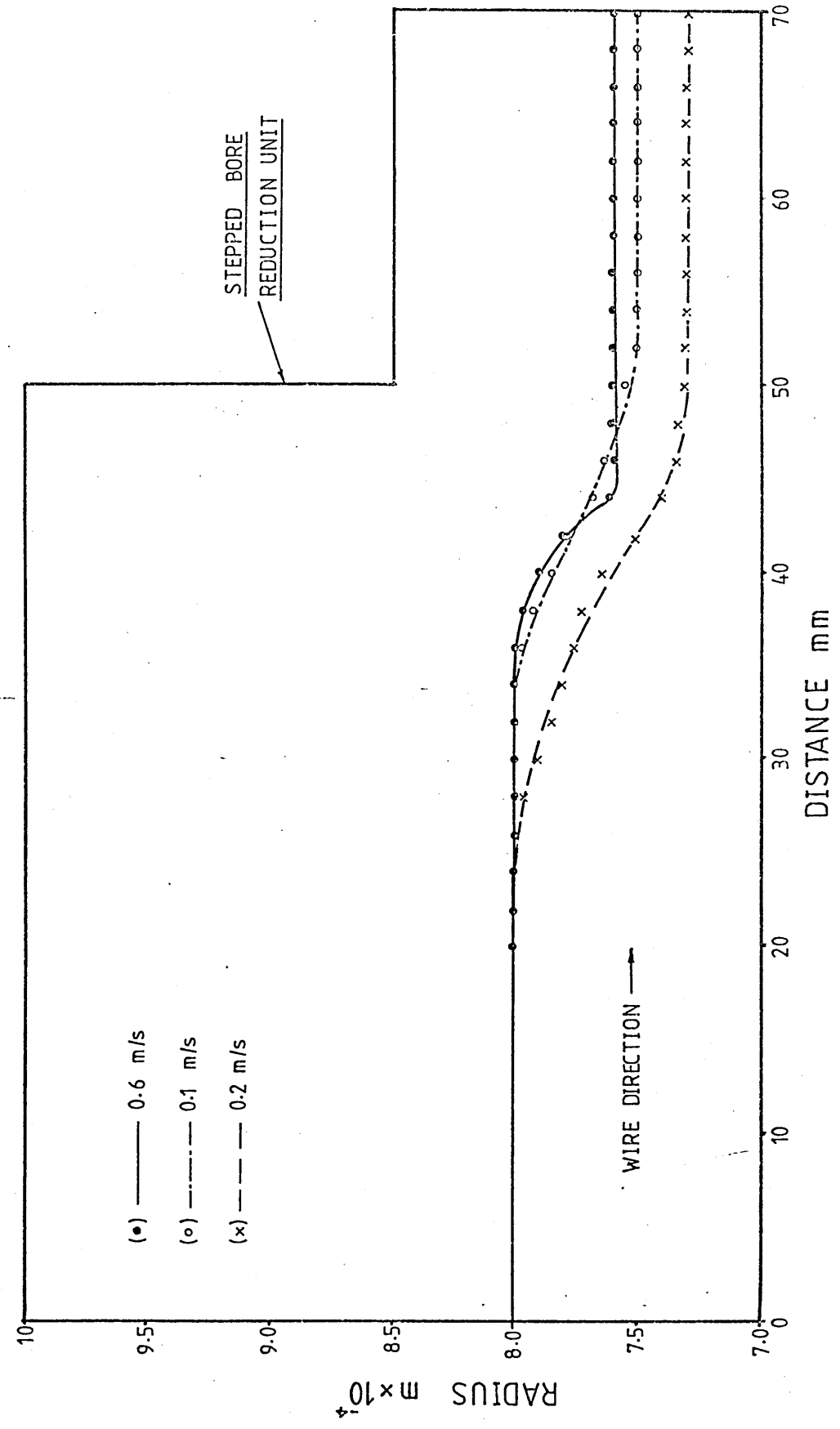

4.5- Evaluation Of The Product Quality.

Deformation of the wire in the conventional drawing process is controlled by the reduction die, hence the amount of deformation is constant at any drawing speed. Also due to the presence of a boundary lubricant, wires with shiny surfaces are produced owing to metal to metal contacts inside the die. In the die-less drawing process however, the formation of the effective die is dependant upon speed, therefore the amount of deformation in the wire varies with the drawing speed. The diameter of the finished product is also dependant on the accuracy of the effective die formed in the unit. Therefore it proved necessary to carry out qualitative assessments of the wires reduced by both systems to evaluate the acceptability of the products from the die-less system. Hence the following tests were conducted;

4.5.1- Roundness Tests.

Roundness of the received wires (reduced by the conventional methods) were measured and compared to those reduced using the stepped bore reduction unit. These tests were carried out employing a Tylor Hobson roundness tester (type Talyrond with reference computer). Results are classified according to the wire materials:

1- Copper wire

Figure 58 shows roundness test of the received copper wire. An average error of about 0.0015 mm may be noticed

from the reference circle and the trace of error produced a rather smooth curve. When this wire was reduced by the stepped bore reduction unit, roundness tests produced slightly different traces which are shown in figures 59 to 61. A typical error of about 0.0015 mm was found to be common in all tests.

2- Mild steel wire

Roundness tests carried out for mild steel wires produced similar traces of error as shown in figures 62 to 65. An average error of about 0.003 mm was measured for the received wire (see figure 62). This error was reduced to about 0.002 mm when mild steel wire was reduced using the stepped pressure chamber.

3- 18/8 Stainless steel wire

The results of roundness tests for this wire was found to be similar to those of mild steel wire. The supplied wire showed an average error of about 0.002 mm. This magnitude of error remained approximately constant for the wires drawn at 0.5 m/s and 1.0 m/s with WVG 23 and KM 61 polymers respectively. The wire reduced at 1.0 m/s with WVG 23 polymer showed a comparatively larger error of about 0.003 mm. these results are shown in figures 66 to 69.

4.5.2- Examination Of The Uniformity Of The Wire Diameter.

Diameter of the drawn wires, reduced by the conventional

method and the die-less system, were examined over long lengths at one meter intervals and the percentage variations from the mean diameter were calculated. Figures 70(a) and 70(b) show these variations for copper wire. The received wire exhibited frequent departure from the mean diameter and a typical maximum of 0.4% error was noted over 20 m length. The frequency of variations of diameter was reduced for wires drawn by the stepped bore reduction unit and a typical maximum of about 0.6% was measured over the same sample length.

Figure 71 shows these variations for mild steel wire. The measurements of the wire diameter from the received coil showed a possible error of about 0.7% from the mean diameter. When this wire was drawn using the stepped bore reduction unit, variations of the diameter remained as frequent as those for received wire, but the magnitudes of the errors were increased, a typical of which was about 2%. Samples used for these tests were of 15 m lengths.

4.5.3- Micro-Examination Of The Surface Finish Of The Wires.

A scanning electron microscope was employed which allowed detailed study of the magnified surfaces of the wires. A magnification factor of X450 was used which provided a general view of the wire surfaces. Results are catagorised according to the wire materials and are presented as follows;

1- Copper wire

Plate 17 shows the surface of the wire reduced by the

conventional drawing methods. Grooves were observed on an even surface which appeared to be deep into the material. When this wire was drawn at 1.0 m/s with WVG 23 polymer at temperature of 130° C, an uneven (matt) surface was produced as shown in plate 18. Plate 19 is taken from surface of the copper wire drawn at 0.5 m/s using WVG 23 polymer at 130° C. The amount of deformation at this speed was more than that of 1.0 m/s, therefore the surface was found to be more uneven compared to plate 18. The surface finish of the copper wire drawn at 0.5m/s with KM 61 polymer at 200° C is shown in plate 20. The surface characteristics were found to be similar to that of plate 19.

2- Mild steel wire.

Mild steel wires were received with a protective layer of oil on the surface which had to be removed prior to the test runs for the adhesion between the wire and the polymer melt to take place. This wire prepration has been described in chapter 3.

Plate 21 shows the surface of the mild steel wire when the layer of oil was removed (etched). Discontinuous grooves of different depth and width were found to make the matrix of the surface. The result of deformation at drawing speed of 1.0 m/s was that a different wire surface was produced. On a porous surface, elongated and well defined grooves were noticed which are clearly shown in plate 22. When this wire was drawn at 0.5 m/s with KM 61 polymer, more wavy and uneven surface was formad with continuous and smoother grooves as shown in plate 23. The surface of the

mild steel wire was completely altered when it was drawn at 0.5 m/s with WVG 23 polymer at temperature of 130° C. This is shown in plate 24 which exhibits a uniform surface, accommodating longitudinal grooves of different sizes.

3- 18/8 Stainless steel wire.

The magnified surface of the supplied wire is shown in plate 25. Short and narrow grooves next to each other were found to make the matrix of the surface. The character of surface was slightly altered when the stainless steel wire wes drawn at 0.5 m/s with WVG 23 polymer at 130° C as shown in plate 26. Grooves of different sizes were observed on the wire which were lesser in numbers than those in plate 25. Plate 27 shows surface of the stainless steel wire drawn at 1.0 m/s with WVG 23 polymer. On a wavy surface, patches of metal were observed amongst small grooves. The wire surface drawn at 1.0 m/s with KM 61 polymer is shown in plate 28. This surface texture was found to be very similar to that of plate 25.

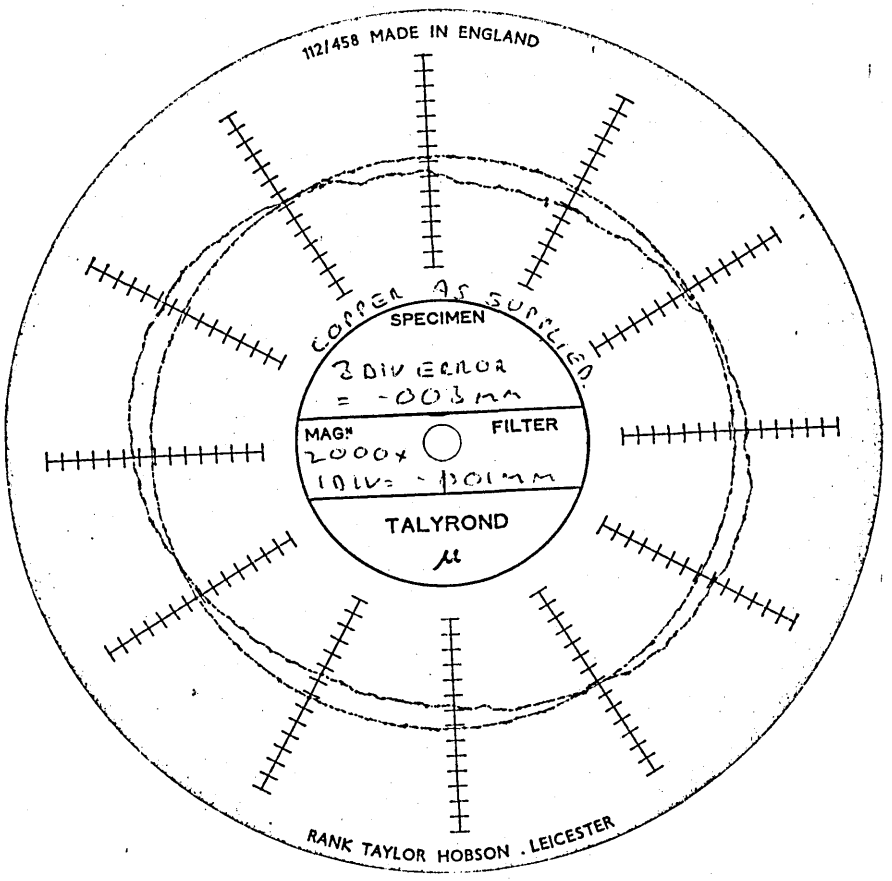

FIG58: ROUNDNESS TEST ON RECEIVED COPPER WIRE

1 DIV=0.001 mm

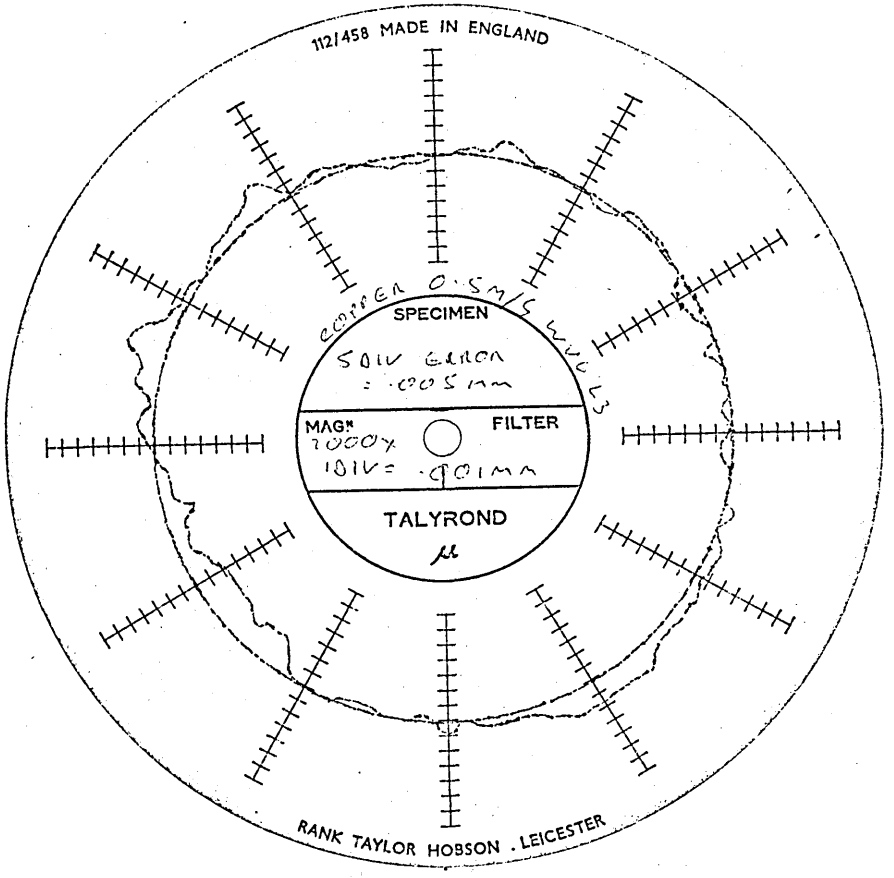

FIG59: ROUNDNESS TEST ON COPPER WIRE DRAWN AT 0.5 m/s WITH WVG23, 130°C - 17% REDUCTION IN AREA

1 DIV = 0.001 mm

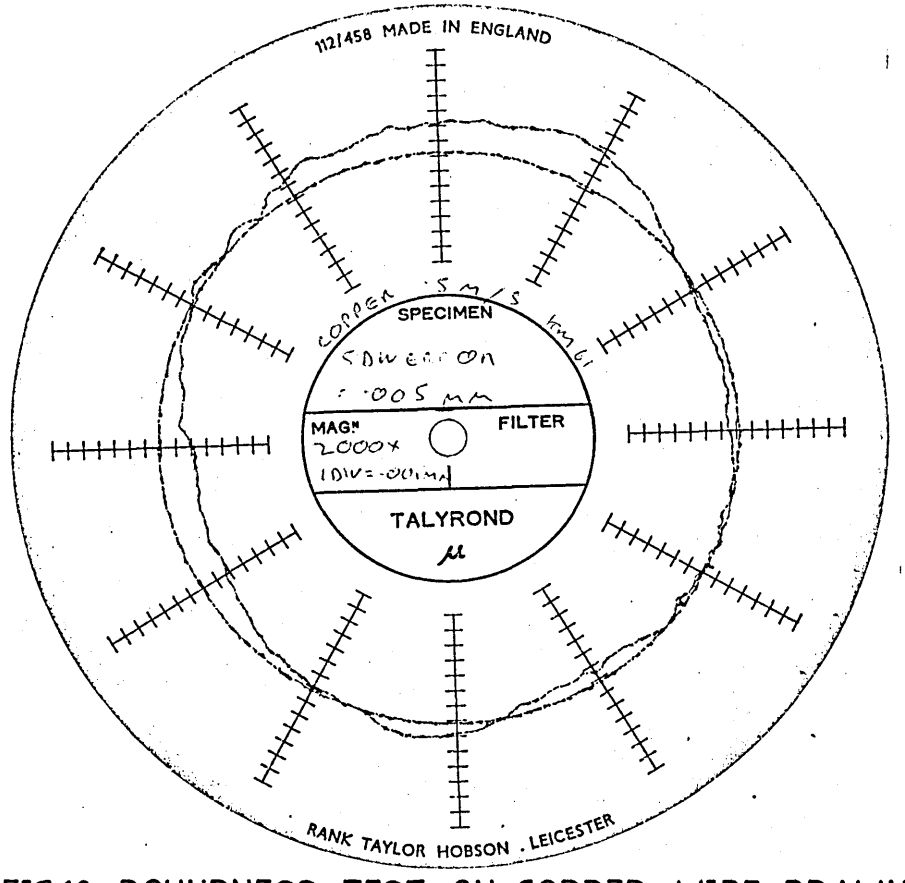

FIG60: ROUNDNESS TEST ON COPPER WIRE DRAWN AT 0·5 m/s WITH KM61, 200°C - 20 % REDUCTION IN AREA

1 DIV = 0·001 mm

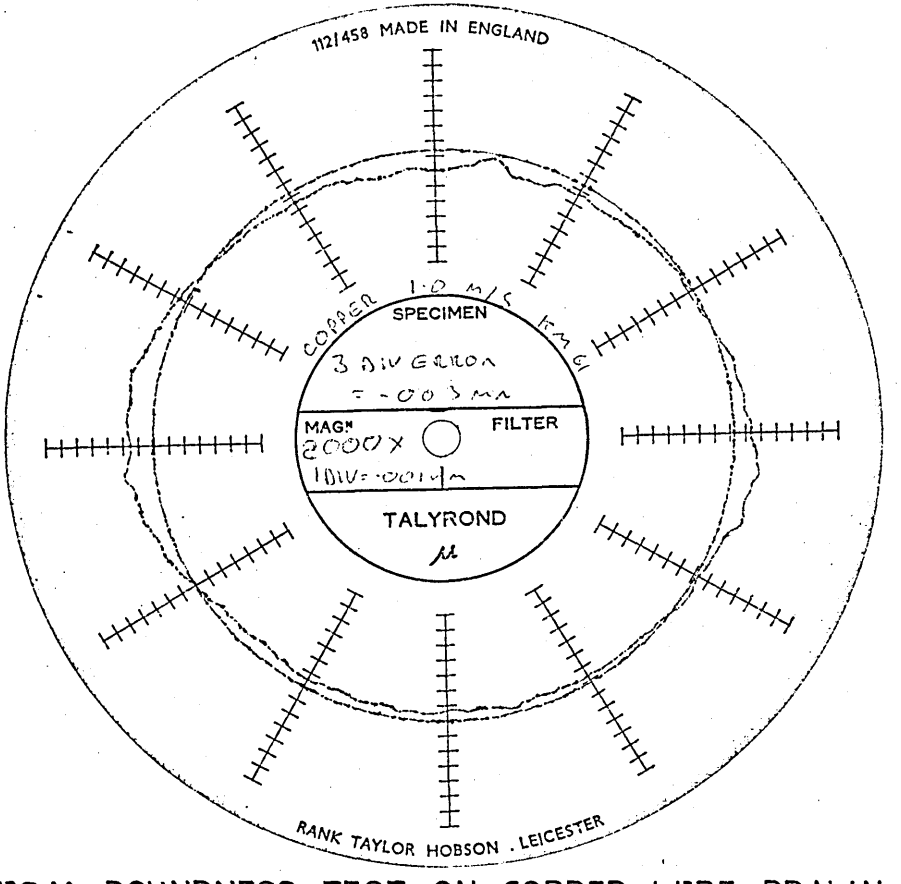

FIG61: ROUNDNESS TEST ON COPPER WIRE DRAWN AT 1·0 m/s WITH KM61, 200°C - 18 % REDUCTION IN AREA

1 DIV= 0·001 mm

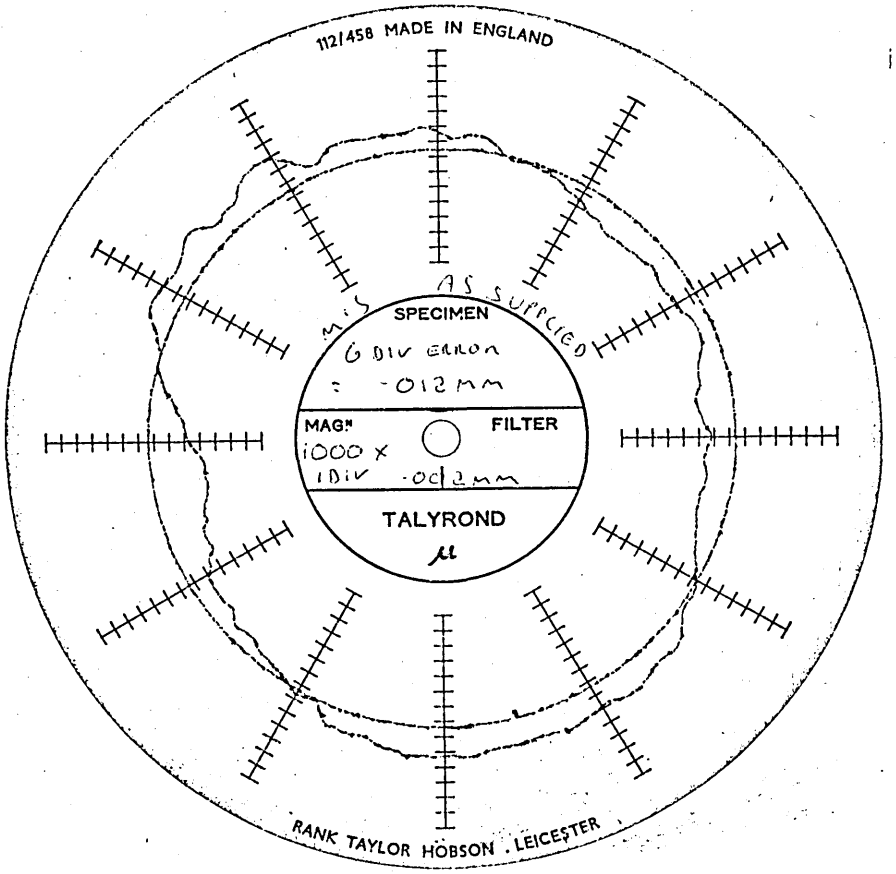

FIG 62: ROUNDNESS TEST ON RECEIVED MILD STEEL WIRE

1 DIV = 0·002 mm

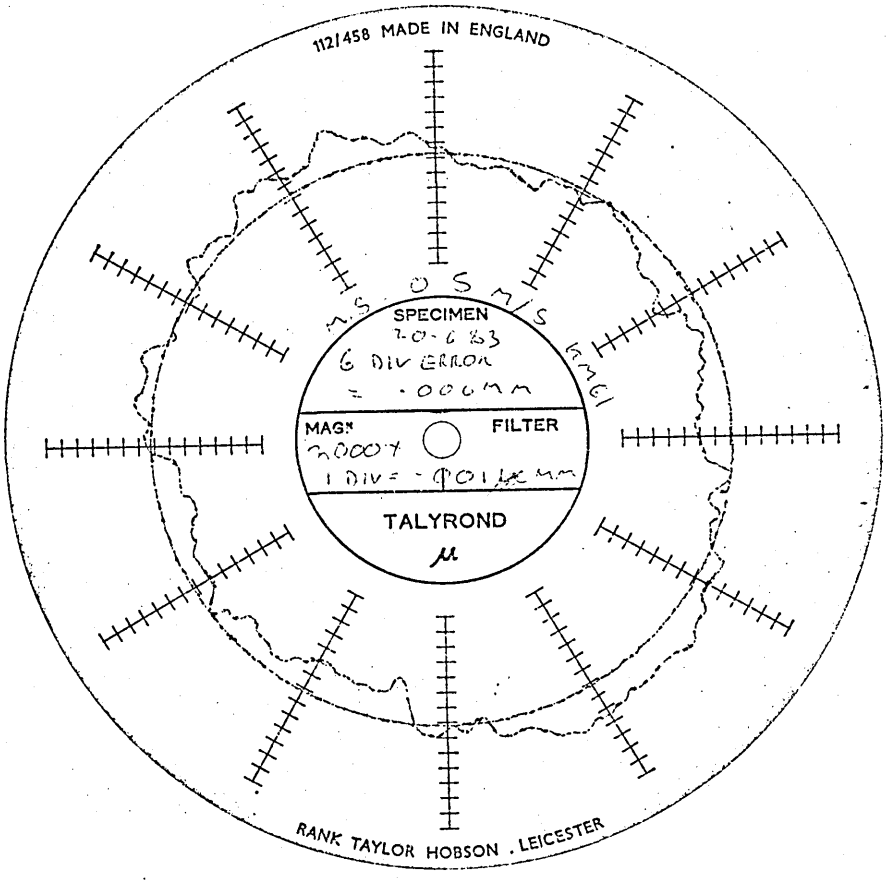

FIG 63: ROUNDNESS TEST ON MILD STEEL WIRE DRAWN AT 0·5 m/s WITH KM61, 200°C 11% REDUCTION IN AREA

1 DIV = 0·001 mm

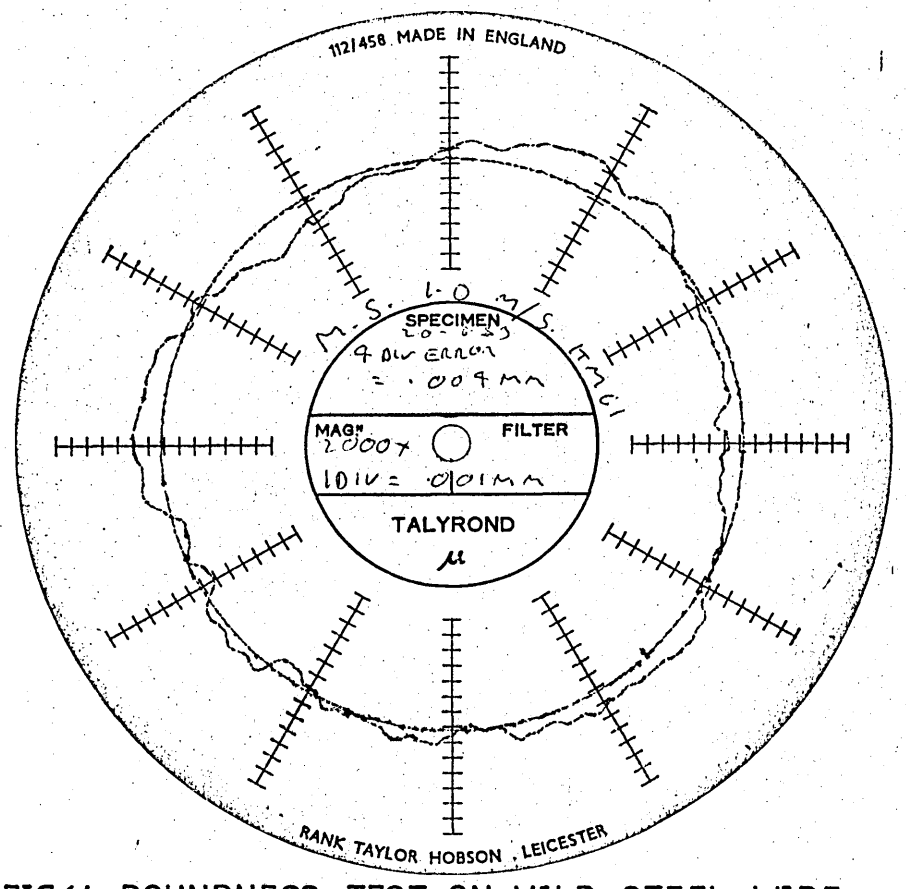

FIG64: ROUNDNESS TEST ON MILD STEEL WIRE DRAWN AT 1·0 m/s WITH KM61, 200°C 11% REDUCTION IN AREA

1 DIV=0·001 mm

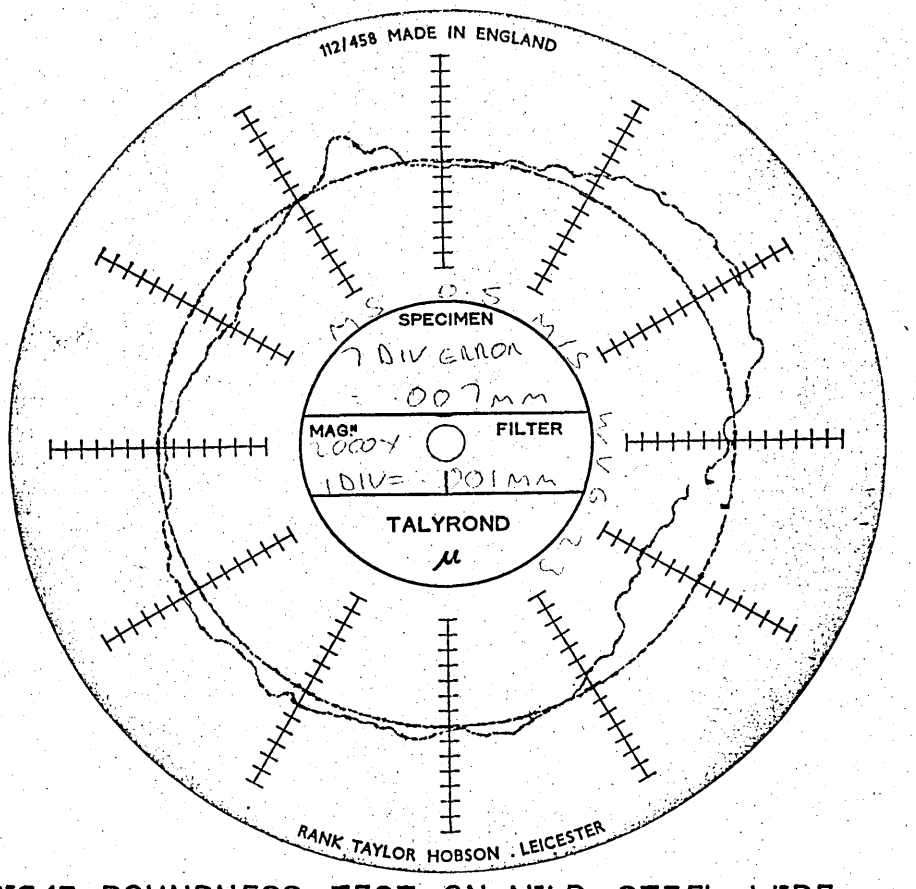

FIG65: ROUNDNESS TEST ON MILD STEEL WIRE DRAWN AT 0·5 m/s WITH WVG23, 130°C - 15% REDUCTION IN AREA

1 DIV=0·001 mm

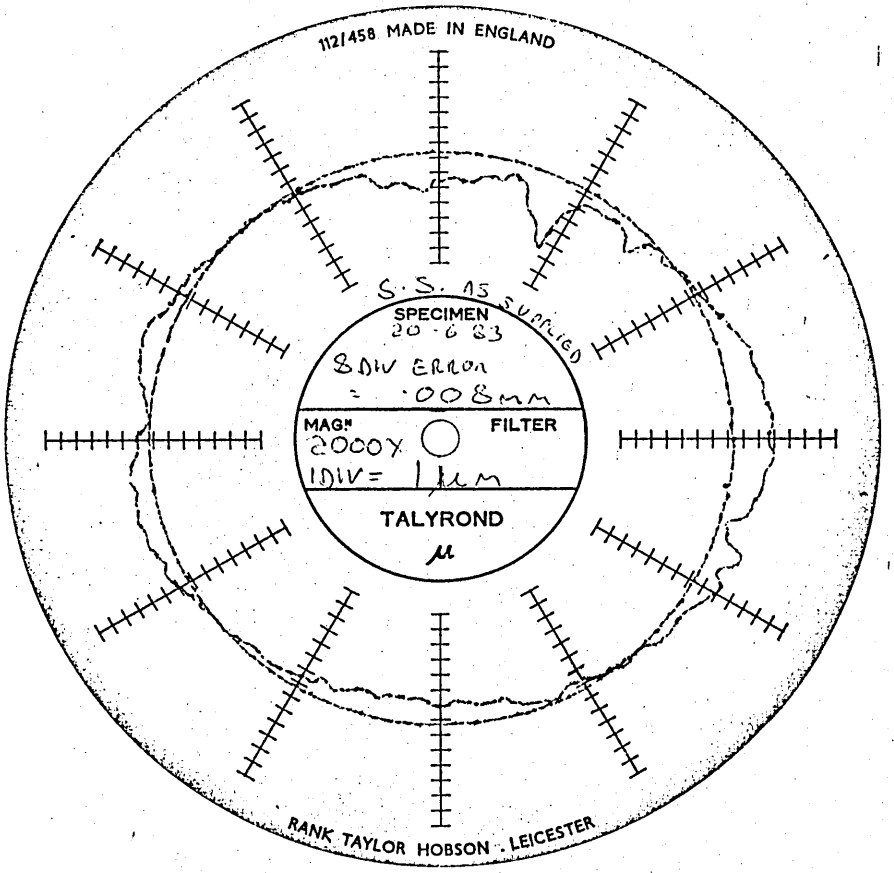

FIG 66: ROUNDNESS TEST ON RECEIVED 18/8 STAINLESS STEEL WIRE

1 DIV = 0.001 mm

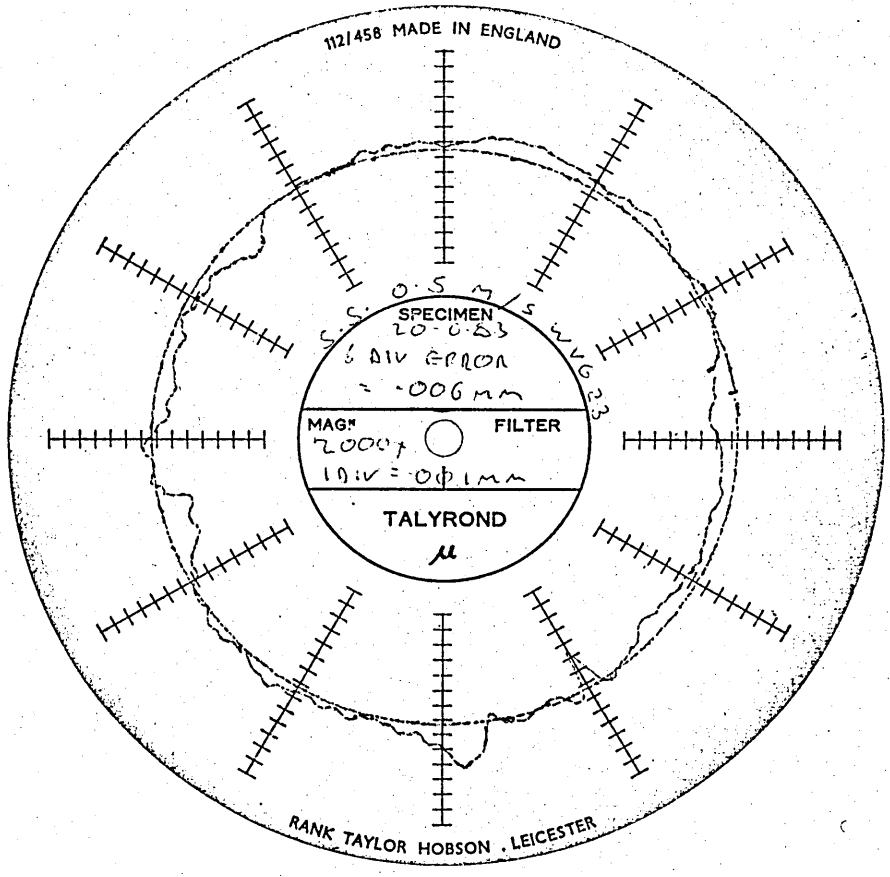

FIG 67: ROUNDNESS TEST ON 18/8 STAINLESS STEEL WIRE DRAWN AT 0.5 m/s WITH WVG23, 130°C - 20% REDUCTION IN AREA

1 DIV = 0.001 mm

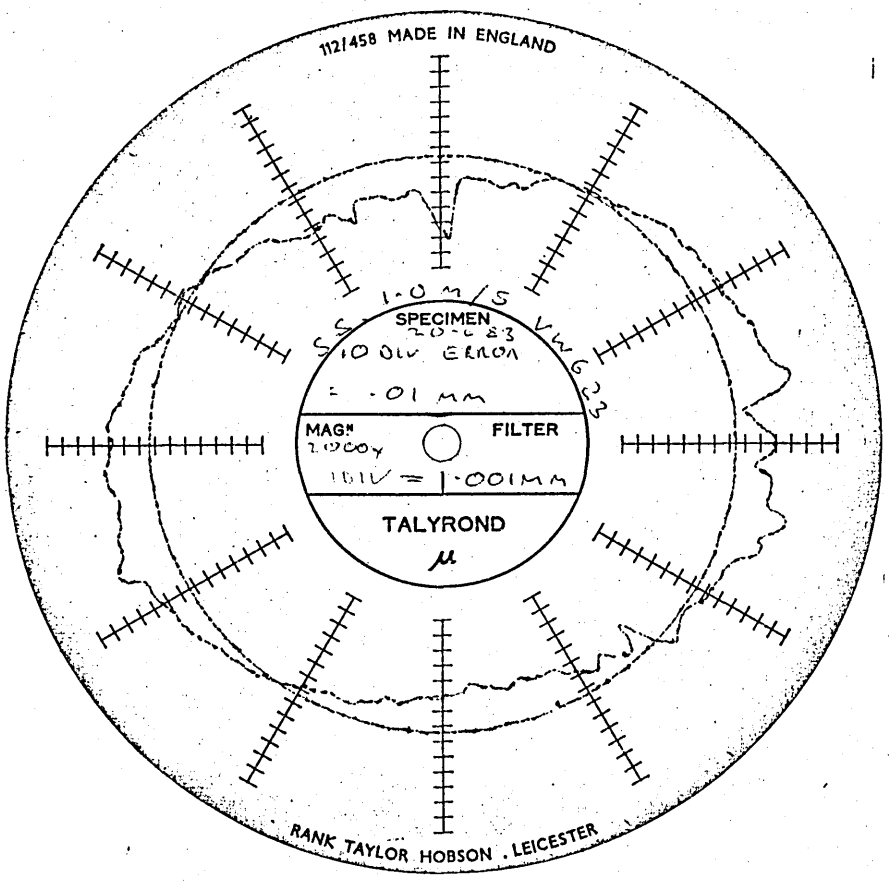

FIG68: ROUNDNESS TEST ON 18/8 STAINLESS STEEL WIRE DRAWN AT 1·0 m/s WITH WVG23, 130°C - 5% REDUCTION IN AREA

1 DIV = 0·001 mm

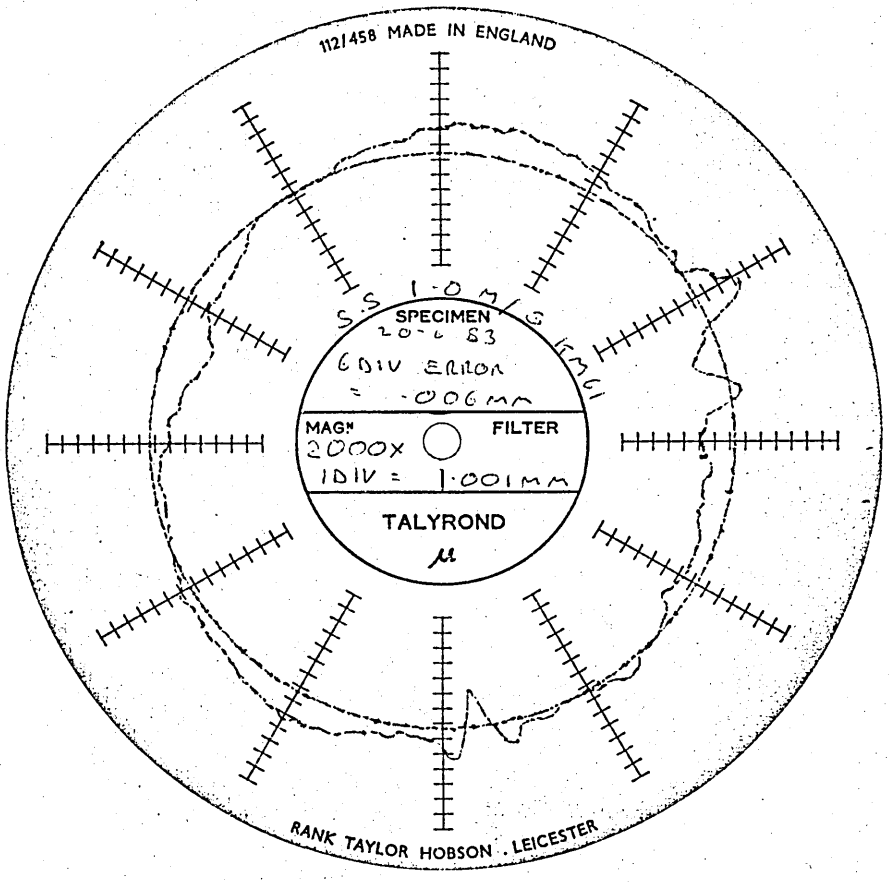

FIG69: ROUNDNESS TEST ON 18/8 STAINLESS STEEL WIRE DRAWN AT 1·0 m/s WITH KM61, 200°C - 13% REDUCTION IN AREA

1 DIV = 0·001 mm

FIG 70(a) : VARIATIONS OF DIAMETER FOR COPPER WIRE

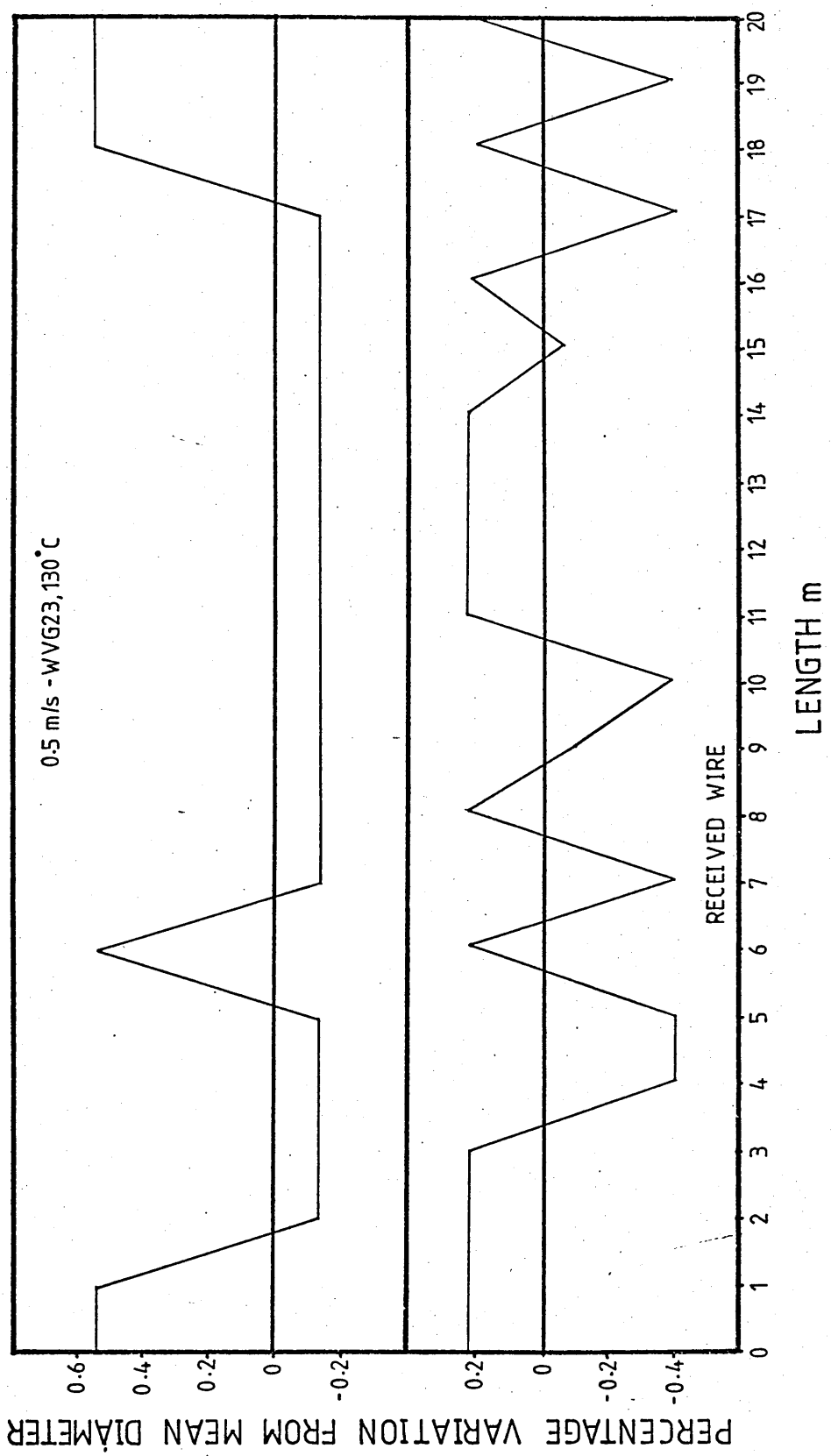

FIG 70(b) : VARIATIONS OF DIAMETER FOR COPPER WIRE

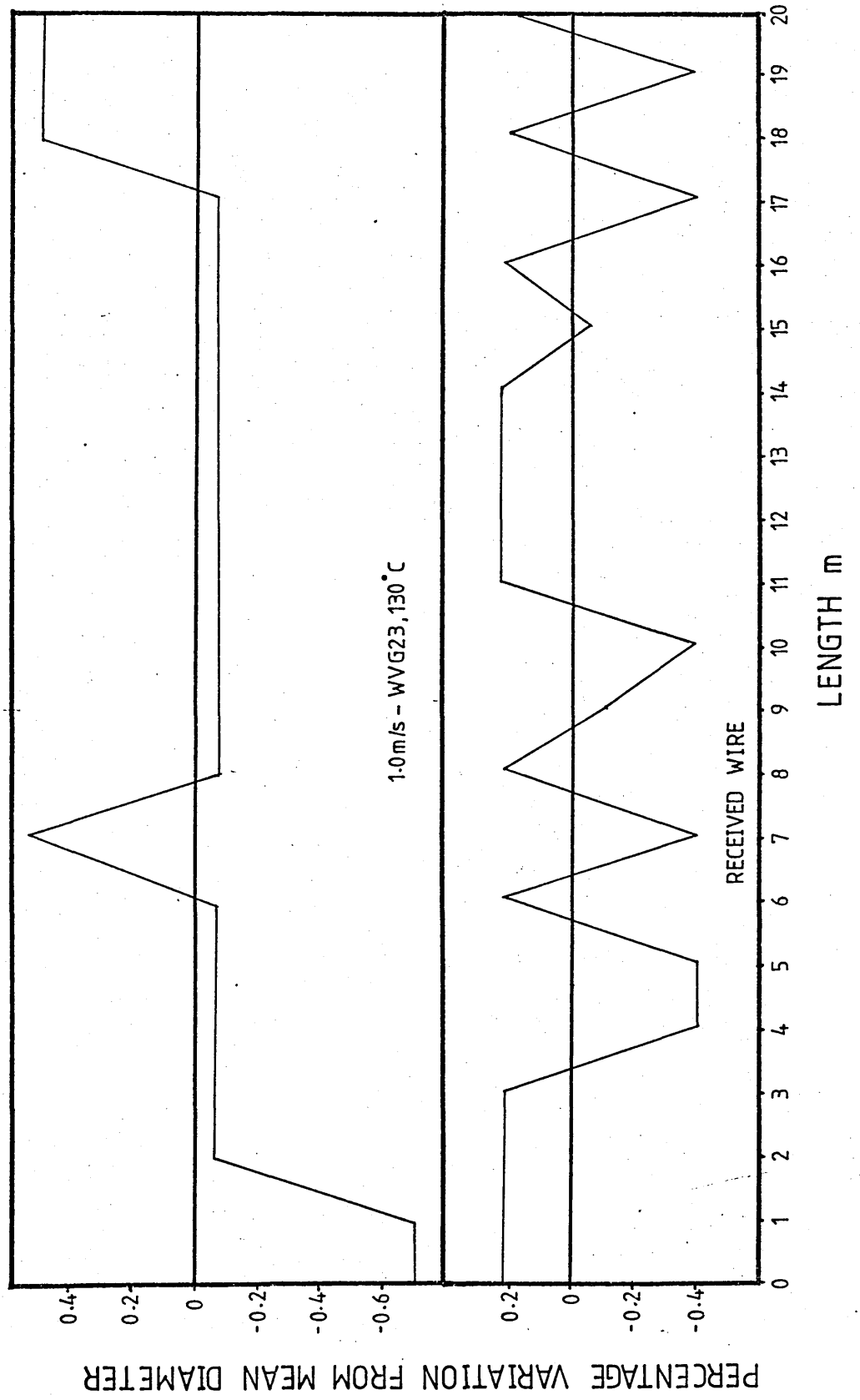

FIG 71: VARIATIONS OF DIAMETER FOR MILD STEEL WIRE

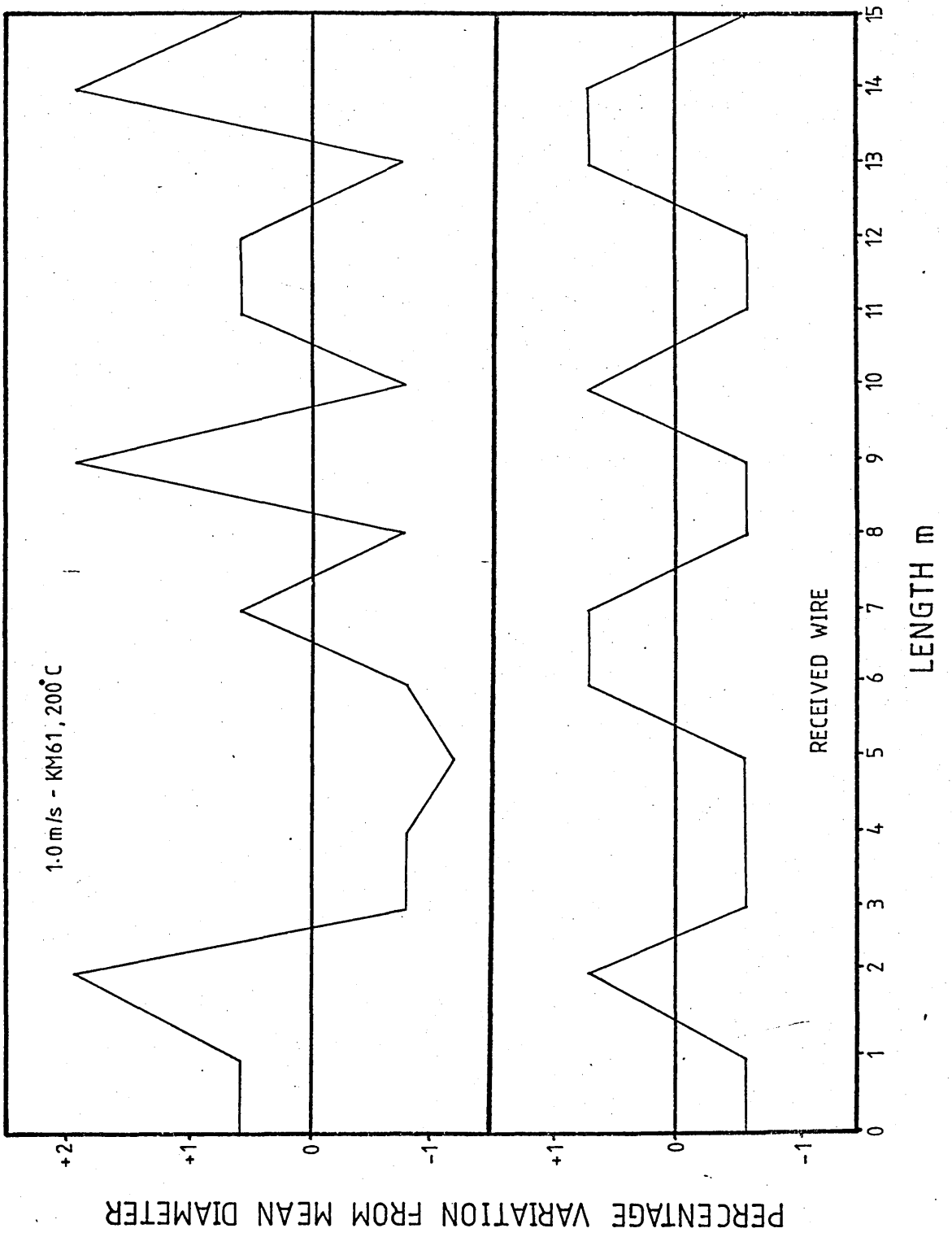

PLATE 17 : SURFACE FINISH OF COPPER WIRE AS RECEIVED - X 450

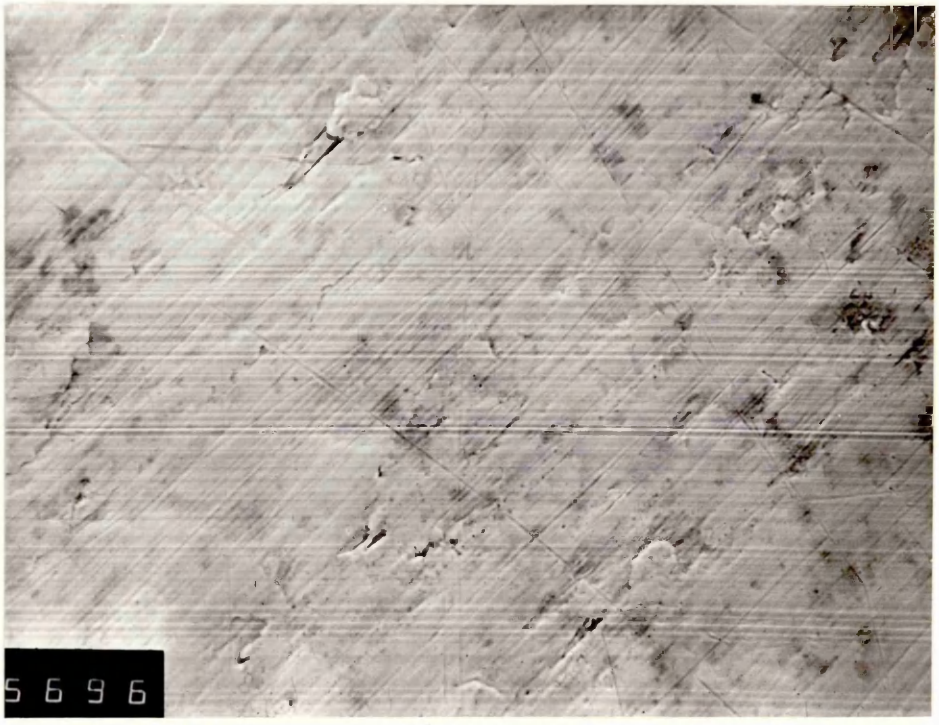

PLATE 18 : SURFACE FINISH OF COPPER WIRE DRAWN AT 1.0 m/s WITH WVG23, 130 °C - 11% REDUCTION IN AREA - X 450

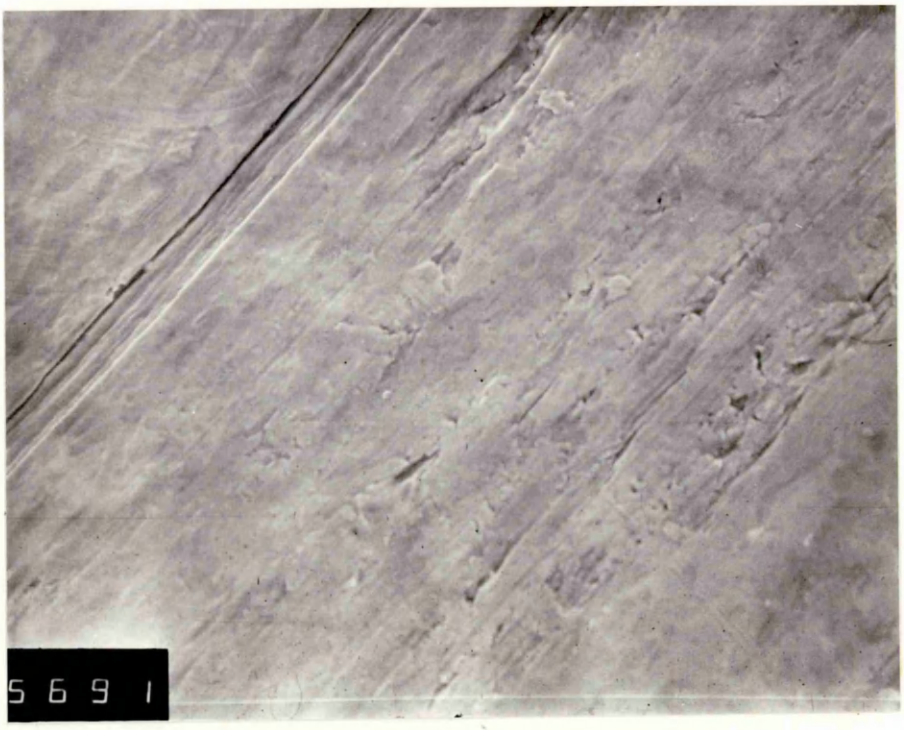

PLATE 19 : SURFACE FINISH OF COPPER WIRE DRAWN AT 0·5 m/s WITH WVG23, 130°C - 17 % REDUCTION IN AREA - X450

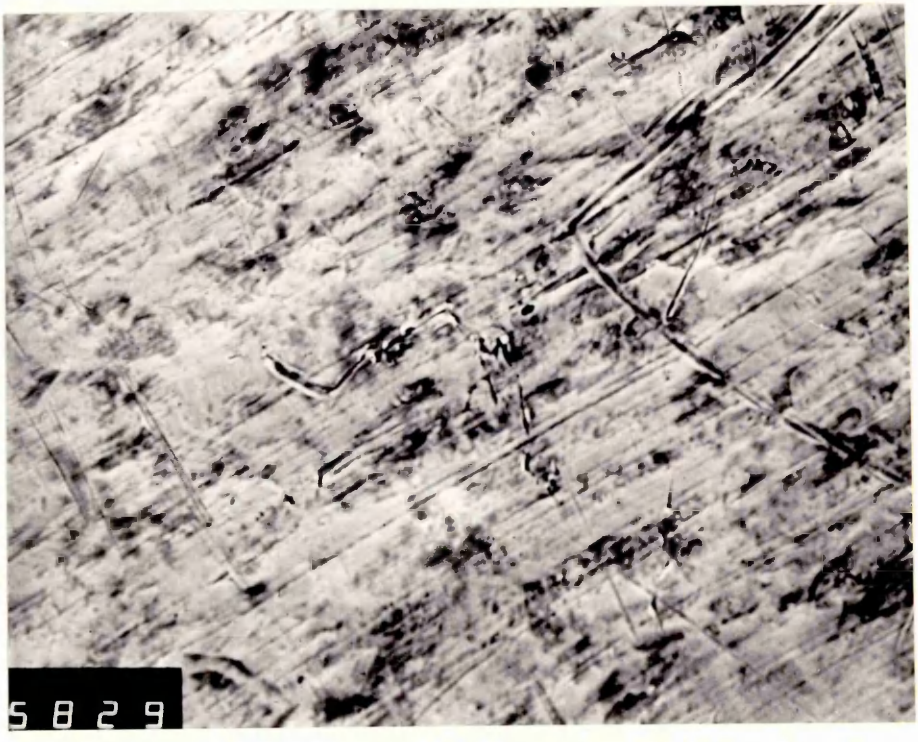

PLATE20 : SURFACE FINISH OF COPPER WIRE DRAWN AT 0·5 m/s WITH KM61, 200°C - 20% REDUCTION IN AREA - X450

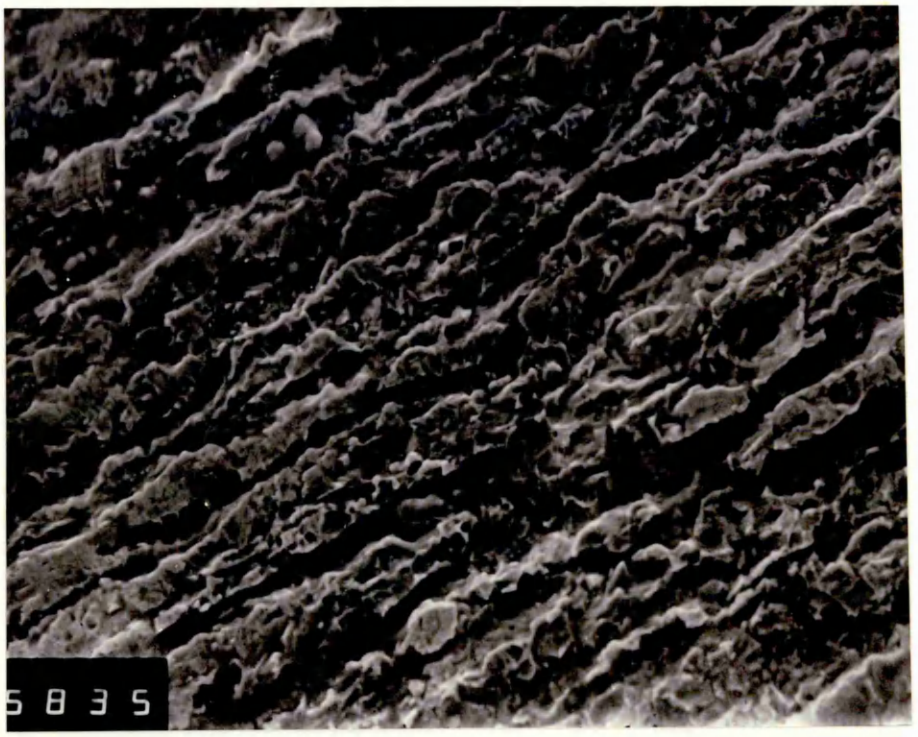

PLATE21: SURFACE FINISH OF MILD STEEL WIRE (ETCHED ONLY) - X 450

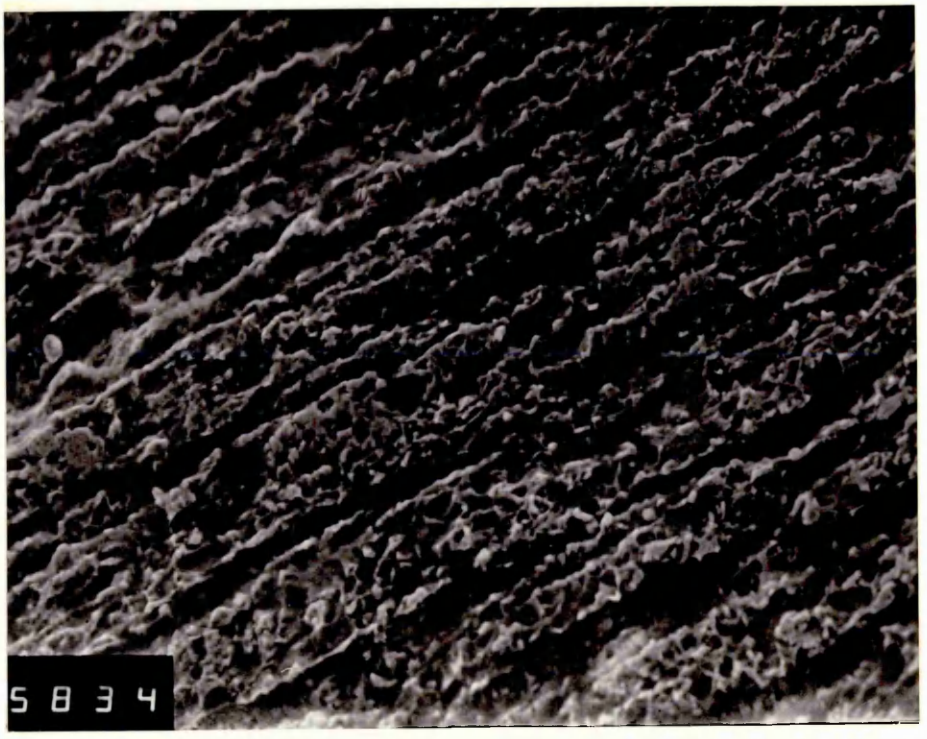

PLATE22: SURFACE FINISH OF MILD STEEL WIRE DRAWN AT 1·0 m/s WITH KM61, 200 °C - 11% REDUCTION IN AREA - X450

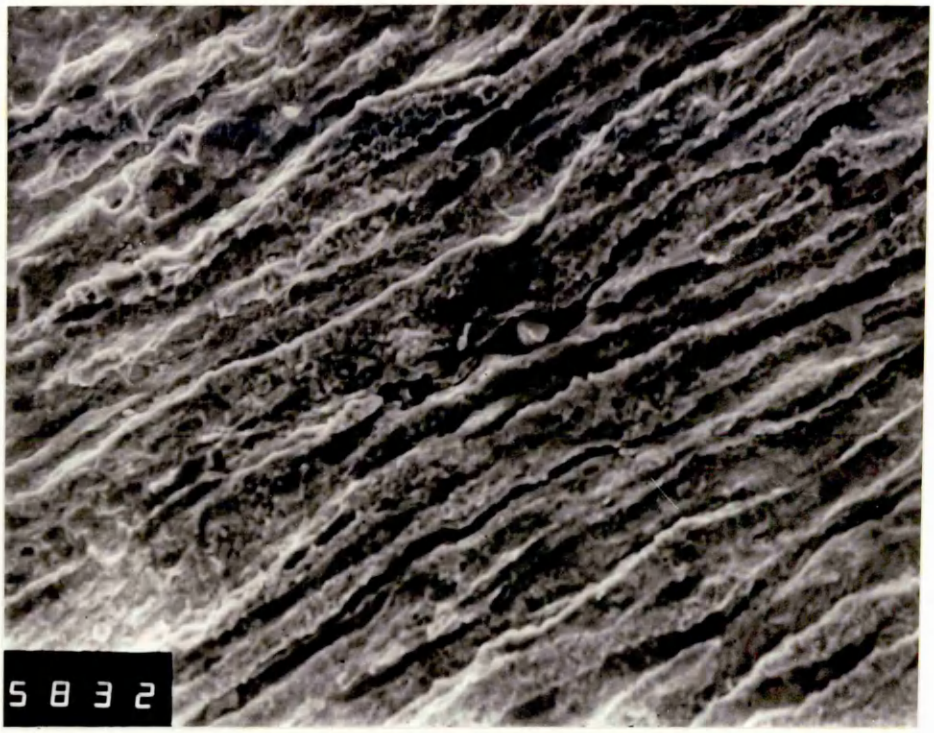

PLATE 23 : SURFACE FINISH OF MILD STEEL WIRE DRAWN AT 0·5 m/s WITH KM61, 200°C - 11% REDUCTION IN AREA - X450

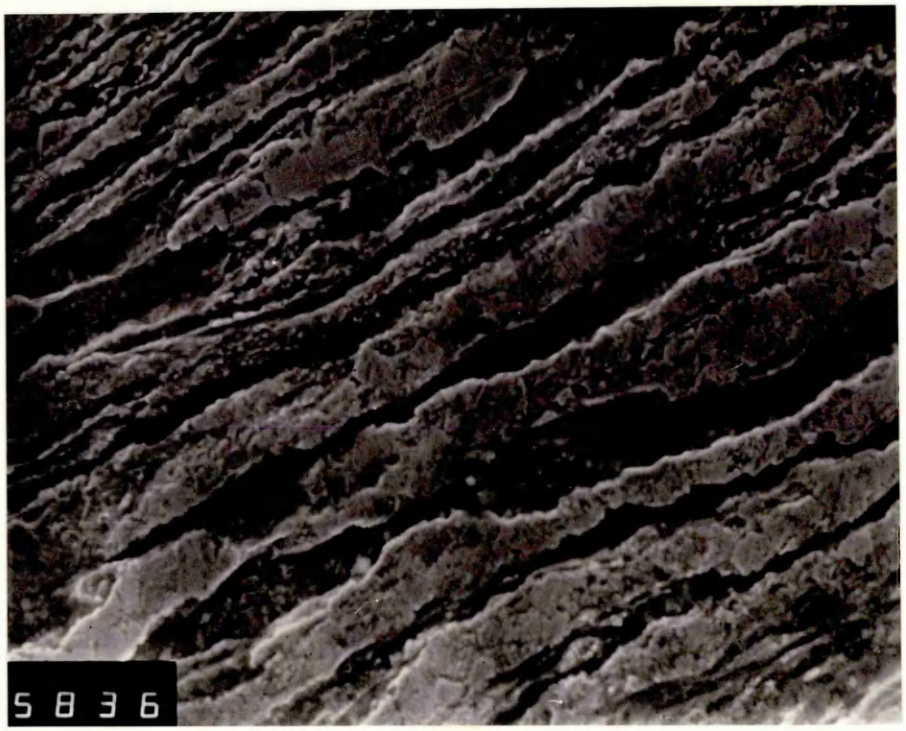

PLATE 24 : SURFACE FINISH OF MILD STEEL WIRE DRAWN AT 0·5 m/s WITH WVG23, 130°C - 15% REDUCTION IN AREA - X450

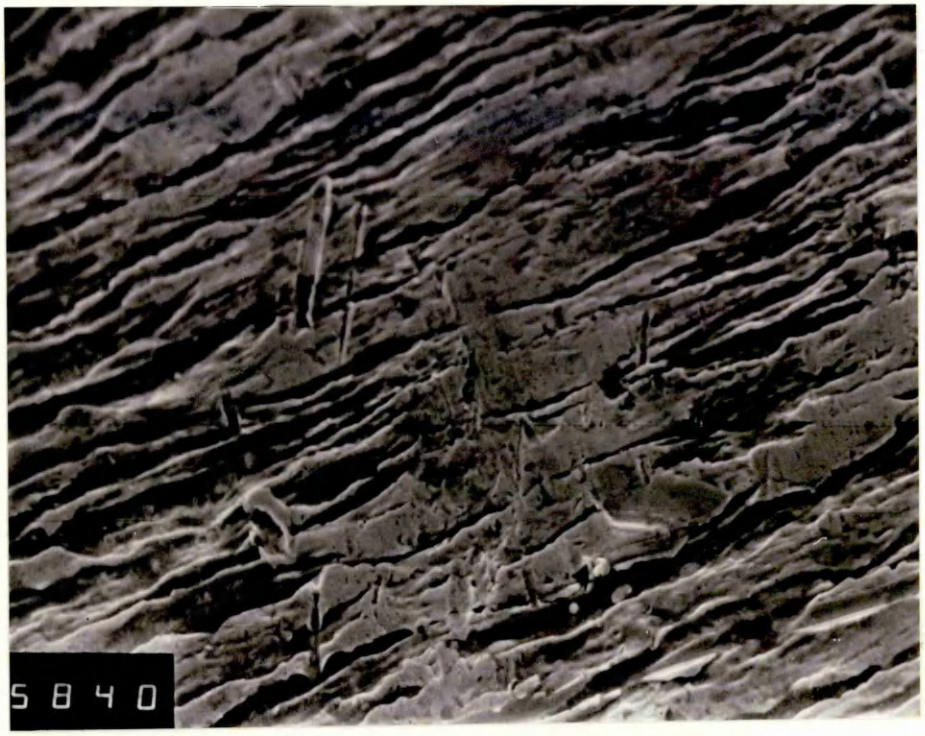

PLATE 25 : SURFACE FINISH OF 18/8 STAINLESS STEEL WIRE AS RECEIVED - X450

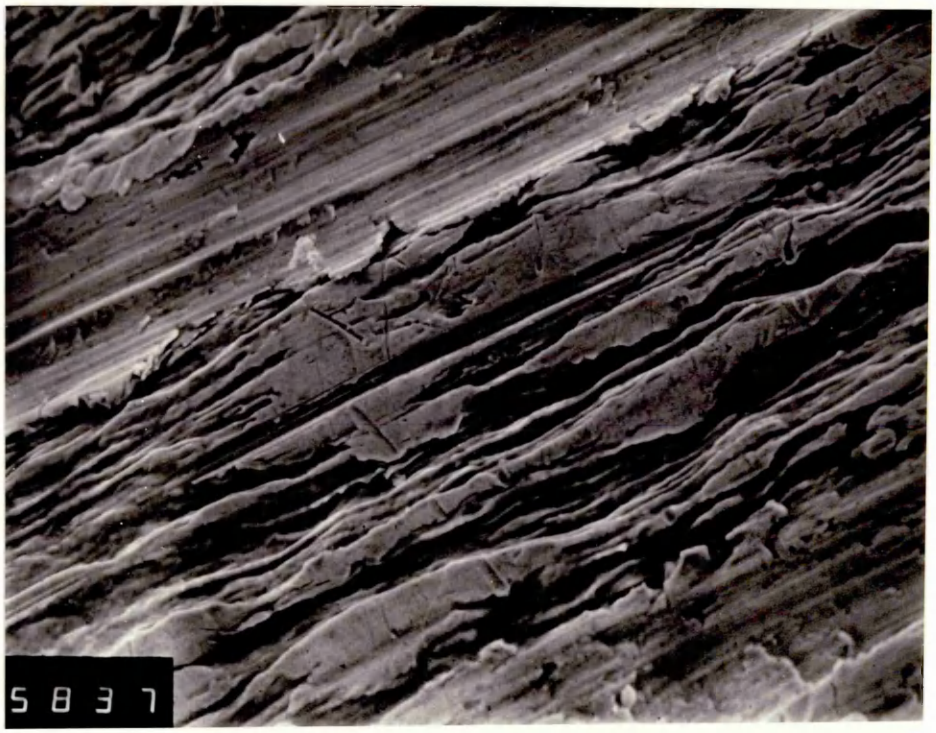

PLATE 26 : SURFACE FINISH OF 18/8 STAINLESS STEEL WIRE DRAWN AT 0·5 m/s WITH WVG23, 130° C - 20% REDUCTION IN AREA - X450

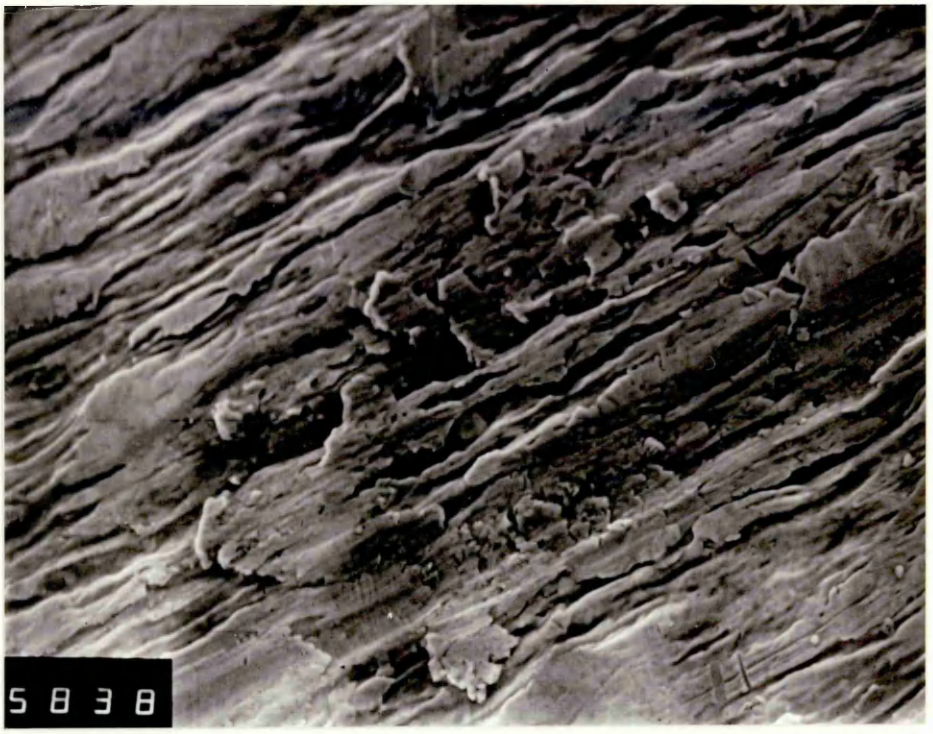

PLATE 27 : SURFACE FINISH OF 18/8 STAINLESS STEEL WIRE DRAWN AT 1·0 m/s WITH WVG23, 130°C - 5·0% REDUCTION IN AREA - X450

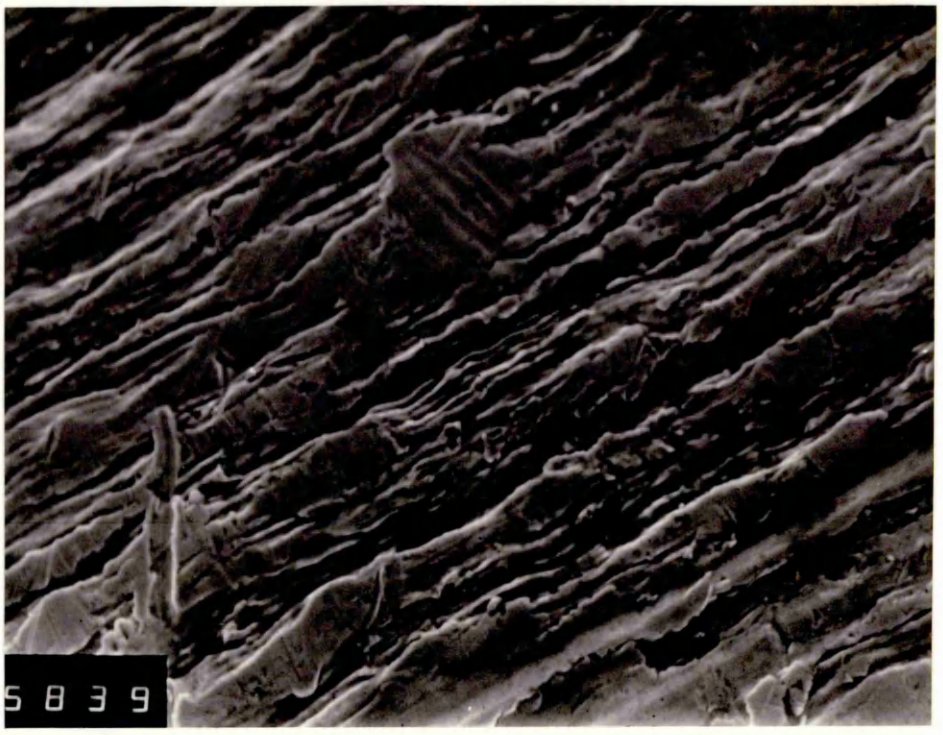

PLATE 28 : SURFACE FINISH OF 18/8 STAINLESS STEEL WIRE DRAWN AT 1·0 m/s WITH KM61, 200°C - 13 % REDUCTION IN AREA - X450

4.6- Results Of Multi-pass Tests.

Performance of the stepped bore reduction unit, in terms of reducing the wire diameter, was found to be poor at higher drawing speeds especially when harder materials were used.

Tests were conducted to investigate the feasibility of a multi-unit system in which higher deformations was thought to be obtainable. Wire was drawn through the stepped bore reduction unit number of times, simulating a multi-unit system, and the reduction in area was measured at each pass. Pressure medium used for these tests was KM 61 polymer which provided comparatively higher results during the previous tests.

Mild steel wire was drawn at 1.0 m/s consecutively and prior to each test run, polymer coating on the wire was removed. This was repeated until no further reduction in the diameter was measured. Table below shows the obtained results in details;

Test no. (pass)	Wire dia. (mm)	Reduction in area per pass	Gap ratio h_1/h_2
0	1.60	0.0%	4.0
1	1.46	17.0%	2.25
2	1.44	2.7%	2.15
3	1.42	2.7%	2.0
4	1.42	0.0%	2.0

Total reduction in area = 21.36%

The above experiment was repeated again for the mild steel wire and this time the polymer coating was allowed to remain on the wire prior to each run. The amount of reduction in area per pass was found to increase significantly but wire fracture repeatedly occured in the third pass. Table below gives details of these tests;

Test no. (pass)	Wire dia. (mm)	Reduction in area per pass
0	1.60	0.0%
1	1.47	15.5%
2	1.36	14.4%
3	1.27	12.3%

Total reduction in area = 36.2%

In previous tests it was observed that mild steel wire was not reduced in diameter at drawing speed of 4.0 m/s. Therefore the above experiment was carried out in order to investigate the performance of the multi-unit system at this drawing speed. Although wire breakage was occuring in the third pass, the obtained results were found to be very encouraging. Table below shows the results;

Test no. (pass)	Wire dia. (mm)	Reduction in area per pass
0	1.60	0.0%
1	1.53	7.4%
2	1.46	9.0%
3	1.41	6.7%

Total reduction in area = 21.4%

The above results confirmed that a multi-unit drawing system, consisting of die-less pressure chambers and polymer melt as a pressure medium, could be operated successfully in reducing the wire diameter. This system could usefully be employed at higher drawing speeds where a single unit was found to fail to reduce the diameter of harder wire materials.

CHAPTER 5 : Plasto-Hydrodynamic Analysis Of The Wire Drawing Using The Stepped Bore Reduction Unit.

5.1- Critical Review Of The Previous Analyses.

5.2- Analysis.

5.1- Critical Review Of The Previous Analyses.

The analyses presented by previous researchers relate to the drawing of wire through a conventional reduction die preceded by a pressure tube. Oil or soap powder have been used for lubrication purposes and it is only recent that polymer melts have been introduced as lubricants in wire drawing.

Christopherson and Naylor (4) presented a simplified analysis of the wire drawing process in which they assumed that wire takes an eccentric position inside the narrow tube. Their equations contained the pressure and the flow of lubricant as two dependant variables, neither of which could be calculated unless one was known from experiment. The limitations of the Christopherson and Naylor's solution were later removed by Tattersall (6), who developed a theory which permited calculation of both the pressure and the flow of lubricant from independant variables. He divided the nozzle/die unit into three separate zones, i)- the cylindrical tube, ii)- inlet part of the die where the wire remains undeformed and iii)- the deformation zone. He assumed that the wire travels centrally down the tube and included the coefficient of pressure on viscosity into the analysis.

Bloor etal (8) carried out an analytical study on the strip drawing process using a tapered die (this can also be applied to wire drawing). They divided the die into four regions, i)- undeformed part, ii)- deformation zone, iii)- plastic zone and iv)- stess relaxation zone. The coefficient of pressure on viscosity was also taken into

account.

Osterle and Dixon (9) presented a plasto-hydrodynamic solution of wire drawing process assuming that the wire deforms according to the shape of the die. In their analysis the combined effect of pressure and temperature on the viscosity of lubricant was incorporated.

All the above analyses were based on oil lubrication using the concept of apparent viscosity. Polymer melt as a lubricant in wire drawing was introduced by Thompson and Symmons (14) in conjunction with a pressure tube and a reduction die. They assumed that the polymer melt could be treated as a Newtonian fluid, using the concept of apparent viscosity. They also introduced critical and subcritical flow of polymer melt in their analysis. Stevens (15), using the work of Thompson and Symmons, presented a Newtonian plasto-hydrodynamic solution in wire drawing for polymer melt lubrication examining the theoretical coat thickness of the polymer. More recently Crampton (16) has introduced a non-Newtonian analysis of wire drawing process for polymer melt lubrication incorporating the effect of pressure and shear rate on the viscosity of the polymer melt. He also included strain hardening and strain rate sensitivity of the deforming metal together with the critical and subcritical flow of polymer into the analysis. He carried out an extensive amount of experimental work investigating various aspects of wire drawing process with polymer melt lubrication which substantiated his analytical work. Crampton showed that the wire was deformed plastically in the pressure tube taking the shape of an effective die of variable angle. He therefore assumed that the reduction die was of secondary

importance which virtually acted as a seal. A mathematical model of the effective die was proposed based on the experimentally measured profile of the deforming wire. The position at which the deformation of wire commenced or terminated were also determined experimentally.

In the present study the geometrical configuration is different from those discussed above. All the above analyses refer to systems where a conventional reduction die is used whose minimum bore size is always smaller than the incoming wire diameter. In the present system no reduction die is used and the minimum bore size of the stepped bore reduction unit is greater than the diameter of the undeformed wire. A different approach is therefore necessary to analyse the deformation process.

A non-Newtonian plasto-hydrodynamic analysis of the wire drawing process is presented for a stepped bore reduction unit in which polymer melt is used as the pressure medium. The effects of shear rate and pressure on the viscosity of the polymer together with the limiting shear stress are included in the analysis. Also strain hardening and strain rate sensitivity of the wire material are incorporated in the solution.

The present analysis predicts the pressure in the melt, stress in the wire, position at which the wire yields plastically in the unit, the subsequent deformation profile of the wire, coating thickness and the percentage reduction in area.

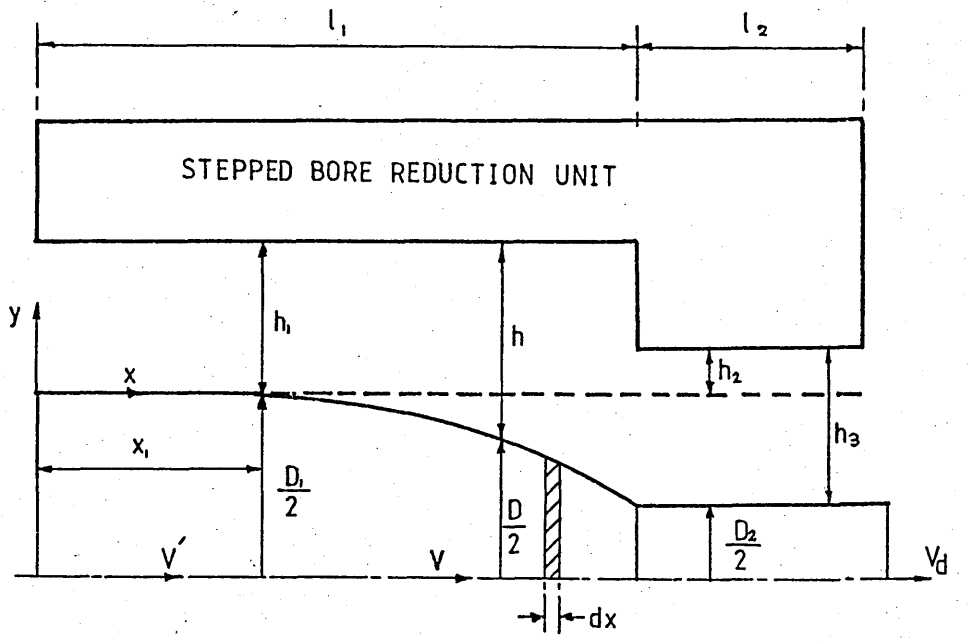

(a)

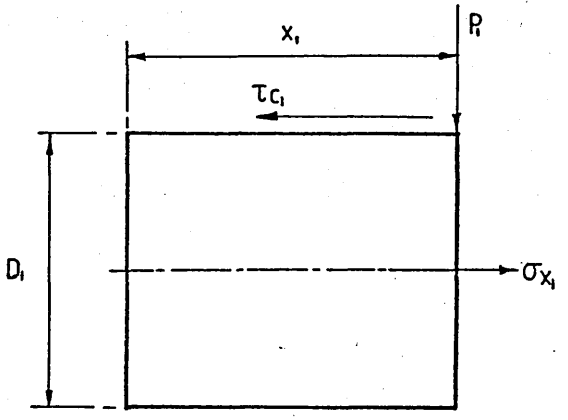

(b)

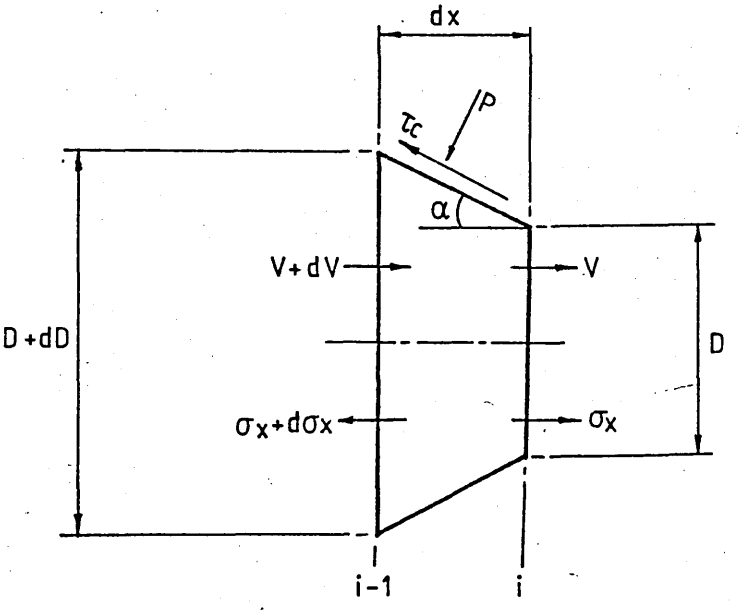

(c)

FIG72: GEOMETRY USED IN THE ANALYSIS

5.2- Analysis.

The following analysis is based on the geometrical configuration shown in figure 72. To formulate the analysis the following assumptions were made:

i)- Flow of polymer melt is isothermal.

ii)- Flow of polymer melt is laminar.

iii)- Flow of polymer melt is axial.

iv)- Thickness of the polymer layer is small compared to the dimensions of the stepped bore reduction unit.

v)- Deformation of the wire takes place isothermally.

Analysis of the stepped bore reduction unit is presented in three parts;

1- Determination of the pressure in the unit prior to deformation of the wire.

2- Prediction of the yielding position of the wire in the unit.

3- Deformation zone.

1- Determination of the pressure in the unit.

An emperical equation relating shear stress and shear rate of polymer melts was suggested by Rabinowitsch (35) in the form;

$$\tau + K\tau^3 = \eta \frac{dU}{dy} \qquad \text{.....(1)}$$

This equation was later used by Hung and Muster (36) to determine the non-Newtonian flow in a step bearing and also by Swamy etal (37) to calculate the load capacity of a finite width journal bearing. Other workers have also used this equation to analyse the behaviour of non-Newtonian fluids (16,38). Flow of polymer melt in the stepped bore reduction unit is divided into two sections, first section being the entry part of the unit before the step and second section being the tube after the step. Considering the first part of the unit in figure 72(a), the steady state flow of the polymer gives;

$$(\frac{dP}{dx})_1 = (\frac{d\tau_1}{dy})_1$$

Integrating with respect to y gives;

$$\tau_1 = \acute{P}_1 y + \tau_{c1} \qquad \text{.....(2)}$$

where $\acute{P}_1 = (\frac{dP}{dx})_1$

and τ_{c1} is the shear stress on the wire at y=0.

Substituting equation (2) into (1) becomes;

$$\acute{P}_1 y + \tau_{c1} + K(\acute{P}_1^3 y^3 + \tau_{c1}^3 + 3\acute{P}_1^2 y^2 \tau_{c1} + 3\tau_{c1}^2 \acute{P}_1 y) = \eta (\frac{dU}{dy})_1$$

Integration with respect to y gives;

$$U_1 = \frac{\acute{P}_1 y^2}{2\eta} + \frac{\tau_{c1} y}{\eta} + \frac{K}{\eta}(\frac{1}{4}\acute{P}_1^3 y^4 + \tau_{c1}^3 y + \acute{P}_1^2 y^3 \tau_{c1} + \frac{3}{2}\tau_{c1}^2 \acute{P}_1 y^2) + \text{const.}$$

$$\text{.....(3)}$$

Considering the boundary conditions.

Two conditions may be considered, at speeds where slip does not occur and at speeds where slip occurs. For conditions of no-slip,

at $y=0$ $\quad U_1 = \acute{V}$ $\quad (a_1)$ and

at $y=h_1$ $\quad U_1 = 0$ $\quad (b_1)$

where $\acute{V}$ is the velocity of the undeformed wire. Substituting condition (a_1) into equation (3) becomes;

$$U_1 = \frac{\acute{P}_1 y^2}{2\eta} + \frac{\tau_{c1} y}{\eta} + \frac{K}{\eta}\left(\frac{1}{4}\acute{P}_1^3 y^4 + \tau_{c1}^3 y + \acute{P}_1^2 y^3 \tau_{c1} + \frac{3}{2}\tau_{c1}^2 \acute{P}_1 y^2\right) + \acute{V} \qquad \ldots\ldots\ldots(4)$$

Substituting condition (b_1) into equation (4) and rearranging give;

$$\tau_{c1}^3 + \left(\frac{3}{2}\acute{P}_1 h_1\right)\tau_{c1}^2 + \left(\frac{1}{K} + \acute{P}_1^2 h_1^2\right)\tau_{c1} + \left(\frac{\eta \acute{V}}{K h_1} + \frac{\acute{P}_1 h_1}{2K} + \frac{1}{4}\acute{P}_1^3 h_1^3\right) = 0$$

Let $\quad L_1 = \frac{3}{2}\acute{P}_1 h_1$

$$M_1 = \frac{1}{K} + \acute{P}_1^2 h_1^2$$

$$N_1 = \frac{\eta \acute{V}}{K h_1} + \frac{\acute{P}_1 h_1}{2} + \frac{1}{4}\acute{P}_1^3 h_1^3$$

Hence,

$$\tau_{c1}^3 + L_1 \tau_{c1}^2 + M_1 \tau_{c1} + N_1 = 0$$

Let $\quad \tau_{c1} = \varphi_1 - \frac{L_1}{3}$ $\qquad \ldots\ldots\ldots(5)$

Therefore,

$$\varphi_1^3 + A_1\varphi_1 + B_1 = 0 \qquad \ldots\ldots\ldots(6)$$

where $A_1 = \frac{1}{K} + \frac{1}{4}\acute{P}_1^2 h_1^2$

and $B_1 = \frac{\eta \acute{V}}{K h_1}$

Equation (6) has been solved previously by approximation methods (36,37,38) which may be considered under specifically defined conditions. This equation however, is shown to have a definite solution with two imaginary roots and one real root (39), the real root being;

$$\varphi_1 = \left(-\frac{B_1}{2} + \left(\frac{B_1^2}{4} + \frac{A_1^3}{27}\right)^{\frac{1}{2}}\right)^{\frac{1}{3}} + \left(-\frac{B_1}{2} - \left(\frac{B_1^2}{4} + \frac{A_1^3}{27}\right)^{\frac{1}{2}}\right)^{\frac{1}{3}}$$

Substituting for B_1 and A_1 into above equation and combining with equation (5) gives;

$$\tau_{c1} = \left(-\frac{\eta\acute{V}}{2Kh_1} + \left(\frac{\eta^2\acute{V}^2}{4K^2h_1^2} + \frac{1}{27}\left(\frac{1}{K} + \frac{1}{4}\acute{P}_1^2h_1^2\right)^3\right)^{\frac{1}{2}}\right)^{\frac{1}{3}} + \left(-\frac{\eta\acute{V}}{2Kh_1} - \left(\frac{\eta^2\acute{V}^2}{4K^2h_1^2} + \frac{1}{27}\left(\frac{1}{K} + \frac{1}{4}\acute{P}_1^2h_1^2\right)^3\right)^{\frac{1}{2}}\right)^{\frac{1}{3}} - \frac{1}{2}\acute{P}_1 h_1 \qquad \ldots\ldots\ldots(7)$$

Equation (7) enables to calculate shear stress on the wire for the condition that $\acute{P}_1$ is defined. The flow of polymer gives;

$$Q_1 = \int_0^{h_1} U_1 \, dy$$

substituting for U_1 and integrating gives,

$$Q_1 = \frac{\acute{P}_1 h_1^3}{6\eta} + \frac{h_1^2 \tau_{c1}}{2\eta} + \frac{K}{\eta}\left(\frac{1}{20}\acute{P}_1^3 h_1^5 + \frac{1}{2}h_1^2\tau_{c1}^3 + \frac{1}{4}\acute{P}_1^2 h_1^4 \tau_{c1} + \frac{1}{2}\acute{P}_1 h_1^3 \tau_{c1}^2\right) + \acute{V} h_1 \quad \text{.....(8)}$$

Also the steady state flow gives;

$$\frac{d}{dx}\left(Q_1\right) = 0$$

substituting equation (7) into (8) and differentiating gives;

$$\left(\frac{d^2P}{dx^2}\right)_1 = 0$$

hence

$$\left(\frac{dP}{dx}\right)_1 = \acute{P}_1 = \text{constant} = \frac{P_m}{l_1}$$

where P_m is the pressure at the step
and l_1 is the length of the first section of the unit.

As shown above, the pressure profile in the first part of the unit is linear. However P_m can not be determined at this stage since equation (8) contains the unknown variable Q_1 and it must be defined. Continuity of flow gives;

$$Q_1 = Q_2$$

therefore it is necessary to establish the flow equations for the second part of the unit before P_m can be predicted.

The steady state flow in the second part of the unit gives;

$$(\frac{dP}{dx})_2 = - (\frac{d\tau_2}{dy})_2$$

Integration gives,

$$\tau_2 = - \acute{P}_2 y + \tau_{c2} \qquad \text{.....(9)}$$

where $\acute{P}_2 = (\frac{dP}{dx})_2$

and τ_{c2} is the shear stress on the wire at y=0.

Substituting equation (9) into (1) gives;

$$- \acute{P}_2 y + \tau_{c2} + K(- \acute{P}_2^3 y^3 + \tau_{c2}^3 + 3\acute{P}_2^2 y^2 \tau_{c2} - 3\tau_{c2}^2 \acute{P}_2 y) = \eta (\frac{dU}{dy})_2$$

Integration with respect to y gives;

$$U_2 = - \frac{\acute{P}_2 y^2}{2\eta} + \frac{\tau_{c2} y}{\eta} + \frac{K}{\eta}(- \frac{1}{4}\acute{P}_2^3 y^4 + \tau_{c2}^3 y + \acute{P}_2^2 y^3 \tau_{c2} - \frac{3}{2}\acute{P}_2 y^2 \tau_{c2}^2) + \text{cons.}$$

$$\text{.....(10)}$$

Again for the condition of no-slip, boundary conditions are:

at	$y = 0$	$U_2 = \acute{V}$	(a_2)	and
at	$y = h_2$	$U_2 = 0$	(b_2)	

Applying conditions (a_2) in equation (10) gives;

$$U_2 = - \frac{\acute{P}_2 y^2}{2\eta} + \frac{\tau_{c2} y}{\eta} + \frac{K}{\eta}(- \frac{1}{4}\acute{P}_2^3 y^4 + \tau_{c2}^3 y + \acute{P}_2^2 y^3 \tau_{c2} - \frac{3}{2}\acute{P}_2 y^2 \tau_{c2}^2) + \acute{V}$$

$$\text{.....(11)}$$

which upon application of condition (b_2) and rearranging gives;

$$\tau_{c2}^3 + \left(-\frac{3}{2}\acute{P}_2 h_2\right)\tau_{c2}^2 + \left(\frac{1}{K} + \acute{P}_2^2 h_2^2\right)\tau_{c2} + \left(\frac{\eta \acute{V}}{Kh_2} - \frac{1}{4}\acute{P}_2^3 h_2^3 - \frac{\acute{P}_2 h_2}{2K}\right) = 0$$

Let $L_2 = -\frac{3}{2}\acute{P}_2 h_2$

$$M_2 = \frac{1}{K} + \acute{P}_2^2 h_2^2$$

$$N_2 = \frac{\eta \acute{V}}{Kh_2} - \frac{1}{4}\acute{P}_2^3 h_2^3 - \frac{\acute{P}_2 h_2}{2K}$$

Therefore,

$$\tau_{c2}^3 + L_2\tau_{c2}^2 + M_2\tau_{c2} + N_2 = 0$$

Let $\tau_{c2} = \varphi_2 - \frac{L_2}{3}$ .....(12)

hence,

$$\varphi_2 + A_2\varphi_2 + B_2 = 0 \qquad .....(13)$$

Where $A_2 = \frac{1}{K} + \frac{1}{4}\acute{P}_2^2 h_2^2$

and $B_2 = \frac{\eta \acute{V}}{Kh_2}$

Again equation (13) has two imaginary roots and one real root, the real root being;

$$\varphi_2 = \left(-\frac{B_2}{2} + \left(\frac{B_2^2}{4} + \frac{A_2^3}{27}\right)^{\frac{1}{2}}\right)^{\frac{1}{3}} + \left(-\frac{B_2}{2} - \left(\frac{B_2^2}{4} + \frac{A_2^3}{27}\right)^{\frac{1}{2}}\right)^{\frac{1}{3}}$$

substituting for A_2 and B_2 into above equation and substituting for φ_2 into equation (12) gives;

$$\tau_{c2} = \left(-\frac{\eta \acute{V}}{2Kh_2} + \left(\frac{\eta^2 \acute{V}^2}{4K^2 h_2^2} + \frac{1}{27}\left(\frac{1}{K} + \frac{1}{4}\acute{P}_2^2 h_2^2\right)^3\right)^{\frac{1}{2}}\right)^{\frac{1}{3}} + \left(-\frac{\eta \acute{V}}{2Kh_2} - \left(\frac{\eta^2 \acute{V}^2}{4K^2 h_2^2}\right.\right.$$

$$\left.\left. + \frac{1}{27}\left(\frac{1}{K} + \frac{1}{4}\acute{P}_2^2 h_2^2\right)^3\right)^{\frac{1}{2}}\right)^{\frac{1}{3}} + \frac{1}{2}\acute{P}_2 h_2 \qquad \text{.....(14)}$$

Equation (14) predicts shear stress on the wire in the second part of the unit. It is now necessary to define $\acute{P}_2$ before equation (14) can be solved. The flow in the second part is given by;

$$Q_2 = \int_0^{h_2} U_2 \, dy$$

substituting equation (11) into above and integrating gives;

$$Q_2 = -\frac{\acute{P}_2 h_2^3}{6\eta} + \frac{\tau_{c2} h_2^2}{2\eta} + \frac{K}{\eta}\left(-\frac{1}{20}\acute{P}_2^3 h_2^5 + \frac{1}{2}h_2^2 \tau_{c2}^3 + \frac{1}{4}\acute{P}_2^2 h_2^4 \tau_{c2} - \frac{1}{2}\acute{P}_2 h_2^3 \tau_{c2}^2\right)$$

$$+ \acute{V} h_2 \qquad \text{.....(15)}$$

Again from steady state flow,

$$\frac{d}{dx}(Q_2) = 0$$

Thus substituting equation (14) into (15) and differentiating gives,

$$\left(\frac{d^2 P}{dx^2}\right)_2 = 0$$

hence,

$$\left(\frac{dP}{dx}\right)_2 = \acute{P}_2 = \text{constant} = \frac{P_m}{l_2}$$

where P_m is the pressure at the step
and l_2 is the length of the second section of the unit.

It is shown that the pressure profile in the second section of the unit is also linear. It is known that pressure increases the viscosity of polymers and this effect should be included in the analysis for a satisfactory solution. With reference to figure 15 a generalized equation relating viscosity and pressure may be shown to take the form:

$$\eta = \eta_o + \frac{a + b P_m^2}{\dot{\gamma}}$$

where a and b are constants and η_o is the initial viscosity of polymer melt at ambient pressure. $\dot{\gamma}$ is the apparent shear rate and is assumed to be;

$$\dot{\gamma} = \frac{\acute{V}}{h_1}$$

hence, substituting $\dot{\gamma}$ into above equation gives,

$$\eta = \eta_o + \frac{h_1}{\acute{V}} (a + b P_m^2) \qquad .....(16)$$

Equation (16) enables to calculate the viscosity of polymer at known pressure and shear rate. This equation together with equations (7),(8),(14) and (15) may be solved simultaneously. Numerical values of P_m and hence $\acute{P}_1$ and $\acute{P}_2$ may be substituted into the above equations, using an iteration technique, until the equation $Q_1 = Q_2$ is satisfied. Therefore pressure in the unit, viscosity of the polymer

melt and shear stresses on the wire (τ_{c1} and τ_{c2}) can be determined for the wire of rigid material. Having determined the hydrodynamic pressure and the resultant stresses on the wire, it is now necessary to predict the position within the unit at which yielding of the non-rigid wire commences.

ii)- Prediction of the position of yield of wire inside the unit.

Consider a distance X_1 from the entry of the unit where yielding of wire is just commenced (see figure 72(b)). Principal stresses acting on the wire are;

$$\sigma_1 = \sigma_{x1} \qquad \text{and} \quad \sigma_2 = \sigma_3 = -P_1$$

where σ_{x1} is the axial stress and P_1 is the radial pressure at point X_1 . Using the Tresca or Von Mises theory of yielding gives,

$$\sigma_{x1} + P_1 = Y \qquad \text{.....(17)}$$

Equilibrium of forces on the wire in the x direction gives;

$$\sigma_{x1}\left(\frac{1}{4} D_1^2 \pi\right) = (\pi D_1 X_1)\tau_{c1}$$

hence,

$$\sigma_{x1} = \frac{4X_1}{D_1}\tau_{c1} \qquad \text{.....(18)}$$

Also linear pressure distribution gives;

$$\frac{P_1}{X_1} = \frac{P_m}{l_1}$$

or

$$P_1 = \frac{P_m}{l_1} X_1 \qquad \text{.....(19)}$$

The yield characteristics of the wires are shown in figures 24 to 26 to take the form;

$$Y = Y_o + K_o \epsilon^n$$

therefore yielding takes place as soon as

$$Y = Y_o \qquad \text{.....(20)}$$

substituting equations (18) , (19) and (20) into (17) and rearranging, position of yield may be expressed as,

$$X_1 = \frac{Y_o}{\frac{4\tau_{c1}}{D_1} + \frac{P_m}{l_1}}$$

This equation enables to predict the position in the first section of the unit where the wire starts to yield. As soon as yielding occurs, plastic deformation will continue as long as equation (17) is satisfied.

iii)- Deformation zone.

Consider a section of the stepped bore reduction unit within which the wire is deformed as shown in figure 72(c).

Since variations of gap and wire diameter are to be determined theoretically and are not pre-defined as functions of x, the equations containing these variables can not be solved analytically. Hence a finite difference technique is adopted to solve the differential equations governing the deformation zone assuming that between any two points of " dx " distance apart on the deforming wire, the deformation takes place linearly, therefore;

$$\frac{dD}{dx} = \text{constant} = B$$

Expressing this equation in finite difference form gives;

$$\frac{D_{i-1} - D_i}{x_i - x_{i-1}} = B$$

or $$D_i = D_{i-1} - B\,\Delta x \qquad \text{.....(21)}$$

and similarly,

$$dh = \frac{1}{2}\,dD$$

hence,

$$h_i = h_{i-1} + \frac{1}{2}\,B\,\Delta x \qquad \text{.....(22)}$$

where B is the slope of the deformation line within " dx " distance. Cosidering a small section of the deforming wire, the radial equilibrium of forces gives;

$$\sigma_r\,(\pi\,D\,dx) = -\,P\,\left(\frac{\pi\,D\,dx}{\cos\alpha}\right)\cos\alpha + \tau_c\,\left(\frac{\pi D\,dx}{\cos\alpha}\right)\sin\alpha$$

hence,

$$\sigma_r = - P + \tau_c \tan\alpha = - P \left(1 - \frac{\tau_c}{P} \tan\alpha \right)$$

The value of $\frac{\tau_c}{P}$ has been shown to be of the order of 10^{-3} and since α is very small, $\frac{\tau_c}{P} \tan\alpha$ is of the order of 10^{-4} . The term $\frac{\tau_c}{P} \tan\alpha$ is therefore ignored. The principal stresses acting on the wire being;

$$\sigma_1 = \sigma_x \quad , \quad \sigma_2 = \sigma_3 = \sigma_r = - P$$

Therefore using Tresca or Von Mises theory of yielding gives;

$$\sigma_x + P = Y \qquad \text{.....(23)}$$

Equilibrium of forces in the x direction gives;

$$- \sigma_x \left(\frac{1}{4} \pi D^2\right) + \left(\sigma_x + d\sigma_x\right) \frac{\pi}{4} \left(D + dD \right)^2 + P \left(\frac{\pi D \, dx}{\cos\alpha}\right) \sin\alpha$$

$$+ \tau_c \left(\frac{\pi D \, dx}{\cos\alpha}\right) \cos\alpha = 0$$

rearranging and ignoring powers of dD leads to;

$$2 \, dD \, \sigma_x + D \, d\sigma_x + 4 P \, dx \tan\alpha + 4 \, dx \, \tau_c = 0$$

but $\tan\alpha = \frac{dD}{2dx}$ hence,

$$D \, d\sigma_x + 2 \, dD \left(P + \sigma_x \right) + 4 \, dx \, \tau_c = 0$$

substituting for $(P + \sigma_x)$ and rearranging gives;

$$d\sigma_x = -\frac{2\,dD}{D}\,Y - \frac{4\,\tau_c\,dx}{D}$$

This is the governing differential equation for the deformation zone which enables to predict the axial stress in the wire. Re-writing the above equation in finite difference form gives;

$$\sigma_{x_{i-1}} - \sigma_{x_i} = -\frac{2\,(D_{i-1} - D_i)}{D_i}\,Y_i - \frac{4\,\tau_{ci}\,\Delta x}{D_i}$$

or

$$\sigma_{x_i} = \frac{2\,(D_{i-1} - D_i)}{D_i}\,Y_i + \frac{4\,\tau_{ci}\,\Delta x}{D_i} + \sigma_{x_{i-1}} \qquad \text{.....(24)}$$

Equation (24) is a function of shear stress on the wire and it must be determined independently. Equation (7) may be re-written as;

$$\tau_{ci} = \left(-\frac{\eta\,V_i}{2Kh_i} + \left(\frac{\eta^2 V_i^2}{4K^2 h_i^2} + \frac{1}{27}\left(\frac{1}{K} + \frac{1}{4}\acute{P}_i^2 h_i^2\right)^3\right)^{\frac{1}{2}}\right)^{\frac{1}{3}} + \left(-\frac{\eta\,V_i}{2Kh_i} -\right.$$

$$\left.\left(\frac{\eta^2 V_i^2}{4K^2 h_i^2} + \frac{1}{27}\left(\frac{1}{K} + \frac{1}{4}\acute{P}_i^2 h_i^2\right)^3\right)^{\frac{1}{2}}\right)^{\frac{1}{3}} - \frac{1}{2}\acute{P}_i\,h_i \qquad \text{.....(25)}$$

Equation (25) contains the pressure gradient and variation of the wire velocity in the deformation zone and they must be determined separately. Flow of the polymer melt in this region may be expressed as;

$$Q_i = \frac{\acute{P}_i\,h_i^3}{6\,\eta} + \frac{\tau_{ci}\,h_i^2}{2\,\eta} + \frac{K}{\eta}\left(\frac{1}{20}\acute{P}_i^3 h_i^5 + \frac{1}{2}\,h_i^2\tau_{ci}^3 + \frac{1}{4}\acute{P}_i^2 h_i^4\tau_{ci} + \frac{1}{2}\acute{P}_i\,h_i^3\tau_{ci}^2\right)$$

$$+ V_i\,h_i = Q_i$$

rearranging above equation leads to,

$$\left(\frac{Kh_i^5}{20\eta}\right) P_i'^3 + \left(\frac{Kh_i^4\tau_{ci}}{4\eta}\right) P_i'^2 + \left(\frac{h_i^3}{6\eta} + \frac{Kh_i^3\tau_{ci}^2}{2\eta}\right) P_i' + \left(V_i h_i + \frac{h_i^2\tau_{ci}}{2\eta}\right.$$

$$\left. + \frac{Kh_i^2\tau_{ci}^3}{2\eta} - Q_1\right) = 0 \qquad \text{.....(26)}$$

Equations (25) and (26) may be solved simultaneously in order to determine P_i' and τ_{ci} by iterating P_i' at point " i " in the deformation zone. Therefore,

$$P_i' = \frac{P_i - P_{i-1}}{\Delta x}$$

or

$$P_i = P_i' \Delta x + P_{i-1} \qquad \text{.....(27)}$$

Variation of speed of wire in the deformation zone may also be included in the analysis. The continuity of flow of metal through the strip (see figure 72(c)) gives;

$$(V + dV)\frac{\pi}{4}(D + dD) = \frac{\pi}{4} V D$$

rearranging and ignoring powers of dD gives;

$$2\frac{dD}{D} + \frac{dV}{V} + 2\frac{dV}{V}\frac{dD}{D} = 0$$

hence,

$$\frac{dV}{V} = -\frac{2\,dD}{D + 2\,dD}$$

re-writing this equation in finite difference form leads to;

$$\frac{V_{i-1} - V_i}{V_i} = - \frac{2 \left(D_{i-1} - D_i \right)}{D_i + 2 \left(D_{i-1} - D_i \right)}$$

or,

$$V_{i-1} = - \frac{2 \left(D_{i-1} - D_i \right)}{2 D_{i-1} - D_i} V_i + V_i$$

hence,

$$V_i = \frac{V_{i-1}}{1 - \left(\frac{2 \left(D_{i-1} - D_i \right)}{2 D_{i-1} - D_i} \right)} \qquad \text{.....(28)}$$

As mentioned before, the stress-strain relationship of the wire material has been shown to take the form,

$$Y = Y_o + K_o \epsilon^n$$

where $\epsilon = 2 \ln \frac{D_1}{D}$, therefore, (for small die angle)

$$Y = Y_o + K_o \left(2 \ln \frac{D_1}{D} \right)^n$$

This equation in finite difference form is,

$$Y_i = Y_o + K_o \left(2 \ln \frac{D_1}{D_i} \right)^n \qquad \text{.....(29)}$$

The strain rate sensitivity of the wire material may also be included in the analysis. The mean strain rate of the material over a small distance " dx " may be expressed as;

$$\bar{\dot{\epsilon}} = \left(-2 \frac{dD}{D} \right) \frac{1}{dt}$$

or,

$$\bar{\dot{\epsilon}}_{mi} = \frac{1}{x_i - x_{i-1}} \int_{D_{i-1}}^{D_i} \bar{\dot{\epsilon}} \, dx$$

where $x = x_{i-1}$ at $D = D_{i-1}$

and $x = x_i$ at $D = D_i$

hence substituting for $\bar{\dot{\epsilon}}$ gives;

$$\bar{\dot{\epsilon}}_{mi} = \frac{1}{\Delta x} \int_{D_{i-1}}^{D_i} -2 \frac{dD}{D} \frac{dx}{dt}$$

but $\frac{dx}{dt} = V_i$ therefore,

$$\bar{\dot{\epsilon}}_{mi} = - \frac{2V_i}{\Delta x} \int_{D_{i-1}}^{D_i} \frac{dD}{D}$$

Integration gives;

$$\dot{\epsilon}_{mi} = \frac{2V_i}{\Delta x} \ln\left(\frac{D_{i-1}}{D_i} \right) \qquad \text{.....(30)}$$

A flow rule of the form;

$$\frac{Y_d}{Y_s} = S = 1 + \left(\frac{\bar{\dot{\epsilon}}_m}{N}\right)^{1/T}$$

has been proposed (40), where Y_d is the dynamic yield stress and Y_s is the static yield stress of the material. Representing this equation in finite difference form gives;

$$S_i = 1 + \left(\frac{\bar{\dot{\epsilon}}_{mi}}{N}\right)^{1/T}$$

Combining this with equation (29) gives;

$$Y_i = S_i \left(Y_o + K_o \left(2\ln \frac{D_1}{D_i} \right)^n \right) \quad \ldots\ldots\ldots(31)$$

Equation (31) represents the yield stress of the wire, incorporating strain hardening and strain rate sensitivity of the material. Substituting for Y_i into equation (24) gives;

$$\sigma_{xi} = \frac{2\,(D_{i-1} - D_i)}{D_i} S_i \left(Y_o + K_o \left(2\ln \frac{D_1}{D_i} \right)^n \right) + \frac{4\,\tau_{ci}\,\Delta x}{D_i} + \sigma_{xi-1} \quad \ldots\ldots\ldots(32)$$

Also re-writing equation (23) in finite difference notation becomes;

$$P_i + \sigma_{xi} = Y_i \quad \ldots\ldots\ldots(33)$$

Solution procedure.

At any point " i " in the deformation zone, D_i , h_i and V_i may be calculated from equations (21), (22) and (28) respectively for an arbitrary value of B. Substituting values of D_i , h_i and V_i into equations (30) and (31), the yield stress Y_i may be calculated. Also by substituting V_i and h_i into equations (25) and (26) which give P_i' and τ_{ci} simultaneously by iterating for P_i' until equation (26) is satisfied. Hence substituting P_i' into equation (27) gives P_i . Similarly τ_{ci} , D_i and S_i may be substituted into equation (32) to evaluate σ_{xi} . Other variables in the above

equations are the known physical parameters.

Having calculated σ_{xi}, P_i and Y_i ,values of B may be iterated in the above equations until equation (33) is satisfied at point " i " in the deformation zone. This procedure may be repeated in suitable steps of Δx from the position of yield of the wire inside the stepped bore reduction unit where $i = X_1$, up to the step, where $i = l_1 - X_1$. It is assumed that the deformation of wire ceases at the step and validity of this assumption is shown in chapter 6 and also is discussed in chapter 7 . Therefore at the step, when equation (33) is satisfied, the drawing speed, final wire diameter and the coat thickness are given by;

drawing speed $V_d = V_i$

final wire diameter $D_2 = D_1$

coat thickness $h_3 = h_i - h_1 + h_2$

respectively. This analysis thus enables to predict pressure in the melt, stress in the wire and profile of the effective die in the deformation zone.

Condition of slip.

It is known that polymers have a critical shear stress at which slip occurs. It is assumed that slip takes place at the wire-polymer interface only and not at the unit wall-polymer interface. Boundary conditions for slip are;

at $y = h_1$ $U_1 = 0$

and at $y = 0$ $U_1 = V_s$

Therefore equation (8) becomes;;

$$Q_s = \frac{P_1' h_1^3}{6\eta} + \frac{h_1^2 \tau_{ca}}{2\eta} + \frac{K}{\eta}\left(\frac{1}{20} P_1'^3 h_1^5 + \frac{1}{2} h_1^2 \tau_{ca}^3 + \frac{1}{4} P_1'^2 h_1^4 \tau_{ca} + \frac{1}{2} P_1' h_1^3 \tau_{ca}^2 \right)$$

$$+ V_s h_1 \qquad \text{.....(34)}$$

V_s may be determined from no-slip conditions when τ_{ca} is reached the critical value. In references (20 to 25), the critical shear stress is shown to have values between 0.1 to 1.0 MN/m^2 for different polymer melts. When polypropylene polymer was being extruded at 200°C, evidence of slip was observed at about $3.2 \times 10^5 N/m^2$. Also critical shear stress for polyethylene polymer was shown by Westover (34) to take place at about $7 \times 10^5 N/m^2$. Therefore an average shear stress of $5 \times 10^5 N/m^2$ is assumed for the slip in the analysis.

Equation (34) shows that when slip occurs, flow of polymer remains constant and subsequently pressure and shear stress will also remain constant. Hence as drawing speed increases after slip, the reduction in area of the wire should progressively reduce. Equations governing the deformation zone are those derived previously, therefore they are only listed here;

$$D_i = D_{i-1} - B \Delta x \qquad \text{.....(35)}$$

$$h_i = h_{i-1} + \frac{1}{2} B \Delta x \qquad \text{.....(36)}$$

$$V_i = \frac{V_{i-1}}{1 - \left(\frac{2\,(D_{i-1} - D_i)}{2D_{i-1} - D_i} \right)} \qquad \ldots\ldots\ldots(37)$$

$$\bar{\dot{\epsilon}}_{mi} = \frac{2V_i}{\Delta x} \ln \left(\frac{D_{i-1}}{D_i} \right) \qquad \ldots\ldots\ldots(38)$$

$$S_i = 1 + \left(\frac{\bar{\dot{\epsilon}}_{mi}}{N} \right)^{1/T} \qquad \ldots\ldots\ldots(39)$$

$$Y_i = S_i \left(Y_o + K_o \left(2 \ln \frac{D_1}{D_i} \right)^n \right) \qquad \ldots\ldots\ldots(40)$$

$$\sigma_{xi} = 2 \left(\frac{D_{i-1} - D_i}{D_i} \right) S_i \left(Y_o + K_o \left(2 \ln \frac{D_1}{D_i} \right)^n \right) + \frac{4 \tau_{ca} \Delta x}{D_i} + \sigma_{xi-1}$$

$$\ldots\ldots\ldots(41)$$

The procedure for the solution is the same as before. The only exception is that P_i remains constant for every speed increment after the slip. For a suitable step of Δx and an arbitrary value of B, D_i, h_i and V_i may be calculated from equations (35), (36) and (37) respectively. Substituting D_i and V_i into equation (38) gives $\bar{\dot{\epsilon}}_{mi}$ and equation (39) gives S_i . Substituting S_i and D_i into equations (40) and (41), Y_i and σ_{xi} may be calculated. Having calculated Y_i and σ_{xi}, numerical values of B may be iterated in above equations until equation $P_i + \sigma_{xi} = Y_i$ is satisfied. This procedure may be repeated at Δx intervals in the deformation zone from $i = X_1$ upto the step where $i = l_1 - X_1$.

A computer programme was written to solve the relevant equations, the flow chart and listing of which are given in Appendix 4. Results from the analysis are provided in chapter 6.

CHAPTER 6: Results From The Analysis.

6.1- Introduction.

6.2- Theoretical Percentage Reduction In Area.

6.3- Theoretical Coating Thickness.

6.4- Theoretical Yielding Position Of The Wire.

6.5- Theoretical Pressure.

6.6- Theoretical Shear Stress On The Wire.

6.7- Theoretical Stress In The Wire.

6.8- Theoretical Deformation Profile.

6.1- Introduction

A computer programme was written utilizing iteration techniques and finite difference method (based on backward difference) to solve the equations simultaneously. Developments and listing of the computer programme is provided in Appendix 4. Since all the equations were dependent upon speed, they were solved for speeds varying from 0.1 m/s to 4.0 m/s and at 0.1 m/s intervals. Also the equations governing the deformation zone were solved at steps of Δx = 1mm for every speed increment from the position of yield up to the step in the unit where it is assumed that the deformation of wire ceases.

The data below are the known parameters which were used to solve the equations and were varied to show their effect on the performance of the unit.

i)- Dimensions of the stepped bore reduction unit;

$h_1 = 0.0002$ m

$h_2 = 0.00005$ m

$l_1 = 0.05$ m

$l_2 = 0.02$ m

$h_1/h_2 = 4.0$

$l_1/l_2 = 2.5$

ii)- Data for polymer;

$\eta = 110$ NS/m^2

$K = 5 \times 10^{-11}$ m^4/N^2

$a = 120000\ N/m^2$

$b = 4 \times 10^{-11}\ m^2/N$

$\tau_{ca} = 5 \times 10^{5}\ N/m^2$

iii)- Data for copper wire;

$Y_o = 0.5 \times 10^{8}\ N/m^2$

$K_o = 4.4 \times 10^{8}\ N/m^2$

$n = 0.52$

$N = 55000$

$T = 3.8$

$D_1 = 0.0016\ m$

Results from the analysis were obtained in tabulated forms and are represented in graphical forms for convenience.

6.2- Theoretical Percentage Reduction In Area

Figure 73 shows the variations of the percentage reduction in area with drawing speed, comparing the Newtonian and the non-Newtonian solutions. The non-Newtonian solution (I) represents the effect of shear rate on viscosity alone and the non-Newtonian solution (II) represents the combined effect of shear rate and pressure on the viscosity.

The Newtonian solution appeared to estimate higher percentage reduction in area compared to those from the other two solutions. The inclusion of the strain rate sensitivity into the solution made little effect in the

final results.

The non-Newtonian solution (I) commenced from zero at about 0.1 m/s and the predicted percentage reduction in area increased as the drawing speed was increased. The theoretical results were significantly reduced when the strain rate sensitivity of the wire material was included into the analysis. This effect became higher as the drawing speed was increased. Note that the speed at which slip was predicted reduced when the strain rate sensitivity was included in the analysis.

The non-Newtonian solution (II) generally predicted higher percentage reduction in area than those of solution (I) and also introduced slip at slower speeds. The inclusion of the strain rate sensitivity into the analysis again reduced the theoretical results. This theory produced results that showed closer trends to those of the experimental results.

Figures 74 to 86 show the theoretical percentage reduction in area when the input data were varied. These results are presented in three parts as follows;

i)- The effect of the dimensional changes of the unit.

The effect of the dimensional changes in the theoretical results are shown in figures 74 and 75. Different values of gap ratios (h_1/h_2) and length ratios (l_1/l_2) were fed into the equations to show their effect on the predicted percentage reduction in area.

Figure 74 shows the effect of the gap ratio on variations of the percentage reduction in area versus

drawing speed. In order to produce these results h_1 remained constant whilst h_2 was varied. As the gap ratio was increased, the predicted percentage reduction in area also increased and the critical shear stress occured at slower drawing speeds.

The effect of the length ratio on the predicted percentage reduction in area are shown in figure 75. It has been observed experimentally that, the deformation of wire takes place in the first part of the unit, therefore l_2 was kept constant and l_1 was changed to obtain the theoretical results for different length ratios. The results of percentage reduction in area showed similar trends to those of figure 74 ie the higher the length ratio, the higher the deformation of the wire.

ii)-The effect of the polymer material.

Theoretical effect of changing the parameters representing the polymer melt rheology are shown in figures 76 to 80. The effect of temperature in the viscosity of polymer melt was not included in the analysis, therefore the initial viscosity was varied which is assumed to have the effect of temperature change.

Figure 76 shows the theoretical effect of changing the initial viscosity of polymer melt on the percentage reduction in area. An increase in the viscosity caused the percentage reduction in area to increase and also introduced slip at slower drawing speeds.

The theoretical effect of changing shear stress

constant "K" is shown in figure 77 where the percentage reduction in area is shown to increase as "K" was reduced. Also as the result of increase in shear stress constant, the cririical shear stress was predicted to occur at slower drawing speeds. When K = 0, deformation of wire commenced at about 0.1 m/s and rapidly reached to 25% reduction in area at about 0.5 m/s.

Figure 78 shows the effect of the critical shear stress on the predicted percentage reduction in area. A small increase in the magnitude of the limiting shear stress appeared to have a substantial effect on the results. The higher the critical shear stress, the higher the percentage reduction in area before slip takes place. Note that in this case the results followed the same curve before the critical shear stress was reached.

The effect of the viscosity constant on the percentage reduction in area is shown in figure 79. The increase in "a" predicted higher deformation in the wire and note that a large increase in "a" was necessary to introduce a noticeable change in the theoretical results.

Figure 80 shows the effect of the coefficient of pressure on viscosity of polymer melts. Higher values of "b" predicted higher percentage reduction in area. When $b = 6 \times 10^{-11} m^2/N$, slip was shown to occur at very slow drawing speeds and higher results were predicted over the entire range of speed.

iii)- The effect of the wire material.

The yield characteristics of the wire materials were

determined when small samples of the wires were subjected to compression tests. These variables were used in the analysis to investigate their effects on the performance of the stepped bore reduction unit.

Figure 81 shows the theoretical effect of changing the initial yield stress of the wire. The wire material was assumed to act rigidly prior to the deformation. The smaller the initial yield stress, the higher the percentage reduction in area.

The effect of the strain hardening constant on the percentage reduction in area is shown in figure 82. The trends and magnitudes of the theoretical results were found to be similar to those of figure 81.

Figure 83 shows the effect of the strain hardening index on the percentage reduction in area. Higher values of "n" predicted higher deformations.

Figure 84 shows the theoretical effect of changing the strain rate sensitivity constant on the variations of percentage reduction in area. As value of "N" was increased, the predicted reduction in area also increased. Note that a large change in this parameter is necessary to produce a noticeable change in the results.

Variations of the percentage reduction in area due to theoretical effect of changing the strain rate sensitivity index are shown in figure 85. Reduction in "T" predicted smaller deformation in the wire.

The theoretical effect of change in the wire diameter is shown in figure 86. The smaller the wire diameter, the higher the percentage reduction in area.

FIG73: COMPARISON BETWEEN THEORETICAL SOLUTIONS PREDICTING PERCENTAGE REDUCTION IN AREA

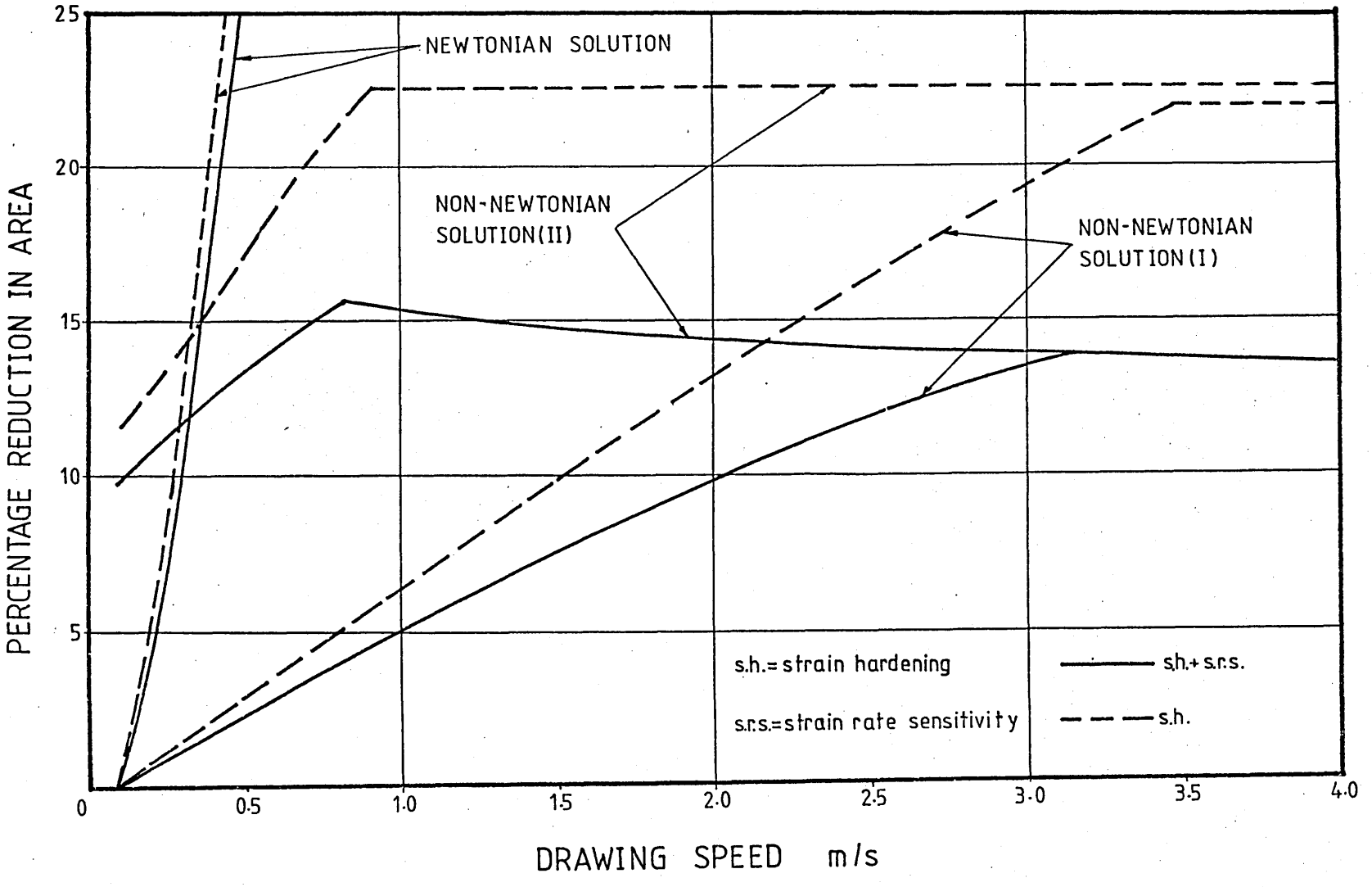

FIG74 : THEORETICAL EFFECT OF GAP RATIO ON PERCENTAGE REDUCTION IN AREA

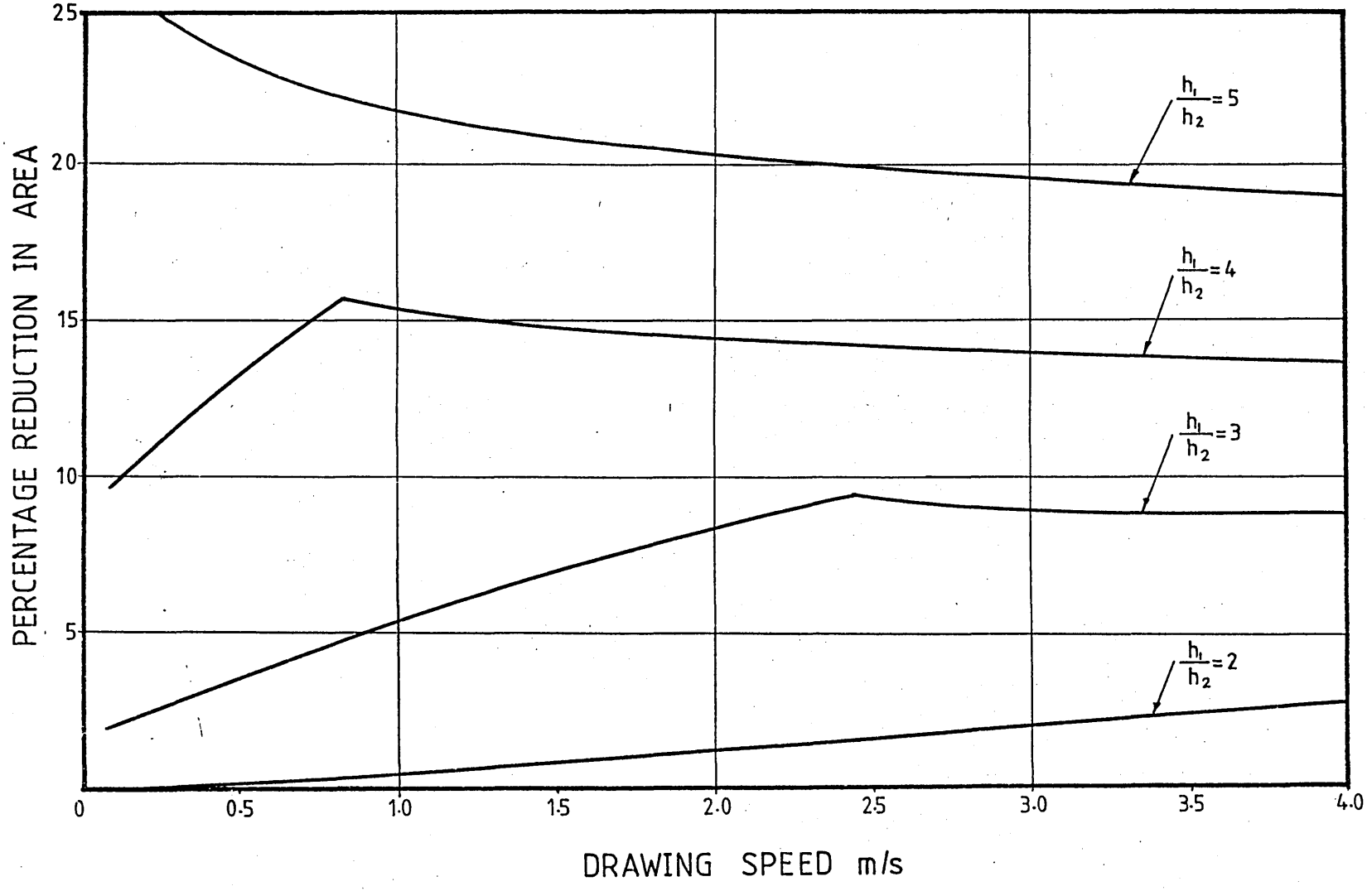

FIG75: THEORETICAL EFFECT OF LENGTH RATIO ON PERCENTAGE REDUCTION IN AREA

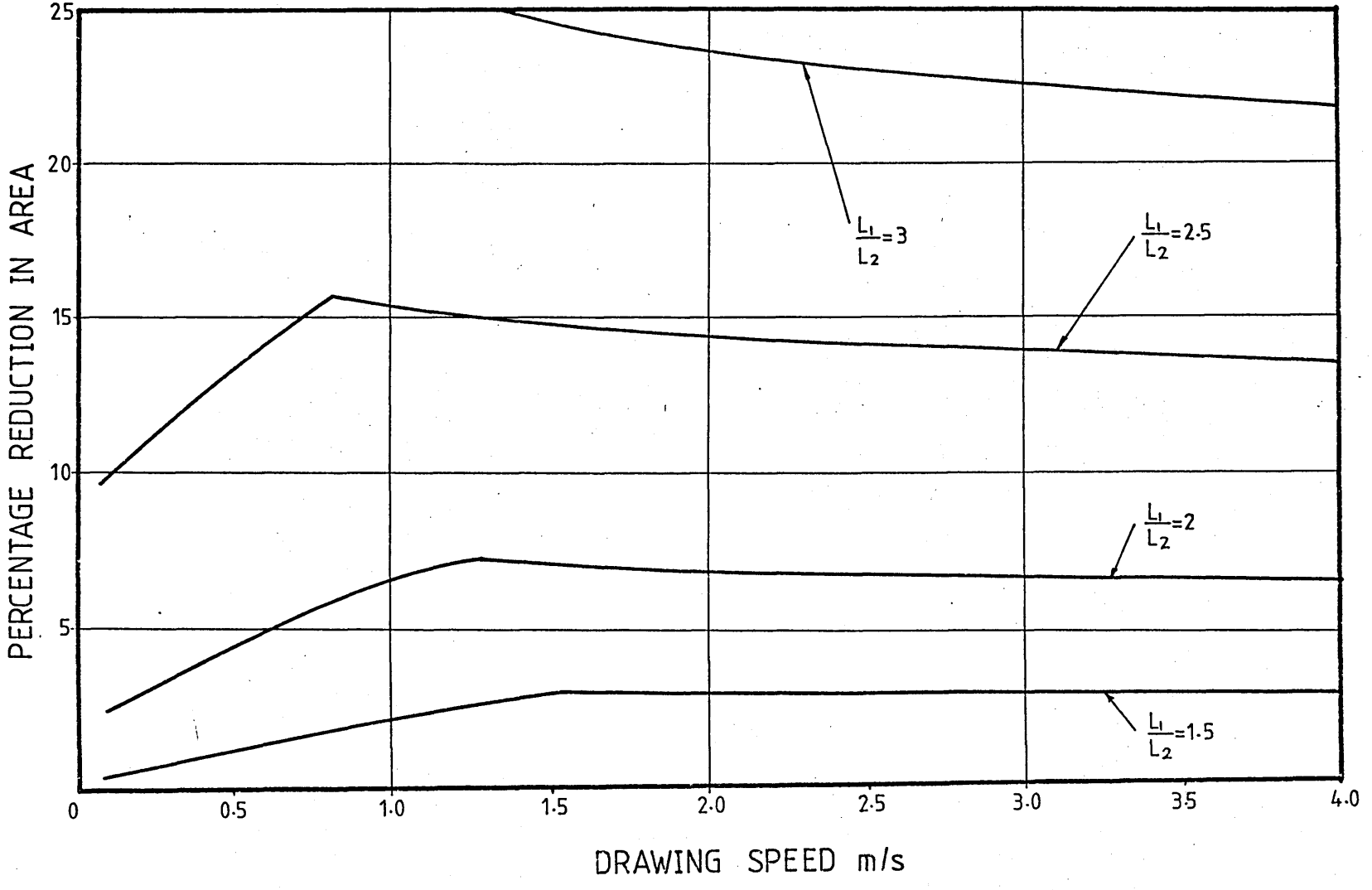

FIG76: THORETICAL EFFECT OF INITIAL VISCOSITY ON PERCENTAGE REDUCTION IN AREA

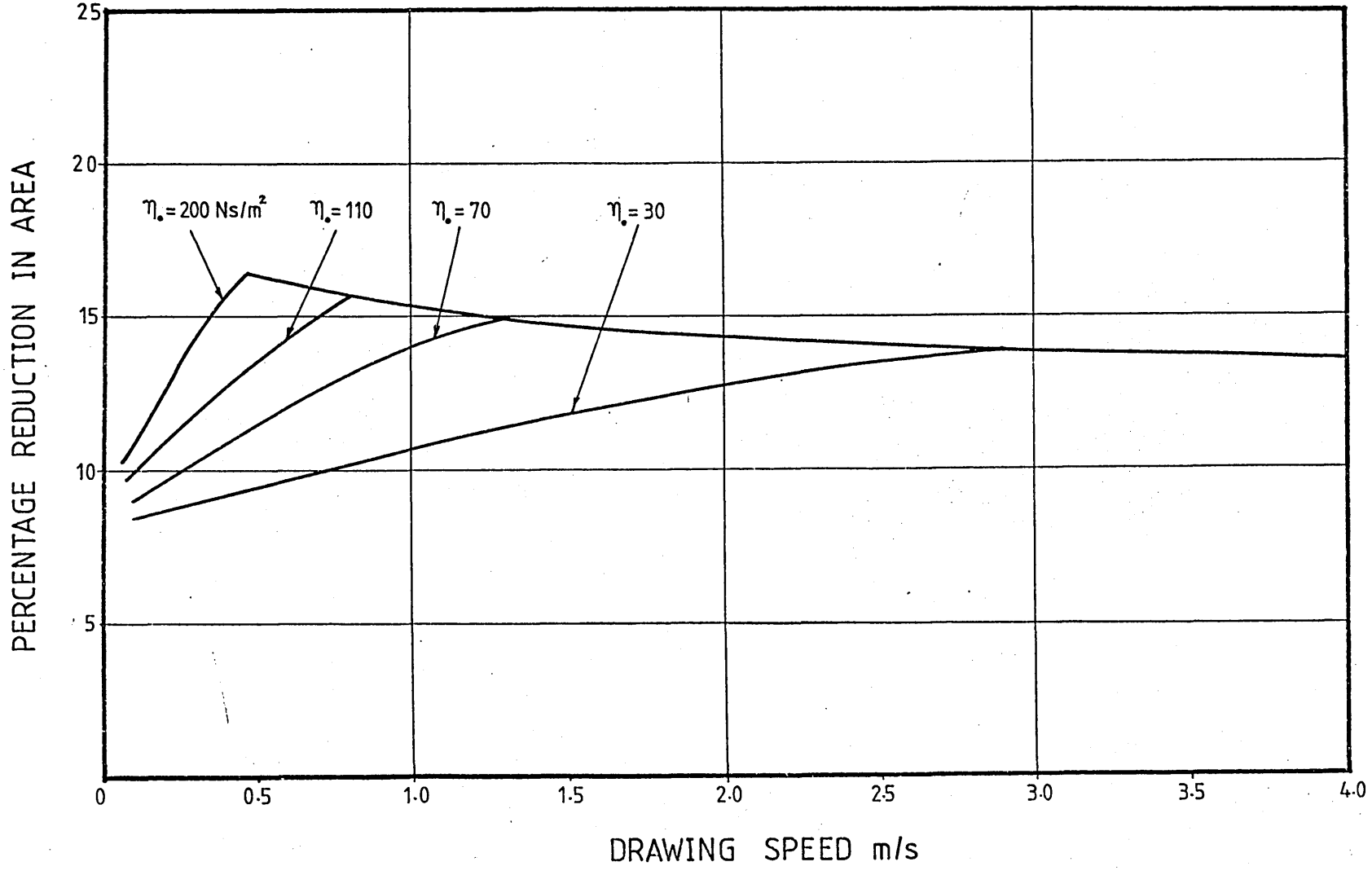

FIG77: THEORETICAL EFFECT OF SHEAR STRESS CONST. ON PERCENTAGE REDUCTION IN AREA

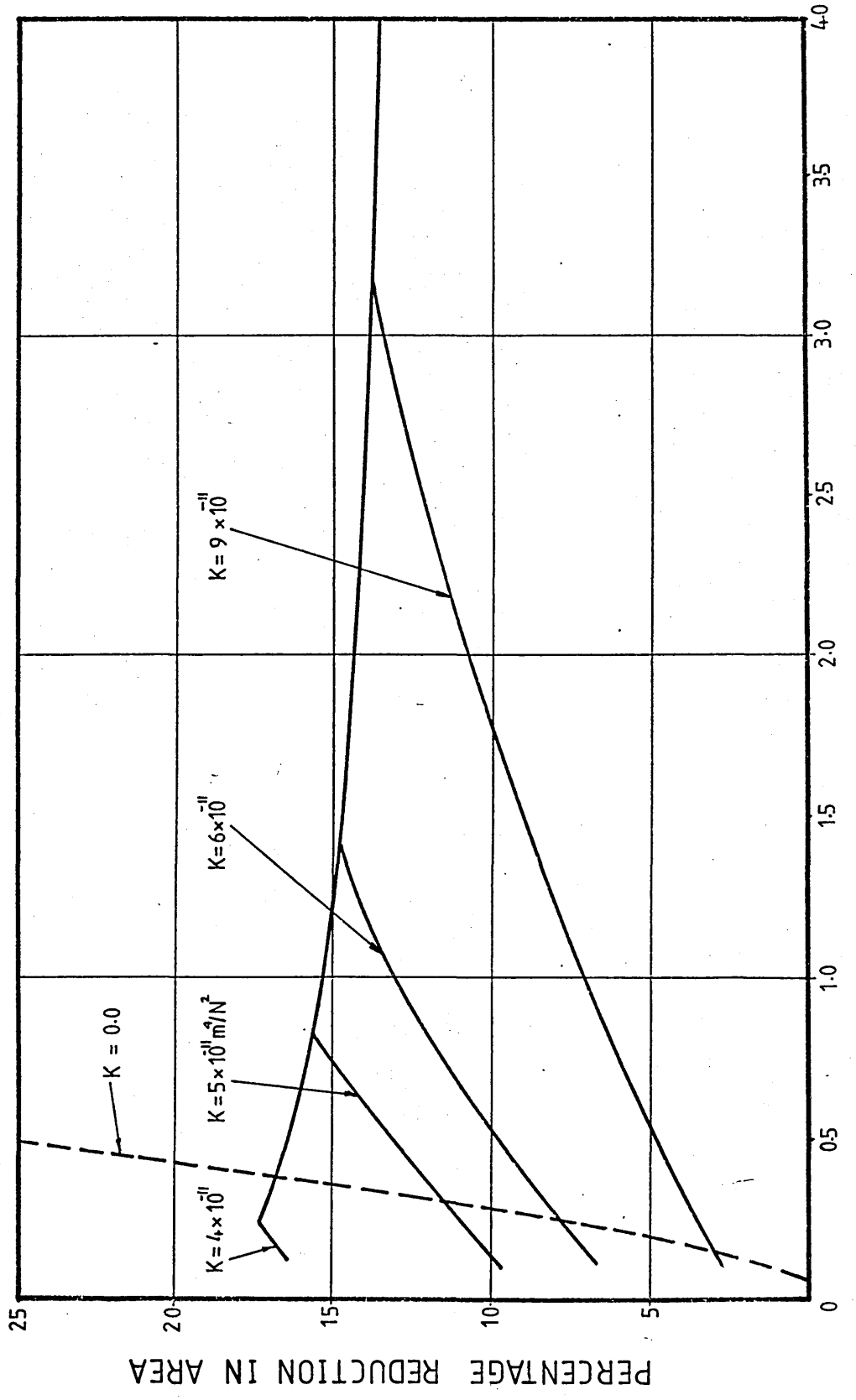

FIG78: THEORETICAL EFFECT OF CRITICAL SHEAR STRESS ON PERCENTAGE REDUCTION IN AREA

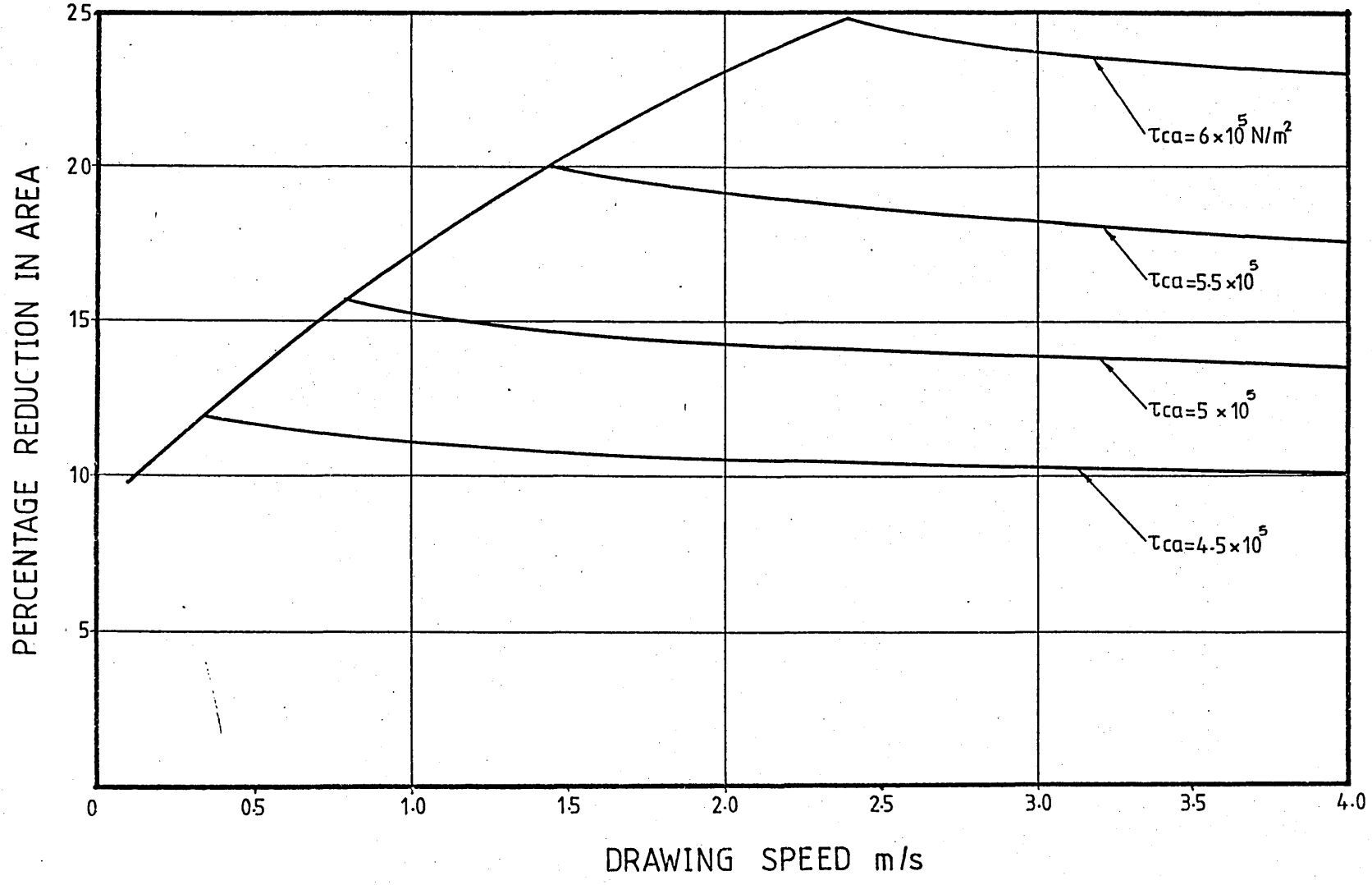

FIG 79 : THEORETICAL EFFECT OF VISCOSITY CONSTANT ON PERCENTAGE REDUCTION IN AREA

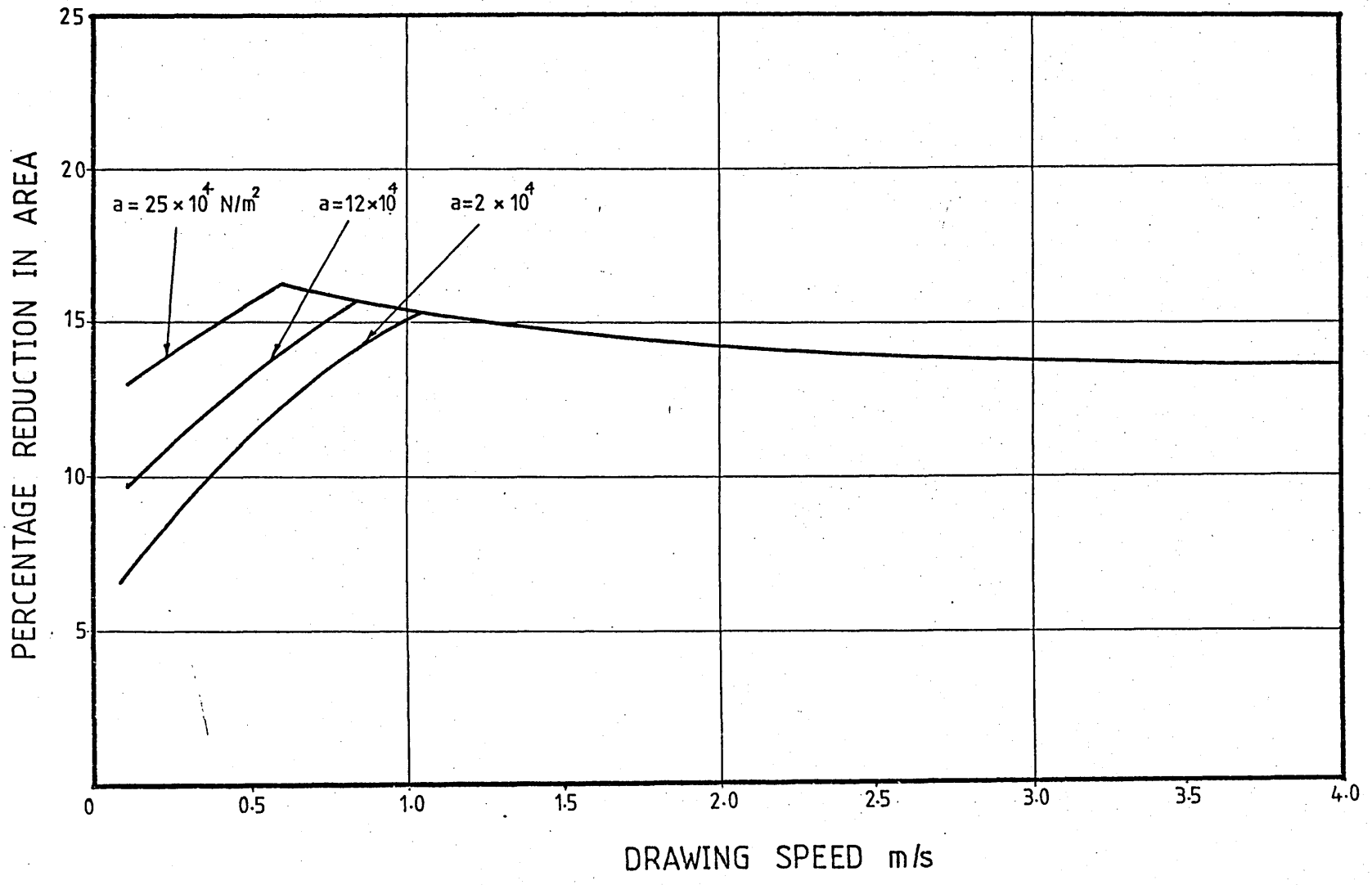

FIG80 : THEORETICAL EFFECT OF PRESSURE COEFFICINT OF VISCOSITY ON PERCENTAGE REDUCTION IN AREA

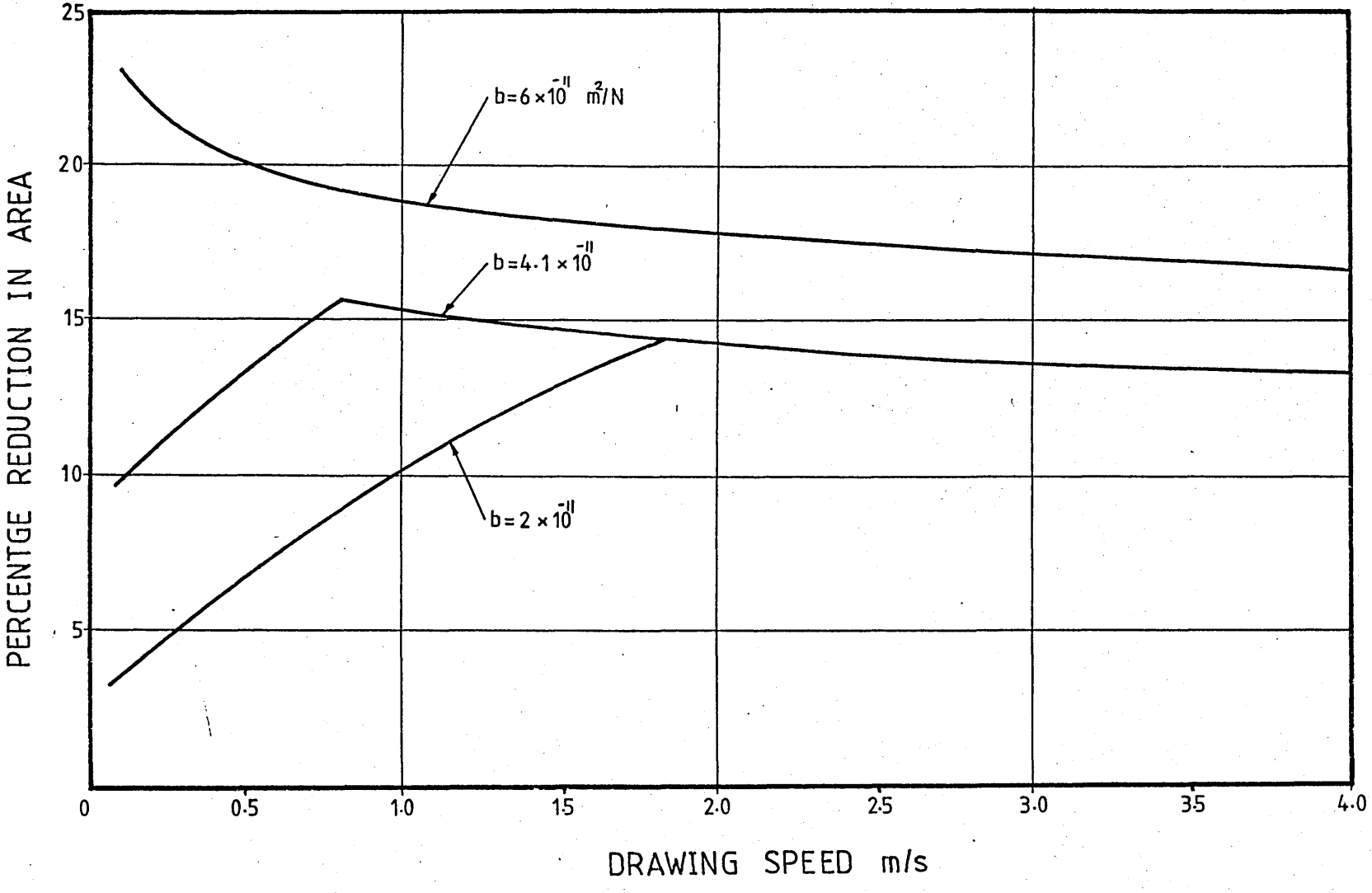

FIG81 : THEORETICAL EFFECT OF INITIAL YIELD STRESS ON PERCENTAGE REDUCTION IN AREA

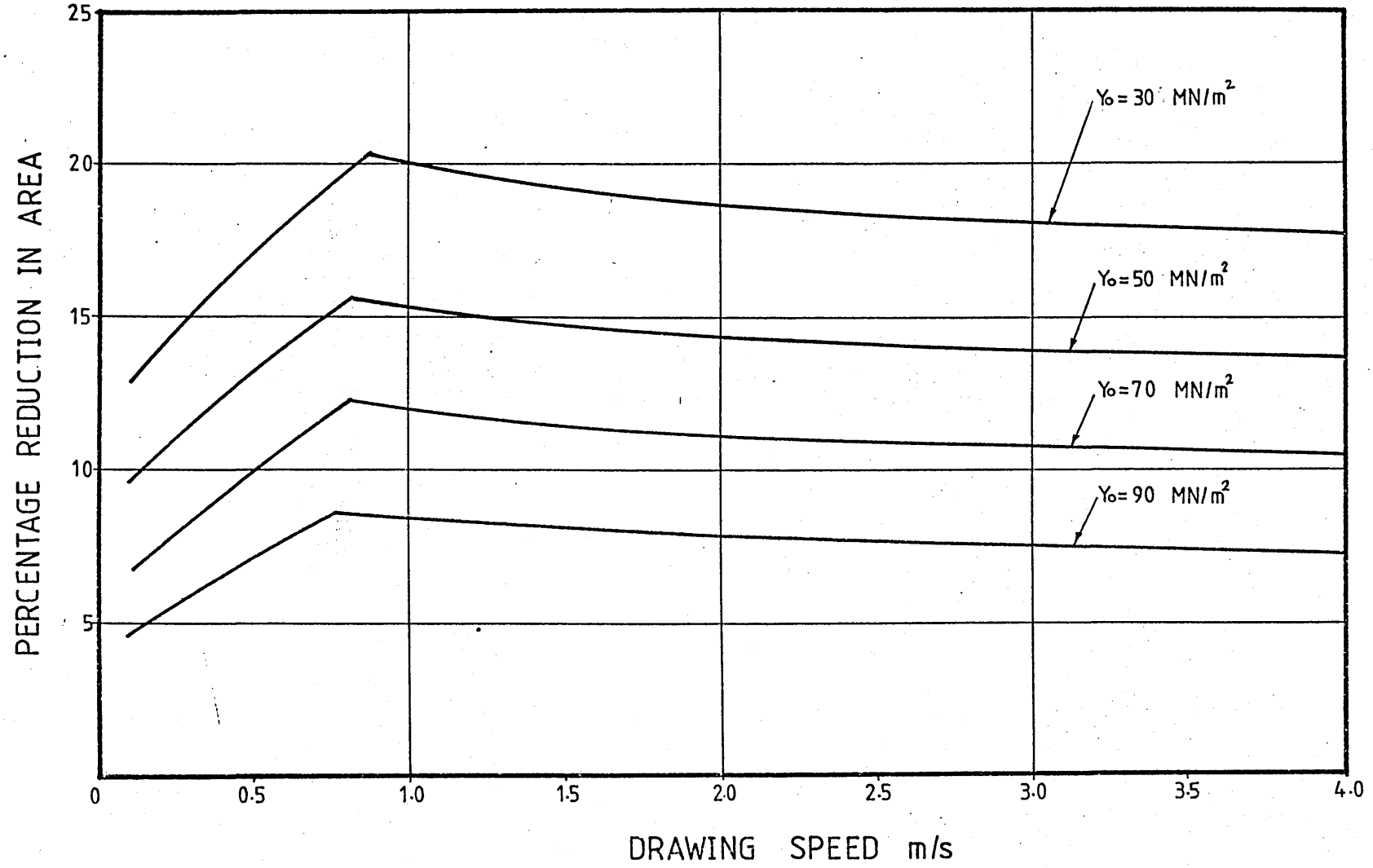

FIG82: THEORETICAL EFFECT OF STRAIN HARDENING CONST. ON PERCENTAGE REDUCTION IN AREA

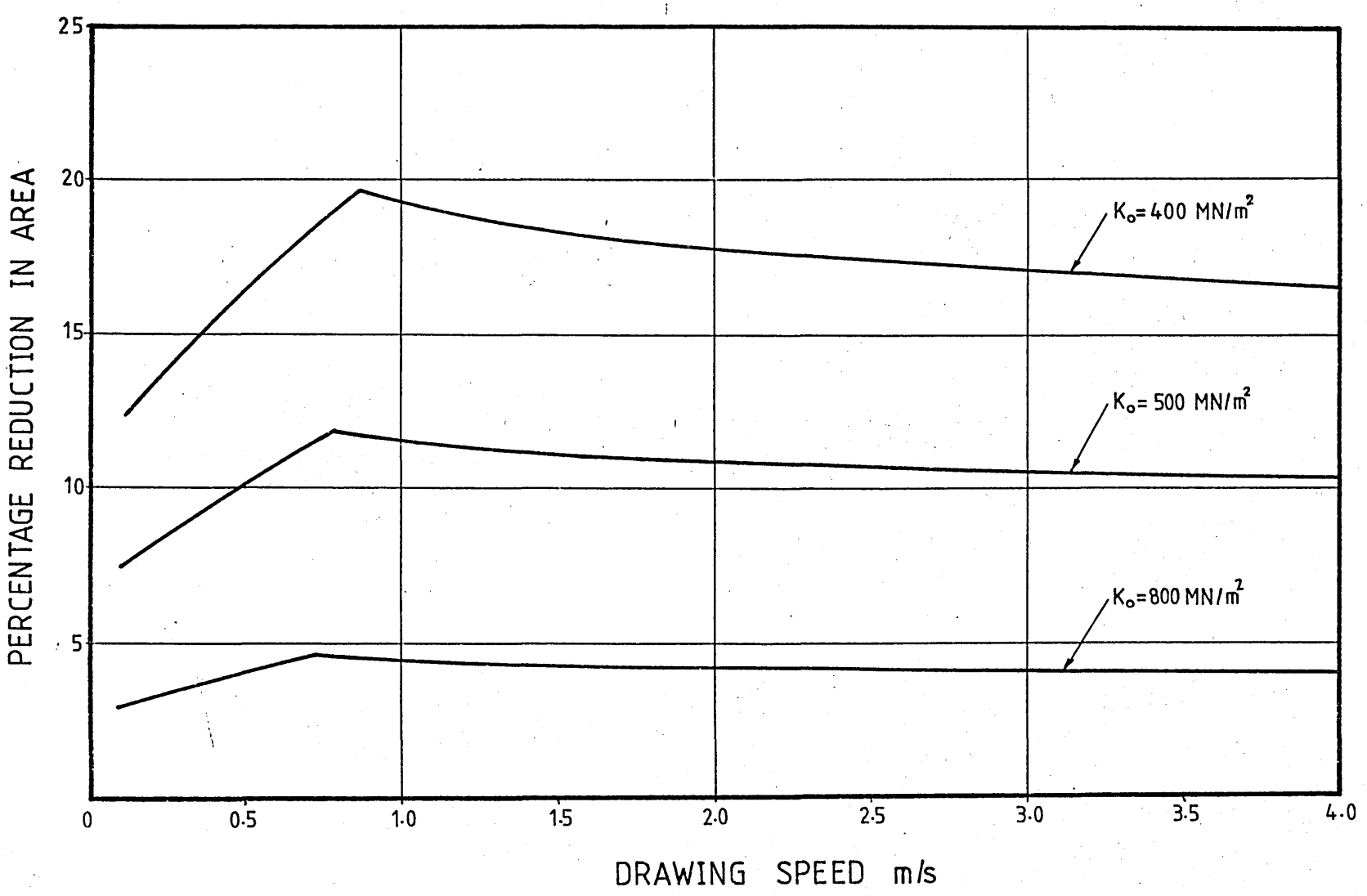

FIG83: THEORETICAL EFFECT OF STRAIN HARDENING INDEX ON PERCENTAGE REDUCTION IN AREA

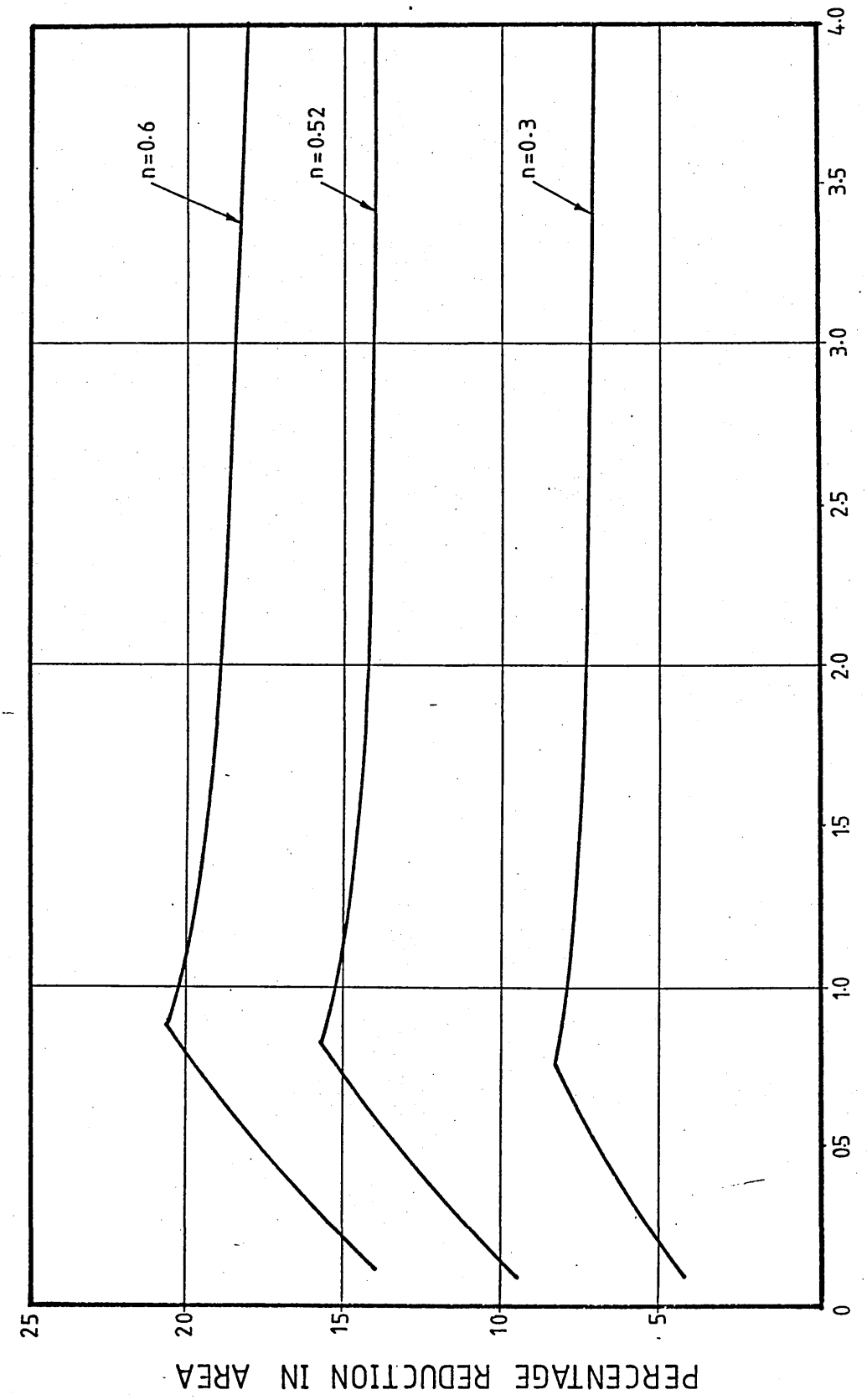

FIG84: THEORETICAL EFFECT OF STRAIN RATE SENSITIVITY CONST. ON PERCENTAGE REDUCTION IN AREA

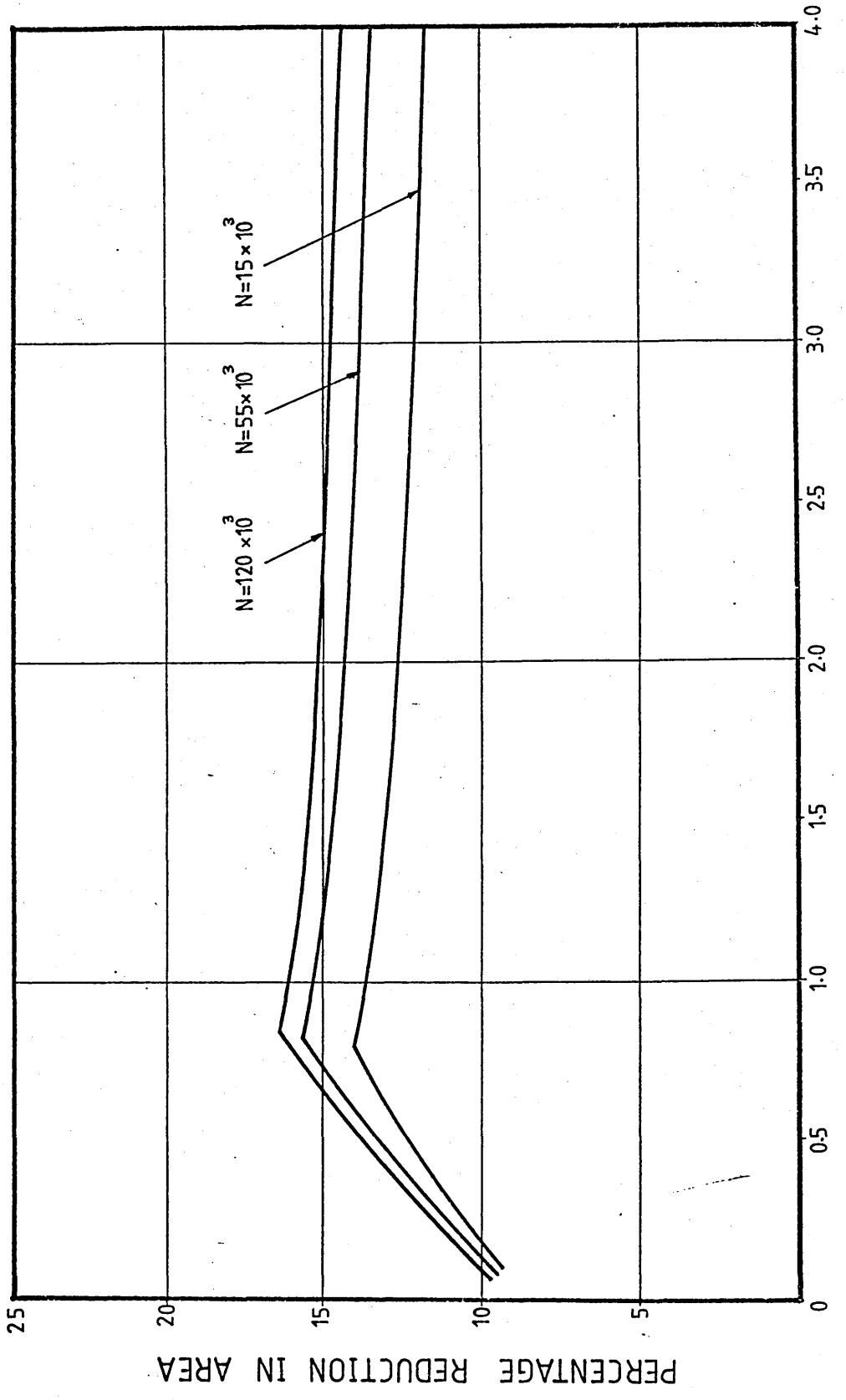

FIG85: THEORETICAL EFFECT OF STRAIN RATE SENSITIVITY INDEX ON PERCENTAGE REDUCTION IN AREA

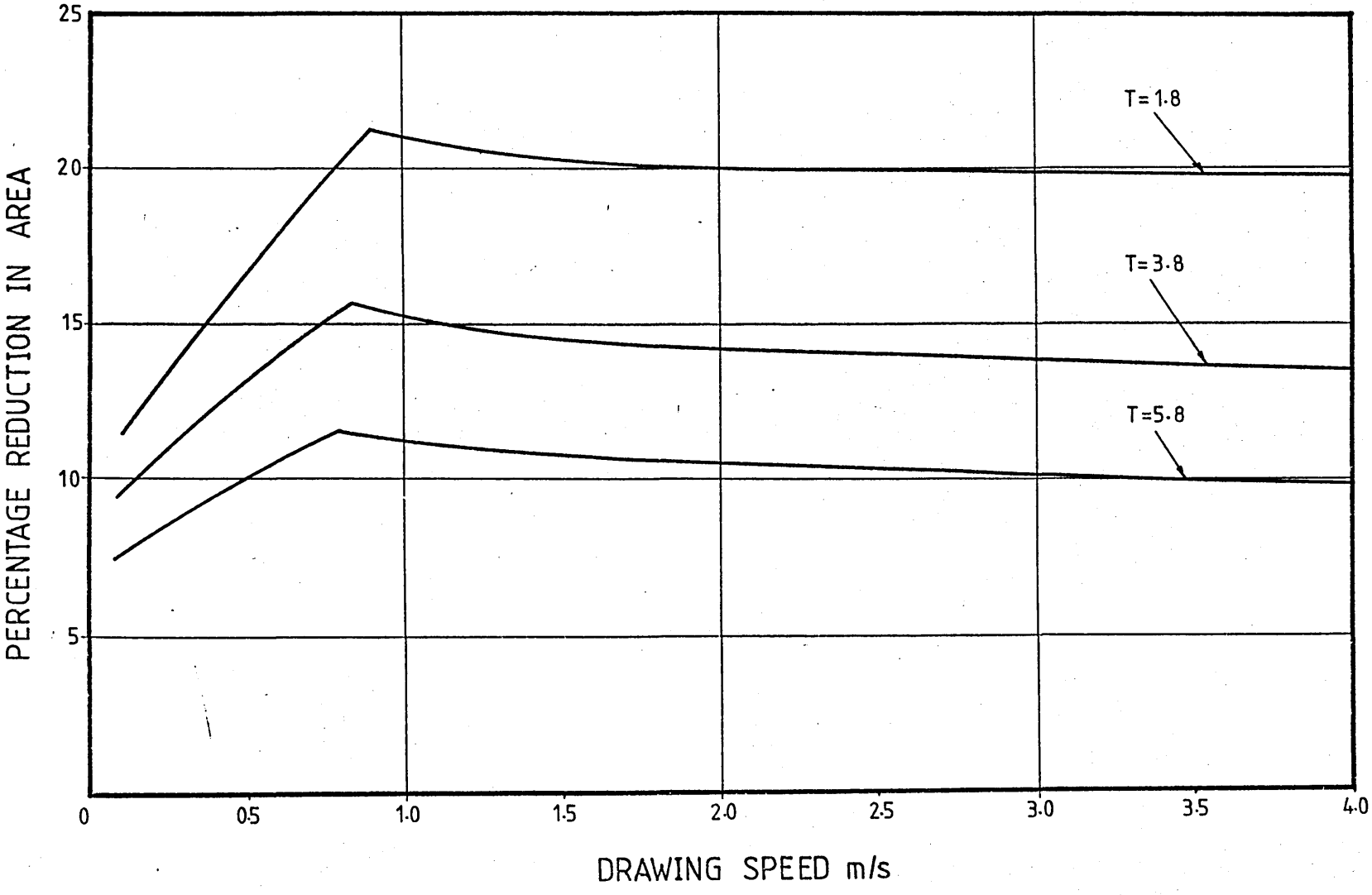

FIG86 : THEORETICAL EFFECT OF WIRE DIAMETER ON PERCENTAGE REDUCTION IN AREA

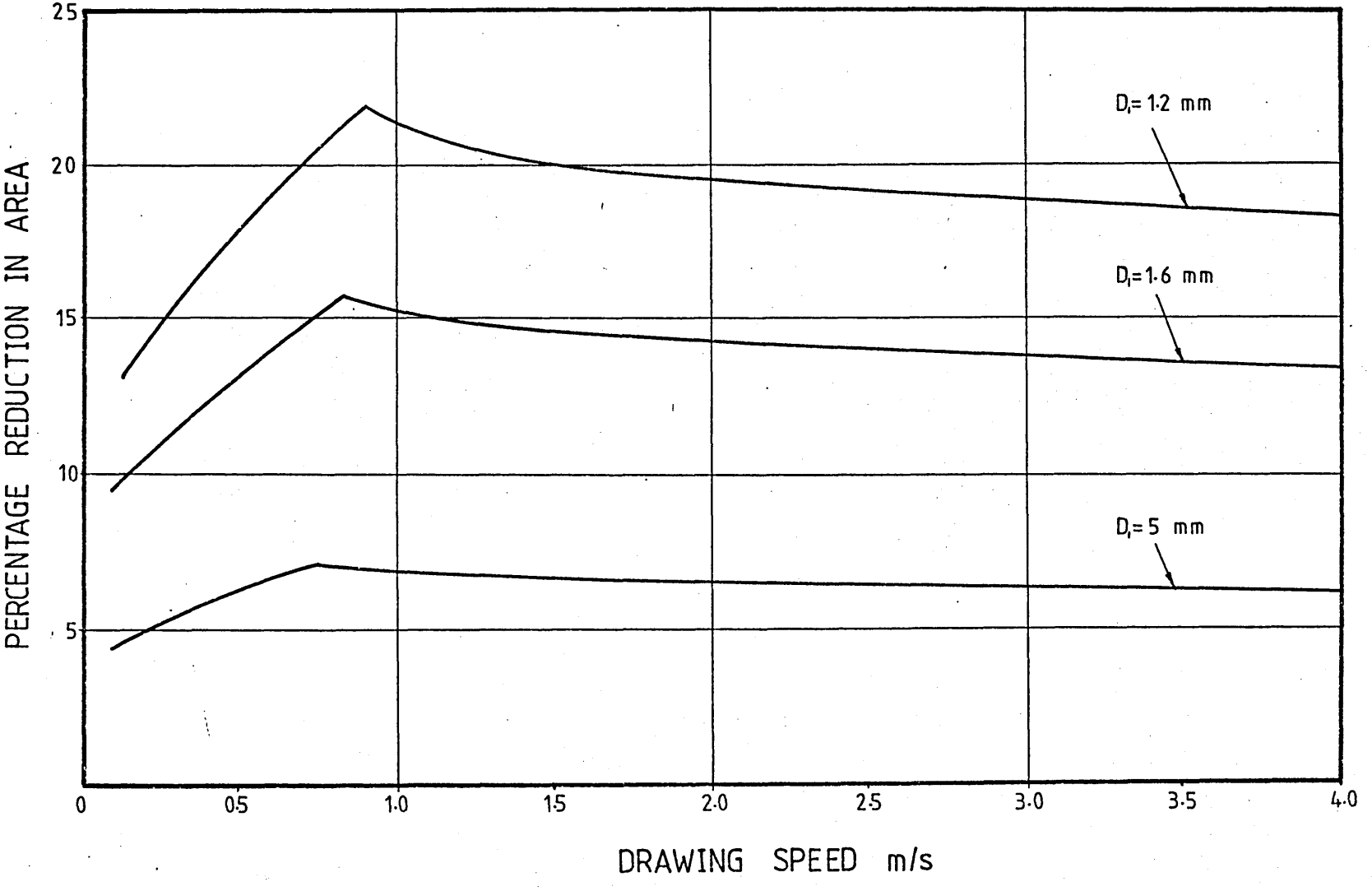

6.3- Theoretical Coating Thickness

Results of the coating thickness exhibited similar trends to those of the percentage reduction in area. This similarity was also observed in the experimental results. Figure 87 shows the variations of the coating thickness versus speed, comparing the Newtonian and the non-Newtonian solutions. The non-Newtonian solution (I) presents the effect of the shear stress on the viscosity and the non-Newtonian solution (II) shows the combined effects of the shear stress and the coefficient of pressure on the viscosity.

The Newtonian solution generally predicted thicker coatings at slower drawing speeds. The effect of strain rate sensitivity introduced little change in the theoretical results.

The non-Newtonian solution (I) shared the same starting point as the Newtonian solution (coat thickness = 0.05mm) and gradually increased as drawing speed was increased. The inclusion of the strain rate sensitivity in the solution, as was observed for the percentage reduction in area, reduced the theoretical results and again this effect became more pronounced at higher drawing speeds.

The non-Newtonian solution (II) predicted higher coating thickness and also showed that critical shear stress took place at slower speeds compared to the non-Newtonian solution (I). The inclusion of the strain rate sensitivity in this solution reduced the theoretical results.

Figures 88 to 100 show the coating thickness predicted when the input data were varied individually and the results are represented in three parts as follows;

i)- The effect of the dimensional changes of the unit.

Dimensions of the stepped bore reduction unit were varied in terms of gap ratios (h_1/h_2) and length ratios (l_1/l_2). Figure 88 shows the effect of the length ratio on the coating thickness. To introduce different length ratios, l_2 was kept constant. These results show that as the length ratio was increased, the coat thickness also increased and the critical shear stress was predicted to occur earlier.

Figure 89 shows the effect of the gap ratio on the coating thickness. Results showed similar trends to those of figure 88. Note that h_1 was kept constant for each gap ratio.

ii)- The effect of the polymer rheology.

Variables presenting the flow characteristics of the polymer melt were determined experimentally using an extrusion rheometer. These parameters were used to investigate the performance of the unit and the results are shown in figures 90 to 94.

Figure 90 shows the effect of the initial viscosity. This effect is equivalent to the temperature change. These results show that as the initial viscosity was increased, the coating thickness increased. At higher drawing speeds

this effect seemed to disappear.

Figure 91 shows the effect of the shear stress constant "K" on the coating thickness. As the value of "K" was reduced, the coating thickness increased and slip occured earlier. Note that the Newtonian solution, unlike other results, shows a sharp increase in coat thickness.

The effect of the critical shear stress on the coating thickness is shown in figure 92. The theoretical results show that as the critical shear stress was increased, the predicted coating thickness also increased before slip occured.

Figure 93 shows the theoretical effect of changing the viscosity constant "a" on the coating thickness of the wire. As value of "a" was increased, the predicted coating thickness increased. Note that like the results obtained for the percentage reduction in area, a large increase in "a" was necessary for a noticeable increase in the coating thickness.

Figure 94 shows the variations of the coating thickness due to the effect of the pressure on the viscosity of the polymer melt.As value of "b" was increased, the predicted coating thickness increased and when $b = 6 \times 10^{-11}$ m^2/N, greater coat thickness was predicted for the entire range of speed.

iii)- The effect of the wire material.

These variables represent the yield characteristics of the wire material which were estimated expirimentally. Variations in coat thickness due to effect of these

parameters are shown in figures 95 to 100..

Figure 95 shows the effect of the initial yield stress of the wire on the predicted coat thickness. In the analysis it was assumed that the wire material was a rigid body before yielding commenced. These results showed that as the initial yield stress was increased, the predicted coat thickness decreased.

Figure 96 shows the effect of the strain hardening constant on the coating thickness. Similar results to those of figure 95 were produced. The effect of the strain hardening index on the coating thickness is shown in figure 97. As the values of "n" were increased, the theoretical coating thickness also increased.

The effect of the strain rate sensitivity constant on the coating thickness is shown in figure 98. An increase in "N" caused the coating thickness to increase. Note that a large increase in the strain rate sensitivity constant was necessary to introduce a noticeable increase in the theoretical coat thickness. Figure 99 shows the effect of the strain rate sensitivity index on the coating thickness. The higher the value of "T", the thinner the coating thickness.

Figure 100 shows the effect of the wire diameter on the coating thickness. These results are in reverse order compared to the corresponding results of the percentage reduction in area (see figure 86). The higher the wire diameter, the thicker the predicted coating on the wire.

FIG87: COMPARISON BETWEEN THEORETICAL SOLUTIONS PREDICTING COATING THICKNESS

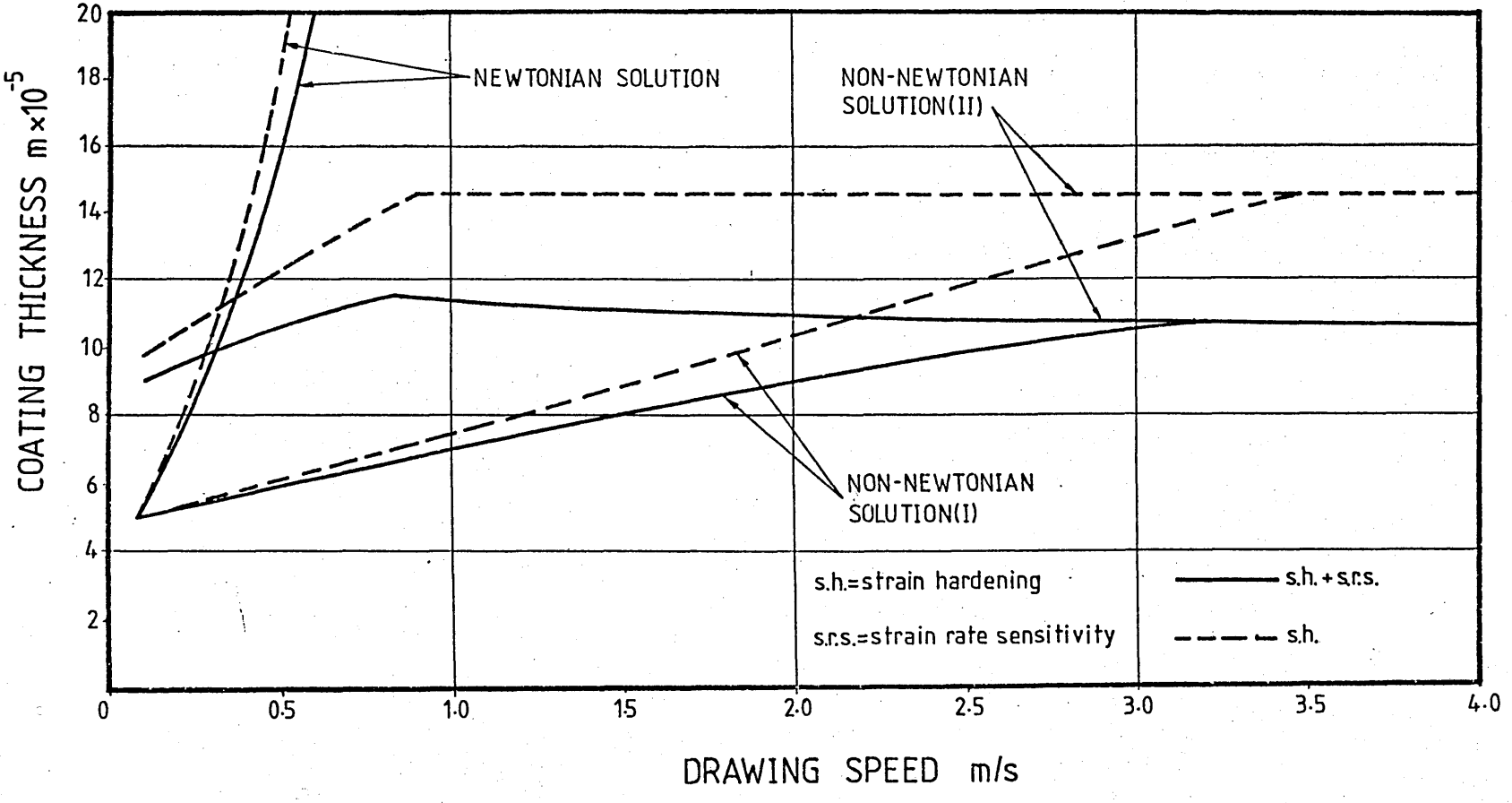

FIG88 : THEORETICAL EFFECT OF LENGTH RATIO ON COATING THICKNESS

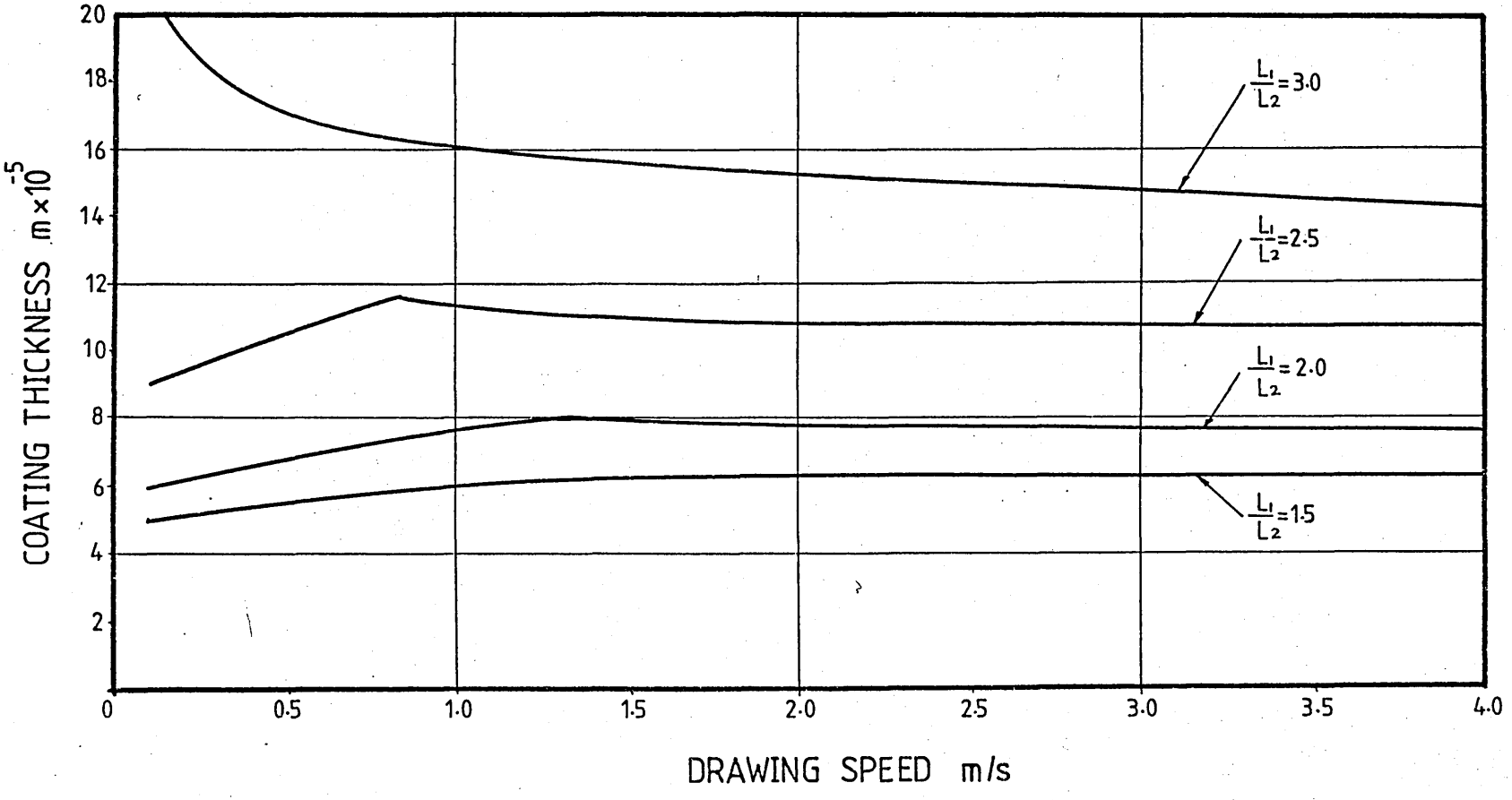

FIG89 : THEORETICAL EFFECT OF GAP RATIO ON COATING THICKNESS

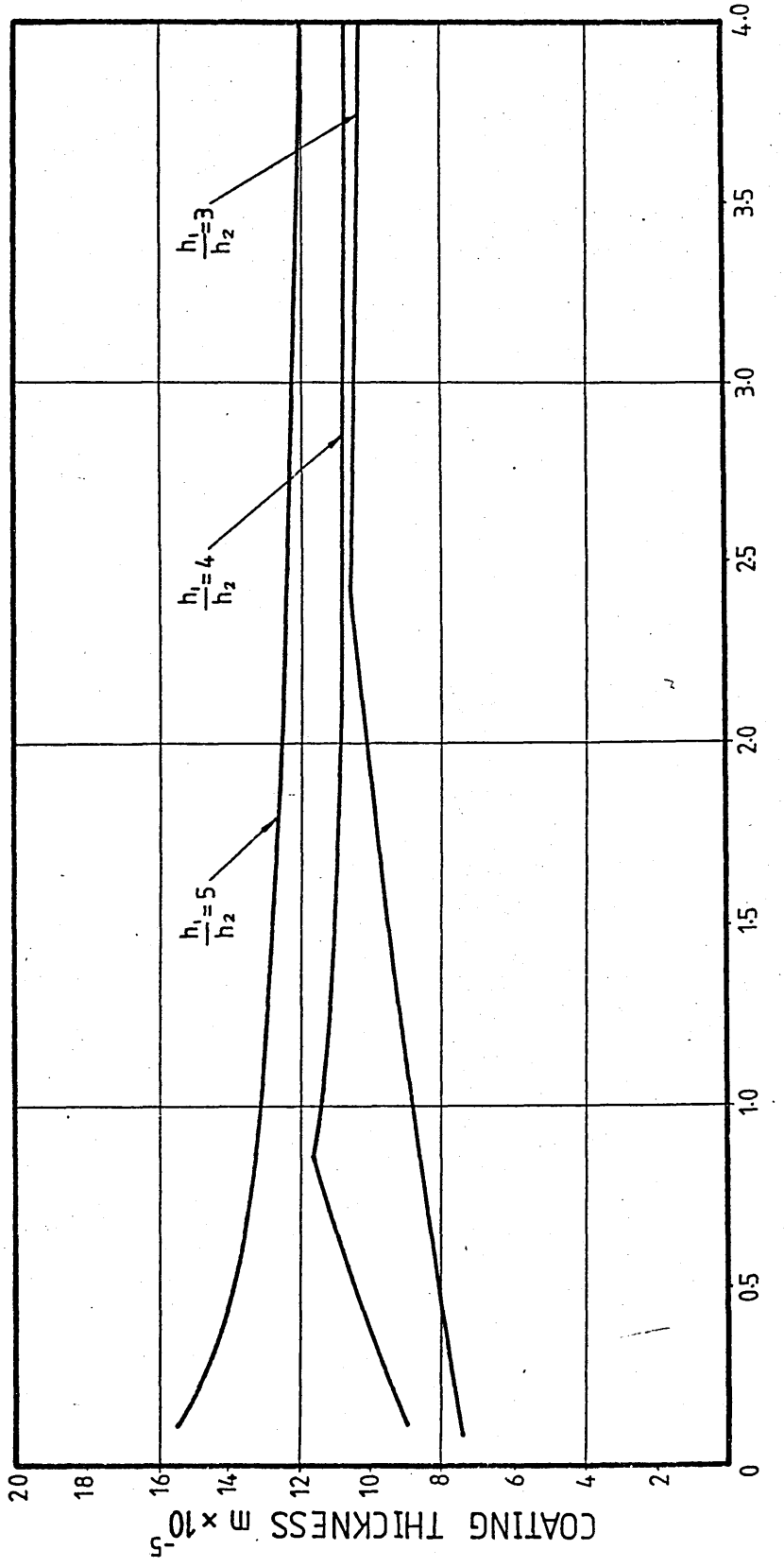

FIG90 : THEORETICAL EFFECT OF INITIAL VISCOSITY ON COATING THICKNESS

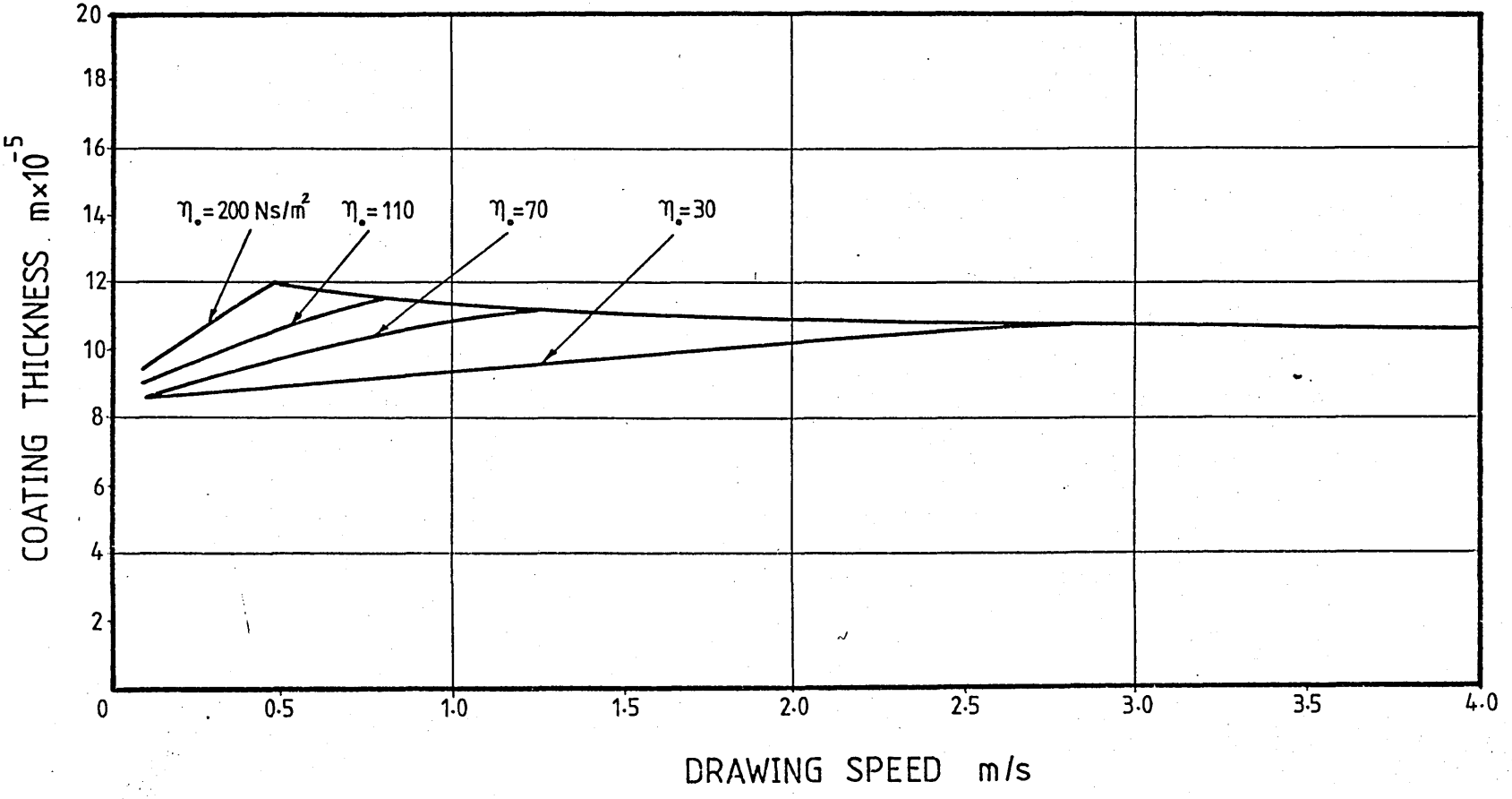

FIG91 : THEORETICAL EFFECT OF SHEAR STRESS CONST. ON COATING THICKNESS

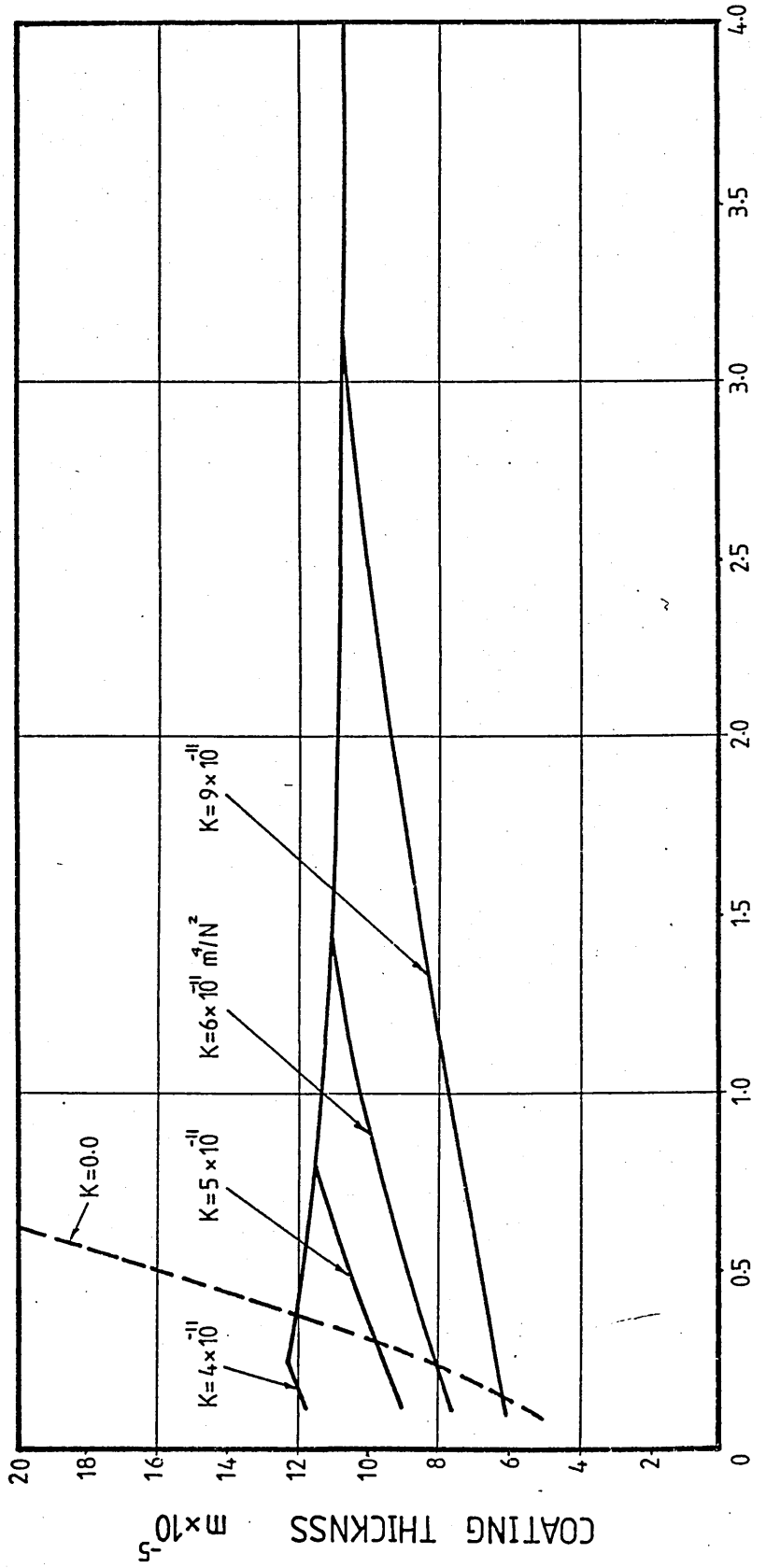

FIG92 : THEORETICAL EFFECT OF CRITICAL SHEAR STRESS ON COATING THICKNESS

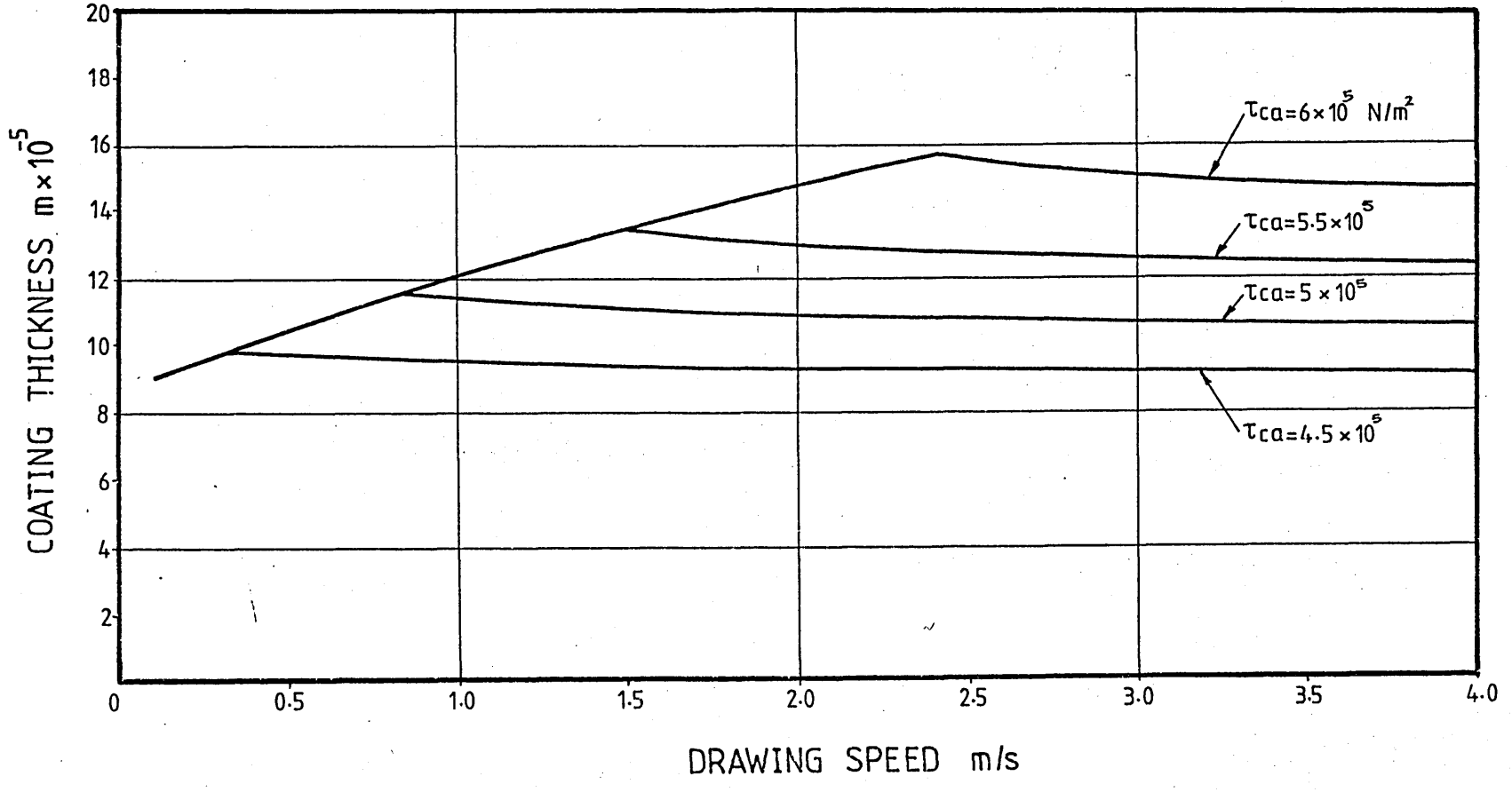

FIG93 : THEORETICAL EFFECT OF VISCOSITY CONST. ON COATING THICKNESS

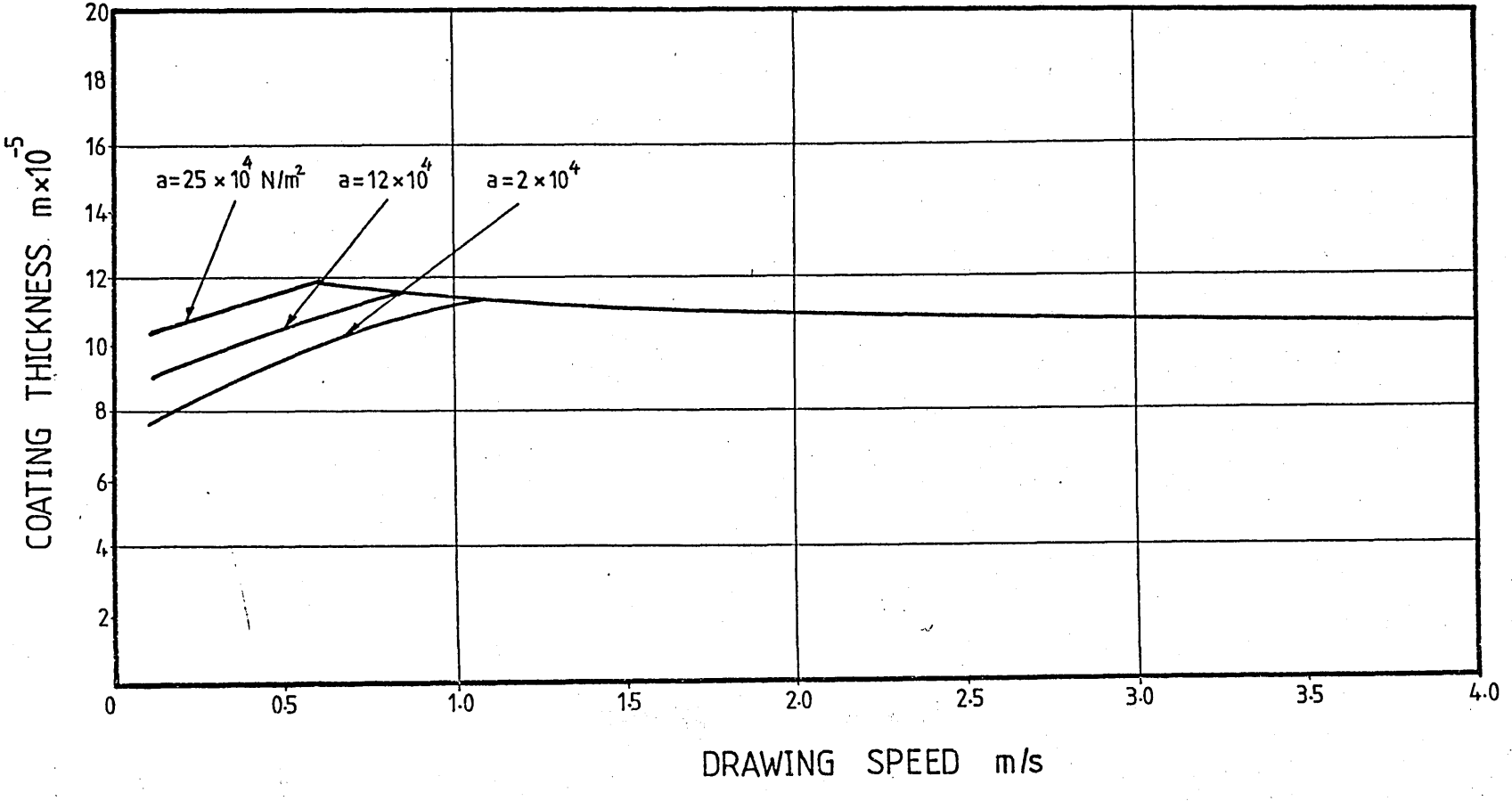

FIG94 : THEORETICAL EFFECT OF PRESSURE COEFFICIENT OF VISCOSITY ON COATING THICKNESS

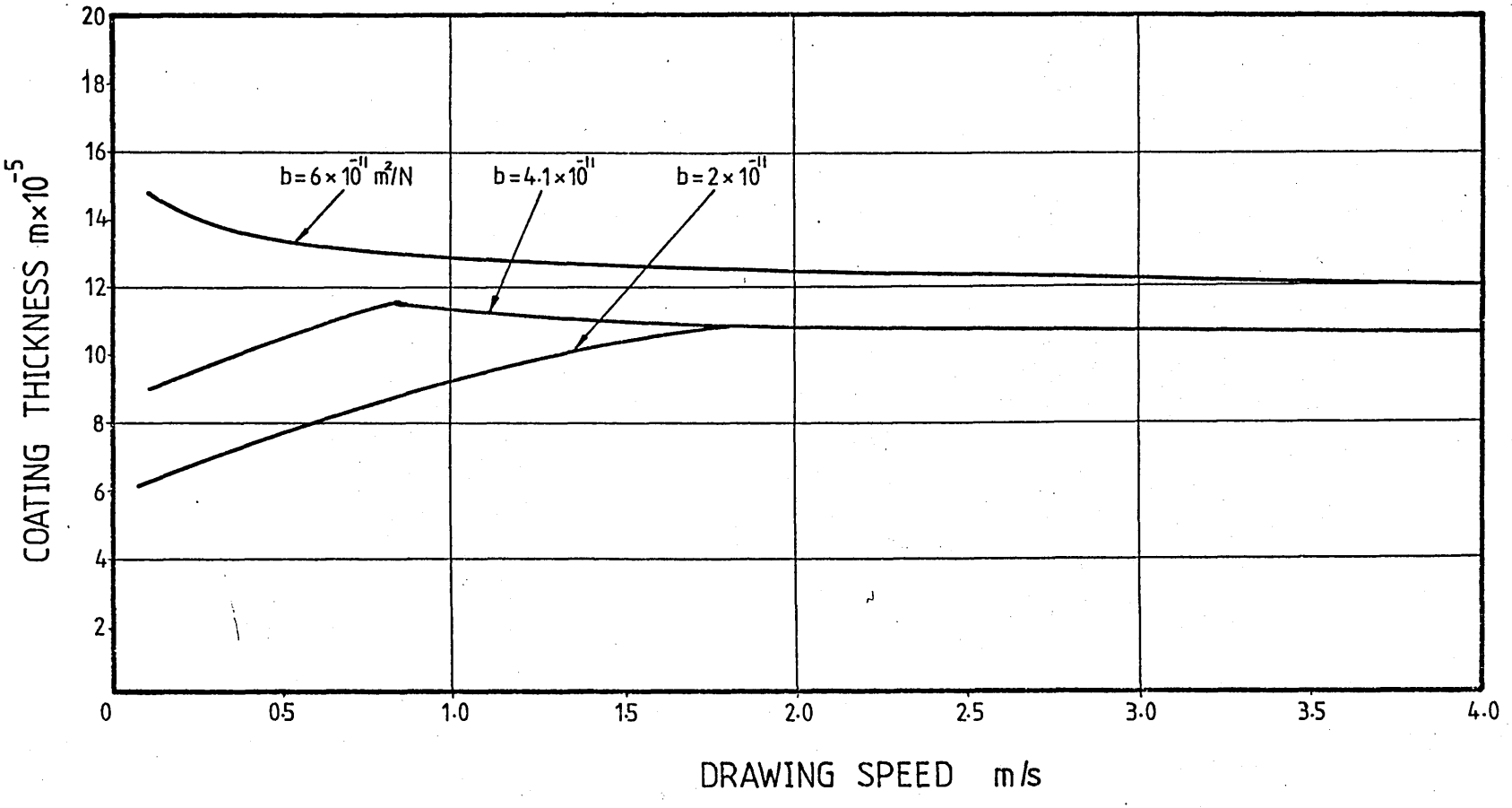

FIG95 : THEORETICAL EFFECT OF INITIAL YIELD STRESS ON COATING THICKNESS

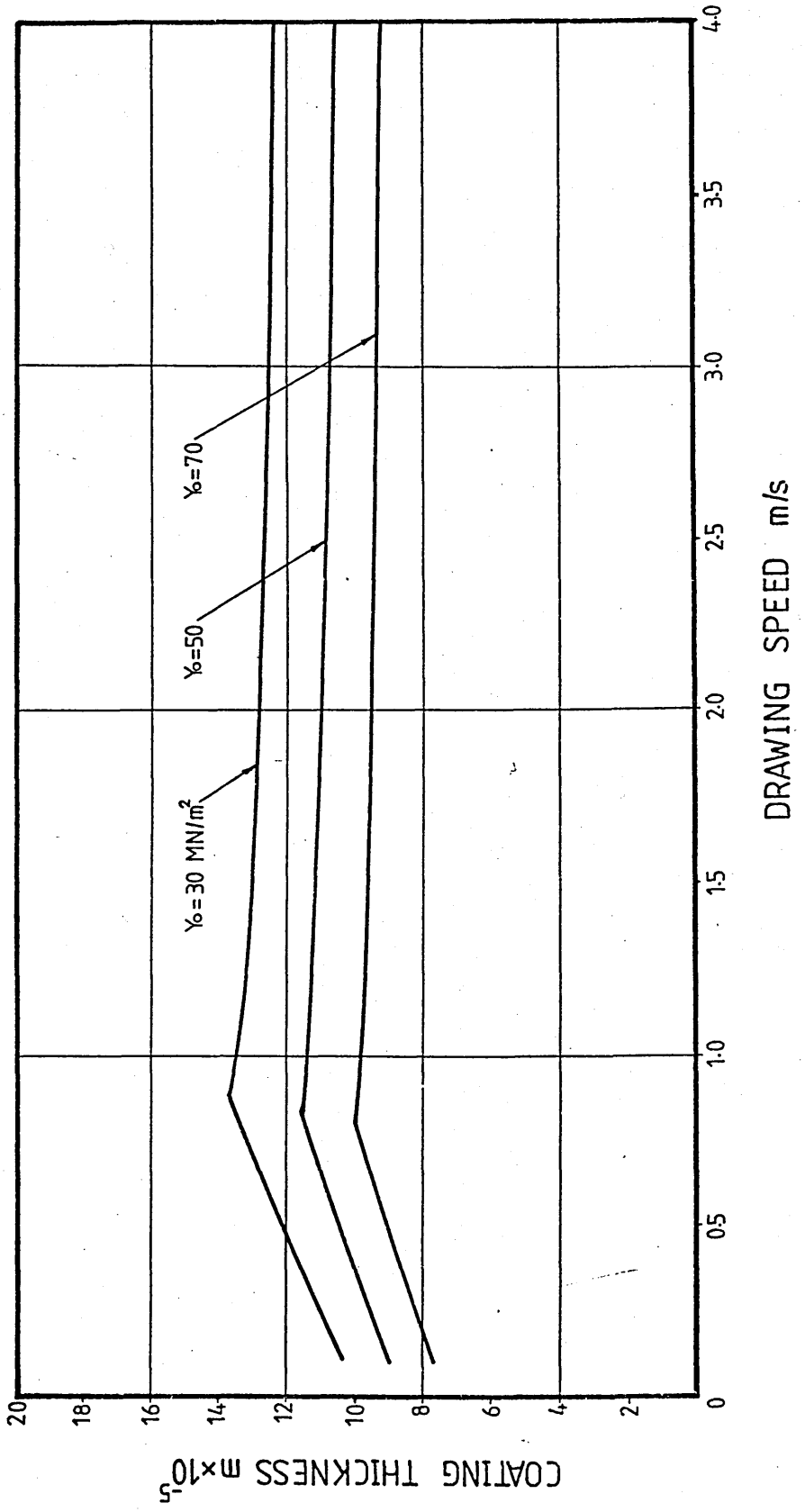

FIG96 : THEORETICAL EFFECT OF STRAIN HARDENING CONST. ON COATING THICKNESS

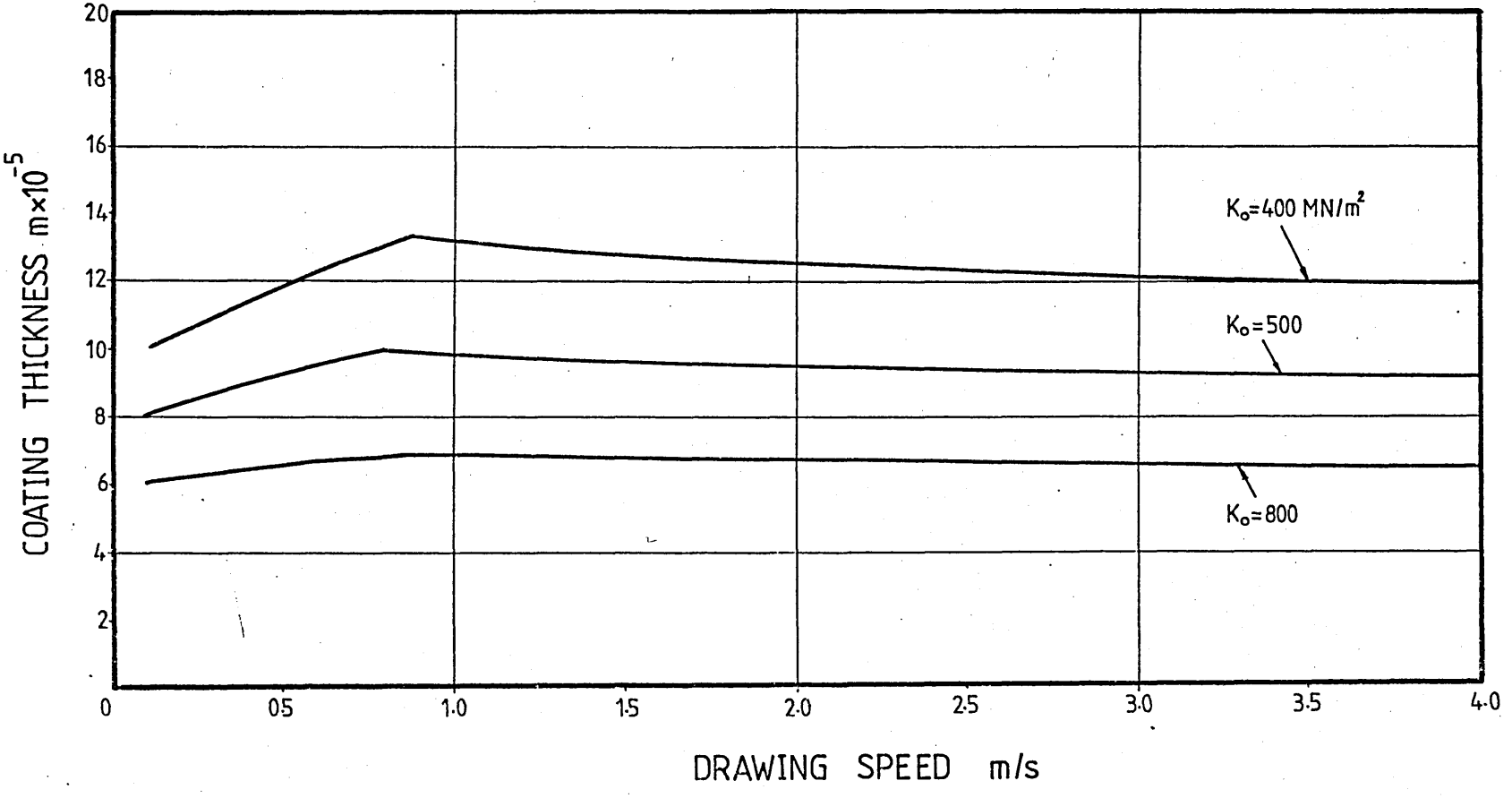

FIG97 : THEORETICAL EFFECT OF STRAIN HARDENING INDEX ON COATING THICKNESS

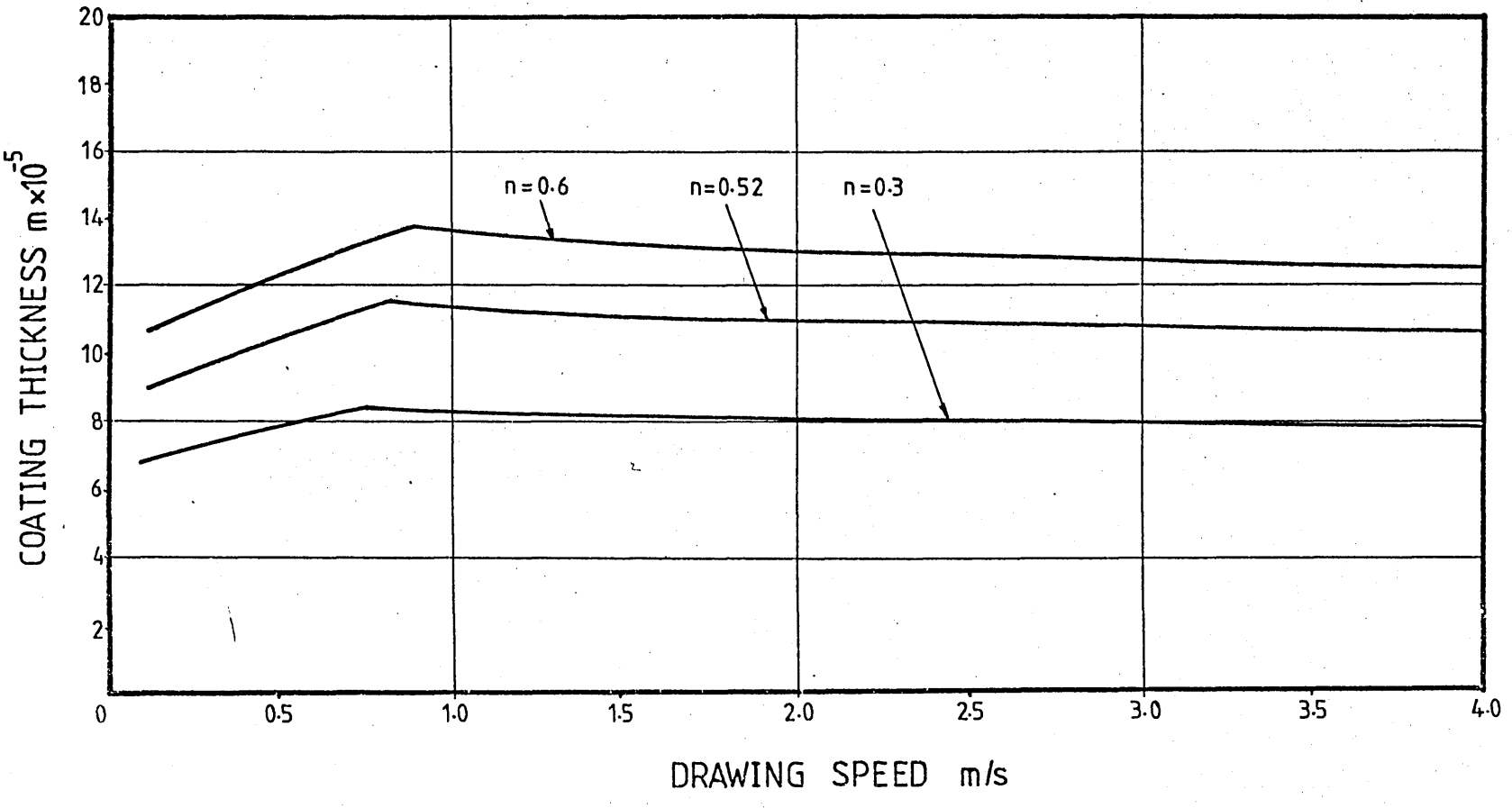

FIG98 : THEORETICAL EFFECT OF STRAIN RATE SENSITIVITY CONST. ON COATING THICKNESS

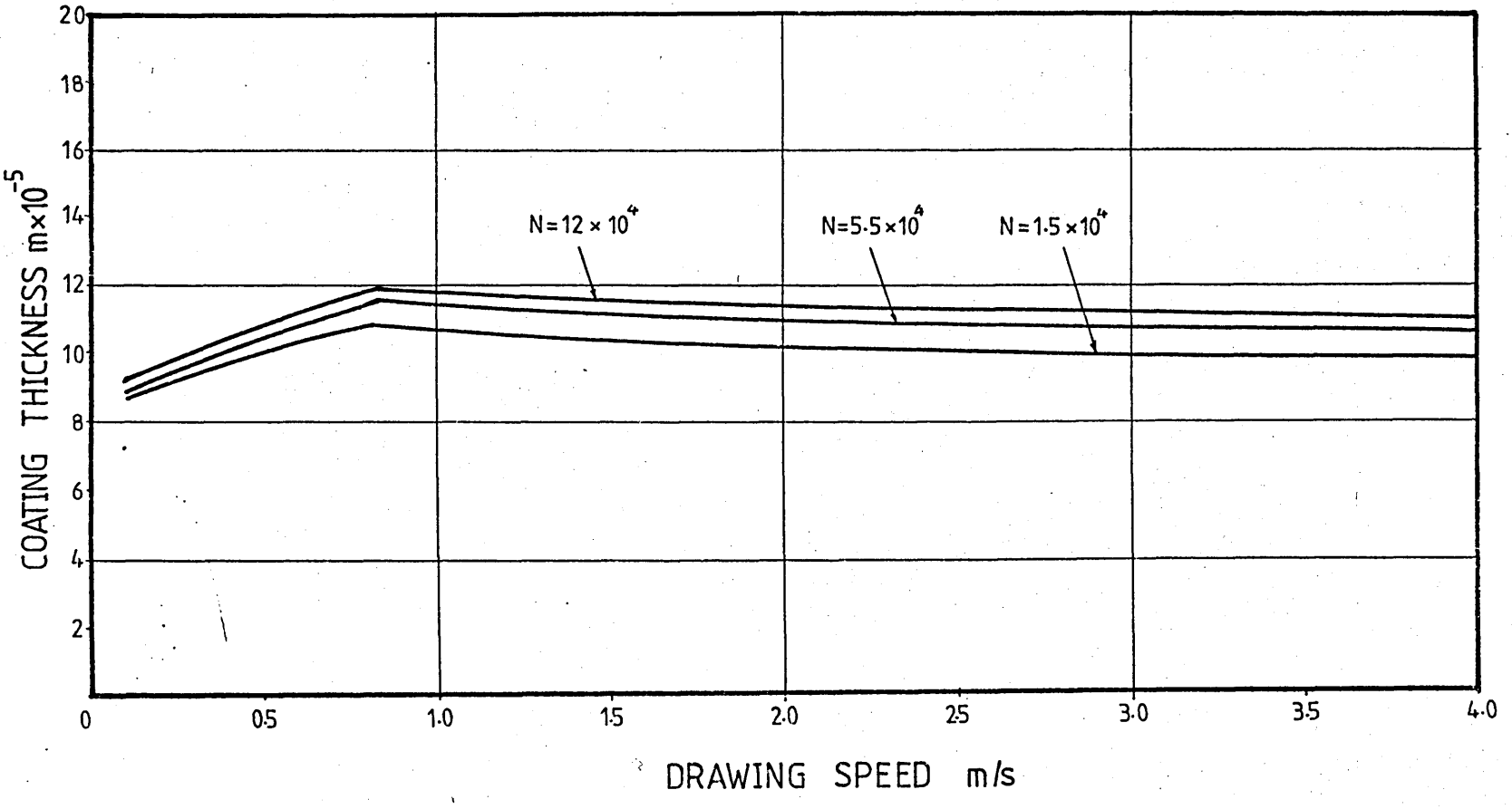

FIG99: THEORETICAL EFFECT OF STRAIN RATE SENSITIVITY INDEX ON COATING THICKNESS

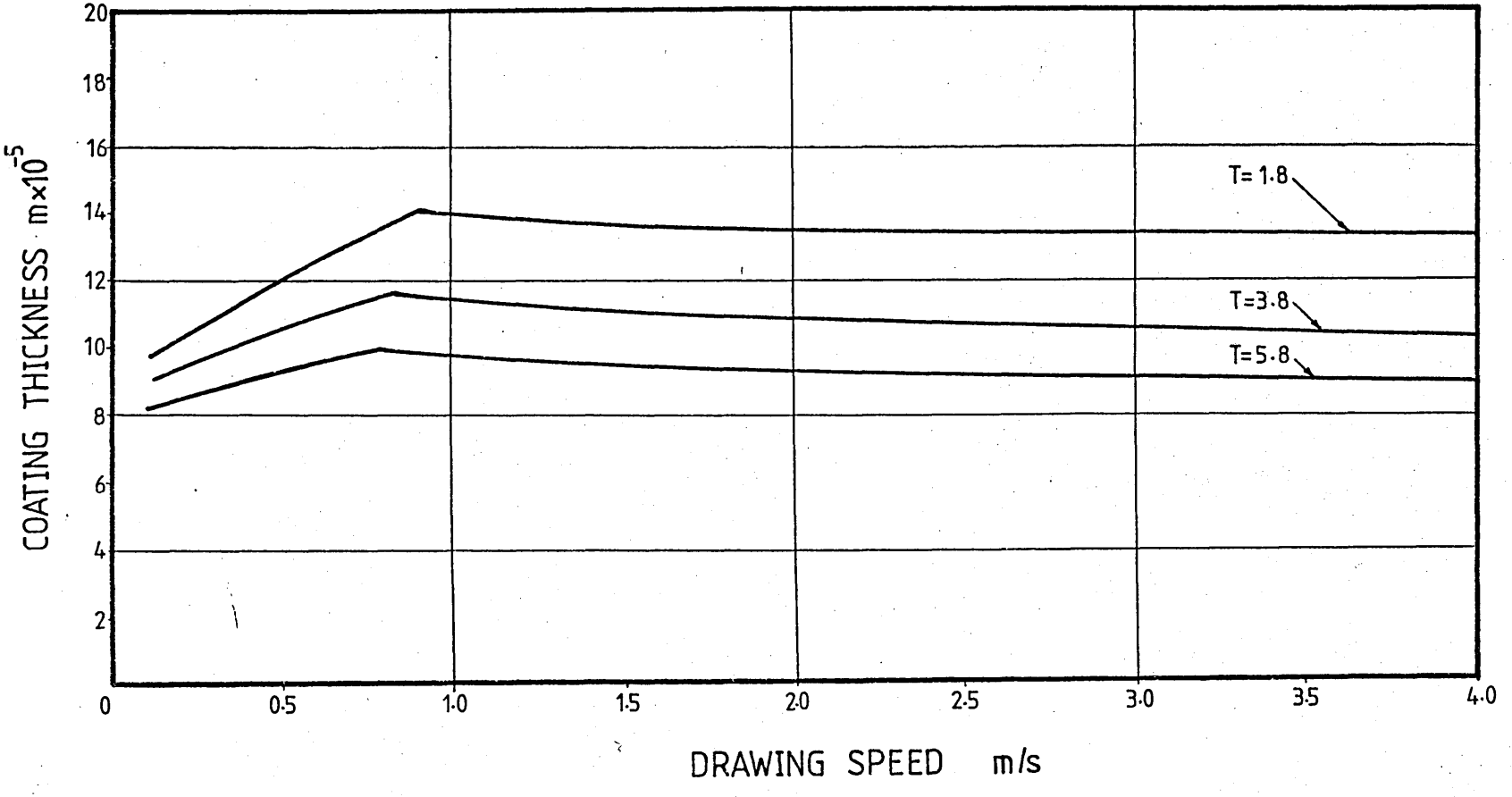

FIG100 : THEORETICAL EFFECT OF WIRE DIAMETER ON COATING THICKNESS

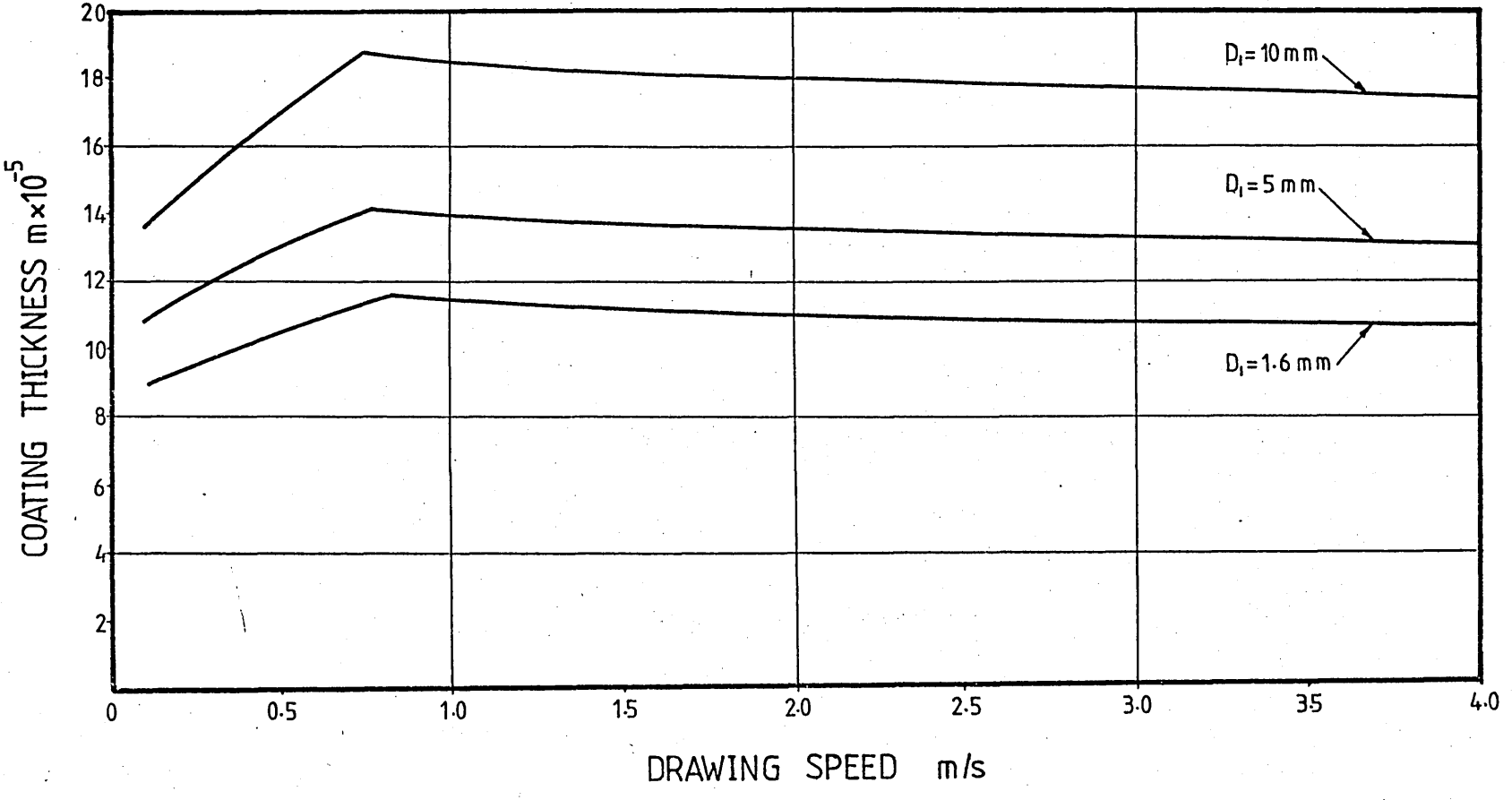

6.4- Theoretical Yielding Position Of The Wire.

Figure 101 shows the position at which the wire in the stepped bore reduction unit yields plastically, predicted by the Newtonian and the non-Newtonian solutions.

The Newtonian solution predicted X_1 to start from the step at slow drawing speed and as the speed was increased the position of yield in the tube reduced in a hyperbolic manner (to about 1mm at 4.0 m/s).

The non-Newtonian solution (I) represents the effect of the shear stress on the viscosity of polymer only. The position of yield predicted by this theory showed similar trends to that of the Newtonian solution and at higher drawing speeds (from 2.0 m/s onwards), X_1 appeared to remain constant at the value of 11mm.

The non-Newtonian solution (II) shows the effects of the shear stress and the pressure on the viscosity of the polymer. The positions at which wire was predicted to yield plastically seemed to be generally constant except at slower drawing speeds which X_1 increased slightly as the drawing speed was reduced.

The effects of the strain hardening and the strain sensitivity of the wire materials were not included in this section since it was assumed that the wire was a rigid body prior to the plastic deformation.

Variations of the input data produced a set of results for X_1 which are shown in graphical forms in figures 102 to 110. Speeds at which the critical shear stress occured are not as easily distinguishable as for the graphs of the coating thickness and the percentage reduction in area.

Again the theoretical results of the yielding position of the wire are presented in three parts as follows;

i)- The effect of the dimensional changes of the unit.

These parameters were changed in terms of the length ratio (l_1/l_2) and the gap ratio (h_1/h_2) which are shown in figures 102 and 103 respectively.

figure 102 shows the theoretical effect of the length ratio on the position of yield of the wire. As this ratio was increased, the undeformed length of the wire (X_1) reduced. For drawing speeds in excess of 1.5 m/s, a constant value of X_1 = 11 mm was predicted for all length ratios. Figure 103 shows the theoretical effect of changing the gap ratio on the position of yield in the unit. The greater the gap ratio, the longer the deformation zone (the smaller the X_1).

ii)- The effect of the polymer melt rheology.

These variables are the initial viscosity (η_o), the non-Newtonian factor (K), the critical shear stress (τ_{ca}), viscosity constant (a) and the pressure coefficient of viscosity (b).

Figure 104 shows the effect of the initial viscosity on the position of yield. For higher values of η_o, X_1 reduced and this became more noticeable at speeds slower than 1.0 m/s. The effect of the shear stress constant (K) on the position of yield of the wire is shown in figure 105. As K was reduced, the undeformed part of the wire was predicted to

reduce. When K = 0, a hyperbolic curve for X_1 was predicted which started from X_1 = 50 mm (step) at slower drawing speeds and reduced to about 1.0 mm at 4.0 m/s.

Figure 106 shows the effect of the critical shear stress on the position of yield of the wire. The higher the critical shear stress, the smaller the X_1. Note that all the curves meet before slip is predicted.

Figure 107 and 108 show the effect of the viscosity constants (a and b) on the position of yield of the wire inside the unit. As the result of increase in both constants (a and b), the predicted position of yield reduced more towards the entry point of the unit. At drawing speed in excess of 1.0 m/s, constant results were obtained for both parameters.

iii)- The effect of the wire material.

Since the wire was assumed to act as a rigid body, the strain hardening and the strain rate sensitivity of the wire were not included in the prediction of the position of yield.

Figure 109 shows the effect of the initial yield stress on the yielding position (X_1). As the initial yield stress was increased, the distance X_1 also increased, reducing the deformation zone. The theoretical effect of changing the wire diameter is shown in figure 110. Smaller wire diameters were predicted to have longer deformation zones. The trends of these results were found to be similar to those of figure 109.

FIG101 : COMPARISON BETWEEN THEORETICAL SOLUTIONS PREDICTING YIELDING POSITION OF WIRE

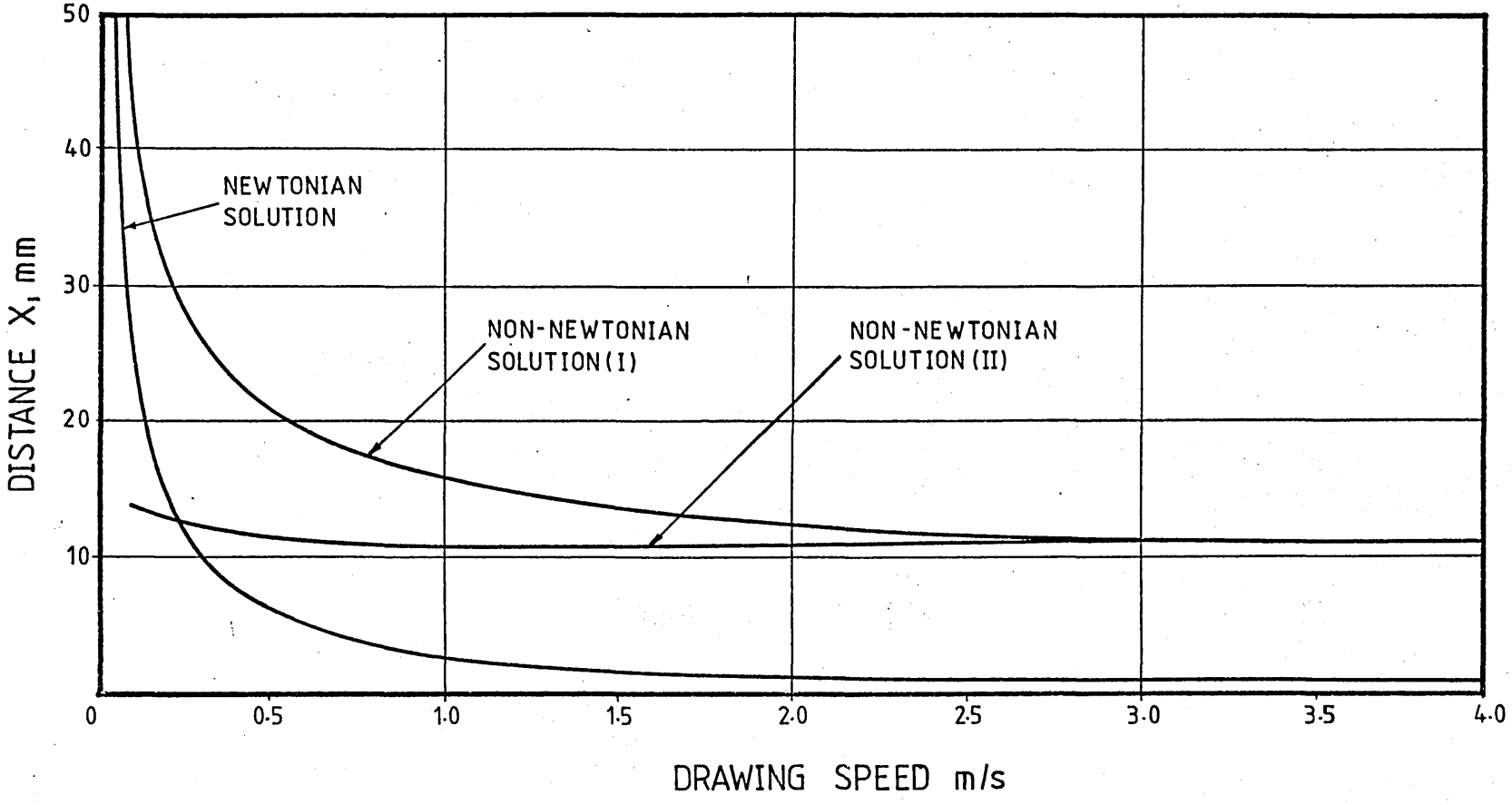

FIG102 : THEORETICAL EFFECT OF LENGTH RATIO ON YIELDING POSITION OF WIRE

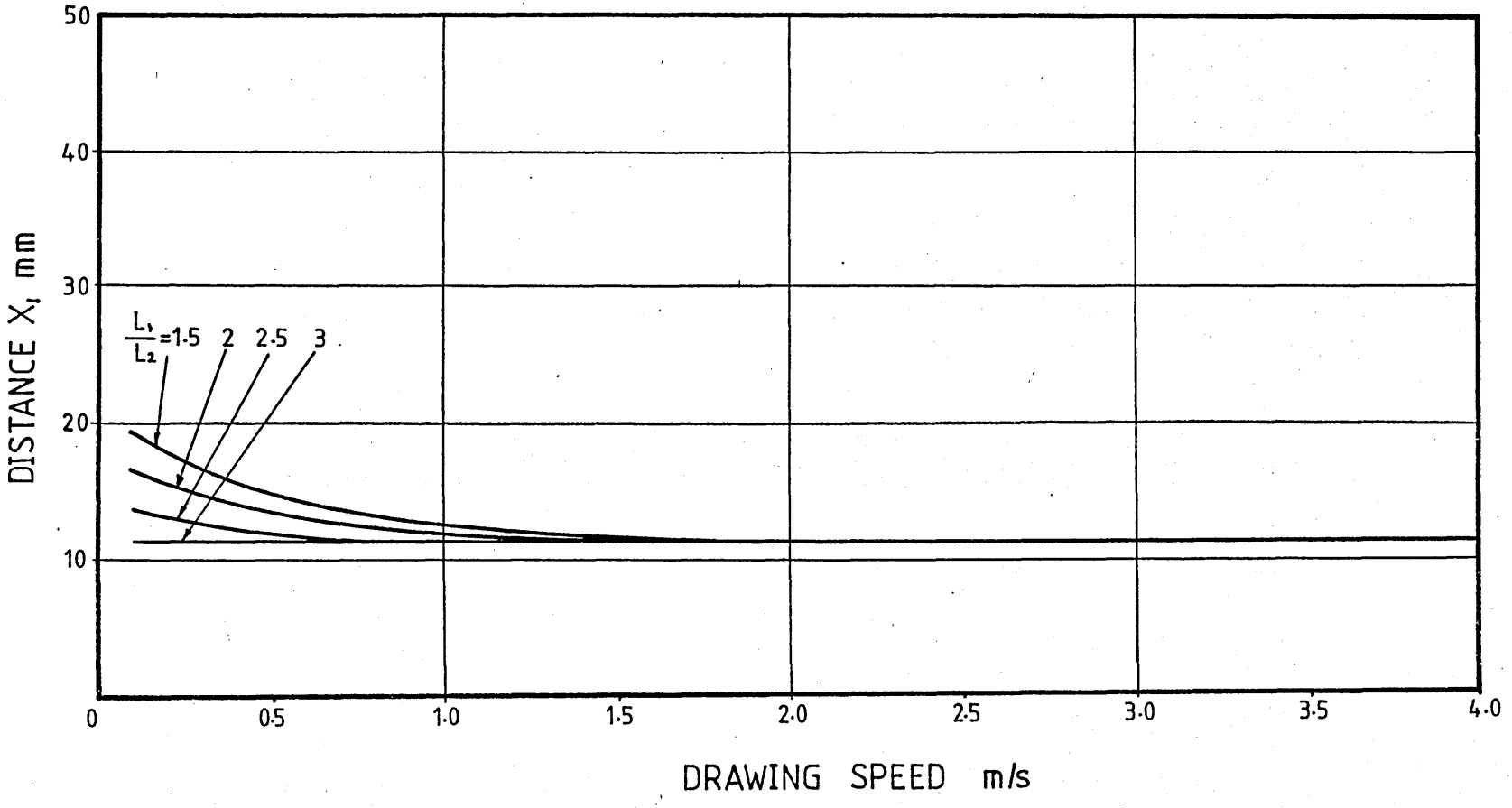

FIG103: THEORETICAL EFFECT OF GAP RATIO ON YIELDING POSITION OF WIRE

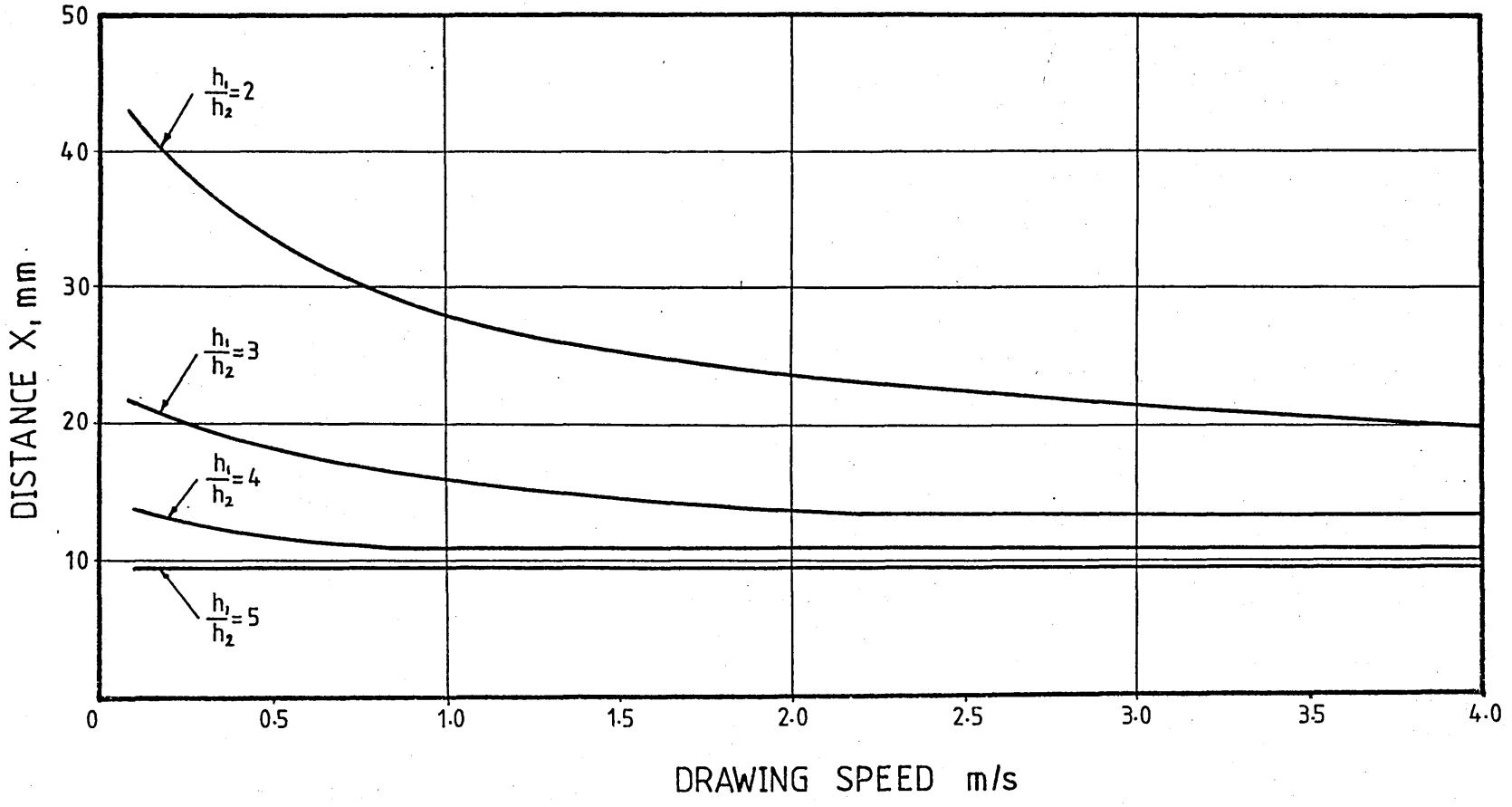

FIG104 : THEORETICAL EFFECT OF INITIAL VISCOSITY ON YIELDING POSITION OF WIRE

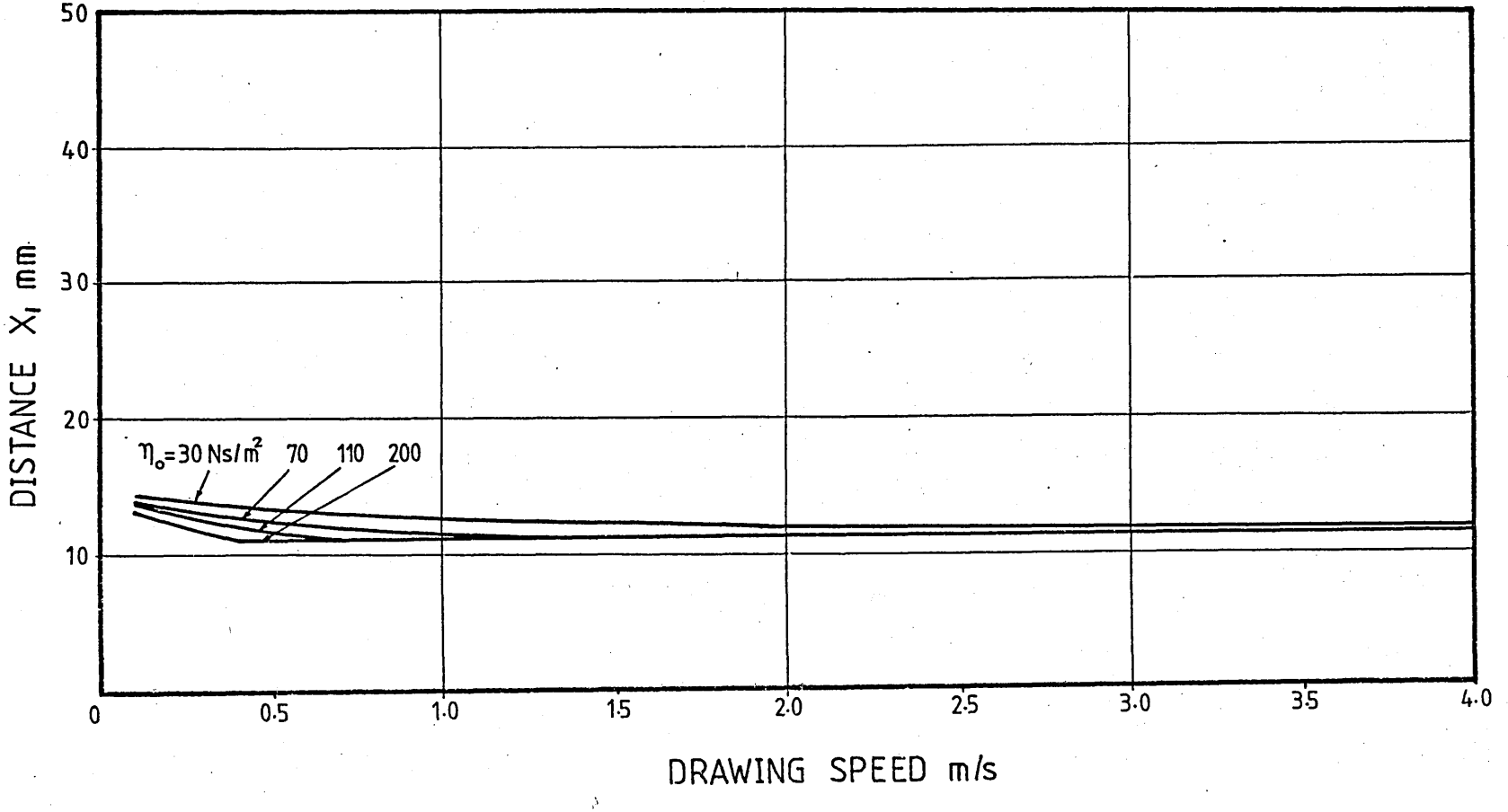

FIG105 : THEORETICAL EFFECT OF SHEAR STRESS CONST. ON YIELDING POSITION OF WIRE

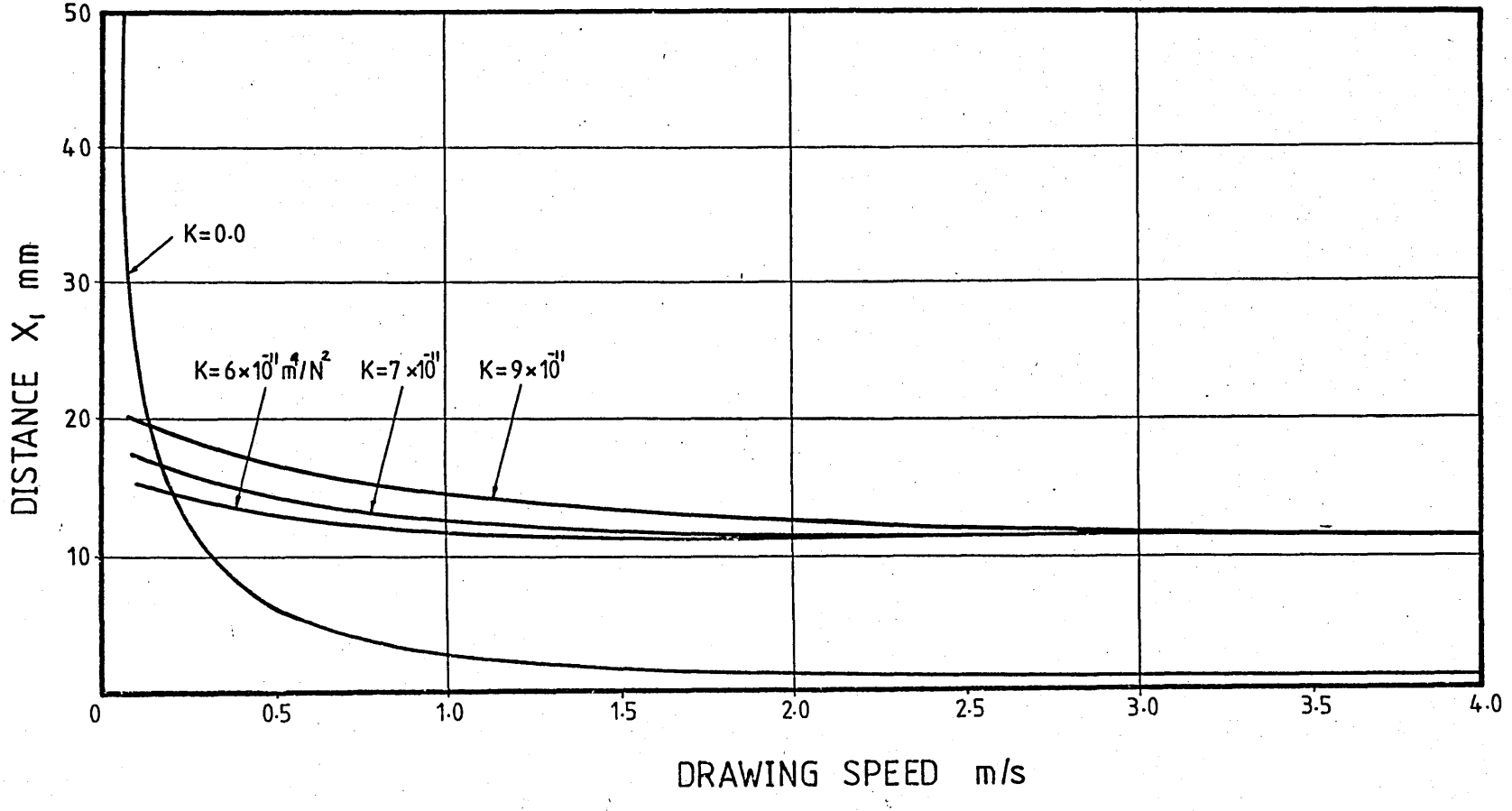

FIG106 : THEORETICAL EFFECT OF CRITICAL SHEAR STRESS ON YIELDING POSITION OF WIRE

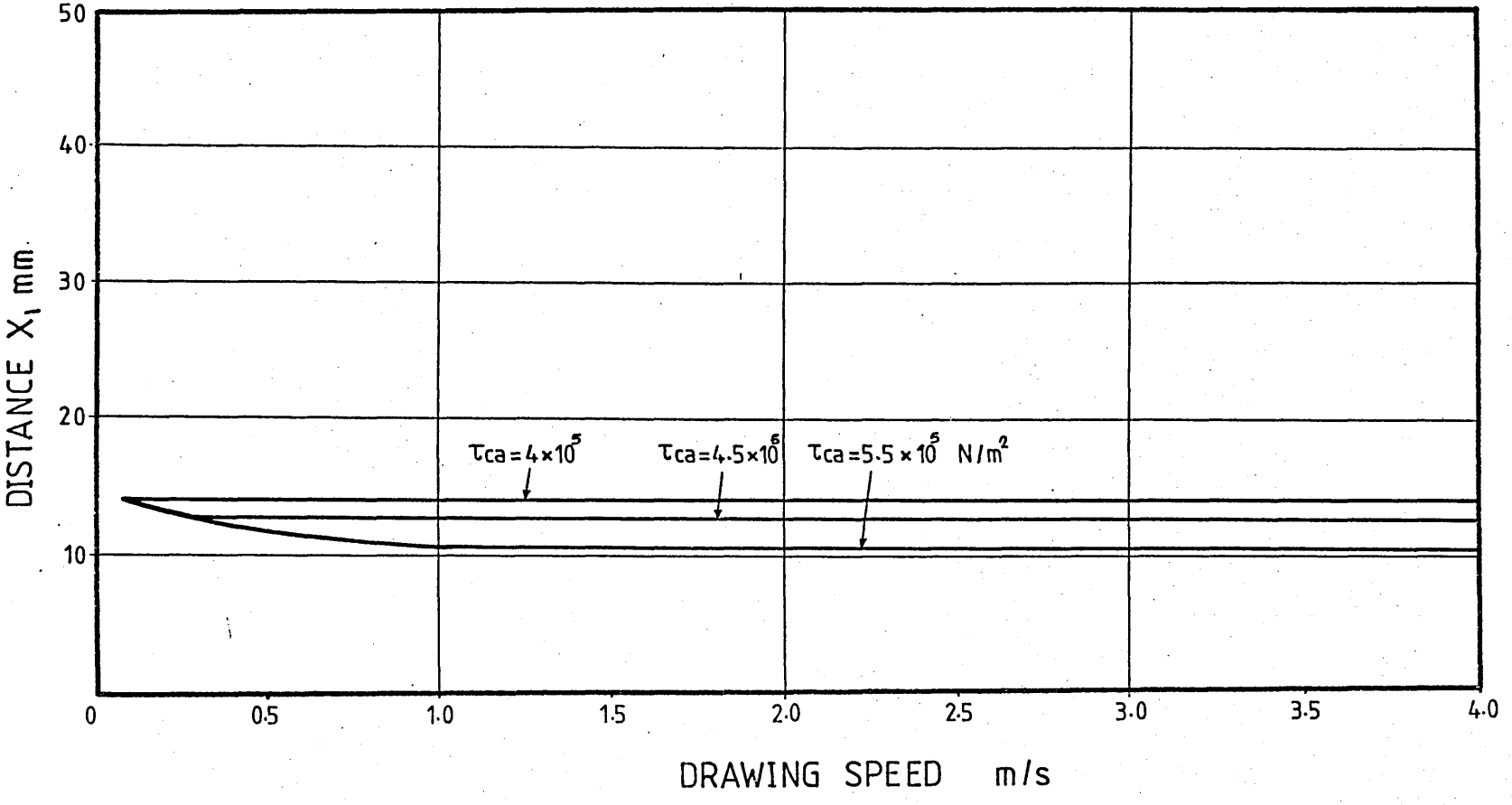

FIG107 : THEORETICAL EFFECT OF VISCOSITY CONST. ON YIELDING POSITION OF WIRE

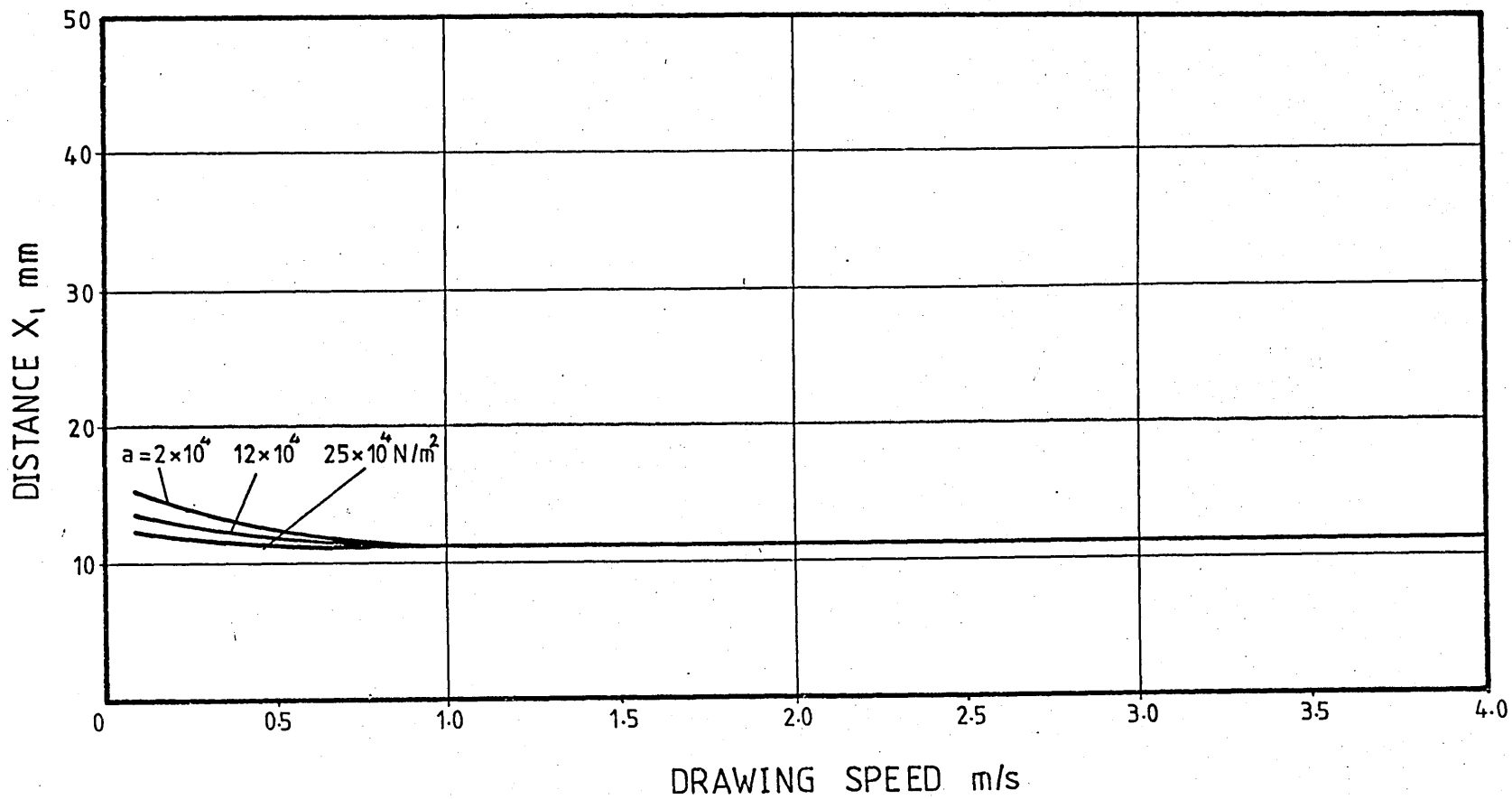

FIG108: THEORETICAL EFFECT OF PRESSURE COEFFICIENT OF VISCOSITY ON YIELDING POSITION OF WIRE

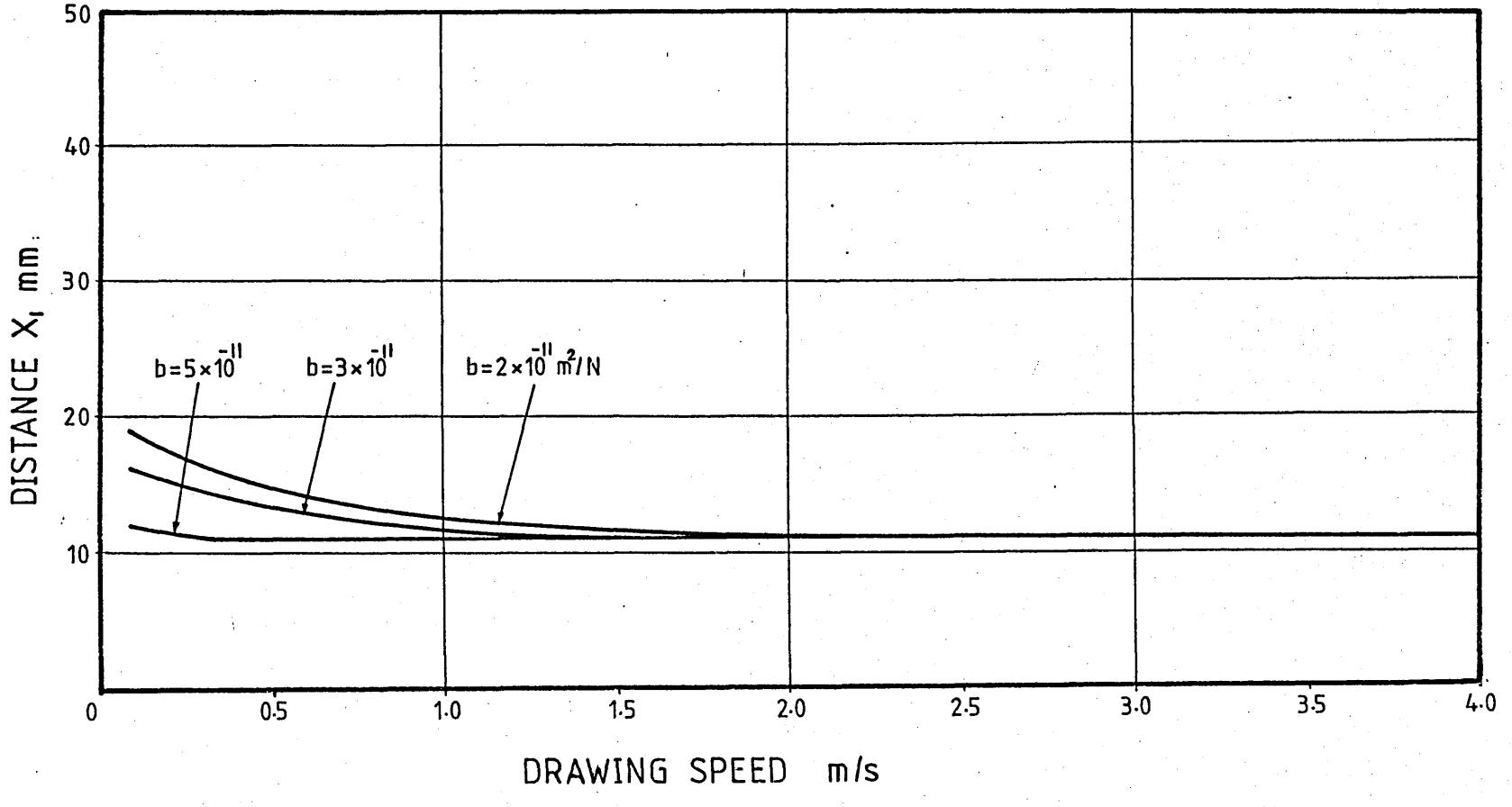

FIG109: THEORETICAL EFFECT OF INITIAL YIELD STRESS ON YIELDING POSITION OF WIRE

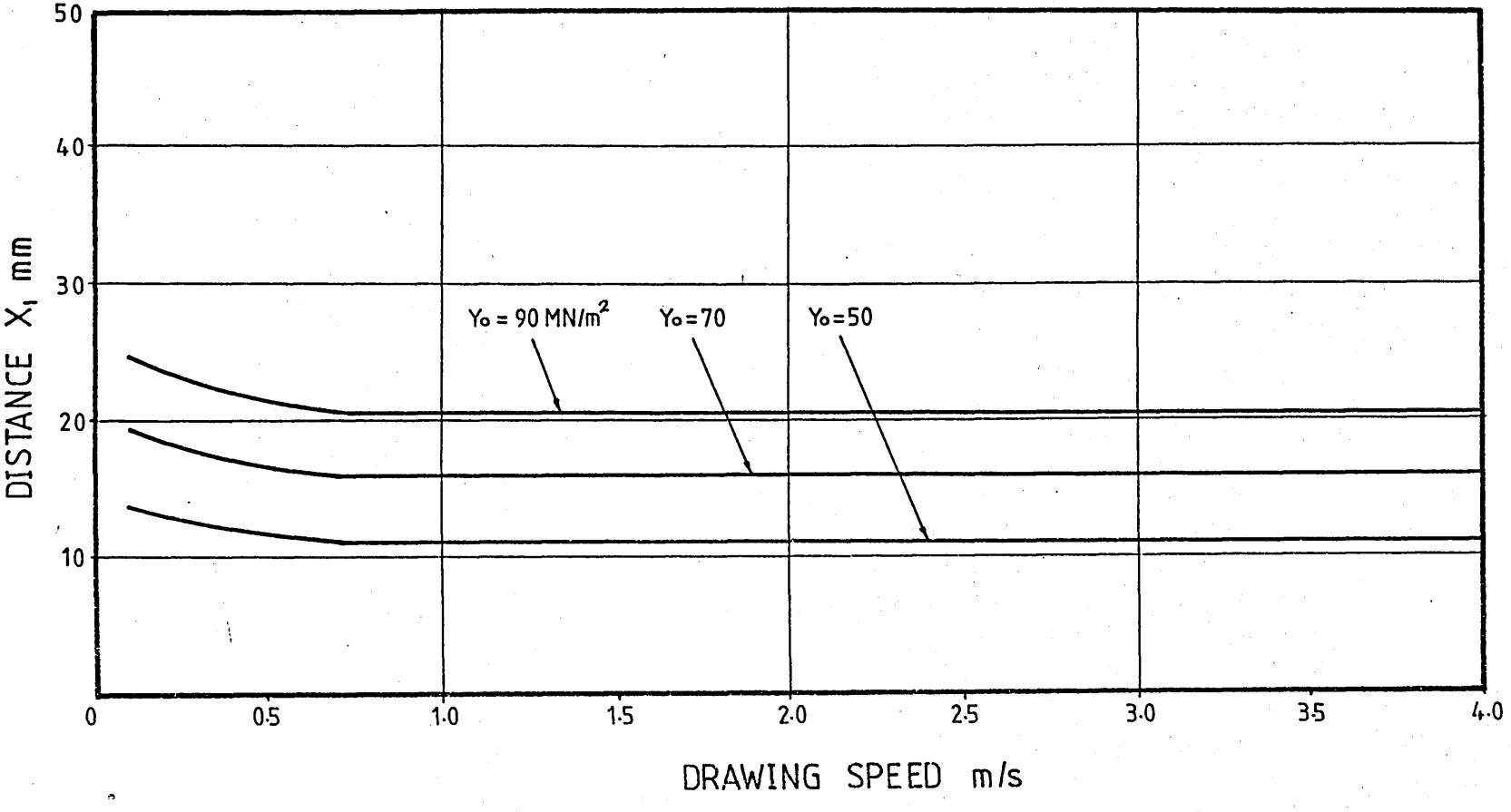

FIG110: THEORETICAL EFFECT OF WIRE DIAMETER ON YIELDING POSITION OF WIRE

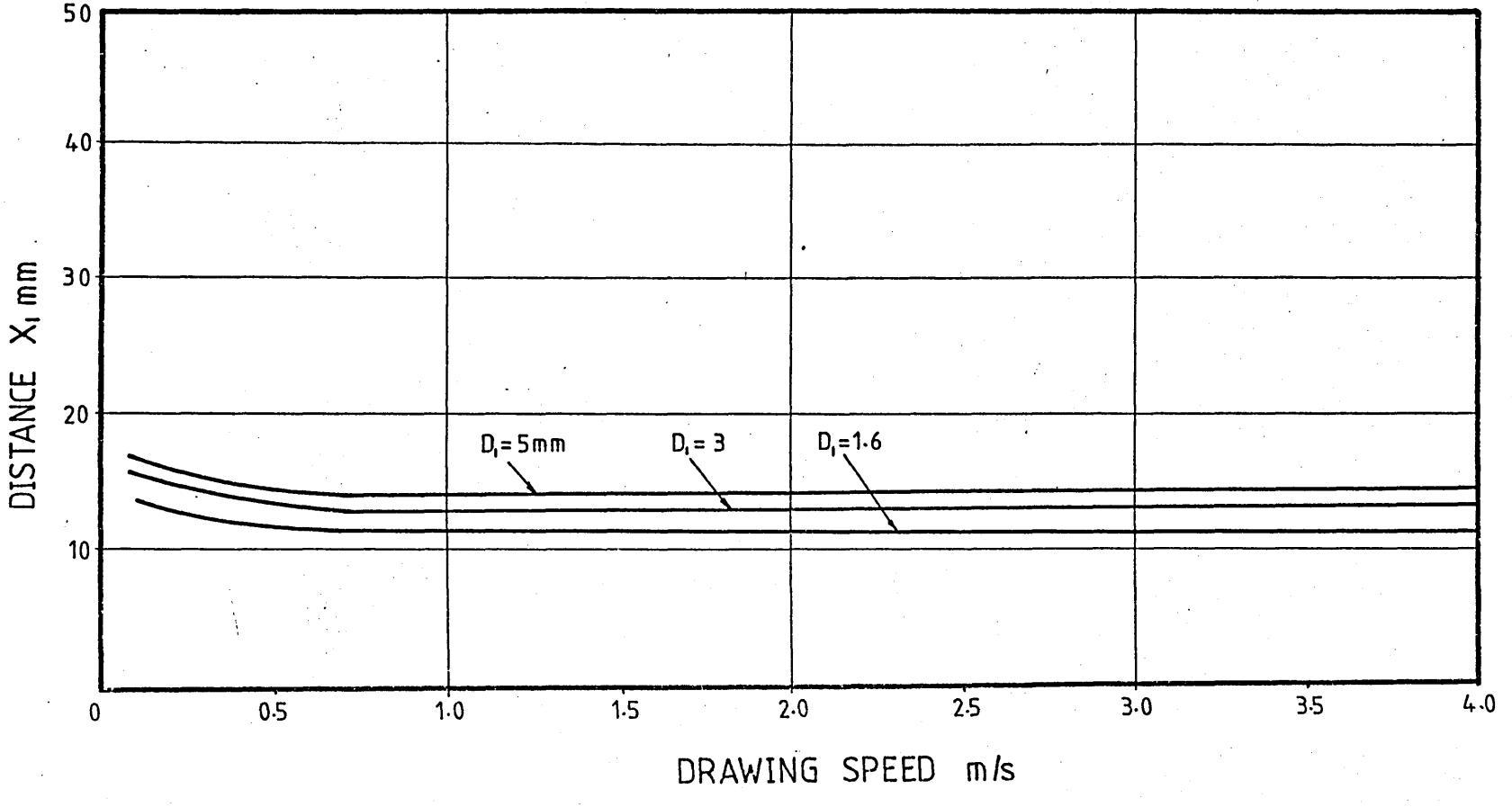

6.5- Theoretical Pressure.

Predicted pressures in the stepped bore reduction unit are presented in graphical forms in this section. It has been shown theoretically that the pressure profile in the unit, prior to deformation of the wire, was linear (similar to that predicted by the Newtonian solution). Pressure profiles with the effect of shear rate on viscosity alone are shown in figure 111 which compares the Newtonian and the non-Newtonian solutions. A large difference became apparent between both solutions and the effect of increasing the non-Newtonian factor "K" was to reduce the predicted pressures.

Figure 112 shows the pressures predicted by both solutions and effect of pressure on the viscosity of the polymer was considered in the non-Newtonian solution. It is clearly shown that the magnitudes of the pressures predicted by the non-Newtonian solution were significantly increased compared to those in figure 111, and again an increase in the parameter "K" caused the pressures to reduce.

Figures 113 and 114 show the pressures versus speed at the step position. Figure 113 shows the effect of shear rate on the viscosity only. As the values of "K" was increased, the pressures reduced and this became more pronounced at higher speeds. The inclusion of the effect of pressure on the viscosity in the non-Newtonian analysis predicted higher theoretical pressures especially at lower drawing speeds (figure 114). Note that as the magnitudes of the pressures increased, slip was predicted at slower speeds.

The above results were obtained such that the change of gap due to deformation of the wire was not included in the solution. It has been shown that as the result of predicted deformation in the wire and hence increse in the gap, the pressure reduced slightly. The variations of the pressure in the unit due to change of gap are shown in chapter 7 when the experimental and the theoretical results are compared.

FIG111 : THEORETICAL PRESSURE DISTRIBUTIONS SHOWING EFFECT OF SHEAR STRESS CONST.

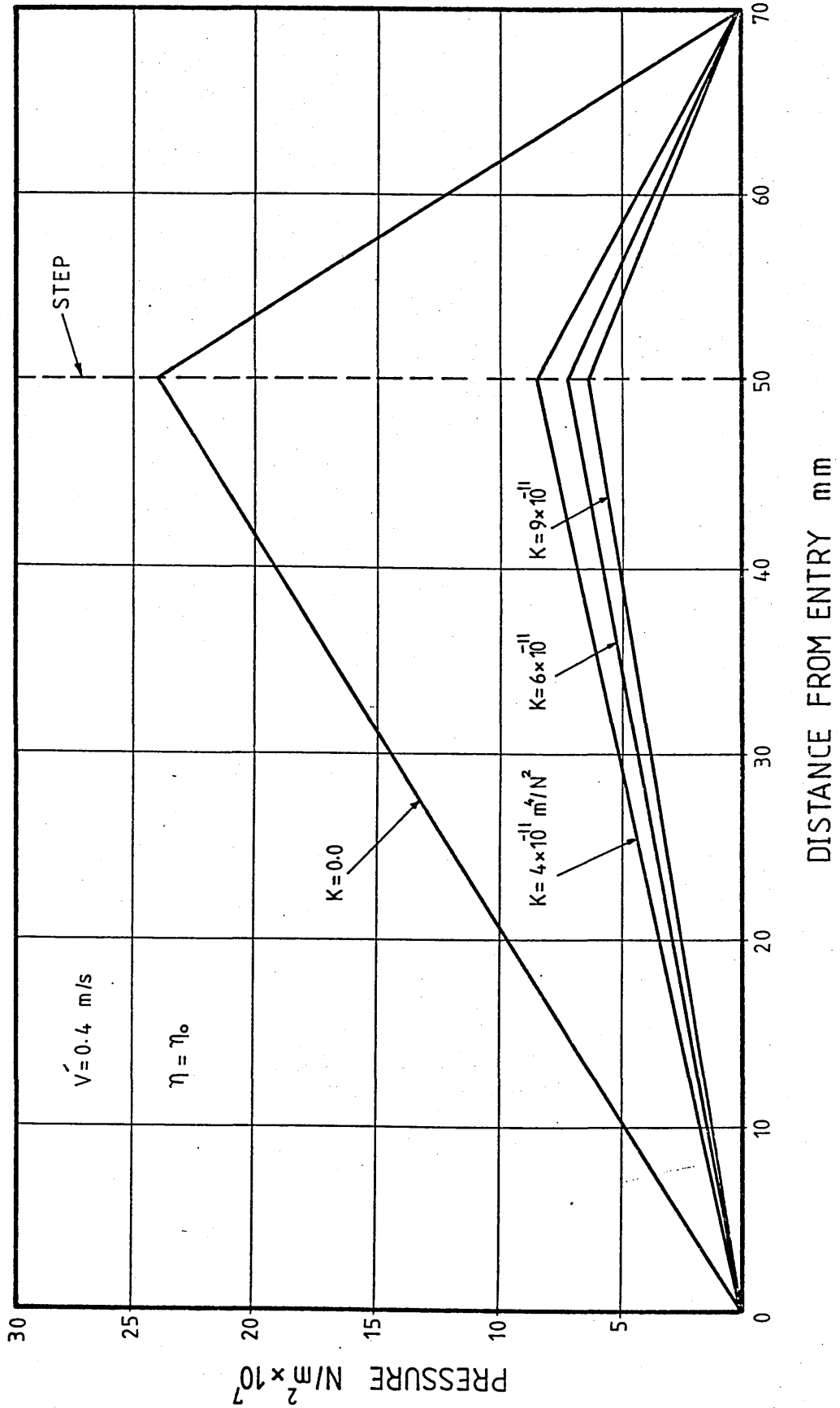

FIG112: THEORETICAL PRESSURE DISTRIBUTIONS SHOWING EFFECT OF PRESSURE ON VISCOSITY

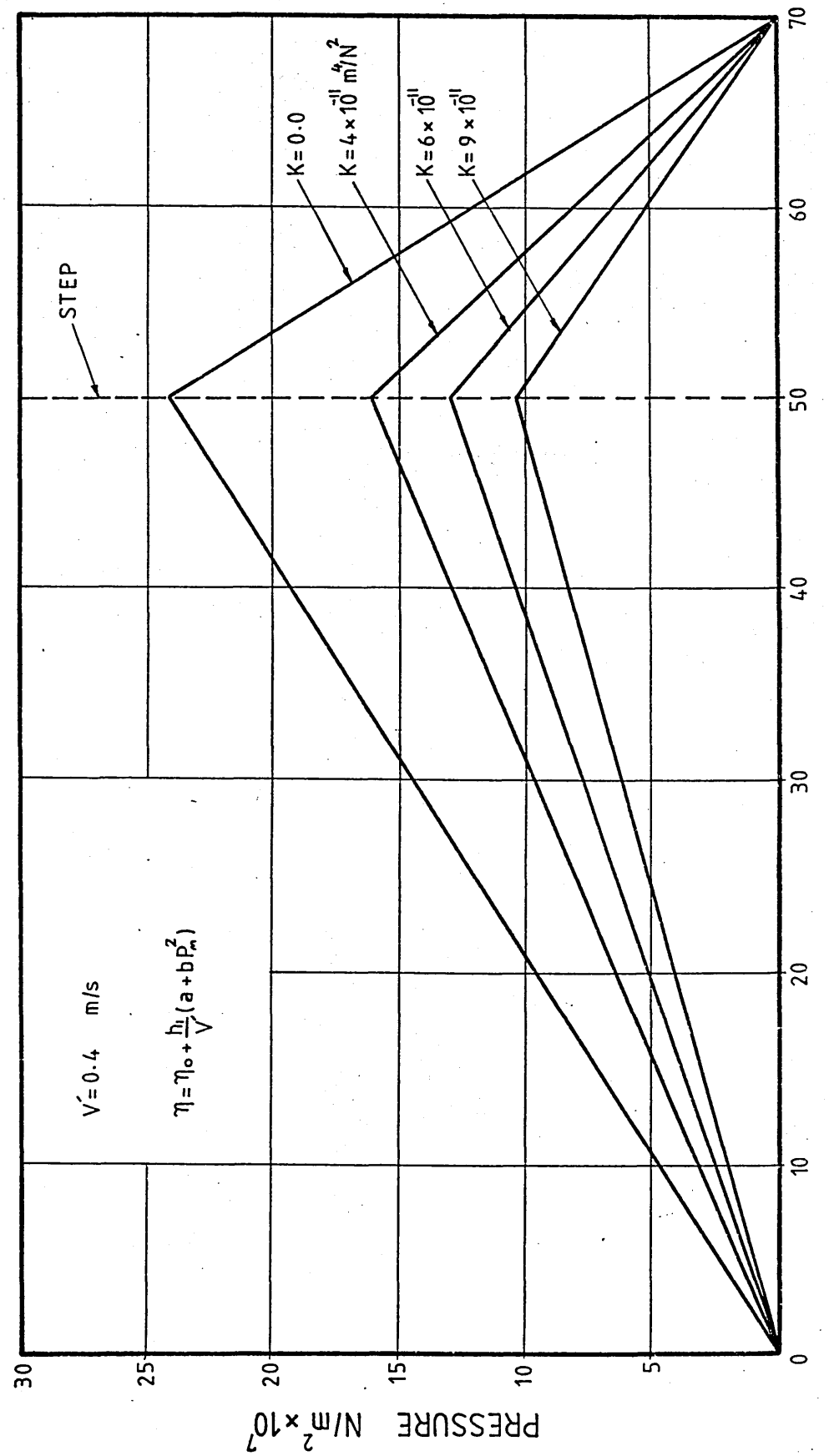

FIG 113 : THEORETICAL PRESSURE VARIATIONS AT STEP WITH EFFECT OF SHEAR STRESS ON VISCOSITY ONLY

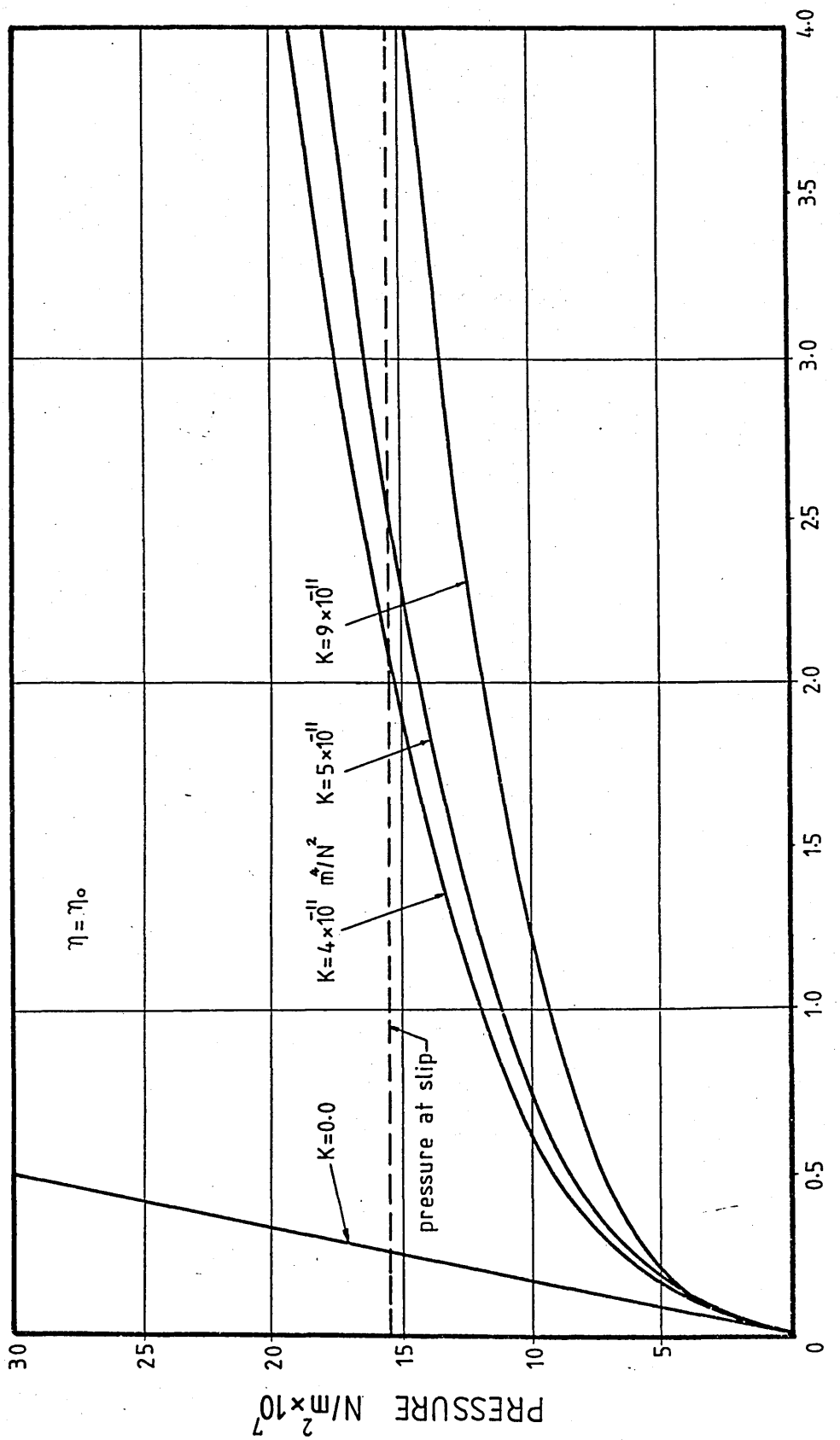

FIG114 : THEORETICAL PRESSURE VARIATIONS AT STEP WITH EFFECT OF PRESSURE ON VISCOSITY

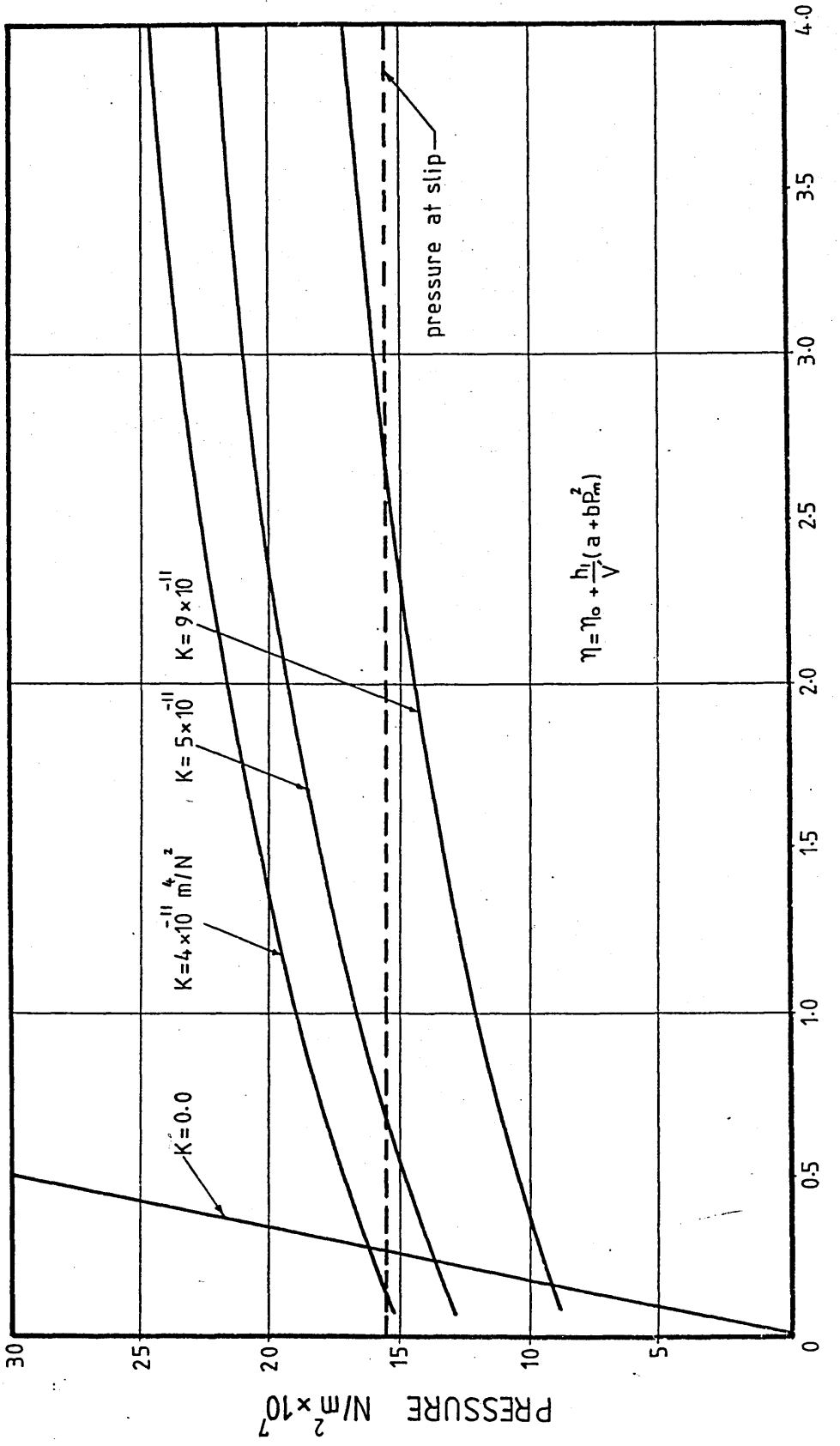

6.6- Theoretical Shear Stress On The Wire.

Shear stress on the wire is a founction of the pressure therefore any decrease in this parameter causes the shear stress to reduce. The combined effects of the pressure and the shear stress result in the yielding of the wire, thus it is essential to understand the role of this stress in more detail.

Figure 115 shows the theoretical shear stress on the wire (τ_{c_1}) in the first part of the unit versus speed, prior to the deformation of the wire. These curves show the effect of the shear rate on viscosity alone. Deterioration of the shear stress due to speed (shear rate) is clearly exhibited and as the non-Newtonian factor "K" was increased, the predicted shear stress decreased and the critical shear stress occured at higher speeds.

Figure 116 shows the theoretical shear stress on the wire in the first part of the unit when the coefficient of pressure on the viscosity was included into the analysis. Again the deformation of wire was not included in these results. A substantial increase in the shear stress was shown to take place especially at slower drawing speeds. Similarly as the non-Newtonian factor "K" was increased, the predicted shear stress decreased and the limiting shear stress was shown to occur at higher speeds. Note that as the result of increase in the viscosity, the critical shear stress was predicted at slower speeds.

Figure 117 and 118 present the theoretical shear stress on the wire in the second part of the unit (τ_{c_2}). Again the change of gap due to deformation of the wire was

not included in these results. The trends of the results were found to be very similar to those of figures 115 and 116 with two significant differences;

i)- The magnitudes of the theoretical shear stress on the wire in the second part of the unit were smaller than those in the first part.

ii)- The theoretical shear stress in the second part of the unit did not reach the critical value even when the effect of pressure on the viscosity was included into the solution.

With reference to the above statements, it may be concluded that slip takes place in the first part of the stepped bore reduction unit only, where the shear stress on the wire in the second part of the unit remains below the critical value. Having examined the shear stress on the wire in both sides of the unit prior to the deformation of the wire, it is now necessary to investigate the behaviour of the shear stress on the wire while the deformation is taking place ie when the gap is increasing.

Figure 119 shows the theoretical shear stress distributions in the unit at two different speeds. The increase in the gap in the first part of the unit caused the shear stress to increase slightly (in the negative direction). After the step, the shear stress on the wire became positive ie in the same direction as the motion of the wire. Note that the increase in speed caused the shear stress to incease on both sides. This interesting result

was infact the basis of the assumption made in chapter 5, that deformation of the wire ceases at the step. In chapter 7 however, this will be discussed in more details.

Figure 120 shows the theoretical shear stress on the wire in the second part of the unit versus speed, when the new gap was introduced due to deformation of the wire. with the effect of shear rate on the viscosity alone (non-Newtonian solution(I)), at slower drawing speeds, the predicted deformation of the wire was small, therefore shear stress was negative. As the drawing speed was increased, the magnitude of the shear stress also increased in negative direction and eventually showed a turning point at about 0.4 m/s. This stress became zero at about 1.7 m/s and after this drawing speed, it remained positive and increased as the drawing speed was increased. Note that the Newtonian solution showed a similar trend with the exception that the turning point took place at about 0.3 m/s and the shear stress became zero at about 0.5 m/s.

The inclusion of the pressure coefficient of viscosity in the analysis (non-Newtonian solution(II)) predicted higher deformations, therefore due to the bigger gaps, the shear stress was positive for all the speeds. Also note that when slip was predicted in the first part of the unit (see figure 116), the positive shear stress in the second part still remained below the critical value.

FIG115: THEORETICAL VARIATIONS OF SHEAR STRESS (τ_{c1}) WITH EFFECT OF SHEAR RATE ON VISCOSITY

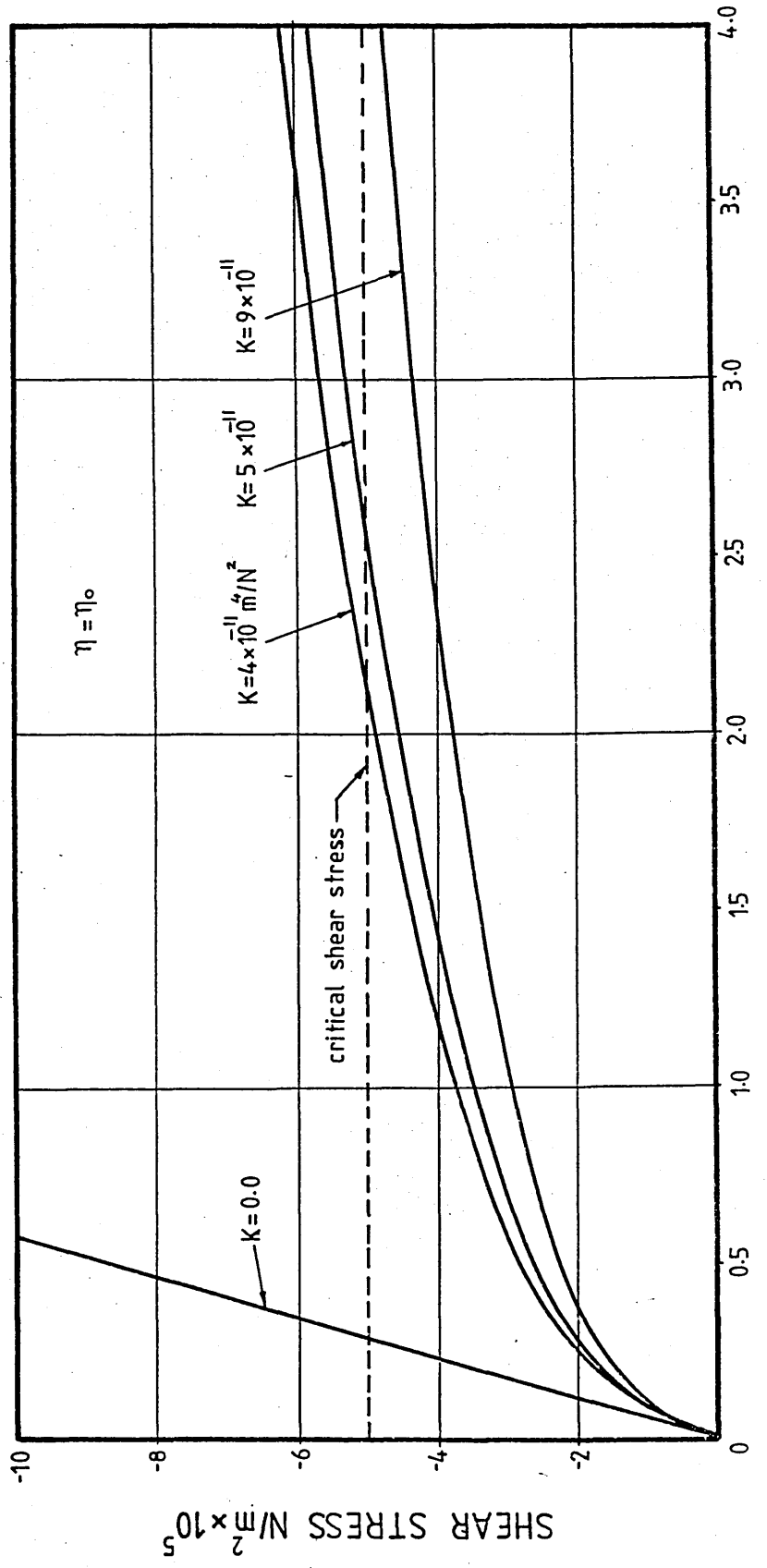

FIG116: THEORETICAL VARIATIONS OF SHEAR STRESS (τ_{c1}) WITH EFFECT OF PRESSURE ON VISCOSITY

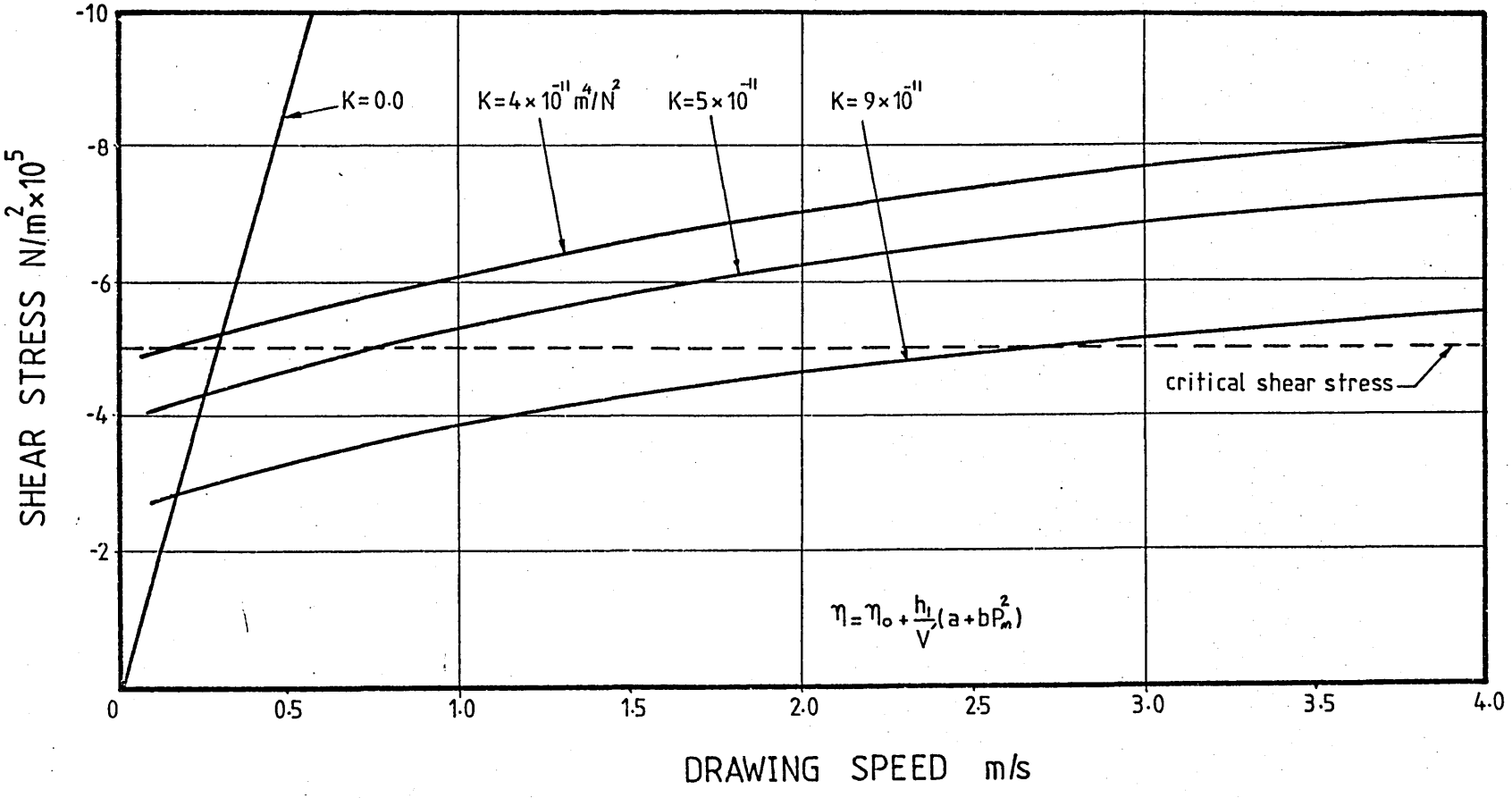

FIG117 : THEORETICAL VARIATIONS OF SHEAR STRESS(τ_{c2}) WITH EFFECT OF SHEAR RATE ON VISCOSITY

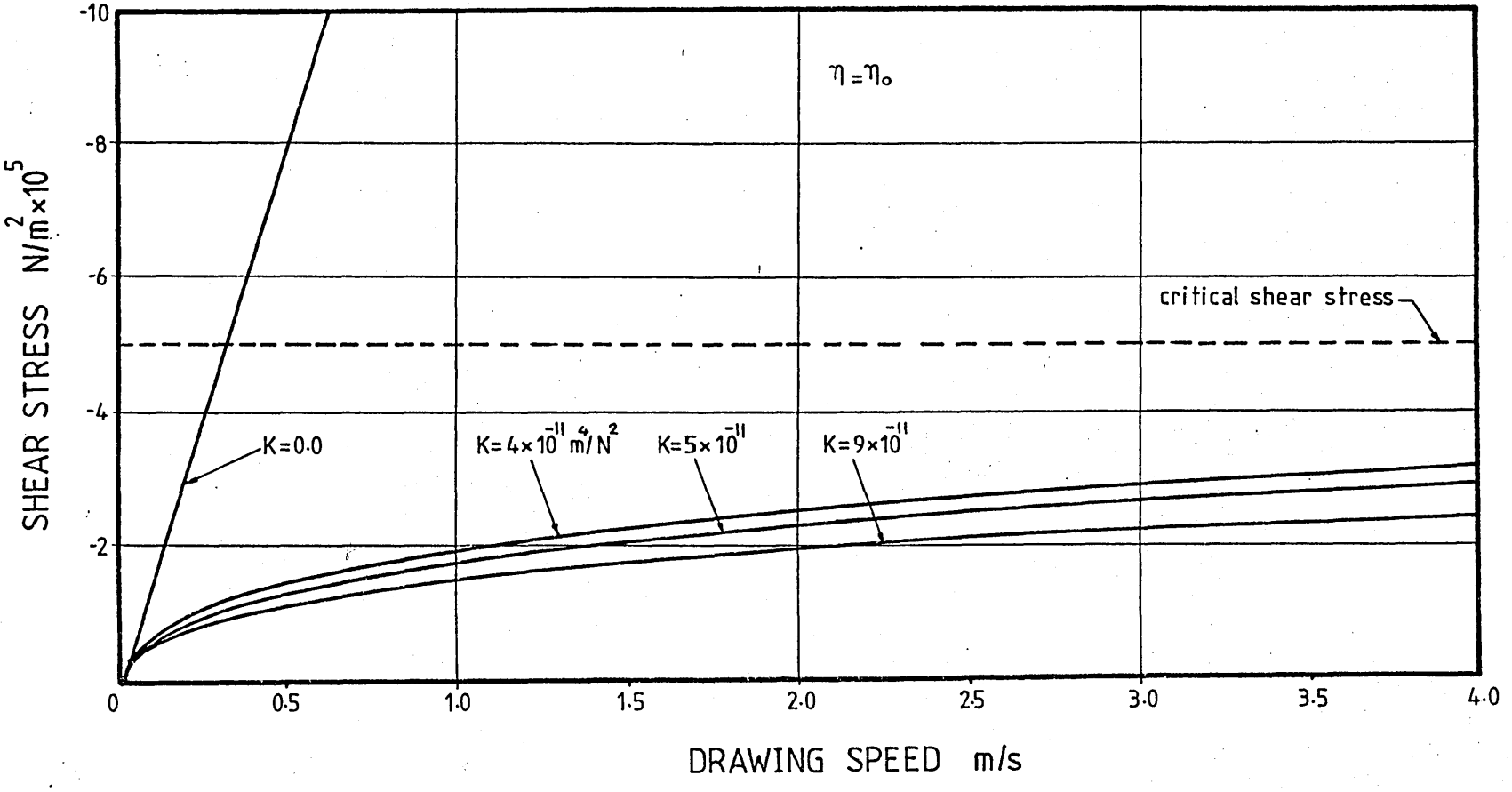

FIG118 : THEORETICAL VARIATIONS OF SHEAR STRESS(τ_{c2}) WITH EFFECT OF PRESSURE ON VISCOSITY

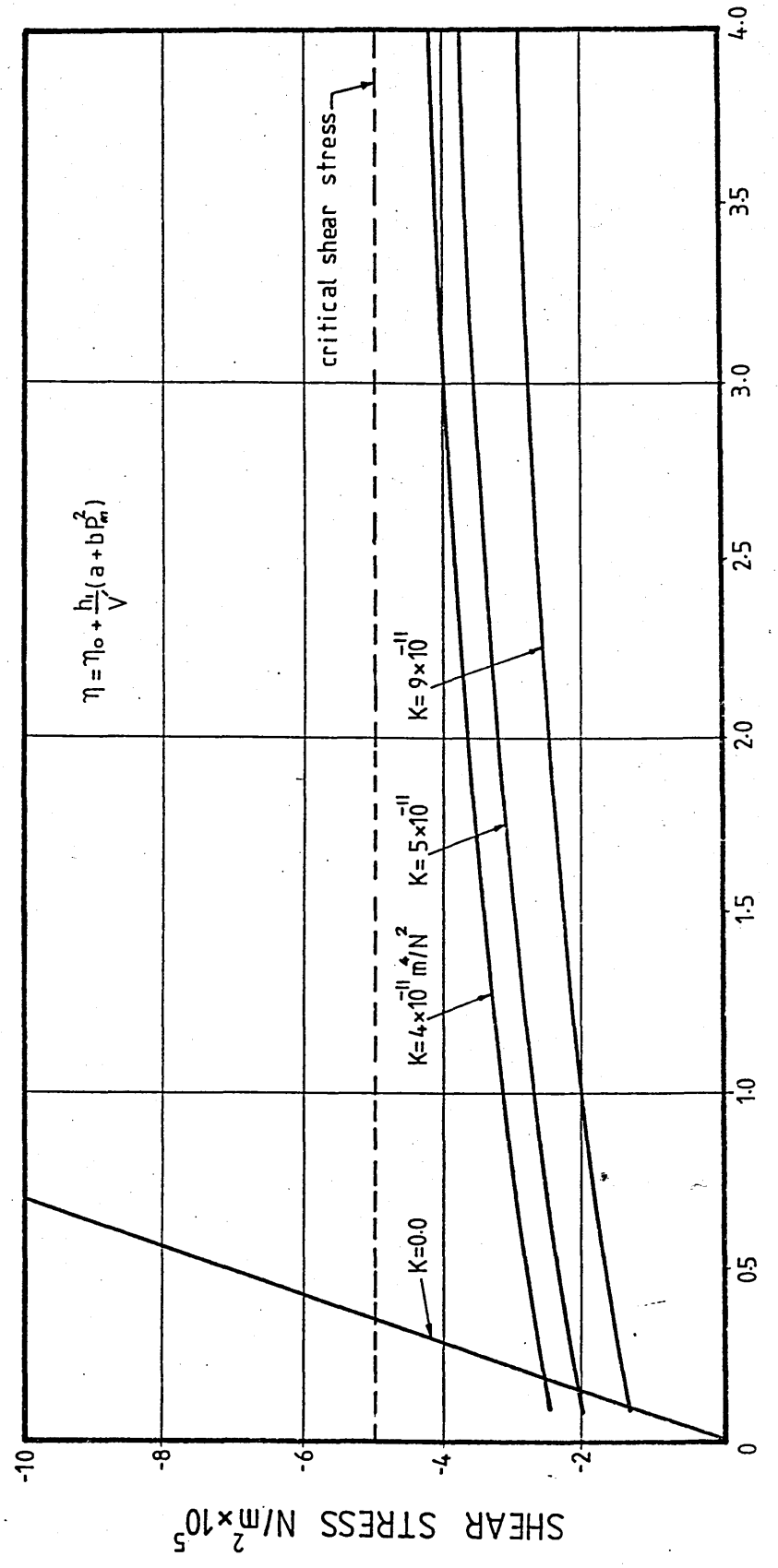

FIG119: THEORETICAL SHEAR STRESS DISTRIBUTIONS ON THE WIRE

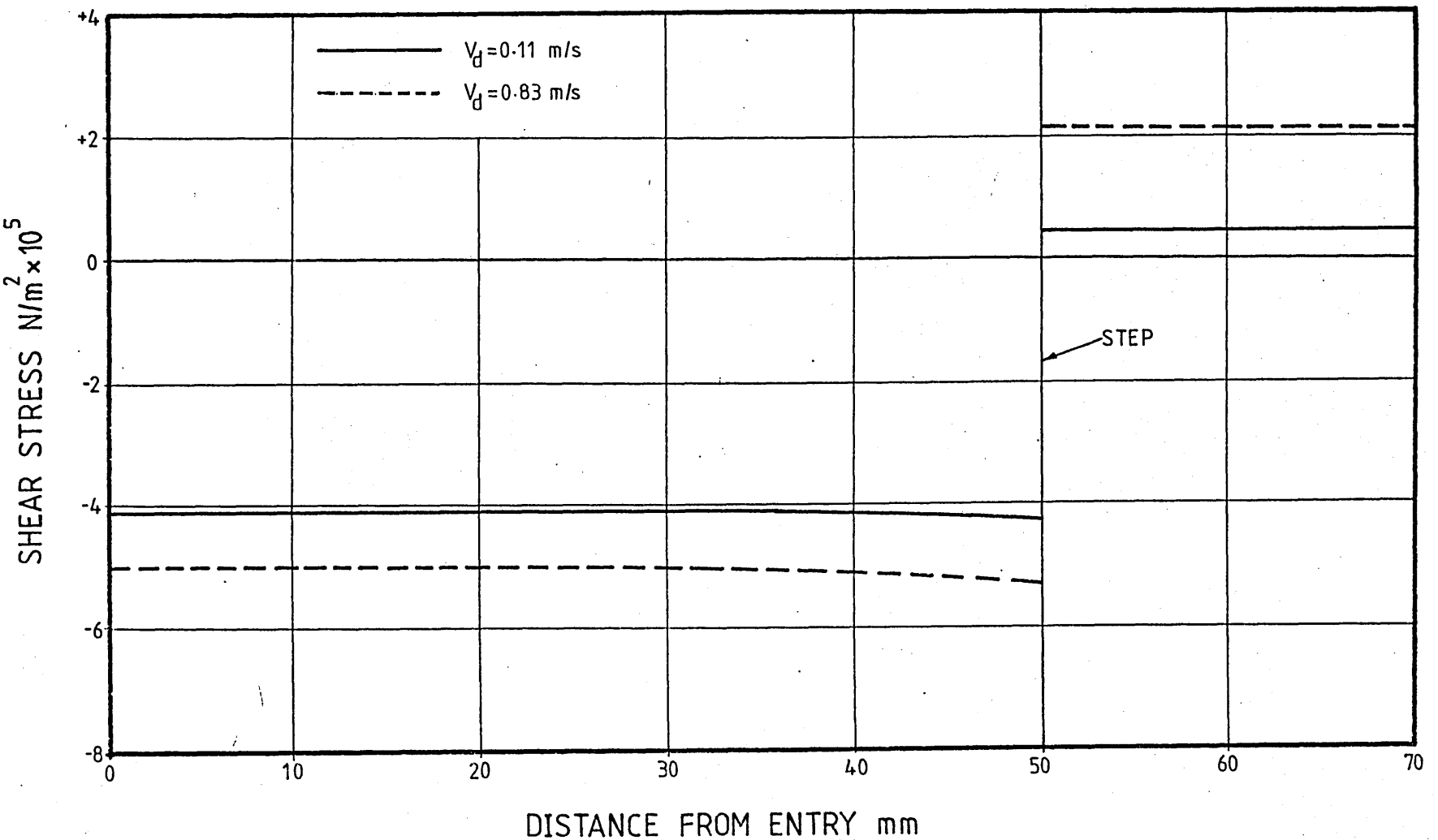

FIG120 : THEORETICAL VARIATIONS OF SHEAR STRESS(τ_{c2}) DUE TO DEFORMATION OF WIRE

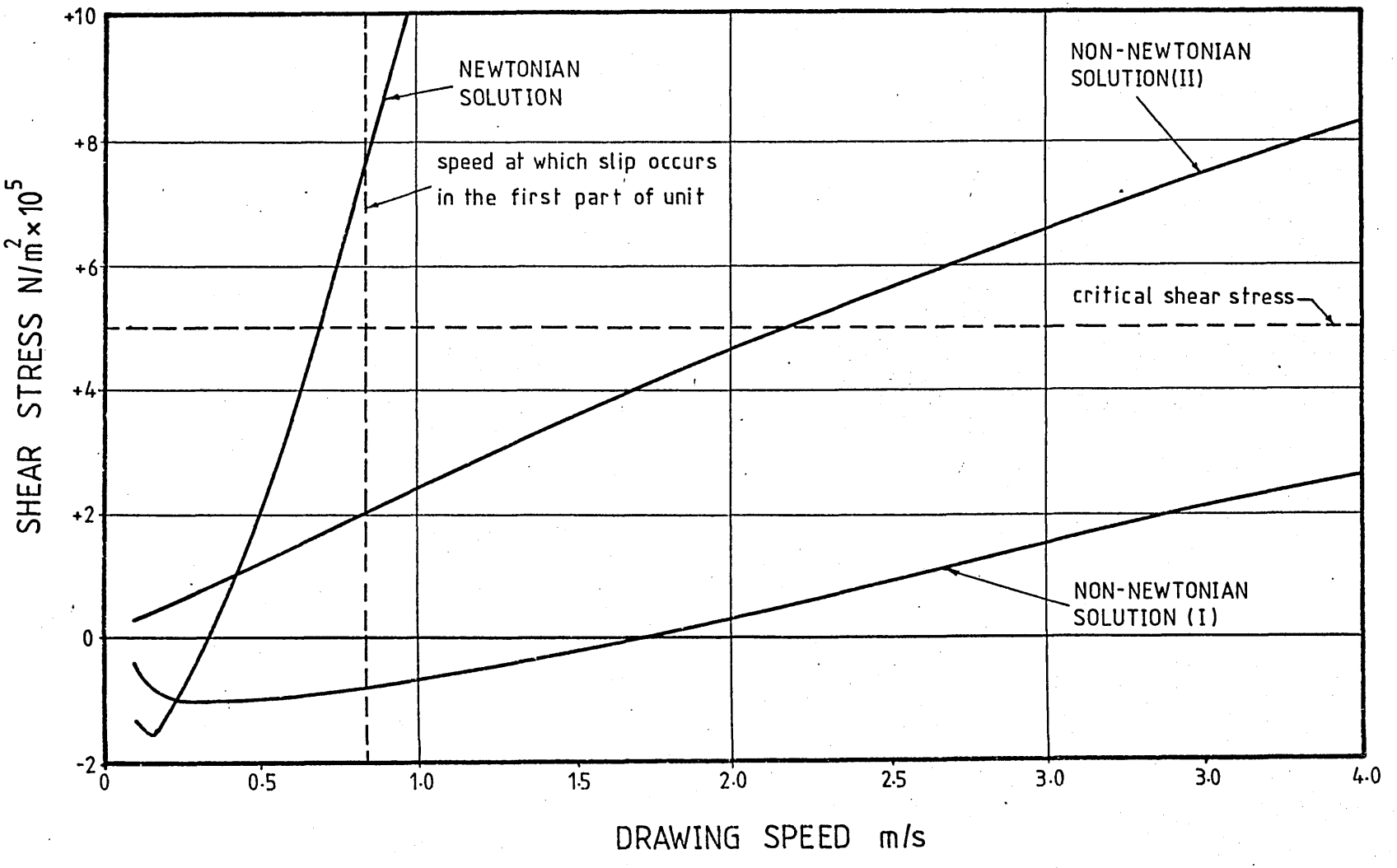

6.7- Theoretical Stress In The Wire.

It has been shown theoretically that according to Tresca or Von Mises theory of yielding, the equation $P + \sigma_x = Y$ must be satisfied for the deformation of wire to continue. Figure 121 shows the predicted axial stress, yield stress and pressure in the stepped bore reduction unit for 15% reduction in area.

The sum of axial stress and the pressure in the first part of the unit, after position of yield, were equal to the flow stress of the wire which they increased non-linearly upto the step. In the second part of the unit, the yield stress was assumed to remain constant since the stress relaxation in the wire was not included in the analysis. Also the axial stress after the step is shown to remain constant. It must be remembered that the shear stress in this section of the unit was predicted to be positive, hence the axial stress should reduce. Since the amount of reduction in the axial stres was found to be negligible, this stress was therefore assumed to remain constant. It was also shown that the pressure decreases after the step, therefore the sum of axial stress and pressure reduced below the yield stress immediately after the step. Hence deformation of the wire was predicted to cease at the step. The experimental results showing the deformation profiles partially confirm the above assumptions.

Figure 121 also shows the effect of the strain hardening and the strain rate sensitivity in the results. It may be noted that for the same amount of reduction in area, higher pressures and axial stresses were required when the strain

rate sensitivity of the wire material was included in the analysis.

6.8- Theoretical Deformation Profile.

The predicted deformation profiles of two drawing speeds are shown in figures 122 and 123 for the copper wire. These results showed that;

i)- A specific deformation profile was predicted for each drawing speed.

ii)- Profiles representing the strain hardening alone showed more deformations than those representing the effect of the strain rate sensitivity of the wire.

FIG121 : THEORETICAL PRESSURE AND AXIAL STRESS DISTRIBUTIONS FOR COPPER WIRE - 15% REDUCTION IN AREA

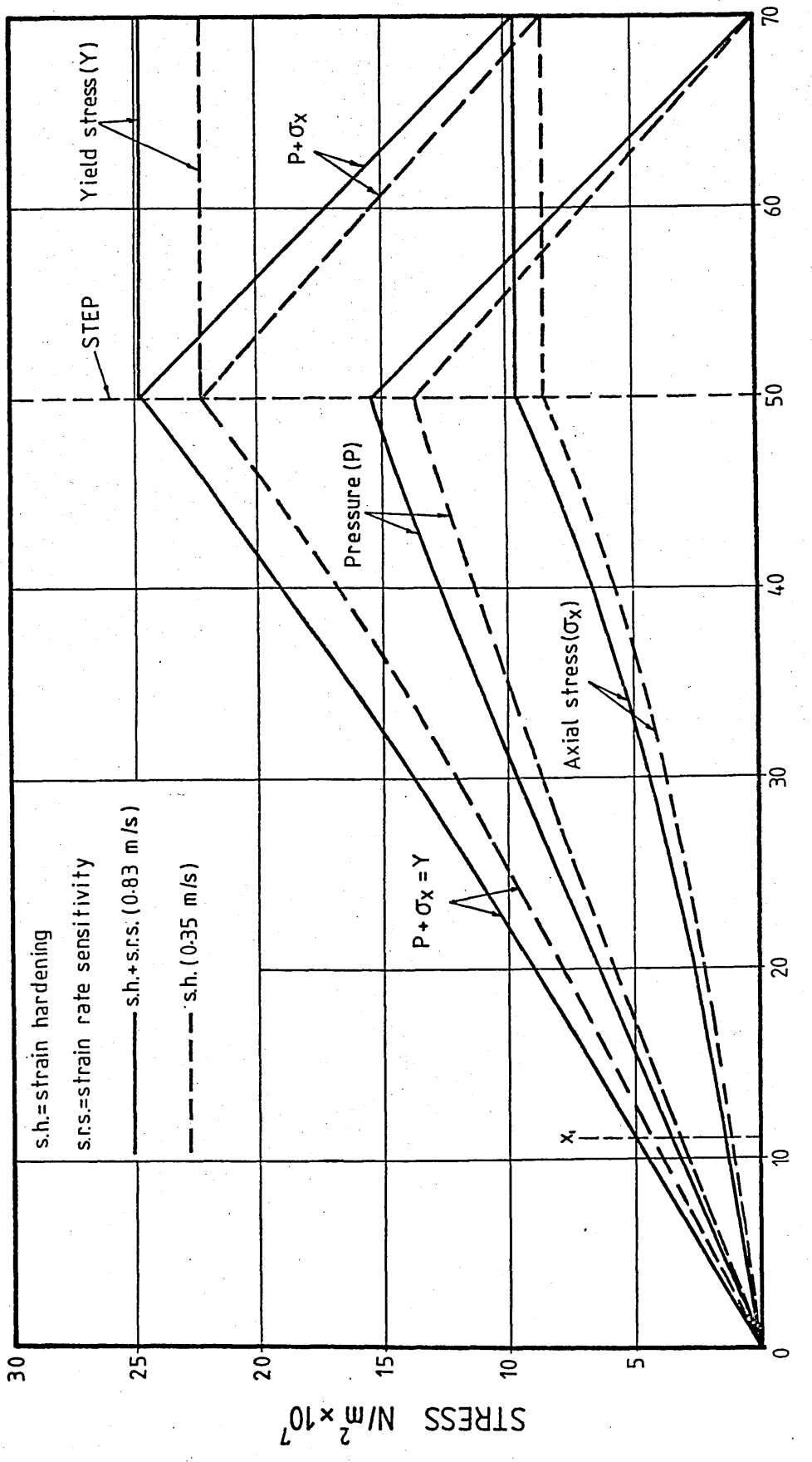

FIG122 : THEORETICAL DEFORMATION PROFILES

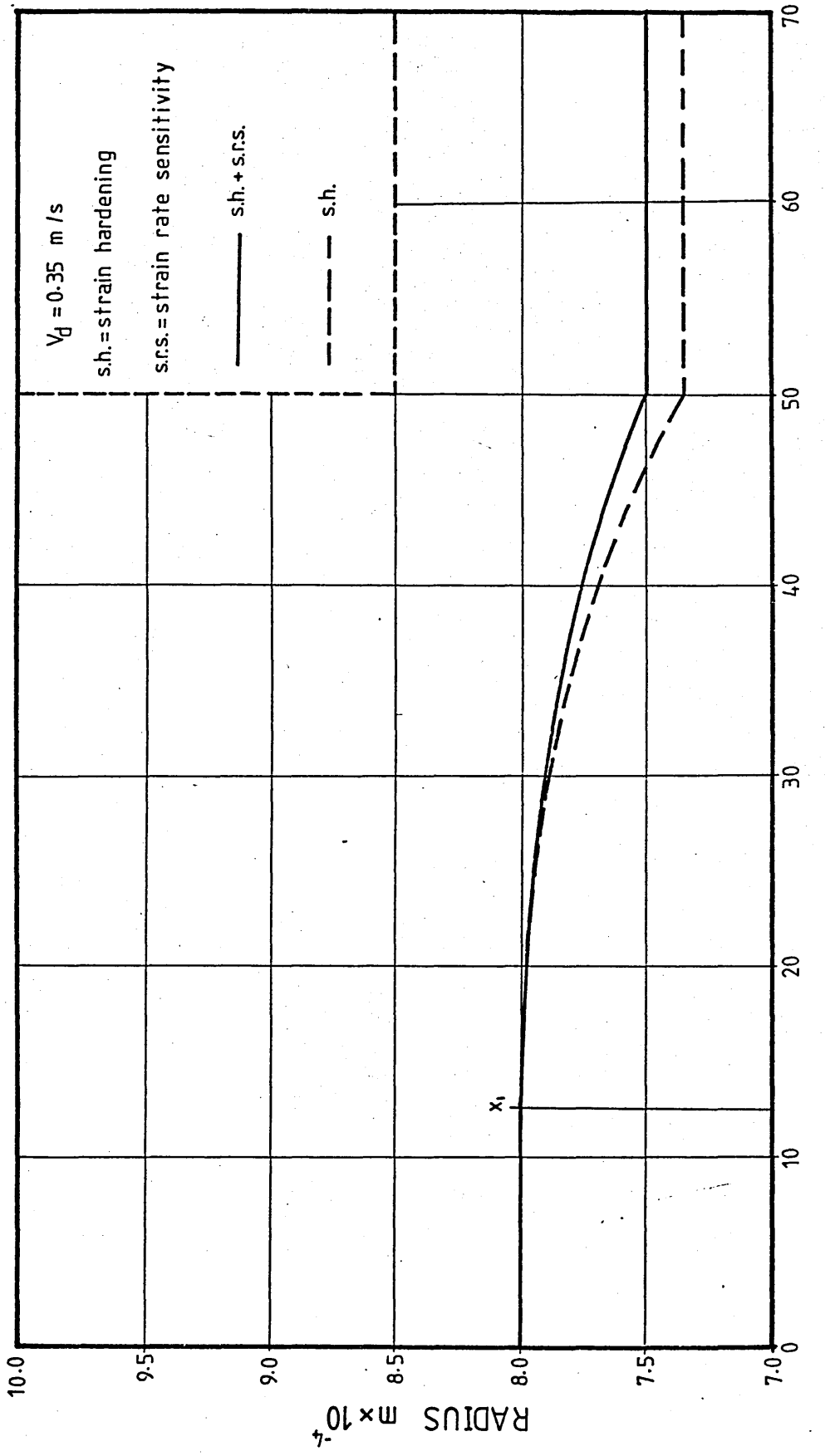

FIG123 : THEORETICAL DEFORMATION PROFILES

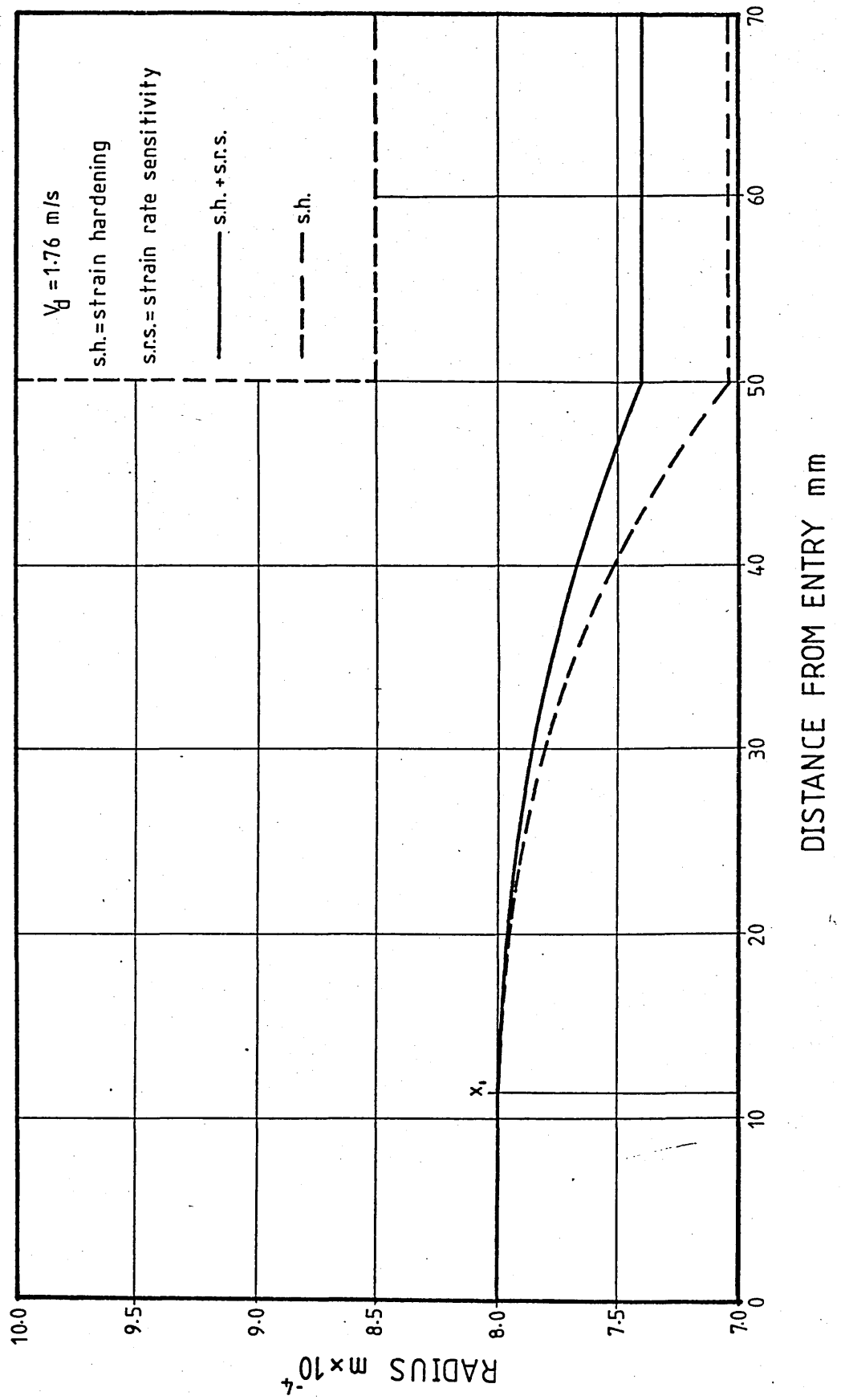

CHAPTER 7: Discussion

7.1- Introduction.

7.2- Error Analysis.

7.3- Discussion On The Test Procedure And The Experimental Results.

7.4- Discussion On The Analysis And The Theoretical Results.

7.5- Comparison Between Theoretical And Experimental Results.

7.6- Recommendations For Future Work.

7.1- Introduction.

The optimisation of the conventional wire drawing process led to the introduction of a novel technique in wire drawing where the reduction die is replaced by the effective die, formed in the stepped bore reduction unit, using a polymer melt acting as a pressure medium. Since the formation of the effective die is dependent upon speed, the amount of deformation of the wire is therefore dependent upon speed. To investigate the performance of the unit, an extensive experimental and theoretical programme was conducted during which a considerable amount of data were obtained. Thus in this chapter, it is aimed to highlight the important results obtained experimentally and theoretically and to carry out a comparison thereby.

The discussion chapter is divided into five sections, error analysis, test procedure and experimental results, analysis and theoretical results, comparison between theoretical and experimental results and recommendations for future work.

7.2- Error Analysis.

Errors always occur in experiments owing to inaccuracies of other variables, however small they may be, which the final results depend upon. Investigation of the probable error is therefore necessary before results can be considered with some degree of confidence.

Theoretical results were predicted using numerical techniques incorporating iterations and finite difference methods since analytical solutions proved difficult to

obtain. An examination of the errors in the results due to method of solution is therefore, necessary before probable errors due to independent variables are estimated. The accuracy of the solution depends upon the errors set to terminate the iteration cycles and also the step size used in the differential equations expressed in finite difference forms.

The tolerated errors for determinations of the pressures in the unit prior to deformation of the wire and in the deformation zone were set to be 10^{-10} between two consecutive cycles before the results were considered sufficiently accurate. A similar procedure was carried out for the equation $P + \sigma_x = Y$ in the deformation zone and in this case the tolerated error in the equation was set to be 10^{-5}. The consistency of the theoretical results were checked when the accepted errors in the solution were altered by $\pm 50\%$. The changes in the final results were found to be negligebly low.

Another area where the accuracy of the solution depends upon, is the step size selected to solve the derived differential equations. All the equations governing the deformation zone were functions of x, therefore at each speed increment, these equations were solved at one millimetre intervals ie Δx = 1mm. It must be remembered that the deformation of wire within Δx is assumed to take place linearly, hence a correct step size was necessary to reduce the amount of errors in the solution. The step size was, therefore, reduced by 50% and 75% and the final and intermediate results were compared to those obtained using the original step size. This test showed that a

negligible change in the predicted results were produced.

The numerical methods adopted to solve the equations were examined and it was found that reasonbly accurate results were obtained due to method of solution. Another equally important area is the experimentally determined variables used in the equations. These parameters may contain small inaccuracies which will introduce some uncertainty in the results and this is aimed to be investigated here.

Dimensions of the stepped bore reduction unit play a very important role in the performance of the unit. Since the polymer had to be heated, the effect of thermal energy on the dimensions of the unit was considered and it was found that the temperature change had little effect on the unit. The accuracy in manufacturing of the unit was then examined. These are;

Input gap (h_1)- This parameter was obtained by measuring the diameter of the wire and diameter of the inlet bore of unit. A hand micrometer was used to measure the wire diameter and ± 0.005mm error is allowed in the reading. Also allowing tolerances of ± 0.002mm for the drilling process, therefore $\pm 3.6\%$ error is estimated for the inlet gap.

Output gap (h_2)- Similar to the input gap and in this case $\pm 13\%$ error is estimated.

Input length (l_1)- It is assumed that the manufactured length of the first part of the unit is within ± 1mm

inaccurate, therefore ±2% error is estimated.

Output length (l_2)- Similar to input length, hence ±5% error is estimated for this length.

Parameters representing the rheology of the polymer melt were determined experimentally using a polymer melt rheometer (see chapter 2). Therefore ±5% error is assigned for the initial viscosity (η_o) and the non-Newtonian factor (K).

Similarly, parameters representing the yield characteristics of the wire materials were determined experimentally using a Hounsfield tensometer (see chapter 4). Again ±5% error is assigned for initial yield stress (Y_o), strain hardening constant (K_o) and the strain hardening index (n).

Considering the above assigned errors, a possible arithmetical error of about±6% could occur in the theoretical results. However a considerable difference has been observed between the theoretical and the experimental results which suggests that the analysis carried out for the stepped bore reduction unit does not represent the actual drawing process. It is believed that the discrepancies have arisen due to the absence of other parameters in the analysis such as the effect of temperature change on the flow properties of the polymer melt and the wire material, stress relaxation of the wire, possible crystallization of the polymer melt at high pressures, slip factor etc. These will be refered to later in this chapter.

7.3- Discussion On The Test Procedure And Experimental Results.

Many interesting results have emerged while carrying out the experimental tests, using the stepped bore reduction unit and polymer melt as a pressure medium. During the course of the experimental programme, parameters such as drawing speed, polymer type, melt temperature, wire material and gap ratio of the unit were varied in order to investigate their effect on the performance of the unit. Diameter of the wire and the length ratio of the unit were kept constant throughout the tests.

Two polymers having different densities and viscosities were selected as pressure medium, one being the Alkathene WVG 23, an ICI polymer with relatively low melt temperature and the other being polypropylene KM 61, a Shell polymer with a higher melt temperature and viscosity. The effect of temperature increase on the performance of the unit was examined using WVG 23 polymer and the effect of change in the gap ratio was examined when KM 61 polymer was used.

The drawing speed was found to have the most dramatic effect on the performance of the unit. This effect is manifested in terms of the shear rates on the viscosity of the polymer which leads to the catastrophic slip in the polymer. Two types of flow of polymer was thought to establish as the drawing speed was increased. These are sub-critical and critical flow which were observed more clearly in the case of WVG 23 polymer. Results of percentage reduction in area, using this polymer, are shown in figures 51 and 52, which show an optimum drawing

speed for each wire material at which the deformation of wire was found to be maximum. This point changed very little when different wire materials were used or temperature of melt was increased. These maximum points are believed to be the transition between the sub-critical and critical flow of the polymer which unfortunately occured at very low shear rates. As soon as critical flow (slip) of polymer was established, the performance of the unit reduced drastically as speed was increased such that at drawing speeds in excess of 1.0 m/s, no further reduction in area was obtained for mild steel wire.

At the drawing speed of 0.8 m/s, a discontinuity in the results of percentage reduction in area, coating thickness, and pressure at position 2 was observed when stainless steel wire was drawn. It is difficult to explain this phenomenon in terms of melt fracture of the polymer melt since the discontinuity occured at speeds higher than those at which slip was thought to be established. With reference to figure 30 (pressure at position 2 (step)), the transition of flow of polymer seemed to take longer than that of percentage reduction in area and as soon as pressure started to reduce in magnitude, the discontinuity occured. The actual mechanism of this behaviour is a matter for conjecture. Very high pressures are thought to be responsible for this discontinuity and will be discussed later. The results of percentage reduction in area versus drawing speed using KM 61 polymer (figures 53 and 54) indicate that, unlike the WVG 23 polymer, the initial flow of polymer and slip are both dependent upon the wire material. Immediately after commencement of the flow of

the polymer, the percentage reduction in area of stainless steel and mild steel wires reduced in a different manner as drawing speed was increased. The transition of flow of polymer was only observed for copper wire which occured at about 0.6 m/s. The reason for the random reduction in area of copper and stainless steel wires, prior to initial flow of the polymer, is thought to be the excess axial stress due to back pull of the polymer. The result of increasing the exit gap was to reduce the deformation of the wire at higher drawing speeds. This may be explained in terms of the pressure generation due to the geometry of the unit ie as the exit gap increases, the flow of polymer is therefore less restricted hence lower pressures are generated which leads to smaller reduction in area.

Polymer coating on the wire is the consequence of this drawing process. The examination of the polymer coating after each test confirmed that continuous and poorly adhered protective layer of polymer was deposited on the wire. The method of measuring the coating thickness is explained in chapter 4. The trends of the results of coating thickness were found to be similar to those of percentage reduction in area. Crampton (16) showed that using WVG 23 polymer as a lubricant in conventional wire drawing, the coat thickness reduced as the drawing speed was increased. He also suggested that the reduction in the thickness of the polymer coating was the consequence of slip in the melt. The transition of flow of polymer however, was not clearly shown in his results. In the case of zero reduction in area, the coating thickness on the stainless steel wire reduced below the gap existing

between the wire and the unit. This provides some evidence for the presence of slip in the unit between the wire and polymer interface.

Shark-skin is another flow defect associated with flow of the polymer melts which appears on the polymer extrudates at shear stresses below the critical value. This was confirmed while KM 61 polymer was being extruded through an extrusion rheometer (see figure 10). It is also shown that the formation of the shark-skin takes place outside the extrusion die (26). With reference to the results of coating thickness however, it may be noticed that shark-skin on the KM 61 polymer were observed at speeds where slip is thought to occur (see figure 49). It is doubted that the condition in an extrusion rheometer can be considered in this particular case since polymer melt was subjected to pressures and shear rates much higher than those applied in an extrusion rheometer.

Drawing load was measured by attaching strain gauges on the support frame which produced a trace on the U.V. paper when it was deflected due to the drawing force. A typical trace of the drawing load is shown in figure 23. Immediately after engaging the clutch, a sudden increase in the drawing load was noticed which was maintained for about half a second before full load was established. The time taken for the development of the flow of the polymer in the unit is thought to be responsible for the delay in the full drawing load. The results of the drawing loads with WVG 23 polymer again showed evidence of the transition between the sub-critical and critical flow of the polymer. The optimum speeds in these results do not correspond to

those of percentage reduction in area and coating thickness (see figure 44). Also prior to initial flow of KM 61 polymer for copper and stainless steel wires, the drawing loads showed random patterns and were lower in magnitudes compared to those when the polymer flow was commenced. This is believed to be due to back pull of the polymer melt which caused random deformation in the wires as shown in figure 45. As soon as flow of polymer started, the drawing load reduced. This again provides a complementary evidence for slip in the unit. The interesting point in these results is the difference between the magnitudes of the drawing loads measured for different wire materials. For example the drawing loads measured for copper wire was less than those measured for stainless steel wire and higher than those for mild steel wire and yet this material was reduced more in diameter than the other two wires. The reason for this phenomenon is a matter of conjecture. Temperature increase in the WVG 23 polymer reduced the viscosity of this polymer which caused less deformation of the copper wire, hence lower drawing loads were measured as shown in figure 43. The decrease in the gap ratio of the unit, when KM 61 polymer was used, increased the drawing load at slower drawing speeds, whereas the amount of deformation in the mild steel wire remained more or less the same. The extra amount of polymer flow in the unit is thought to be responsible for the increase in the drawing load. The increase in the coating thickness on the mild steel wire as the result of increase in the exit gap also provides some evidence for the above suggestion (see figure 50).

Four pressure transducers were mounted on the stepped bore reduction unit and for each speed increment, the trace of pressure at each location was recorded on the U.V. paper which is shown in figure 23. Figures 27 to 42 show the measured pressures for different wire materials and polymers used for the tests. The effect of increase in the melt temperature was to reduce the viscosity of the polymer and hence to reduce the generated pressures. For the same melt temperature however, the measured pressures, especially at position 2 (step), appear to indicate that the magnitude of the pressures were dependent upon the wire materials. This was found to be true for both polymers. When copper wire was drawn, comparetively lower pressures were generated and higher percentage reduction in area were obtained. In the case of mild steel and stainless steel wires, much higher pressures were measured whereas the reduction in area was found to be smaller than those measured for copper wire.

Results of pressure with WVG 23 polymer also provide evidence of transition of flow in the polymer. The optimum speed however, seemed to be slightly different for different positions. The sub-critical and critical flow of KM 61 polymer was not clearly exhibited in the obtained results. The trends of the pressures measured for the copper wire using KM 61 polymer (see figure 29) were found to be similar to those reported by Crampton (16) when WVG 23 polymer was used.

Apart from the shear rate, the magnitudes of the pressures generated during the drawing process are believed to be another reason for slip to occur. Maxwell and Jung (30)

reported that when polystyrene was subjected to the pressure of 150 MN/m^2, the polymer acted like solid material. Pressures measured during the experimental tests, especially at position 2 were found to have similar magnitudes for copper wire and nearly twice as much for stainless steel wire. It will not be surprising if the polymer melt becomes solidified or crystallized under these pressures. The discontinuity in the results of the pressure for stainless steel wire (figure 30) could be related to the above mentioned effects in the polymer at high pressures.

The deformation profiles measured experimentally showed that the formation of the effective die was dependent upon the drawing speed and also varied for different wire materials. In conventional wire drawing process, the deformation of the wire takes the shape of the reduction die, therefore the roundness of the final diameter is decided by the roundness of the reduction die. A qualitative test, therefore was conducted to examine the products obtained using the die-less method. Roundness test was undertaken to check the circularity of the drawn wires and the results showed that the amount of errors measured in the wires, in the case of both polymers, were similar to those drawn by the conventional method (see figure 58 to 69). This seems to suggest that the applied stresses on the wire (pressure and axial stress) were fairly uniform for both polymers. It must be remembered that the accuracy of the dimensions of the unit and concentricity of the wire in the unit, have determining effects on the amount of reduction in the wire.

Another method of examining the uniformity of the axial stress and the pressure in the unit was to draw a long length of the wire and then examine the variations of the final wire diameter over the length of the sample. Any variations of either stresses during the drawing time would be reflected on the variations of the final diameter of the drawn wire. The results of these tests are presented in figures 70 and 71 which show that the fluctuation of these stresses are very little since the magnitudes of the errors measured in the final diameter remained close to those measured in the original wire diameter.

Total elimination of the metal to metal contact in this unique drawing process produced wires of matt surfaces. Photographs of the enlarged surfaces are shown in plates 17 to 29. The mattness effect on the surface of the copper wire drawn by the die-less system was thought to be the wavyness of the surface which became more pronounced as the reduction in area increased. This effect on the surfaces of the mild steel and stainless steel wires was not clearly visible and instead elongated and longitudinal grooves on the surface of the wires was believed to provide the mattness effect on the finished product. Prior to deformation of the wire, the surface was more flatter and these grooves also prevailed.

An attempt was made to investigate the feasibility of a multi-unit drawing process in which more than one unit could be operated simultaneously. This stemmed from the desire to improve the performance of the unit at higher drawing speeds. The first test was carried out such that prior to each run, the polymer coating on the wire was

removed. This method of test showed that with a constant length ratio, there is a gap ratio for which deformation of the wire ceases. At the drawing speed of 1.0 m/s, this gap ratio was found to be 2 with a possible exit gap of 0.14mm. The total reduction achieved in three passes was about 21% which was higher than that obtained from a single unit system. The next test was conducted at the same drawing speed and this time the polymer coating was allowed to remain on the wire. This test produced even higher reduction in area (36%) but the wire breakage occured repeatedly in the second pass. The reason for the wire breakage was thought to be the excess stresses generated in the unit. Since the overall diameter of the wire and the polymer coating was slightly greater than the exit diameter of the unit, the flow of the polymer was more restricted which led to higher pressures and axial stresses, resulting in wire breakage as well as reducing the diameter. A similar test was carried out at drawing speed of 4.0 m/s which provided some encouraging results, proving that a multi-unit system may be operated successfully eliminating the limitations encountered while a single unit was used.

7.4- Discussion On The Analysis And The Theoretical Results.

The present analysis enabled the prediction of the percentage reduction in area, coating thickness, position of yield of the wire within the unit, melt pressure, stress in the wire and the deformation profile of the wire. The following assumptions were made in order to simplify the analysis.

The empirical non-Newtonian equation commonly used to predict the behaviour of the polymer melt, as proposed by Rabinowitsch (35), takes the form;

$$\tau + K\tau^3 = \eta \frac{dU}{dy}$$

This equation was used in the analysis to predict the pressure and the shear stress in the melt within the no-slip range. The non-Newtonian factor "K" and the initial viscosity "η" were both determined experimentally by curve fitting the above equation over the results obtained from the flow characteristics of the polymer melt (see chapter 2). The above equation represents the effect of the shear stress on the viscosity only. It is known that the pressure increases the viscosity of the polymer melt. To incorporate this effect in the analysis, the data provided by Westover (28) for the Alkathene polymer was used to produce figure 15 which shows that the influence of pressure on the viscosity is dependent on the shear rate in the melt. The accuracy of Westover's results is not known and unfortunately the polymer used for his

experiments was not WVG 23 polymer. Therefore this may have introduced some discrepancy in the theoretical results. Using figure 15, a generalized equation was derived to predict the viscosity of the polymer melt at known pressures and shear rates which is shown to take the form;

$$\eta = \eta_o + \left(\frac{a + b\, P_m^2}{\dot{\gamma}} \right)$$

where a and b are constants. $\dot{\gamma}$ is the apparent shear rate in the first part of the unit and is assumed to be $\frac{\acute{V}}{h_1}$. Since it was shown theoretically that slip occurs in the first section of the unit, therefore the apparent shear rate in this part was taken into account. Also the pressure component in the above equation is the one calculated at the step ie the maximum pressure in the unit. An attempt was made to include the effect of the pressure profile into the viscosity in order to predict the variations of viscosity along the unit but it was discarded in view of the fact that the equations became very cumbersome to solve.

Slip in the polymer is believed to occur and the experimental results justified this. The magnitude of the critical shear stress have been estimated to be between 0.1 to 1.0 MN/m^2 (20 to 25). When extruding polypropylene KM 61 polymer, melt fracture (slip) was observed at shear stress of about 0.32 MN/m^2. Westover (28) showed that for Alkathene polymer slip occured at shear stress of about 0.7 MN/m^2. The magnitude of the critical shear stress considered in the analysis was 0.5 MN/m^2. It must be remembered that the pressures and shear stresses

applied on the polymer melt were much greater than those created in an extrusion rheometer, therefore the critical shear stress chosen for the condition of slip was only an approximation. In order to calculate the flow of the polymer melt after slip, a pressure ratio between no-slip and slip of polymer should be known which was not easily determinable. Therefore it was assumed that polymer melt could not accommodate further increase in pressure at the onset of slip and that the flow of polymer melt remained constant for further increase in the drawing speed. The above assumptions permitted the results to be obtained easier after slip was predicted in the unit.

In addition to the above, the following assumptions were also made;

i)- The flow of the polymer melt in the unit is laminar - This seems to be a reasonable assumption since the velocities of the wire are low, viscosity of the polymer is high and the gaps are small.

ii)- The flow of the polymer melt is axial - As soon as the flow through the unit is established, little or no back flow is expected which allowed the flow to be considered as one dimensional.

iii)- The ratio of the thickness of the polymer layer to the dimensions of the unit is small - This enabled the analysis to be conducted in rectangular rather than cylindrical co-ordinates.

iv)- Pressure through the thickness of the polymer layer is constant - This assumption simplified calculation of the pressure in the unit and allowed the viscosity constants to be evaluated.

v)- The flow of the polymer melt through the unit is isothermal - This may introduce some error in the results since viscosity of the fluids are sensitive to the temperature change.

vi)- The deformation of the wire is isothermal - This assumption again may cause some error in the results since it is known that the temperature of the wire increases during the drawing process.

vii)- Slip occurs between the polymer melt-wire interface - A reasonable assumption since the thickness of the polymer coating measured experimentally was found to be less than the gap between the wire and the tube in the case of stainless steel wire.

The analysis of the stepped bore reduction unit was carried out in two parts, i)- the flow of the polymer melt which enabled the pressure in the unit, the shear stress on the wire and the position of yield of the wire in the unit to be calculated and ii)- the deformation zone, which allowed the axial stress, and the deformation profile of the wire to be determined.

The results of the percentage reduction in area showed two zones;

i)- At slower drawing speeds, the percentage reduction in area increased as the drawing speed was increased.

ii)- When slip occured, the percentage reduction in area reduced as the drawing speed was increased further.

As the input parameters were varied the following points became apparent;

a)- The inclusion of the strain rate sensitivity reduced the amount of deformation and had little effect on the critical speed.

b)- Increase in the gap ratio increased the percentage reduction in area and also affected the critical drawing speed. Increasing the length ratio, initial viscosity and pressure coefficient of viscosity had the same effect.

c)- Increase in the non-Newtonian factor, decreased the percentage reduction in area and increased the speed at which the critical shear stress occured.

d)- Increase in the initial yield stress reduced the percentage reduction in area and had little effect on the critical drawing speed. A similar effect was also observed when strain hardening constant, strain hardening index and the strain rate sensitivity constant were increased.

e)- Decreasing the strain rate sensitivity index and the

original diameter of the wire increased the percentage reduction in area.

Some of the above results were expected and others became more apparent as the results were obtained. The inclusion of the strain rate sensitivity for example was expected to reduce the amount of deformation of the wire. This was due to the increase in dynamic yield stress as the drawing speed was increased (see equation 39 in chapter 5). The predicted deformation of the wire seemed to be very sensitive as the exit gap of the unit was reduced. This is shown in figure 74. With the gap ratio of 5, the slip was predicted at very slow drawing speeds and higher percentage reductions in area were obtained since higher pressures were calculated. With the gap ratio of 2 however, the slip was not predicted within the range of the drawing speeds and small deformations were obtained (maximum of about 3%). The increase in initial viscosity icreased the percentage reduction in area and indicated that slip could occur at slower speeds. The length ratio had similar effect on the reduction in area. This was again due to higher pressures predicted in the unit. The reduction in the non-Newtonian factor "K" was also expected to increase the percentage reduction in area as the fluid became more Newtonian.

Another interesting result obtained was the increase in the pressure coefficient of viscosity which simply increased the predicted pressure. When $b = 6 \times 10^{-11}$ m^2/N, slip was shown to occur at very slow speeds. The increase in the initial yield stress of the wire reduced the percentage reduction in area. A similar effect was observed for the strain hardening

constant K_o. The critical drawing speed was found to be affected slightly by changing the above parameters(Y_o, K_o). These parameters simply increased the flow stress of the wire which reduced the amount of deformation. The increase in the strain hardening index "n" however, increased the theoretical percentage reduction in area. This may be explained with reference to figures 24 to 26, which show the yield characteristics of the wires (the interesting similarities may be observed if these results are compared to the flow characteristics of the polymer melts in figures 9 and 10). As the index "n" was increased the stress-strain curves became more parabolic (softer wires), hence lesser stresses were needed for the flow of the material at higher strins.

The strain rate sensitivity constant, if it was increased, would increase the predicted percentage reduction in area. This parameter reduced the effect of the mean strain rate of the deforming wire on the dynamic yield stress of the material (see equation 38 in chapter 5). The increase in the wire diameter reduced the percentage reduction in area and increased the amount of deformation predicted in the wire. The percentage reduction in area was reduced simply because the ratio of the changes in the diameter to the original diameter was reduced. The amount of deformation was increased because the axial stress on the wire was predicted to reduce according to equation 24 in chapter 5. This also reduced the length of the deformation zone but the overall effect was to produce more deformation in the wire.

The trends of the theoreticall results obtained for the

coating thickness were found to be similar to those of the percentage reduction in area as shown in figures 87 to 100. The only exception observed in these results was that the increase in the wire diameter predicted thicker coating on the wire which was found to be in reverse order to the corresponding results of the percentage reduction in area. Similar theoretical results have also been predicted by Crampton (16).

Prediction of the yielding position of the wire in the unit produced another set of interesting results which are shown in figures 101 to 110. It may be noticed that the critical drawing speeds in these results are not easily distinguished. In order to be able to predict the yielding position, it was assumed that the wire was a rigid body before deformation commenced. A reasonable simplification since the amount of elastic strain before plastic deformation was shown to be comparatively small (usually about 0.3%). Therefore the strain hardening and the strin rate sensitivity of the material were not included in the prediction of the position of yield (X_1). The following observations were made as the results were obtained;

i)- The increase in the length ratio reduced the undeformed length of the wire in the unit. The gap ratio, intial viscosity and viscosity constants had similar effect.

ii)- The increase in the non-Newtonian factor "K", increased the undeformed part of the wire. So did the increase in the initial yield stress and diameter of the wire.

A close inspection of the equation predicting X_1 would show that an increase in the initial yield stress simply would increase the undeformed length X_1. Similarly any parameter which predicted higher pressures and shear stresses in the unit, reduced the undeformed length of the wire.

The theoretical results of the pressures showed that as the non-Newtonian factor "K" was reduced, the fluid became more Newtonian and the effect of coefficient of pressure on the viscosity was to generate higher pressures (figures 111 and 112). Both parameters predicted slip at slower drawing speeds as they were increased (figures 113 and 114). A similar prediction was also made for the shear stresses on both side of the unit. The two following observations were made from the results of the shear stresses;

i)- Shear stresses on the wire, prior to deformation, were both negative

ii)- Slip was predicted to occur in the first part of the unit only.

Perhaps one of the most interesting result obtained was the shear stress on the wire in the second part of the unit (τ_{c2}) when the change of gap due to deformation of the wire was taken into account. It was shown that with increasing gap, the shear stress in the first part of the unit increased slightly in the negative direction. This change of gap however, caused the shear stress on the wire in the second part of the unit to become positive ie in the same direction as the motion of the wire. This of course was found to be

dependant upon the amount of deformation. Figure 120 shows that with the effect of pressure on the viscosity (non-Newtonian solution (II)), higher deformations were predicted, hence the shear stress on the wire was always positive. On the other hand, the non-Newtonian solution (I) showed that there was an optimum speed at which the the shear stress on the wire was maximum and negative at about 0.4 m/s. As the deformation of wire increased, the shear stress was predicted to become positive from the drawing speeds in excess of 1.7 m/s.

The positive shear stress in the second part of the unit reduced the axial stress slightly but this effect was found to be negligible compared to the magnitude of the axial stress in the first section of the unit. Therefore the axial stress was assumed to remain constant after the step as shown in figure 121. The yield stress was also assumed to remain constant after the step since the stress relaxation was not taken into account. Considering the above conditions in the unit after the step, the sum of pressure and the axial stress ($P + \sigma_x$) reduced below the yield stress and hence the Tresca or Von Mises yield criterion ($P + \sigma_x = Y$) was not satisfied immediately after the step. The deformation of the wire was therefore assumed to terminate at the step.

The inclusion of the strain rate sensitivity in the analysis increased the yield stress and the axial stress in the wire. Therefore for the same amount of deformation, more pressure was required to reduce the wire diameter.

7.5- Comparison Between The Theoretical And Experimental Results.

In the two previous sections, a discussion of the theoretical and the experimental results was carried out through which some discrepancies became apparent. In this section, it is aimed to out line these discrepancies and discuss the possible cause of their occurance.

Figure 124 shows typical experimental and theoretical results of the percentage reduction in area obtained for the copper wire. At slower drawing speeds, the non-Newtonian analysis appeared to under estimate the reduction in area and at higher drawing speeds, for which the critical shear stress was predicted, over estimated the experimental results. The Newtonian solution however showed a totally different trend compared to the other results.

The error analysis carried out earlier in this chapter indicated that errors could occur in the results due to the inaccuracies in the independant variables. The theoretical variations of the exit gap, in figure 74, showed that the results were very sensitive as the gap ratio was changed. It was predicted that with the gap ratio of 2, small reductions in area were possible and slip did not occur in the entire range of the drawing speeds. The experimental results illustrating the effect of the gap ratio, in figure 54, showed that slip occured at slow speeds and only the limiting drawing speed (when the percentage reduction in area became zero) was reduced due to the reduction in the gap ratio.

The temperature of the melt was also varied during the

experimental tests as shown in figure 51. It was found that the critical drawing speed was not affected greatly by the temperature change and instead the overall percentage reduction in area was reduced.The equivalent theoretical results are shown in figure 76 which were produced by changing the initial viscosity of the polymer melt. The critical shear stress was predicted to occur at higher drawing speeds by reducing the initial viscosity and still over estimating the experimental results at higher speeds.

The effects of other variables were also examined theoretically in order to investigate their influence on the predicted results. The increase in the non-Newtonian factor "K" only reduced the speed at which the critical shear stress was predicted. The viscosity constants "a" and "b" were thought to carry some error since they were evaluated from the available data. A large change in "a" was found necessary for a reasonable change in the theoretical results and the overall trends remained more or less the same as before. Increase in the pressure coefficient of viscosity increased the overall results and predicted slip at slower drawing speeds (see figures 79 and 80).

Parameters representing the flow stress of the wires (Y_o , K_o and n) were determined experimentally and it is belived that they contained very little error. Variations in these parameters also did not reduce the amount of discrepancy existing between the theoretical and the experimental results. A similar observation was made for the parameters representing the strain rate sensitivity of the wire material.

The trends of the results for the coating thickness

were found to be very similar to those of the percentage reduction in area, therefore the above discussion is also applicable for the coat thickness.

Figures 125 to 127 show the theoretical and the experimental pressure profiles at three different drawing speeds. At the drawing speed of 0.22 m/s (figure 125) a reasonably close correlation was observed between the theoretical and the experimental results of copper and mild steel wires. For the 18/8 stainless steel wire however, the measured pressure was found to be much higher than that predicted. At the drawing speed of 1.18 m/s (figure 126) very good agreement appeared to exist between the predicted and the measured results for all three materials. Figure 127 shows the pressure distributions at the drawing speed of 2.9 m/s. The theoretical results seemed to over estimate the experimental results for all three wires.

Also for comparison purposes, the measured and the predicted deformation profiles of the copper wire are shown in figures 128 and 129. At the slower drawing speeds (0.22 m/s figure 128), the measured profile showed that yielding occured nearer to the step and that the deformation took place in a much steeper manner, producing higher reduction in the diameter than that predicted theoretically. At slightly higher speed (0.48 m/s, figure 129), a good correlation was observed between the experimental and the theoreticall results especially the profile presenting the strain hardening of the wire alone. An attempt was made to obtain the theoretical deformation profile of the mild steel and the stainless steel wires and to compare them with the measured profiles (as shown in chapter 4). The analysis

predicted very little deformation for both materials, hence the above comparison was carried out for the copper wire only.

FIG124 : COMPARISON BETWEEN EXPERIMENTAL AND THEORETICAL RESULTS

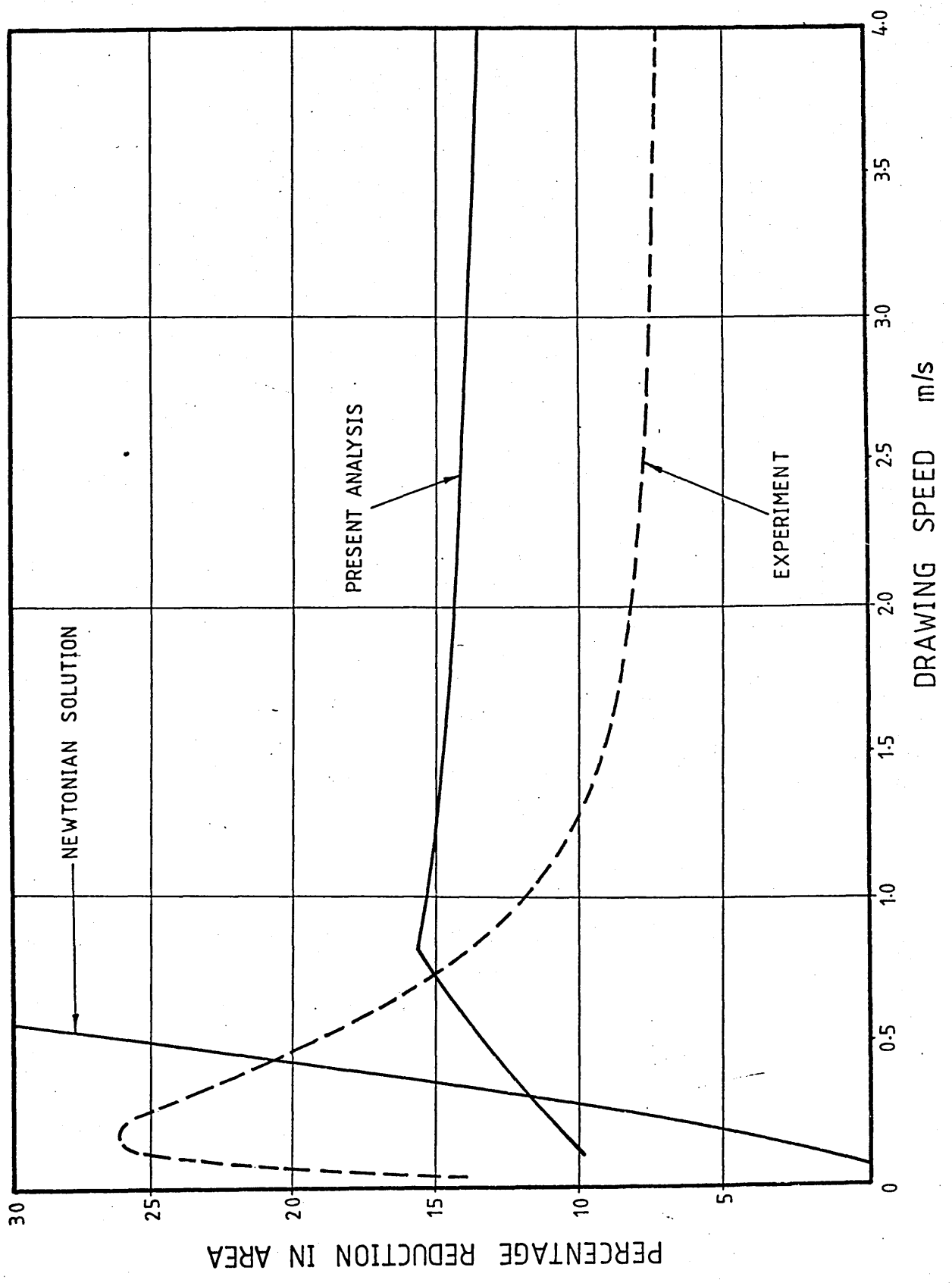

FIG125:PRESSURE DISTRIBUTIONS

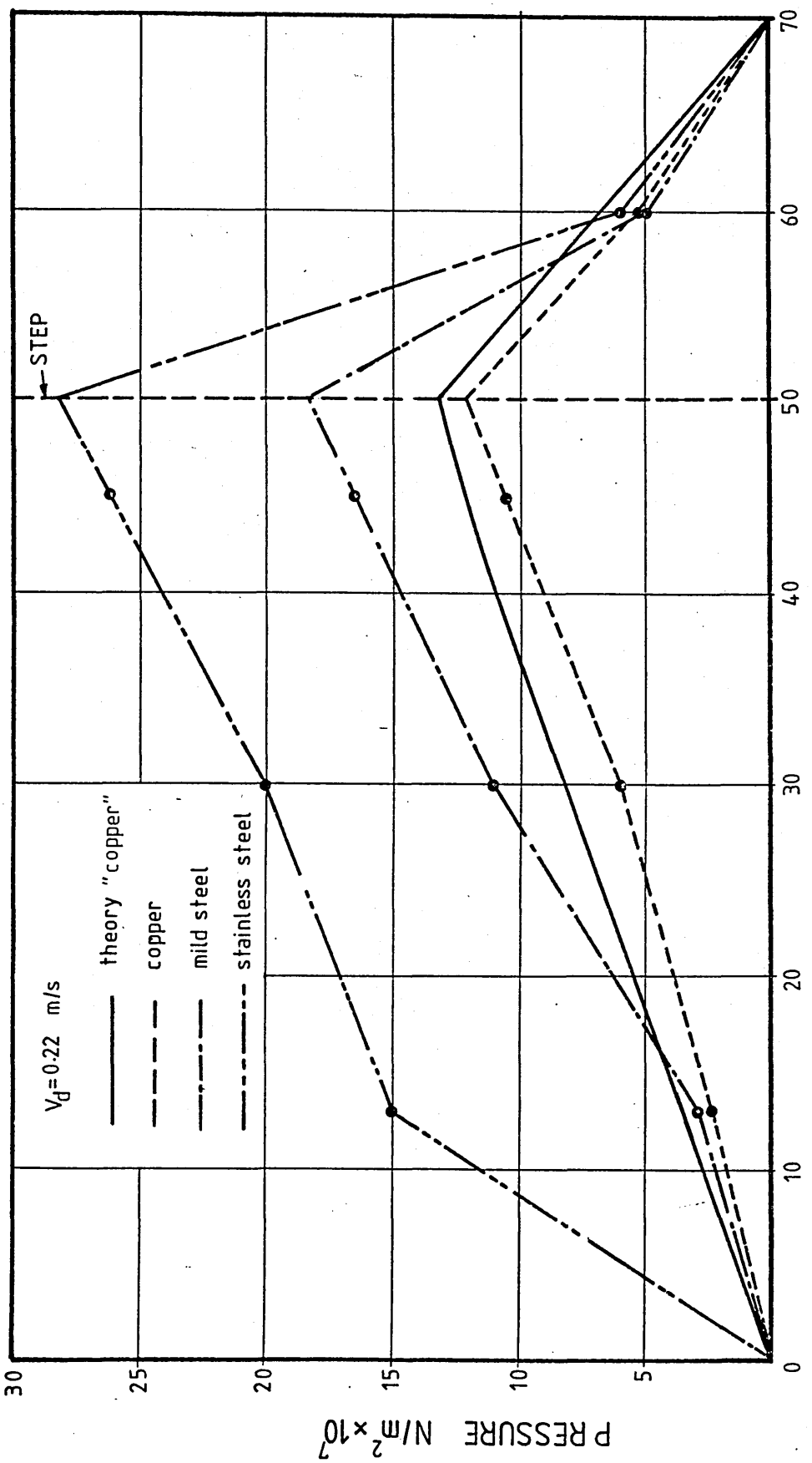

FIG126 : PRESSURE DISTRIBUTIONS

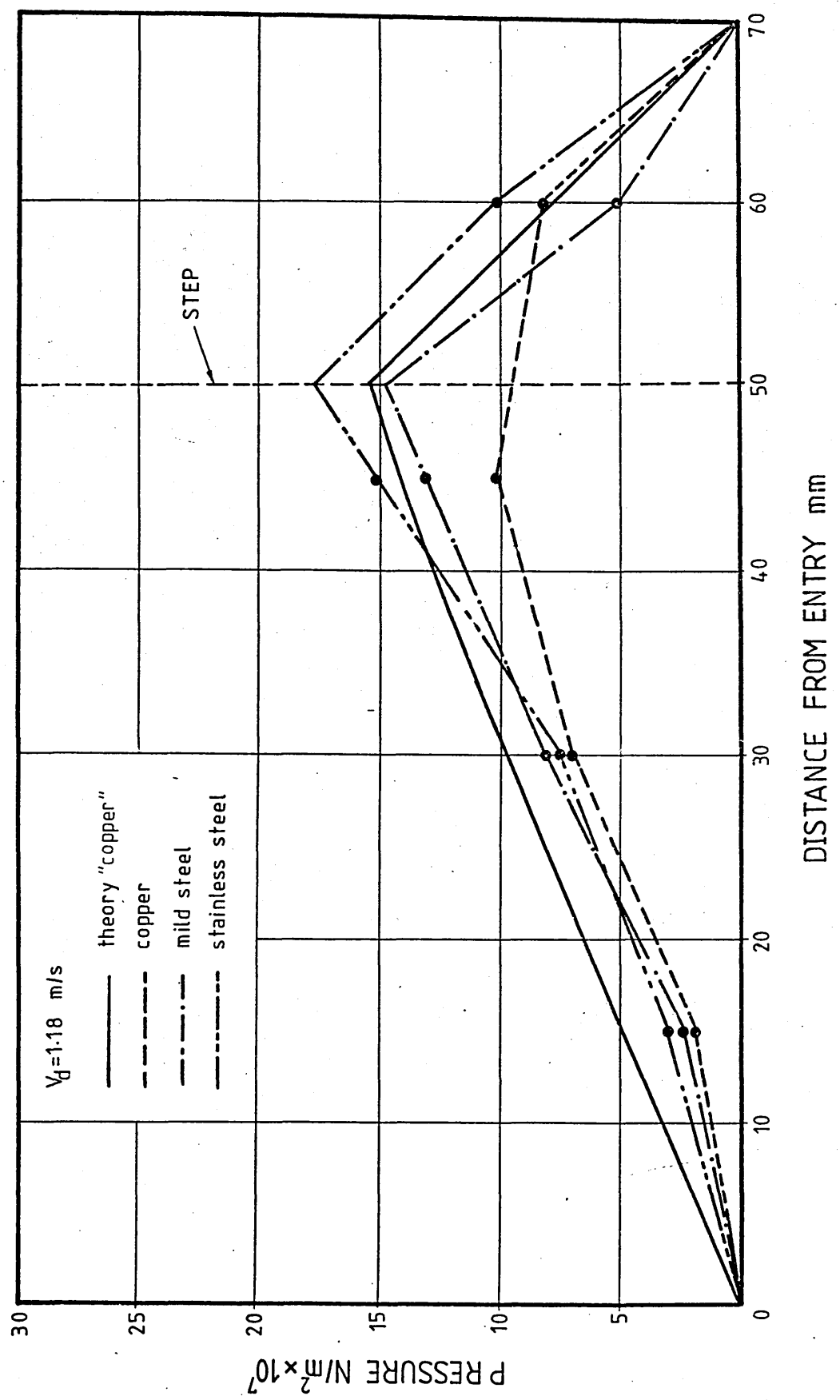

FIG127: PRESSURE DISTRIBUTIONS

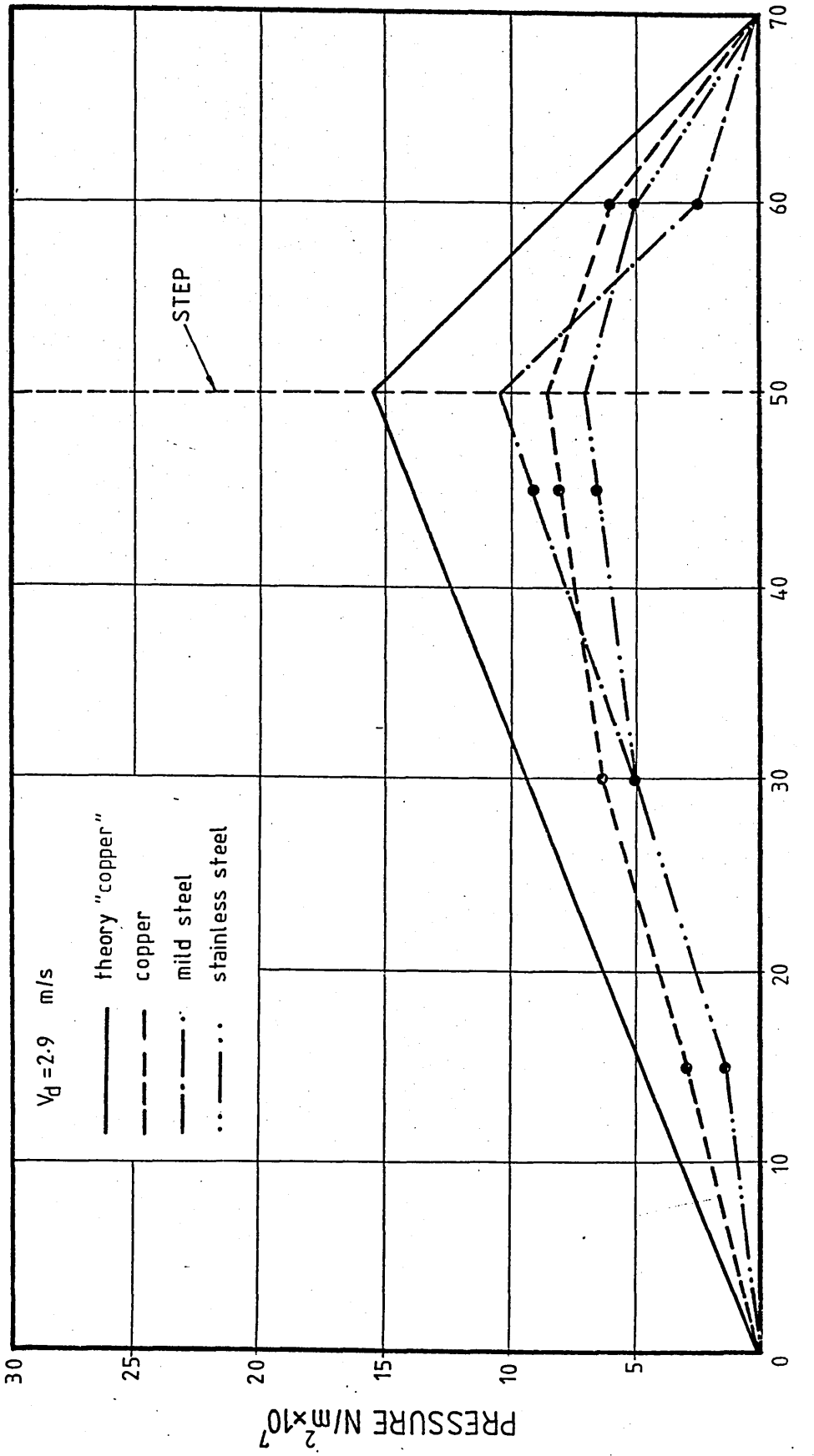

FIG128: DEFORMATION PROFILES FOR COPPER WIRE

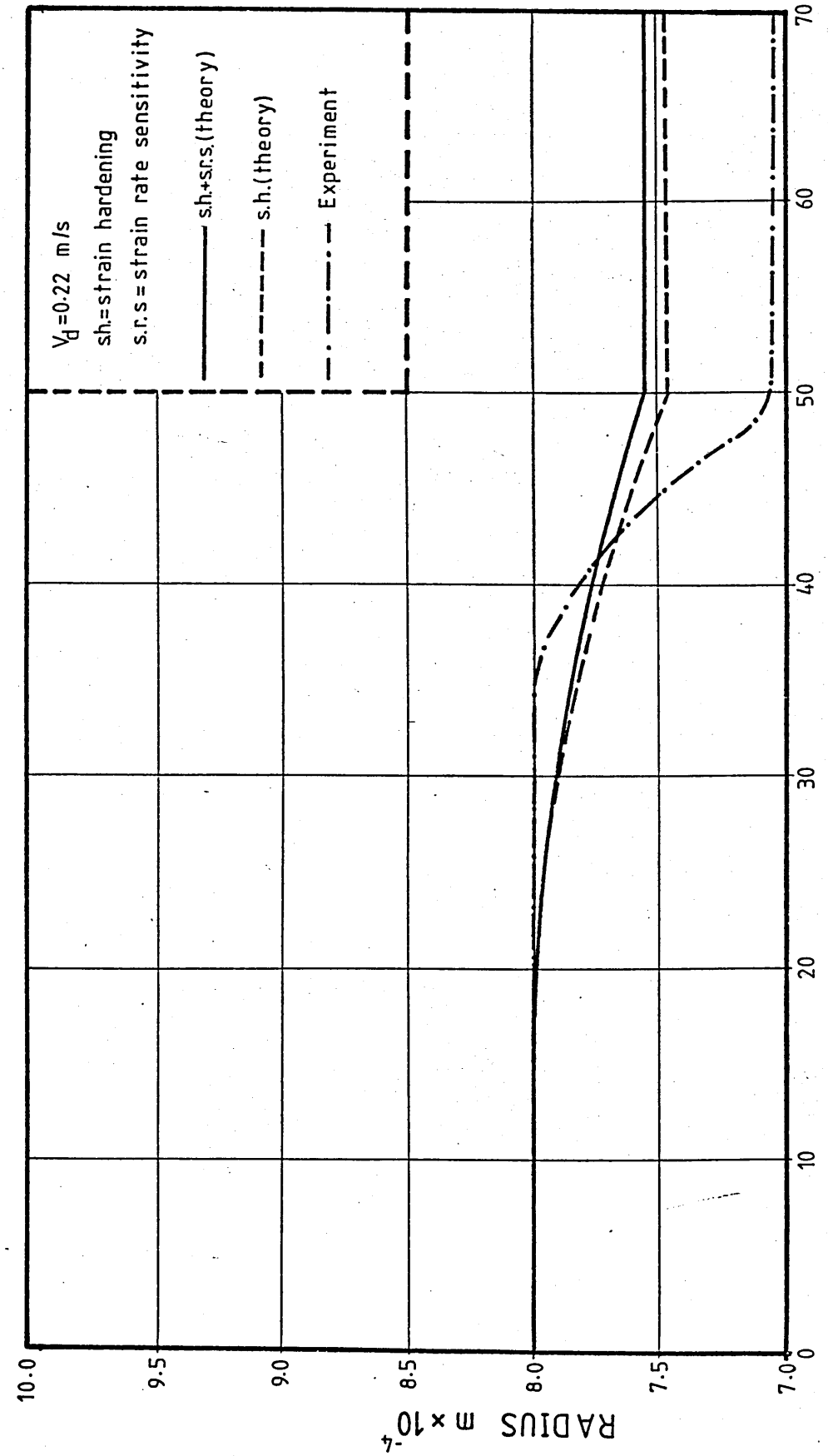

FIG129 : DEFORMATION PROFILES FOR COPPER WIRE

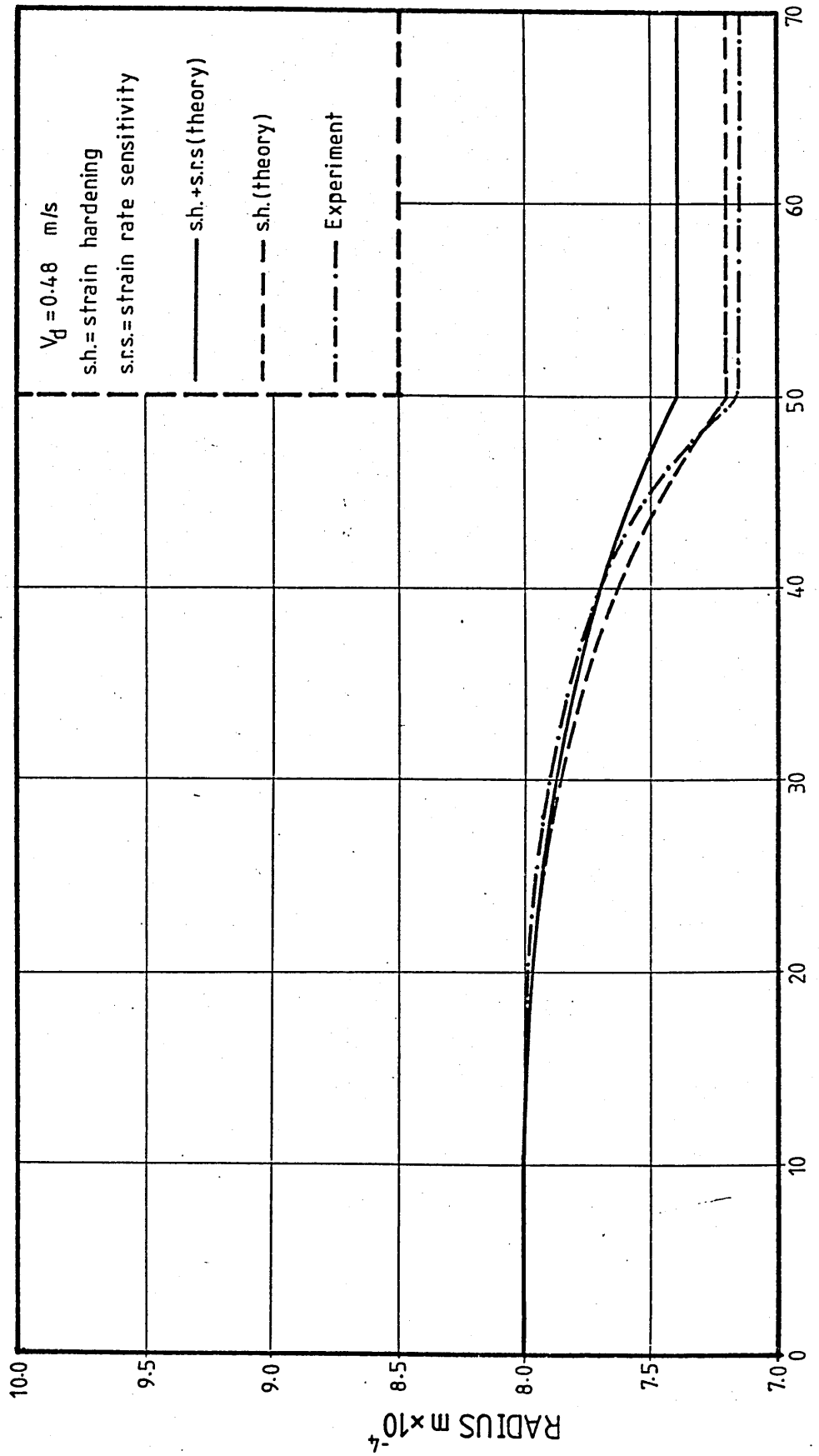

7.6- Recommendations For Future Work.

A unique wire drawing technique has been developed in which many problems and limitations associated with the conventional wire drawing process have been eliminated. This is achieved by removing the reduction die hence preventing metal to metal contact taking place. The only limitation observed was the reduction in the deformation of the wire diameter at higher drawing speeds due to the higher shear rates imposed on the polymer melt. In the analysis, it was attempted to incorporate as many factor as possible, but further works may be usefully conducted in the following areas;

1- Experimentally.

The deformation of the wire takes place in the unit according to the effective die formed by the pressure medium. The resistance to the shear rate is solely dependent upon the type of pressure medium used in the unit. It is well known that the polymer melts are shear thinning fluids and no polymer melts have been found to perform other-wise. However in reference 19, it is reported that certain polymer solutions are shear thickening fluids (dilatant). It is thought that if a dilatant pressure medium could be used;

i)- The need for heating the polymer could be dispensed with to reduce the cost of the operation.

ii)- The problem of slip may be solved hence improving the performance of the unit at higher drawing speeds.

In addition to the above, higher viscosity polymer melts could be used in order to increase the limiting drawing speeds (where the reduction in area becomes zero) for harder wire materials.

The multi-pass tests (see chapter 4) showed that the performance of the unit could be improved significantly at higher speeds where little or no deformation was obtained when a single unit was used. Undoubtedly the multi-pass tests have provided many interesting and encouraging results. To explore the full potential of such a system, much more tests should be carried out not only on the different pressure mediums, but also on units of different geometry. Examples for the latter are units of tapered bore geometry (some of the results of which are provided in Appendix 2) and units of combined geometry (tapered and stepped bore).

Since the quality of the product is of utmost importance, methods of controlling the process should be looked at in order to produce wires of desired qualities in terms of consistency in the diameter and cross-section over long lengths.

2- Theoretically.

In the present study, the amount of heat lost in the melt during the drawing was considered to be negligible. The viscosity of the fluids are known to be sensitive to temperature change, hence a relation-ship predicting the

viscosity change due to the temperature variation may improve the theoretical results.

The equation predicting the viscosity of the polymer melt in the unit accommodates the pressure calculated at the step. It would provide more accurate results if the pressure profile is taken into account in order to predict variation of the viscosity inside the unit.

If nothing, very little is known when slip takes place in the polymer melt. When the critical shear stress is reached, the pressure is assumed to remain constant as the drawing speed increases further. It would again reduce the errors in the theoretical results if a slip factor could be assigned to ascertain the pressure in the unit when slip is predicted.

Conclusions.

A die-less wire drawing system has been developed, as an alternative to the conventional drawing process, consisting of a stepped bore reduction unit and polymer melt as a pressure medium. In the die-less drawing process, since the bore size of the unit was greater than the wire diameter, the metal to metal contact was eliminated. Therefore a leader wire was no longer needed prior to the drawing operation and also wire fracture during the start-up was overcome.

Copper, mild steel and stainless steel wires were reduced successfully and the experimental work has shown that the amount of deformation was much higher at slower drawing speeds. The only draw back was the fact that at higher drawing speeds, the obtainable reduction in area was significantly reduced. The performance of the unit was partially improved at higher speeds by employing a higher viscosity polymer melt. Further investigations on viscous pressure mediums should remove this limitation.

A multi-unit drawing system was also simulated using identical units in order to increase the limiting operational drawing speeds after which no reductions in area were obtained. This problem again was partially overcome and further work on this particular area should give improved results.

The quality of the wires drawn by the die-less method were found to be comparable to those drawn using the conventional reduction dies.

The analysis tended to under estimate the experimental results at slower drawing speeds and over estimate the measured results at higher speeds.

1- WISTREICH, J.G.
"The Fundamentals Of Wire Drawing"
Metallurgical Review, 1958, vol. 3, No 10.

2- WISTREICH, J.G.
"ABC Of Better Lubrication And Cooling In Steel Wire Drawing"
1959, Nov., Wire, pg. 1486.

3- JOHNSON, W. & MELLOR, P.B.
"Engineering Plasticity"
Pg. 321 - 323, 1972.

4- CHRISTOPHERSON, D.G. & NAYLOR, P.B.
"Promotion Of Fluid Lubrication In Wire Drawing"
Proc. Inst. Mech. Eng., (1955), 169, 643.

5- WISTREICH, J.G.
"Lubrication In Wire Drawing"
Wear, March 1957, pg. 505 - 511.

6- TATTERSALL, G.H.
"Hydrodynamic Lubrication In Wire Drawing"
J. Mech. Eng. Sc., vol. 3, No 4, 1961, pg. 378.

7- CHU, P.S.
"Theory Of Lubrication Applied To Pressure Nozzle Design In Wire Drawing"
Proc. Inst. Mech. Eng., vol. 181, pg. 3, (1966-67).

8- BLOOR, M., DOWSON, D. & PARSON, B.
"An Elasto-Plasto-Hydrodynamic Lubrication Analysis Of The Plane Strain Drawing Process"
J. Mech. Sc., vol 12, No 3, 1970.

9- OSTERLE, J.F. & DIXON, J.R.
"Viscous Lubrication In Wire Drawing"
ASLE Trans. 5, pg. 233 - 241, 1962.

10- WILSON, W.R.D. & WALOWIT, J.A.
"An Isothermal Hydrodynamic Lubrication Theory For Hydrostatic Extrusion And Drawing Process With Conical Dies"
Journal Of Lubrication Technology, January 1971.

11- CHO, N.S. & YANG, Y.
"Analysis Of Hydrodynamic Extrusion Through Optimised Curved Dies"
Int. J. Mech. Sci., vol 24, No 10, pg. 589 - 595, 1982.

12- MIDDLEMISS, A.
"Hydrostatic Lubrication For Drawing Steel Wire"
Tribology In Iron And Steel Works, ISI, publication 125.

13- ORLOV, S.I., KOLMOGROV, V.L., URAL'SKLL, V.I.
& STUKALOV, V.T.
"Integrated Development And Introduction Of New High-Speed Mills And Hydrodynamic Lubrication System For Drawing Wires"
Steel In The USSR., vol 10, pg. 953 - 956, 1974.

14- THOMPSON, P.J. & SYMMONS, G.R.
"A Plasto-Hydrodynamic Analyais Of The Lubrication And Coating Of Wire Using Polymer Melt During Drawing"
Proc. Inst. Mech. Eng., vol 191, 13/77, 1977.

15- STEVENS, A.J.
"A Plasto-Hydrodynamic Investigation Of The Lubrication And Coating Of Wire Using A Polymer Melt During Drawing"
M.Phil. Thesis, Sheffield City Polytechnic, 1979.

16- CRAMPTON, R.
"Hydrodynamic Lubrication And Coating Of Wire Using A Polymer Melt During Drawing Process"
Ph.D. Thesis, Sheffield City Polytechnic, 1980.

17- DIENES, G.J.
Applied Phys., 24, 779, 1953.

18- BRYDSON, J.A.
"Flow Properties Of Polymer Melts"
Published By Plastic Institute, London, Illiffe Books, 1970.

19- GOGOS, G.G.
"Principles Of Polymer Processing"
pg. 147 - 149, 1979.

20- CLEGG, P.L.
"Elastic Effect In The Extrusion Of Polythene"
Rheology Of Elastomers, Pergammon Press, London, 1957.

21- SPENCER, R.S. & DILLON, R.E.
"The Viscous Flow Of Molten Polystyrene"
J. Colloid Sci.,vol 3, pg. 163, 1948.

22- BAGLEY, E.B.
"The Seperation Of Elastic And Viscous Effect In Polymer Flow"
Trans. Of The Society Of Rheology, vol 31, pg. 355 - 368, 1961.

23- BAGLEY, E.B. & SCHRABER, H.P.
"Effect Of Die Entry On Polymer Melt Fracture And Extrusion Distorsion"
Trans. Of The Society Of Rheology V, pg. 341 - 353, 1961.

24- HOWELLS, E.R. & BENBOW, J.J.
"Flow Defects In Polymer Melts"
ICI Publication, August 1962.

25- METZNER, A.B.
"Fracture Of Non-Newtonian Fluids At High Shear Stresses"
Industrial And Eng. Chemistry, vol 50, No 10, 1958.

26- BENBOW, J.J. & LAMB, P.
"New Aspect Of Melt Fracture"
SPE Trans., January 1963, pg. 7.

27- LUPTON, J.M. & REGESTER, J.W.
"Melt Flow Of Polyethylene At High Rates"
Polymer Eng. And Science, pg. 235, October 1965.

28- WESTOVER, R.F.
"The Significance Of Slip In Polymer Melt Flow"
Polymer Engineering And Science, pg. 83, January 1966.

29- MAXWELL, B. & MATSUKA, S.
"Bulk Compressibility Of Polymers At Fabricating Temperatures"
SPE Journal, pg. 27, Feb 1957.

30- MAXWELL, B. & JUNG, A.
"Hydrostatic Pressure Effect On Polymer Melt Viscosity"
Modern Plastic, pg. 174, Nov. 1957.

31- PENWELL, R.C. & PORTER, R.S.
"Determination Of The Pressure Coefficient And Pressure Effects In Capillary Flow"
Journal Of Polymer Science, Part A-2, vol 9, pg. 731 - 745, 1971.

32- CHOI, S.Y.
"Determination Of Melt Viscosity As A Function Of Hydrostatic Pressure In An Extrusion Rheometer"
J. Of Polymer Sci., Part A-2, vol 6, pg. 2043 - 2049, 1968.

33- COGSWELL, F.N.
"The Influence Of Pressure On The Viscosity Of Polymer Melts"
Plastics And Polymers, 39, Feb. 1973.

34- WESTOVER, R.F.
"Effect Of Hydrostatic Pressure On Polymer Melt Rheology"
SPE Technical Papers, vol 6, 80-1, 1960.

35- RABINOWITSCH, B.
"Uber Die Viskostat Und Elastizitat Von Solen"
Z. Phys. Chem.(1929), A145, pg. 141.

36- HUNG, D. & MUSTER, D.
"Non-Newtonian Flow In Infinite Length Step Shaped Bearings"
Naval Research Report, No 17, University Of Houston, 1-14, 1969.

37- SWAMY, S.T.N., PRABU, B.S. & RAO, B.V.A.
"Calculated Load Capacity Of Non-Newtonian Lubricant In Finite Width Journal Bearings"
Wear, vol 31, pg. 277 - 285, 1975.

38- HSU, Y.C. & SAIBEL, E.
"Slider Bearing Performance With A Non-Newtonian Lubricant"
ASLE Transaction, 8, pg. 191 - 194, 1965.

39- REKTERYS, K.
"Survey Of Applicable Mathematics"
Illiffe Publications, pg. 77 - 79, 1969.

40- HASHMI, M.S.J.

"Strain Rate Sensitivity Of Commercially Pure Copper At Room Temperature And Strain Rate Of Up To 10^6 Per Second" Sheffield City Polytechnic Technical Report No SCP/MPE/R10, Oct. 1978.

APPENDIX 1: Description Of The Extrusion Rheometer Used To Determine The Flow Characteristics Of The Polymer Melts.

Instrumentations.

A Devenport Extrusion Rheometer was used to determine the flow characteristics of Alkathene WVG 23 and polypropylene KM 61 polymers. The results have been shown graphically in chapter 2 and the description of the apparatus and the experimental procedure are explained in this section.

Figure A1 shows the schematic diagram of the extrusion rheometer which basically consisted of a heater chamber, a motor driven piston, a quartz pressure transducer and a variable heating system. The temperature in the melt could be varied within the range of 100 $^{\circ}$C to 300 $^{\circ}$C using a heater controller. The piston was driven vertically into the chamber by an electrically controlled variable speed motor. The speed of the piston could be set for any rate upto 25 cm/min and the actual speed was directly indicated on a tachometer. The pressure transducer was located in the body of the melt chamber so that the pressure in the melt was measured as near to the extrusion die as possible.

Test Procedure.

The pressure transducer on the rheometer was calibrated using an oil chamber and a calibrated pressure gauge. The heater on the melt chamber was then switched on and set at the desired temperature. When the set temperature was reached, the melt chamber was supplied with the polymer granules and sufficient time was allowed for the polymer to reach the molten state. The piston was then set in motion and both, the speed of the piston and the pressure in the melt were

recorded. These measurements were repeated at small intervals upto the shear rate of 2×10^4 s^{-1}. This shear rate is equivalent to the apparent shear rate applied to the polymer melt in the first section of the stepped bore reduction unit at the maximum drawing speed of 4.0 m/s. These measurements were later converted to shear stresses and shear rates using the following equations supplied by the manufacturer;

$$\text{Shear Stress} = \frac{P\ r}{2\ l}$$

$$\text{Shear Rate} = \frac{V}{16.5326\ \ r^3}$$

Where;

P is the pressure in the melt

r is the radius of the extrusion die.

l is the length of the extrusion die.

V is the velocity of the piston.

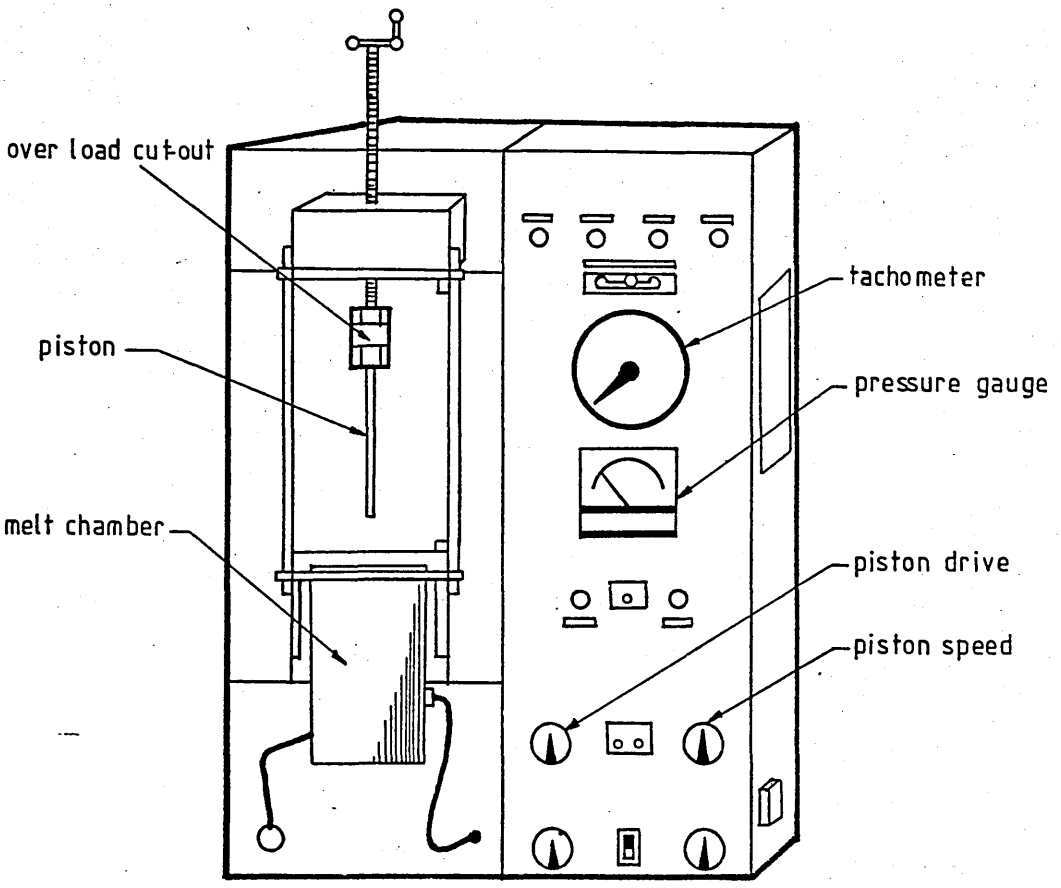

FIG A1 : SCHEMATIC DIAGRAM OF THE EXTRUSION RHEOMETER

APPENDIX 2: Experimental Results Obtained Using The Tapered Bore Reduction Unit.

A tapered bore reduction unit was designed and manufactured while carrying out the initial feasibility study of the die-less drawing process (see chapter 3). Dimensional details and assembly of the unit are shown in figures 18 and 20 respectively. Also plate 7 shows a section view of the manufactured unit. The pressure medium used with the tapered bore reduction unit was Alkathene WVG 23 polymer. The results of percentage reduction in area, coating thickness, drawing load and pressure are presented here in graphical forms for convenience. Copper wire of 1.6 mm diameter was used for these tests..

Figure A2 shows the results of percentage reduction in area versus speed at two different melt temperatures (130°C and 180°C). At slower drawing speeds, deformation of wire increased as the speed was increased. A maximum reduction in area was obtained at about 0.2 m/s for 130°C and at about 0.3 m/s for 180°C. The deformation of copper wire reduced as the drawing speed was increased further. Approximately constant reduction in area was obtained at speeds in excess of 1.5 m/s for both melt temperatures. these were 5% for 130°C and 3.5% for 180°C. The interesting similarities may be observed when these results are compared with those in figure 51 which shows the results of percentage reduction in area obtained using the stepped bore reduction unit.

Figure A3 shows the coating thickness measured at the temperatures of 130°C and 180°C. The trends of these results are very close to those of percentage reduction in area as shown in figure A2. Maximum coating thickness were found to be about 0.135 mm at 130°C and about 0.09 mm at 180°C. No

sharkskin effect was observed on these coatings.

Figure A4 shows the drawing loads measured for tests conducted at the melt temperature of 180°C. The drawing load increased from about 20 N at very slow speeds to about 100 N at the drawing speed of 4.0 m/s. Results of drawing loads measured with the stepped bore reduction unit also showed similar trend at the same melt temperature (see figure 43).

Figure A5 shows the pressures recorded in the tapered pressure chamber at temperature of 180°C. These measurements were taken at three different positions and the number on each curve refers to the location of the pressure transducer mounted on the unit as shown in figure 20. Maximum pressures were recorded at position 1 which increased as the drawing speed was increased. A maximum pressure of 70 MN/m^2 was measured at drawing speed of 0.5 m/s. At speeds in excess of 1.5 m/s, a steady pressure of 60 MN/m^2 was noted for this position. Pressures at positions 2 and 3 increased as the drawing speed was increased. Again approximately constant pressures were recorded at drawing speeds in excess of 1.0 m/s for both positions. These were 25 MN/m^2 for position 2 and 15 MN/m^2 for position 3. A similar trend was noticed for the pressures measured in the stepped bore reduction unit at positions 2 and 4 , at the same melt temperature as shown in figure 27. Note that the magnitudes of the pressures are also close in both cases.

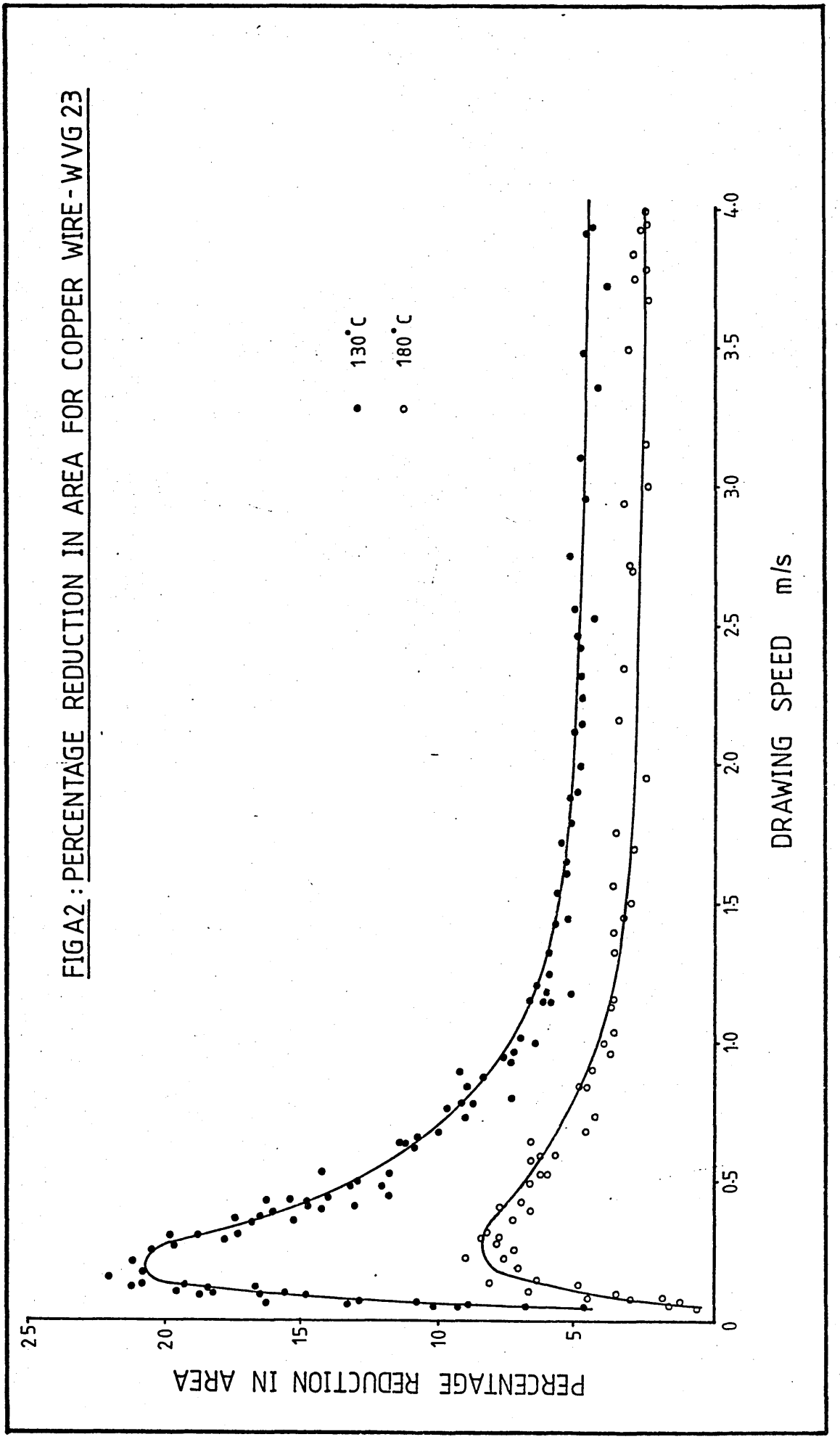
FIG A2 : PERCENTAGE REDUCTION IN AREA FOR COPPER WIRE - W VG 23
PERCENTAGE REDUCTION IN AREA
25
20
15
10
5
0
130°C
180°C
0.5
1.0
1.5
2.0
2.5
3.0
3.5
4.0
DRAWING SPEED m/s

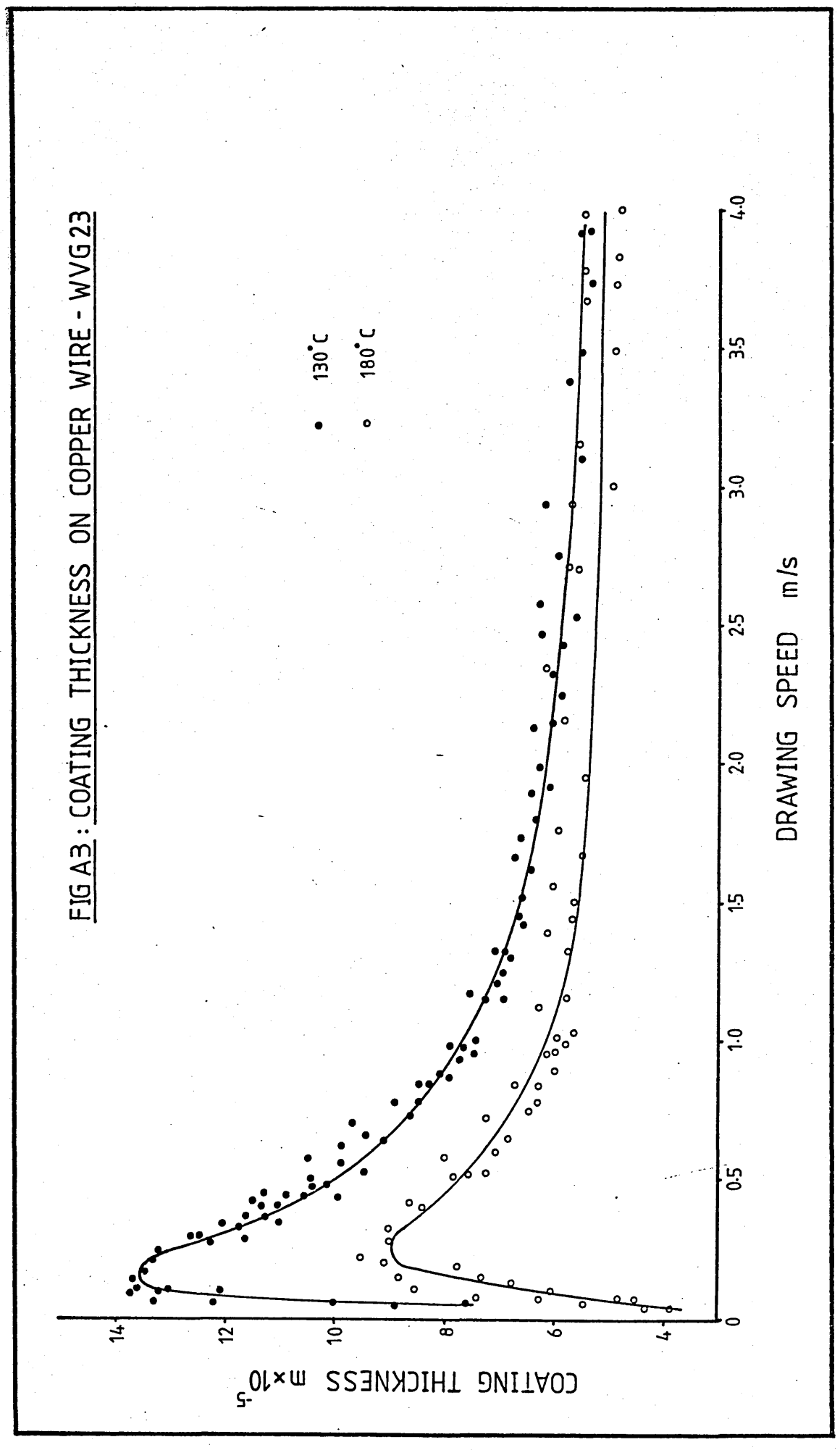
FIG A3 : COATING THICKNESS ON COPPER WIRE - WVG 23
130°C
180°C
COATING THICKNESS m×10⁵
14
12
10
8
6
4
0
0.5
1.0
1.5
2.0
2.5
3.0
3.5
4.0
DRAWING SPEED m/s

FIG A4 : DRAWING LOAD FOR COPPER WIRE - WVG 23, 18°C

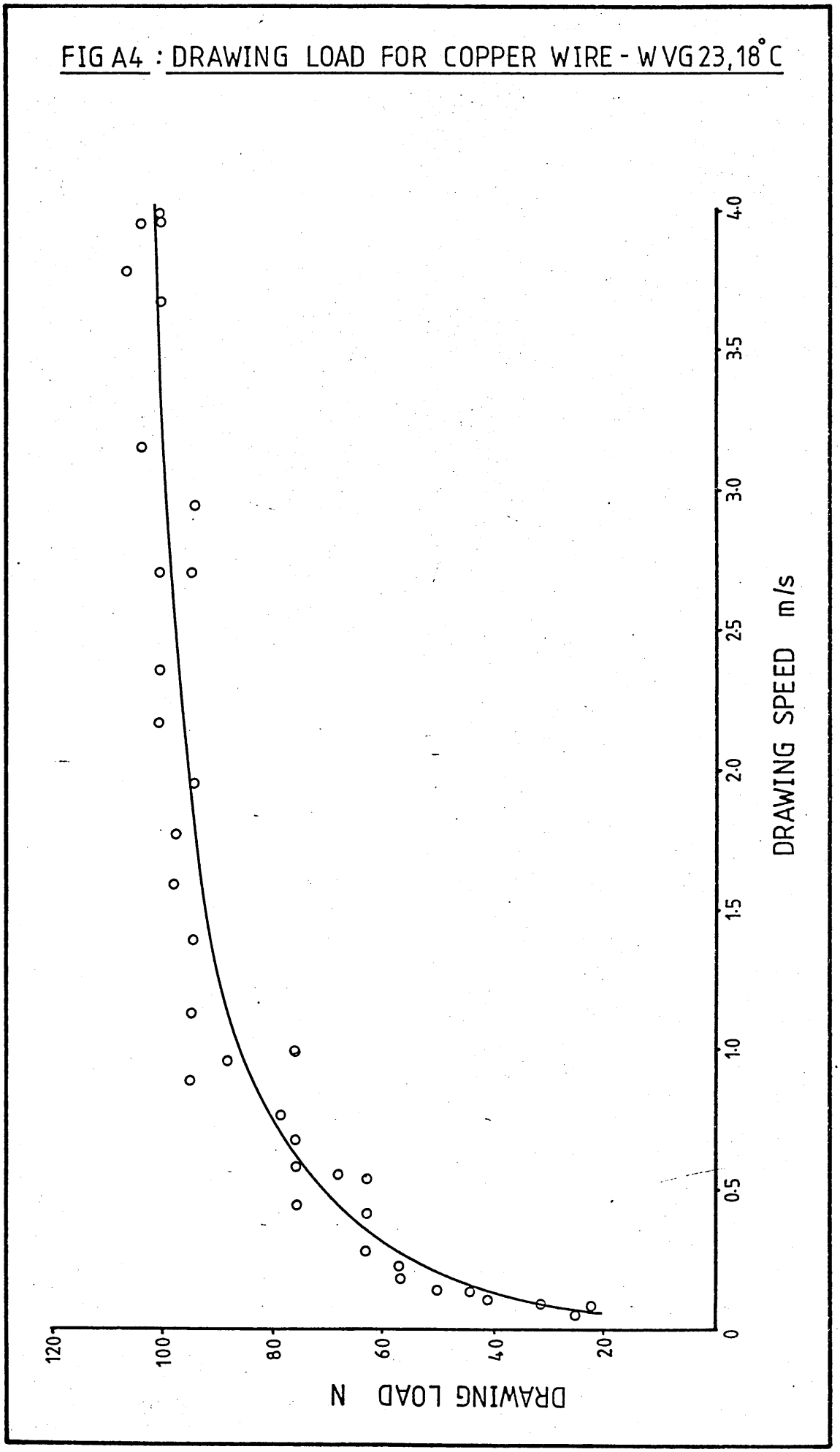

FIGA5 : PRESSURE VARIATIONS FOR COPPER WIRE - WVG23, 180°C

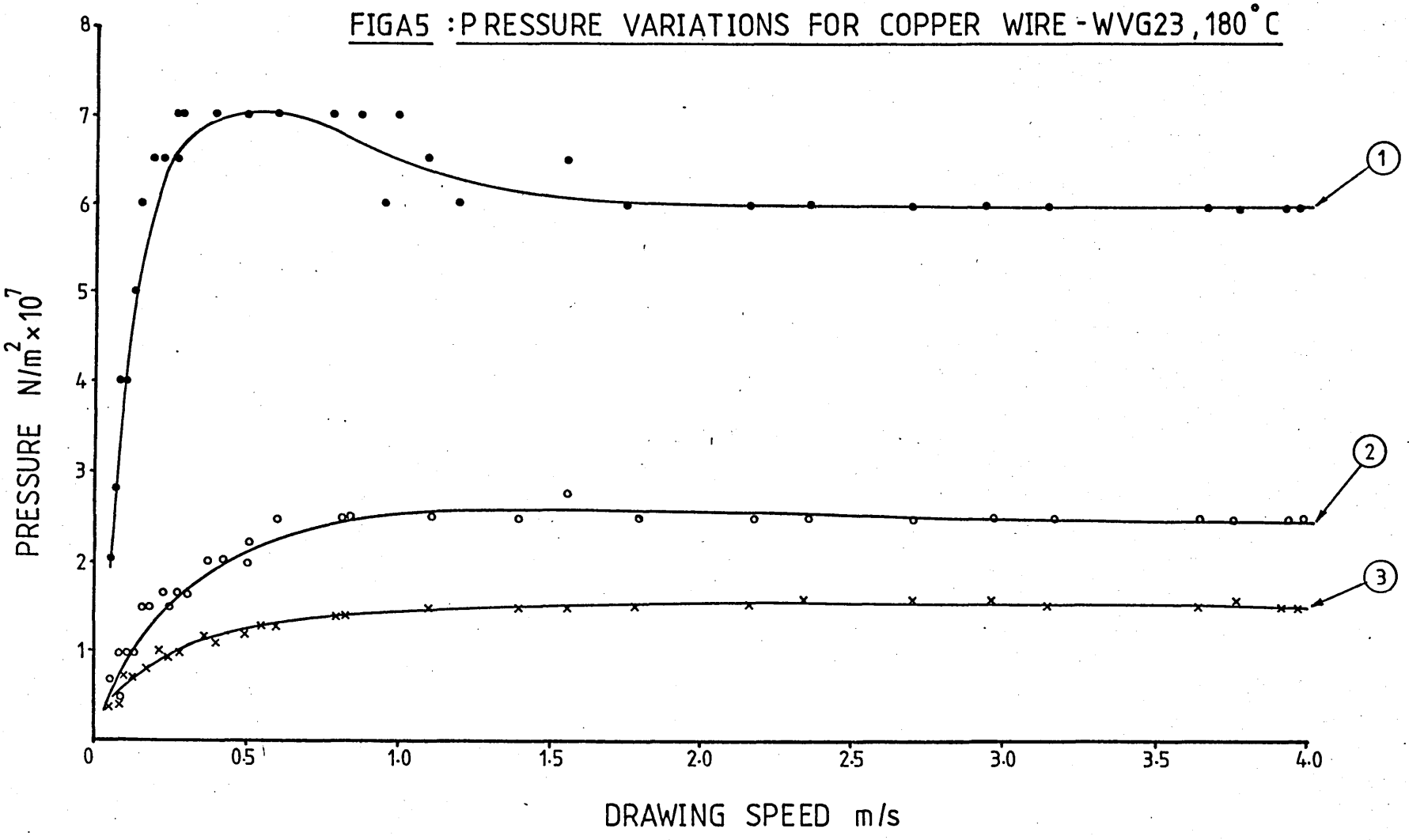

APPENDIX 3: Newtonian Analysis.

A Newtonian solution was developed for the stepped bore reduction unit based on the constant viscosity. The geometry shown in figure 72 was used for this analysis. The assumptions made in deriving the non-Newtonian solution in chapter 5 are also applicable here.

The equilibrium of the flow of polymer melt in the first part of the unit gives;

$$(\frac{dP}{dx})_1 = (\frac{d\tau}{dy})_1$$

Integration with respect to y gives;

$$\tau_1 = P_1' y + \tau_{c1} \qquad \text{.....(3.1A)}$$

where $P_1' = (\frac{dP}{dx})_1$

and τ_{c1} is the shear stress on the wire at y=0.
The relationship between the shear stress and the rate of shear for the Newtonian fluid is given by;

$$\tau = \eta (\frac{dU}{dy}) \qquad \text{.....(3.2A)}$$

Substituting equation (3.1A) into (3.2A) and integrating with respect to y gives;

$$U_1\eta = \frac{1}{2}P_1 y^2 + \tau_{c1} y + \text{cons.} \qquad \text{.....(3.3A)}$$

Boundary conditions are;

at $y = 0$ $U_1 = \acute{V}$ (a_3) and

at $y = h_1$ $U_1 = 0$ (b_3)

Applying boundary condition (a_3) in equation (3.3A) and rearranging gives;

$$U_1 = \frac{\acute{P}_1 y}{2\eta} + \frac{\tau_{c1} y}{\eta} + \acute{V} \qquad \text{.....(3.4A)}$$

Applying condition (b_3) in equation (3.4A) yields;

$$\tau_{c1} = -\frac{1}{2}\acute{P}_1 h_1 - \frac{\acute{V}\eta}{h_1} \qquad \text{.....(3.5A)}$$

The flow of polymer melt in the first part of the unit is given by;

$$Q_1 = \int_0^{h_1} U_1 \, dy$$

Substituting equation (3.4A) into above and integrating gives;

$$Q_1 = \frac{\acute{P}_1 h_1^3}{6\eta} + \frac{\tau_{c1} h_1^2}{2\eta} + \acute{V} h_1$$

and substituting for τ_{c1} into above equation gives;

$$Q_1 = -\frac{\acute{P}_1 h_1^3}{12\eta} + \frac{1}{2}\acute{V} h_1 \qquad \text{.....(3.6A)}$$

Similarly the flow and shear stress in the second part of the unit are;

$$Q_2 = \frac{\acute{P}_2 h_2^3}{12\eta} + \frac{1}{2}\acute{V} h_2 \qquad \text{.....(3.7A)}$$

and $\tau_{c2} = \frac{1}{2}\acute{P}_2 h_2 - \frac{\acute{V}\eta}{h_2}$ .....(3.8A)

respectively. The steady state flow in the unit gives;

$$\frac{d}{dx}(Q_1) = \frac{d}{dx}(Q_2) = 0$$

Therefore differentiating equation (3.6A) with respect to x gives;

$$\frac{d}{dx}(\acute{P}_1) = 0 \quad \text{or} \quad \acute{P}_1 = \text{constant} = \frac{P_m}{l_1}$$

where P_m is the pressure at the step and l_1 is the length of the unit before the step. Also differentiating equation (3.7A) with respect to x yields;

$$\frac{d}{dx}(\acute{P}_2) = 0 \quad \text{or} \quad P_2 = \text{constant} = \frac{P_m}{l_2}$$

where l_2 is the length of the unit after the step. Continuity of flow in the unit gives;

$$Q_1 = Q_2 \qquad \text{.....(3.9A)}$$

Substituting equations (3.6A) and (3.7A) into (3.9A) and also substituting for $\acute{P}_1$ and $\acute{P}_2$, pressure at the step prior to deformation of wire is given by;

$$P_m = \frac{6\eta\acute{V}(h_1 - h_2)}{\frac{h_1^3}{l_1} + \frac{h_2^3}{l_2}} \qquad \text{.....(3.10A)}$$

With reference to figure 72 part (b), the equilibrium

of forces acting on the wire in the first part of the unit gives;

$$\sigma_{x1} = \frac{4\,\tau_{c1}}{D_1}\,X_1$$

and $$P_1 = \frac{P_m}{l_1}\,X_1$$ as before.

Position of yield of the wire in the unit , according to the Tresca or Von Mises yielding theory ($P + \sigma_x = Y$) gives;

$$X_1 = \frac{Y_o}{\frac{P_m}{l_1} + \frac{4\,\tau_{c1}}{D_1}} \qquad \text{.....(3.11A)}$$

Equations governing the deformation zone, apart from those representing the flow of the polymer melt, are the same equations derived for the non-Newtonian analysis in chapter 5. Therefore they are only listed here in finite difference forms. Variations of the wire diameter, the gap and the wire velocity are;

$$D_i = D_{i-1} - B\,\Delta x \qquad \text{.....(3.12A)}$$

$$h_i = h_{i-1} + \frac{1}{2}B\,\Delta x \qquad \text{.....(3.13A)}$$

$$V_i = \frac{V_{i-1}}{1 - \left(\frac{2\,(D_{i-1} - D_i)}{2D_{i-1} - D_i}\right)} \qquad \text{.....(3.14A)}$$

respectively. The pressure gradient and the pressure in the deformation zone with reference to equation (3.6A) are;

$$P_i' = \frac{12\eta}{h_i^3}\left(\frac{V_i h_i}{2} - Q_1\right) \qquad \text{.....(5.15A)}$$

and $$P_i = P_i' \Delta x + P_{i-1} \qquad \text{.....(3.16A)}$$

respectively. Also the shear stress on the wire in the deformation zone is;

$$\tau_{ci} = -\frac{1}{2} P_i' h_i - \frac{V_i \eta}{h_i} \qquad \text{.....(3.17A)}$$

Similarly, the axial stress in the wire is given by;

$$\sigma_{xi} = 2\left(\frac{D_{i-1} - D_i}{D_i}\right) Y_i + \frac{4\tau_{ci}\Delta x}{D_i} + \sigma_{xi-1} \qquad \text{.....(3.18A)}$$

The yield stress of the wire gives;

$$Y_i = S_i\left(Y_o + K_o\left(2\ln\frac{D_1}{D_i}\right)^n\right) \qquad \text{.....(3.19A)}$$

wher $$S_i = 1 + \left(\frac{\dot{\bar{\epsilon}}_{mi}}{N}\right)^{1/T} \qquad \text{.....(3.20A)}$$

and $$\dot{\bar{\epsilon}}_{mi} = \frac{2V_i}{\Delta x} \ln\frac{D_{i-1}}{D_i} \qquad \text{.....(3.21A)}$$

as before. At any point within the deformation zone the Tresca or Von Mises theory of yielding gives;

$$P_i + \sigma_{xi} = Y_i \qquad \text{.....(3.22A)}$$

Iteration technique and finite difference method (based on back ward difference) may be used to determine the variables in the deformation zone.

For an arbitrary value of "B" and a step size of Δx, D_i and h_i may be calculated from equations (3.12A) and (3.13A) respectively. D_i and h_i may be substituted into equation (3.14A) which gives V_i . By substituting V_i and h_i into equation (3.15A) gives P_i and hence from equation (3.16A), P_i may be calculated. Similrarly by substituting P_i V_i and h_i into equation (3.17A) gives τ_{ci} . Equation (3.19A) gives Y_i upon substitutions for D_i and S_i . Also σ_{xi} may be calculated by substituting for D_i , τ_{ci} and Y_i in equation (3.18A).

Having calculated P_i , σ_{xi} and Y_i , they may be substituted into equation (3.22A). The error in this equation may be reduced to the desired level by iterating "B" into the above equations. The equation ($P_i + \sigma_{xi} = Y_i$) may be satisfied in the deformation zone from $i = X_1$ upto the step where $i = l_1 - X_1$. This procedure may be repeated at each speed increments.

A computer programme was written to solve the above equations simultaneously. Flow chart and listing of the programme is provided in figure A6. Results from the Newtonian analysis are presented in chapter 6.

FIG A6 : FLOW CHART AND LISTING OF THE PROGRAMME FOR THE NEWTONIAN ANALYSIS

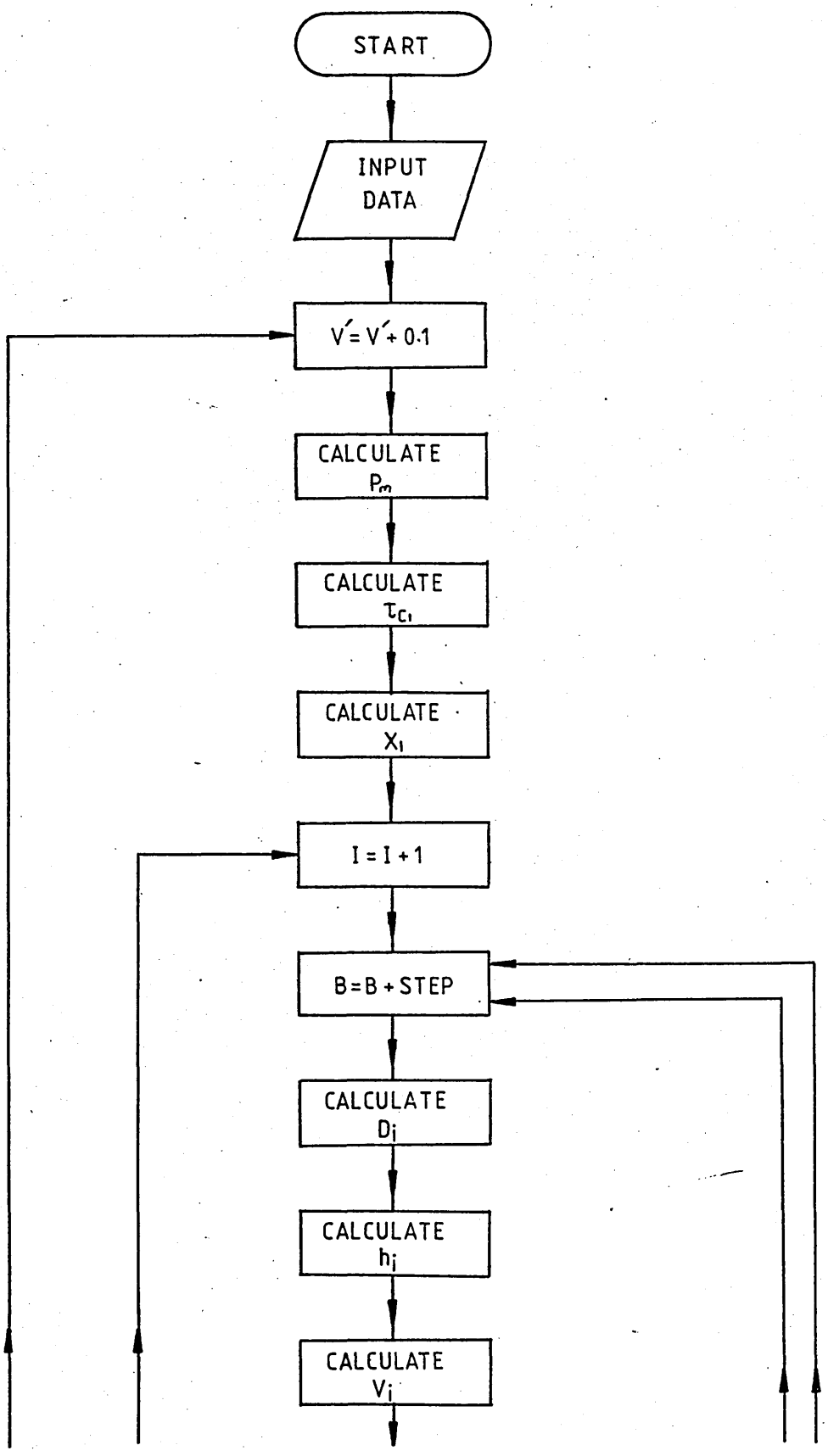

FIG A6 CONTINUED·····

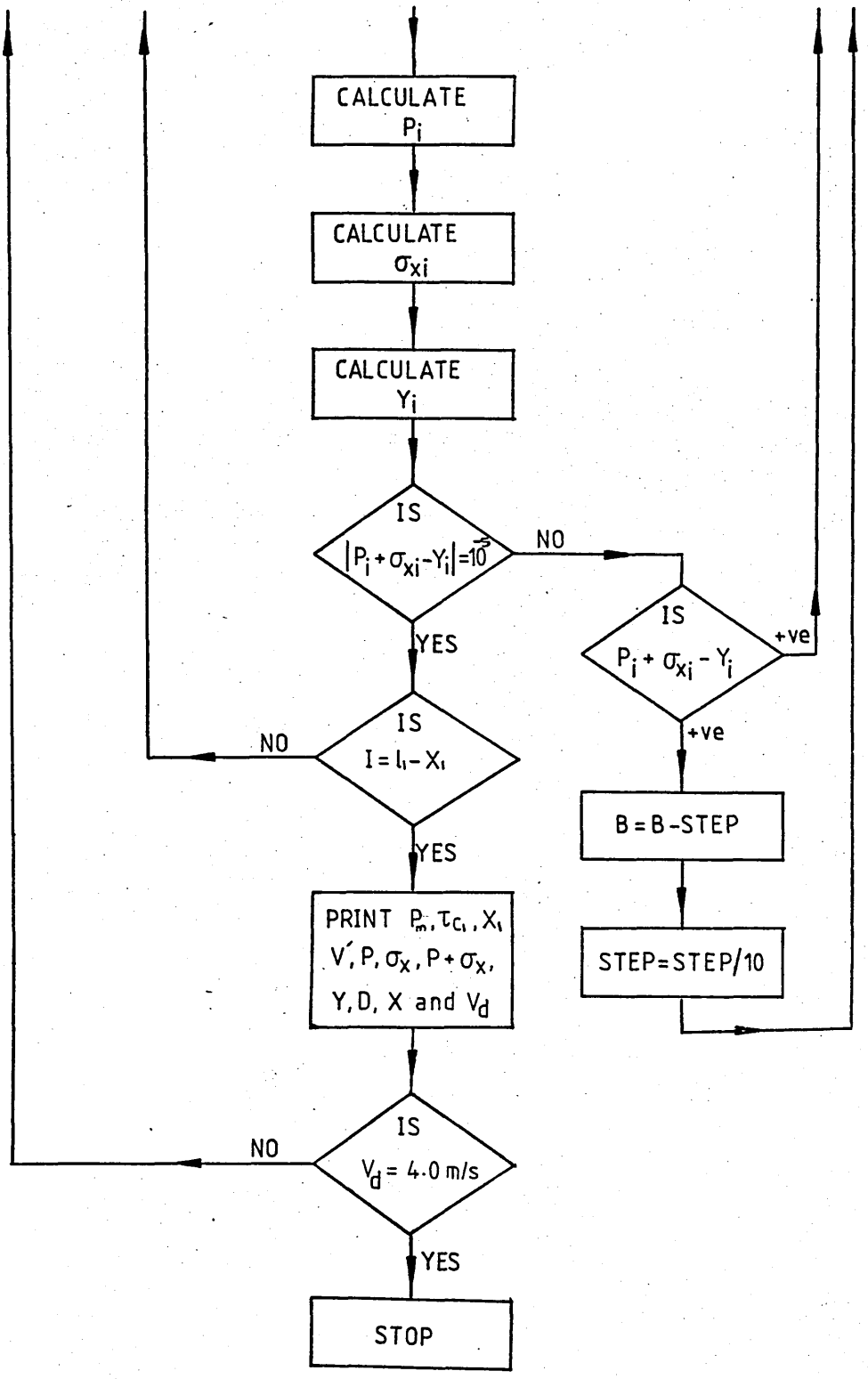

FIG A6 CONTINUED .....

```
      DIMENSION P(500),S(500),X(500),D(500),H(500),PS(500)
      DIMENSION Y(500),V(500),E(10000)
      DOUBLE PRECISION D,EMB
5     WRITE(6,10)
10    FORMAT(1HO,'THIS PROGRAMME CALCULATES THEORETICAL',/,
     &1X,'PERCENTAGE REDUCTION IN AREA OF A STEPPED BORE',/,
     &1X,'REDUCTION UNIT USING NEWTONIAN SOLUTION.',////,
     &1X,'INPUT VISCOSITY OF THE LUBRICANT.')
      READ(5,*)VIS
      WRITE(6,20)
20    FORMAT(1HO,'INPUT INITIAL YIELD OF THE WIRE "YO"',/,
     &1X,'MATERIAL CONSTANT "K" AND STRAIN INDEX "N"',/,
     &1X,'RESPECTIVELY.')
      READ(5,*)YO,TER,F
      WRITE(6,30)
30    FORMAT(1HO,'INPUT L1 ,L2 ,H1 AND H2 IN METERS.')
      READ(5,*)AL1,AL2,H1,H2
      WRITE(6,40)
40    FORMAT(1HO,'INPUT INITIAL DIAMETER OF WIRE IN METERS.')
      READ(5,*)D1
      WRITE(6,50)
50    FORMAT(1HO,'INPUT STRAIN SENSITIVITY COSTANTS "N" AND "T"')
      READ(5,*)TU,BA
      WRITE(6,60)
60    FORMAT(1HO,'TO INCLUDE STRAIN RATE SENSITIVITY ,',/,
     &1X,'TYPE 1,OTHERWISE TYPE 0 .')
      READ(5,*)AA
      WRITE(6,70)
70    FORMAT(1HO,'TO PRINT PRESSURE AND STRESS OVER THE DEFORMATION ZON
     &',/,1X,'TYPE 1 ,OTHERWISE TYPE 0 .')
      READ(5,*)BB
75    DO 200 L=1,40
      VEL=VEL+0.2
      PM=6*VIS*VEL*(H1-H2)/((H1**3)/AL1+(H2**3)/AL2)
      TC1=-(VIS*VEL/H1)-(PM*H1/(2*AL1))
      X1=YO/((PM/AL1)+(4*ABS(TC1)/D1))
      WRITE(6,80)
80    FORMAT(1HO,'**********************************************************
     &**********************')
      WRITE(6,90)PM,VEL,TC1,X1
90    FORMAT(1H ,'PM=',F10.0,2X,'VEL=',F4.2,2X,'TC1=',F9.0,2X,
     &'X1=',F8.5)
      IF(X1.GT.AL1)GOTO 75
      REP=INT(X1*1000)+1
      N=AL1*1000-REP
      P(1)=(PM*X1)/AL1
      S(1)=4*ABS(TC1)*X1/D1
      PS(1)=P(1)+S(1)
      Y(1)=YO
      D(1)=D1
      H(1)=H1
      X(1)=X1
      V(1)=VEL
      DX=0.001
      DO 140 M=1,N
      J=M+1
```

FIG A6 CONTINUED·····

```
      STEP=1E-04
      REM=1E-10
      B=0.0
      K=0
100   B=B+STEP
      K=K+1
      X(J)=X(J-1)+DX
      D(J)=D(J-1)-(B*DX)
      IF(D(J).LT.0)GOTO 210
      H(J)=H(J-1)+0.5*DX*B
      V(J)=V(J-1)/(1-(2*(D(J-1)-D(J))/((2*D(J-1))-D(J))))
      DP=(PM*(H1**3)/(AL1*(H(J)**3)))+6*V(J)*VIS*(H1-H(J))
      P(J)=DP*DX+P(J-1)
      STRS=0.0
      IF(AA.NE.1)GOTO 110
      EMB=2*V(J)*(DLOG(D(J-1)/D(J)))/DX
      STRS=(EMB/TU)**(1/BA)
110   Y(J)=(1+STRS)*(YO+(TER*((2*(DLOG(D(1)/D(J))))**F)))
      S(J)=2*((D(J-1)-D(J))/D(J))*Y(J)+(4*DX*ABS(TC1)/D(J))+S(J-1)
      PS(J)=P(J)+S(J)
      RES=PS(J)-Y(J)
      E(K)=ABS(RES)
      RES1=E(K)-E(K-1)
      IF(ABS(RES1).LE.REM)GOTO 130
      IF(RES)120,130,100
120   B=B-STEP
      STEP=STEP/10
      GOTO 100
130   CONTINUE
140   CONTINUE
      HH=H(J)-H1+H2
      WRITE(6,150)HH
150   FORMAT(1H ,'H=',F10.8)
      IF(BB.NE.1)GOTO 180
      I=M+1
      DO 170 J=1,I
      WRITE(6,160)P(J),S(J),PS(J),Y(J),X(J),D(J)
160   FORMAT(1H ,'P=',F10.0,2X,'S=',F10.0,2X,'P+S=',F10.0,2X,'Y='
     &,F10.0,2X,'X=',F6.4,2X,'D=',F9.7)
170   CONTINUE
180   PRA=(1-((D(J)**2)/(D1**2)))*100
      WRITE(6,190)PRA
190   FORMAT(1HO,'PRA=',F8.5,1X,'%')
      WRITE(6,205)V(J)
205   FORMAT(1HO,'VD=',F4.2)
200   CONTINUE
210   WRITE(6,220)
220   FORMAT(1HO,'WIRE BREAKS AT THIS SPEED.')
      WRITE(6,230)
230   FORMAT(1HO,'TO RUN THIS PROGRAMME AGAIN TYPE 1,',/,
     &1X,'OTHERWISE TYPE 0.')
      READ(5,*)CC
      IF(CC.EQ.1)GOTO 5
      STOP
      END
```

APPENDIX 4: Flow Chart And Listing Of The Computer Programme For The Non-Newtonian Analysis.

FIG A7 : FLOW CHART AND LISTING OF THE PROGRAMME FOR THE NON-NEWTONIAN ANALYSIS

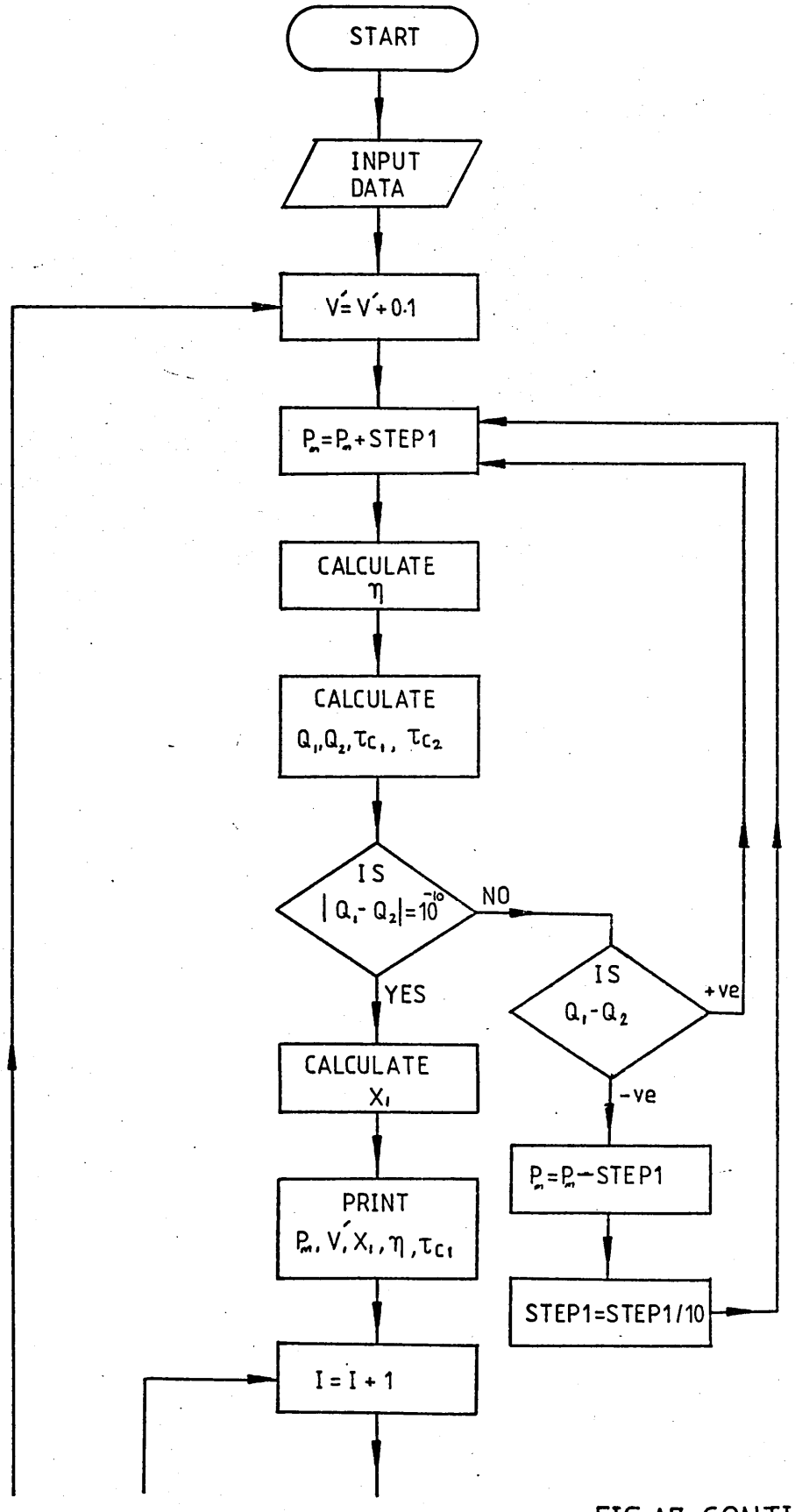

FIG A7 CONTINUED.....

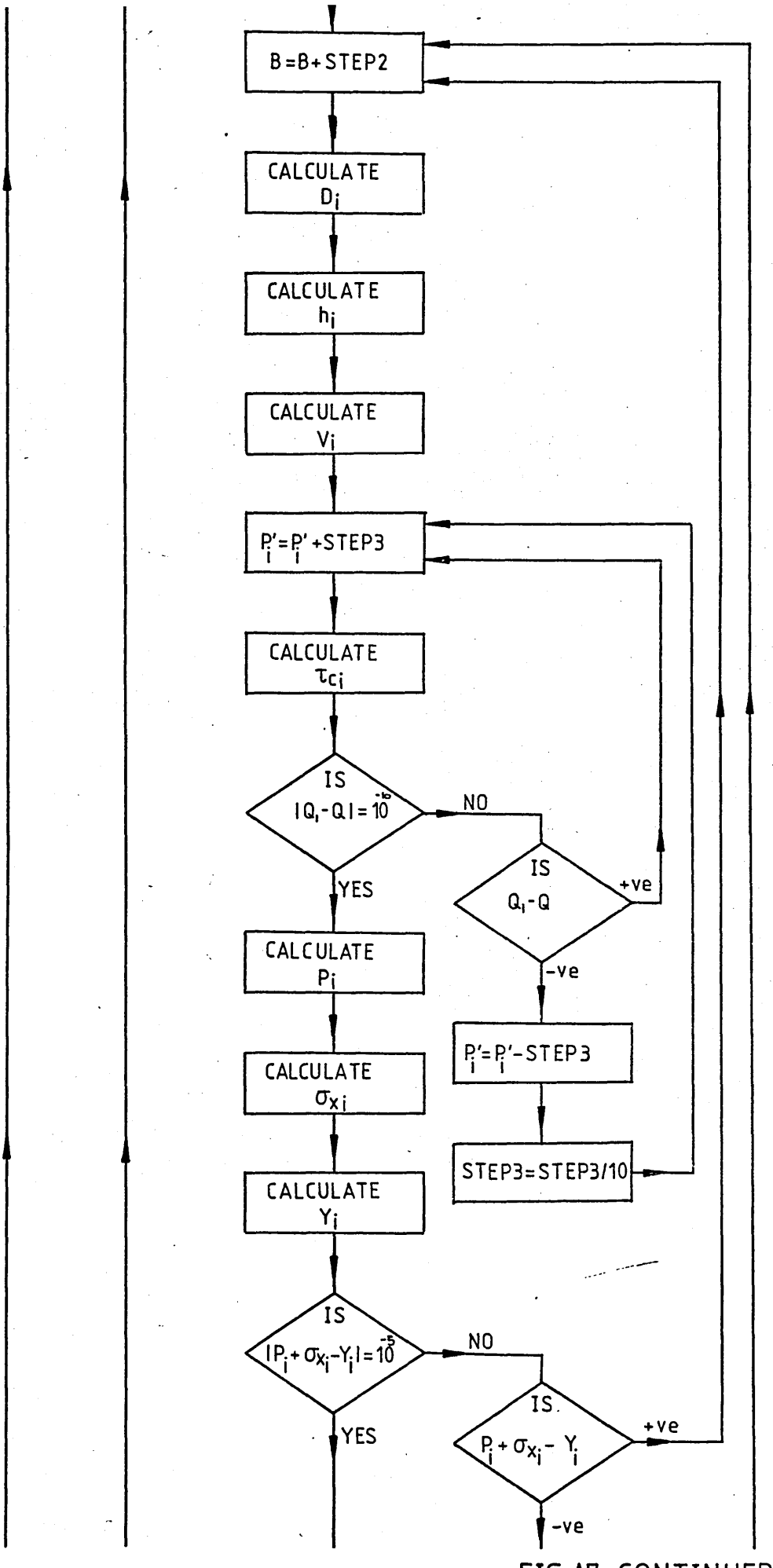

FIG A7 CONTINUED.....

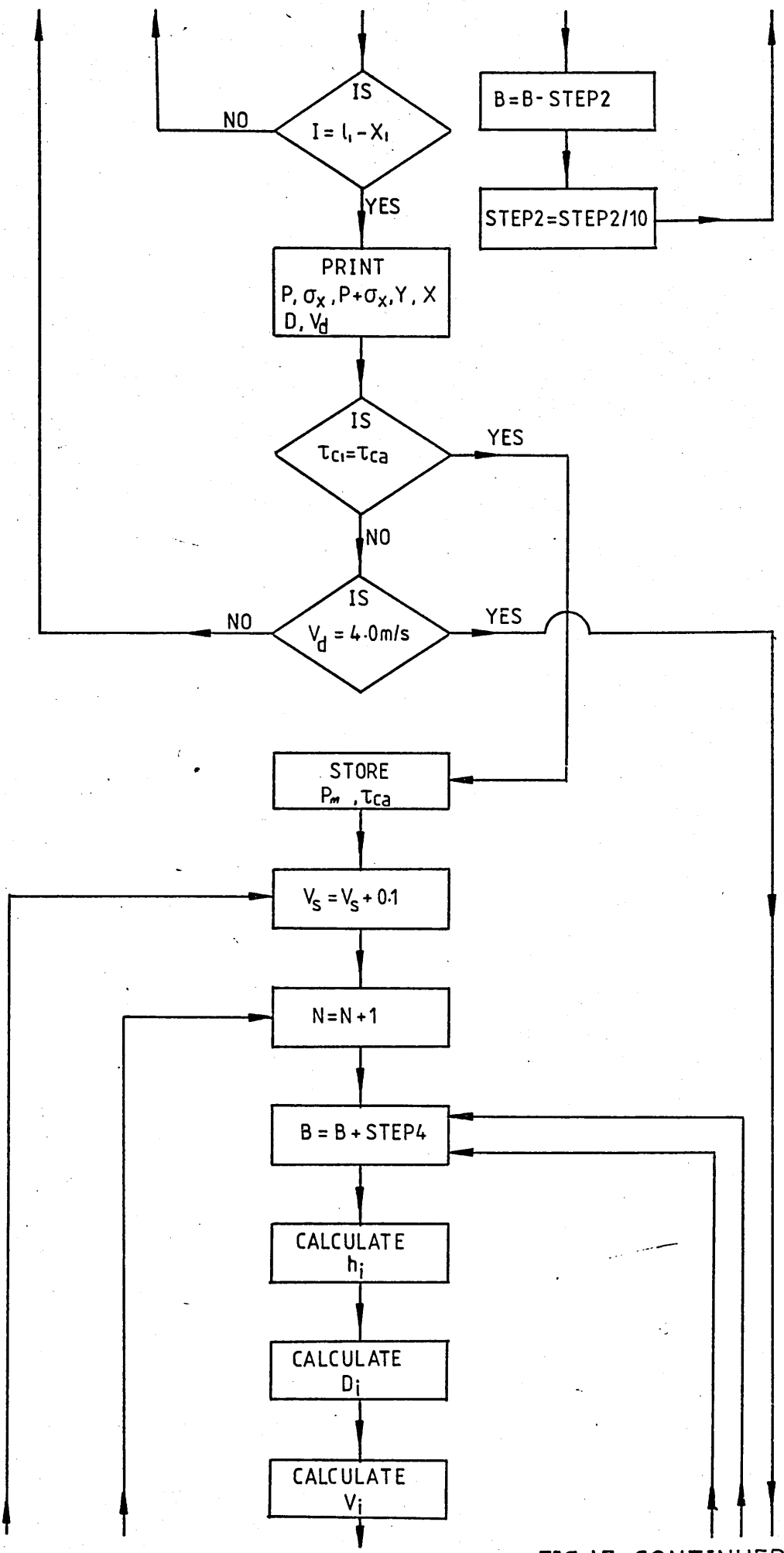

FIG A7 CONTINUED·····

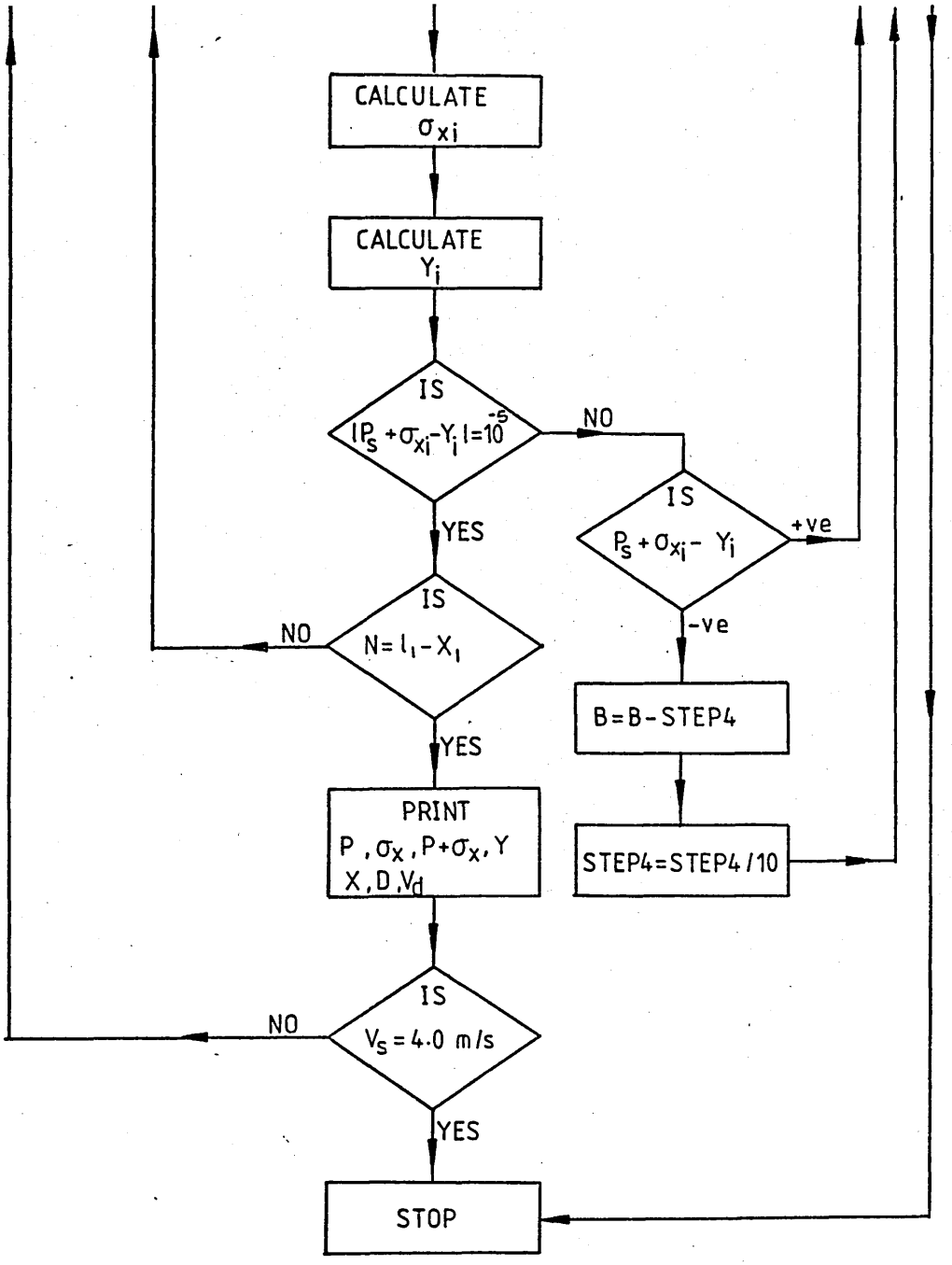

FIG A7 CONTINUED·····

```
      DIMENSION P(500),S(500),PS(500),X(500),Y(500),D(500),H(500)
      DIMENSION E(100),E2(100),E3(10000),V(50),E10(10000)
      DOUBLE PRECISION POIS1,QUET1,T11,T12,PHY1
      DOUBLE PRECISION POIS2,QUET2,T21,T22,PHY2
      DOUBLE PRECISION POIS3,QUET3,T31,T32,PHY3
      DOUBLE PRECISION EMB,D
      WRITE(6,10)
10    FORMAT(1HO,'THIS PROGRAMME CALCULATES THEORETICAL',/,
     &1X,'PERCENTAGE REDUCTION IN AREA ATTAINABLE IN A',/,
     &1X,'STEPPED REDUCTION UNIT FOR POLYMER MELT LUBRICATION.')
20    WRITE(6,30)
30    FORMAT(1HO,'INPUT SHEAR STRESS CONSTANT "K",VISCOSITY OF',/,
     &1X,', POLYMER AND CRITICAL SHEAR STRESS "TCA" RESPECTIVELY.')
      READ(5,*)PC,AVIS,TCA
      WRITE(6,40)
40    FORMAT(1HO,'INPUT INITIAL YIELD OF THE WIRE "YO",',/,
     &1X,'MATERIAL CONSTANT "K" AND STRAIN INDEX "N"',/,
     &1X,'RESPECTIVELY.')
      READ(5,*)YO,TER,F
      WRITE(6,50)
50    FORMAT(1HO,'INPUT L1,L2,H1 AND H2 IN METERS.')
      READ(5,*)AL1,AL2,H1,H2
      WRITE(6,60)
60    FORMAT(1HO,'INPUT INITIAL DIAMETER OF WIRE IN METERS.')
      READ(5,*)D1
      WRITE(6,70)
70    FORMAT(1HO,'INPUT STRAIN SENSITIVITY CONSTANTS "N" AND "T" .')
      READ(5,*)TU,BA
      WRITE(6,80)
80    FORMAT(1HO,'TO INCLUDE STRAIN RATE SENSITIVITY,TYPE 1,',/,
     &1X,'OTHERWISE TYPE 0.')
      READ(5,*)AA
      WRITE(6,90)
90    FORMAT(1HO,'TO PRINT OUT THE PRESSURE & STRESS',/,
     &1X,'OVER THE DEFORMED LENGTH TYPE 1,OTHERWISE 0.')
      READ(5,*)DR
      VEL=0.0
      TC1=0.0
100   DO 290 I=1,40
      VEL=VEL+0.1
      P1=0.0
      SRT=VEL/H1
      STEP1=1E07
      REM1=1E-10
      J1=0
110   P1=P1+STEP1
      J1=J1+1
      VIS=AVIS+((((P1**2)*(4.1E-11))+120000)/SRT)
      DP1=P1/AL1
      POIS1=(4+(PC*(DP1**2)*(H1**2)))/(12*PC)
      QUET1=(VIS*VEL)/(2*PC*H1)
      T11=-QUET1+(DSQRT((POIS1**3)+(QUET1**2)))
      T12=QUET1+(DSQRT((POIS1**3)+(QUET1**2)))
      PHY1=(T11**0.3333)-(T12**0.3333)
      TC1=PHY1-(DP1*H1*0.5)
      Q1=((DP1*(H1**3))/(6*VIS))+(TC1*(H1**2)/(2*VIS))+(VEL*H1)+
```

FIG A7 CONTINUED·····

```
     &(PC/VIS)*(((DP1**3)*(H1**5)/20)+((TC1**3)*(H1**2)/2)+
     &((DP1**2)*(H1**4)*TC1*0.25)+(0.5*(TC1**2)*DP1*(H1**3)))
      DP2=P1/AL2
      POIS2=(4+(PC*(DP2**2)*(H2**2)))/(12*PC)
      QUET2=(VIS*VEL)/(2*PC*H2)
      T21=-QUET2+(DSQRT((POIS2**3)+(QUET2**2)))
      T22=QUET2+(DSQRT((POIS2**3)+(QUET2**2)))
      PHY2=(T21**0.3333)-(T22**0.3333)
      TC2=PHY2+(DP2*H2*0.5)
      Q2=-((DP2*(H2**3))/(6*VIS))+(TC2*(H2**2)/(2*VIS))+(VEL*H2)+
     &(PC/VIS)*(-((DP2**3)*(H2**5)/20)+((TC2**3)*(H2**2)*0.5)+
     &((DP2**2)*(H2**4)*TC2*0.25)-(0.5*(TC2**2)*DP2*(H2**3)))
      RES1=Q1-Q2
      E(J1)=ABS(RES1)
      FIX=E(J1)-E(J1-1)
      IF(ABS(FIX).LE.REM1)GOTO 130
      IF(RES1)120,130,110
120   P1=P1-STEP1
      STEP1=STEP1/10
      GOTO 110
130   WRITE(6,140)
140   FORMAT(1HO,'**********************************************************
     &**********************')
      X1=YO/((P1/AL1)+(4*ABS(TC1)/D1))
      WRITE(6,150)P1,TC1,VIS,X1,VEL
150   FORMAT(1HO,'PM=',F10.0,2X,'TC1=',F8.0,2X,'VIS=',F8.2
     &,2X,'X1=',F8.5,2X,'VEL=',F4.2)
      IF(X1.GT.AL1)GOTO 100
      REP=(INT(X1*1000.0)+1)
      N=AL1*1000.0-REP
      P(1)=(P1*X1)/AL1
      Y(1)=YO
      S(1)=(4*ABS(TC1)*X1)/D1
      PS(1)=P(1)+S(1)
      D(1)=D1
      H(1)=H1
      V(1)=VEL
      X(1)=X1
      DX=0.001
      DO 230 M=1,N
      J=M+1
      PP=M
      STEP4=1E-03
      REM4=1E-05
      B=0.0
      K=0
160   B=B+STEP4
      K=K+1
      X(J)=X(J-1)+DX
      D(J)=D(J-1)-(B*DX)
      IF(D(J).LT.0)GOTO 300
      H(J)=H(J-1)+0.5*B*DX
      V(J)=V(J-1)/(1-(2*(D(J-1)-D(J))/((2*D(J-1))-D(J))))
      DP=0.0
      REM3=1E-10
      STEP3=5E08
```

FIG A7 CONTINUED·····

```
      K1=0
170   DP=DP+STEP3
      K1=K1+1
      POIS3=(4+(PC*(DP**2)*(H(J)**2)))/(12*PC)
      QUET3=(VIS*V(J))/(2*PC*H(J))
      T31=-QUET3+(DSQRT((POIS3**3)+(QUET3**2)))
      T32=QUET3+(DSQRT((POIS3**3)+(QUET3**2)))
      PHY3=(T31**0.3333)-(T32**0.3333)
      TC=PHY3-(DP*H(J)*0.5)
      RES2=((DP*(H(J)**3))/(6*VIS))+(TC*(H(J)**2)/(2*VIS))+(V(J)*H(J))
     &+(PC/VIS)*(((DP**3)*(H(J)**5)/20)+((TC**3)*(H(J)**2)/2)+
     &((DP**2)*(H(J)**4)*TC/4)+((TC**2)*DP*(H(J)**3)/2))-Q1
      E2(K1)=ABS(RES2)
      FIX2=E2(K1)-E2(K1-1)
      IF(ABS(FIX2).LE.REM3)GOTO 190
      IF(RES2)180,190,170
180   DP=DP-STEP3
      STEP3=STEP3/10
      GOTO 170
190   P(J)=DP*DX+P(J-1)
      STRS=0.0
      IF(AA.NE.1)GOTO 200
      EMB=2*V(J)*(DLOG(D(J-1)/D(J)))/DX
      STRS=(EMB/TU)**(1/BA)
200   Y(J)=(1+STRS)*(YO+(TER*((2*(DLOG(D(1)/D(J))))**F)))
      S(J)=2*((D(J-1)-D(J))/D(J))*Y(J)+(4*DX*ABS(TC)/D(J))
     &+S(J-1)
      PS(J)=P(J)+S(J)
      RES3=PS(J)-Y(J)
      E3(K)=ABS(RES3)
      RES4=E3(K)-E3(K-1)
      IF(ABS(RES4).LE.REM4)GOTO 220
      IF(RES3)210,220,160
210   B=B-STEP4
      STEP4=STEP4/10
      GOTO 160
220   CONTINUE
230   CONTINUE
      HH=H(J)-H1+H2
      WRITE(6,240)HH
240   FORMAT(1H ,'H=',F10.8)
      IF(DR.NE.1)GOTO 270
      I1=M+1
      DO 260 J=1,I1
      WRITE(6,250)P(J),S(J),PS(J),Y(J),X(J),D(J)
250   FORMAT(1H ,'P=',F10.0,2X,'S=',F10.0,2X,'P+S=',F10.0,
     &2X,'Y=',F10.0,2X,'X=',F6.4,2X,'D=',F8.6)
260   CONTINUE
270   PRA=(1-((D(J)**2)/(D1**2)))*100
      WRITE(6,280)PRA
280   FORMAT(1HO,'PRA=',F6.3,1X,'%')
      WRITE(6,285)V(J)
285   FORMAT(1HO,'VD=',F4.2)
      IF(ABS(TC1).GT.TCA)GOTO 320
290   CONTINUE
      GOTO 440
```

FIG A7 CONTINUED·····

```
300   WRITE(6,310)
310   FORMAT(1HO,'WIRE BREAKS AT THIS SPEED.')
      GOTO 440
320   WRITE(6,330)
330   FORMAT(1HO,10X,'$$$$$$$$$$CONDITION OF SLIP IS DETECTED.$$$$$$$$$
     &')
      DO 430 II=1,40
      VEL=VEL+0.1
      V(1)=VEL
      DO 380 M=1,N
      J=M+1
      STEP10=1E-03
      REM10=1E-05
      B10=0.0
      K10=0
340   B10=B10+STEP10
      K10=K10+1
      D(J)=D(J-1)-(B10*DX)
      H(J)=H(J-1)+0.5*B10*DX
      V(J)=V(J-1)/(1-(2*(D(J-1)-D(J))/((2*D(J-1))-D(J))))
      STRS=0.0
      IF(AA.NE.1)GOTO 350
      EMB=2*V(J)*(DLOG(D(J-1)/D(J)))/DX
      STRS=(EMB/TU)**(1/BA)
350   Y(J)=(1+STRS)*(YO+(TER*((2*(DLOG(D(1)/D(J))))**F)))
      S(J)=2*((D(J-1)-D(J))/D(J))*Y(J)+(4*DX*ABS(TC1)/D(J))+S(J-1)
      PS(J)=P(J)+S(J)
      RES10=PS(J)-Y(J)
      E10(K10)=ABS(RES10)
      RES20=E10(K10)-E10(K10-1)
      IF(ABS(RES20).LE.REM10)GOTO 370
      IF(RES10)360,370,340
360   B10=B10-STEP10
      STEP10=STEP10/10
      GOTO 340
370   CONTINUE
380   CONTINUE
      H10=H(J)-H1+H2
      PRA=(1-((D(J)**2)/(D1**2)))*100
      WRITE(6,390)VEL,PRA,H10,V(J)
390   FORMAT(1HO,'VEL=',F4.2,5X,'PRA=',F6.3,1X,'%',5X,
     &'H=',F10.8,5X,'VD=',F4.2)
      IF(DR.NE.1)GOTO 420
      I10=M+1
      DO 410 J=1,I10
      WRITE(6,400)P(J),S(J),PS(J),Y(J),X(J),D(J)
400   FORMAT(1H ,'P=',F10.0,2X,'S=',F10.0,2X,'P+S=',F10.0,2X
     &,'Y=',F10.0,2X,'X=',F6.4,2X,'D=',F8.6)
410   CONTINUE
420   CONTINUE
      IF(V(J).GT.4.0)GOTO 440
430   CONTINUE
440   WRITE(6,450)
450   FORMAT(1HO,'TO RUN THIS PROGRAMME AGAIN TYPE 1,OTHERWISE 0.')
      READ(5,*)CC
      IF(CC.EQ.1)GOTO 20
      STOP
      END
```

APPENDIX 5: Experimental Results Obtained Using The Stepped And The Tapered Bore Reduction Units In Tabular Form.

This Appendix contains the most important experimental results which are classified and tabulated as follows;

i)- Results of the stepped bore reduction unit.

Table 1 : Copper wire - WVG 23, 180° C.

Table 2 : Copper wire - WVG 23, 130° C.

Table 3 : Mild steel wire - WVG 23, 130° C.

Table 4 : 18/8 Stainless steel wire - WVG 23, 130° C.

Table 5 : Copper wire - KM 61, 200° C.

Table 6 : Mild steel wire - KM 61, 200° C.

Table 7 : 18/8 Stainless steel wire - KM 61, 200° C.

Table 8 : Mild steel wire - KM 61, 200° C -(h_1/h_2=2.0).

ii)- Results of the tapered bore reduction unit.

Table 9 : Copper wire - WVG 23, 130° C.

Table 10: Copper wire - WVG 23, 180° C.

Table 1 : Copper wire - WVG 23, 180° C.

Speed m/s	% Reduction in area	Coating thickness mm	Drawing load N	Pressure $N/m^2 \times 10^7$			
				1	2	3	4
0.052	2.45	0.0352	57	1.2	1.5	3.0	1.2
0.081	2.50	0.0375	65	2.1	4.0	3.5	1.0
0.126	4.57	0.0455	82	3.9	5.0	4.5	1.25
0.152	6.0	0.053	106	4.8	6.0	5.0	1.25
0.20	7.27	0.060	123	6.0	6.0	5.5	1.3
0.25	6.67	0.060	123	6.0	6.0	5.0	1.25
0.30	7.0	0.060	123	6.0	6.0	5.0	1.25
0.356	6.0	0.057	123	6.0	6.0	4.0	1.5
0.40	6.0	0.050	123	6.0	6.0	5.0	1.5
0.44	4.87	0.056	130	5.5	6.0	4.0	1.5
0.53	4.87	0.056	131	4.5	6.0	4.5	1.5
0.26	6.10	0.0613	105	7.5	7.0	4.5	1.5
0.32	7.3	0.069	105	8.1	7.0	4.5	1.5
0.40	6.1	0.065	111	7.8	7.0	4.5	1.5
0.50	6.1	0.062	111	7.5	7.0	4.0	1.5
0.60	6.0	0.063	117	6.9	7.0	4.0	1.5
0.70	4.9	0.054	117	6.6	7.0	4.0	1.5
0.80	4.9	0.058	111	6.3	7.0	4.0	1.5
0.98	4.87	0.056	111	5.4	7.0	4.0	1.5
1.16	4.87	0.055	92	4.5	7.0	4.0	1.5
1.30	4.87	0.054	118	4.8	7.0	4.0	1.5
1.54	4.87	0.053	98	4.2	6.5	4.5	1.5
1.66	4.57	0.052	98	4.5	7.0	4.0	1.5
1.84	4.57	0.052	105	4.2	7.0	4.0	1.5
2.0	4.87	0.052	105	3.6	7.0	4.0	1.5
0.83	4.57	0.057	108	1.8	8.0	6.0	2.5
0.98	4.57	0.055	127	7.2	7.5	5.5	3.0
1.20	4.87	0.054	127	7.25	7.5	6.5	2.5
1.43	3.67	0.053	127	6.2	7.5	6.0	2.5
1.66	4.87	0.053	127	6.3	7.5	6.0	2.7
1.76	4.87	0.052	127	6.1	7.25	6.2	2.5
2.0	4.57	0.051	127	6.0	7.5	6.0	2.5

table 1 continued

2.31	4.57	0.0512	127	6.3	7.5	6.0	2.5
2.6	4.27	0.051	127	5.5	7.5	6.0	2.5
2.8	4.27	0.050	127	5.5	7.5	6.0	2.5
3.25	4.27	0.049	133	5.5	7.5	6.0	2.5
3.5	4.0	0.049	133	5.5	7.5	6.0	2.5
3.9	3.67	0.0476	133	5.5	7.5	6.0	2.5
4.14	4.0	0.051	133	5.5	7.5	6.0	2.5

Table 2 : Copper wire - WVG 23, 130° C.

Speed m/s	% Reduction in area	Coating thickness mm	Drawing load N	Pressure $N/m^2 \times 10^7$			
				1	2	3	4
0.05	10	0.086					
0.08	16	0.104					
0.09	14.88	0.102					
0.13	16	0.105					
0.15	14.8	0.099					
0.18	14.88	0.10					
0.22	14.23	0.098					
0.27	12.5	0.088					
0.34	11.4	0.090					
0.39	11.4	0.087					
0.44	13.7	0.096					
0.55	8.87	0.073					
0.63	7.73	0.066					
0.74	8.4	0.072					
0.28	22.7	0.095					
0.31	22.9	0.138					
0.37	21.59	0.132					
0.47	19.38	0.122					
0.513	16.44	0.109					
0.60	13.73	0.095					
0.67	12.5	0.09					
0.80	9.8	0.083					
1.30	9.73	0.075					
1.24	10.83	0.077					
1.16	9.8	0.076					
1.06	10.48	0.078					
0.91	10.4	0.080					
0.86	10.68	0.081					
0.67	9.73	0.083					
0.63	9.88	0.081					
0.28	23.7	0.14					
0.37	22.7	0.137					

table 2 continued

0.38	22.21	0.130		
0.55	18.13	0.111		
0.70	17.5	0.109		
0.83	13.87	0.095		
0.85	13.44	0.090		
1.0	12.87	0.090		
1.17	11.41	0.080		
1.42	10.83	0.075		
1.29	10.83	0.078		
1.16	12.58	0.083		
1.04	12.58	0.085		
0.90	12.58	0.088		
0.78	15.45	0.10		
0.054	18.15	0.093		
0.08	18.91	0.133		
0.10	25.0	0.138		
0.134	26.84	0.143		
0.165	25.84	0.143		
0.21	26.64	0.141		
0.26	26.90	0.146		
0.33	25.48	0.142		
0.40	24.44	0.133		
0.45	22.89	0.132		
0.527	21.12	0.127		
0.77	19.95	0.116		
0.88	18.35	0.11		
0.05	19.26	0.113		
0.07	16.53	0.122		
0.087	23.0	0.134		
0.10	23.57	0.135		
0.124	24.24	0.134		
0.15	26.64	0.146		
0.83	10.51	0.081		
0.942	11.0	0.082		
1.16	11.82	0.10		
1.11	11.0	0.082		
1.41	10.8	0.078		
1.67	10.21	0.074		

table 2 continued

1.96	9.63	0.069					
2.17	8.67	0.067					
2.43	8.75	0.067					
2.68	8.45	0.064					
2.9	7.27	0.059					
3.0	7.27	0.059					
3.47	7.2	0.062					
3.89	7.27	0.058					
4.26	7.27	0.058					
0.80	12.25	0.083	158	7.5	11.0	9.0	2.5
0.93	10.8	0.078	158	8.0	9.5	8.5	3.0
1.14	8.75	0.07	152	7.5	9.5	9.5	3.0
1.32	8.45	0.066	152	7.0	9.5	8.0	3.0
1.5	7.56	0.062	145	7.0	9.5	8.0	3.0
1.81	7.0	0.061	145	6.75	9.0	8.0	2.5
2.0	7.0	0.06	145	6.25	8.5	7.0	2.0
2.28	7.0	0.06	146	6.25	8.5	7.0	2.5
2.63	6.67	0.056	145	6.2	8.5	7.0	2.5
3.0	6.67	0.056	145	5.75	8.0	7.0	2.0
3.31	6.97	0.055	145	5.87	8.0	6.5	2.5
3.68	6.37	0.052	152	6.75	8.0	7.0	2.5
3.91	6.37	0.053	152	6.75	8.0	6.6	3.0
0.27	20.1	0.124	120	5.0	9.5	6.0	2.5
0.36	20.0	0.121	114	8.5	10.5	6.5	2.5
0.43	19.6	0.123	120	6.2	11.0	6.6	2.5
0.54	17.66	0.111	108	9.25	11.5	6.0	2.5
0.66	16.81	0.10	108	10.0	12.5	7.0	2.5
0.7	17.0	0.11	101	7.5	12.5	7.0	2.5
0.84	11.8	0.088	108	7.2	10.0	7.0	2.5
0.97	10.0	0.081	101	7.0	9.5	6.0	2.5
1.17	9.33	0.074	102	7.0	9.0	7.0	2.5
1.35	8.45	0.065	95	6.0	8.5	6.5	2.5
1.57	7.56	0.065	95	5.7	8.0	6.0	2.5
1.77	7.27	0.064	95	6.2	8.0	6.0	2.5
1.85	7.27	0.064	102	6.2	7.5	6.0	2.5
1.98	7.0	0.061	102	5.7	8.0	6.0	2.5
0.05	13.11	0.056	118	2.0	9.0	6.0	4.0
0.06	21.87	0.136	130	2.5	8.5	8.0	4.5

table 2 continued

0.06	21.87	0.136	130	2.5	8.5	8.0	4.5
0.08	22.0	0.139	137	3.0	10.5	7.0	2.5
0.09	25.25	0.145	138	2.5	10.0	7.0	2.5
0.126	27.17	0.158	138	3.25	10.0	8.0	2.5
0.14	26.18	0.149	130	4.0	10.0	7.0	2.5
0.184	25.31	0.145	130	4.5	10.5	7.0	2.5
0.23	24.71	0.152	125	5.0	11.5	6.0	2.5
0.24	22.0	0.127	130	6.0	11.5	6.0	2.5
0.33	22.1	0.13	118	6.0	12.0	7.0	2.5
0.42	20.16	0.122	118	6.2	12.5	7.0	2.5
0.51	17.24	0.111	111	6.7	12.5	7.0	2.5
0.60	15.68	0.10	105	7.5	12.5	7.0	2.5
0.73	11.1	0.086	98	8.0	11.5	7.0	3.0

Table 3 : Mild stwwl wire - WVG 23, 130° C.

Speed m/s	% Reduction in area	Coating thickness mm	Drawing load N	Pressure $N/m^2 \times 10^7$			
				1	2	3	4
0.05	13.0	0.11	158	3.0	15.0	12.0	2.5
0.068	15.9	0.12	164	2.5	13.5	13.0	4.0
0.10	17.9	0.115	152	2.7	13.0	13.0	5.0
0.125	21.6	0.13	159	3.7	15.0	13.0	5.0
0.17	21.8	0.136	160	4.5	17.5	12.0	4.0
0.21	21.5	0.128	152	5.7	17.5	10.0	3.5
0.27	20.0	0.124	133	6.5	18.5	10.0	2.5
0.30	17.7	0.113	140	7.0	18.0	10.0	2.5
0.35	18.4	0.122	140	7.5	18.5	10.0	3.5
0.50	15.9	0.104	126	4.2	20.0	9.0	2.5
0.51	13.0	0.096	126	7.5	19.0	9.0	2.5
0.57	14.0	0.10	126	6.5	13.5	9.0	2.5
0.05	18.4	0.145	154	3.0	14.0	11.0	2.5
0.07	18.4	0.138	184	2.5	14.0	11.0	4.0
0.08	20.2	0.143	184	3.0	14.5	10.0	5.0
0.11	20.4	0.133	184	3.0	14.0	12.0	4.0
0.14	21.7	0.142	184	4.0	15.0	12.0	3.5
0.16	21.0	0.132	190	3.0	16.0	11.0	3.0
0.20	21.0	0.133	177	2.5	14.0	10.0	3.0
0.26	21.23	0.127	177	3.7	17.5	10.0	2.0
0.33	20.7	0.129	165	5.75	18.0	10.0	2.0
0.37	19.28	0.122	158	5.5	17.5	10.0	2.5
0.47	17.0	0.105	140	6.2	16.5	9.0	2.5
0.56	13.4	0.089	127	5.7	17.0	9.0	2.5
0.67	14.7	0.10	127	4.5	16.5	9.0	2.0
0.70	12.54	0.088	127	5.0	19.0	10.0	3.0
0.80	13.0	0.093	120	3.7	18.0	9.0	2.5
0.94	9.16	0.08	114	4.0	15.0	7.0	2.5
0.314	16.5	0.12	133	6.25	17.5	8.0	2.0
0.38	14.8	0.10	140	7.2	16.0	7.0	2.0
0.42	13.0	0.10	120	7.5	17.0	8.0	2.5
0.56	11.3	0.095	127	7.5	15.5	8.0	2.0

table 3 continued

0.64	5.35	0.075	114	8.0	15.5	7.0	2.5
0.79	4.12	0.07	114	7.5	15.0	6.5	2.5
0.94	0.0	0.053	114	5.0	11.5	6.0	2.5
0.97	0.0	0.053	108	6.7	13.5	7.0	2.5
1.08	0.0	0.054	114	5.2	13.5	6.5	2.5
1.22	0.0	0.049	108	6.2	13.5	6.0	2.5
1.42	0.0	0.045	89	1.5	9.5	4.0	2.0
1.48	0.0	0.047	114	3.5	11.5	7.0	2.5
1.61	0.0	0.046	108	4.0	12.5	6.0	2.5
1.77	0.0	0.048	95	4.2	10.0	6.5	2.5
1.93	0.0	0.050	95	3.75	10.5	7.0	2.5
0.26	19.88	0.134	184	1.5	12.5	10.0	2.5
0.34	18.7	0.13	171	5.5	11.8	10.0	2.5
0.49	14.8	0.12	152	5.0	17.0	9.0	2.5
0.62	12.18	0.104	146	6.25	17.5	8.0	2.0
0.8	8.13	0.088	127	7.5	13.5	8.0	2.5
0.90	5.0	0.073	121	6.5	15.0	7.5	2.5
1.0	2.0	0.06	108	4.2	12.5	8.0	3.0
1.2	0.0	0.056	121	6.2	11.5	7.5	2.5
1.34	0.0	0.051	114	6.25	13.0	7.0	2.5
1.51	0.0	0.055	114	5.7	11.5	7.0	3.0

Table 4 : 18/8 Stainless steel wire - WVG 23, 130° C.

Speed m/s	% Reduction in area	Coating thickness mm	Drawing load N	Pressure $N/m^2 \times 10^7$			
				1	2	3	4
0.05	5.25	---	226	5.0	12.0	12.0	7.5
0.068	8.15	---	250	7.0	11.5	12.0	5.0
0.08	8.97	---	264	7.0	11.0	13.0	5.0
0.10	17.31	---	300	7.0	22.5	15.0	3.0
0.13	16.53	---	324	12.5	24.0	19.0	3.5
0.16	18.77	0.115	320	10.0	25.0	20.0	8.5
0.217	18.77	0.114	350	12.5	26.5	21.0	4.0
0.28	20.0	0.123	350	12.5	27.5	20.0	6.0
0.36	19.8	0.124	317	12.5	29.5	13.0	2.5
0.41	18.7	0.116	295	12.5	29.0	13.0	1.0
0.52	11.67	0.10	270	12.5	24.0	10.0	3.5
0.05	6.37	---	289	4.0	13.0	10.0	5.0
0.07	8.16	---	280	1.6	12.0	8.0	5.0
0.10	17.1	---	340	2.8	23.0	15.0	6.0
0.113	16.8	---	360	4.0	25.0	15.0	6.5
0.16	20.45	---	377	5.0	30.0	18.0	10.0
0.19	20.5	---	360	6.0	30.0	20.0	11.5
0.25	19.88	---	354	7.5	30.0	20.0	11.5
0.28	21.0	0.122	362	7.5	32.0	20.0	15.0
0.35	20.0	---	325	7.5	35.0	22.0	16.0
0.40	19.33	0.113	340	7.5	30.0	20.0	15.0
0.46	17.66	0.11	265	9.0	30.0	15.0	8.5
0.52	19.88	0.117	285	9.0	32.0	14.0	7.5
0.60	17.66	0.119	230	9.0	30.0	13.0	3.5
0.67	16.66	0.125	230	8.5	30.0	13.0	3.5
0.97	3.66	0.063	200	8.0	17.0	9.0	2.5
1.10	9.63	0.082	200	4.2	17.0	9.0	3.0
1.3	1.84	0.054	173	8.0	15.0	7.0	2.5
1.5	6.0	0.054	145	9.0	18.0	6.0	2.2
1.62	0.0	0.051	173	3.0	17.0	7.0	1.0
0.61	20.4	0.131	260	9.0	40.0	16.0	1.3
0.73	17.66	0.117	230	9.0	35.0	12.0	3.0

table 4 continued

0.84	4.42	0.062	220	7.5	16.0	10.0	2.8
0.95	4.87	0.065	196	7.5	17.0	8.0	2.7
1.0	2.45	0.055	196	7.5	16.0	9.0	2.7
1.13	2.45	0.055	196	7.5	14.0	7.0	2.7
1.3	1.23	0.053	183	7.5	13.0	7.0	2.5
1.4	1.84	0.052	177	7.5	13.0	7.0	2.5
0.05	2.5	0.048	248	3.9	13.0	10.0	4.0
0.07	15.4	0.162	327	4.5	23.0	15.0	6.5
0.10	14.26	0.145	300	4.8	26.0	14.0	3.0
0.13	25.4	0.13	300	5.4	28.0	16.0	7.0
0.16	19.88	0.152	295	6.6	27.0	14.0	6.0
0.20	19.2	0.141	288	7.8	31.0	21.0	1.4
0.6	16.0	0.111	216	12.0	30.0	10.0	3.0
0.8	2.45	0.055	183	10.0	15.0	7.0	3.0
1.0	0.0	0.053	157	11.0	12.0	7.0	2.5
1.2	0.0	0.050	137	9.0	11.0	6.0	2.2
1.4	0.0	0.049	136	10.0	10.5	6.0	2.2
1.6	0.0	0.047	130	8.1	10.0	5.5	2.0
1.8	0.0	0.043	131	7.8	9.5	5.5	2.0
2.0	0.0	0.045	125	6.3	9.0	5.0	2.0
2.2	0.0	0.044	125	6.0	8.0	5.0	1.7
2.4	0.0	0.043	125	6.0	8.0	5.0	1.7
2.6	0.0	0.043	131	6.0	8.5	5.0	2.0
2.8	0.0	0.043	125	5.7	8.2	5.0	1.7
3.0	0.0	0.042	125	5.4	8.0	5.0	1.5

Table 5 : Copper wire - KM 61, 200° C.

Speed m/s	% Reduction in area	Coating thickness mm	Drawing load N	Pressure $N/m^2 \times 10^7$			
				1	2	3	4
0.05	14.55	---	188	---	---	---	---
0.08	9.63	---	260	---	---	---	---
0.167	10.8	---	204	---	---	---	---
0.23	5.83	---	107	---	---	---	---
0.30	7.56	---	171	---	---	---	---
0.42	19.88	0.118	220	4.5	10.0	8.0	5.0
0.52	20.0	0.116	213	3.0	8.0	7.0	6.0
0.615	22.0	0.122	204	4.5	10.0	8.0	4.5
0.05	10.2	---	133	---	---	---	---
0.08	13.7	---	126	---	---	---	---
0.11	7.0	---	154	---	---	---	---
0.167	10.8	---	161	---	---	---	---
0.40	18.9	0.112	196	4.2	12.0	9.0	5.0
0.50	20.0	0.111	182	3.6	8.0	7.0	4.0
0.57	20.0	0.112	182	2.6	8.0	6.0	5.0
0.7	21.2	0.115	175	2.4	9.0	7.0	5.0
0.78	20.7	0.118	210	2.1	9.0	5.0	3.5
1.0	18.22	0.105	267	3.6	6.0	3.0	2.5
1.4	16.8	0.099	235	1.8	6.0	3.5	2.0
1.61	17.1	0.102	212	1.8	6.0	4.0	2.5
2.0	14.26	0.092	204	1.5	5.0	4.0	3.0
2.4	11.6	0.08	188	2.4	5.0	4.0	3.0
2.73	11.1	0.083	188	3.0	7.0	5.0	3.0
3.26	10.1	0.077	173	2.4	4.0	6.0	2.5
3.34	10.0	0.074	173	3.0	8.0	6.0	3.5
3.77	9.63	0.068	157	2.4	8.0	7.0	3.5
0.82	20.16	0.115	321	3.6	10.0	6.0	2.5
0.95	19.33	0.111	312	3.9	10.0	4.0	1.75
1.2	18.22	0.104	285	3.3	10.0	4.0	1.5
1.42	18.0	0.106	250	3.9	11.0	4.0	2.5
1.7	15.4	0.098	241	4.5	11.0	5.0	2.5
2.0	14.83	0.095	223	3.9	11.0	5.0	3.0

table 5 continued

2.34	13.4	0.088	223	6.0	15.0	10.0	3.5
2.66	12.0	0.083	205	4.8	10.0	5.0	3.0
3.13	9.63	0.075	205	5.4	8.0	6.0	3.0
3.52	9.34	0.075	196	5.1	10.0	6.0	3.0
3.82	8.75	0.07	196	3.9	8.0	4.0	3.5
4.14	8.17	0.07	196	3.9	8.0	6.0	3.5

Table 6 : Mild steel wire - KM 61, 200° C.

Speed m/s	% Reduction in area	Coating thickness mm	Drawing load N	Pressure $N/m^2 \times 10^7$			
				1	2	3	4
0.05	8.61	0.085	200	6.0	10.0	4.0	0.5
0.075	13.0	0.096	217	6.0	10.0	4.0	1.0
0.13	17.2	0.12	224	5.1	13.0	9.0	4.5
0.20	17.4	0.125	210	7.5	16.0	12.0	5.5
0.26	13.2	0.113	210	7.5	17.0	12.0	6.5
0.33	10.4	0.10	203	7.5	14.0	12.0	7.5
0.42	12.2	0.103	203	6.0	12.0	10.0	6.0
0.52	10.7	0.102	203	4.5	16.0	10.0	5.0
0.58	10.4	0.099	196	5.4	15.0	11.0	6.0
0.68	10.1	0.103	196	6.6	18.0	11.0	6.0
0.05	19.7	0.138	139	6.9	18.0	15.0	3.5
0.08	25.0	0.158	222	5.4	15.0	14.0	4.0
0.14	19.4	0.133	215	9.0	17.0	15.0	4.5
0.20	16.3	0.12	215	6.0	12.0	11.0	6.0
0.28	14.0	0.112	196	4.0	20.0	18.0	6.5
0.35	12.0	0.109	203	9.0	16.0	14.0	8.0
0.45	11.0	0.102	184	7.5	30.0	20.0	6.5
0.52	11.3	0.10	190	6.9	20.0	20.0	7.0
0.70	11.0	0.103	209	4.5	20.0	10.0	6.5
0.8	11.0	0.11	205	10.0	24.0	12.0	6.0
1.0	11.0	0.105	215	10.0	24.0	12.0	6.0
1.2	9.2	0.094	214	9.5	25.0	12.0	4.5
1.4	10.1	0.096	208	11.0	25.0	15.0	5.5
1.6	10.4	0.096	202	10.0	26.0	14.0	5.0
1.8	9.2	0.092	205	10.2	25.0	11.0	4.0
2.0	10.1	0.088	215	5.1	27.0	14.0	5.0
2.2	8.3	0.084	210	5.1	28.0	13.0	5.0
2.4	8.8	0.074	190	4.2	30.0	13.0	5.0
2.6	3.12	0.064	170	3.9	33.0	12.0	5.0
2.8	2.18	0.061	164	3.6	31.0	11.0	4.5
3.0	0.0	0.053	164	3.5	28.0	9.0	4.5
3.2	0.0	0.057	164	3.0	29.0	7.0	4.0
3.4	0.0	0.052	157	2.1	25.0	9.0	3.5

Table 7 : 18/8 Stainless steel wire - KM 61, 200° C.

Speed m/s	% Reduction in area	Coating thickness mm	Drawing load N	Pressure $N/m^2 \times 10^7$			
				1	2	3	4
0.05	2.45	---	124	---	---	---	---
0.07	2.45	---	85	---	---	---	---
0.10	1.53	---	78	---	---	---	---
0.15	3.70	---	52	---	---	---	---
0.20	20.4	0.118	405	9.6	21.0	15.0	8.0
0.25	19.66	0.113	412	7.0	32.0	16.5	7.2
0.32	19.6	0.103	400	6.0	30.0	16.0	7.0
0.40	18.77	0.096	347	5.0	28.0	18.0	7.5
0.50	19.88	0.096	347	9.5	31.0	20.0	6.0
0.60	19.6	0.010	320	10.0	33.0	17.0	6.5
0.80	15.6	0.091	255	9.6	31.0	15.0	7.5
1.0	14.26	0.096	248	9.0	33.0	14.0	9.0
1.2	14.26	0.098	222	9.0	32.0	16.0	9.0
0.78	10.8	0.095	400	12.0	32.0	14.0	5.5
1.2	7.27	0.082	361	6.0	30.0	13.0	3.0
1.57	2.75	0.066	330	6.0	28.0	13.0	3.0
1.88	4.5	0.069	290	6.0	26.0	11.0	5.0
2.12	3.0	0.063	267	4.0	24.0	12.0	4.0
2.4	2.75	0.06	259	11.0	23.0	11.0	4.0
2.8	5.3	0.061	228	9.0	21.0	10.0	4.0
3.0	1.23	0.055	220	10.0	21.0	11.0	4.0
3.2	0.61	0.053	212	10.0	19.0	9.5	3.5
3.4	0.0	0.052	212	10.0	19.0	10.0	3.5

Table 8 : Mild steel wire - KM 61, 200° C -($h_1/h_2 = 2$)

Speed m/s	% Reduction in area	Coating thickness mm	Drawing load N	Pressure $N/m^2 \times 10^7$			
				1	2	3	4
0.05	11.0	0.124	273	3.0	9.0	8.0	3.0
0.08	17.4	0.132	315	3.0	10.0	10.0	2.5
0.13	17.4	0.111	330	2.4	8.8	8.0	3.5
0.17	16.3	0.116	315	1.5	9.0	8.0	5.0
0.24	15.1	0.118	308	3.6	11.0	9,0	6.5
0.33	12.77	0.108	280	2.4	12.0	9.0	6.0
0.41	12.18	0.106	238	1.8	12.0	10.0	6.0
0.52	11.3	0.101	217	1.9	12.0	10.0	8.0
0.62	11.4	0.102	210	2.0	15.0	13.0	8.0
0.73	9.8	0.105	182	5.1	15.0	10.0	7.0
0.80	11.8	0.103	234	6.0	20.0	15.0	10.0
1.0	11.0	0.108	240	6.6	20.0	13.0	9.0
1.2	8.6	0.11	234	6.9	22.0	13.0	6.0
1.4	5.88	0.10	211	6.6	22.0	12.0	5.0
1.6	5.2	0.102	204	7.2	22.0	12.0	5.0
1.8	2.5	0.096	189	7.5	21.0	12.0	4.5
2.0	1.25	0.091	174	7.2	18.0	10.0	4.5
2.2	0.0	0.088	166	6.0	15.0	9.0	4.0
2.4	0.0	0.085	159	4.8	12.0	8.0	3.0
2.6	0.0	0.081	143	3.0	8.0	5.0	2.5
2.8	0.0	0.083	138	2.5	7.0	4.5	2.5
3.0	0.0	0.082	140	2.4	7.0	4.7	2.5

Table 9 : Copper wire - WVG 23, 130° C.

Speed m/s	% Reduction in area	Coating thickness mm	Drawing load N	Pressure $N/m^2 \times 10^7$			
				1	2	3	4
0.28	18.0	0.123					
0.30	19.87	0.126					
0.32	17.5	0.117					
0.34	17.2	0.12					
0.36	15.3	0.112					
0.4	13.0	0.104					
0.44	11.9	0.095					
0.47	13.0	0.104					
0.52	11.9	0.095					
0.58	9.5	0.088					
0.64	11.53	0.09					
0.80	7.44	0.074					
0.88	10.7	0.079					
0.96	8.0	0.075					
1.17	5.22	0.064					
1.30	6.07	0.068					
1.24	6.07	0.071					
1.15	6.07	0.071					
0.98	7.45	0.077					
0.93	7.22	0.07					
0.83	9.0	0.085					
0.78	9.0	0.088					
0.73	9.0	0.083					
0.70	10.8	0.097					
0.66	10.8	0.095					
0.58	13.11	0.105					
0.50	13.0	0.10					
0.45	15.4	0.114					
0.40	14.3	0.11					
0.85	9.4	0.084					
0.96	7.12	0.074					
1.0	6.5	0.08					

table 9 continued

1.18	6.0	0.075		
1.26	6.0	0.069		
1.33	6.6	0.071		
1.44	5.33	0.066		
1.65	5.34	0.067		
1.88	6.0	0.064		
1.99	4.83	0.062		
2.12	5.77	0.064		
2.46	5.0	0.062		
2.57	5,17	0.063		
3.0	4.87	0.062		
3.35	4.27	0.058		
3.92	4.76	0.056		
3.75	4.04	0.054		
3.49	4.87	0.055		
3.10	4.87	0.055		
2.75	5.33	0.059		
2.53	4.38	0.055		
2.42	4.91	0.057		
2.24	4.87	0.058		
2.14	4.87	0.060		
1.79	5.17	0.063		
1.53	5.64	0.065		
1.43	5.8	0.066		
1.30	6.0	0.068		
1.21	6.37	0.073		
1.15	6.6	0.073		
1.0	6.7	0.074		
0.95	7.64	0.077		
0.05	4.66	0.076		
0.055	6.85	0.089		
0.057	9.24	0.10		
0.06	13.3	0.122		
0.098	16.4	0.133		
0.11	19.6	0.137		
0.12	21.75	0.14		
0.15	20.7	0.138		
0.176	20.8	0.135		

table 9 continued

0.20	17.0	0.115		
0.25	20.0	0.132		
0.28	17.3	0.11		
0.30	19.7	0.113		
0.35	16.8	0.11		
0.46	16.3	0.109		
0.50	16.3	0.106		
0.73	11.3	0.08		

Table 10 : Copper wire - WVG 23, 180° C.

Speed m/s	% Reduction in arae	Coating thickness mm	Drawing load N	Pressure $N/m^2 \times 10^7$			
				1	2	3	4
0.057	1.84	0.043					
0.061	1.84	0.054					
0.081	3.0	0.063					
0.09	4.60	0.074					
0.114	6.7	0.085					
0.15	8.2	0.088					
0.21	9.1	0.09					
0.22	9.36	0.095					
0.29	8.5	0.09					
0.32	8.5	0.09					
0.4	6.7	0.084					
0.42	7.0	0.081					
0.51	6.1	0.078					
0.58	6.7	0.081					
0.59	6.24	0.08					
0.65	6.73	0.08					
0.05	6.40	0.075	25	2.0	0.7	0.5	
0.08	1.23	0.045	22	2.8	0.5	0.5	
0.10	1.84	0.048	31	4.0	1.0	0.7	
0.104	3.6	0.06	41	4.0	1.0	0.75	
0.134	5.0	0.07	47	5.0	1.0	0.7	
0.15	6.4	0.073	50	6.0	1.5	0.9	
0.19	7.2	0.077	57	6.5	1.5	0.9	
0.22	7.7	0.076	57	6.5	1.7	1.0	
0.26	7.3	0.079	63	6.5	1.5	1.0	
0.28	7.88	0.078	63	7.0	1.7	1.0	
0.30	7.88	0.08	63	7.0	1.7	1.0	
0.37	7.3	0.077	63	7.0	2.0	1.1	
0.41	7.88	0.076	63	7.0	2.0	1.1	
0.49	6.77	0.074	63	7.0	2.0	1.2	
0.53	6.4	0.072	63	7.0	2.2	1.3	
0.60	5.8	0.07	63	7.0	2.5	1.3	

table 10 continued

0.84	4.77	0.062	63	7.0	2.5	1.4
0.28	5.5	0.072	76	7.0	1.7	1.0
0.30	5.5	0.072	76	7.0	1.7	1.0
0.33	5.4	0.067	76	7.0	1.7	1.0
0.37	5.9	0.073	79	7.0	1.7	1.1
0.40	5.4	0.07	76	7.0	2.0	1.1
0.44	5.5	0.07	76	7.0	2.0	1.1
0.52	4.3	0.065	76	7.0	2.0	1.2
0.58	4.3	0.066	76	7.0	2.0	1.2
0.68	4.6	0.065	76	6.5	2.2	1.2
0.76	4.3	0.064	77	7.0	2.25	1.3
0.88	3.0	0.058	76	7.0	2.25	1.3
1.03	3.0	0.058	76	7.0	2.4	1.3
1.13	3.6	0.063	95	6.5	2.5	1.4
1.39	3.67	0.061	95	6.0	2.5	1.5
1.57	3.6	0.06	95	6.0	2.8	1.5
1.76	3.67	0.06	98	6.0	2.5	1.5
1.95	3.45	0.054	95	5.0	1.5	0.9
2.16	3.4	0.058	101	6.0	2.5	1.5
2.35	3.36	0.06	101	6.0	2.5	1.6
2.71	3.21	0.057	95	6.0	2.5	1.6
2.94	3.36	0.057	95	6.0	2.5	1.6
3.15	2.45	0.055	104	6.0	2.5	1.5
3.67	2.45	0.055	101	6.0	2,5	1.6
3.94	2.45	0.055	104	6.0	2.5	1.6
4.0	2.45	0.055	101	6.0	2.5	1.6

APPENDIX 6: Papers published.

A NOVEL TECHNIQUE OF WIRE DRAWING

M. S. J. Hashmi†‡ G. R. Symmons†‡ H. Parvinmehr†

In the conventional wire drawing process the reduction is achieved by pulling the wire through a tapered die. The minimum bore size of such a die is always smaller than the inlet wire diameter. A suitable lubricant is used to reduce the die wear and drawing load and to produce a good surface finish. Nevertheless, the problem of die wear and wire breakage during start-up is always present.

In this paper a new technique of wire drawing is being reported which eliminates the problem of wear and breakage during start-up and also the need to have the diameter of the leading end of the wire reduced for easy insertion through the die. The reduction of the wire diameter is affected by means of the hydrodynamic action of a polymer melt lubricant in conjunction with a long tapering tube, the diameter of the tube being greater than the nominal wire diameter. Reductions in area of up to 21 per cent can be obtained in one single pass using this dieless reduction unit.

1 INTRODUCTION

Although wire drawing is one of the earliest crafts in metal forming, no significant development of the process took place until the beginning of this century and only single-die machines were used. Later on multi-die machines and tungsten-carbide dies were introduced, but the operating principle remained the same, namely, the wire is pulled through a tapered reduction die and the material deforms plastically whilst passing through the die. The die in this case acts primarily to reduce the wire diameter to a specific size with an acceptable surface finish.

Normally the die has a trumpet shaped bore with a conical portion which serves to deform the wire. The total die angle can have values between 5 and 25 degrees and the possible reduction in area at each die varies from about 10 to 45 per cent. In industrial wire drawing practice lubrication is used to reduce the drawing load and die wear and hence improve the machine life and surface finish of the product.

Usually, boundary lubrication is affected by pre-treating the wire and applying a suitable lubricant along the die and wire interface. The die wear however, is still at a significantly high level. In attempting to reduce the die wear to a lower level an alternative lubrication system was introduced by Christopherson and Naylor (1)§ who placed a long close fitting tube before the die, thus effectively sealing it on to the inlet side of the die. This assembly facilitated hydrodynamic lubrication to be achieved using oil.

It was necessary, however, to provide a leader to the full size wire to encourage effective lubrication at the starting condition. As oil is not a good boundary lubricant, some die wear was still prevalent. Modifications to the above hydrodynamic system and other designs of lubricating systems have been considered; for example, combined hydrostatic and hydrodynamic lubrication and the double-die system. However, the problem of breakage during start-up and the need for a leader to the full wire size was still not solved.

A programme of research has been undertaken at the Sheffield City Polytechnic with a view to introducing alternative lubricating systems in wire drawing which would have very different characteristics from those currently in use. It has been shown that a pressure tube based on the work of reference (1) improved some of the operating characteristics when polymer melt was used as lubricant (2)–(4). On the basis of experimental evidence it is apparent that the deformation of the wire commences in the tube itself before reaching the reduction die, which effectively acts only as a seal. Under these conditions the die geometry becomes of secondary importance and deformation actually takes place as if an effective die of continuously changing die angle is being used.

The polymer melt, in addition to acting as a lubricant, was also found to form a coating on the drawn wire. This coating was thought to be useful in protecting the wire against corrosion and also as a lubricant during any subsequent forming operation, e.g., bending or cold heading. This research has shown that, using a polymer melt, successful hydrodynamic lubrication can be attained during wire drawing thus eliminating die wear except at the start-up. However, the problem of breakage during start-up and the need for the leader to the full wire size still remained. Further, adhesion between the coating and the drawn wire was found to be poor. Despite all these, the results were very stimulating and lead the authors to believe that effective reduction of the wire should be possible using a polymer melt in conjunction with a tubular conical reduction unit only, thus eliminating the need for a conventional reduction die. Furthermore, the least diameter of the conical reduction unit could be greater than the nominal wire diameter.

Such a possibility would be useful in a number of ways in solving the problems associated with the conventional wire drawing process, e.g., die wear, initial wire breakage, and the need for a leader wire. Since the diameter at the exit end of the dieless reduction unit is greater than that of the wire, metal to metal contact, and hence wear, would no longer be a problem. As no conventional reduction die is used, the need for a leader wire and breakage during start-up would also be eliminated. With these aims an experimental programme was undertaken, the technique and results of which are discussed in the following sections.

2 EXPERIMENTAL PROCEDURE AND EQUIPMENT

Experimental work was carried out using a purpose built wire drawing machine which incorporates the dieless

The MS. of this paper was received at the Institution on 21st August 1981 and accepted for publication on 20th January 1982.

† *Department of Mechanical and Production Engineering, Sheffield City Polytechnic.*

‡ *Member of the Institution.*

§ *References are given in the Appendix.*

0022-2542/82/0300-0001 $02.00

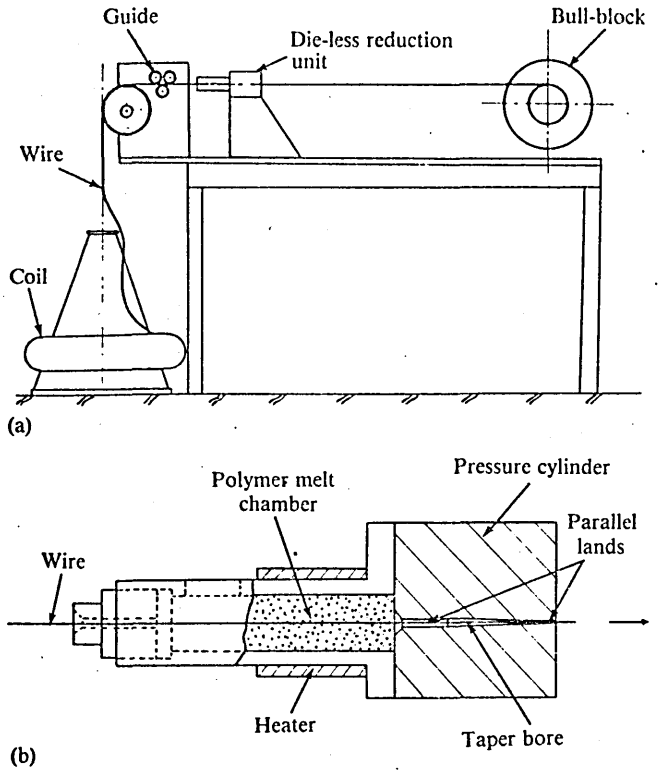

Fig. 1. Schematic diagram showing: (a) the wire drawing arrangement, (b) the details of the die-less reduction unit

reduction unit (DRU) and permits a wire drawing speed range of 0·054–4·0 ms^{-1} to be achieved. The schematic diagram of the drawing machine is shown in Fig. 1(a). The reduction unit, which consists of the conical tube and a melt chamber, is rigidly attached to the drawing machine bench. Details of the DRU is shown in the schematic diagram in Fig. 1(b). The undeformed wire passes through the melt chamber before undergoing deformation within the DRU. The melt chamber is kept filled with molten polymer by means of a heater. The 56 mm long bore of the DRU consists of three different sections, a parallel section, at the inlet side of length 16 mm and diameter 2·75 mm, a conical section of length 34 mm and another parallel section at the outlet side of length 5 mm and diameter 1·72 mm.

The diameter of the copper wire used in 1·625 mm. A low density polyethylene (Alkathene WVG23) with a specific gravity of 0·93 was used as the lubricant/coating material. Tests were carried out mainly at 130°C for the results presented in this paper. For general observations of the process tests were also carried out at other temperatures up to 200°C.

To start a run the wire is fed through the melt chamber and then through the DRU before being attached to the motorized winding drum. The wire while passing through the melt chamber drags along molten polymer into the DRU where hydrodynamic action is generated and reduction of the wire diameter takes place. The overall diameter of the coated wire at the outlet side of the DRU is controlled by the diameter of the parallel section at the outlet side of the DRU.

3 RESULTS AND DISCUSSION

Copper wire of nominal diameter 1·625 mm with stress–strain properties as shown in Fig. 2 was drawn at speeds

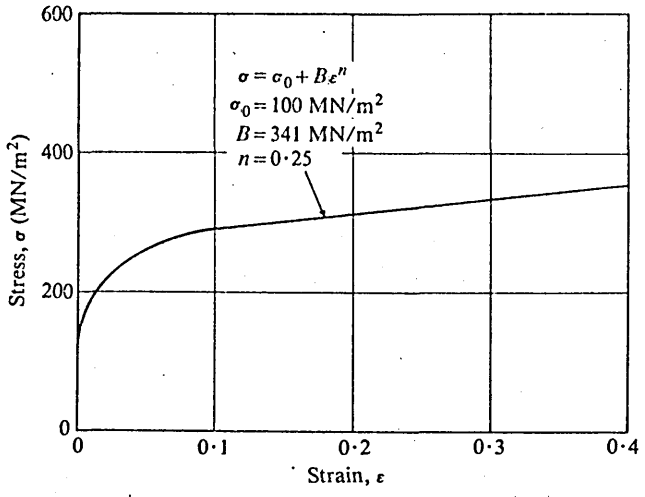

Fig. 2. Stress–strain diagram for the copper wire material

varying from 0·054 to 4·0 ms^{-1}. With the start of each run the hydrodynamic action of the polymer lubricant gives rise to an effective die profile within the DRU. In order to demonstrate any variation in the shape of this effective die profile, the process was stopped suddenly by instantaneously cutting off the wire during a number of runs at different drawing speeds. The wire was then taken out of the DRU and measurements were taken over the deformation zone. The results are plotted in Fig. 3 which shows profiles corresponding to three different drawing speeds. It is interesting to note that the effective die profile changes with speed but not in a linear manner. The profiles corresponding to the drawing speeds of 0·057 ms^{-1} and 1·3 ms^{-1} are shallower than that at drawing speed of 0·21 ms^{-1}. At least three tests were carried out at the same drawing speed. Measurements were taken of the drawn wire diameter from each test and the percentage reduction in area was calculated. These results are shown in Fig. 4 which shows the variation of the percentage reduction in area with drawing speed. It is evident that for certain drawing conditions a maximum reduction in area of up to 21 per cent can be obtained in one pass at drawing speed of around

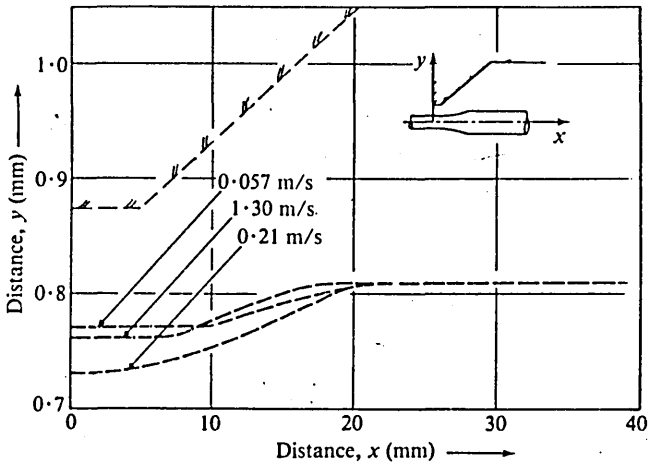

Fig. 3. Effective die profile corresponding to three different drawing speeds

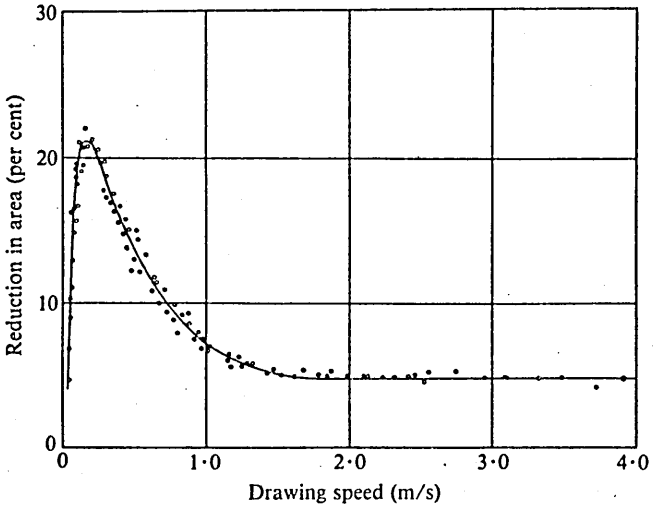

Fig. 4. The variation of reduction in area with drawing speed

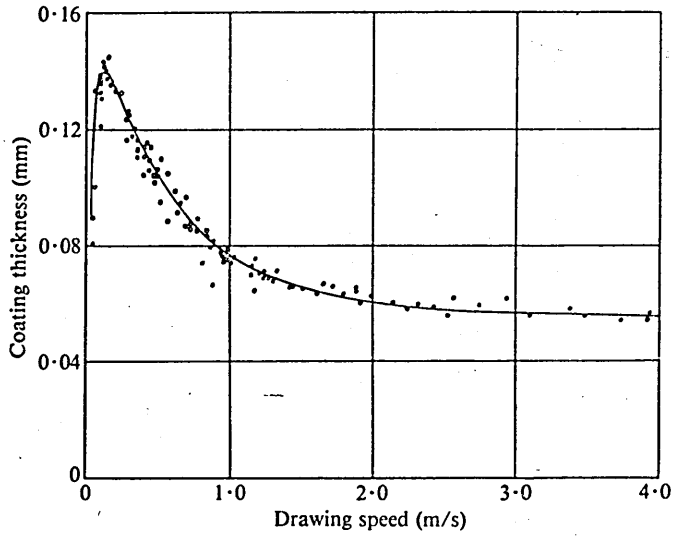

Fig. 5. The variation of coating thickness with drawing speed

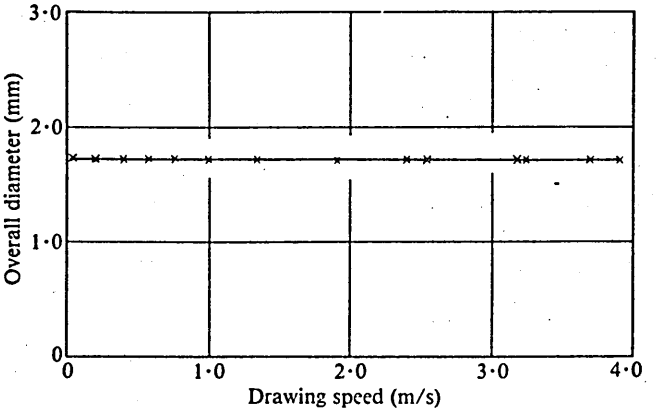

Fig. 6. Plot of overall diameter of the drawn and coated wire against drawing speed

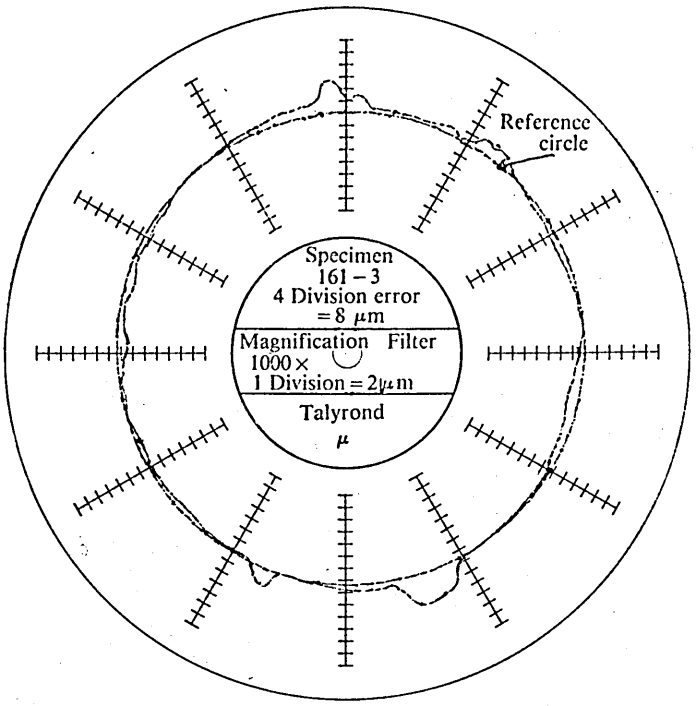

Drawing speed 0·054 m/s Reduction 4·66 per cent

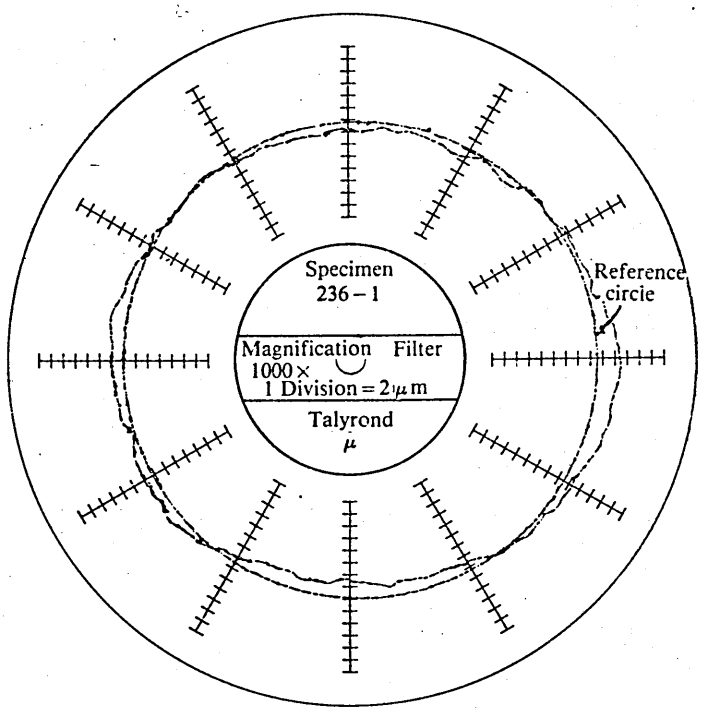

Drawing speed 0·40 m/s Reduction 22 per cent

Fig. 7. Roundness of the drawn wire corresponding to different reductions in area

0·20 ms^{-1}. It is also evident that the reduction in area is very sensitive to the variation of drawing speed at the lower end of the speed range of up to about 1·00 ms^{-1}. For drawing speeds greater than 1·00 ms^{-1} the reduction in area is insensitive to the variation in drawing speed and a steady value of about 5 per cent reduction in area is obtainable.

The thickness of the polymer coat was measured from the wires drawn at different speeds and the results are shown in Fig. 5. It is evident that the coat thickness varies in the same manner as the reduction in area. The speed at which maximum reduction in area is obtained,

corresponds to that at which the maximum coat thickness is obtained. A thinner coat is obtained at higher drawing speeds when the reduction in area is also less. It seems, therefore, that the drawn wire diameter and the coat thickness are complementary to each other in making up the overall diameter of the coated wire since no variation in the overall diameter was observed over the entire range of drawing speeds. This is evident from Fig. 6 which shows a plot of the overall diameter of the coated drawn wire against the drawing speed.

The overall diameter of the coated wire is controlled by the outlet diameter of the DRU. It should, therefore, be possible to simultaneously draw and coat wires to close specifications, in one single pass through a DRU.

In order to establish the uniformity of roundness along the length of the drawn wire, measurements were taken over a length of a number of specimens drawn at different speeds. The results of such measurement are shown in Fig. 7. It is evident that wires of acceptable roundness are produced at the various drawing speeds under consideration.

A number of observations were also made during the experimental programme. These may be enumerated as follows:

(i) there were no breakages during start-up for all the tests carried out at temperatures of up to 200°C,
(ii) there is no metal to metal contact during test runs and hence no wear,
(iii) there is no need for a leader wire to start a test run.

4 CONCLUSIONS

Copper wire has been drawn using a novel technique in which a dieless reduction unit in conjunction with a polymer melt as lubricant/coating material replaced the conventional reduction die.

Experimental results show that reductions in area of around 21 per cent are obtainable in one pass with reasonable dimensional accuracy.

It is also evident that the technique should be suitable for simultaneous reduction and production of coated wires.

The process eliminates the need for a leader wire, prevents breakage during start-up, and eliminates the use of conventional reduction die and, hence, the problem of die wear.

APPENDIX

REFERENCES

(1) CHRISTOPHERSON, D. G. and NAYLOR, H., 'Promotion of fluid lubrication in wire drawing', *Proc. Instn mech. Engrs*, 1955, **169**, 643–653.

(2) SYMMONS, G. R., STEVENS, A. J., and THOMPSON, P. J., 'Hydrodynamic lubrication and coating of wire using a polymer melt during the drawing operation', *Wire Industry*, 1978, 469–483.

(3) CRAMPTON, R., SYMMONS, G. R., and HASHMI, M. S. J., 'A non-Newtonian plasto-hydrodynamic analysis of the lubrication and coating of wire using a polymer melt during drawing', Int. Symposium Metal Working Lubrication, San Francisco, USA, August 1980, p. 107.

(4) HASHMI, M. S. J., CRAMPTON, R., and SYMMONDS, G. R., 'Effects of strain hardening and strain rate sensitivity of the wire material during drawing under non-Newtonian plasto-hydrodynamic lubrication conditions', *Int. J. Mach. Tool Des. Res.*, 1981, **21**, 71–86.

Plasto-hydrodynamic, dieless wire drawing: theoretical treatment and experimental results

G R SYMMONS, M S J HASHMI, and H PARVINMEHR

SYNOPSIS

A novel technique of drawing wires is described in which no conventional reduction dies are used. The wire is passed through a reduction unit having stepped parallel bores filled with polymer melts, the smallest bore diameter being greater than the initial nominal wire diameter. The reduction of the wire diameter is affected by means of the plasto-hydrodynamic action of the polymer melt within the reduction unit.

Experiments show that reductions in area in excess of 20 per cent can be obtained in one single pass when copper and mild steel wires are drawn. Furthermore, it is also observed that the use of this novel dieless reduction unit eliminates the problem of wear and breakage during start-up and also the need to have the diameter of the leading end of the wire reduced for easy insertion through the die used in conventional wire drawing.

Tests carried out on the drawn wire show that the process yields products of comparable mechanical and metallurgical properties as those obtained using conventional drawing process.

Analytical solutions are presented which enable prediction of the product sizes for given drawing speeds and other parameters. Agreement between the theory and experiment is found to be reasonably close.

THE AUTHORS are all in the Department of Mechanical and Production Engineering at the Sheffield City Polytechnic, UK.

INTRODUCTION

For conventional wire drawing the wire is pulled through tungsten-carbide tapered reduction dies on multi-die machines and the material deforms plastically whilst passing through the dies. The die in this case acts primarily to reduce the wire diameter to a specific size with an acceptable surface finish. Normally a die has a trumpet shaped bore with a conical portion which serves to deform the wire and the possible reduction in area at each die may vary from about 5 to 45 per cent.

In industrial wire drawing practice lubrication is used to reduce the drawing load and die wear and hence improve the machine life and surface finish of the product. Boundary lubrication is affected by pre-treating the wire and applying a suitable lubricant at the die-wire interface. The die wear, however, is still a major cause of concern and in order to reduce it an alternative lubrication system was suggested in Ref.(1) in which a long close fitting tube was placed before the die to facilitate hydrodynamic lubrication to be achieved using oil.

It was necessary, however, to provide a leader to the full size wire in order to induce effective lubrication at the starting condition. Nevertheless some die wear was still present. Modifications to the above hydrodynamic system and other designs of lubricating systems have been considered; for example, combined hydrostatic and hydrodynamic lubrication and the double-die system (2). However, the problem of breakage during start-up and the need for a leader to the full wire size was still not solved.

In an attempt to introduce alternative lubricating systems in wire drawing which would have very different characteristics from those currently in use further research was undertaken based on the system proposed in reference (1) but using polymer melt as the lubricant (3-5). On the basis of the experimental evidence it became apparent that the deformation of the wire commences in the tube itself before reaching the reduction die and the die effectively acts as only a seal. Under these conditions the die geometry becomes of secondary importance and deformation actually takes place as if an effective die of continuously changing die angle is being used. The polymer melt was acting as the lubricant at the same time forming a thin coating on the drawn wire.

This coating was thought to be useful in protecting the wire against corrosion during storage and also as a lubricant during any subsequent forming operation, eg bending or cold heading. It has also been shown that, using a polymer melt, successful hydrodynamic lubrication can be attained during wire drawing thus eliminating die wear except at the start-up. However, the problem of breakage during start-up and the need for the leader to the full wire size still remained.

The results of this research stimulated the authors to believe that reduction of the wire diameter should be possible using a polymer melt in conjunction with a tubular orifice only, thus eliminating the need for a conventional reduction die. Such a possibility should be useful in a number of ways in solving the problems associated with the conventional wire drawing process, eg die wear, initial breakage and the need for a leader wire. Since the diameter at the exit end of the dieless reduction unit would be greater than that of the undeformed wire, the need for a leader wire and breakage during start-up would be eliminated. Furthermore, in the absence of metal to metal contact, wear will no longer be a problem. With these aims in mind experimental programmes were undertaken using (i) a conical die-less reduction unit and (ii) a stepped bore die-less reduction unit. The results of the tests with the conical bore die-less reduction unit have previously been published in reference (6).

In this paper we shall present the experimental results carried out on copper and mild steel wires using the stepped bore cylindrical die-less reduction unit. Analysis of the process has been carried out and is also presented in this paper.

EXPERIMENTAL PROCEDURE AND EQUIPMENT

A purpose built wire drawing machine was used to carry out the experimental work. Fig.1(a) shows a schematic diagram of the drawing machine which incorporated a coil holder, the die-less reduction unit (DRU) and a bull-block. The machine permitted a wire drawing speed range of 0.05-4.0 ms^{-1} to be achieved. The DRU, which consists of the stepped bore cylinder and a melt chamber, is rigidly attached to the drawing machine bench. The relative bore sizes of the DRU were determined arbitrarily and could have been varied. In the present case, however, all the experiments were carried out using only one unit of fixed bore sizes. Effect of the bore sizes on the performance are currently being investigated and the results will be reported at a later date. Details of the DRU is shown in the schematic diagram in Fig.1(b).

The polymer melt chamber is attached to the DRU and is heated by a jacket type electrical heating element. Granular polymer is fed through a hopper to the melt chamber where it melts and is kept at a predetermined constant temperature level of 130°C. The polymer used in this study was a low density type polyethylene (Alkathene WVG23) with a specific gravity of 0.93. Tests were carried out on 1.62 mm diameter copper and 1.58 mm diameter mild steel wires. The melt temperature was kept at 130°C for all the tests reported in this paper.

To start a test run the wire is fed through the melt chamber and through the DRU whose smallest bore size is greater than the nominal diameter of the inlet wire. The wire is then attached to the motorized winding drum. When the process is started the wire while passing through the melt chamber drags along molten polymer into the DRU where hydrodynamic action generates pressure and reduction in the wire diameter takes place. The amount of reduction in area depends on the speed of drawing for given DRU geometry and polymer melt rheology at the test temperature but the overall diameter of the coated wire is controlled by the smallest bore size at the exit end of the DRU.

EXPERIMENTAL RESULTS

Copper and mild steel wires of nominal diameter 1.62 mm and 1.58 mm respectively were drawn at speeds varying from 0.05 to 4.00 ms^{-1}. The true stress-strain properties of the wire materials were determined by performing compression tests on small specimens prepared from the wires. These curves are shown in Fig.2(a) and (b) for copper and mild steel respectively. In order to establish the profile of the effective die within the DRU the process was stopped suddenly by instantaneously cutting off the wire during a test run. The wire was then taken out of the DRU and measurements were taken over the deformation zone.

Results of such measurements on mild steel wires drawn at various speeds are shown in Fig.3. which shows a number of typical deformation profiles in relation to the profile of the stepped bore DRU. Copper and mild steel wires were drawn at speeds varying from 0.05 to 4.0 ms^{-1}.

NOTATION

A	Material constant
D	Diameter of the wire
R	Radius of the wire
Y	Flow stress of the wire material
b	Factor determining theoretical profile
h_1	Gap between the undeformed wire and inlet bore of DRU
h_2	Gap between the undeformed wire and outlet bore of DRU
h_3	Gap between the deformed wire and outlet bore of DRU
l_1	Length of the DRU before the step
l_2	Length of the DRU after the step
n	Material constant
p	Pressure at any point in DRU
p_m	Maximum pressure if no deformation occurs
p_s	Maximum pressure if deformation occurs
v	Drawing speed
x_1	Length of undeformed wire in the DRU
x	Distance from x_1 when deformation occurs
ξ	Polymer viscosity
σ	Axial stress in the wire
τ	Shear stress along wire surface

Measurements taken on the drawn wires show that a maximum of about 26 per cent in reduction in area is obtained with copper wire and about 22 per cent in mild steel wire in one pass. However, for the given experimental conditions these maximum reductions in area occur at drawing speeds of about 0.20 ms^{-1} and falls sharply at higher drawing speeds. For copper wires the reduction in area falls down to about 8 per cent corresponding drawing speeds ranging from 1.0 to 4.0 ms^{-1}. This can be seen in Fig.4(a). However, as can be seen in Fig.4(b), the reduction in area for mild steel wires drop down to nothing at drawing speeds in excess of about 1.0 ms^{-1}. A number of tests were carried out at each drawing speed and the result is very repeatable for both the copper and mild steel wires.

The drawing load was measured by means of a peizo-electric load washer placed between the DRU and its fixtures to the drawing bench. The plots of such measured drawing loads against the drawing speed for the copper the mild steel wires are shown in Fig.5(a) and (b) respectively. These figures show that the drawing load is maximum when the reduction in area is maximum, ie at drawing speed of about 0.2 ms^{-1}.

Hydrodynamic pressure generated within the DRU during the drawing process was measured at four different locations using pressure transducers fitted into the DRU. Fig.6(a) and (b) show such pressure distributions along the length of the DRU when copper and mild steel wires respectively were drawn at 0.6 ms^{-1}. This figure indicates that pressure increases to maximum at around the location where the bore size changes; the pressure then falls to zero over the length of the smaller bore size of the DRU. The measured maximum pressure for copper was found to be about 1200 Bars whilst that for mild steel was found to be about 1800 Bars. Each of these pressure values was averaged from a number of pressure readings taken under similar test conditions.

ANALYSIS

In this section we shall describe an attempt to theoretically analyse the deformation process which takes place within the DRU. In references (7) and (8) analytical solutions were presented of the deformation process during drawing of the wire through a conventional reduction die incorporated pressure tube which was also filled with polymer melt. In the present case a different approach had to be taken as no physical reduction die is present and also that the minimum bore size of the DRU is slightly larger than the nominal wire diameter before any deformation takes place.

The present analysis requires the following assumptions to be made:

(i) the polymer melt has Newtonian characteristics
(ii) flow of the polymer melt is laminar
(iii) flow of the polymer melt is axial
(iv) the thickness of the polymer layer is small compared with bore size of the DRU
(v) pressure in the polymer melt is uniform in the thickness direction at any point along the length of the DRU
(vi) the deformation profile within the DRU may be described by $y = R_1 - bx^2$ (see Fig.7(a)).

Referring to Fig.7(a) which depicts the deformation mode, the Reynold's Equation for a Newtonian fluid may be written as

$$\frac{\partial}{\partial x}\left(h^3\frac{\partial p}{\partial x}\right) = \frac{\partial}{\partial x}(6\xi v h) \quad \ldots\ldots(1)$$

where $h = h_1 + bx^2$

Now for a given velocity, v and polymer viscosity, ξ, equation (1) becomes

$$\frac{\partial}{\partial x}\left(h^3\frac{\partial p}{\partial x}\right) = 6\xi v\frac{\partial h}{\partial x}.$$

But $\frac{\partial h}{\partial x} = 2bx$,

hence $\frac{\partial}{\partial x}\left(h^3\frac{\partial p}{\partial x}\right) = 6\xi v(2bx)$

which upon integration becomes

$$h^3\left(\frac{\partial p}{\partial x}\right) = 6\xi v b x^2 + c \quad \ldots\ldots(2)$$

Noting that $h = h_1 + bx^2$ and applying the boundary condition that $\frac{\partial p}{\partial x} = P_m/l_1$ at $x = 0$, the constant c is given by

$$c = h_1^3\left(\frac{\partial p}{\partial x}\right)$$

where P_m is the maximum pressure at the end of l_1 when no deformation occurs. Equation (2) then becomes,

$$\frac{\partial p}{\partial x} = 6\xi v\frac{bx^2}{(h_1 + bx^2)^3} + (P_m/l_1)\frac{h_1^3}{(h_1 + bx^2)^3} \quad \ldots(3)$$

Equation (3) may be integrated by substituting $a^2 = h_1/b$, so that the expression for the pressure becomes

$$p = 6\xi v\left\{\frac{\tan^{-1}(x/a)}{8a^3b^2} + \frac{(x^3 - a^2x)}{8a^2b^2(a^2 + x^2)^2}\right\} + (p_m/l_1)(h_1^3/b^3)\left\{\frac{3\tan^{-1}(x/a)}{8a^5} + \frac{(5a^2x + 3x^3)}{8a^4(a^2 + x^2)^2}\right\} + K \quad \ldots\ldots(4)$$

where K is the constant of integration.

Applying the boundary condition that at $x = 0$ where plastic deformation starts, the pressure $p = (p_m x_1/l_1)$ the const K is evaluated, so that equation (4) becomes

$$p = 6\xi v\left\{\frac{\tan^{-1}(x/a)}{8a^3b^2} + \frac{(x^3 - a^2x)}{8a^2b^2(a^2 + x^2)^2}\right\} + \frac{p_m}{l_1}\left\{x_1 + \frac{3a\tan^{-1}(x/a)}{8} + \frac{5a^4x + 3a^2x^3}{8(a^2 + x^2)^2}\right\} \quad \ldots(5)$$

Equation (5) gives the pressure distribution along the length $(l_1 - x_1)$ within the DRU and up to the step. The parameter p_m for the case when no deformation takes place within the length l_1 may easily be shown to be

$$p_m = 6\xi v(h_1 - h_2)/\{(h_1^3/l_1) + (h_2^3/l_2)\} \quad \ldots\ldots(6)$$

Also, the shear stress on the wire surface when no deformation takes place may be expressed as

$$\tau_1 = -\frac{h_1}{2}\left(\frac{\partial p}{\partial x}\right) - \frac{\xi v}{h_1} \quad \ldots\ldots(7)$$

But $\frac{\partial p}{\partial x} = p_m/l_1$ is constant and hence

$$\tau_1 = -\frac{p_m h_1}{2l_1} - \frac{\xi v}{h_1} \quad \ldots\ldots(7i)$$

According to Maxwell von-Mises or Tresca yield criterion for cylindrical deformation

$$\sigma_1 - \sigma_3 = Y_o \quad \ldots\ldots(8)$$

Now, $\sigma_x = -\frac{4\tau_1 x_1}{D_1}$ and $p = \frac{P_m x_1}{l_1}$, where x_1 is the length of the undeformed part of the wire within the DRU. Substituting for σ_x and p in equation (8) we obtain,

$$x_1 = Y_o/(p_m/l_1 - 4\tau_1/D_1) \quad \ldots\ldots(9)$$

Equation (9) in conjunction with equations (6) and (7) permits calculation of x_1 for known drawing speed, v.

The expression for the shear stress on the surface of the deformed wire may be given by equation (7) by simply replacing τ_c for τ_1 and h for h_1, thus

$$\tau_c = -\frac{h}{2}(\partial p/\partial x) - \xi v/h \quad \ldots\ldots(10)$$

Now, substitution for $(\partial p/\partial x)$ from equation (3) after writing $(h_1/b) = a^2$ and for $h = h_1 + bx^2 = b(a^2 + x^2)$ into equation (10) we get

$$\tau_c = -\frac{\xi v(a^2 + 4x^2)}{b(a^2 + x^2)} - \frac{p_m h_1 a^4}{2l_1(a^2 + x^2)^2} \quad \ldots\ldots(11)$$

Now, the axial force equilibrium condition for a small element of the wire shown in Fig.7(b), gives

$$d\sigma_x = -2\frac{dD}{D}(Y + \tau_c\cot\alpha) \quad \ldots\ldots(12)$$

hence $dD = -4bxdx$, $\tan\alpha = \frac{dD}{2dx} = -2bx$ and $\cot\alpha = -\frac{1}{2bx}$

Substituting for dD, $\cot\alpha$, τ_c in equation (12) we obtain

$$d\sigma_x = -\frac{8bxYdx}{(D_1 - 2bx^2)} + \frac{4\xi v(a^2 + 4x^2)dx}{b(D_1 - 2bx^2)(a^2 + x^2)^2} + \frac{2p_m h_1 a^4 dx}{l_1(a^2 + x^2)^2(D_1 - 2bx^2)} \quad \ldots\ldots\ldots\ldots(13)$$

At this stage let us introduce the strain hardening property of the wire material by substituting

$$Y = Y_o + A\varepsilon^n = Y_o + A[2\ln\{D_1/(D_1 - 2bx^2)\}]^n \ldots(13i)$$

into equation (13), where A and n are the material constants. Hence,

$$d\sigma_x = -\frac{8bxY_o dx}{(D_1 - 2bx^2)} - \frac{8bxA[2\ln\{D_1/(D_1-2bx^2)\}]^n dx}{(D_1-2bx^2)} + \frac{4\xi v(a^2+4x^2)dx}{b(D_1-2bx^2)(a^2+x^2)^2} + \frac{2p_m h_1 a^4 dx}{l_1(a^2+x^2)^2(D_1-2bx^2)} \quad \ldots\ldots\ldots(14)$$

Integrating equation (14) by use of partial fraction the expression for the axial stress is obtained as

$$\sigma_x = -2Y_o\ln(D_1-2bx^2) - \frac{2A}{(n+1)}[2\ln(D_1-2bx^2)]^{n+1} - \frac{4\xi v}{b}\{\frac{4b(2D_1+a^2b)}{\sqrt{2bD_1}(D_1+2ba^2)^2}\ln\left(\frac{\sqrt{D_1} + x\sqrt{2b}}{\sqrt{D_1+2bx^2}}\right) + \frac{(5D_1-2ba^2)}{2a(D_1+2ba^2)}\tan^{-1}\frac{x}{a} - \frac{3x}{2(D_1+2ba^2)(a^2+x^2)}\} + \frac{2p_m h_1}{l_1}\{\frac{a^2x}{2(D_1+2ba^2)(a^2+x^2)} + \frac{a(D_1+6ba^2)}{2(D_1+2ba^2)^2}\tan^{-1}\frac{x}{a} + \frac{4a^4b^2}{\sqrt{2bD_1}(D_1+2ba^2)^2}\ln\left(\frac{\sqrt{D_1} + x\sqrt{2b}}{\sqrt{D_1-2bx^2}}\right)\} + k \quad \ldots(15)$$

where K is the constant of integration. Applying the boundary condition; when $x = 0$, $\sigma_x = \frac{4\tau_1 x_1}{D_1}$ into equation (15) the constant K is obtained as

$$K = \frac{4x_1\tau_1}{D_1} + 2Y_o\ln D_1 + \frac{2A}{(n+1)}[2\ln(D_1)]^{n+1} \quad \ldots(16)$$

which upon sibstitution in equation (15) yields

$$\sigma_x = 2Y_o\ln\left(\frac{D_1}{D_1-2bx^2}\right) + \frac{4\xi v}{b}\{\frac{(2D_1+ba^2)}{\sqrt{2bD_1}(D_1+2ba^2)^2}\ln\left(\frac{\sqrt{D_1} + x\sqrt{2b}}{\sqrt{D_1-2bx^2}}\right) + \frac{5D_1-2ba^2}{2a(D_1+2ba^2)^2}\tan^{-1}\frac{x}{a} - \frac{3x}{2(D_1+2ba^2)(a^2+x^2)}\} + 2P_m\frac{h_1}{l_1}\{\frac{a^2x}{2(D_1+2ba^2)(a^2+x^2)} + \frac{a(D_1+6ba^2)}{2(D_1+2ba^2)^2}\tan^{-1}\frac{x}{a} + \frac{4a^4b^2}{\sqrt{2bD_1}(D_1+2ba^2)^2}\ln\left(\frac{\sqrt{D_1} + x\sqrt{2b}}{\sqrt{D_1 - 2bx^2}}\right)\} + \frac{2A}{(n+1)}[2\ln\left(\frac{D_1}{D_1-2bx^2}\right)]^{n+1} + \frac{4x_1}{D_1}\tau_1 \quad \ldots\ldots\ldots(16)$$

$$p + \sigma_x = Y_o + A\varepsilon^n = Y_o + A(2\ln\frac{D_1}{D_1-2bx^2})^n \quad \ldots\ldots(17)$$

Equation (17) when substitutions are made for p and σ_x from equations (5) and (16) respectively, may be iterated to establish the value of b for given drawing speed and DRU geometry. Once the value of 'b' is established the deformation profile is obtained and the reduction in area at any point for $x_1 < x < l_1$ is given by

$$PRA = \{(D_1 - 2bx^2)/D_1\}^2 \times 100 \quad \ldots\ldots\ldots\ldots(18)$$

where PRA = percentage reduction in area.
It is assumed that no further deformation takes place after the step within the DRU and hence the maximum reduction in area is given by

$$PRA = [\{D_1 - 2b(l_1-x_1)^2\}/D_1]^2 \times 100 \quad \ldots\ldots\ldots\ldots(19)$$

The maximum pressure, P_s, at the step is obtained by substituting $x = (l_1-x_1)$ in equation (5) when the value of 'b' is already determined. The axial stress σ_s at the step is obtained from equation (16) by substituting for $x = (l_1-x_1)$. The drawing stress, σ_d, at the exit end of the DRU is then given by

$$\sigma_d = \sigma_s + \sigma_x' \quad \ldots\ldots\ldots\ldots(20)$$

where
$$\sigma_x' = -\frac{4\tau_2 l_2}{\{D_1 - b(l_1-x_1)^2\}}$$
$$\tau_2 = -\frac{h_3}{2}\left(\frac{\partial p}{\partial x}\right) - \frac{\xi v}{h_3}$$
$$= \frac{h_3 P_s}{2l_2} - \frac{\xi v}{h_3}, \text{ since } \frac{\partial p}{\partial x} = -P_s/l_2 \quad \ldots\ldots\ldots(21)$$
$$h_3 = h_2 + b(l_1-x_1)^2$$

RESULTS AND DISCUSSIONS

Theoretical results were obtained on the basis of the above analysis for copper and mild steel wires. The length of the wire from the inlet side of the DRU to the point where plastic deformation commences was calculated using equation (9) for drawing speeds of up to 4 ms^{-1} and the results are shown in Fig. 8(a) for both the copper and mild steel wires. As expected the length of undeformed wire within the DRU is greater for mild steel than that for copper for any given drawing speed.

The pressure distribution within the DRU was calculated for a number of theoretical deformation profiles ('b' values) corresponding to a given drawing speed and the results can be seen in Fig.8(b). The value of the polymer viscosity, ξ, was taken as 118 Nsm^{-2} at the melt temperature of 130°C. The pressure increases linearly up to the point where deformation commences then falls linearly to zero at the exit end of the DRU. The deformation profiles, calculated theoretically show very close similarity with those observed experimentally for both the copper and mild steel wires. A number of such profiles calculated for different drawing speeds are shown in Fig.9 (see also Fig.3).

The drawing load was calculated using equation (20) for drawing speeds of up to 4.0 ms^{-1} and is shown in Fig.10 for mild steel and copper. These results do not agree well with

experimental drawing load (see Figs. 5(a) and (b)) occurs at drawing speed of about 0.2 ms^{-1} after which it decreases to a lower value. Theoretically this value is reached at drawing speed of about 1.2 ms^{-1} after which the drawing load keeps on increasing. The theoretically calculated percentage reduction in area for copper and mild steel for different drawing speeds were found to be different from what was observed experimentally. Such results shown in Fig.11 indicates that the reduction in area increases with drawing speed at a greater rate and reaches a magnitude of about 25 per cent corresponding to a drawing speed of 1.2 ms^{-1}. However, unlike the experimentally observed results, the theoretically calculated reduction in area keeps on increasing, although at a slower rate, with increasing drawing speed. We should note that the experimentally observed maximum reduction in area takes place at around 0.2 ms^{-1} drawing speed.

There could be a number of factors contributing towards such discrepancy. Firstly, we assumed the polymer melt to behave like a Newtonian fluid, whilst in practice it would more likely behave as a non-Newtonian fluid. Furthermore, no provision was made in this analysis of the possibility that during the deformation process a critical shear stress value may be reached as well as the fact that slip at the metal fluid boundary may occur at some stage. This aspects need further attention at experimental level and then the analysis should be modified accordingly.

CONCLUSIONS

Copper and mild steel wires have been successfully drawn using a stepped bore die-less reduction unit (DRU) in conjunction with a polymer melt.

Reductions in area in excess of 20 per cent was possible in a single pass both with copper and mild steel wires. The process eliminates the need for a leader wire, prevents breakage during start-up and eliminates the use of conventional reduction dies and hence the problem of die wear. Theoretical analysis of the process based on Newtonian fluid behaviour of the polymer melt predicts deformation profile which are in close agreement with those observed experimentally. However, the theory, as it stands, is found to be inadequate to accurately predict the drawing load and the percentage reduction in area at drawing speeds in excess of about 1.2 ms^{-1}.

REFERENCES

1. Christopherson, D.G. and Naylor, H., 'Promotion of fluid lubrication in wire drawing', Proc. Instn. Mech. Engrs, 1955, vol.169, 643-653.

2. Middlemiss, A., 'Hydrodynamic lubrication for drawing of steel wire', Tribology in Iron and Steel Works, ISI Publications 125, 47-54.

3. Symmons, G.R., Stevens, A.J. and Thompson, P.J., 'Hydrodynamic lubrication and coating of wire using a Polymer melt during the drawing operation', Wire Industry, 1978, 469-483.

4. Crampton, R., Symmons, G.R. and Hashmi,M.S.J., 'A non-Newtonian plasto-hydrodynamic analysis of the lubrication and coating of wire using a polymer melt during drawing', Int. Symposium Metal Working Lubrication, San Francisco, USA, August 1980, p107.

5. Hashmi, M.S.J., Crampton, R. and Symmons, G.R., 'Effects of strain hardening and strain rate sensitivity of the wire material during drawing under non-Newtonian plasto-hydrodynamic lubrication conditions', Int. J. Mach. Tool Des. Res., 1981, vol.21, 71-86.

6. Hashmi, M.S.J., Symmons, G.R. and Parvinmehr, H., 'A novel technique of wire drawing', JMES, Instn. Mech. Engrs. 1982, vol.24, 1-4.

A patent application is currently being prepared for the experimental process described in this paper

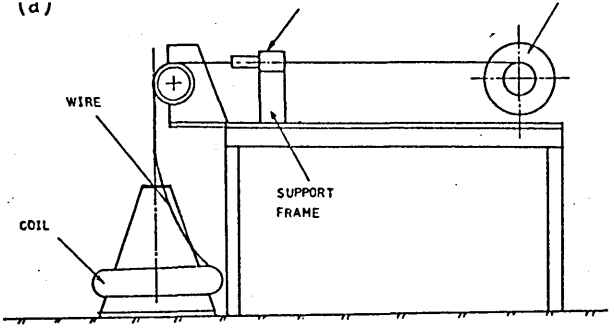

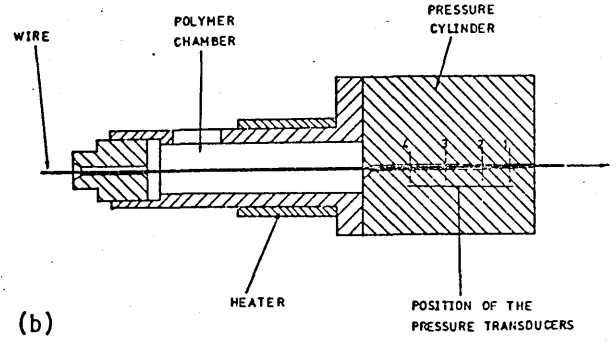

Fig.1 Schematic diagram showing (a) the drawing machine and (b) the DRU and polymer melt assembly.

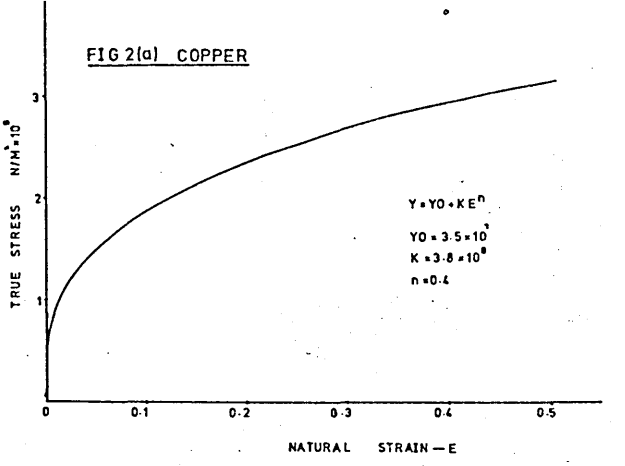

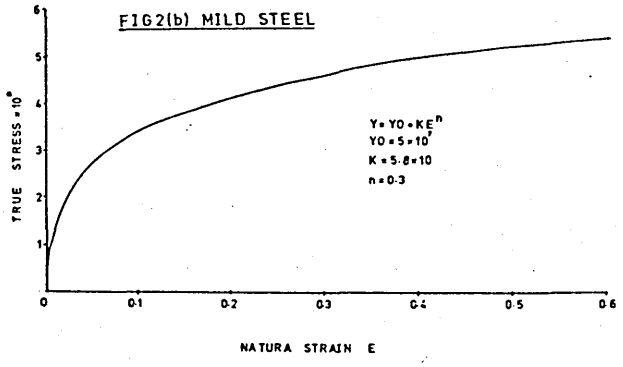

Fig.2 Showing the stress-strain curves for (a) copper and (b) mild steel.

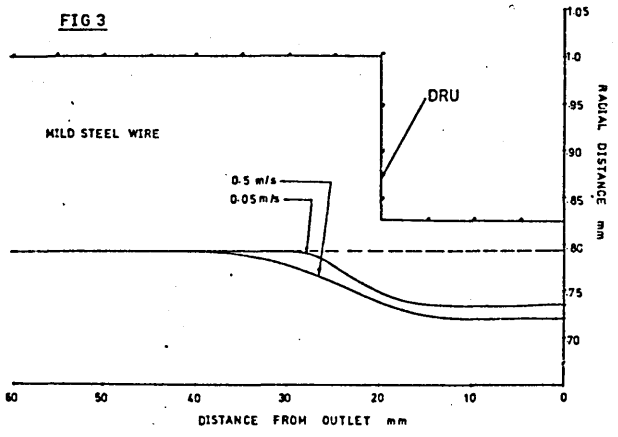

Fig.3 Showing typical deformation profiles for mild steel wires.

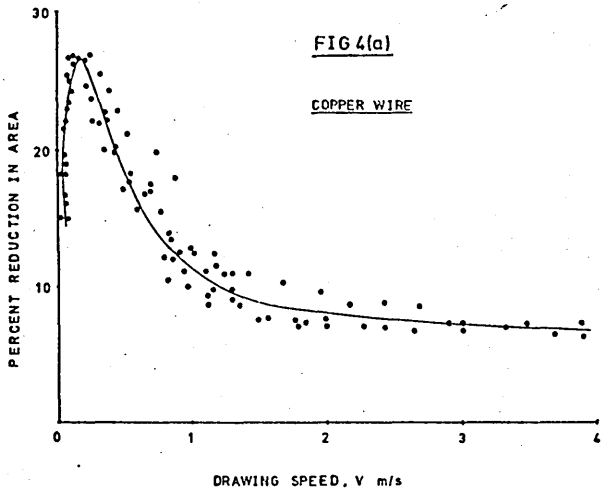

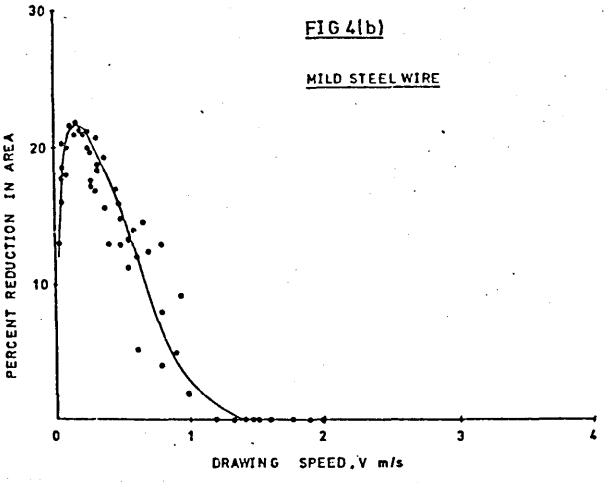

Fig.4 Percentage reduction in area against drawing speed for (a) copper and (b) mild steel wires.

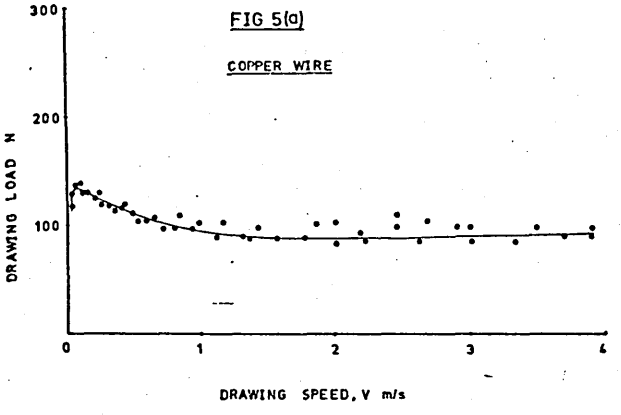

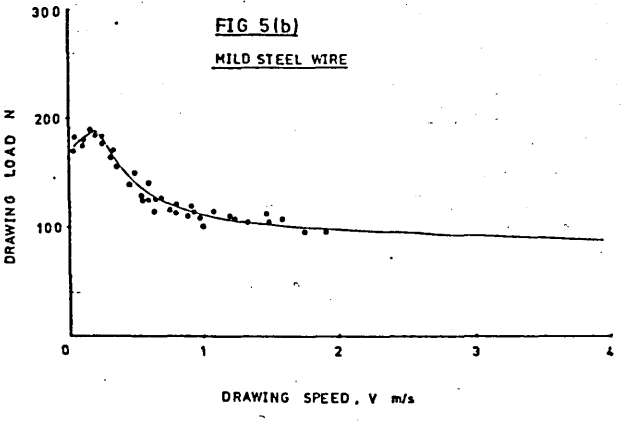

Fig.5 Showing drawing load against drawing speed for (a) copper and (b) mild steel wires.

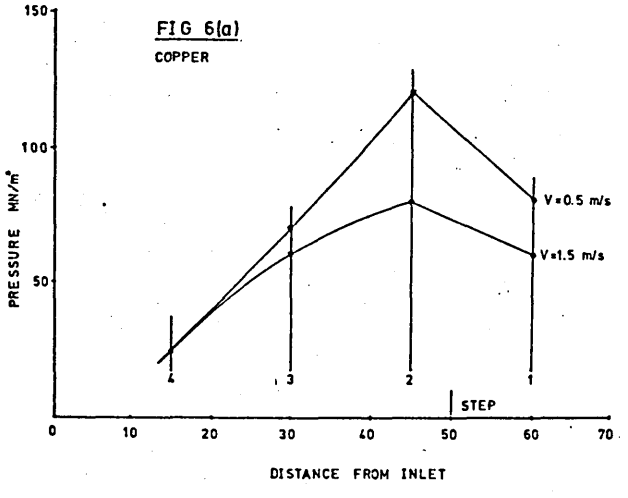

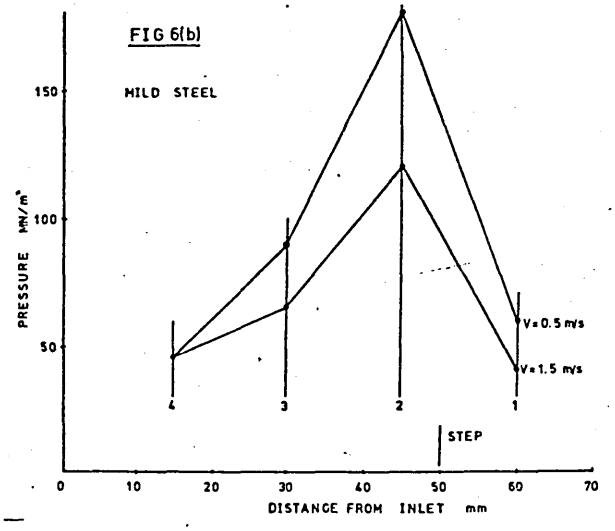

Fig.6 Experimentally measured pressure distributions along the DRU when (a) copper and (b) mild steel wires are drawn.

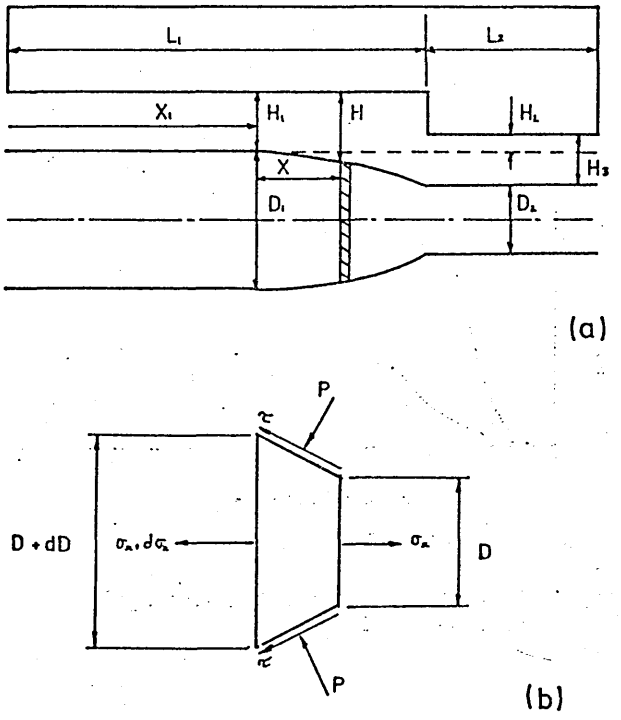

Fig.7 Showing (a) theoretically assumed deformation mode within the DRU, (b) stresses acting on an element of the wire.

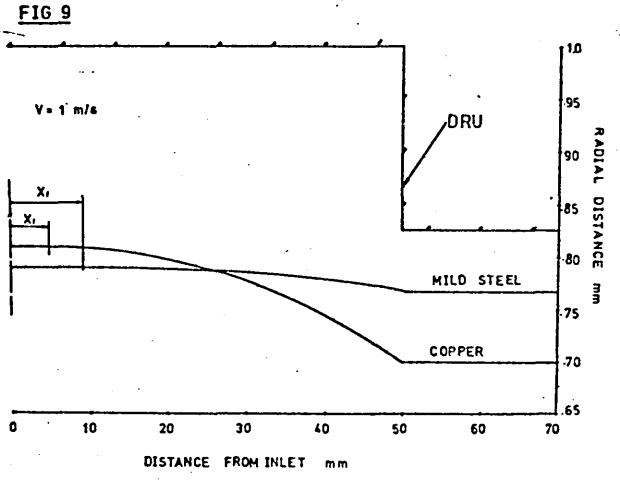

Fig.9 Showing theoretically predicted deformation profiles.

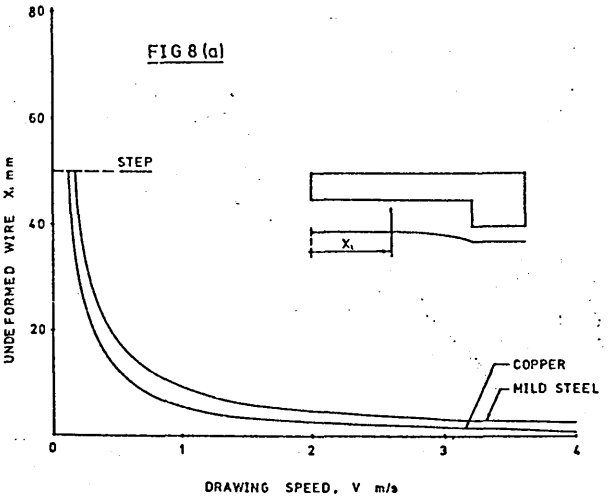

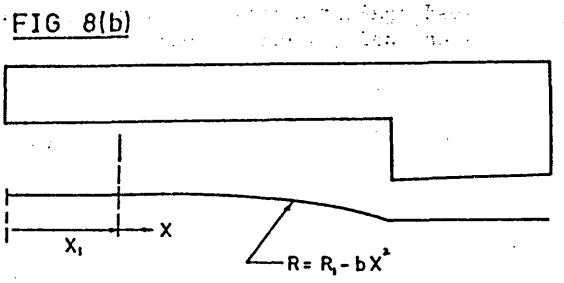

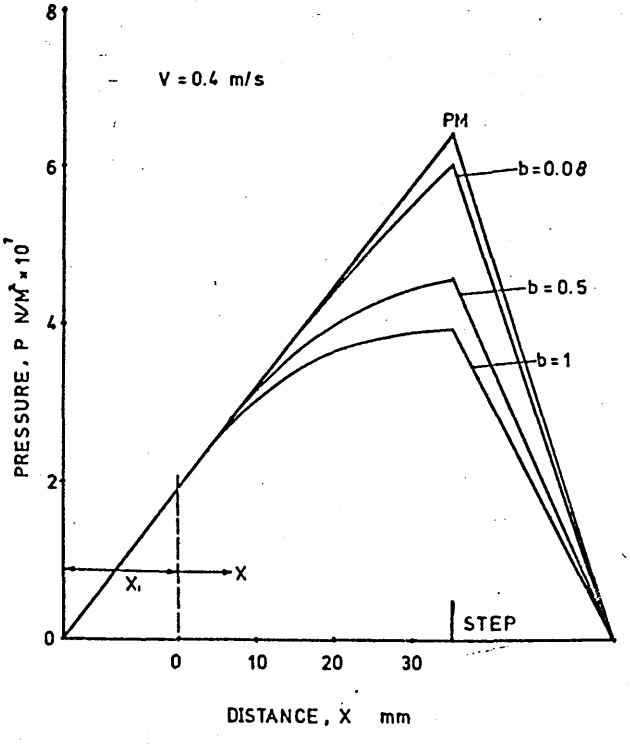

Fig.8 Showing (a) the graph of undeformed length, x, against drawing speed and (b) the effect of deformation profile on pressure.

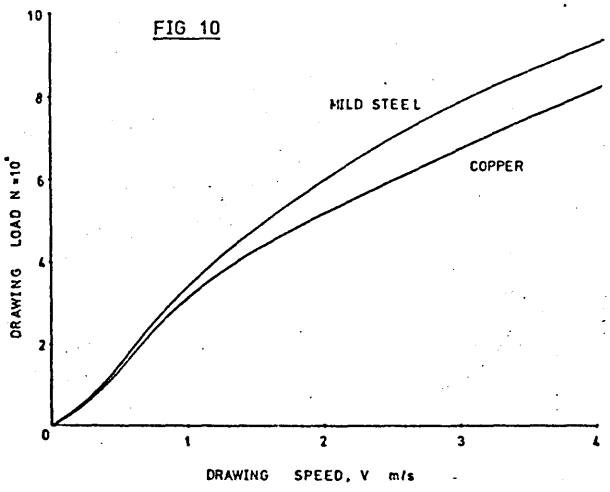

Fig.10 Showing theoretically calculated drawing load against drawing speed for (a) mild steel and (b) copper wires.

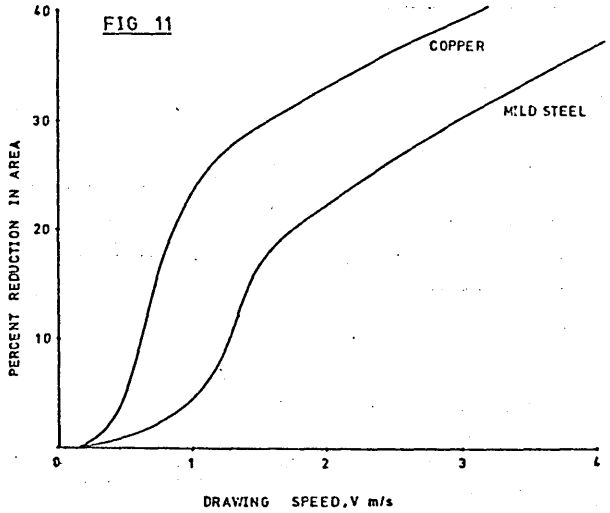

Fig.11 Percentage reduction in area against drawing speed.